Expansive Soils

Recent advances in characterization and treatment

Edited by
Amer Ali Al-Rawas & Mattheus F.A. Goosen

Expansive Soils

BALKEMA - Proceedings and Monographs
in Engineering, Water and Earth Sciences

Expansive Soils

Recent advances in characterization and treatment

Editors

Amer Ali Al-Rawas

Department of Civil and Architectural Engineering,
College of Engineering, Sultan Qaboos University,
Sultanate of Oman

Mattheus F.A. Goosen

School of Science and Technology, University of Turabo,
Puerto Rico, USA

Taylor & Francis
Taylor & Francis Group
LONDON / LEIDEN / NEW YORK / PHILADELPHIA / SINGAPORE

Published by: Taylor & Francis/Balkema
P.O. Box 447, 2300 AK Leiden, The Netherlands
e-mail: Pub.NL@tandf.co.uk
www.balkema.nl, www.tandf.co.uk, www.crcpress.com

British Library Cataloguing in Publication Data
A catalogue record for this book is available from the British Library

Library of Congress Cataloging in Publication Data
Expansive soils: recent advances in characterization and treatment / editors: Amer Ali Al-Rawas, Mattheus F. A. Goosen.
p. cm.
Includes index.
1. Soil consolidation. 2. Swelling soils. I. Al-Rawas, Amer Ali.
II. Goosen, Mattheus F.A.

TE210.4.E96 2006
624.1'5136–dc22 2005035532

ISBN10 0–415–39681–6 ISBN13 978–0–415–39681–3

Contents

List of contributors ix
Preface xi

PART 1
Nature, identification, and classification of expansive soils 1

1 Geology, classification, and distribution of expansive soils and rocks: a case study from the Arabian Gulf 3
AMER A. AL-RAWAS, MATTHEUS F.A. GOOSEN, AND GHAZI A. AL-RAWAS

2 Identification and classification of expansive soils 15
SUDHAKAR M. RAO

3 Prediction and classification of expansive clay soils 25
AGUS SETYO MUNTOHAR

4 Overview of mineralogy of bentonites: genesis, physicochemical properties, industrial uses, and world production 37
RICHARD PŘIKRYL

5 Swelling in non-vertisolic soils: its causes and importance 55
MIGUEL ANGEL TABOADA AND RAÚL SILVIO LAVADO

PART 2
Volume change characteristics 79

6 ESEM study of structural modifications of argillite during hydration/dehydration cycles 81
JOËLLE DUPLAY, GERMAN MONTES-HERNANDEZ, AND LUIS MARTINEZ

7 **Large-scale odometer for assessing swelling and consolidation behavior of Al-Qatif clay** 85
SHAHID AZAM

8 **Water sorption and dilatation of bentonites and montmorillonite-rich clays** 101
RADEK HANUS, IRENA KOLAŘÍKOVÁ, AND RICHARD PŘIKRYL

PART 3
Swelling potential measurement 115

9 **ESEM–DIA method to estimate swelling–shrinkage of raw and cation-saturated bentonite** 117
GERMAN MONTES-HERNANDEZ

10 **Effect of remolding techniques on soil swelling and shear strength properties** 127
MOUSA F. ATTOM, MAJED M. ABU-ZREIG, AND MOHAMMED TALEB OBAIDAT

11 **Swelling rate of expansive clay soils** 139
ROSLAN HASHIM AND AGUS SETYO MUNTOHAR

12 **Swelling behavior of Ankara Clay: predictive techniques, damage details, and swelling maps** 149
ZEYNAL ABIDDIN ERGULER AND RESAT ULUSAY

13 **Prediction of swelling characteristics with free swell index** 173
BHYRAVAJJULA R. PHANIKUMAR

PART 4
Advanced techniques for swelling potential assessment 185

14 **Remote sensing of expansive soils: use of hyperspectral methodology for clay mapping and hazard assessment** 187
SABINE CHABRILLAT AND ALEXANDER F.H. GOETZ

15 **Spectroscopy as a tool for studying swelling soils** 211
PATRICK CHEGE KARIUKI, KEITH SHEPHERD, AND FREEK VAN DER MEER

16 **Finite element analysis of piers in expansive soils** 231
YAHIA E.-A. MOHAMEDZEIN

17 Prediction of swelling pressure of expansive soils using Neural Networks 245
YAHIA E.-A. MOHAMEDZEIN, RABAB IBRAHIM, AND ASSIM ALSANOSI

18 Shrinkage strain characterization of expansive soils using digital imaging technology 257
ANAND J. PUPPALA, SIVA PATHIVADA, VENKAT BHADRIRAJU, AND LAUREANO R. HOYOS

PART 5
Site characterization 271

19 Swelling behavior of expansive shale: a case study from Saudi Arabia 273
ABDULLAH I. AL-MHAIDIB

20 Volume change characteristics of compacted Ankara clay 289
ERDAL COKCA AND OZLEM CORA

21 Influence of trees on expansive soils in southern Australia 295
DONALD A. CAMERON, MARK B. JAKSA, WAYNE POTTER, AND AARON O'MALLEY

PART 6
Lime stabilization 315

22 Stabilization of expansive Ankara Clay with lime 317
MEHMET CELAL TONOZ, CANDAN GOKCEOGLU, AND RESAT ULUSAY

23 Lime stabilization of expansive clay 341
ZALIHE NALBANTOGLU

24 Combined lime and polypropylene fiber stabilization for modification of expansive soils 349
ANAND J. PUPPALA, EKARIN WATTANASANTICHAROEN, AND ALI PORBAHA

PART 7
Cement-stabilization 369

25 Assessment of anisotropic behavior of swelling soils on ground and construction work 371
EVANGELOS I. STAVRIDAKIS

26 Stabilization of problematic soils using cement and lime **385**
EVANGELOS I. STAVRIDAKIS

27 Influence of sand content on strength and durability of cement-acrylic resin treated soil **399**
COSTAS A. ANAGNOSTOPOULOS

28 Physical and engineering properties of cement stabilized soft soil treated with acrylic resin additive **405**
COSTAS A. ANAGNOSTOPOULOS

PART 8
Other treatment methods **417**

29 Pozzolanic stabilization of expansive soils **419**
P.V. SIVAPULLAIAH

30 Swelling characteristics and improvement of expansive soil with rice husk ash **435**
AGUS SETYO MUNTOHAR

31 Effects of addition of fly ash on swell potential of an expansive soil **453**
DEVRIM TURKER AND ERDAL COKCA

32 Dynamic characterization of chemically modified expansive soil **465**
LAUREANO R. HOYOS, PHONLAWUT CHAINUWAT, AND ANAND J. PUPPALA

33 Assessment of seasonal effects on engineering behavior of chemically treated sulfate-rich expansive clay **483**
LAUREANO R. HOYOS, ARTHIT LAIKRAM, AND ANAND J. PUPPALA

PART 9
Construction techniques and remedial measures **505**

34 Granular pile-anchors: an innovative foundation technique for expansive soils **507**
BHYRAVAJJULA R. PHANIKUMAR AND RADHEY S. SHARMA

Index 523

Contributors

Majed M. Abuzreig, Jordan University of Science and Technology, Irbid, Jordan

Abdullah I. Al-Mhaidib, King Saud University, Riyadh, Saudi Arabia

Amer Ali Al-Rawas, Sultan Qaboos University, Al-Khoud, Sultanate of Oman

Ghazi A. Al-Rawas, Sultan Qaboos University, Sultanate of Oman

Assim Alsanosi, University of Khartoum, Khartoum, Sudan

Costas A. Anagnostopoulos, Aristotle University of Thessaloniki, Thessalonica, Greece

Mousa F. Attom, Jordan University of Science and Technology, Irbid, Jordan

Shahid Azam, University of British Columbia, Vancouver, Canada

Venkat Bhadriraju, University of Texas at Arlington, USA

Donald A. Cameron, University of South Australia, Australia

Sabine Chabrillat, GeoForschungsZentrum (GFZ) Potsdam, Germany

Phonlawut Chainuwat, PSA Engineering, Texas, USA

Erdal Cokca, Middle East Technical University, Ankara, Turkey

Ozlem Cora, Middle East Technical University, Ankara, Turkey

Joelle Duplay, Centre de Géochimie de la Surface, Strasbourg, France

Zeynal Abiddin Erguler, Hacettepe University, Ankara, Turkey

Alexander F.H. Goetz, University of Colorado, USA

Candan Gokceoglu, Hacettepe University, Ankara, Turkey

Mattheus F.A. Goosen, University of Turabo, Gurabo, Puerto Rico

Radek Hanus, Charles University, Prague, Czech Republic

Roslan Hashim, University of Malaya, Kuala Lumpur, Malaysia

Laureano R. Hoyos, University of Texas at Arlington, USA

Rabab Ibrahim, Al-Amin Engineering Company, Khartoum, Sudan

Mark B. Jaksa, University of Adelaide, Australia

Patrick Chege Kariuki, International Livestock Research Institute (ILRI), Kenya

Irena Kolaříková, Charles University, Prague, Czech Republic

Arthit Laikram, University of Texas at Arlington, USA

Raúl Silvio Lavado, Universidad de Buenos Aires, Argentina

Luis Martinez, Universite Henri Poincare, Nancy, France

Freek van der Meer, Delft University of Technology, Delft, The Netherlands

Yahia E.-A. Mohamedzein, Sultan Qaboos University, Al-Khoud, Sultanate of Oman

German Montes-Hernandez, Centre de Géochimie de la Surface, Strasbourg, France

Agus Setyo Muntohar, Muhammadiyah University of Yogyakarta, Indonesia

Zalihe Nalbantoglu, Eastern Mediterranean University, Gazimagusa, Mersin 10, Turkey

Mohammed T. Obaidat, Jordan University of Science and Technology, Irbid, Jordan

Aaron O'Malley, University of South Australia, Australia

Siva Pathivada, University of Texas at Arlington, USA

Bhyravajjula R. Phanikumar, GMR Institute of Technology, India

Ali Porbaha, California Department of Transportation, USA

Wayne Potter, University of South Australia, Australia

Richard Přikryl, Charles University, Prague, Czech Republic

Anand J. Puppala, University of Texas at Arlington, USA

Sudhakar M. Rao, Indian Institute of Science, Bangalore, India

Radhey S. Sharma, Louisiana State University, USA

Keith Shepherd, World Agroforestry Centre (ICRAF), Kenya

P.V. Sivapullaiah, Indian Institute of Science, Bangalore, India

Evangelos I. Stavridakis, Aristotle University of Thessaloniki, Greece

Miguel Angel Taboada, Universidad de Buenos Aires, Argentina

Mehmet Celal Tonoz, Hacettepe University, Ankara, Turkey

Devrim Turker, Middle East Technical University, Ankara, Turkey

Resat Ulusay, Hacettepe University, Ankara, Turkey

Ekarin Wattanasanticharoen, University of Texas at Arlington, USA

Preface

Expansive soils are a worldwide problem. The estimated damage to buildings, roads, and other structures built on expansive soils, for example, exceeds 15 billion dollars in the US annually. Such soils are considered natural hazards that pose challenges to civil engineers, construction firms, and owners. In some underdeveloped countries, buildings were constructed without any knowledge of the presence of expansive soils. This was in part due to a lack of historical evidence. With the rapid development in urban infrastructure, expansive soil problems have become more evident. There is therefore a need to address the problems associated with these soils.

Expansive soils occur in many parts of the world but particularly in arid and semi-arid regions. In these regions, evaporation rates are higher than the annual rainfall so that there is almost always a moisture deficiency in the soil. The addition of water will cause ground heave in soils possessing swelling potential. Semi-arid regions are characterized by short periods of rainfall followed by long periods of draught causing cyclic swelling and shrinking phenomena. The ground heave that results from soil swelling potential is a multifactorial phenomenon that involves a combination of the type of material, type and amount of clay minerals, microfabric, initial moisture content, and initial dry density.

Considerable research has been reported on expansive soils over the past three decades. The last international conference on expansive soils was held in Dallas, Texas, USA in 1992. The 6th International Conference on Expansive Soils was held in New Delhi in January 1988. Several textbooks on expansive soils are also available: *Foundations on Expansive Soils* by Chen, F.H., Elsevier 1988; *Expansive Soils: Problems and Practice in Foundation and Pavement Engineering* by Nelson, J.D. and Miller, D.J., John Wiley & Sons, Inc. 1992; *Construction of Buildings on Expansive Soils* by Sorochan, E.A., Aa Balkema January 1991; and *Behaviour of Saturated Expansive Soil and Control Methods – Revised and Enlarged Edition* by Katti, R.K./Katti, D.R./Katti, A.R., Routledge 2002. Since the most recent comprehensive publication is several years old, a book is now needed that updates the state-of-the-art knowledge in this area.

This book provides a broad coverage of recent advances in the characteristics and treatment of expansive soils. There are nine parts each with specific chapters. It starts with an overview section (Part 1) on the nature, identification, and classification of expansive soils. Parts 2 and 3 deal with volume change characteristics and swelling potential measurements, respectively. Part 4 covers advanced techniques for swelling potential assessment. Such tests are important for assessing the actual swelling potential of the soil and estimating ground heave. Part 5 on site characterization presents field measurements of soil swelling potential and suction. The next three parts deal with lime stabilization, cement stabilization, and

other treatment methods. Chemical stabilization, for example, has gained wide attention as a successful technique for treating expansive soils. In the final section (Part 9), the performance of engineering structures built on expansive soils such as buildings, houses, embankments, and roads, is evaluated. Remedial measures used to address soil swelling problems are also described.

The intended audience for this book includes researchers, practicing engineers, contractors, postgraduate and undergraduate students, and others working in expansive soils. The authors hope that the information provided in this book will help to promote a better understanding of expansive soils, contribute toward their treatment, and thereby reducing or minimizing their effects. The views expressed in the chapters of this book are those of the authors and do not necessarily reflect those of their respective institutions. The authors hope that this book will contribute to the advancement in research in expansive soils and help engineers in the development of practical solutions to expansive soil problems.

Amer Ali Al-Rawas
Sultan Qaboos University, Al-Khoud, Sultanate of Oman
Mattheus F.A. Goosen
University of Turabo, Gurabo, Puerto Rico
2005

Part I

Nature, identification, and classification of expansive soils

Chapter 1

Geology, classification, and distribution of expansive soils and rocks

A case study from the Arabian Gulf

Amer A. Al-Rawas,[1] *Mattheus F.A. Goosen,*[2] *and Ghazi A. Al-Rawas*[3]

Summary

The chapter presents an overview of the geology, classification, and distribution and swelling potential of expansive soils and rocks from the Arabian Gulf country of Oman. After a description of the geological setting of case study area, the origin and types of soils and rocks encountered in areas of building damage were identified. A typical soil/rock profile at an area with a known expansive soil problem, describing the expansive materials was presented. Using an empirical relationship, data from 56 construction sites was employed to classify broadly the likely swelling potential of the regional soils. Maps showing the geographical distribution of expansive soils and rocks, their swelling potential, and the geology of the regions were developed. These maps were based on information from soil laboratory tests, reported occurrences, and local geological conditions.

Introduction

Expansive soils and rocks are generally found in arid and semiarid regions, such as in the Arabian Gulf. These soils and rocks undergo volumetric changes upon wetting and drying, thereby causing ground heave and settlement problems. This characteristic causes considerable construction defects if not adequately taken care of. The case study area, Oman, has witnessed rapid development in the past three decades. Many projects such as government buildings, houses, and roads have been constructed in the first two decades without any knowledge of the existence of expansive soils and rocks, which in a large part was due to a lack of historical evidence of any expansive soil and rock problems. As a result, some of these structures have developed severe cracking and in a few cases, the distress has been so severe that buildings have had to be abandoned (Figure 1.1). As a consequence of the structural damage, the potential problems associated with expansive soils and rocks have been recognized and preventative measures are being incorporated into new designs and construction works.

This chapter describes the geological settings in the case study area, Oman, and the origin and types of soils and rocks encountered in areas of building damage. Furthermore, it

[1] Sultan Qaboos University, Oman; email: ameraar@squ.edu.om
[2] University of Turabo, Puerto Rico; email: mgoosen@suagm.edu
[3] Sultan Qaboos University, Oman; email: ghazi@squ.edu.om

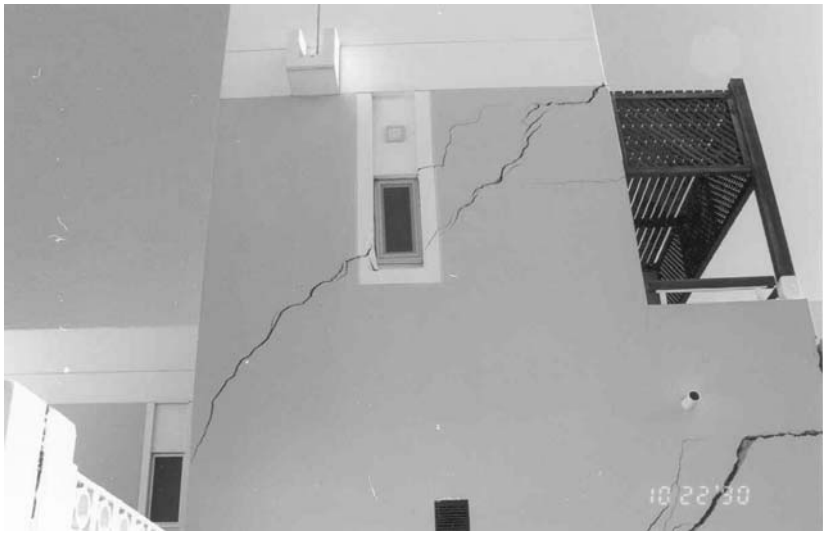

Figure 1.1 Structural cracks in a villa in case study area at Al-Khod (northern Oman).

classifies the likely swelling potential of the regional soils using empirical relationships and employing geotechnical data from 56 sites.

Geological setting of case study area

Oman, which occupies the southeastern corner of the Arabian Peninsula, covers an area of about 310,000 km^2. The country has a unique geological setting characterized by two mountain areas, one in the north of the country (i.e. Oman Mountains) and the other in the south (i.e. Dhofar Mountains) with elevations up to 3,000 m, and vast, generally flat, central plains, between 50 and 250 m above sea level (Le Metour *et al.*, 1995) (Figure 1.2).

The regional geology of northern Oman is dominated by the Oman Mountains which are geologically different from the rest of the Arabian Peninsula and can be divided into three major tectonostratigraphic sequences: the autochthonous sequence, the allochthonous sequence, and the autochthonous sedimentary cover. Extensive folding, domal uplift, and subsequent erosion have resulted in exposures and geological windows throughout the total succession of sedimentary and igneous rocks down into the underlying metamorphic and crystalline basement (Glennie *et al.*, 1974). A brief description of the three sequences follows.

The autochthonous sequence, which is exposed in the central Oman Mountains, is composed of the crystalline basement complex in Jebel Ja'alan and Qalhat areas, the metamorphics in Saih Hatat, and the clastic rocks and platform carbonates in Jebel Akhdar and Jebel Nakhl. This prePermian sequence is overlain unconformably by about 3,000 m

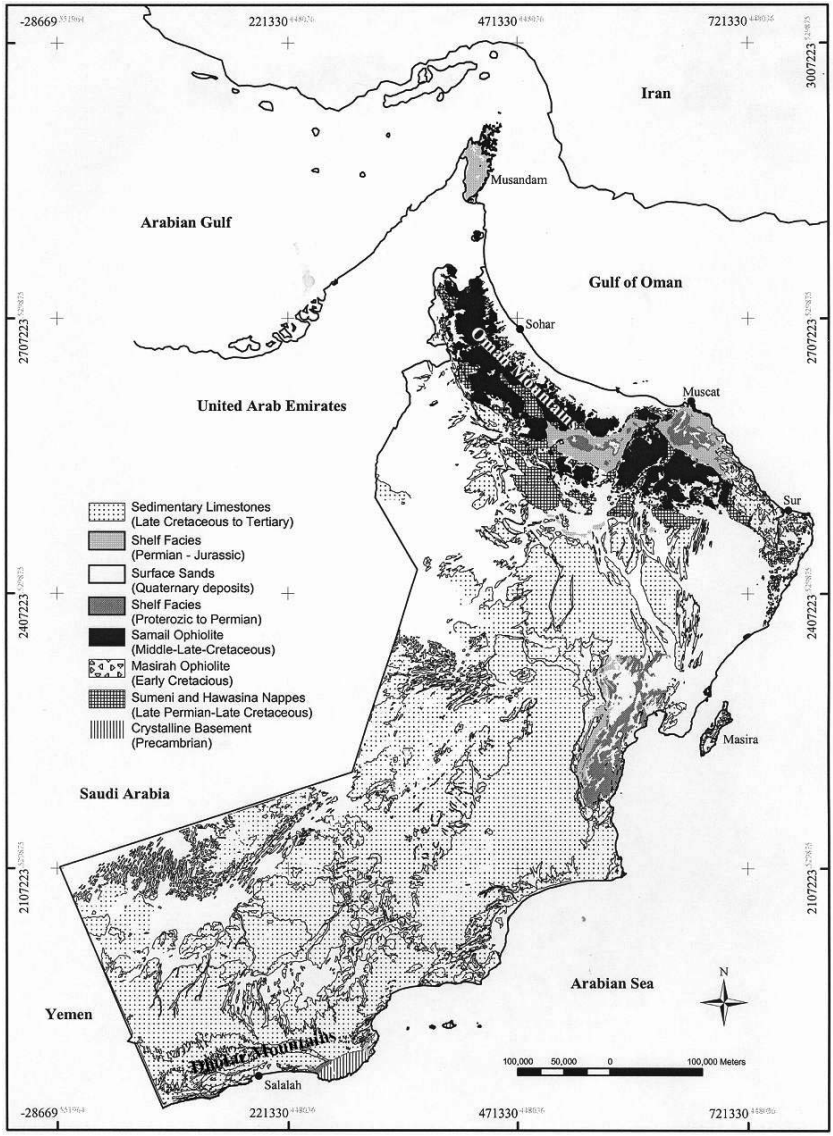

Figure 1.2 Geology of case study area, Oman.

Source: El-Baz, 2002.

of the Hajar Supergroup (middle Permian to middle Cretaceous) which is composed of shallow marine shelf carbonate rocks.

In the late Cretaceous, an allochthonous thick sequence of oceanic lithosphere and marine sediments has been thrust onto the continental margin of the southeastern Arabian Plate from an ocean in the north. These nappes comprise the Hawasina Complex and Semail Ophiolite. The Hawasina Complex (late Permian to mid-Cretaceous) consists of deep-sea sediments. The Semail Ophiolite (late Cretaceous), which tectonically overlies the Hawasina Complex, consists of a thick series of basic and ultrabasic igneous rocks.

The autochthonous sedimentary sequence (late Cretaceous and early Tertiary) unconformably overlies the autochthonous and allochthonous sequences described in the previous paragraphs. It consists mainly of conglomerates and shallow marine limestones. The Oligocene sediments of this sequence include large boulders of ophiolite, some of which have been altered into clays.

The regional geology of southern Oman (i.e. Dhofar) is composed essentially of a broad Cretaceous–Tertiary carbonate platform (Cavelier *et al.*, 1985) which is almost everywhere marine in character and in places in excess of 4,000 m thick. This platform is limited to the south, at the edge of the Arabian Sea by a near-continuous, 250 km-long line of thick late Paleocene/early Eocene limestone cliffs of the Umm er Radhuma Formation (BRGM, 1987). The lithostrategraphic units of the region can be divided into pre-Cretaceous, Cretaceous, Tertiary, and Quaternary. A brief description of these units follows.

The pre-Cretaceous units underlie all the Cretaceous deposits and comprise of three types: the Murbat crystalline rocks (pre-Cambrian to early Paleozoic), the El Hota – Ain Sarit Formation (late pre-Cambrian to early Cambrian), and the Murbat Sandstone Formation (Carboniferous to Permian). The Cretaceous deposits overlie unconformably the pre-Cretaceous formations. It is represented, from base to top, by the Qishn, Kharfot, Dhalqut, Qitqawt, Samhan, and Sharwayn formations.

The Tertiary deposits comprise, from base to top, the Umm er Radhuma, Rus, and Dammam formations (BGRM, 1987). They are overlain by the Aydim, Zalumah, and Ashawq formations of late Eocene and Oligocene age which only occur in southern Dhofar. The Tertiary succession is completed by the Mughsayl and Adawnib formations, overlain by the Nar Formation. The Quaternary deposits are heterogeneous in nature and of different origins. They comprise alluvial deposits, colluvial deposits, eolian deposits, and travertine and littoral marine deposits.

Expansive soils and rocks

The problems of ground heave experienced in the case study area, Oman, are predominately related to the presence of smectite clay minerals within Tertiary and Quaternary soils. Al-Rawas *et al.* (1998) investigated the mineralogical composition of expansive soils and rocks from different sites in northern Oman using the X-ray diffraction (XRD) technique. The XRD tests were performed on oriented samples (approximately <2 μm). They found that smectite (montmorillonite) constitutes the major clay mineral. They also indicated the presence of illite, palygorskite, and kaolinite clay minerals in the samples but in relatively small quantities. It is widely recognized that the formation of the smectite group is greatly influenced by the composition of the parent rocks. Donaldson (1969) and Van der Merwe

(1964) have indicated that the decomposition of basic and ultrabasic igneous rock can result in the formation of residual soils containing montmorillonite.

Ultrabasic igneous rocks are well represented in the region by the widespread exposure of Samail ophiolite. This formation is also thought to be the main source of clastic materials forming part of the Tertiary sedimentary cover along the foothills of the Oman Mountains and in the region surrounding Duqm (Figure 1.2). Within the conglomerates, it is apparent that clay mineral has resulted from the in situ weathering and alteration of the ultrabasic clasts. In contrast, within the fine grained mudstones and argillaceous limestones, which also occur within this sequence, the mineral appears to have originated at the time of deposition, having been washed into the area from source material in the mountains. Recent colluvium that has accumulated in low-lying depressions and wadis, contain smectite minerals from a similar source. It may also be possible for expansive clay minerals to occur within other geologic formations other than the Tertiary and Quaternary.

The expansive soils and rocks in Oman are generally variable with changes in color, structure, and lithology. The main expansive materials are: bentonitic mudstones, marls and silty mudstones, argillaceous dolomitic limestones, and altered conglomerates. These materials were found in areas where expansive soils and rocks problems were evidenced such as in Al-Khod and Al-Murtafah (northern Oman) which are about 45 and 35 km west of Muscat, respectively (YRM International, 1986; Al-Rawas *et al.*, 1998). The expansive soils and rocks at Al-Khod and Al-Murtafa'a areas were tentatively dated as middle to late Oligocene passing into Miocene by Y.R.M. International (1986) and as Pliocene by BRGM (1986). A brief description of the expansive soils and rocks follows. Typical soil/rock profiles are shown in Figure 1.3.

There are two varieties of bentonitic mudstones. The first variety occurs as a thinly laminated silty, quartz-rich, lithiclastic stratum with small lenses of light greyish-green color. The second variety of bentonitic mudstone is green, homogeneous, and very fine grained. It forms blocky beds and, on wetting the surface, exfoliates prior to complete breakdown. The marls are light green and brown in color, blocky in structure, and associated with abundant fibrous gypsum. The silty mudstones are interbedded with the marls. They are dark greenish-brown in color, and highly fissured.

The argillaceous dolomitic limestones expansive deposit is a brownish to light yellow medium to very fine grained rock with clayey lenses. It occurs as well-bedded closely jointed and highly fissured material. The altered conglomerates vary in color, but generally have a greenish hue. The clasts are mainly ultrabasic in origin and are of medium gravel size. They are derived mainly from the rocks of the ophiolite suite. The conglomerates have been subjected to strong in situ weathering and alteration.

The term "desert fill" describes aeolian and reworked calcareous sediments as well as in situ weathered materials which fills topographic depressions. Desert fill occurs as a light greenish-brown poorly sorted sand comprising carbonatic and ophiolitic material of the conglomerates. Desert fill covers low-lying areas.

Distribution of expansive soils and rocks

To investigate the distribution of expansive soils and rocks, site investigation data were collected from 56 construction sites in the case study area. The soils and rocks data available

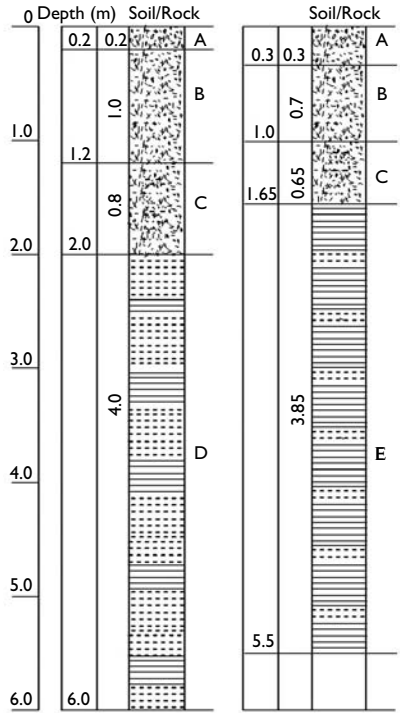

Figure 1.3. Soil/rock profiles at Al-Khod, northern Oman.

Notes

A Loose to medium dense, brown, grey, silty, fine to medium SAND and GRAVEL with occasional cobbles.
B Medium dense to dense, brown/light grey very silty slightly clayey SAND with gravel and lumps of cemented sand.
C Dense, brown/light grey, very silty sandy CLAY with occasional fine gravel and gypsum evaporite matrix.
D Very stiff to hard, light brown to dark brown, light grey, silty CLAY with layers of mudstone and some gypsum crystals at joint places.
E Hard, dark brown, highly weathered MUDSTONE with bands of silty CLAY.

included basic soils properties, such as Atterberg limits and particle size distributions, from a wide range of soil and rock lithologies. These data have been used, together with reported information on swelling potential obtained from some sites, to predict the swelling potential and distribution of expansive soils and rocks.

Soil swelling potential was initially determined using three empirical relationships as developed by Seed *et al.* (1962), Van der Merwe (1975), and Dakshanamurthy and Raman (1973). From the results, it was evident that there was a considerable variation in swell potential predicted by these methods. The final choice was based on the recommendations

of the detailed study of all three methods by Bucher and Sailie (1984). They reported that the classification of Dakshanamurthy and Raman (1973) yielded the best correlation with direct measurements of the swell potential.

For the purpose of this study, the Dakshanamurthy and Raman (1973) classification ranges were slightly modified to reflect the quantity and variability of soil data. Instead of five classifications, the *high, very high*, and *extra high* ranges were incorporated into one *high* range; the *low* and *medium* divisions remain unchanged. To classify the swell potential of the site rather than an individual sample, sites which have samples lying in more than one range were classified by the highest range in each case. For example, if samples from a site had swelling potentials in the low and medium range, the site would have been classified as medium. This classification system acknowledged the impersistence of many of the swelling soils, in so far as the numerical dominance of data in any one particular swelling range did not necessarily reflect the critical engineering behavior of the site.

For convenience, the sites were divided into seven geographical regions consisting of Muscat, Al-Batinah, Al-Sharqiya, Al-Dhahira, Al-Dakhiliya, Al-Wusta, and Dhofar. The regions, location of sites investigated, and range of soil properties are given in Table 1.1. The results are also presented as maps showing the geographical distribution of expansive soils and rocks, their swelling potential, and the geology of the regions (Figures 1.4 to 1.7).

Samples from the Muscat region possessed a swelling potential range of low–high. The majority of the samples lay within the high range, with the remaining data distributed relatively evenly between the medium and low ranges. A swell pressure up to 3,100 kN/m^2 was measured for samples from Al-Murtafah while at Al-Khod the measured swell pressure ranged from 10 to 200 kN/m^2. Samples within the high range originated mainly from Tertiary deposits. A similar trend was shown in the Al-Dhahira, Al-Wusta, and Al-Batinah regions with the majority of samples lying in the high swelling potential range. Samples from Duqm (Al-Wusta) showed a swell pressure up to 3,500 kN/m^2. In this case, geologic period of high swelling samples covered the Upper Cretaceous and Tertiary.

The Al-Dakhiliya region had a relatively even distribution of samples within the medium and high swelling potential with the majority of the sites showing a low swelling potential. The majority of samples from the Al-Sharqiya region lay in the medium swelling potential range. The geological period identified with this region, Upper Cretaceous to Quaternary, was much longer than those of regions with higher swelling potentials. A similar swelling potential was also indicated from the Al-Batinah region.

Al-Rawas and Woodrow (1992) developed a map showing the geographical distribution of swelling soils and their swelling potential in northern-Oman based distribution of geological formation of expansive nature, prediction of swelling potential from basic geotechnical properties, and reports of expansive soils damage. Based on the maps shown in Figures 1.4 to 1.7, there appears to be a correlation between the geological period and the swelling potential of the soils. Samples classified as having a high swelling potential were almost exclusively associated with Tertiary rocks and Quaternary deposits. Furthermore, Figures 1.4 to 1.7 show the number of predicted occurrences for each swelling potential at each site for the whole case study area. Thus, it is a significant refinement of the Al-Rawas and Woodrow map.

Table 1.1 Properties of engineering soils from sites in case study area of Oman

Region	*No.*	*Sites*	*Soil description*	*Depth (m)*	*<75 μm (%)*	*Liquid limit (%)*	*Plastic limit (%)*	*Plasticity index (%)*	*Class.*	*Swell (%)*	*Swell pressure (kPa)*	*Geological age*	*Swelling potential*
Muscat	1	Jebro	Clayey sand	1.0	16.6	29	18	11	SC			UC	L (1)
	2	Al-Khwair	Silty sand, clay	2.5–4.5		26–28	18–21	6–9	SC			T–Q	L (3)
	3	Ghubrah	Fine sand	6.0–6.5		29	19	10	SC			T–Q	L (1)
	4	Qurum	Silty clay, limestone	1.0–5.8		29–73	17–27	7–46	GC, SW			T	L (3), M (1), H (1)
	5	Qurayat	Silty clayey sand		53	28	21	7	SC			T	L (1)
	6	Al-Hail	Clayey sandy gravel	0.5	4	47	30	17	SW			T–Q	M (1)
	7	Ruwi	Sandy gravely clay	0.4	37	39	22	17	SC			T	M (1)
	8	Mutrah	Clayey sand	6.0		41	24	17	SC			UC	M (1)
	9	Al-Bustan	Silty sand	0.6–5.0	20	27–91	18–77	9–14	SM, SC			T–Q	L (1), H (5)
	10	Al-Ansab	Clay, mudstone	1.5–5.0		34–74	19–37	14–37	CH, SC			T	L (1), M (5), H (8)
	11	Al-Khod	Clay, mudstone, gypsum	1.0–4.0	81–89	41–107	29–54	5–58	MH	1.5–50	10–200	T	M (4), H (17)
	12	Al-Murtafah	Clay, mudstone, gypsum	2.0–14.2		53–103	18–43	25–60	CH	1.0–15	10–3,000	T	H (30)
	13	Darsait	Silty sand, siltyclay	4.0–7.0		40–41	22–25	15–19	CL	3.8–14.4	23–48	UC	M (2)
	14	Azaiba	Gravel, clayey sand	0.5	2–4	47–51	30–31	17–20	GW, SW			T–Q	M (1), H (1)
	15	Asseeb	Clayey silt, silty sand	0.5–8.6	7–30	26–130	17–53	9–77	CL, SC			T–Q	L (2), M (2), H (6)
Al-Batinah	16	Halban	Silty clay, conglomerate	0.3–0.8	74	44	30	14	ML		30–35	C–J	M (1)
	17	Al-Khaburah	Clay, fine sand	0.0–1.5	17–71	37–62	25–43	11–23	ML			T–Q	M (4), H (1)
	18	Saham	Sandy silty clay	1.0	96	53	25	30	CH			T–Q	H (1)
	19	Al-Musnah	Sandy silty clay	0.7–1.7	62	59	42	17	MH			T–Q	H (1)
	20	Sohar	Silty sand, sandy clay	1.5–8.0	19.7	25–68	18–37	7–34	CL, SC		4.7	T–Q	L (6), M (7)
	21	Majees	Sand, silt, clay	3.5–17		34–68	19–35	13–34	MH, SC				L (1), M (2), H (4)
	22	Arrustaq	Silty sand	1.0–2.0	6–10	27–51	17–36	10–15	GC			UC	L (2), M (4), H (1)
	23	Birka	Sandy silty clay	0.8	76–84	24–35	19–21	3–17	ML, CL			T–Q	L (1), M (1)
	24	Liwa	Sandy silty clay	0.0–1.5		23–37	21–26	2–11	ML			T–Q	L (1), M (1)
	25	Shinas	Silty sand	0.7–2.6		21–48	17–31	3–18	ML			T–Q	L (1), M (3)
	26	Assuwayq	Sandy silty clay	0.8–3.5	70–77	21–84	14–46	7–35	MH, CL			T–Q	L (5), H (12)
Al-Sharqiya	27	Samad Alshan	Sandy gravel with clay	0.5–2.0		26–34	19–24	7–10	ML, CL			UC	L (3)
	28	Sinaw	Silty clay	2.5–5.0		36–50	26–33	10–17	MC			Q	M (2)
	29	J.B.B.B. Ali	Clay silt, gypsum	2.0–4.3		43–73	21–33	22–40	SC			UC	M (3), H (1)

	30	Sur	Clay, limestone	0.2–0.3		27–43	19–27	6–16	CL			T	L (2), M (1)
	31	Al-Qabil	Clay, evaporties	0.9–2.9		37–53	24–31	11–27	SC			UC	M (4), H (1)
Al-Dhahira	32	Ibri	Siltstone, gypsum	0.5–5.0	15–27	38–48	23–27	15–21	SM			T	M (4)
	33	Fahud	Silty clay, mudstone	1.2–12.3		65–140	30–78	20–2	CH		18–107	T	H (9)
	34	Yibal	Clay, mudstone, marl	0.8–5.2		54–113	32–55	6–58	SC, MH		38–110	Q	H (7)
	35	Yanqul	Silty sand, clay	0.8–1.3	6–11	24–42	17–25	6–17	GC, SC			UC	L (2), M (1)
Al-Dakhiliya	36	Qarn Alam	Sandy soil	0.5–1.0	9–41	24–43	18–24	6–19	SM, SC			Q	L (4), M (1)
	37	Bahla	Clayey sand, clayey silt	1.3–2.0		28–56	22–41	6–15	SM		20	UC	L (1), H (1)
	38	Bid Bid	Sandy soil	0.4–0.6	6–19	26–33	19–22	7–12	GM, SM			UC	L (3)
	39	Samail	Silty sand	0.7–0.9	5–11	27–32	12–22	9–15	GW, SC			UC	L (3)
	40	Nizwa	Silty sand	0.6	10–69	32–35	10–23	9–25	CL, SC			UC	L (3)
	41	Ghaba	Silty sand	0.5–0.7	36–39	31–42	16–34	8–15	SM			Q	M (2)
	42	Qarat Al-Milh	Silty sand, gypsum	0.4–0.7	39–60	31–68	16–47	15–21	SC, MH				L (1), M (7), H (1)
	43	Manah	Clay, mudstone	1.5–6.7		52–86	25–60	22–30	CH			UC	H (5)
	44	Adam	Sandy gravel, gypsum	0.5–1.0	4–29	33–68	22–47	13–21	GW, SM			C–J	L (2)
Al-Wusta	45	Haima	Sand, marl, gypsum	0.3–1.4	50–87	27–74	15–42	11–32	SM, CL			Q	L (1), H (1)
	46	Duqm	Stiff clay	1.9–4.6		30–117	14–56	13–74	CH	0.4–30	62–3500	UC–T	H (5)
	47	Ras Madraka	Clay, conglomerate	1.5–3.0		26–59	16–42	10–23	CL, MH				L (1), H (2)
Dhofar	48	Salalah	Sand, clay, mudstone	1.0–10	10–21	20–147	16–77	6–70	GC, ML				L (10), M (7), H(1)
	49	Mughsayl	Red clay, marl	0.5–1.0	19–64	27–124	18–65	5–59	GC, CL				L (2), M (4), H (2)
	50	Raysut	Sand, silt, limestone	6.5	81	30–112	25–52	5–60	ML				L (1), H (1)
	51	Wadi Sahanot	Sandy gravel and clay	0.9	27	32	21	11	GC				L (1)
	52	Wadi Nahiz	Stiff silty clay	1.0–3.0	3.7–48	30–51	20–25	10–28	SM, GC				L (2), M (2), H(1)
	53	Montasar	Marls, limestone	0.5–2.0	29–50	18–38	11–25	7–13	SM, SC				M (2)
	54	Thamarit	Sand, clay, gypsum	1.2		39	27	12	CL				M (1)
	55	Tawsinat	Silt, clay, evaporites	1.0–3.3		35–56	24–36	11–20	SM				L (1), M (2), H (1)
	56	Wadi Mitan	Clay and limestone	1.65		51	37	14	SM				H (1)

Notes
Class. = Classification; L = Low; M = Medium; H = High; Q = Quaternary; T = Tertiary; UC = Upper Cretaceous; C–J = Cenomanian to Jurassic.

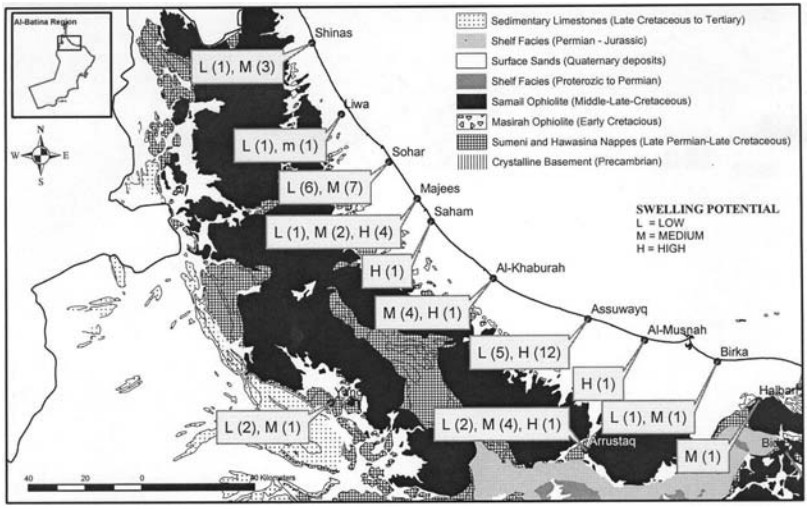

Figure 1.4 Geographical distribution of expansive soils and rocks combined with regional geology for Al-Batinah region.

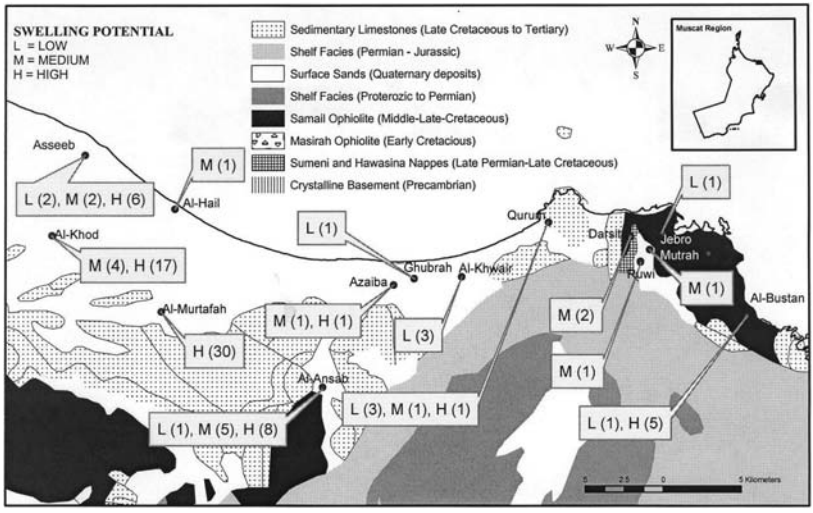

Figure 1.5 Geographical distribution of expansive soils and rocks combined with regional geology for Muscat region.

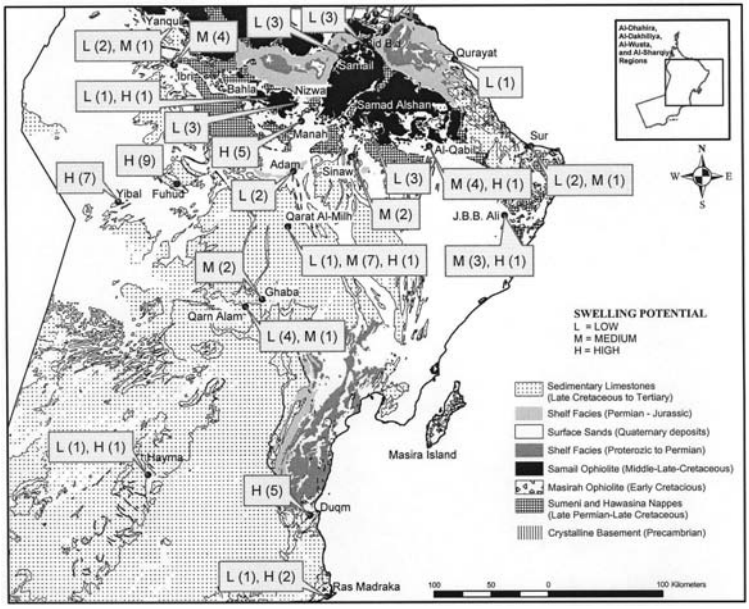

Figure 1.6 Geographical distribution of expansive soils and rocks combined with regional geology for Al-Dhahira, Al-Dakhiliya, Al-Wusta, and Al-Sharqiya regions.

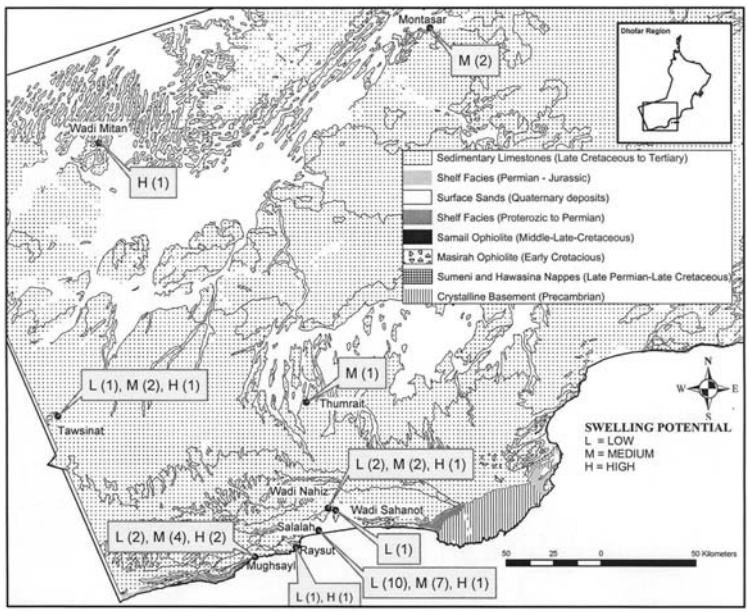

Figure 1.7 Geographical distribution of expansive soils and rocks combined with regional geology for Dhofar region.

Conclusions

The unique geology of the case study area, Oman, has resulted in construction problems associated mainly with expansive soils and rocks within Tertiary rocks and Quaternary deposits. The main types of expansive materials identified were: bentonitic mudstones, marls and silty mudstones, argillaceous dolomitic limestones, altered conglomerates, and desert fill derived from these materials. It was suggested that the principal mechanism of swelling was related to the presence of smectite clay minerals. A secondary mechanism may be due to over-consolidation and the presence of gypsum. Maps have been developed to show the geographical distribution of expansive soils and rocks, their swelling potential, and the geology of the regions. These maps are based on information from soil laboratory tests, reported occurrences, and local geological conditions.

References

Al-Rawas, A.A. and Woodrow, L.K.R. 1992. The distribution of expansive soils in Oman. Proceedings of the 7th International Conference on Expansive Soils, Dallas, USA, 3–5 August, Vol. 1, pp. 432–437.

Al-Rawas, A.A., Ingeborg, G., and McGown, A. 1998. Geological and engineering characteristics of expansive soils and rocks in Northern Oman. *Engineering Geology*, Elsevier Science Publishers, The Netherlands, ISSN 0013–7952, Vol. 50, pp. 267–281.

BRGM. 1986. *Mineral report*. Bureau De Recherches Geologiques Et Minieres. Ministry of Petroleum and Minerals, Sultanate of Oman, pp. 50–62.

BRGM. 1987. Geological study of mineral occurrences of Southern Dhofar. Bureau De Recherches Geologiques Et Minieres, 87 OMN 062, for Directorate General of Petroleum and Minerals, Ministry of Petroleum and Minerals, Sultanate of Oman, p. 111.

Bucher, F. and Sailie, E.L. 1984. Swelling behaviour of tropical black clays. Proceedings of the 8th Regional Conference for Africa on Soil Mechanic and Foundation Engineering, Harare, 81–86.

Cavelier, C., Platel, J.P., Roger, J., Berthiaux, A. and Robelin, C. (1985). Stratigraphie et histoire geologique du Dhofar (Sultanat d'Oman) depuis la transgression cretacee: Principaux Resultats Scientifiques et Techniques du.

Dakshanamurthy, V. and Raman, V. 1973. A simple method of identifying an expansive soil. Soils and Foundations, Japanese Society of SMFE, 13, 1, March, 97–104.

Donaldson, G.W. 1969. The occurrences of problems of heave and the factors affecting its nature. 2nd. International Research and Engineering Conference on Expansive Clay Soils, A & M Press, Texas, 25–36.

Glennie, K.W., Boeuf, M.G.A., Hughes Clarke, M.W., Moody-Stuart, M., Pilaar, W.F.H., and Reinhardt, B.M. 1974. Geology of the Oman Mountains. Verhandelingen Van het Koninklijk, Nederlands Geologisch Mijnbouwkundig Genootschap, 1, 31, 182.

Le Metour, J., Michel, J.C., Bechennec, F., Platel, J.P., and Roger, J. 1995. Geology and Mineral Wealth of the Sultanate of Oman. Ministry of Petroleum and Minerals Geological Documents, Ministry of Petroleum and Minerals, Sultanate of Oman, p. 285.

Seed, H.B., Woodward, R.J., and Lundgren, R. 1962. Prediction of swelling potential for compacted clays. Journal of S.M.F. Division, ASCE, 88, SM3, 53–87.

Van der Merwe, D.H. 1964. The weathering of some basic igneous rocks and their engineering properties. The Civil Engineer in South Africa, 213–222.

Van der Merwe, D.H. 1975. Contribution to speciality Session B, Current theory and practice for building on expansive Clays. Proceeding of 6th Regional Conference for Africa on SMFE, Durban, 2. 166–167.

YRM. International. 1986. *Site Geology and Geotechnics*, Sultan Qaboos University.

Chapter 2

Identification and classification of expansive soils

Sudhakar M. Rao[1]

Summary

The swelling tendencies of expansive soils are quantified by the swell potential and swelling pressure parameters. The swell pressure of a soil is the external pressure that needs to be placed over a swelling soil to prevent volume increase, while the swell potential of an expansive soil is the magnitude of heave of a soil for a given final moisture content and loading condition. These expansive soil parameters can be directly estimated in the laboratory from special oedometer tests or indirectly from the index properties of the soils and the differential free swell test. However, swell potentials based on index properties are in far excess of the oedometer swell potentials. The soil properties, external pressure, and wetting–drying process affect the swell potential and swell pressure of expansive soils.

Introduction

Expansive soils are mostly found in the arid and semi-arid regions of the world. The presence of montmorillonite clay in these soils imparts them high swell–shrink potentials (Chen, 1988). Low rainfall has hindered the weathering of the active montmorillonite mineral into low active clay types such as illite and kaolinite. Further, the rainfall has not been sufficient to leach the clay particles far enough so that the overburden pressure can control the swell.

Expansive soils cover nearly 20% of the landmass in India and include almost the entire Deccan plateau, Western Madhya Pradesh, parts of Gujarat, Andhra Pradesh, Uttar Pradesh, Karanataka, and Maharastra (Gopal Ranjan and Rao, 1991). The swelling soils are commonly known by the name of black cotton soils. For swelling to occur, these soils must be initially unsaturated at some water content. If the unsaturated soil gains water content, it swells. On the other hand, if a decrease in water content occurs the soil shrinks. A major concern in geotechnical engineering is identification of expansive soils and estimation of their swelling magnitudes when subjected to changes in environment (Subba Rao and Satyadas, 1987; Day, 1994; Al-Homoud *et al.*, 1995).

The study reported in this chapter focuses on the identification, classification, and estimation of swell potential and swell pressures of expansive soils.

[1] Civil Engineering, Indian Institute of Science, Bangalore 560012; email: msrao@civil.iisc.ernet.in

Swell pressure and swell potential

Swelling pressure is a very useful index of the trouble potential of an expansive soil. This pressure is the maximum force per unit area that needs to be applied over a swelling soil to prevent volume increase. A swelling pressure of less than 20 kPa may not be regarded as of much consequence. The swell potential of a soil in comparison is the magnitude of heave of a soil for a given final water content and loading condition. Specially designed oedometer tests have been found quite useful to determine the magnitudes of these parameters for expansive soils (ASTM D 4546–90 Standard Test Method for One Dimensional Swell or Settlement Potential of Cohesive Soils).

Oedometer test procedures

The initial water content and void ratio should be representative of the in situ soil immediately prior to construction. In case where it is necessary to use disturbed soil samples, the soil sample should be compacted to the required field density and water content in a Proctor Compaction mould. The swell potential and swell pressure of a soil specimen can be determined by any of the three methods specified by ASTM Standards (ASTM D 4546–90 Standard Test Method for One Dimensional Swell or Settlement Potential of Cohesive Soils).

Method A

The seating pressure (at least 1 kPa) is applied to the clay specimen. After the initial deformations at the seating pressure are complete, the specimen is inundated with water in the oedometer cell and is allowed to swell vertically. The time-swell curve typically consists of three regions. An initial swell region, primary swell region, and secondary swell region (Figure 2.1). The minor initial swell is attributed to swelling of the macrostructure, while the major primary swell and minor secondary swell is attributed to microstructural swelling (Rao *et al.*, 2006). The specimen is stepwise loaded after primary swell is complete using a

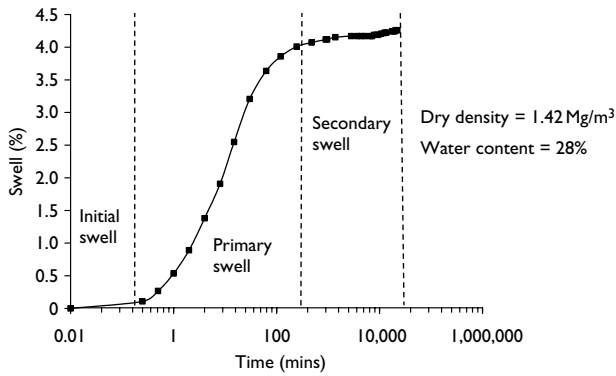

Figure 2.1 Time-swell behavior of compacted black cotton soil.

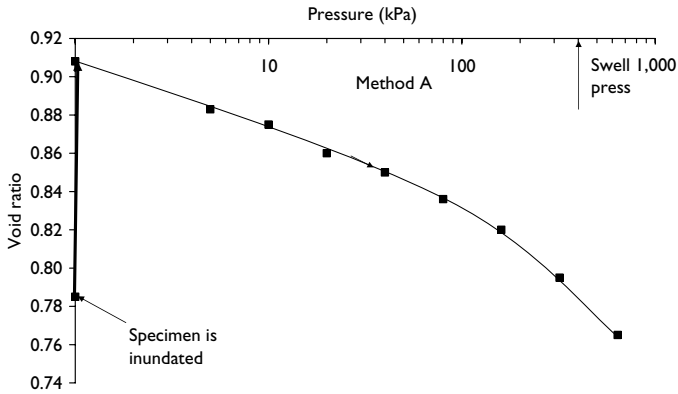

Figure 2.2 Estimation of swell potential and swell pressure by Method A.

load increment ratio of unity. The loading process is continued till the swollen specimen regains its initial void ratio/height. The external pressure needed to regain the initial void ratio e_0, defines the swell pressure of the specimen (Figure 2.2).

The swell potential at the seating pressure relative to the initial void ratio e_0 is given as:

$$\text{Swell potential (\%)} = \frac{e_{se} - e_0}{1 + e_0 \times 100} \tag{2.1}$$

where e_{se} is void ratio after stabilized swell at seating pressure and e_0 is the initial void ratio of the soil specimen at the seating pressure. This test method measures (a) the percent heave of the specimen at the seating pressure and (b) the swell pressure of the specimen (Figure 2.2).

Method B

A vertical pressure exceeding the seating pressure is applied to the specimen. The magnitude of vertical pressure (σ_{v0}) is usually equivalent to the in situ overburden pressure, or structural loading or both. After the axial deformations under the vertical pressure σ_{v0} are complete, the specimen is inundated with water and axial swelling deformations of the specimen are recorded until primary swell is complete. After completion of primary swell, the specimen is stepwise loaded till the pre-wetting void ratio (e_{v0}) corresponding to the vertical pressure σ_{v0} is attained (Figure 2.3). The pressure needed to regain the void ratio e_{v0} defines the swell pressure of the specimen. This test method measures (a) the percent heave for vertical pressure usually equivalent to the estimated in situ vertical overburden pressure and other vertical pressures up to the swell pressure and (b) the swell pressure of the specimen (Figure 2.3). The swell potential at the vertical pressure σ_{v0}, relative to e_{v0} is given as:

$$\text{Swell potential (\%)} = \frac{e_{se} - e_{v0}}{1 + e_{v0} \times 100} \tag{2.2}$$

where e_{se} is the void ratio after stabilized swell at the vertical pressure σ_{v0} and e_{v0} is the initial (pre-swollen) void ratio at the vertical pressure σ_{v0}.

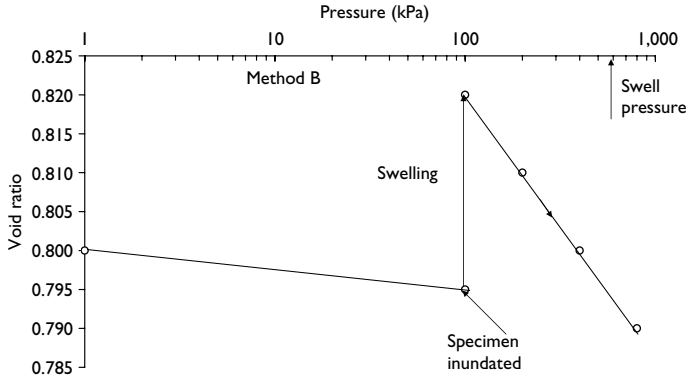

Figure 2.3 Estimation of swell potential and swell pressure by Method B.

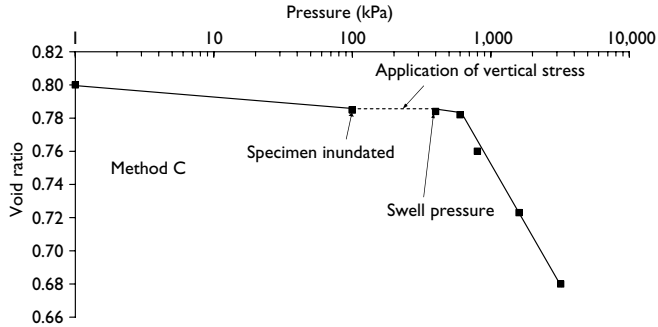

Figure 2.4 Estimation of swell pressure by Method C.

Method C

A vertical pressure (σ_1) equivalent to the estimated vertical in situ pressure or swell pressure is applied to the specimen. After completion of axial deformations under the vertical pressure σ_1, the specimen is inundated with water. Increments of vertical stress are applied to the wetted specimen to prevent any swell. Variations from the dial gage readings at the time the specimen is inundated at stress σ_1 shall be preferably kept within 0.005 mm and not more than 0.01 mm. The vertical pressure at which the wetted specimen shows no further tendency to swell defines the swell pressure of the specimen. The specimen is stepwise loaded following no further tendency to swell. The applied load increments should be sufficient to define the maximum curvature on the consolidation curve and to determine the slope of the virgin compression curve (Figure 2.4).

Table 2.1 Classification of expansive soils

Degree of expansion	*Holtz and Gibbs' (1956) classification of percent swell*	*Seed* et al's *(1962) classification of percent swell*
Low	0–10	0–1.5
Medium	10–20	1.5–5
High	20–35	5–25
Very high	>35	>25

Table 2.2 Identification criteria for expansive clays

Colloid content (%)	*Plasticity index (%)*	*Shrinkage limit (%)*	*Degree of expansion*	*Probable expansion (% total volume change)*
<15	<18	<10	Low	<10
13–23	15–28	10–20	Medium	10–20
20–31	25–41	20–30	High	20–30
>28	>35	>30	Very high	>30

Source: After Holtz and Gibbs, 1956.

Expansivity classification

Based on the oedometer swell potential values, Holtz and Gibbs (1956) and Seed *et al.* (1962) have classified the relative expansivity of the swelling soils. Holtz and Gibbs' (1956) classification is based on the swell potentials of undisturbed specimens that were inundated under 1 psi (approximately 7 kPa) pressure. Seed *et al.* (1962) criterion is based on the swell potential of remoulded specimens that were compacted at their Standard Proctor MDD (maximum dry density) and OMC (optimum moisture content) values and inundated under 1 psi pressure. Table 2.1 gives the expansivity categories proposed by these workers.

Indirect evaluation of swell potentials

Besides direct quantification of swell potentials from the oedometer tests, it is also possible to indirectly estimate the degree of expansivity of clay soils from their index properties or from the differential free swell test. The Atterberg limits and swell potentials of clays depend on the quantity of water that clay can imbibe. The higher the plasticity index, the greater the quantum of water that can be imbibed by the soil and hence the greater would be its swell potential. Likewise, a low shrinkage limit indicates that a soil would begin to swell at low water content. The colloid content ($< 1\ \mu m$) constitutes the most active part of the soil contributing to swelling and a high colloid content naturally means a greater possibility of expansion. Together, the United States Bureau of Reclamation uses these three parameters to indicate the criterion for identification of expansive soils, which are reproduced in Table 2.2.

Similarly, the Van Der Merwe method (Van Der Merwe, 1964) evolved from empirical relationships between the degree of expansion, the plasticity index, the percent clay

fraction, and the surcharge pressure. The total heave at the ground surface is found from the relation:

$$\Delta H = \sum_{D=1}^{D=n} F \times \text{PE} \tag{2.3}$$

where, ΔH = total heave, inches; D = depth of soil layer in increments of 1 foot increment at the deepest level; F = reduction factor for surcharge pressure and $F = 10^{-D/20}$; PE = potential expansiveness in inch/foot of depth. The PE values are found by assumed values of PE = 0, 1/4, 1/2, and 1 inch/foot for low, medium, high, and very high levels, respectively of potential expansiveness as depicted in Figure 2.5.

Besides using the index properties, the swell potential of clay soils can be indirectly estimated from the differential free swell (DFS) test (IS 2720 Part 40–1977 Determination of Free Swell Index of Soils). In this method, two oven-dried samples weighing 10 g each and passing through 425 μm sieve are taken. One sample is put in a 100 ml graduated glass cylinder containing kerosene (nonpolar liquid) and the other sample is put in a similar cylinder containing distilled water. Both the samples are stirred and left undisturbed for 24 hours and then their volumes are noted. The DFS is expressed as:

$$\text{DFS} = \frac{\text{Soil volume in water} - \text{Soil volume in kerosene}}{\text{Soil volume in kerosene}} \times 100\% \tag{2.4}$$

The degree of expansivity and possible damage to lightly loaded structures may be qualitatively assessed from Table 2.3. In areas where the soils have high or very high DFS values, conventional shallow foundations may not be adequate.

Table 2.4 predicts the swell potential based on the index properties for three black cotton soil specimens from Karnataka, India using the Holtz and Gibbs' (1956) criteria for indirect

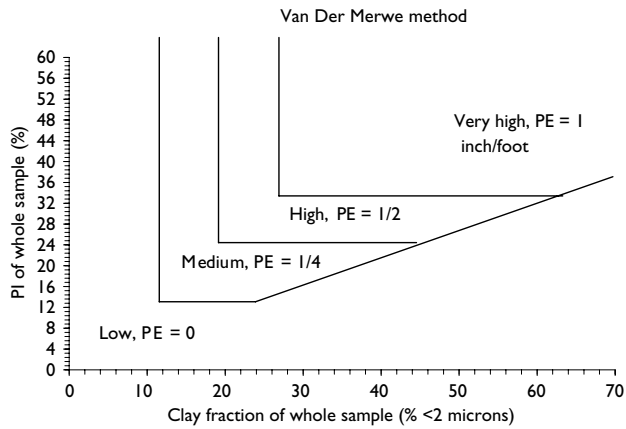

Figure 2.5 Expansivity classification by the Van Der Merwe method (PE = potential expansivity).

Table 2.3 Degree of expansiveness and free swell

Degree of expansiveness	*DFS (%)*
Low	<20
Moderate	20–35
High	35–50
Very high	>50

Table 2.4 Estimation of swell potential of black cotton soil specimens based on index properties

Soil No.	*Clay content (%)*	*Plasticity index (%)*	*Shrinkage limit (%)*	*Probable expansion (%)*
1	61	46	10	>30
2	59	71	8	>30
3	55	61	10	>30

Source: After Holtz and Gibbs, 1956.

Table 2.5 Oedometer swell potentials of black cotton soils

Soil No.	*Dry density (mg/m^3)*	*Moisture content (%)*	*Swell potential (%)*
1	1.34	32	5.2
2	1.37	30	4
3	1.35	33	5
3	1.35	28	10
3	1.42	28	11
3	1.42	23	16

estimation of swell potentials. Table 2.5 presents the oedometer swell potentials of the compacted black cotton soil specimens using ASTM method A. The percent swell predicted by the index properties (Table 2.4) far exceeds the oedometer swell potentials (Table 2.5). Further, variations in compaction conditions impact the oedometer swell potentials of the compacted black cotton soil specimens (Soil No. 3, Table 2.5). For example, an increase in compaction water content from 28 to 33% at dry density of 1.35 g/cc reduces the swell potential of Soil No. 3 from 10 to 5%. Indirect predictions based on index properties are insensitive to variations in initial soil conditions.

Factors influencing swell potential and swell pressure

The swell potential and swell pressure are dependant on several factors namely the type and amount of clay minerals present, the initial dry density (void ratio) and water content of the soil specimen, the nature of pore fluid, the type of exchangeable cations, the overburden pressure, and the wetting and drying effects (Yong and Warkentin, 1975; Subba Rao and

Satyadas, 1987; Chen, 1988; Nelson and Miller, 1992; Day, 1994, Al-Homoud *et al.*, 1995; Subba Rao *et al.*, 2000). The swell potential and swell pressure are known to increase with increase in clay content and dry density and decrease with increase in initial water content, overburden pressure, pore salt concentration, and exchangeable cation valence (Holtz and Gibbs, 1956; Seed *et al.*, 1962; Mitchell, 1976; Chen, 1988). It has hence been suggested that clay soils could be compacted at water contents in excess of their OMC values to control their swell potentials (Gromko, 1974).

However, clay soils in arid and semi-arid regions are subjected to cycles of wetting and drying in the field due to climatic variations. The data of Day (1994), Al-Homoud *et al.* (1995), and Subba Rao *et al.* (2000) have illustrated that cyclic wetting and drying overrides the influence of initial water content and void ratio on the swell potentials of expansive clays. Figures 2.6 and 2.7 illustrate the impact of one drying cycle on the swell potentials of compacted black cotton soils from Karnataka. Table 2.6 provides the index properties of black cotton Soil Nos 4 and 5 from Karnataka. Figure 2.6 presents the vertical swell potential as a function of compaction water content for specimens of Soil No. 4 compacted to a dry density of 1.3 Mg/m^3. Figure 2.7 presents the vertical swell potentials as a function of compaction water content for specimens of Soil No. 5 compacted to a dry density of 1.24 mg/m^3. The compacted specimens in Figures 2.6 and 2.7 were flooded at the nominal pressure of 6.25 kPa. Expectedly in both figures, the drier specimen exhibits a larger swell potential at a given dry density on first wetting. After attaining maximum swelling on first wetting, the compacted specimens were subjected to full drying at 45°C in the oedometer assemblies. The fully dried specimens were re-wetted by inundating the oedometer assemblies with water.

Trends of results are distinctly different from the results of first wetting. Figure 2.6 shows that specimens of Soil No. 4 that were compacted wet of OMC swell more than the specimens that were compacted dry of OMC on second wetting. Similar trends of results are observed with specimens of Soil No. 5 in Figure 2.7. The results in Figures 2.6 and 2.7 bring out that though immediate control of vertical swell potential can be achieved by compacting

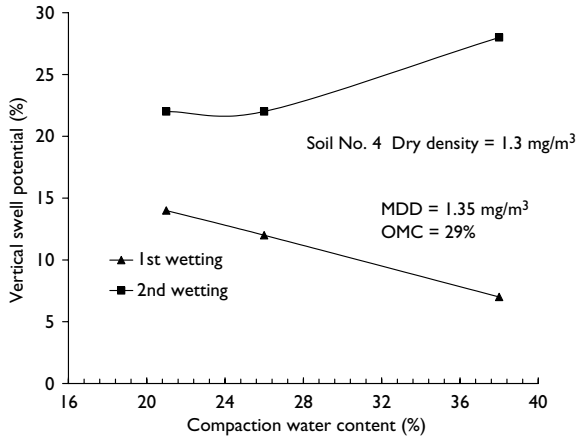

Figure 2.6 Effect of one-wetting cycle on swell potential of Soil No. 4.

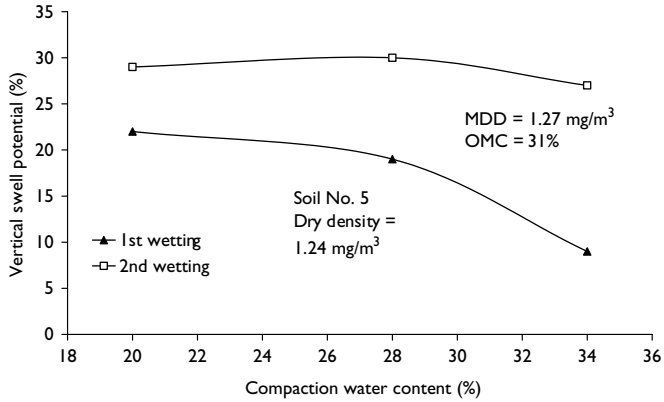

Figure 2.7 Effect of one-wetting cycle on swell potential of Soil No. 5.

Table 2.6 Black cotton soil specimens used in oedometer tests

Soil No.	4	5
Liquid limit (%)	75	103
Plasticity index (%)	44	51
Grain size distribution (%)		
Sand	15	0
Silt	30	34
Clay	55	66
Standard proctor characteristics		
Maximum dry density (MDD) mg/m^3	1.35	1.27
Optimum moisture Content (OMC) (%)	29	31

the expansive soil specimen wet of OMC, this benefit is lost on drying of the specimen. One cycle of drying causes the specimen compacted wet of OMC to swell much more than the specimens compacted dry of OMC on second wetting.

Conclusions

The tendency of expansive soils to increase their volume when they come in contact with water is quantified by the swell potential and swell pressure parameters. These parameters in turn can be directly quantified in the laboratory by three different oedometer tests. Alternatively, the swell potentials can be indirectly estimated from the index property values or from differential free swell test. The swell potentials estimated from index properties overestimate the swell potentials of expansive clays. Swell potentials estimated from index properties are insensitive to the influence of initial soil conditions (i.e. dry density, water content) on the swell potentials of the soil. The soil properties, external pressure, and

wetting–drying impact the swell potential and swelling pressure parameters. Under these circumstances, care must be taken to simulate the field conditions as closely as possible in the laboratory tests. In particular, immediate control of vertical swell potential achieved through compacting the expansive soil specimen wet of OMC is lost on single drying of the specimen.

References

Al-Homoud, A.S. Basma, Husein Malkavi, and Al-Bashabshah, M.A. (1995). Cyclic swelling behaviour of clays. *Journal of Geotechnical Engineering, ASCE* 121, 582–585.

Chen, F.H. (1988). *Foundations on Expansive Soils*, Elsevier, New York.

Day, R.W. (1994). Swell-shrink behaviour of compacted clay. *Journal of Geotechnical Engineering, ASCE* 120, 618–623.

Gopal Ranjan and Rao, A.S.R. (1991). *Basic and Applied Soil Mechanics,* Wiley Eastern, New Delhi.

Gromko, G.J. (1974). Review of expansive soils. *Journal Geotechnical Division, ASCE* 100, 667–687.

Holtz, W.G. and Gibbs, H.J. (1956). Engineering properties of expansive clays. *Transactions of the American Society of Civil Engineers* 121, 641–663.

Mitchell, J.K. (1976). *Fundamentals of Soil Behaviour*, John Wiley, New York.

Nelson, J.D. and Miller, D.J. (1992). *Expansive Soils Problems and Practices in Foundation and Pavement Engineering*, John Wiley, New York.

Rao, S.M., Thyagaraj, T., and Thomas, H.R. (2006). Swelling of compacted clay under osmotic gradients. Geotechnique (revised manuscript under review).

Seed, M.B., Woodward, R.J., and Lundgren, R. (1962). Prediction of swelling potential of compacted soils. *Journal of Soil Mechanics and Foundation Engineering, ASCE* 85, 86–128.

Subba Rao, K.S. and Satyadas, G.C. (1987). Swelling potentials with cycles of swelling and partial shrinkage. *Proceedings 6th International Conference on Expansive Soils*, vol. 1, New Delhi, 137–142.

Subba Rao, K.S., Rao, S.M., and Gangadhara, S. (2000). Swelling behaviour of desiccated clay. *ASTM Geotechnical Testing Journal* 23, 193–198.

Van Der Merwe, H. (1964). The prediction of heave from plasticity index and the percentage clay fraction of the soils. *The Civil Engineer, South African Institute of Civil* Engineers 6, 103–107.

Yong, R.N. and Warkentin, B.P. (1975). *Soil Properties and Behaviour*, Elsevier, New York.

Chapter 3

Prediction and classification of expansive clay soils

Agus Setyo Muntohar[1]

Summary

This chapter deals with the prediction and classification of the degree of expansiveness of clay soil. Statistics analysis was introduced as a simple technique for identifying and predicting the degree of swelling. There were three properties which were most strongly correlated to swelling potential (i.e. plasticity index, liquid limit, and clay fraction). In general, the models in the current study showed good correlation compared with previous models cited in the literature. The multiple linear regression model gave the best-fit for all soil conditions.

Introduction

Expansive soils are a world wide problem (Seed *et al.*, 1962; Kormonik and David, 1969; Al-Rawas *et al.*, 1998; Alawaji, 1999; Cokca, 2001; Erguler and Ulusay, 2003; Muntohar and Hashim, 2003). Principally, swelling occurs when water infiltrates between the clay particles, causing them to separate. Several attempts have been made by researchers to obtain time-swell relationships for expansive soils. Some progress has been made toward characterizing swelling characteristics, despite the complexity of the behavior. Seed *et al.* (1962) reported that the time required for completion of swelling is relatively long.

Many tests and methods have been developed for estimating shrink–swell potential. These include both indirect and direct measurements. Indirect methods involve the use of soil properties and classification schemes to estimate shrink–swell potential. Direct methods provide actual physical measurements of swelling. Several laboratory methods have been developed to directly determine the swelling a soil undergoes as the moisture content changes. These include free swell, expansion index, consolidation-swelling, California Bearing Ratio (CBR), potential volume change (PVC), and coefficient of linear extensibility (COLE).

Currently, no one method of soil analysis estimates the shrink–swell potential accurately for all soils. Soil scientists recognize that shrink–swell behavior can be best predicted by examining a combination of physical, chemical, and mineralogical soil properties. Determining these properties and establishing a shrink–swell model that can be extrapolated

[1] Department of Civil Engineering, Muhammadiyah University of Yogyakarta, Building F1, 3rd floor. Jl. Ringroad Selatan, Taman Tirto, Yogyakarta, Indonesia. 55183. Email: muntohar@umy.ac.id

across the same or similar parent materials is needed. Some researchers consider that this swelling potential can be linked to a single parameter.

This chapter deals with the prediction and classification of the degree of expansiveness of clay soil. Statistics analysis is introduced as a simple technique for identifying and predicting the degree of swelling.

Potential of volume change

Holtz and Gibbs (1956), Altmeyer (1955), Seed *et al.* (1962), and Daksanamurthy and Raman (1973) have evolved different methods to identify expansive soils based on the percentage of clay content, shrinkage limits (both volumetric and linear), plasticity index, liquid limit, and shrinkage index. Accordingly, they classified soils into low, medium, high, and very high degrees of potential expansiveness (Figures 3.1, 3.2, and 3.3). However, as

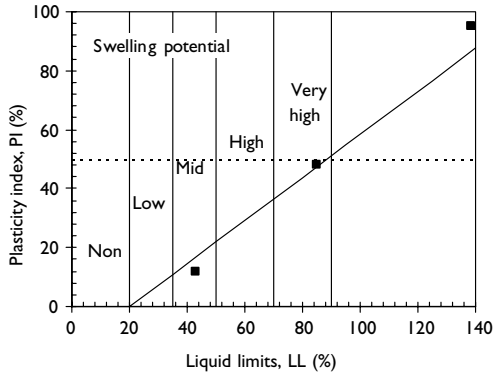

Figure 3.1 Chart for potential expansiveness of soil.
Source: Daksanamurthy and Raman, 1973.

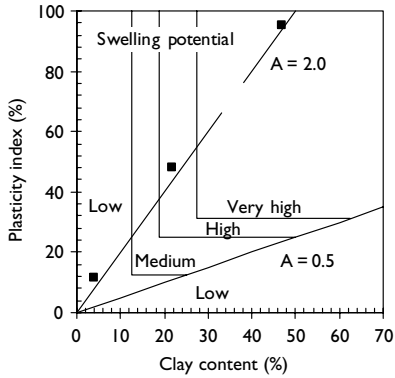

Figure 3.2 Potential expansiveness of expansive soil.
Source: Williams, 1957.

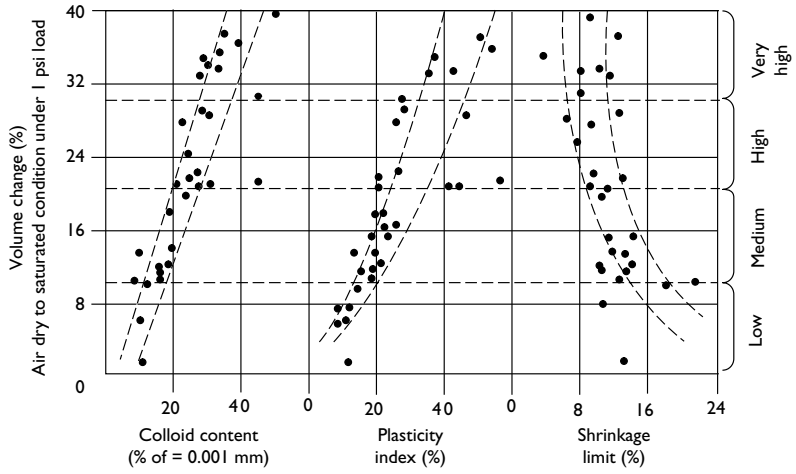

Figure 3.3 Relation of volume change to colloid content, plasticity index, and shrinkage limit.
Source: Holtz and Gibbs, 1956.

Table 3.1 Classifications for degree of expansion (swelling potential)

Degree of expansion	*Chen (1983)*	*Seed* et al. *(1962)*	*Daksanamurthy and Raman (1973)*	*USBR (Holtz and Gibbs, 1956)*
Very high	LL > 60	PI >35	LL > 70	CC > 28
High	40 < LL ≤ 60	20 < PI ≤ 35	50 < LL ≤ 70	20 < CC ≤ 31
Medium	30 ≤ LL ≤ 40	10 ≤ PI ≤ 20	35 < LL ≤ 50	13 ≤ CC ≤ 23
Low	LL < 30	<10	20 ≤ LL ≤ 35	CC < 13

with most soil systems, the activity classification scheme does not accurately estimate shrink–swell potential in mixed mineralogy soils. Parker *et al.* (1977) found that the activity index was too imprecise for both mixed and montmorillonitic mineralogy soils to be useful. However, Schreiner (1988) observed consistent trends in soil and bentonite/sand mixtures using the activity index as an indicator of shrink–swell potential.

The classification of potential expansiveness does not give the same assessment of the swelling potential. It cannot conclude precisely the degree of volume change for particular soils as presented, for example, in Table 3.1. Seed *et al.* (1962) have also correlated the swelling potential with the degree of expansion values used by USBR as presented in Table 3.2. The boundaries defining these ranges are plotted in Figure 3.4.

Indirect estimation of swelling parameters

In view of the difference that has been observed between the directly measured values of the swelling parameters and the values output by the earlier models, the first idea was to fit the models in question. The literature contains a considerable number of empirical techniques for assessing the swelling potential of soils, which correlated with consistency limits, moisture content, dry density, and depth of the soil samples (Seed *et al.*, 1962; Chen, 1983;

Table 3.2 Classification of degree of expansion

Degree of expansion	*Swelling potential (%)*
Very high	>25
High	5–25
Medium	1.5–5
Low	0–1.5

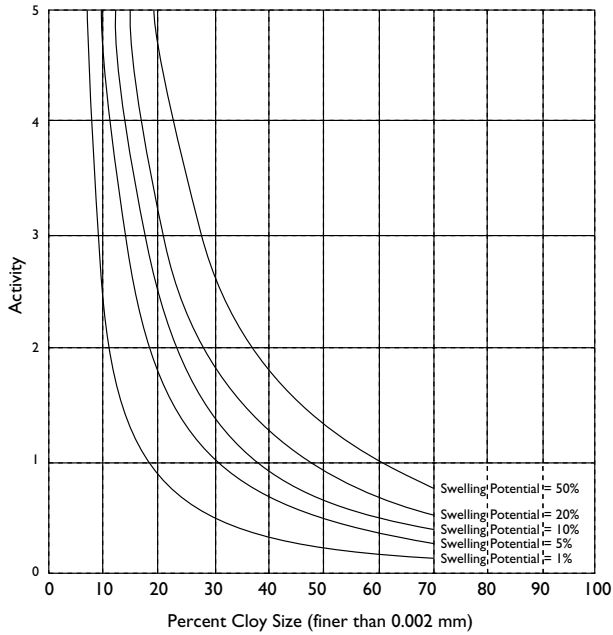

Figure 3.4 Classification chart for swelling potential.
Source: Seed *et al.*, 1962.

Basma *et al.*, 1995; Djedid, 2001). Thomas (1998) proposed an expansive soil rating system, termed as the *Expansive Soil Index (ESI)*. The model was developed as a function of using the soil properties most correlated with shrink–swell potential such as the ratio 2:1 between smectite and vermiculite minerals, swell index, liquid limit, and cation exchange capacity (CEC). The model gave expansive soil potential ratings (ESI) for each soil series.

Seed's model (Seed *et al.*, 1962) and Chen's model (Chen, 1983) are very simple. They used plasticity index parameters. Their models are given by Equations 3.1 and 3.2, respectively.

$$\mathrm{SP} = 60K\,(\mathrm{PI})^{2.44} \tag{3.1}$$

$$\mathrm{SP} = B\,e^{A(\mathrm{PI})} \tag{3.2}$$

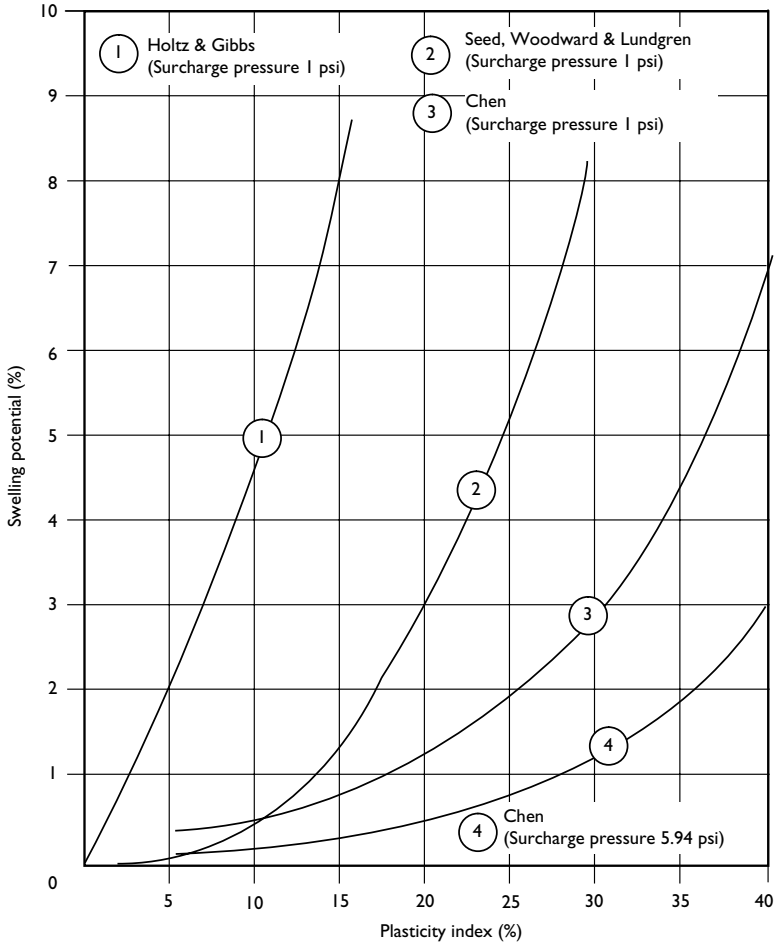

Figure 3.5 Correlations between swelling potential and plasticity index.
Source: Reproduced from Chen, 1983.

where, SP is swelling potential plasticity index. Figure 3.5 shows the correlations between swelling potential and plasticity index that given by some researchers. $K = 3.6 \times 10^5$, $A = 0.0838$, $B = 0.2558$ are constants, and PI is plasticity index.

Data analysis

Data used in this study consisted of 115 pairs and was compiled from many references (Seed *et al.*, 1962; Kormonik and David, 1969; Al-Rawas *et al.*, 1998; Alawaji, 1999; Cokca, 2001; Erguler and Ulusay, 2003; Muntohar and Hashim, 2003). Table 3.3 presents the data source

Table 3.3 Number of data used for model

Source of data	*Number of data*
Current research data	7
Alawaji (1999a)	10
Attom *et al.* (2001)	3
Çokça (2001)	1
Zeynal and Ulusay (2003)	20
Seed *et al.* (1962)	12
USBR (quoted by Seed *et al.*, 1962)	28
Total data	81

Table 3.4 Proposed empirical model for predicting swelling potential

No.	*Models*	*Regression statistics*	*Regression ANOVA*
1	Variable: plasticity index (PI)	$R^2 = 0.58$	df = 1
(a)	$SP = 1.035(PI)^{0.816}$	Ad. $R^2 = 0.57$	F = 109.24
		$S\epsilon = 7.85$	$P_v < 0.0001$
(b)	$SP = 10.106e^{0.056(PI)}$	$R^2 = 0.444$	df = 1
		Ad. $R^2 = 0.44$	F = 63.12
		$S\epsilon = 9.04$	$P_v < 0.0001$
(c)	$SP = 2.231 + 0.453$ (PI)	$R^2 = 0.563$	df = 1
		Ad. $R^2 = 0.56$	F = 102.08
		$S\epsilon = 9.04$	$P_v < 0.0001$
2	Variable: clay fraction (CF)	$R^2 = 0.226$	df = 1
(a)	$SP = 2.919(CF)^{0.535}$	Ad. $R^2 = 0.22$	F = 23.08
		$S\epsilon = 10.66$	$P_v < 0.0001$
(b)	$SP = 11.418e^{0.0135(CF)}$	$R^2 = 0.152$	df = 1
		Ad. $R^2 = 0.15$	F = 14.22
		$S\epsilon = 11.16$	$P_v < 0.0001$
(c)	$SP = 7.518 + 0.323(CF)$	$R^2 = 0.192$	df = 1
		Ad. $R^2 = 0.18$	F = 18.77
		$S\epsilon = 10.89$	$P_v < 0.0001$
3	Variable: liquid limit (LL)	$R^2 = 0.546$	df = 1
(a)	$SP = 0.109(LL)^{1.236}$	Ad. $R^2 = 0.54$	F = 95.03
		$S\epsilon = 8.16$	$P_v < 0.0001$
(b)	$SP = 6.871e^{0.0149(LL)}$	$R^2 = 0.466$	df = 1
		Ad. $R^2 = 0.46$	F = 69.10
		$S\epsilon = 8.85$	$P_v < 0.0001$
(c)	$SP = 0.393(LL) - 6.298$	$R^2 = 0.56$	df = 1
		Ad. $R^2 = 0.55$	F = 100.53
		$S\epsilon = 8.04$	$P_v < 0.0001$
4	Multiple linear regression:	$R^2 = 0.613$	df = 3
	$SP\ (\%) = 0.171CF + 0.0012LL + 0.409PI - 1.869$	R^2 Adj. = 0.60	F = 40.608
		$S\epsilon = 7.64$	$P_v < 0.0001$

Notes
Coefficient of confidence level (α) = 0.05; SP is swelling potential (%); Sε: Standard error.

that was used in the study. Preliminary statistics test was carried out for screening the variables used in the models. The variables, which only had good correlation with swelling potential, were chosen as independent variables. They were plasticity index (PI), liquid limit (LL), clay fraction (CF), dry density (γ_d), and water content (w). Due to the large variability of dry density and water content data, both variables were rejected as independent variables.

Data analysis was considered in two stages (i.e. learning and validating). As much as 81 data samples were randomly used for formulating the empirical model in the learning stage. The other data was used for validating. The two most common empirical models, linear and nonlinear, were fitted to the data using a single independent variable. These were developed using SigmaPlot Ver 6.1. Multiple independent variables or multiple linear regression were also established for developing empirical models to indicate reliable assessment of swelling potential of a soil. The general models are given as follows:

- Linear (single): $y = b_0 + b_1 t$
- Power: $y = b_0 t^{b_1}$
- Exponential: $y = b_0 e^{(b_1 t)}$
- Multiple linear: $y = b_0 + b_1 t_1 + b_2 t_2 + b_3 t_3$

The results of the statistical analysis are presented in Table 3.4.

Discussion

Empirical models

The evaluation of swell behavior of a soil using undisturbed samples and specialized swell tests is a difficult and expensive process for practicing engineers and small builders. Therefore, there is a need for simple routine tests that can be performed on disturbed engineered samples to achieve the same purposes. The empirical models appearing in the literature are primarily related to prediction of swelling and swelling pressure from index properties of soils. Sometimes, the empirical models proposed cannot be applied appropriately to all soils due to different soil conditions and testing procedures.

The data used, here, was compiled from different determinations of swelling and index properties. It was hoped that the models would be acceptable and generalized. Figure 3.6 shows the correlation between predicted-swelling and actual (measured) swelling. The figure plotted all the data used (i.e. 115 data samples were used in learning and validating). The dashed line shows the correlation between measured and predicted swell. It was expected that correlation should have lain on the 45° line (1 : 1 line), which refers to the colinearity of model. The figure illustrates that proposed empirical models, given in Table 3.3, give good correlations. The dash lines in Figures 3.6a, 3.6b, and 3.6c were laid down in the colinearity range of 0.5–0.8. The empirical model, proposed by Seed *et al.* (1962), as shown in Figure 3.6d, showed a very weak correlation in which the correlation was below line 0.5. It indicated that the proposed equation by Seed *et al.* (1962) is only appropriate for a measured-swelling of less than 30%. In our study, the multiple linear regression method (Equation 3.4, in Table 3.4) indicated a best-fit correlation. In general, the model can be used for all soil conditions.

In the current study, multiple regression analysis was considered to derive an equation that can be used to predict swelling potential from several index and physical properties. The

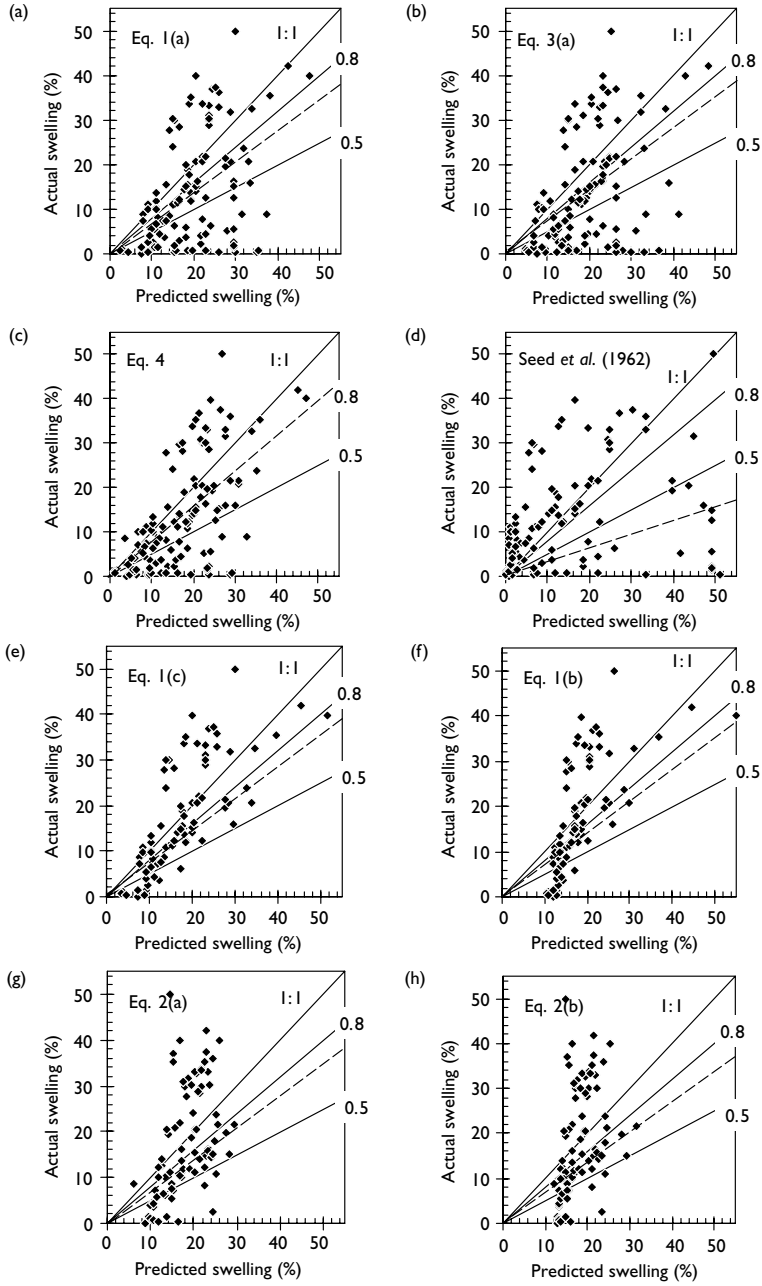

Figure 3.6 Correlation of proposed empirical model and actual swelling.

use of multiple regression statistics is very important in reducing the number of variables that are considered to be an independent source of information. These variables are reduced to only 3 or 4 which adequately explains the variation in swelling properties of the soils.

Many trials were carried out to correlate the swelling parameters to a combination of variables. The test of hypothesis of a linear model involved testing for significance of regression and testing on individual regression coefficients (Montgomery, 2001). For the proposed model, since *P*-value (P_v) is considerably smaller than the confidence level ($\alpha = 0.05$), the null hypothesis (H_0: $\mu_1 = \mu_2$) was rejected, indicating a strong correlation between each variable. For all statistical models, single or multiple linear regressions, satisfactorily fulfilled the F-test.

The coefficient of determination (R^2) has been used as a global statistic to assess the fit of the model. However, this value will increase when a regressor is added. In this model, the R^2 for a single variable is 0.192 (Equation 2c in Table 3.4). When added with two other variables it increases to 0.60. It showed significance. It can be concluded that swelling potential is linearly related to CF, LL, or PI. Testing of individual regression coefficient requires that at least one of the variables contributes significantly to the model. It has been observed that the CF and PI imply a significant contribution, since the standard error was 0.0661and 0.141 respectively, and the *P*-value was less than $\alpha = 0.05$ (Table 3.5). The coefficients of variables lie in the range of 95% confidence level. The overall test indicated that the variables fulfilled the requirements of the *t*-test and *F*-test.

Classification degree of swell

The empirical models have indicated that the multiple linear regression model gives the best-fit correlation for prediction of swelling potential of expansive soil. Furthermore, qualitative measurement is also needed to classify the degree of swelling. The measurement was determined based on the normal probability plot as shown in Figure 3.7. The measurement was simply divided into four regions based on the 25% percentile (Quartile), 50% percentile (Mean), and 75% percentile data. The classification of degree of expansiveness (swelling) is presented in Table 3.6. The determination is quite high compared to the category that was given by USBR in Table 3.2.

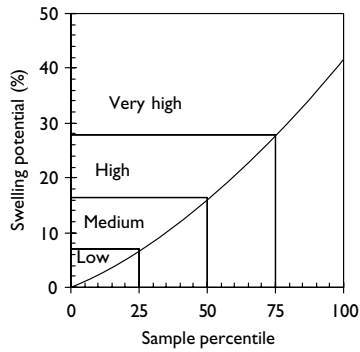

Figure 3.7 Normal probability plot and qualitative measurement of swelling potential.

Table 3.5 Analysis of variance (ANOVA) multiple linear regression

Variables	*Coefficients*	*Standard error*	*t-stat*	*P-value*	*Lower 95%*	*Upper 95%*
Intercept	−1.8695	3.1612	−0.5913	0.5559	−8.1644	4.4253
CF	0.1707	0.0661	2.5804	0.0117	0.0389	0.3023
LL	0.00124	0.1320	0.00947	0.9925	−0.2616	0.2640
PI	0.4092	0.1406	2.9105	0.0047	0.1292	0.6890

Table 3.6 Category for swelling potential classification

Proposed model	*USBR**	*Expansiveness remarks*
SP < 8.68	SP < 1.5	Low
8.68 ≤ SP 15.1	1.5 ≤ SP < 5	Medium
15.1 ≤ SP ≤ 28.8	5 ≤ SP ≤ 15	High
SP > 28.8	SP > 25	Very high

Notes
SP: swell potential (%); * Seed, *et al.* (1962).

Table 3.7 Predicted swelling potential and classification of soil used in the study

Soil code	*Clay fraction (CF)%*	*Liquid limit (LL) %*	*Plasticity index (PI) %*	*Predicted swelling potential (SP)%*	*Remarks*
KB1	26.9	76.9	37.5	18.2	High
KB2	30.0	89.7	47.5	22.8	High
KB3	32.5	106.8	62.4	29.3	Very
KB4	39.0	121.5	78.4	37.0	Very
SB1	4.0	42.9	21.8	7.8	Low
SB2	21.7	85.1	57.9	25.6	High
SB3	47.0	138.3	95.1	45.2	Very

It can be noted that the models and classification devised in this study are a simple predictive tool for assessing swell potential of a given soil, both undisturbed and remoulded specimens. Using the proposed model (Table 3.5), the swelling potential of the soil used in this study can be predicted and then classified as presented in Table 3.7.

Conclusions

Index and physical properties of soil are useful indicators to estimate engineering and swelling properties. There are three properties, which are most strongly correlated to swelling potential, PI, LL, and CF. The proposed models in the current study, showed good correlation compared with previous models cited in the literature. The multiple linear regression model gave the best-fit for all soil conditions. The classification of degree of expansiveness (i.e. swelling) has been well devised based on the statistical analysis. The degree of swelling can be classified into four distinct levels, low, medium, high, and very high.

Acknowledgments

The author gratefully appreciates the funding provided by the Ministry of Science, Technology, and Environmental (MOSTE) Malaysia through Intensify Research for Priority Area (IRPA) RM#8 and the University of Malaya through Short-Term IRPA Fund (Vot-F) 2002/2003. Sincere thanks go to Ir. Dr Roslan Hashim, Professor of University of Malaya, for his discussion.

References

Alawaji, H.A. (1999), Prediction of swell characteristics of sand – bentonite mixtures, *Proceedings of 11th Asian Regional Conference on Soil Mechanic and Geotechnical Engineering*, Vol. 1, Seoul, pp. 35–37.

Al-Rawas, A.A., Guba, I., and McGown, A. (1998), Geological and engineering characteristics of expansive soils and rock in northern Oman, *Engineering Geology*, Vol. 50, pp. 267–281.

Altmeyer, W.T. (1955), Discussion of engineering properties of expansive clays, *Transaction ASCE*, Vol. 81 (658), pp. 17–19.

Basma, A.A., Al-Hamoud, A.S., and Malkawi, A.H. (1995), Laboratory assessment of swelling pressure of expansive soils, *Applied Clay Sciences*, Vol. 9, pp. 355–368.

Chen, F.H. (1983), *Foundation on Expansive Soils*, Elsevier Scientific Publishing Co., New York, USA.

Çokça, E. (2001), Use of class C-Fly Ashes for the stabilization of an expansive soils, *Journal of Geotechnical and Geoenvironmental Engineering, ASCE*, Vol. 127 (7), pp. 568–573.

Daksanamurthy, V. and Raman, V. (1973), A simple method of identiying an expansive soil, Soil and Foundations, *Japanese Society of Soil Mechanic and Foundation Engineering*, Vol. 13 (1), pp. 97–104.

Djedid, A., Bekkouche, A., and Aissa Mamoune, S.M. (2001), Identification et prévision du gonflement de quelques sols de la région de Tlemcen, Algérie, *Bulletin des Laboratories des Ponts et Chaussées*, Vol. 233, pp. 69–77.

Erguler, Z.A. and Ulusay, E. (2003), A simple test and predictive models for assessing swell potential of Ankara (Turkey) clay, *Engineering Geology*, Vol. 67, pp. 331–352.

Holtz, W.G. and Gibbs, H.J. (1956), Engineering properties of expansive clays, *Transaction ASCE* Vol. 121, pp. 641–677.

Kormonik, A. and David, D. (1969), Prediction of swelling pressure of clays, *Journal of Soil Mechanics and Foundation Division ASCE*, Vol. 95 (SM1), pp. 209–225.

Montgomery, D.C. (2001), *Design and Analysis of Experiments*, 5th Edn., John Wiley & Son's Inc., New York, USA.

Muntohar, A.S. and Hashim, R. (2003), *Swelling Behavior of Engineered Clay Soil*, The Second International Conference on Advances in Soft Soil Engineering and Technology, 2–4 July, Kuala Lumpur, Malaysia.

Parker, J.C., Amos, D.F., and Kaster, D.L. (1977), An evaluation of several methods of estimating soil volume change, *Soil Science Society American Journal,* Vol. 41, pp. 1059–1064.

Schreiner, H.D. (1988), Identification and classification of expansive soils, In Varma, C.V.J. (ed.), *Proceeding of 6th International Conference on Expansive Soils*, New Delhi, India, pp. 23–29.

Seed, H.B., Woodward, R.J., and Lundgren, R. (1962), Prediction of swelling potential for compacted clays, *Journal of Soil Mechanics and Foundation Division ASCE*, Vol. 88 (SM3), pp. 53–87.

Thomas, P.J. (1998), *Quantifying Properties and Variability of Expansive Soils in Selected Map Units*, Ph.D Dissertation, Virginia Polytechnic Institute and State University, Blacksburg, Virginia, p. 79.

Williams, A.A.B. (1957), *Discussion on the Prediction of Total Heave from the Double Oedometer Test*, Symposium on Expansive Clays, South African Instituion of Civil Engineer, p. 57.

Chapter 4

Overview of mineralogy of bentonites

Genesis, physicochemical properties, industrial uses, and world production

Richard Přikryl[1]

Summary

The aim of this chapter was to give an overview of the mineralogy and chemistry of smectite-rich rocks, their genesis, important physical and physico-chemical properties, industrial and commercial uses, and principal deposits and world production. There are three major uses of bentonites: as a filler, as a binder, and as an adsorbent/absorbent. It is hoped that this review will give a more fundamental insight into how this resource functions as well as clarifying the important applications of this valuable commodity.

Introduction

Natural sodium bentonite is a high swelling clay composed mainly of sodium montmorillonite. There are three major uses of bentonites (*s.l.* (*sensu lato*)): as a filler, as a binder, and as an adsorbent/ absorbent (Andrews, 1992). Bentonite production has recently been reported from 43 countries reaching 10.4 Mt/year (data for 2002). In Europe, important bentonite deposits are located in the Mediterranean area (Sardinia, Spain, and Greece). Significant Central European deposits can be found in Germany (Bavaria – area of Mainburg, Moosburg, and Landshut), Czech Republic (West Bohemia), Slovakia, and Hungary.

Smectites are one group in the broad family of clay minerals and represent the dominant crystalline (mineral) phase forming bentonites and related rocks. Chemical characteristics of bentonites and smectite-rich clays are similar. Smectites are common minerals formed by hydrothermal alteration (argillitization) under specific conditions. The controlling factor is the pH of the environment with an optimum range of 5–7. Various natural environments of bentonite formations range from precipitation of smectites at sea floor at temperatures of about +3°C (Cole, 1985) to hydrothermal systems with temperatures below 200°C. At higher temperatures, smectites quickly transform to mixed-layer minerals and chlorites (Kristmannsdottir, 1979). Bentonite (*s.l.*) deposits reflect complex conditions of the origin of smectite group minerals. Smectites generally form from various rocks under medium intensity weathering conditions typical for temperate climates and moderate drainage of weathering profile (Jackson, 1959). Some of the most important bentonite formations (e.g. located in Wyoming and Oregon, USA) were formed by post-depositional weathering of airborne and

[1] Institute of Geochemistry, Mineralogy and Mineral Resources, Faculty of Science, Charles University in Prague, Albertov 6, 128 43 Prague 2, Czech Republic; phone: + 420–221951500, fax: + 420–221951496, e-mail: prikryl@natur.cuni.cz

water transported volcanic ash in shallow lacustrine and sea water (Jeans *et al.*, 1977; Altaner and Grim, 1990; Elzea and Murray, 1990). In situ alteration of volcanic glass in aqueous environment presents the most common process of bentonite formation (Grim and Güven, 1978).

Smectites with Na^+ exchangeable cation show higher swelling capacity and excellent colloidal properties in comparison to that of smectites with Ca^{2+} exchangeable cation. Cation exchange capacity is probably the most important physico-chemical characteristic of smectite-rich rocks. This property is linked to their chemical activity and common cation substitutions. The specific surface area (total surface including particle external surface and area of interlayer faces) is one of the fundamental factors influencing swelling, colloidal, and rheological properties of bentonites.

There are a variety of industrial applications for special varieties of bentonites. White bentonites or speciality clays (Clarke, 1985; Russell, 1991), for example, have found high value uses as electrical ceramics, pharmaceuticals, cosmetics, toiletries, and detergents. Expansive clays – bentonites *s.l.* – play an important role as engineered barriers that must act as isolation and retardation envelopes (Savage *et al.*, 1999) of canisters containing spent nuclear fuel. This means providing sufficient mechanical stability and preventing groundwater flow from surrounding environment to the canister.

The aim of this chapter is to give an overview of the mineralogy and chemistry of smectite-rich rocks, their genesis, important physical and physico-chemical properties, industrial and commercial uses, and principal deposits and world production.

Bentonites

Bentonite is a rock composed almost entirely of crystalline clay minerals from the smectite family. It is formed by in situ weathering processes. According to the geological understanding of their genesis, bentonites are formed by devitrification and chemical alteration of igneous materials – usually tuffs or volcanic ash of basic composition containing principal amount of volcanic glass (Ross and Shannon, 1926). This process occurs at the place of original volcanic eruption and is not accompanied by any significant transport of weathered material to another sedimentary basin. Bentonite holds its name after Fort Benton (Montana, USA). The term, first applied by Knight (1898) for highly plastic and swelling clays from the Upper Cretaceous sediments quarried in Rock River (Wyoming, USA), is recently used for almost any smectite-rich materials regardless of their true genesis (compare Elzea and Murray, 1994).

Smectite-rich or montmorillonitic clays (Konta, 1973) represent raw material showing composition and properties similar to that of bentonites. Nevertheless, transport of smectites and their deposition in sedimentary basin are vital for their formation. According to the geological understanding, these deposits can be considered as true secondary deposits of smectite-rich rocks. Sedimentary montmorillonitic clays are derived, in most of the cases but not always, from bentonites.

In technical practice, the general term bentonite is used for any smectite-rich material regardless of genesis and occurrence of the deposit (Grim, 1973; Elzea and Murray, 1994). Technological criteria serve also as a common classification criterion (e.g. foundry bentonites and bentonites for other applications as used by the Czech Geological Survey (Kavina *et al.*, 2002)). Evidently, one of the many industrial uses cannot be applied for the raw material with so many diverse industrial applications. More comprehensive classification of smectite-rich rocks was suggested during the last decade (Andrews, 1992; Elzea and Murray, 1994; Manning 1995). Compilation of these sources is summarised in Table 4.1.

The categorization is based on mineralogy (type of smectite), chemistry (type of exchangeable cation), treatment of natural material (i.e. improvement of material quality), and geographic location of major deposits (mainly used in USA and UK).

Natural sodium bentonite is a high swelling clay composed mainly of sodium montmorillonite. Organophilic bentonite (organoclay) represents sodium bentonites with organic cations adsorbed to increase special properties. Natural calcium bentonite containing calcium montmorillonite exhibit several time less swelling potential (also called sub-bentonite) compared to that of natural sodium bentonite. Improvement of this property (by reaction of soda with Ca-bentonite) produces sodium-exchanged bentonite (for other synonyms see Table 4.1). White bentonite is high brightness calcium bentonite. Natural calcium bentonites are often treated by acids to enhance sorption properties (acid activated bentonite). Potassium bentonite (metabentonite) is of less commercial interest due to the presence of mixed (smectite–illite) structures that decrease unique properties of true bentonites.

Geographic terms are namely applied in USA (Wyoming or western bentonite, Mississippi or southern or Texas bentonite) and in UK (fuller's earth) with dissimilar meaning of the later term. The term fuller's earth used mainly in UK (Manning, 1995) is derived from its former use – cleaning or "fulling" of wool by peoples termed "fullers" (Hosterman and Patterson, 1992). This clay has found, however, numerous other applications and the term fuller's earth recently refers to any naturally active material (see Table 4.1 for non-smectite materials) having the ability to decolorize and purify liquids (Nutting, 1943;

Table 4.1 Terminology of smectite-rich rocks of commercial interest

Dominant mineral	*Dominant exchangeable cation*	*Term for natural material according to properties*	*Term for artificial material*	*Geographical term*
Smecties				
Sodium montmorillonite	Na^+	Sodium b., swelling b., high swelling b.	Sodium-activated b., sodium exchanged b., synthetic b., engineered b., organophilic b., organoclay	Wyoming b. (USA), Western b. (USA), bentonite
Calcium montmorillonite	Ca^{2+}	Calcium b., non-swelling b., low swelling b., sub-bentonite, white b.	Acid-activated b.	Mississippi b. (USA), southern b. (USA), Texas b. (USA), fuller's earth (UK), bentonite (other countries)
Magnesium montmorillonite	Mg^{2+}	Saponite, armargosite		
Potassium montmorillonite	K^+	Potassium b., non-swelling b., metabentonite,		
Lithium montmorillonite	Li^+	Hectorite		
Non smectites				
Attapulgite		Palygorskite		Fuller's earth (USA)
Sepiolite		Meerschaum (lumps)		
Sodium sepiolite		Loughlinite		

Source: (Based on Andrews, 1992; Elzea and Murray, 1994; Manning, 1995; Kendall, 1996.) Note that this classification do not differentiate genetic aspects of these rocks and all materials are termed bentonites.

Hosterman and Patterson, 1992). Classification of fuller's earth shows similar duplication and overlapping as for bentonite. Fuller's earth used for oil processing is classified as naturally active clay (Elzea and Murray, 1994). When treated with acid, it becomes activated clay (Torok and Thompson, 1972). Bleaching earth (bleaching clay) is applied for both naturally active and activated clay (Rich, 1960). A more general term, "absorbent clay" (Nutting, 1943), covers both types of fuller's earth if used for variety of absorbing purposes different from oil processing. Other terms applied to the bentonites are loosely used synonyms (Andrews, 1992) like volcanic clay, soap clay, and mineral soap. Alternative classifications covered other properties of smectite-rich materials like their ability to be activated (Nutting, 1943; Ross, 1964) or swelling, colloidal, adsorptive, and osmotic properties (Davis and Vacher, 1940). These are not common in recent literature.

Mineralogy and chemistry of smectite-rich rocks

Smectites

Smectites are one group in the broad family of clay minerals and represent the dominant crystalline (mineral) phase forming bentonites and related rocks. The atomic structure of smectites is composed of stacked units comprising octahedrally coordinated ions (so called O units) occurring between two sheets of tetrahedrally coordinated ions (so called T units) composed of six-fold hexagonal rings of silica tetrahedra (Güven, 1991). TOT units are basic structural units of smectites (Figure 4.1).

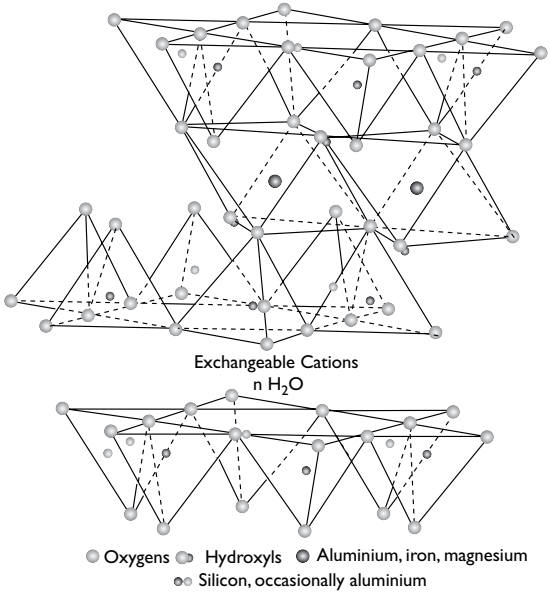

Figure 4.1 Crystal structure of smectite clay minerals (e.g. montmorillonite) showing basic TOT unit and interlayer space.
Source: Adopted and modified after Elzea and Murray, 1994.

Table 4.2 Classification of natural smectites

Ratio between tetrahedral (x_t) and octahedral (x_o) charges	*Diocathedral smectites*		*Triocathedral smectites*	
	Dominant octahedral cation(s)	*Mineral name*	*Dominant octahedral cation(s)*	*Mineral name*
$x_o/x_t > 1$	$Al^{3+}(R^{2+})$	montmorillonite	$Mg^{2+}(Li^{+})$	hectorite
$x_o/x_t 1$	Al^{3+}	beidellit	Mg^{2+}	saponit
	Fe^{3+}	nontronit	Zn^{2+}	*sauconite*
	Cr^{3+}	*volkonskoite*		
	V^{3+}	*vanadium smectite*		

Source: (Modified after Güven, 1991.) Less common minerals are given in italics.

The structural subdivision of smectites depends on the occupation of octahedral networks by cations (Table 4.2). If 2 of 3 sites are occupied by trivalent cations, the network is called dioctahedral. In trioctahedral smectites, all three sites hold divalent cations (Güven, 1991). The cation substitutions (tetrahedral substitutions of R^{3+} cations for Si^{4+}, octahedral substitutions of R^{+} cations for R^{2+}, cation in trioctahedral and R^{2+} cations for R^{3+} in dioctahedral smectites), octahedral vacancies, and deprotonation of hydroxyls (loss of H^{+}) are responsible of negative layer charges (Güven, 1991; Velde, 1995). The surface negative charges (chemical activity) are balanced by loosely bound (by Vaan der Wals forces) hydrated (Na^{+}, Ca^{2+}, Mg^{2+}) and non-hydrated (K^{+}) cations, and water molecules on tetrahedral sheets between two adjacent TOT units (compare Figure 4.1). Depending on these cations, either one molecule of water (for Na^{+}) or two molecules of water (for Ca^{2+} and/or Mg^{2+}) can enter the TOT interspace (Elzea and Murray, 1994). Loosely bound cations also specify basic natural types of bentonites (Table 4.1).

The classification of smectites is based, along with di- or trioctahedral nature of the octahedral sheets, on the sources and sites of excess layer charges, relative amounts of charges in the tetrahedral and octahedral networks, and on dominant octahedral cation (Güven, 1991). For dioctahedral smectites (Grim and Kulbicki, 1961; Schultz, 1969) (Figure 4.2), the ionic substitutions and octahedral versus tetrahedral charges lead to the subdivision based on:

- Wyoming type montmorillonite (numerous bentonite deposits in Wyoming, USA);
- Otay type montmorillonite (bentonite deposit Otay, California, USA);
- Cheto (Chambers) type montmorillonite (low swelling montmorillonite from Cheto deposit, Arizona, USA);
- Tatatilla type montmorillonite (Vera Cruz, Mexico);
- Fe-rich montmorillonite;
- Beidellite; and finally
- Fe-rich beidellite.

Mg- and Fe-smectites (Wyoming type, Cheto type, Fe-rich montmorillonite) form from intermediate or basic rock precursors (andesites, basalts), whereas Al-smectites (beidellite, Tatatilla type) are genetically related to rhyolitic rocks (Christidis and Dunham, 1993a,b;

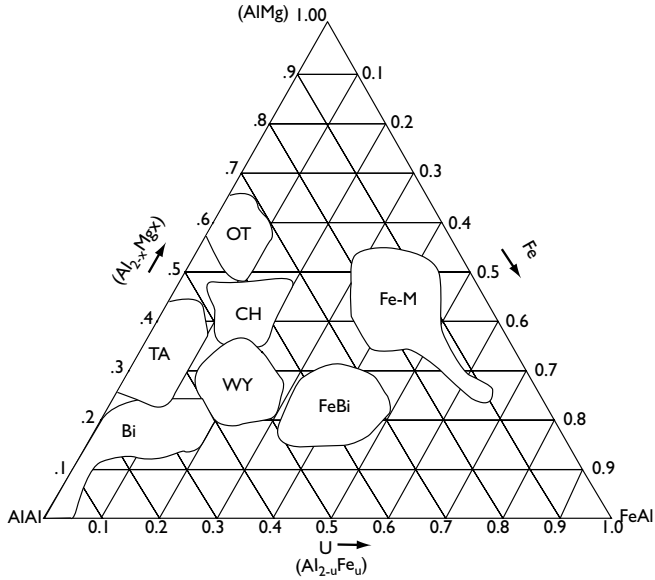

Figure 4.2 Plot showing major groups of dioctahedral aluminous smectites according to substitutions of Al, Fe, and Mg.

Source: Plot after Güven, 1991, mineral fields constructed according to data given by Grim and Kulbicki, 1961; Schultz, 1969; Weaver and Pollard, 1975.

Notes
TA: Tatatilla-type montmorillonite; OT: Otay-type montmorillonite; CH: Cheto-type montmorillonite; WY: Wyoming-type montmorillonite; Fe-M: Fe-rich montmorillonite; Bi: Beidellite; FeBi: Ferric beidellite.

Christidis *et al.*, 1995; Christidis and Scott, 1997). Trioctahedral smectites are subdivided into three major groups based on the dominant octahedral cations and genesis (Güven, 1991): Mg-smectites with Li^+ substitution (mainly hectorite, after Hector bentonite deposit, California, USA) formed in Mg-rich environments; transition metals (Ni, Co, Zn, Cu, Mn, Fe, etc.) smectites found around ore bodies, and in laterites and saprolites of ultramafic rocks; and Fe-Mg smectites (saponite) common in nature as authigenic clay minerals formed by the alteration of basic volcanic rocks.

Chemical characteristics of bentonites and smectite-rich clays are almost similar to those of smectite group of clay minerals. As shown earlier, these include ion-exchange ability that evidently affects physical properties like viscosity and thixotropy. Chemical composition of selected bentonites, smectite-rich clays, and smectites is given in Table 4.3.

Theoretical chemical composition of dioctahedral smectites (montmorillonite, beidellite, and nontronite) can be generally expressed as (after Elzea and Murray, 1994):

$$[Al_xFe_yMg_z)_{2.00}(Si_{4.00-(u+v)}\,Fe_vAl_u)O_{10}\,(OH)_2]M^+_{u+v+z}$$

Table 4.3 Chemical composition of smectites, bentonites and related rocks (data in wt %)

Sample	*1*	*2*	*3*	*4*	*5*	*6*	*7*	*8*	*9*	*10*	*11*	*12*	*13*	*14*	*15*
SiO_2	51.14	59.72	50.20	53.96	40.72	53.95	50.01	38.59	61.77	62.23	60.80	69.6	75.03	73.04	67.74
Al_2O_3	19.76	18.22	16.19	15.44	4.96	0.14	3.89	13.36	19.85	21.03	22.15	16.3	13.72	12.20	16.79
TiO^2	—	—	0.20	0.19	0.02	3.04	>0.04	0.31	0.24	n.d.	n.d.	0.29	0.17	0.18	0.13
Fe_2O_3	0.83	4.15	4.13	1.12	29.57	0.03	0.21	3.41	1.95	1.75	2.06	1.17	1.51	2.73	1.19
FeO	—	—	—	Tr.	0.71	—	—	—	n.d.	0.48	0.36	0.04	—	—	—
MnO	Tr.	—	—	—	—	—	—	—	n.d.	n.d.	n.d.	0.01	0.03	0.01	0.02
MgO	3.22	2.08	4.12	6.99	0.74	25.89	25.61	1.18	5.56	5.70	4.44	3.56	1.82	2.28	1.99
CaO	1.62	1.46	2.18	0.80	1.98	0.16	1.31	0.94	1.89	0.00	3.74	1.73	0.56	0.70	1.43
K_2O	0.11	0.54	0.16	0.54	—	0.23	—	0.18	0.09	0.00	n.d.	0.15	2.33	0.19	2.30
Na_2O	0.04	2.70	0.17	0.94	—	—	—	0.01	0.07	0.65	n.d.	0.33	0.29	0.40	1.94
P_2O_5	—	—	—	—	—	—	—	—	—	—	—	0.03	0.01	0.01	n.d.
Li_2O	—	0.14	—	—	—	1.22	—	—	n.d.	n.d.	n.d.	—	—	—	—
ZnO	—	—	—	—	—	—	—	23.50	n.d.	n.d.	n.d.	—	—	—	—
SO_3	—	0.59	—	—	—	—	—	—	n.d.	n.d.	n.d.	—	—	—	—
CO_2	—	—	—	—	—	—	—	—	—	—	—	0.16	—	—	—
H_2O^-	14.81	5.87	15.58	14.22	15.46	9.29	12.02	8.05	9.49	8.41	7.08	—	—	—	—
H_2O^+	7.99	5.55	7.57	6.34	6.66	5.61	7.28	10.39	7.72	7.38	8.02	—	—	—	—
LOI	—	—	—	—	—	—	—	—	—	—	—	7.50	4.98	7.37	7.43
$\sum$	99.75	101.02	100.50	100.54	100.82	99.56	100.37	99.92	—	—	—	100.87	100.45	99.11	100.82

Source: Data adopted from: 1 – montmorillonite from Montmorillon, France (Ross and Hendricks, 1945); 2 – swelling bentonite composed essentially of montmorillonite from Colony, Wyoming, USA (Andrews, 1992); 3 – sub-bentonite composed essentially of montmorillonite from Polkville, Mississippi, USA (Ross and Hendricks, 1945); 4 – sub-bentonite composed essentially of montmorillonite from San Diego county, California, USA (Ross and Hendricks, 1945); 5 – nontronite, USA (Ross and Hendricks, 1945); 6 – hectorite, Hector, California, USA (Andrews, 1992); 7 – saponite, Milford, Utha, USA (Cahoon, 1954); 8 – sauconite, Liberty mine, Meekers Grove, Wisconsin, USA (Ross, 1964); 9 – clay fraction from Cheto deposit, Arizona, USA (Grim and Kulbicki, 1961); 10 – clay fraction from Otay deposit, California, USA (Grim and Kulbicki, 1961); 11 – crude clay from Tatatilla, Vera Cruz, Mexico (Grim and Kulbicki, 1961); 12 – STx-1 montmorillonite standard from Gonzales County, Texas, USA (van Olphen and Fripiat, 1979); 13 – white bentonite rich in beidellite and Tatatilla type montmorillonite from Ano Komia deposit, Milos, Greece (Christidis and Scott, 1997); 14 – bentonite rich in Cheto type montmorillonite from Zoulias deposit, Milos, Greece (Christidis and Scott, 1997); 15 – white bentonite rich in Cheto type montmorillonite from Prassa deposit, Kimolos, Greece (Christidis and Scott, 1997).

Trioctahedral smectites (hectorite, saponite) show theoretical structural formula:

$$[Mg_{3.00-z}Li_z)_{2.00}(Si_{4.00-u}Al_u)O_{10}\,(OH)_2]M^+_{u+z}$$

Other minerals

Other non-clay crystalline phases are commonly found in bentonites. These can be subdivided in the following categories (Elzea and Murray, 1994): residual phases of volcanic origin; secondary minerals (weathering products) formed by transformation of original volcanic rocks or during their diagenesis (in situ formation); and detritic admixtures (later transported material to existing bentonites and montmorillonite clays).

The first group is represented by feldspars, biotite, quartz (or silica in general), amphiboles, and accessory minerals (e.g. magnetite, apatite, zircon). The low temperature transformation of original volcanic rocks leads to the formation of secondary phases – non-smectite clay minerals (kaolinite group minerals, illite), amorphous SiO_2, calcite, zeolites, and/or sulphates.

Genesis of smectite-rich rocks

Various natural environments of bentonite formations range from precipitation of smectites at sea floor at temperatures of about +3°C (Cole, 1985) to hydrothermal systems with temperatures below 200°C. At higher temperatures, smectites quickly transform to mixed-layer minerals and chlorites (Kristmannsdottir, 1979). At laboratory conditions, smectites have grown from temperatures +25°C (Noll, 1936) to more than 1000°C (Yamada *et al.*, 1994).

Bentonite (*s.l.*) deposits reflect complex conditions of the origin of smectite group minerals. The weathering environment produces the widest variety of these phyllosilicates. Smectites generally form from various rocks under medium intensity weathering conditions typical for temperate climate and moderate drainage of weathering profile (Jackson, 1959). Smectite, either detrital or authigenic, makes up a common part of continental and marine sedimentary sequences. In diagenesis, fully expandable dioctahedral montmorillonites disappear near 100°C at depths of about 2 km at low geothermal gradient (Burst, 1959; Perry and Hower 1970; Weaver and Beck, 1971 among others). Hydrothermal alteration zones present another environment where economically important deposits can form. Even in this specific case, smectite formation is again limited by temperature. Smectite therefore never occurs in the innermost hydrothermal alteration zone (Shirozu, 1978).

Basin-weathered volcano-sedimentary deposits

Some of the most important bentonite formations (e.g. located in Wyoming and Oregon, USA) were formed by post-depositional weathering of airborne and water transported volcanic ash in shallow lacustrine and sea water (Jeans *et al.*, 1977; Altaner and Grim, 1990; Elzea and Murray, 1990). Formation of this rock type was possible only if all the following factors existed (Manning, 1995): existing source of volcanic ash; accumulation of this ash in the depositional basin; transformation of volcanic ash to smectite clay in the presence of sea water (necessity of alkaline brines); and protection of newly formed mineral assemblage from erosion (mechanical destruction) or further change (mineral transformation due to burial of smectites in greater depths and their consequent conversion to mixed illite-smectite or illite clays – compare, for example, Hower *et al.*, 1976).

This specific type of bentonite deposit is differentiated from the others by two factors. First, accumulation of volcanic ash in depositional basin can be preceded by transport (mainly in air) accompanied by sedimentary sorting (by size, density etc.) which can later facilitate ash weathering. Second, deposition of ash in the presence of marine water (alkaline water with excess of Na^+ cation) promotes formation of sodium (Wyoming) type bentonite (rich in montmorillonites with Na^+ exchangeable cation). Weathered volcanoclastic rocks are major bentonite deposits *s.s*. (*sensu stricto*). The most important deposits are located in Wyoming (MT, USA) forming individual beds within the Upper Cretaceous marine sediments.

In situ-weathered volcano-sedimentary deposits

In situ alteration of volcanic glass in aqueous environment presents the most common process of bentonite formation (Grim and Güven, 1978). Residual volcanic ashes deposited on the slopes of volcanic cones or in maars represent another *s.s*. bentonite deposits. The absence of natural transport and sorting mechanisms during the deposition of volcanic ash did not allow for effective separation of impurities. Smectites with Ca^{2+} and/or Mg^{2+} cations preferentially occur because the weathering process takes place at subsurface terrestrial conditions with brines rich in Ca^{2+} and/or Mg^{2+}. Typical deposits of this type are bound to the neovolcanic Tertiary sequences in central Europe (Bohemian Massif – Czech Republic), south-west Europe (Cabo de Gata in Spain – Benito *et al.*, 1998), or Africa (e.g. Libya).

Hydrothermal deposits

Smectites are common minerals formed by hydrothermal alteration (argillitization) under specific conditions. The controlling factor is pH of the environment with optimum range 5–7. The increase of acidity (pH = 4.5–5) leads to the preferred formation of kaolinite instead of smectites (Drits and Kossovskaja, 1990). The temperature conditions are extrapolated up to 160°C (Reyes, 1990) although no thermometer is available (Šucha, 2001). Smectites formed from hydrothermal alteration may produce economically significant resources (Grim and Güven, 1978; Manning, 1995) similar to hydrothermal kaolin deposits (Bristow, 1993). These deposits are generally small in extent forming alteration patterns associated within and/or around structural features (namely joints). Massive changes of parent rock similar to that of Kuroko-type deposits (Chamley, 1989) seem to be economically significant. Smectites (sometimes accompanied with zeolites) occur in the outer alteration zone (zone I) (Shirozu, 1978). Important bentonite resources of this type have been reported from Japan (Na-bentonites formed from altered ryolitic tuffs on west Honshu), Italy (Ca-bentonite from trachytic volcanic ash on Sardinia – Annedda, 1956), and Greece (Ca-bentonite from dacite and related tuffs on Milos – Christidis and Dunham 1993a). For Spanish bentonites, hydrothermal origin is considered as well (Martin-Vivaldi and Linares, 1968).

Sedimentary deposits

Sedimentary smectite-rich clays can be formed by redeposition of primary types of bentonite deposits or by accumulation of smectites formed, for example, during pedogenesis. These deposits can be probably found in many sedimentary environments (mainly intracontinental) adjacent to volcanic terranes where bentonites coming from in situ weathering process occur. Although written evidence on this distinct type of bentonite *s.l*. is missing in

the international literature, there must be numerous deposits. Some of the Czech deposits (e.g. Maršov in South Bohemia or Zelená in West Bohemia) represent accumulation of smectites by sedimentary process (Přikryl *et al.*, 2003).

Physical and physico-chemical properties of smectite-rich rocks

Unique physical and physico-chemical properties of smectite-rich rocks result from a combination of chemical phenomena and mineralogical composition (crystal size below 2 μm, specific structure of smectites, ion substitution in crystal structure, and presence of cations or water in the interlayer). Proportion and type of exchangeable cations influence surface chemistry of clay particles and their charge. This, in reverse, determines clay reactivity with water (Foster, 1953; Van Olphen, 1977; Alther, 1986; Lagaly, 1989; Velde, 1995). The most important feature is the colloidal nature of smectites (Ross, 1964; Wayland, 1971; Andrews, 1992; Giese and van Oss, 2002). This arises from weathering of original alumosilicates giving rise to particles ranging from 1–100 μm. Electrochemical energy of these particles is activated when mixed with water resulting in dilatancy (swelling capacity), viscosity (resistance to flow), and thixotropy (gelling strength).

Smectites with Na^+ exchangeable cation show higher swelling capacity and excellent colloidal properties in comparison to that of smectites with Ca^{2+} exchangeable cation. This fact, experimentally approved, is explained by presence of Na^+, its charge, and hydration (Elzea and Murray, 1994). Smectite-rich rocks can form colloidal gels exhibiting thixotropy (ability of some gels become fluid when agitated and revert). Aqueous suspensions of bentonite show greater viscosities, gel strength (difference in yield value immediately after agitation and standing for 10 minutes – Harben, 2002), and thixotropies than any other clay (Andrews, 1992). Thixotropy of sodium bentonites is higher than of calcium bentonites (Rogers, 1963).

Smectites are highly hygroscopic. Finely ground and dried smectites with Ca^{2+} exchangeable cation absorb moisture rapidly. Smectites with Na^+ exchangeable cation show an even greater absorption capacity (Andrews, 1992). Dehydratation of smectite-rich materials occurs in several steps if subjected to heat. At 100–150°C pore moisture escapes resulting in shrinkage (free moisture varies in the range 3–10%). Temperature in the range of 100–500°C results in the expelling of the interlayer water and consequent disappearance of swelling properties (rate of loss of swelling properties varies with exchangeable cation – for smectites with Na^+ occurs at 390–490°C, for smectites with Ca^{2+} at 300–390°C) (Hofmann and Endell, 1939). Temperatures in the range of 400–750°C lead to the removal of hydroxyl ions out of crystal structure. At 550°C bloating or expansion often occurs (due to expulsion of water and alkalies).

Cation exchange capacity, that is, ability to exchange of ionic species is probably the most important physico-chemical characteristic of smectite-rich rocks. This property is linked to their chemical activity and common cation substitutions. The ions or molecular species are attracted by a charged surface of clay particles (process of adsorption) or to the internal surface of clay particles (process of absorption) (Velde, 1995). About 80% of exchange capacity is due to the cation substitution in smectites crystal structure, the remaining 20% is linked to the charges at the edge of clay particles (Weaver and Pollard, 1975). The common range of cation exchange capacity of montmorillonite (the most common smectite mineral) is 70–130 (maximum 145) meqv/100 g (Weaver and Pollard, 1975).

Table 4.4 Specific surface area of clay minerals

Type of clay mineral	*1*	*2*
Na-montmorillonite	—	727
Ca-montmorillonite	800	733
Illite	150	84
Kaolinite	50	219

Source: Data in m^2/g. 1 – theoretical data after Moorlock and Highley (1991); 2 – experimental data after Gilchrist *et al.* (1993).

Specific surface area (total surface including particle external surface and area of interlayer faces) is one of the fundamental factors influencing swelling, colloidal, and rheological properties. Specific surface area is measured either from adsorption isothermes – for example, BET method (Brunauer *et al.*, 1938) or dye absorption technique (Gungor and Tulun, 1996). The specific surface area from BET method represents predominantly the surface area of meso- and macropores (radii >2 nm). Structural parameters of micropores (pores radii <2 nm) are commonly determined from the CO_2 isotherms at the temperature of 298 K within a pressure range from 0 to 1000 mbars. The measured isotherms are evaluated according to Dubinin's theory of volume filling and basic parameters like volume of micropores, surface area, and distribution of micropores can be computed using Dubinin's and Medek's equations (Dubinin, 1967; Medek, 1977).Technique of determination can seriously influence results (Table 4.4). Value of specific surface area is often used during preliminary evaluation of maximum smectite content in raw material (Moorlock and Highley, 1991; Christidis and Scott, 1993).

Uses of smectite-rich rocks

There are three major uses of bentonites (*s.l.*): as a filler, as a binder, and as an adsorbent/absorbent (Andrews, 1992) (Table 4.5). Specific areas of application are dependent on actual properties of the raw material that can be improved by various treatments. Properties of non-sodium bentonites are commonly improved by sodium activation, during which part of Ca^{2+} is exchanged for Na^{+}. Acid activation is conducted on calcium bentonite to increase its specific surface area and sorptive properties (Adams, 1987; Christidis *et al.*, 1997; Christidis and Kosiari, 2003). Most recently, interlayer cations are exchanged for positively charged organic species to produce organically activated bentonites (Boyd and Jaynes, 1994).

Along with major industrial applications depicted in Table 4.5, numerous other uses can be found for special varieties of bentonites. White bentonites or speciality clays (Clarke, 1985; Russell, 1991) found high value industrial uses for electrical ceramics, pharmaceuticals, cosmetics, toiletries, and detergents.

Role of smectite-rich rocks in nuclear waste treatment

Commonly proposed treatment of high level radioactive waste is based on its deposition in solid bedrock at great depths of about 500–1000 m. This approach, also called Swedish concept (SKB, 1995), ensures isolation of such a waste from surrounding environment

Table 4.5 Major areas of industrial application of bentonite *s.l.*

Industry	*Acid activated*	*Untreated*	*Sodium activated*	*Organically activated*
Food production	Fats and oils – refining, decolourising, stabilizing			
Beverages	Wine – fining Other beverages – purifying Beer – stabilization			
Water	Adsorption of impurities; coagulation of bacteria			
Chemical	Catalyst carrier; insecticides/fungicides; dehydrating agents; water purification; waste adsorbent; extender and emulsifier for rubber, linoleum and oilcloth production			
Petroleum	Refining: decolorising; purifying oils, fats, and waxes; catalysts			
Cleaning	Dry-cleaning fluid regeneration	Polishes; additives to washing and cleaning agents; filler in soap production		
Paper	Pigment/color developer for copying paper; opacity improvement; smoothness; printing softness; process water purification			
Pharmaceuticals		Earths and medicaments filler; creams; cosmetics (mud packs)		
Waste disposal		Sealing liners for landfill sites; composite geotextile/clay liners; barriers in radioactive waste disposal		
Construction and civil engineering		Supporting suspensions for cut-off diaphragm wall construction; antifriction agents for shaft sinking; additive to concrete and mortar; impermeabilization of ground soil		
Underground construction		Grouting material (swelling in fissures)		
Agriculture, horticulture, animal care		Soil improvement; composting; feed pellets; cat litter; liquid manure treatment; diluent for pesticides and herbicides		
Drilling		Borehole scavenging for salt water	Drill fluid formulation	
Tar			Emulsification and thixotroping of tar–water emulsions; tar and asphalt coating	
Paint/varnish			Extender; thickening; thixotroping; stabilizing and anti-setting (suspending) agents	
Foundries		Binder for special moulding sands	Binder for synthetic moulding sands	Binder for anhydrous casting sands
Ore production		Binder for ore pelletizing		
Ceramics		Plasticizer of ceramic compounds; suspending agent for procelain enamels and glazes; improvement of strength; fluxes		
Fire control	Water carrier in air fire fighting			

Source: Compiled and adopted after Ross, 1964; Fleming, 1972; O'Driscoll, 1988; Andrews, 1992; Manning, 1995.

(geosphere, hydrosphere, atmosphere, and biosphere). Expansive clays – bentonites *s.l.* – play important role in the concept of engineered barriers that must act as an isolation and retardation envelopes (Savage *et al.*, 1999) of canisters containing spent nuclear fuel. The isolation means providing sufficient mechanical stability and preventing groundwater flow from

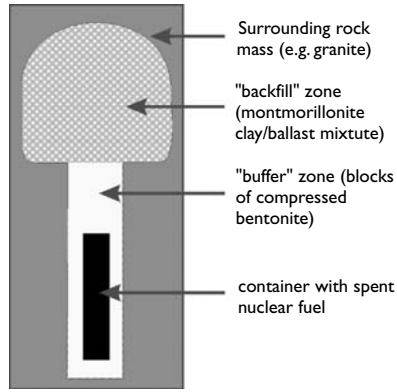

Figure 4.3 Schematic cross-section of shaft containing spent nuclear fuel, engineered barriers (including buffer zone), and of access tunnel filled by the "backfill" material. This repository facility is placed 500–1,000 m bellow ground arising demand for about 2 Mt of high quality smectite-rich sealing material for each repository.

Source: Modified after Savage *et al.*, 1999 and Přikryl *et al.*, 2003.

surrounding environment to the canister. Retardation function is required for collapsed canisters (e.g. due to corrosion). Retardation properties of the barrier consist of resistance to chemical and mineralogical alteration during the life of repository, and sufficient sorption capacity (ability to prevent escape of radio nuclides to the surrounding environment).

Engineered barriers are used in two distinct zones – buffer and backfill (Figure 4.3). Buffer consists of manufactured blocks composed of highly compacted bentonite with sodium exchangeable cation (NAGRA, 1985). This type of bentonite was selected due to its higher ability to swell in comparison to bentonites containing calcium exchangeable cations. The backfill part of the multibarrier means backfilling of excavated accessory tunnels and shafts. Depending on size of the repository, the amount of material for backfilling can vary from about 0.5 to 2 mil m^3 (Lopez *et al.*, 1987). The qualitative requirements will be probably less strict than those for buffer zone materials but still need detailed research. Evidently, bentonites with calcium exchangeable cation fit perfectly to the backfilling material due to optimum ratio of properties and price.

Principal deposits and world production

Besides USA, which has almost 40% of world production, commercially significant deposits of bentonite are found in many other countries. Bentonite production has recently been reported from 43 countries reaching 10.4 Mt/year (data for 2002). Fuller's earth production (Table 4.6) presents an additional 3.89 Mt of raw material (data for 2002). In Europe, important bentonite deposits are located in the Mediterranean area (Sardinia, Spain, and Greece). Significant Central European deposits can be found in Germany (Bavaria – area of Mainburg, Moosburg, and Landshut), Czech Republic (West Bohemia), Slovakia, and Hungary. Europe bentonite production makes about 30% of world total (Table 4.7).

Table 4.6 World production of fuller's earth

Country	*1998*	*1999*	*2000*	*2001*	*2002*[e]
Algeria	3,942	2,489	3,431	3,254	3,521
Argentina[e]	1,500	1,500	1,500	1,500	1,500
Australia (attapulgite)	15,670	5,639	5,600	5,600	6,000
Germany[e]	600,000	500,000	500,000	500,000	500,000
Italy	30,000	30,000	30,000	30,000	30,000
Mexico	48,016	47,522	51,685	148,194	150,000
Morocco (smectite)	27,650	21,956	30,665	40,664	42,243
Pakistan	14,659	15,565	15,288	15,000	15,000
Poland	5,400	5,000	29,700	29,000	NA
Senegal (attapuglite)	80,000	136,000	131,000	130,000	176,454
South Africa (attapulgite)	7,830	7,067	7,337	9,229	7,990
Spain (attapulgite)[e]	90,000	90,000	90,000	90,000	90,000
United Kingdom	95,000	75,000	66,000	52,000	44,000
United States	242,000	2,560,000	2,910,000	2,890,000	2,730,000
World total	3,380,000	3,560,000	3,920,000	4,000,000	3,890,000

Source: Compiled from Steblez, 2001; Virta, 2002 e – estimates. All data in metric tons.

Table 4.7 World production of bentonite *s.l.*

Country	*1998*	*1999*	*2000*	*2001*	*2002*[e]
Europe					
Bosnia[e]	800	800	800	800	800
Bulgaria	176,000	232,000	296,000	308,000	250,000
Croatia	7,581	8,441	10,013	10,580	11,204
Cyprus	121,000	138,853	167,500	126,000	125,000
Czech Republic	125,000	160,000	280,000	250,000	250,000
Germany	509,000	477,000	465,000	448,000	500,000
Greece	950,000	1,049,650	1,148,694	1,150,000	1,150,000
Hungary	17,000	16,000	15,000	30,400	30,000
Italy	592,000	600,000	600,000	600,000	500,000
Macedonia	30,000	30,000	30,000	30,000	30,000
Poland	5,400	5,000	29,700	29,000	30,000
Romania	25,434	19,577	35,789	24,779	15,402
Serbia and Montenegro	68	77	75	75	75
Slovakia	81,010	64,390	66,528	82,915	NA
Spain	193,000	190,000	90,152	90,000	150,000
Ukraine	300,000	300,000	300,000	300,000	300,000
Europe subtotal	3,133,293	3,291,788	3,535,251	3,480,549	3,342,481
Africa					
Algeria	15,655	15,491	22,708	21,286	27,178
Egypt	33,000	50,000	50,000	50,000	50,000
Kenya	—	—	64	50	50
Morocco	33,311	36,528	43,152	71,741	65,754
Mozambique	10,448	10,828	16,144	1,611	1,600
South Africa	48,382	49,261	85,187	108,300	218,512
Zimbabwe	135,785	140,000	140,000	—	—
Africa subtotal	276,581	302,108	357,255	252,988	363,094

(continued)

Table 4.7 Continued

Country	*1998*	*1999*	*2000*	*2001*	*2002*[e]
Asia					
Armenia	3,000	3,493	2,807	3,000	3,000
Burma	1,066	998	978	900	900
Commonwealth of Independent States	600,000	700,000	750,000	750,000	750,000
Georgia	11,000	9,891	7,084	7,000	7,000
Indonesia	840	5,213	5,000	5,000	5,000
Iran	83,279	4,957	70,000	80,000	80,000
Japan	443,566	428,247	415,115	405,738	400,000
Pakistan	14,196	15,349	27,700	27,000	28,000
Philippines	3,900	1,844	2,800	5,128	5,500
Turkey	567,708	899,614	636,273	674,178	559,224
Turkmenistan	50,000	50,000	50,000	50,000	50,000
Asia subtotal	1,778,555	2,119,606	1,967,757	2,007,944	1,888,624
America					
Argentina	131,320	128,809	123,092	104,335	88,685
Brazil	220,000	274,623	273,975	160,381	165,000
Chile	721	1,104	1,314	1,695	632
Guatemala	2,278	4,301	3,317	3,000	3,100
Mexico	185,729	208,611	269,730	415,133	400,000
United States	3,382,000	4,070,000	3,760,000	3,970,000	3,970,000
America subtotal	3,922,048	4,687,448	4,431,428	4,654,544	4,627,417
Australia and Oceania					
Australia	104,000	180,000	180,000	180,000	200,000
New Zealand	14,000	15,000	10,000	10,000	7,800
World total	9,228,477	10,595,950	10,481,691	10,586,025	10,429,416

Source: Compiled from Steblez, 2001; Virta, 2002.

Note
e – estimates. All data in metric tons.

In closing, this chapter has provided an overview of the mineralogy and chemistry of bentonites, their genesis, their physical and physico-chemical properties, commercial and industrial uses, and principle deposits and world production. It is hoped that this review has provided a more fundamental insight into how this resource functions as well as clarifying the important applications of this valuable commodity.

References

Adams J.M., 1987. Synthetic organic chemistry using pillard, cation exchanged and acid-treated montmorillonite catalysts – a review. *Applied Clay Science*, 2: 309–342.

Altaner S.P. and Grim R.E., 1990. Mineralogy, chemistry and diagenesis of tuffs in the sucker creek formation (miocene) eastern Orgeon. *Clays and Clay Minerals*, 38: 561–572.

Alther G.R., 1986. The effect of exchangeable cations on the physicochemical properties of Wyoming bentonites. *Applied Clay Science*, 1: 273–284.

Andrews P.R.A., 1992. *Summary report No. 17: Bentonite, Fuller's Earth and Kaolinite*. CANMET, Ottawa, Canada, p. 185.

Annedda V. 1956. Deposits of bentonite in Sadali and Vallanova Sarda territories, Sardinia. *Resuconti Association Min. Sarda*, 60: 50–59.

Benito R., Garcia-Guinea J., Valle-Fuentes F.J., and Recio P., 1998. Mineralogy, geochemistry and uses of the mordenite-bentonite ash-tuffs beds of Los Escullos, Almería, Spain. *Journal of Geochemical Exploration* 62: 229–240.

Boyd S.A. and Jaynes W.F., 1994. Role of layer charge in organic contaminant sorption by organoclays. In: Mermut A.R. (ed.), *Layer Charge Characteristics of 2:1 Silicate Clay Minerals*. CMS Workshop Lectures, 6, Clay Minerals Society, Bloomington, Indiana, pp. 47–77.

Bristow C.M., 1993. The genesis of the China clays of south-west England – a multistage story. In: H. Murray, Bundy W., Harvey C. (eds), *Kaolin Genesis and Utilization*. Special Publication No. 1, The Clay Minerals Society, Boulder, pp. 171–203.

Brunauer S., Emmett P.H., and Teller E., 1938. Adsorption of gases in multimolecular layers. *Journal of American Chemical Society* 60: 309–324.

Burst J.F., 1959. Postdiagenetic clay mineral environmental relationships in the Gulf Coast Eocene. *Clays and Clay Minerals*, 6: 327–341.

Cahoon H.P., 1954. Saponite near Milford, Utah. *American Mineralogist*, 39: 222.

Chamley H., 1989. *Clay Sedimentology*. Springer Verlag, Berlin.

Christidis G. and Dunaham A.C., 1993a. Compositional variations in smectites: Part I. Alteration of intermediate rocks. A case study from Milos Island, Greece. *Clay Minerals*, 28: 255–273.

Christidis G. and Dunaham A.C., 1993b. Compositional variations in smectites: Part II. Alteration of acidic precursors. A case study from Milos Island, Greece. *Clay Minerals*, 32: 253–270.

Christidis G.E. and Kosiari S., 2003. Decolorization of vegetable oils: a study o mechanism of adsorption of β-carotene by an acid-activated bentonite from Cyprus. *Clays and Clay Minerals*, 51(3): 327–333.

Christidis G. and Scott P.W., 1993. Laboratory evaluation of bentonites. *Industrial Minerals*, 311: 51–57.

Christidis G. and Scott P.W., 1997. The origin and control of colour of white bentonites from the Aegean islands of Milos and Kimolos, Greece. *Mineralium Deposita*, 32: 271–279.

Christidis G., Scott P.W., and Marcopoulos T., 1995. Origin of the bentonite deposits of eastern Milos, Aegean, Greece: geological, mineralogical and geochemical evidence. *Clays and Clay Minerals*, 43(1): 63–67.

Christidis G., Scott P.W., and Dunham A.C., 1997. Acid activation and bleaching capacity of bentonites from the islands of Milos and Chios, Aegean, Greece. *Applied Clay Science*, 12: 329–347.

Clarke G.M., 1985. Special clays. *Industrial Minerals*, 216: 25–51.

Cole T.G., 1985. Composition, oxygen isotope geochemistry, and origin of smectite in the metalliferous sediments of the Bauer Deep, southeast Pacific. *Geochimica et Cosmochimica Acta*, 49: 221–235.

Davis C.W. and Vacher H.C., 1940. *Bentonite: it's properties, mining, preparation and utilization*. U.S.Bureau of Mines Technical Paper 609.

Drits V.A. and Kossovskaja A.G., 1990. *Clay Minerals: Smectites and Mixed Layer Formations*. Nauka, Moscow, pp. 212 (In Russian).

Dubinin M.M., 1967. Adsorption in micropores. *Journal of Colloid and Interface Science* 23: 487.

Elzea J.M., and Murray H.J., 1990. Variation in the mineralogical, chemical and physical properties of the Cretaceous Clay Spur bentonite in Wyoming and Montana. *Applied Clay Science*, 5: 229–248.

Elzea J. and Murray H.H., 1994. Bentonite. In: D.D. Carr (ed.), *Industrial Minerals and Rocks*. 6th ed., Society for Mining, Metallurgy, and Exploration, Littleton. pp. 233–246.

Fleming R.F.S., 1972. Calcium and sodium bentonite – Uses and consumption. *Industrial Minerals*, 63: 21–35.

Foster M.D., 1953. Geochemical studies of clay minerals: II. Relation between ionic substitution and swelling in montmorillonites. *American Mineralogist*, 38(11–12): 994–1006.

Giese R.F. and van Oss C.J., 2002. *Colloid and Surface Properties of Clays and Related Minerals*. Marcel Dekker, Inc., New York, p. 295.

Gilchrist G.F.R., Gamble D.S., Kodama H., and Khan S.U., 1993. Atrazine interactions with clay minerals: kinetics and equilibria of sorption. *Journal of Agricultural and Food Chemistry*, 41: 1748–1755.

Grim R.E., 1973. Technical properties and application of clays and clay minerals. *Proceedings of the International Clay Conference 1972* (*AIPEA*), Madrid, pp. 719–721.

Grim R.E. and Güven N., 1978. *Bentonites. Geology, Mineralogy, Properties, and Uses*. Elsevier, New York, p. 256.

Grim R.E. and Kulbicki G., 1961. Montmorillonite: high temperature reactions and classification. *American Mineral*. 46: 1329–1369.

Gungor N. and Tulun T., 1996. Evaluation of sodium and calcium bentonites for industrial application. *Journal of Science and Industrial Research*, 55: 268–273.

Güven N., 1991. Smectites. In: Bailey S.W. (ed.) Hydrous Phyllosilicates. *Reviews in Mineralogy*, 19, 2nd ed., Mineralogical Society of America, Washington, pp. 497–559.

Harben P.W., 2002. *The Industrial Minerals Handybook*. 4th ed., Industrial Minerals Information, Surrey, p. 412.

Hoffman V. and Endell J., 1939. Die Abhangiglaet des Kationaustausches und der Quellung bei Montmorillonit von der Vorsitzung. *Z. Ver. Deutsche Chemiker* 10.

Hosterman J.W. and Patterson S.H., 1992. *Bentonite and Fuller's Earth Resources of the United States*. U.S. Geological Survey Professional Paper 1522, U.S. Government Printing Office, Washington, p. 45.

Hower J., Eslinger E.V., Hower M.E., and Perry E.A., 1976. Mechanism of burial metamorphism of argillaceous sediment: 1. Mineralogical and chemical evidence. *Geological Society of American Bulletin,* 87: 725–737.

Jackson M.L., 1959. Frequency distribution of clay minerals in major soil groups as related to factors of soil formation. *Clays and Clay Minerals*, 6: 133–143.

Jeans C.V., Merriman R.J., and Mitchell J.G., 1977. Origin of middle Jurassic and Lower Cretaceous Fuller's Earths in England. *Clay Minerals*, 12: 11–44.

Kavina P., Starý J., and Vaněček M., 2002. *Mineral Commodity Summaries of the Czech Republic*. Czech Geological Survey, Prague, p. 180 (In Czech).

Kendall T., 1996. Bentonite. Major market review. *Industrial Minerals*, 344: 25–37.

Knight W.C., 1898. Bentonite. *Engineering and Mining Journal*, 66(17): 491.

Konta J., 1973. *Quantitative System of Residual Rocks, Sediments and Volcanoclastic Deposits*. Charles University, Prague, p. 375 (In Czech).

Kristmannsdottir H., 1979. Alteration of basaltic rocks by hydrothermal activity at 100–300 °C. *Proceedings of the 6th International Clay Conference*, Oxford, U.K., 1978, pp. 359–367.

Lagaly G., 1989. Principles of flow of kaolin and bentonite dispersions. *Applied Clay Science*, 4: 105–123.

Lopez R.S., Yong R.N., Boonsinsuk P., Card E.C., and White P., 1987. Development of materials specifications and emplacement procedures for backfilling nuclear fuel waste vaults. *Bulletin IAEG*, 36: 43–50.

Manning D.A.C., 1995. *Introduction to Industrial Minerals*. Chapman & Hall, London, p. 276.

Martin-Vivaldi J.L., and Linares G.J., 1968. Los Bentonitas de Cabo de Gata: Il Yacimiento de Palma del Muerto. *Span. Institute Geologico y Minero Boletin*, 79(6): 65–71.

Medek J., 1977. Possibility of micropore analysis of coal and coke from the carbon dioxide isotherme. *Fuel*, 56: 131–133.

Moorlock B.S.P., Highley D.E., 1991. *An appraisal of fuller's earth resources in England and Wales*. British Geological Survey Technical Report WA/92/75, p. 87.

NAGRA, 1985. *Project "Gewähr 1985", Feasibility and safety studies for final disposal of radioactive wastes in Switzerland*. Nagra, Wettingen.

Noll W., 1936. Synthese von Montmorilloniten. *Chemie der Erde*, 10: 129–154.

Nutting P.G., 1943. *Absorbent clays, their distribution, properties, production, and uses*. U.S. Geological Survey, Bulletin 928-C, pp. 127–221.

O'Driscoll M., 1988. Bentonite; overcapacity in need of markets. *Industrial Minerals* 250: 43–67.
Perry E.A. and Hower J., 1970. Burial diagenesis in Gulf Coast pelitic sediments. *Clays and Clay Minerals*, 18: 165–178.
Přikryl R., Hanus R., and Kolaříková I., 2003. Genesis of Czech bentonites related to their use in engineered barriers for nuclear waste disposal. *Applied Earth Science (Trans. Inst. Min. Metall. B)*, 112(2): B138–B140.
Reyes A.G., 1990. Petrology of Philippine geothermal system and the application of alteration mineralogy to their assessment. *Journal of Volcanic and Geothermal Research*, 43: 279–309.
Rich A.D., 1960. Bleaching clay. In: Gillson J.L. (ed.), *Industrial Minerals and Rocks*. 3rd ed., AIME, New York, pp. 93–101.
Rogers W.F., 1963. *Composition and Properties of Oil Well Drilling Fluids*. Gulf Publ. Co., Houston.
Ross J.S., 1964. *Bentonite in Canada*. Mines Branch Monograph 873, CANMET, Energy, Mines and Resources, Canada.
Ross C.S. and Hendricks S.B., 1945. *Minerals of the montmorillonite group*. U.S. Geological Survey Professional Paper 205-B, U.S. Government Printing Office, Washington.
Ross C.S. and Shannon E.V., 1926. The minerals of bentonite and related clays and their physical properties. *American Ceramic Society Journal*, 9(2): 77–96.
Russell A., 1991. Speciality clays. Market niches taken by unique properties. *Industrial Minerals*, 285: 49–61.
Savage D., Lind A., and Arthur R.C., 1999. *Review of the properties and uses of bentonite as a buffer and backfill material*. SKI Report 99:9. Swedish Nuclear Fuel and Waste Management Company, Stockholm.
Schultz L.G., 1969. Lithium and potasium absorption, dehydroxylation temperature and structural water content of aluminous smectites. *Clays and Clay Minerals*, 19: 137–150.
Shirozu H., 1978. Wall rock alteration of Kuroko deposits. In: Sudo T., Shimoda S. (eds), *Clays and Clay Minerals of Japan*. Elsevier, Amsterdam, pp. 127–145.
SKB, 1995. *Treatment and final disposal of nuclear waste: Programme for encapsulation, deep geologic disposal, and research, development and demonstration*. SKB RD&D Programme 95. Swedish Nuclear Fuel and Waste Management Company, Stockholm.
Steblez W.G., 2001. The mineral industries of the Czech Republic, Hungary, Poland, and Slovakia. *Minerals Yearbook*, Vol. III, p. 27 available from http://mineral.usgs.gov/minerals/pubs
Šucha V., 2001. *Clays in geological processes*. Acta Geologica Univ. Com. Seria Monografie, Bratislava, p. 159 (In Slovak).
Torok A. and Thompson T.D., 1972. Activated bleaching earth for the future. *Translated ASME-AIME*, 252: 15–17.
van Olphen H., 1977. *An Introduction to Clay Colloid Chemistry*. 2nd edn, John Wiley and Sons, New York, p. 318.
van Olphen H., and Fripiat J.J., eds, 1979. *Data Handbook for Clay Materials and Other Non-Metallic Minerals*. Pergamon Press, New York.
Velde B., ed., 1995. *Origin and Mineralogy of Clays*. Springer, Berlin, p. 334.
Virta R.L., 2002. Clay and shale. Minerals Yearbook, Vol. I, p. 27; available from http://mineral.usgs.gov/minerals/pubs
Wayland T.E., 1971. Geological occurrence and evaluation of bentonite deposits. *Society of Mining Engineers (AIME)*, 250: 120–132.
Weaver C.E. and Beck K.C., 1971. Clay-water diagenesis during burial: how mud becomes gneiss. *Geological Society of American Special Papers*, 134.
Weaver C.E. and Pollard L.D., 1975. *The Chemistry of Clay Minerals*. Elsevier, Amsterdam, p. 213.
Yamada H., Nakazawa H., and Hashizume H., 1994. Formation of smectite crystals at high pressures and temperatures. *Clays and Clay Minerals*, 42: 674–678.

Chapter 5

Swelling in non-vertisolic soils

Its causes and importance

Miguel Angel Taboada[1] *and Raúl Silvio Lavado*[1]

Summary

The aim of this chapter was to give insight into soil swelling behavior in non-vertisols on the basis of studies in the Pampas region of Argentina. Vertisols have clayey texture and definite swelling mineralogy, and as a result, they are extensively swelling, and undergo normal shrinkage with no air pore entrance during drying. Non-vertisols, in contrast, behave differently, depending on which factor determines their volume change. When this factor is an inherent soil property, like the amount of swelling clay, the process does not differ from that operating in vertisols. This is shown by results from studies in Pampas silty loams. When the swelling factor is not an inherent soil property, such as in the case of trapped air in natric soils from the flooding Pampa, soil swelling is due to a process of air inflation during flooding.

Introduction

Soil volume changes upon desiccation or rewetting, take place in all soils that contain organic matter and/or clay. In fact, this phenomenon is not restricted to clayey soil systems, since even sandy soils crack over much larger volumes than clayey soils (Wilding, 2004). However, expansive soils have been traditionally included in vertisol order, which also comprises associated vertic intergrades (Dudal and Eswaran, 1988). Vertisols which have a minimum clay content of 30% in the upper 18 cm of their profile, normally develop drying cracks (Soil Survey Staff, 1998, 1999). They develop extensive volume change due to shrink/swell processes, which causes significant bulk density variations during their water content (θ) variation range, and develop desiccation cracks on drying (Coulombe *et al*., 2000). Soil volume changes can then be regarded as taking place in vertisols and in non-vertisols.

According to the FAO-Unesco Soil Map of the World (www.fao.org), vertisols are estimated to occupy 308.5 Mha (10^6 ha), which corresponds to 2.36% of the ice-free land area in the globe. The rest of the surface is covered by non-vertisols (Coulombe *et al*., 2000). Most of the knowledge on soil volume changes was developed in vertisols and related soils (Yule and Ritchie, 1980; Jayawardane and Greacen, 1987; Mc Garry and Malafant, 1987; Coughlan *et al*., 1991). Non-vertisols have always received considerable less attention in the

[1] Facultad de Agronomía, Universidad de Buenos Aires. Av. San Martín 4453, C1417DSE Buenos Aires, Argentina; e-mail: mtaboada@agro.uba.ar

literature, even less in terms of their volumetric response to wetting–drying cycles. It was generally assumed that, because of a non-definite swelling mineralogy of clays, non-vertisols have moderate swelling behavior (Jayawardane and Greacen, 1987).

The aim of this chapter is to give additional insight into soil swelling behavior in non-vertisols, on the basis of our own research experience in the Pampas region of Argentina.

Case study: non-vertisols of Pampas region of Argentina

The Pampas region of Argentina is a large, temperate plain, covered by originally fertile soils, and composed of different subregions (Figure 5.1). Soils are developed on loess-like sediments during the Quaternary, under the effect of grassland vegetation and changing climatic regimes (INTA, 1990; Soriano *et al*., 1991). This general picture does not differ from that commonly found in other temperate plains of the globe. The region is covered by

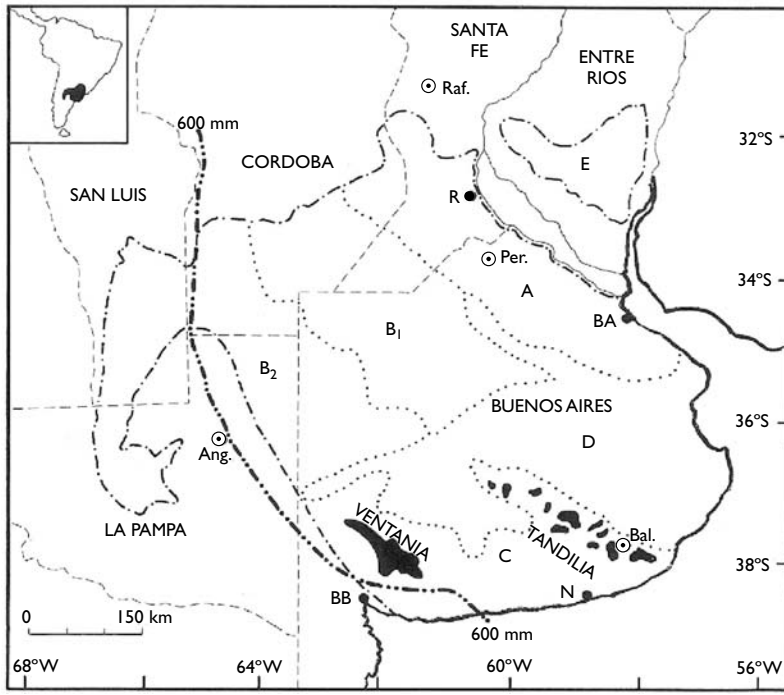

Figure 5.1 Subdivision of the Pampas region.

Source: Hall *et al.* (1992).

Notes

A. Rolling Pampa; B. Inland Pampa (B_1. Plane, B_2. Western); C. Southern Pampa; D. Flooding Pampa; E. Mesopotamian Pampa. Regional limits (– . – .), Subregional (. . . .) e Interprovince (– – –). Mean annual isohyets) (–..–). Populations (•): Ang, Anguil; BA, Buenos Aires; Bal, Balcarce; BB, Bahía Blanca; N, Necochea; Per, Pergamino; Raf, Rafaela; R, Rosario.

different associations of soils (scale 1:500.000), as shown by the Soil Map of the Buenos Aires Province (INTA, 1990; Hall *et al*., 1992) (Figure 5.2). It can be seen that vertisols only prevail in the northeast of the region, while in the rest there are different great groups of mollisols (US Soil Taxonomy). For the present study, two large subregions can be identified in the map. They are: the so-called rolling Pampa, which is covered by highly productive Argiudolls having silty loam texture in their A horizon; and the flooding Pampa, which is covered by halo-hydromorphic soils standing out Natraquolls and Natraqualfs (Figure 5.2). Their soils do not have vertisolic features, such as high clay contents, slickensides, visible drying cracks, and *gilgai* microrelief (Iñíguez and Scoppa, 1970; Lavado and Camilión, 1984; INTA, 1990).

In both Pampas regions the soils are affected by physical degradation, because of soil cultivation in one case (rolling Pampa) and because of cattle grazing in the other (flooding Pampa). Due to their different inherent properties and external factors, different responses to wetting–drying cycles can be expected in the soils of each region. In this chapter we aim to show the swelling behavior, and its consequences for the recovery of a degraded soil

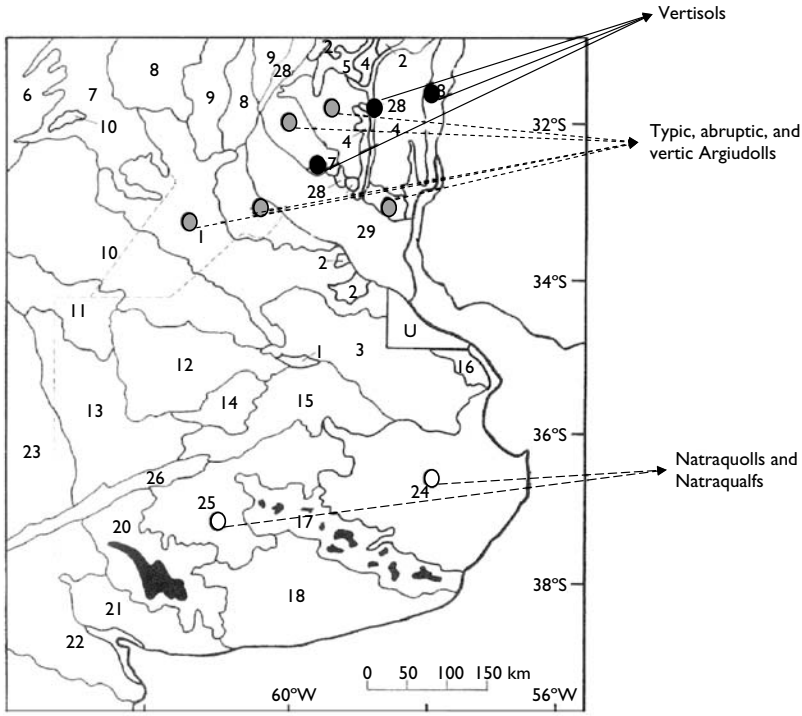

Figure 5.2 The main Soil Associations of the Buenos Aires Province and adjacent areas identified by numbers. Only the names of the studied Great Soil Groups are shown.

Source: Hall *et al.* (1992).

structure of two non-vertisolic soils. In both cases soil swelling is related to made-man or climatic factors, rather than to inherent soil properties.

Content and clay mineralogy in Pampas mollisols

The general clay mineralogy of Pampas soils shows the predominance of illite with minor quantities of kaolinite and montmorillonite (Iñíguez and Scoppa, 1970; Soriano *et al*., 1991). Their A horizons have abundant clay illite, while the B horizons have a better degree of crystallinity and increasing amounts of expansive minerals. Thus, the fine (0.2–0.08%) and very fine clay (<0.08 u) fractions of the argillic (B) horizons of most soils from the Pampas plain are composed mainly of smectite formed under an illuvial process. Several authors suspected the occurrence of amorphous minerals in some deep horizons (BC or C). In some soils large amounts of swelling minerals are found in the Bt horizons, whereas in others the expansive minerals are found mainly in the deeper B3 or C horizons. Some authors suggested that this differential distribution could either be due to the limited transformation of montmorillonite to illite in alkaline or poor drainage environment or the limitation of the differential clay leaching because of the poor internal drainage. The latter hypothesis is reflected in the low degree of crystallinity of the minerals in the deep horizons, affected by the water table and the reducing environment (Lavado and Camilión, 1984; Taboada *et al*., 1988). The fine silt fraction (2–20 μm) is an important component of topsoils (>50% by weight). It is largely composed by phytollites (Cosentino and Pecorari, 2002).

Figure 5.3 shows X-difractograms performed in topsoil and subsoil horizons of a flooding Pampa Natraquoll (Taboada *et al*., 1988). The content of swelling minerals (smectites or irregular, interstratified swelling clays) reaches its maximum in the Ah and BA horizons, although it is lower than 50%. There were only definite reflections of smectites in the BA horizon. In the below lying horizons, soil minerals have less reflections, with a high degree of non-definition and low abundance. The illite, a mineral that has the major crystalline perfection, is the dominant species throughout the profile. Its abundance is more evident in the Bt horizon. In Figure 5.4, O.A. Barbosa (unpublished) shows an X-diffractogram of clay illite sampled in a silty loam Argiudoll from the rolling Pampa.

Theory

Processes taking place during drying and wetting

The process of swelling is mainly caused by the intercalation of water molecules, which enter to the inter-plane space of smectitic clay minerals (Schafer and Singer, 1976; Low and Margheim, 1979; Parker *et al*., 1982). The expansive characteristics of smectites are affected by the nature of adsorbed ions and molecules. Smectite increases its plane spacing as a result of the loss of adsorbed cations. Different processes take place when a swelling soil dries or swells. On drying, the soil decreases its volume by shrinkage, and desiccation cracks appear because of internal stresses in the shrunken and dried soil mass. These cracks are created in pre-existing planes of weakness within soil clods (Towner, 1987, 1988; Hallett and Newson, 2005). As a result of shrinkage, soil decreases its height by subsidence. On wetting the soil increases its volume by swelling, the cracks are closed, and soil level rises. When a dry soil wets, it undergoes three dimensional (3-D) volumetric expansions, in a first stage. This is because its desiccation cracks are still open. In a second stage, after desiccation cracks are

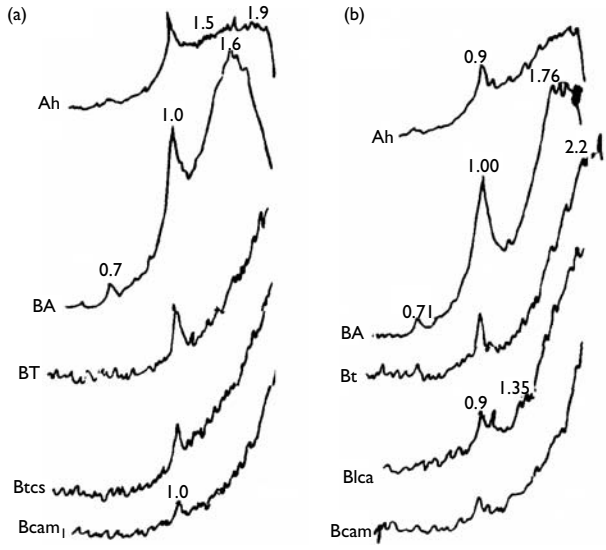

Figure 5.3 X-diffractograms of oriented clays of a Typic Natraquoll. (a) Air dry soil samples; (b) soil samples saturated with ethylene-glycol. Unities in nm.

Source: Taboada *et al*., 1988.

closed, soil volumetric expansion is only one dimensional (1-D), causing the rising of the soil level.

Soil volumetric changes may cause both unfavorable and favorable effects on human activities. Unfavourable effects are the destruction of buildings, roads and pipelines, and the leaching of fertilizers and chemicals below the root zone through desiccation cracks (bypass flow) in cropped soils. In these soils horizontal cracks break capillary flux of water. On the other hand, swelling clays can be used to seal landfills storing hazardous wastes. This sealing avoids the downward migration of contaminants to groundwater. In cropped soils, the development of a dense pattern of cracks on drying improves water drainage and soil aeration, and decreases surface runoff in sloped areas. Soil cracking is closely related to the recovery of porosity damages by compaction. A dense network of fine microcracks is developed within the dried and shrunken soil mass, thus allowing the recovery of soil aggregates and related pores (Dexter, 1988).

J.M. Oades (1993) classified the soils in three textural groups, according to their response to wetting–drying cycles. In this classification, *sands* (<15% clay) and *clays* (>35% clay) are two extreme cases because of their null or maximum respective response to wetting–drying cycles. In the middle of these groups is the textural group of *loams* (15–35% clay), which is characterized by its moderate response to wetting–drying cycles. Loam soils evolved under grassland vegetation, and its structural dynamics are envisaged as a result of the combined action of wetting–drying cycles and biological stabilization, such as also happens in non-vertisols of the Pampas region of Argentina (Taboada *et al*., 2004).

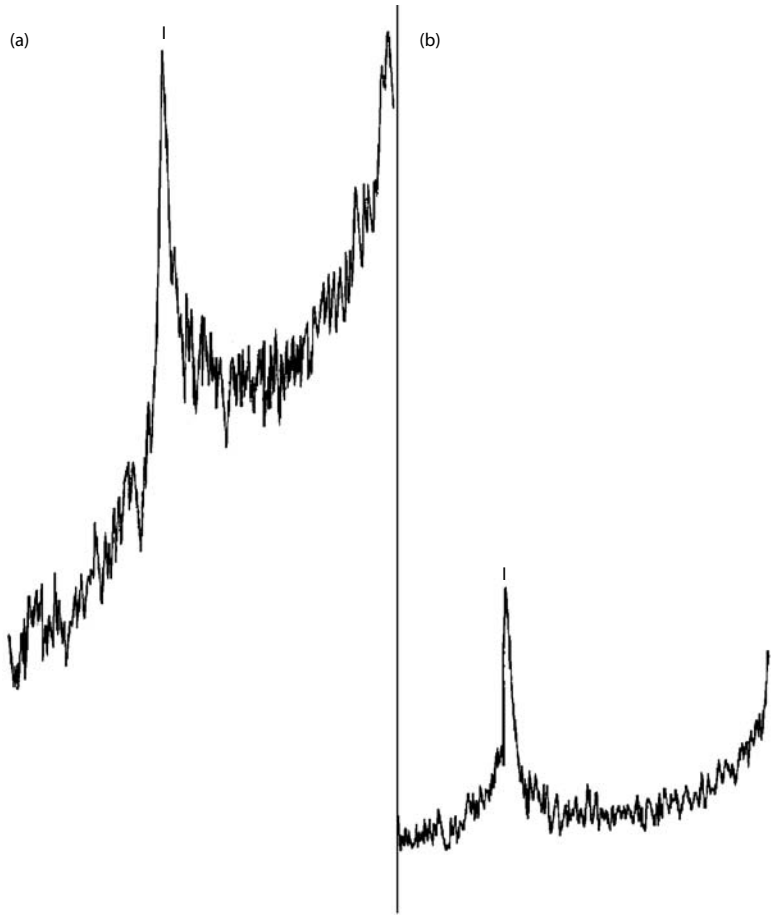

Figure 5.4 X-diffractograms of clay illite in a Pampas silty loam. (a) Nomal; (b) calcinated at 550°C. Source: O.A. Barbosa, unpublished.

Shrinkage curves and shrinkage indices

Soil volumetric changes can be investigated either by the shrinkage of natural clods on drying under controlled laboratory conditions (Mc Garry and Daniells, 1987; Mc Garry and Malafant, 1987; Coughlan *et al*., 1991), or by the repeated sampling of soil cores in the field (Jayawardane and Greacen, 1987; Taboada *et al*., 2001). In both cases, the inverse of bulk density (i.e. soil specific volume, v) is plotted to the volumetric water content (θ) of the soil. Fitted straight lines allow the identification of different shrinkage zones (Figure 5.2).

Table 5.1 Soil shrinkage indexes and derived variables defined from a theoretical shrinkage curve

Indices	
θ_B	θ at the limit of normal swelling
θ_A	θ at the air entry point, i.e. the end of residual shrinkage
n	slope of the line B→A (normal shrinkage)
r	slope of the line A→α (residual shrinkage)
ν_B	specific volume at the limit of normal swelling
ν_A	specific volume at the air entry point
α	specific volume at zero water content
P_B	specific volume of air filled pores at B
P_A	specific volume of air filled pores at A
P_α	specific volume of air filled pores at α
θ_B-θ_A	difference between θ at the limit of normal swelling and θ at the air entry point, i.e. range of u in the normal shrinkage zone

Source: Figure 5.5.; Mc Garry and Daniells, 1987.

Normal shrinkage (B→A) is characterized by equivalent decreases in both ν and θ on drying, and so, by no air entrance to soil pores (McGarry and Daniells, 1987; Coughlan *et al*., 1991). In the drier range of the θ variation, soil ν decreases on drying are lower or even null. Residual shrinkage (A→α) allows air entrance to soil pores, and hence the creation of air filled porosity. In order to facilitate this discussion, McGarry and Daniells (1987) derived several indices and related variables from the shrink data of natural soil clods (Table 5.1).

In non-vertisols, soil volume decreases during drying have less magnitude than water volume decreases. This process which is known as *residual* or *irreversible* soil shrinkage, allows for air entrance to soil pores (Mc Garry and Daniells, 1987; Gibbs and Reid, 1988; Coughlan *et al*., 1991). This creation of air filled porosity is closely related to the potential recovery of a deteriorated soil structure (Gibbs and Reid, 1988).

Clod shrinkage characteristic of cropped Pampas silty loams

Argiudolls covering the region have silty loam texture in their topsoil. After long-term continuous cropping using conventional tillage practices (e.g. mouldboard- and disc-ploughing), they show varying soil degradation levels (Senigagliesi and Ferrari, 1993). Three soil degradation levels can be identified in the field, as shown by Table 5.2 (adapted from Barbosa *et al*., 1997). Figure 5.6 shows idealized soil profiles characterizing the three study situations. Most soils have undergone significant organic carbon losses, which caused the deterioration of topsoil structure (Moderate degradation). The most serious degradation process is water erosion (Senigagliesi and Ferrari, 1993). Soil losses by laminar erosion shallowed A horizons, which often become mixed with the underlying Bt horizon during ploughing (Severe degradation). In this situation, the top horizon has significantly higher clay content and prismatic structure, and X-ray-diffraction analysis shows the predominance

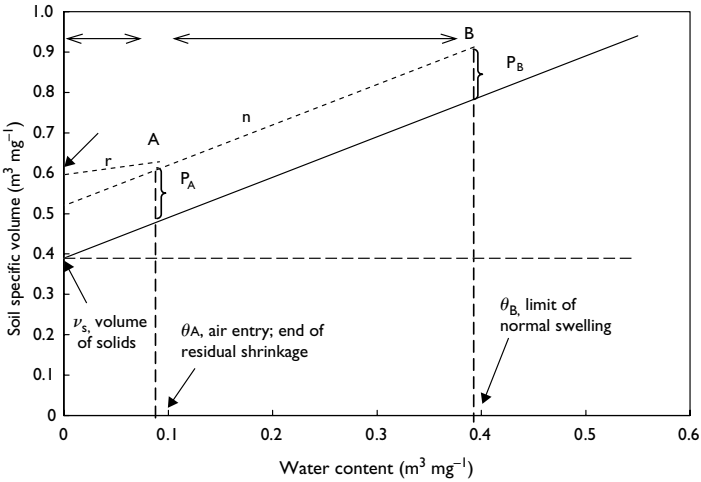

Figure 5.5 Theoretical shrinkage curve showing the different shrinkage zones, and the indices and derived variables of shrinkage. Symbols defined in Table 5.1.

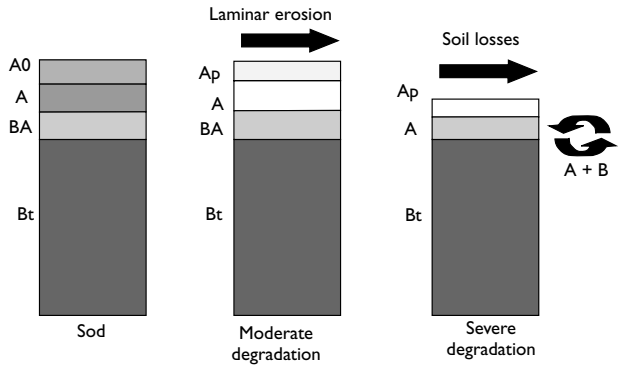

Figure 5.6 Idealization of soil profiles in non degraded (Pasture), moderately and severely degraded situations.

of open illite and interstratified swelling clay minerals (Table 5.3). In contrast, clay mineralogy in the nondegraded and moderately degraded soils are composed of illite (95%) and kaolinite (5%) (Table 5.3). Because of its swelling clay mineralogy, the severely degraded soil is the only one with a measurable swell–shrink index (Table 5.2).

The aim of this section is to understand whether soil degradation levels affect soil structural recovery capacity during the wetting and drying cycles in these soils, and to what extent this can be improved by the enrichment of topsoil with swelling clays. Results were published by Barbosa *et al*. (1999).

Table 5.2 Soil properties in studied sites

Soil	*Pasture*		*Moderate degradation*		*Severe degradation*	
Soil horizon	*A1*	*A2*	*Ap*	*A2*	*Ap*	*A2*
Soil depth (m)	0–0.27	0.27–0.40	0–0.18	0.18–0.32	0–0.08	0.08–0.17
Structural form	Subang Bk	Subang Bk	platy	Subang Bk	platy	Prisms
Total organic C ($g\ kg^{-1}$)	30, 0c	18, 6b	18, 5b	15, 7b	14, 3a	12, 0a\
Clay (%)	29, 5b	29, 6b	26, 4a	26, 7a	28, 8b	35, 8c
Silt (%)	58, 8b	58, 4b	61, 7c	60, 2c	55, 4a	49, 8a
Textural class	Silty clay loam	Silty clay loam	Silty loam	Silty loam	Silty clay loam	Silty clay loam
Water retention at −33.3 kPa (v/v)	0.446c		0,351a		0,361b	
Swell–shrink index	−0.07a	−0.04a	−0.08a	−0.07a	−0.20b	−0.29c

Note
Different letters indicate significantly different means between horizons are at the 0.05 probability level.

Table 5.3 Clay mineralogy in topsoil horizons under different soil degradation levels

	Horizons	*Clay mineralogy* *I Illite K Kaolinite*
	Ap	I 95% K 5%
Pasture	A2	I 95% K 5%
	B1	I 100% with somewhat open structure
	Bt	I open + swelling interstratified
Moderate degradation	Ap	I 95%
	A2	I 100% hydromica
Severe	Ap	I 95%
degradation	A2	I open + swelling interstratified

Source: Barbosa *et al.*, 1997.

Clod shrinkage characteristics

The shrinkage curve of the Bt horizon is shown in Figure 5.7. This curve is similar to that found in extensively swelling soils, which have slickensides and drying cracks in their profile. Clod shrinkage was normal (slope, $n \approx 1$) during most of the water content, θ, variation range. As shown by a low air entry point ($<0.2\ g\ g^{-1}$), residual shrinkage only occurred at very low water contents.

Clod shrinkage curves are shown from both A0 or Ap horizons and the A1 horizon lying immediately below. It can be seen that clod shrinkage curves differed because of the different degradation levels (Figure 5.8). The curves of the nondegraded (pasture) and moderate degraded sites have residual and normal shrinkage zones. It becomes evident that the wider volumetric variation range of the severely degraded soil has shrinkage curves very similar to that obtained in the clayey Bt horizon. This agrees with SSI indexes of this soil which are about

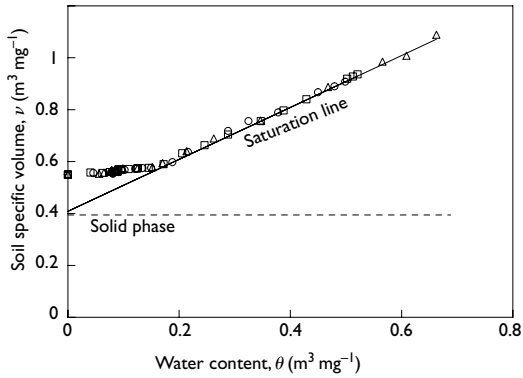

Figure 5.7 Clod shrinkage characteristic of a Bt horizon of a Peyrano series typic argiudol.
Source: Barbosa *et al*., 1999.

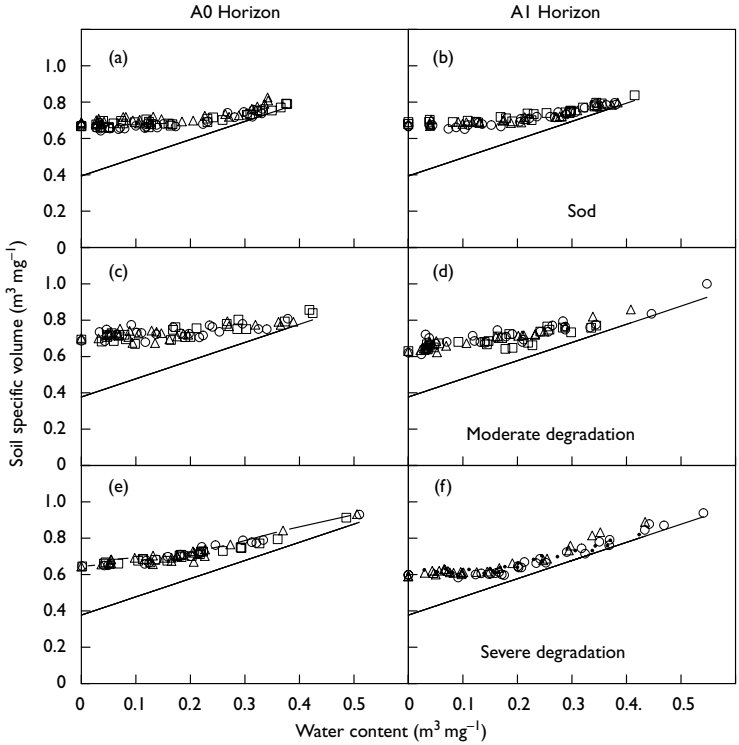

Figure 5.8 Soil shrinkage curves in the A0 y A1 horizons of a Peyrano silty clay Loam, under pasture (non degraded) (a, b), moderately degraded (b, c), and severely degraded (d, e) situations.
Source: Barbosa *et al*., 1999.

20 times higher than those in the pasture and moderately degraded situations (Table 5.2). This is due to the consequences of the mixture between the shallow, eroded A horizon with the below lying Bt horizon during tillage, which causes clay enrichment in top soil (Figure 5.6).

From these clod shrinkage curves, the indexes proposed by Mc Garry and Daniells (1987) were derived. As shown, not all of them differ among sites with different degradation levels. Soil volume at zero water content, α, and the air entry point, θ_A, show no significant differences between the nondegraded and moderately degraded soils, but are significantly lower in the severely degraded soil (Figure 5.8a). The slope, n, increases significantly from the nondegraded to the severely degraded soil. The same happens with the normaly range (Figures 5.8c and d). The severely degraded soil reaches significantly higher volume, ν_B, and water content, θ_B, when swollen at maximum. It can be concluded that clay enrichment (severe degradation) accentuates soil swelling ($>\nu_B$ and θ_B and normalcy range), but does not improve air filled porosity.

We also investigated soil cracking patterns after 4 and 8 months of wetting–drying (W/D) cycles in the nondegraded and severely degraded soils, in both moist and dry soil conditions (Figure 5.9a through h). No difference in soil cracking was observed after 4 and 12 months of W/D cycles, at both moist (a, c, e, and g) and dry (b, d, f, and h) soil conditions. This indicated that the creation of all desiccation cracks took place within the first four months of the experiment. Likewise, we also found in the same silt loam no additional aggregation due to the extra eight months of W/D cycles (Taboada *et al*., 2004). The soil cracking pattern was similar between the three studied degradation levels. Despite the higher clay content and SSI index of the severely degraded soil (Tables 5.2 and 5.3), there was no effect on the soil cracking pattern.

We also measured the mean width, length, and depth of desiccation cracks, and calculated their volume after 4 and 12 months under W/D cycles (Figure 5.10 a through h). As happened with cracking patterns, similar crack dimensions were found at 4 and 12 months. All cracks dimensions increased from the nondegraded to the severely degraded soil, showing that the induced textural change of this soil enlarged the cracks. However, it did not change their pattern or distribution within the dry and shrunken soil.

These results allowed us to analyze, and even refute, some preexisting ideas about the structural behavior of silty loams. First, though having a low swell–shrink index, Pampas silty loams can develop normal and residual shrinkage during drying. This means that these soils are not completely rigid, as supposed, but are moderately swelling (Jayawardane and Greacen, 1987). Second, clay enrichment caused by textural mixtures during tillage did not lead to a more dense microcracking (and more air filled porosity), but only to more normal swelling. The degraded soil has more expansion, but it persists a dense soil mass only subdivided by large cracks, as shown in Figure 5.11. Therefore, the low regeneration capacity of Pampas silty loams is not due to the lack of swelling clays. A soil swell–shrink index was proposed as a means to characterize the aptitude of soils to be managed without periodic tillage (e.g. zero tillage, direct drilling) (Taboada *et al*., 1998). Taking into account the present results, the SSI is not always suitable for characterizing pore regeneration capacity. A soil horizons mixture is not a suitable practice for improving topsoil structure in Pampas silty loams.

Soil volume changes caused by air entrapment in natric soils

The flooding Pampa is a large wetland region, covered by different kind of salt affected and natric soils (Figure 5.2). Natraquolls and Natraqualfs do not occur in patches, but in

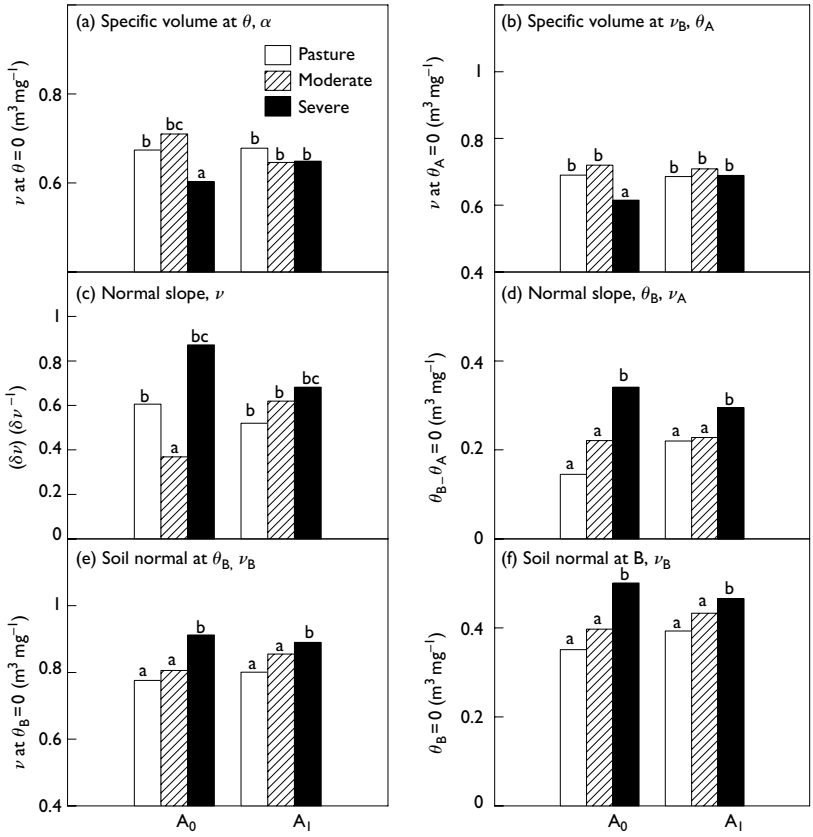

Figure 5.9 Soil shrinkage indexes obtained from shrinkage curves (see Figure 5.8) of A0 and A1 horizons of Peyrano silty loam, under non degraded (Pasture) (a, b), moderately degraded (c, d), and severely degraded (d, e) situations. Different letters indicate significant ($P < 0.05$) diffences between soils.

Source: Barbosa *et al.*, 1999.

continuous surfaces. For instance, the General Guido Series (Typic Natraquoll) covers more than 200,000 hectares in the region (Lavado and Taboada, 1988; INTA, 1990). These soils are mainly covered by native grasslands, which are periodically ponded (<15 cm water height) during winter–spring periods. These wide soil water content variations lead to noticeable soil volume changes, which resemble those of vertisols despite the soils (as in the rest of the Pampas region) not having definite smectitic clay mineralogy (Iñíguez and Scoppa, 1970; Lavado and Camilión, 1984). In this section, we aim to describe the causes by which these non-vertisolic soils develop noticeable volume changes in the Flooding Pampa of Argentina.

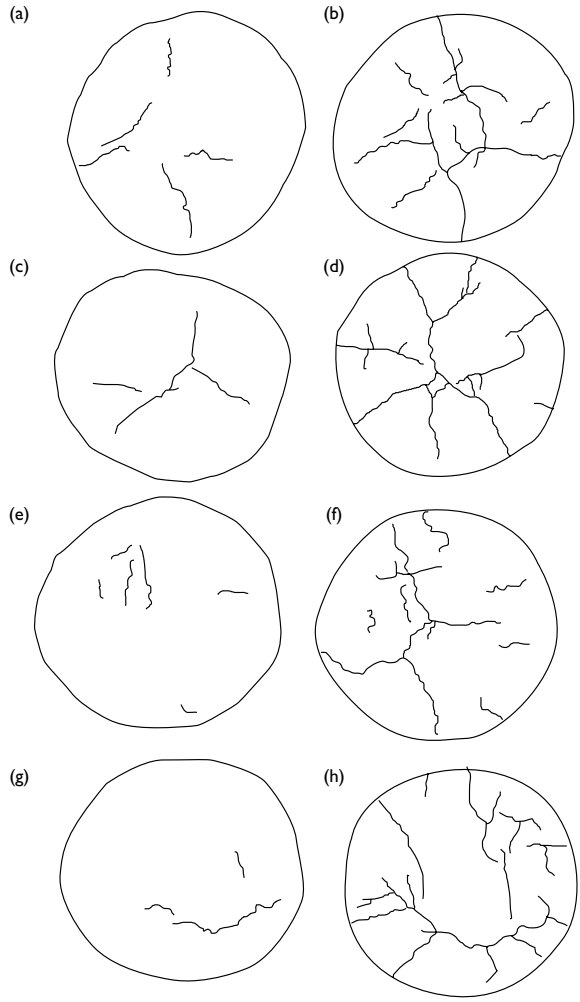

Figure 5.10 Width (a, b), depth (c, d), length (e, f) and calculated volume (g, h) of desiccation cracks in non degraded, moderately degraded and severely degraded situations of a Peyrano Series silty loam (Barbosa and Taboada, unpublished). Results after 4 months at left side of the Figure; results after 12 months at the right side.

Studies were performed in two sites covered with untilled grassland soils. They were a General Guido Series soil (Typic Natraquoll) and a Chelforó Series soil (Mollic Natraqualf). The main properties of both soils are given in Table 5.4. Both of them have no vertic features (i.e. slickensides, visible cracks), throughout their profile (Lavado and Camilión, 1984; Taboada *et al*., 1988).

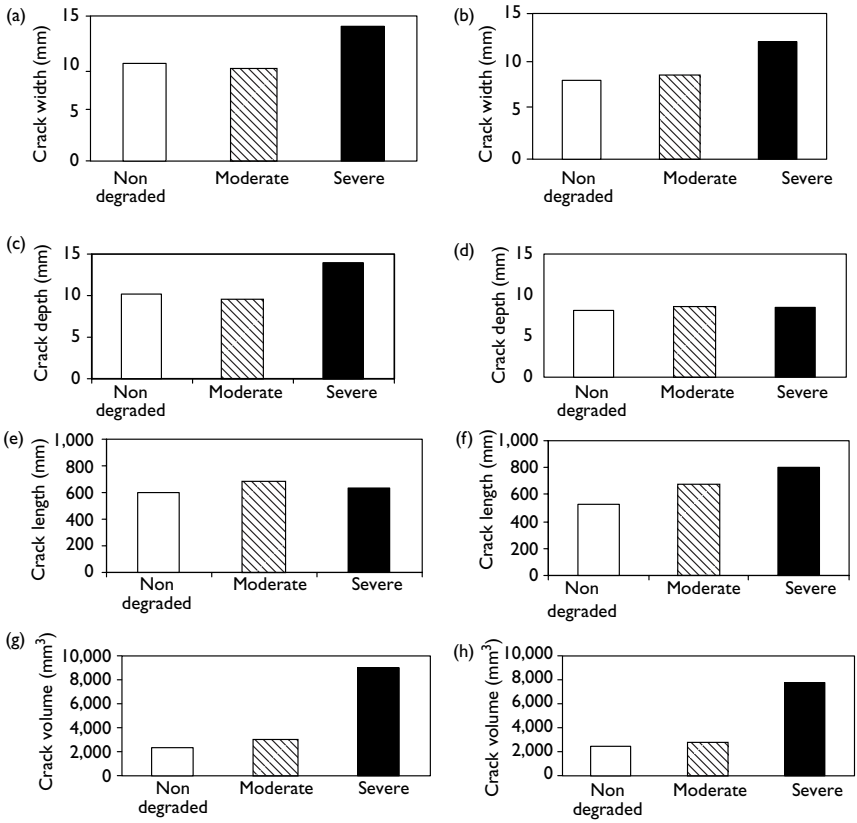

Figure 5.11 Size order of cracks at moist (left side) and dry (right side) soil conditions. (a) and (b); (c) and (d) idem severely degraded soil; (e) and (f) pasture soil after 12 months wetting-drying (W/D) cycles; (g) and (h) idem severely degraded soil

Source: Barbosa and Taboada, unpublished.

As already commented, the soils had non-vertisolic features and no swelling clay mineralogy (Lavado and Camilión 1984; Taboada *et al*., 1988). Despite, significant bulk density (BD)–gravimetric water content (θ_w) relationships were determined by Taboada *et al*. (1988), according to the following polynomial function:

$$BD = 1.2 + 0.0008\,\theta_w - 0.0002\,\theta_w^2 \quad R^2 = 0.89^{***} \tag{5.1}$$

Clod shrinkage curves obtained under controlled laboratory conditions, and the derived indexes showed the influence of inherent soil properties on soil volume changes (Figure 5.12a through d; Table 5.5). The shrinkage characteristics of natural clods had two distinct zones (i.e. zero and residual shrinkage) in surface and Bt horizons. Both soils had low proportion

Table 5.4 Soil properties in surface (Ah and E) and Bt horizons of the studied soils

Horizon (w/w)	*Depth (m)*	*Structure*	*Clay <2 μm (% w/w)*	*Silt 2–50 μm*	*pH (in paste)*	*Organic C (% w/w)*	*SAR*
Typic Natraquoll, General Guido Series							
Ah	0–0.13	Subang blocks	22,8	41,3	6.0	3,5	6,8
Bt	0.21–0.32	Prisms	34.0	36,7	7,2	0,5	17,4
Typic Natraqualf, Chelforó Series							
E	0–0.11	Subang blocks	18,5	42.0	8,2	1,2	7,8
Bt	0.19–0.40	Prisms	48,3	37,2	9.0	0,9	33,9

Source: Taboada *et al*., 2001.

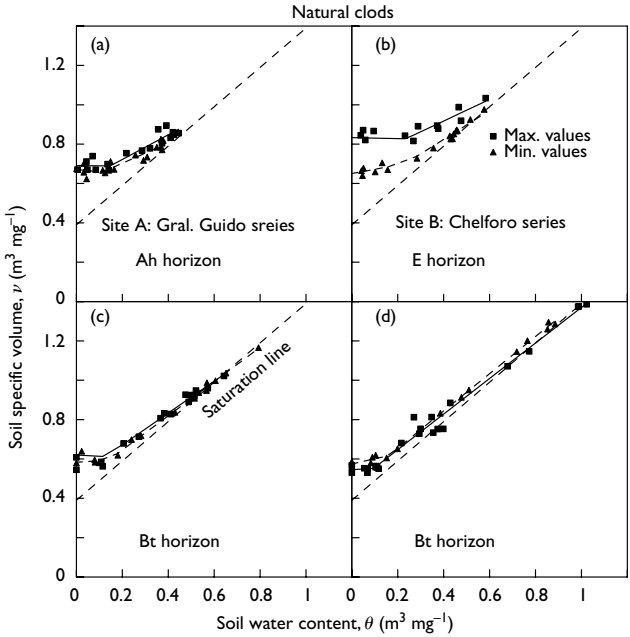

Figure 5.12 Shrinkage curves of natural clods of surface (a and b) and Bt horizons (c and d) of soils in sites A (Typic Natraquoll) and B (Mollic Natraqualf).

Source: Taboada *et al*., 2001.

of expansible clay (Lavado and Camilión, 1984; Taboada *et al*., 1988). Therefore, surface clods had slopes, n, of about 0.5–0.6 showing residual shrinkage during most of the drying phase (Table 5.5). The specific volume of air filled pores increased as the clods dried ($P_B < P_A < P_\alpha$).

Table 5.5 Shrinkage indices in clods of surface and Bt horizons of the soils of sites A and site B

Indices	*Site A: typic Natraquoll*				*Site B: Mollic Natraqualf*			*Site A vs Site B*	
	General Guido Series				*Chelforó series*			*Surface*	*Bt*
	Horizons				*Horizons*			*Significance*	*Significance*
	Units	*A*	*Bt*	*P<*	*E*	*Bt*	*P<*		
θ_B	($m^3\ mg^{-1}$)	0,410	0,715	**	0,580	0,955	***	***	*
θ_A	($m^3\ mg^{-1}$)	0,131	0,135	ns	0,215	0,127	*	**	ns
n		0,572	0,840	*	0,642	0,924	*	ns	ns
r		−0,064	−0,027	ns	0,096	0,171	ns	ns	ns
ν_B	($m^3\ mg^{-1}$)	0,840	1,095		*	0,985	1,345	***	**
ν_A	($m^3\ mg^{-1}$)	0,679	0,604	*	0,754	0,585	**	ns	ns
α	($m^3\ mg_{-1}$)	0,681	0,600	ns	0,751	0,560	*	ns	ns
P_B	($m^3\ mg^{-1}$)	0,040	0,005	ns	0,030	0,015	ns	ns	ns
P_A	($m^3\ mg^{-1}$)	0,159	0,089	*	0,159	0,078	ns	ns	ns
P_α	($m^3\ mg^{-1}$)	0,291	0,220	*	0,371	0,180	ns	ns	ns
θ_B-θ_A	($m^3\ mg^{-1}$)	0,280	0,581	*	0,365	0,828	*	**	*

Notes
***, **, and * mean significant differences between horizons at P <0.001, <0.01, and <0.05, respectively.
ns means not significantly different between soils.

The θ–ν relationships obtained in field cores, and the derived indexes (Figures 5.13a through d; Table 5.5), differed greatly from those obtained in clod shrinkage curves. Differences between shrinkage indexes obtained in the laboratory and in the field are also shown by Table 5.5. The clods of our soils always had less shrinkage than field cores. Moreover, θ–ν functions fitted in the field deviated from the theoretical saturation line as the soils wetted, unlike the functions fitted in the clods which deviated as the soils dried (Figures 5.12a through d). The specific volume of air filled pores at the end of swelling, PB, which never surpassed 0.04 v/v in wet clods, was as high as 0.20–0.35 v/v in surface and Bt horizons sampled by cores in the field (Table 5.5). This suggested a process of air entrapment within soil pores during soil wetting. As a result, in the field air filled porosity was the highest at the maximum swelling limit ($P_B > P_A > P_\alpha$). Soil swelling under such conditions must be regarded as a process of "inflation" of pore space by entrapped air (Gäth and Frede, 1995). The influence of trapped air can be assessed from the magnitude of slopes, n. They were about 1.5 in both surface horizons, and about 2 in both Bt horizons (Table 5.5). Due to these higher than one slope, our soil volumetric changes can be considered abnormal.

Results showed that the inherent soil properties (e.g. soil texture, clay percentage, sodium adsorption ratio) exerted virtually no influence on soil swell–shrink capacity in the field.

Sources of trapped air

In the study area, during winter – spring the water table rises from more than a 2 m depth up to about 0.65 m, where the bottom of the impervious Btk horizon checks further water

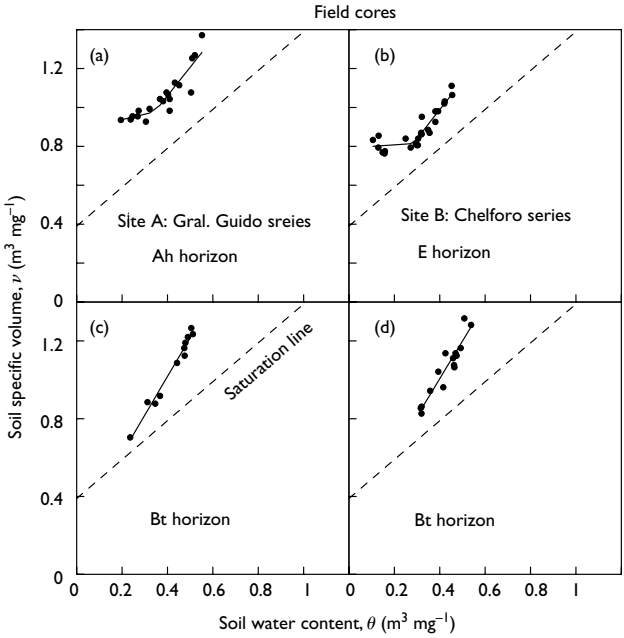

Figure 5.13 Soil specific volume – water content relationships from repeated core sampling in the field of surface (a and b) and Bt horizons (c and d) of soils in sites A (Typic Natraquoll) and B (Mollic Natraqualf).

Source: Taboada *et al.*, 2001.

table rises. Figure 5.14 shows the variation of water table depth and the specific volume of air filled pores in the Ah, BA, and Bt horizons showing the typic water regime of the region.

A conceptual model describing the changes taking place in the soil profile is proposed (Figure 5.15).

In this model, the water table is deep as usual at the end of a summer period (Lavado and Taboada, 1988), and there is groundwater recharge by rain water through preferential flow paths. During autumn and winter the water table rises close to the soil surface, where it reaches the bottom of the impervious Btk horizon. This horizon prevents further water table rises up to the soil surface, so that groundwater below it is under pressure. The specific volume of air filled pores makes a peak in the Bt horizon, showing air entrapment ahead of the rising water table. The soil condition changes to "air-occluded," which reduces greatly the dissipation of pore pressure (Chen and Yu, 1995). Therefore, the air within soil pores can not escape to the atmosphere and becomes trapped, likely under pressure. The rain excess under such conditions creates a "perched" water table over the impervious Btk horizon, which results in surface ponding with rain water during

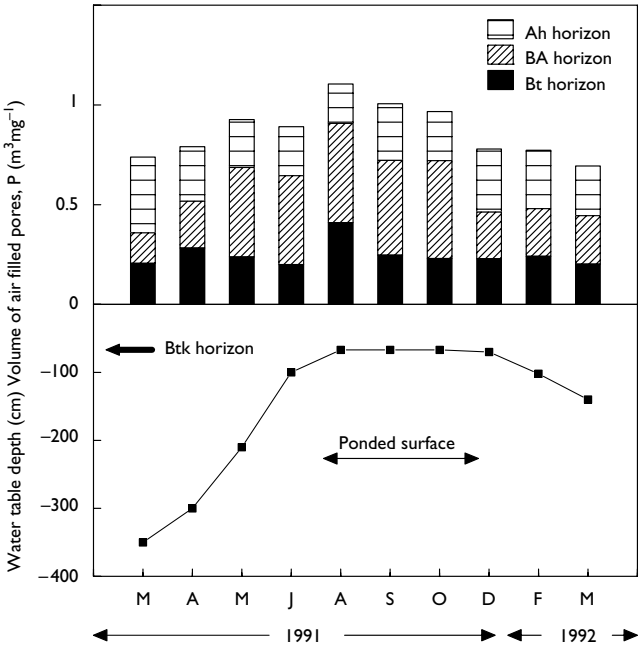

Figure 5.14 Water table depth and volume of air filled pores in the upper three horizons of the soil of site A (typic Natraquoll).

Source: Taboada *et al.*, 2001.

winter and most of spring. During ponding, trapped air is redistributed upward from the Bt horizon to the overlying BA and Ah horizons and a rapid increase in air filled porosity is observed at the same time. This causes soil swelling due to "air inflation," as represented by Figure 5.15.

Our unusually high entrapped air volumes at the maximum swollen condition, P_B, can be regarded as the result of two coincident wetting fronts during winter – spring periods (Lavado and Taboada, 1988). Air bubbles entrapped between the ponded soil surface and the rising water table could not escape, showing that the "air breaking value" was not reached in our study site (Wang *et al.*, 1998). This explains why air entrapment exerted so great an influence on the swelling of our soils.

Taboada and Lavado (1993) reported that in this Natraquoll, the volume of pores >30 μm was decreased by trampling in dry conditions. This damage only affected the first 8 cm of soil depth. In the same way, aggregate stability under grazing increased when the soil was wet and decreased when the soil was dry. The following polynomial function was obtained between soil water content (θ) and the mean weight diameter (MWD) of wet sieved aggregates:

$$\text{MWD (mm)} = 3.78 + 0.065\,\theta - 0.00085\,\theta^2 \quad R^2 = 0.74^* \tag{5.2}$$

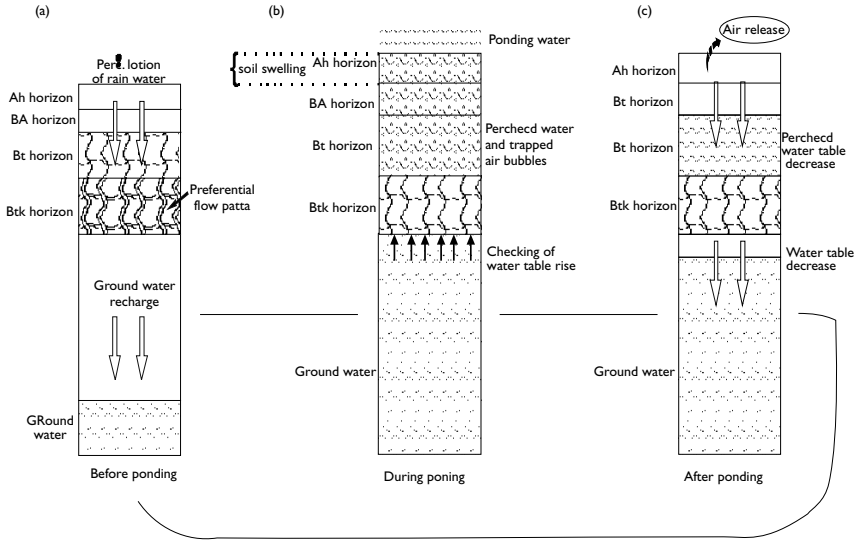

Figure 5.15 Conceptual model describing the process of soil swelling because of air entrapment. (a) Before ponding: free water and air movements throughout the profile (bio-opened system); (b) During ponding: soil swelling by air trapped within water table perched over the impervious Btk horizon (air-occluded system); (c) After ponding: soil shrinkage after perched water and water table decreases, and rapid air escape to the atmosphere.

Source: Taboada *et al*., 2001.

According to the fitted function, soil water content accounted for 74% of the variation of aggregate stability under grazing. These results on aggregate MWD and those previously reported on soil porosity agree well. Our results showed detrimental effects by trampling during the summer when the soil was dry.

Figure 5.16 shows a conceptual model that postulates decreases in structural stability resulting from crushing air filled pores by cattle hooves. This yields smaller water-stable aggregates, as shown by the higher proportion of aggregates <0.3 mm usually found in the soil of the grazed area compared to the soil in the enclosure area. Only at low water contents was the structure of the topsoil destabilized by grazing. The recovery of structural stability began in the fall and was completed in the winter, when the soil was ponded.

The structural recovery results from swelling, when the smaller aggregates created by trampling of dry soil are bound again into larger structural units. Macroporosity recovers after ponding because of the mellowing of topsoil aggregates (Taboada and Lavado 1993; Taboada *et al*., 1999). Soil mellowing consists in the partial slaking of aggregates carried to high water contents. Topsoil structural improvement found during ponding in this site thus appears as a consequence of soil inflation (Gäth and Frede 1995). In our case, grazing effects on soil structural unit size were temporary and disappeared within the first year of grazing exclusion.

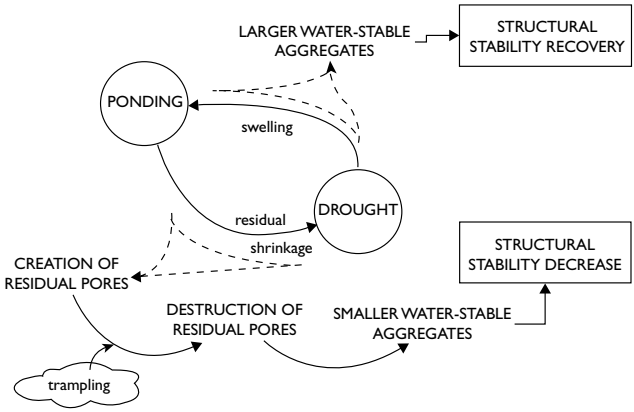

Figure 5.16 Conceptual model showing the process of soil structural destabilization when the soil dries and the process of structural recovery when soil wets.

Source: Taboada *et al.*, 1999.

It can be concluded that air entrapment due to water table rises from depth and surface ponding was the main factor determining the swelling of soils. While most soils have less than normal volumetric changes, our studied soils developed abnormal swelling. These results may contribute to the development of a model that explains the structural behavior of seasonally ponded soils. Soil volume changes taking place in vertisols and non-vertisols are summarized in Figure 5.17.

Concluding remarks

Vertisols are well known for soil swelling, which is mainly caused by inherent soil properties. In fact, vertisols have clayey texture and definite swelling mineralogy, and as a result, they are extensively swelling, and undergo normal shrinkage with no air pore entrance during drying. Non-vertisols, in contrast, behave differently, depending on which factor determines their volume change. When this factor is an inherent soil property, like the amount of swelling clay, the process does not differ from that operating in vertisols. This is shown by our results in Pampas silty loams, which naturally have little to moderate swelling behavior. Only when degraded, and their shallow topsoil is enriched with swelling clay from subsoil during tillage, do they acquire an extensive swelling behavior like that found in vertisols. However, this soil swelling does not result in a desirable creation of fine microcracks which improve the low porosity recovery capacity of these silty loams.

When the swelling factor is not an inherent soil property, such as the case of trapped air in natric soils from the flooding Pampa, then this leads to an accentuation of soil swelling. This is due to a process of air inflation during flooding, when air becomes trapped between two wetting fronts existing in the field (i.e. surface ponding and water table rises). But unlike what happened in cropped soils, in this seasonally ponded area, the accentuation of

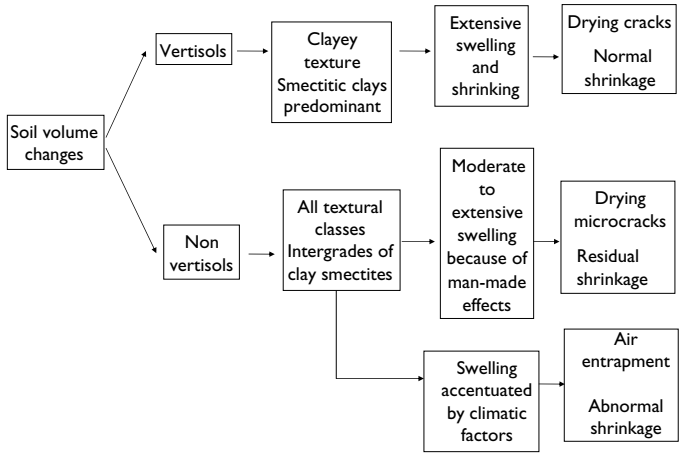

Figure 5.17 Schematic diagram showing different kind of soil volume changes.

soil swelling determines a fast recovery of soil pores previously damaged by trampling. This results in lowland grassland soils providing additional soil swelling. Clay content and mineralogy are not the only reasons causing noticeable soil volume changes.

References

Barbosa O.A., Taboada M.A., Rodríguez M.B., and Cosentino D.J., 1997. Regeneración de la estructura en un suelo franco limoso de la Pampa Ondulada en diferentes fases de degradación, Ciencia del Suelo 15, 81–88.

Barbosa, O.A., Taboada, M.A., and Cosentino, D.J., 1999. Contracción al secado de agregados en diferentes fases de degradación de un suelo limoso de la pampa Ondulada. Ciencia del Suelo 17, 1–7.

Chen, Y.J., Yu, P.J., 1995. Pore pressure dissipation features of an unsaturated compacted soil. In: Alonso, E.E., Delage, P. (eds), *Unsaturated Soils*. A.A. Balkema, Rotterdam, pp. 439–445.

Cosentino, D.J. and Pecorari, C., 2002. Limos de baja densidad: impacto sobre el comportamiento físico de los suelos de la región pampeana. Ciencia del Suelo 20, 9–16.

Coughlan, K.J., Mc Garry, D., Loch, R.J., Bridge, B., and Smith, G.D., 1991. The measurement of soil structure – Some practical initiatives. Australian Journal of Soil Research 29, 869–889.

Coulombe, C.E., Wilding, L.P., and Dixon, J.B., 2000. Vertisols. In: Malcom E. Sumner, (Ed. in.Chief). *Handbook of Soil Science*, CRC Press, New York, pp. 269–286.

Dexter, A.R., 1988. Advances in characterization of soil structure. Soil and Tillage Research, 199–238.

Dudal, R. and Eswaran, H., 1988. Distribution, properties and classification of Vertisols. In: L.P. Wilding and R. Puentes (eds). Vertisols: Their Distribution Properties, Classification and Management. Tech. Mono. N° 18, Texas A & M Printing Center, College Station, TX, pp. 1–22.

Gäth, S. and Frede, H.G., 1995. Mechanisms of air slaking. In: Hartge, K.H., Stewart and B.A. (eds), *Soil Structure: Its Development and Function*. C.R.C. Lewis Publishers, Boca Raton, Florida, pp. 159–173.

Gibbs, R.J. and Reid, J.B.,1988. A conceptual model of changes in soil structure under different cropping systems. *Advances in Soil Science* 8, 123–149.

Hall, A.J., Rebella, C.M., Ghersa, C.M., and Culot, J. Ph., 1992. Field-crop systems of the Pampas. In: C.J. Pearson (ed.). *Ecosystems of the Worlds*. Field Crop Ecosystems, Elsevier, Amsterdam pp. 413–450.

Hallett, P.D. and Newson, T.A., 2005. Describing soil crack formation using elastic – plastic fracture mechanics. *European Journal of Soil Science* 56, 31–38.

Iñiguez, A.M. and Scoppa, C.O., 1970. Los minerales de arcilla en los suelos "Zonales" ubicados entre los ríos Paraná y Salado Provincia de Buenos Aires. RIA, Serie 3, Clima y Suelo, Vol. VII, N° 1.

INTA, 1990. Atlas de suelos de la República Argentina. Tomo I y II. G.N. Moscatelli (ed.). SAGyP-INTA. Proyecto PNUD Argentina 85/019, Buenos Aires.

Jayawardane, N.S. and Greacen, E.L., 1987. The nature of swelling in soils. *Australian Journal of Soil Research* 25, 107–113.

Lavado, R.S. and Camilión, M.C., 1984. Clay minerals in Argentine salt – affected soils. *Clay Research* 3, 68–74.

Lavado, R.S. and Taboada, M.A., 1988. Water, salt and sodium dynamics in Natraquoll in Argentina. *Catena* 15, 577–594.

Low, P.F. and Margheim, J.F., 1979. The swelling of clay: I. Basic concepts and empirical equations. *Soil Science Society of America Journal* 43, 473–481.

Mc Garry, D. and Daniells, I.G., 1987. Shrinkage curves indices to quantify cultivation effects on soil structure of a Vertisol. *Soil Science Society of America Journal* 51, 1575–1580.

Mc Garry, D. and Malafant, K.W.J. 1987. The analysis of volume change in unconfined units of soil. *Soil Science Society of America Journal* 51, 290–297.

Oades, J.M., 1993. The role of biology in the formation, stabilization and degradation of soil structure. *Geoderma* 56, 377–400.

Parker, J.C., Amos, D.F., and Zelazny, L.W., 1982. Water adsorption and swelling of clay minerals in soil systems. *Soil Science Society of America Journal* 46, 450–456.

Schafer, W.M. and Singer, M.J., 1976. Influence of physical and mineralogical properties on swelling of soils in Yolo County, California. *Soil Science Society of America Journal* 40, 557–562.

Senigagliesi, C. and Ferrari, M.,1993. Soil and crop responses to alternative tillage practices. In: Buxton, D.R., Shibles, R., Forsberg, R.A., Blad, B.L., Asay, B.H., Paulsen, G.M., and Wilson, R.F. (eds), *International Crop Science I*. Crop Science Society of America, Madison, Wisconsin, pp. 27–35.

Soil Survey Staff, 1998. Keys to Soil Taxonomy (Eighth Edition). USDA–NRCS, Washington, DC, 326 p.

Soil Survey Staff, 1999. Soil Taxonomy. A Basic System of Soil Classification for Making and Interpreting Soil Surveys. Second Edition. Agr. Handbook N° 436. USDA–NRCS, Washington, DC, 869 p.

Soriano, A., León, R.J.C., Sala, O.E., Lavado, R.S., Deregibus, V.A., Cauhépé, M.A., Scaglia, O.A., Velázquez, C.A., and Lemcoff, J.H., 1991. Rio de la Plata grasslands. en R.T. Coupland (ed.) Temperate Subhumid Grasslands. Ecosystems of the World. Vol. 8, *Natural Grasslands*. A. 367–407. Elsevier Scientific Publishing Co, Amsterdam.

Taboada, M.A. and Lavado, R.S., 1993. Influence of trampling on soil porosity under alternate dry and ponded conditions. *Soil Use and Management* 9, 139–143.

Taboada, M.A. and Lavado, R.S., and Camilión, M.C., 1988. Cambios volumétricos en un Natracuol típico. *Ciencia del Suelo* 6, 151–158.

Taboada, M.A., Micucci, F.G., Cosentino, D.J., and Lavado, R.S., 1998. Comparison of compaction induced by conventional and zero tillage in two soils of the Rolling Pampa of Argentina. *Soil and Tillage Research* 49, 57–63.

Taboada, M.A., Lavado, R.S., Svartz, H., and Segat, A.M.L., 1999. Structural stability changes in a grazed grassland Natraquoll of the Flooding Pampa (Argentina). *Wetlands* 19, 50–55.

Taboada, M.A., Lavado R.S., Rubio G., and Cosentino D.J., 2001. Soil volumetric changes in natric soils caused by air entrapment following seasonal ponding and water table. *Geoderma* 101, 49–64.

Taboada, M.A., Barbosa O.A., Rodríguez M.B., and Cosentino D.J., 2004. Mechanisms of aggregation in a silty loam under different simulated management regimes. *Geoderma* 123, 233–244.

Towner G.D., 1987. The mechanisms of cracking of drying clay. Journal of Agricultural. *Engineering Research* 36, 115–124.

Towner G.D., 1988. The influence of sand and silt-size particles on the cracking during drying of small clay-dominated aggregates. *Journal of Soil Science* 39, 347–356.

Wang, Z., Feyen, J., van Genutchen, M.Th., and Nielsen, D.R., 1998. Air entrapment effects on infiltration rate and flow instability. *Water Resources Research* 34, 213–222.

Yule, D.F. and Ritchie, J.T., 1980 . Soil shrinkage relationships of Texas vertisols: I. Small cores. *Soil Science Society of America Journal* 44, 1285–1291.

Wilding, L., 2004. Advances in the knowledge base of vertisols: Genesis, classification, distribution and management. Revista Científica Agropecuaria, Facultad de Ciencias Agropecuarias – UNER 8, 45–54.

Part 2

Volume change characteristics

Chapter 6

ESEM study of structural modifications of argillite during hydration/dehydration cycles

Joëlle Duplay,[1] *German Montes-Hernandez,*[1] *and Luis Martinez*[2]

Summary

The aim of the study reported in this chapter was to observe at the micrometer scale, changes in both clay structure and texture of the Callovo-Oxfordian argillite (East argillite) when subjected to hydration/dehydration cycles. This was undertaken using an Environmental Scanning Electron Microscope (ESEM) which allows direct observations of the system under controlled relative humidities within the microscope chamber. The study points out the importance of hydration/dehydration cycling on the porosity and texture of clays within the argillite. An important question is whether the swelling clays will change their properties after long-term hydration/dehydration cycles.

Introduction

It is well known that clays are very sensitive to their environment and especially to variations in temperature, pressure, humidity, and fluid composition. Cycles of hydration/dehydration influence the swelling behavior and also the structure and texture of clays as shown by Ben Rhaiem *et al.* (1986). Hydration/dehydration cycles in soils may also lead to the transformation of smectite to illite (Andreoli *et al.*, 1989) and thus induce significant structural and textural reorganization of the material.

In a porous rock, the degree of hydration/dehydration is primarily influenced by the abundance and mineralogy of the swelling clays present. In low permeability clay-rich lithologies sensitive to hydrothermal changes, clay minerals contribute to the mechanical behavior of the rock (e.g. porosity, permeability, plasticity, shear strength) when it is subject to inflowing water or imbibition. Changes in hydration conditions can therefore lead to significant modifications of porosity and the clay texture, as demonstrated on Tournemire mudstone composed of clay minerals (55%) and quartz (45%), carbonates, K-feldspar, and pyrite (Charpentier *et al.*, 2003).

The aim of the study reported in this chapter was to observe at the micrometer scale, changes in both clay structure and texture of the Callovo-Oxfordian argillite (East argillite) when subjected to hydration/dehydration cycles. This was undertaken using an ESEM which

[1] EOST, Centre de Géochimie de la Surface, UMR 7517 du CNRS, 1 rue Blessig 67084 Strasbourg Cédex France, jduplay@illite.u-strasbg.fr

[2] G2R, UMR G2R/7566 Faculte des Sciences, Universite Henri Poincare, Nancy 1, BP 239; Bd des Aiguillettes, 54506 Vandoeuvre les Nancy Cedex France Nancy.

Table 6.1 Mineralogical composition of Callovo-Oxfordian argillites observed by ESEM

Sample	*Core*	*Depth (m)*	*Composition (%)*			
			Clay minerals	*Carbonates*	*Quartz*	*Other*
HTM983	HTM102	399	50	21	22	7
HTM80743	HTM102	466	55	16	21	8
EST2159	EST104	447	26	23	40	11

Source: Andra, 1996.

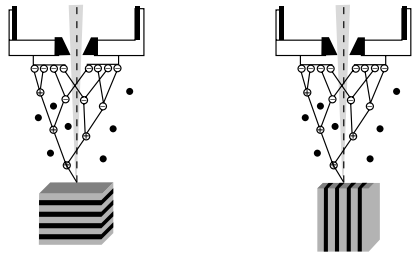

Figure 6.1 ESEM beam and water molecules orientation: (a) perpendicular to the bedding anisotropy, where the argillite is less sensitive to the wet atmosphere; (b) parallel to the bedding anisotropy where the argillite is more sensitive to wet atmosphere.

Source: Montes, 2002.

allows direct observations of the system under controlled relative humidities within the microscope chamber.

Methodology

Argillites of East France are characterized by a range of different mineralogical compositions and clay abundance with depth. We observed the behavior of argillite lithologies from 399 m and 466 m depths within the HTM borehole (HTM 983 and 80743), lithologies which contain 50% clay content and significant quantities of carbonates and quartz (EST2154) (Table 6.1). The clay minerals are composed of illite, kaolinite, chlorite, and 10% interstratified illite/smectite.

The samples were submitted to 3 to 4 cycles of hydration and dehydration, with conditions ranging from 0% to 80% relative humidity. We also monitored the sensitivity to hydration/dehydration reactions as a function of the initial permeability of the lithology (Figure 6.1) by orientating the sample so that the water molecules were either perpendicular or parallel to the bedding anisotropy.

Results and discussion

Figure 6.2 illustrates the main observations of the "East" argillites submitted to hydration/dehydration cycles. Initially the clay-rich argillites (HTM 983 and 80743) swelled significantly

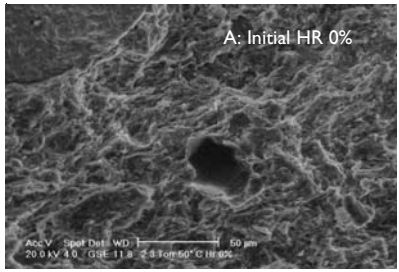

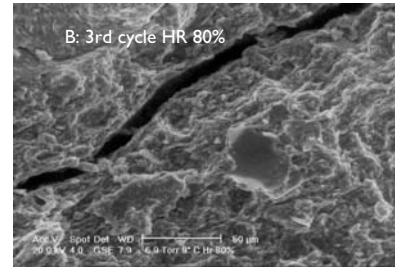

Beam parallel to the bedding anisotropy of clay rich argillite (HTM 80743)

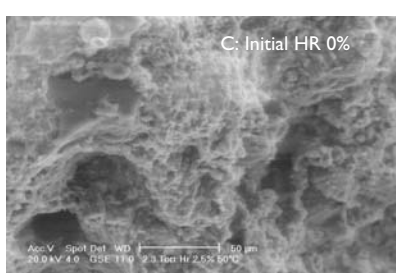

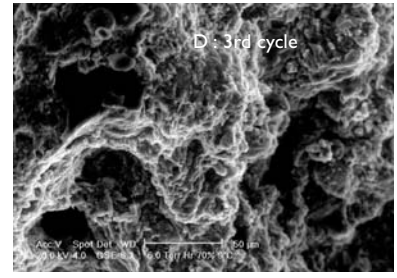

Beam parallel to the bedding anisotropy of quartz and carbonate rich mudstone (EST2159)

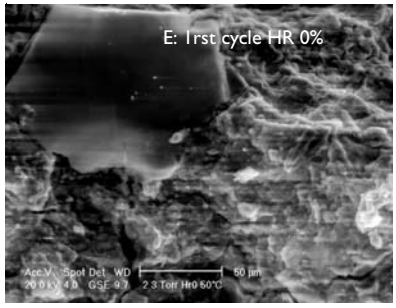

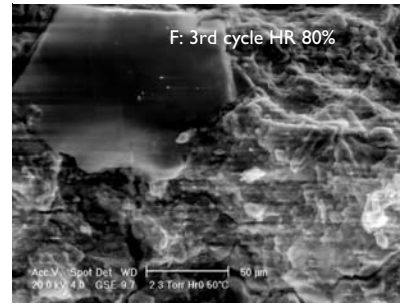

Beam perpendicular to the bedding anisotropy of clay rich argillite (HTM 983)

Figure 6.2 Influence of the mineralogy of the argillite (A to D) and permeability anisotropy (A, B, E, and F) on swelling behavior during hydration/dehydration cycles.

and were very sensitive to hydration/dehydration cycles as shown in Figure 6.2 (A, B, E, and F). In Figure 6.2B, the formation of a fissure could be observed after 3 cycles, which remained even when the clays were rehydrated (80% relative humidity). It appeared the sample could not recover its initial structure and porosity after the third hydration/dehydration cycle.

A different behavior was observed for the carbonate and quartz-rich argillites (EST2154). The initial structure appeared unaffected by hydration/dehydration cycling (pictures C and D) even if the sample was aligned with the permeability anisotropy. This behavior was taken to

reflect the influence of the hard minerals, namely quartz or calcite, which favor the formation of fissures (Figure 6.1 E and F). In the clay-dominant argillite fissure can form even in less favorable orientation conditions.

In closing, these observations point out the importance of hydration/dehydration cycling on the porosity and texture of clays within the argillite. An important question is whether the swelling clays will change their properties after long-term hydration/dehydration cycles.

References

Andra (1996). Rapport Andra/DIR/96/1138.

Andreoli C.Y., Robert M., and Pons C.H. (1989). First steps of smectite-illite transformation with humectation and desiccation cycles. *Applied Clay Science*, 4, 5–6, 423–435.

Ben Rhaiem H., Tessier D., Pons C.H., and Ben Haj A. (1986). Comportement hydrique et évolution structurale et texturale des montmorillonites au cours d'un cycle de dessication-humectation. I-Cas des montmorillonites calciques. *Clay Miner*, 21, 9–29.

Charpentier D., Tessier D, and Cathelineau M. (2003). Shale microstructure evolution due to tunnel excavation after 100 years and impact of tectonic paleo-fracturing. Case of Tournemire, France. *Engineering Geology*, 70, 55–69.

Montes-Hernandez G. (2002) Thesis, ULP Strasbourg, p. 150.

Chapter 7

Large-scale odometer for assessing swelling and consolidation behavior of Al-Qatif clay

Shahid Azam[1]

Summary

Heave, settlement, and lateral distress are the major geotechnical problems associated with expansive soils in the Arabian Gulf coastal region. Geology, climate, environment, and topography influenced the development of expansive minerals in many indigenous soils. This study investigated the swelling and consolidation behavior of undisturbed field samples of Al-Qatif clay using the constant volume method. Large-scale circular and square samples were tested in a highly instrumented large-scale odometer fabricated at King Fahd University of Petroleum and Minerals (KFUPM). Results indicated that soil structure governs the engineering behavior of local over-consolidated clay deposits. The vertical swelling pressure of the clay measured 555 kPa for the conventional circular sample and was reduced by 35% and 60% for the large-scale circular and square samples, respectively. The lateral swelling pressure was one-third the vertical swelling pressure and the swelling index was one-third the compression index for the investigated soil.

Introduction

Expansive soils are infamous for causing heave and settlement problems in many parts of the globe (Chen, 1988). Sustainable engineering solutions to these problems are provided by regional approaches because of their effective capture of indigenous geological settings, climatic and environmental conditions, and construction practices. Al-Qatif clay represents a typical expansive soil generally encountered in the Arabian Gulf coastal region. This over-consolidated clay is extremely fissured in the natural unsaturated state and exhibits alternate volume changes in all directions when the water content is altered. The volume change capacity is due to the high amount of constituent expansive minerals such as smectite and illite (Azam, 2003). Due to recent construction activity related to oil production in Al-Qatif, there was an exigent need for the direct determination of the swelling and consolidation behavior of local clay sediments.

Figure 7.1 gives the generalized map of the study area. The town of Al-Qatif is located at latitude 26°31′ N and longitude 50°01′ E. Expansive soils in and around the town are derived from argillaceous deposits of the Permian, the Cretaceous, and the Tertiary

[1] Department of Mining Engineering, University of British Columbia, Vancouver, Canada; email: azam@mining.ubc.ca

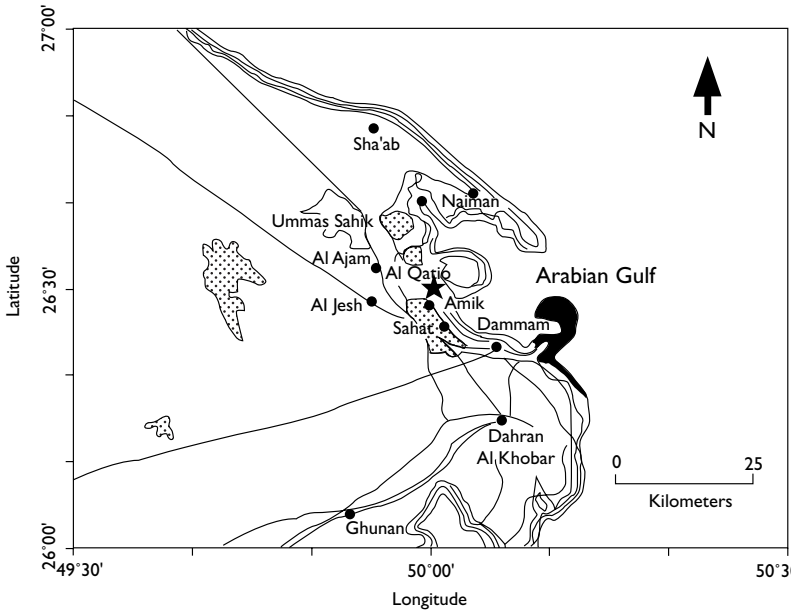

Figure 7.1 Generalized map of the Arabian Gulf coastal region.

(Saint-Marc, 1978). The presence of soil discontinuities such as joints and fissures in the desiccated surface layers in situ clearly indicates that the clay is highly over-consolidated. Parent materials associated with indigenous soils include calcareous sedimentary rocks composed of shale, limestone, marl, and chert (Abduljauwad, 1994). These geological materials were converted to clays by both physical and chemical weathering processes (Potter *et al*., 1980). Expansive minerals were formed under conditions of extreme disintegration, strong hydration, restrained leaching, and an abundance of Na^{+}, Ca^{2+}, Mg^{2+}, SO_4^{2+}, and Fe^{3+} in the pore water (Mitchell, 1993). Geology, hot and arid climate, alkaline environment, and flat topography of the region provided favorable conditions for clay mineral evolution in Al-Qatif soils.

Damages caused by swelling and consolidation of Al-Qatif clay fall into two general categories. Those in the vertical direction include cracks in masonry fences, grade beams, and members of reinforced concrete; uplift and subsidence of floating slabs on grade; and heave and settlement of pavements and walkways. Likewise, horizontal distress is observable in several abutments for road drainage structures and in retaining walls for stabilizing slopes (Azam, 1997). These tribulations are brought about by water infiltration due to rising water table that saturates the predominantly unsaturated soils under the extreme degree of aridity prevalent in the region. Groundwater rise is brought about by both natural and anthropogenic activity. Natural causes include seasonal climatic variations in temperature, precipitation, and relative humidity, all of which can alter the rate of evapo-transpiration and root activity. Man-made causes comprise of lawn watering, utility leakages, and over-irrigation in

the growing urban community. The resulting problems in structures, pavements, and retaining walls are multiplied manifold when the supporting or the supported soils are periodically and/or differentially wetted and dried. Abduljauwad (1994) reported the demolition of 40 unserviceable residential units out of a total of 574 constructed on expansive soils in the town of Al-Qatif.

This study was prompted by the need to understand the swelling and consolidation behavior of Al-Qatif clay thereby providing a guide for construction on similar soils in the region. To capture the influence of the highly fissured nature of this over-consolidated soil, large-scale undisturbed field samples were retrieved from a test pit. A large-scale odometer was fabricated to determine the volume change behavior of the soil under in situ conditions using large-scale circular and square molds. The samples were highly instrumented to measure the swelling pressure in both the vertical and lateral directions. Results of the large-scale odometer were compared with a conventional odometer that used a circular ring.

Geology and environment

The eastern part of the Arabian Peninsula, known as the Arabian Shelf, comprises of sedimentary soils from the Cambrian to the Quaternary (Abduljauwad, 1994). The strata dip gently at a slope of 1 m/km toward the east and northeast and eventually merge with the Arabian Gulf (Slater, 1983). The Shelf geology includes argillaceous shale and calcareous materials such as dolomitic limestone, marl, and chert in several formations of the Phanerozoic succession (Saint-Marc, 1978). The present day coastal clay deposits such as those found in Al-Qatif gradually evolved as a result of geological and weathering processes. Deformational processes like glacial activity and alternate seawater transgressions occurred during the Late Pleistocene and the Holocene (Al-Sayari and Zotl, 1978). In the marine depositional environment of the Arabian Gulf, these processes caused extensive reworking of the parent argillaceous and calcareous materials and intermixing with the newly forming evaporitic sediments (Al-Amoudi and Abduljauwad, 1995). Subsequent physical and chemical weathering of the resulting soils was mainly governed by the climatic and environmental conditions prevalent in the region.

The environment of the Arabian Gulf basin was clearly favorable to expansive mineral development because of an abundance of clay forming ions in the pore water of the sedimenting materials. Chemical analyses of the present day groundwater (brine) indicated the presence of the following ions (parts per thousand): Na^+ (78.8), K^+ (3.1), Ca^{2+} (1.5), Mg^{2+} (10.3), Cl^- (157.2), and SO_4^{2-} (5.5) and a pH of 6.9 (Azam, 1997). The specific gravity and dynamic viscosity of the brine at 20°C was earlier reported to be 1.207 and 1943 $\mu Ns/m^2$ as compared with 0.998 and 1009 $\mu Ns/m^2$ for distilled water (Al-Amoudi and Abduljauwad, 1995). Restrained mobility of this highly alkaline water in the basin valley inhibited sediment leaching thereby facilitating the evolution of expansive minerals in regional clayey soils (Azam and Al-Shayea, 1999).

The Arabian Gulf lies in the northern tropical zone and falls within the hot-arid climate region. A comparison between the average annual rainfall (5 cm) and the average annual rate of evaporation (125 cm) indicates the extreme degree of aridity of the area, as defined by Fookes (1978). Rainfall is scanty and sporadic and is thinly spread between December and March, but it is not unusual for the region to go for several successive months without any precipitation (Al-Amoudi and Abduljauwad, 1995). Although the average temperature of the area ranges from 15°C to 45°C, this range is much wider along the inland margins of the

Gulf where the temperature can reach 50°C during summer days and may drop to 0°C during winter nights. Relative humidity varies between 50% and 80% and usually remains on the high side for most of the summer months. This harsh climate rendered the present-day coastal sediments of the region in a highly desiccated state.

Soil characteristics

Table 7.1 summarizes the characteristics of Al-Qatif clay. The exposed strata at the sampling site constituted greenish brown clay with limestone intercalation up to a depth of 3 m. According to Abduljauwad (1994), this soil layer is underlain by highly inter-bedded green clay containing silty sand seams up to 10 m depth. The measured water content (w) for the top 1 m to 3 m of the deposit averaged 42%. With a degree of saturation (S) of 77%, the surface layer appeared desiccated and exhibited soil discontinuities. A visual survey of the exposed cutting showed extensive variation in the dip angles of fissures with respect to the horizontal. Azam (1997) reported that the specific gravity (G_s) and the dry unit weight (γ_d) of Al-Qatif clay are 2.75 and 1.1 g/cm^3, respectively. From knowledge of γ_d, the in situ soil void ratio (e_0) was determined to be 1.5. This high void ratio is derived from the high amount of small clay particle sizes associated with various clay minerals.

The major constituents of Al-Qatif clay include smectite, illite, and dolomite. Palygorskite, quartz, and gypsum collectively amount to about 15% by weight of the soil. The presence of dolomite in this soil is related to the parent calcareous materials whereas minor minerals have formed as a result of complex chemical reactions between the brine and the host sediment during evaporation (Azam, 2003). The high cation exchange capacity

Table 7.1 Characteristics of Al-Qatif clay

Characteristic	*Value*	*Reference*
In situ conditions		Azam (1997)
Color	Greenish brown	
Water content, w (%)	42	
Specific gravity, Gs	2.75	
Dry unit weight, γ_d (g/cm^3)	1.1	
Degree of saturation, S (%)	77	
Void ratio, e_0	1.5	
*Soil composition**		Azam (2003)
Smectite (%)	50	
Illite (%)	20	
Dolomite (%)	10	
Palygorskite, Gypsum, Quartz	15	
Cation exchange capacity, *CEC* (cmol (+)/kg)	148	
Soil consistency		Azam and Al-Shayea (1999)
Liquid limit, w_l (%)	150	
Plastic limit, w_p (%)	55	
Plasticity index, I_p (%)	95	
Shrinkage limit, w_s (%)	20	

Note
* Mineral quantities are variable by ± 5.

(*CEC*) of Al-Qatif clay is mainly derived from the expansive clay minerals such as smectite and illite. According to Abduljauwad (1994), Na^+ is the predominant exchangeable cation in local calcareous soils.

The high values of liquid limit (w_l), plastic limit (w_p), and plasticity index (I_p) along with the low shrinkage limit (w_s) indicate the high water intake and water holding capacity of Al-Qatif clay (Azam and Al-Shayea, 1999). These characteristics are governed by the presence of monovalent exchangeable cations such as Na^+ and the large specific surface areas of the clay particles (Van Olphen, 1977). Using the free swell odometer test, Azam (2003) determined the swelling potential and the compression index (C_c) of Al-Qatif clay as 34.3% and 1.166, respectively.

Methodology

The laboratory investigations were aimed at understanding the swelling and consolidation behavior of Al-Qatif clay using high quality undisturbed block samples. At the site, a 3 m deep rectangular test pit (4 m × 5 m) was excavated using a Poclain Series 90 backhoe. The bottom of the test pit was cleaned and leveled and a stainless steel box was slowly pushed into the ground to retrieve individual samples. The soil around the box was dug out to isolate the sample from the parent soil. A stainless steel plate was fastened to the box and the latter was carefully inverted. To preserve the in situ water content, the sample was wrapped with cheesecloth and painted with molten wax. A number of samples were extracted and transported to the KFUPM Geotechnical Laboratory and were stored at 25°C in a humidity chamber.

The swelling and consolidation characteristics of the clay were determined using a conventional circular ring as well as large-scale circular and square molds. All of the specimens were prepared according to the ASTM Standard Test Methods for One-Dimensional Swell or Settlement Potential of Cohesive Soils (D4546-96) and the ASTM Test Method for One-Dimensional Consolidation Properties of Soils (D2435-96). The large-scale samples were carefully trimmed to fit in the large-scale molds. Before conducting the odometer tests, the specimens were subjected to a seating stress of 7 kPa that closely corresponded to the in situ effective stress acting on the soil.

Conventional and large-scale odometer tests were performed using the constant volume method. Figure 7.2 shows the large-scale odometer fabricated at the KFUPM workshop. The large-scale samples were mounted on the odometer that used a pneumatic loading system to prevent vertical expansion of the specimen when flooded with water; a load cell connected to a data logger measured the pressure required to prevent expansion. After the swelling pressure was fully developed, the submerged specimens were loaded and unloaded following the usual consolidation test procedure. Changes in volume during the consolidation stage were recorded by Linear Variable Displacement Transducers (LVDT) connected to a data logger that, in turn, was linked to a portable computer.

Figure 7.3 illustrates the large-scale circular and square samples in the stainless steel molds. The molds were reinforced by stiffeners to prevent bulging due to the expected high lateral swelling pressures. Table 7.2 compares the geometry of the conventional and the large-scale samples. The height of the latter samples was 8.5 cm and their diameter or side was 30 cm wide. These dimensions ensured a constant height-to-diameter or height-to-side ratio for all of the samples. With respect to the conventional sample, the contact areas were in excess of 18 times and 23 times for the large-scale circular and square samples, respectively.

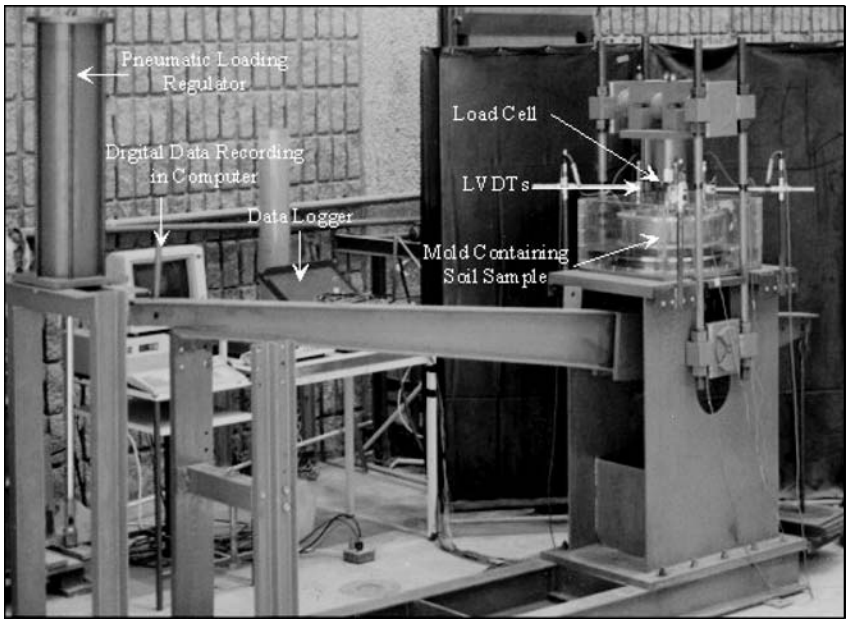

Figure 7.2 The large-scale odometer.

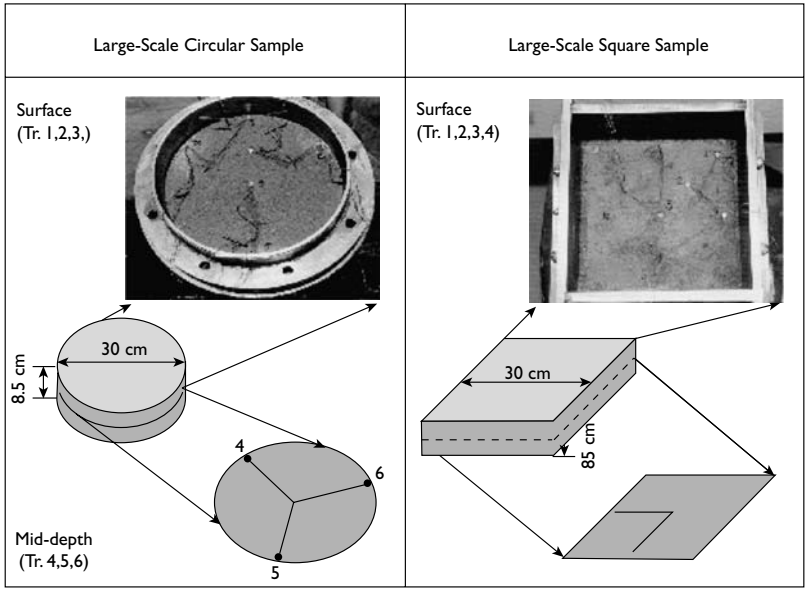

Figure 7.3 Spatial distribution of pressure transducers in large-scale samples.

Table 7.2 Comparison of sample geometry

Parameter	*Conventional sample (Circular)*	*Large-scale samples*	
		Circular	*Square*
Sample height (cm)	1.95	8.50	8.50
Sample diameter or side (cm)	7	30	30
Top and bottom contact area (cm^2)	77	1,414	1,800
Wall contact area (cm^2)	43	801	1,020
Height/diameter or height/side	0.28	0.28	0.28
Normalized top and bottom contact	1.0	18.4	23.4
Normalized wall contact	1.0	18.6	23.7

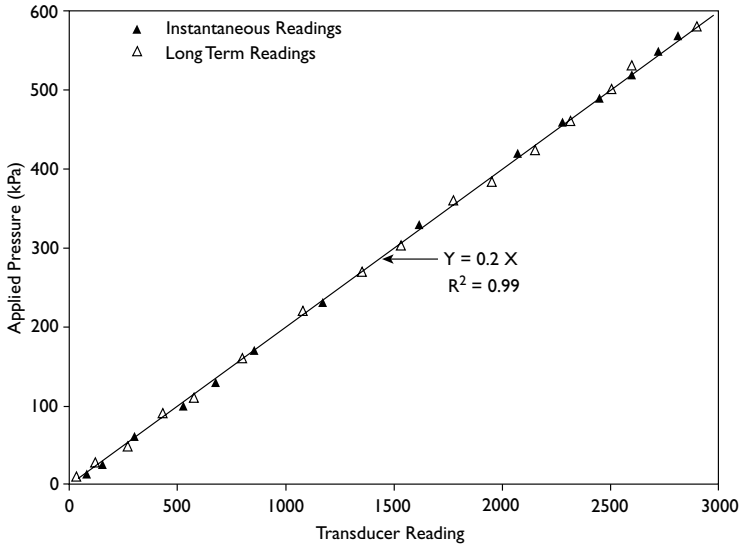

Figure 7.4 Calibration data for a typical pressure transducer.

To monitor the development of swelling pressure in the vertical and lateral directions, ENTRAN (EPN-300-100) pressure transducers were installed in the large-scale samples at several specified locations. The miniature strain sensors employed a high-sensitivity semiconductor bridge and compensated for thermal changes in the environment. The pressure transducers were 10.2 mm in diameter and 3.8 mm in thickness. The transducer sensitivity and range were of the order of 25 mV/kPa and 700 kPa, respectively.

Figure 7.3 shows the spatial arrangement of transducers in the large-scale samples. For the circular sample, three surface transducers were installed radially at an equal separation distance and three mid-depth transducers were installed circumferentially 120° apart. For the square sample, three surface transducers were installed diagonally at an equal separation distance whereas one surface transducer was installed on the side; two transducers were

installed at mid-depth along two adjacent sides. To embed the transducers and the attached electrical wiring, indentations were made in the soil using a sharp knife. This activity was performed carefully to ensure minimum sample disturbance. The surface and mid-depth transducers measured the vertical swelling pressure and the lateral swelling pressure, respectively.

Transducer readings in the large-scale tests were corrected using appropriate calibration factors. Figure 7.4 gives instantaneous and long-term calibration data for a typical transducer. Each transducer was put in a closed chamber and a data logger recorded the instantaneous readings as air pressure was applied. Likewise, these transducers were installed in a soil sample and loaded incrementally similar to a consolidation test in an odometer ring. The long-term transducer readings and the applied pressure pertained to the cessation of sample deformation. The data from both calibration methods was always in good agreement and calibration factors for individual transducers were usually in the range of 0.2 ± 0.01.

Results and discussion

Expansive minerals such as smectite and illite can undergo large volume increases when inundated with water. Due to their negatively charged surfaces and large specific surface areas, these clay minerals adsorb water along the 001 interlayer spacing (Van Olphen, 1977). Surface hydration causes the individual clay platelets to push apart from one another. High swelling pressures are developed when this expansive movement of the clay particles is restrained (Chen, 1988). Figure 7.5 gives the constant volume test results in the form of void ratio versus effective stress. The vertical swelling pressure pertained to the maximum value obtained from the initial straight-line portion of the curve. The vertical swelling pressure of Al-Qatif clay measured 555 kPa in the conventional circular sample whereas the large-scale circular and square samples recorded 360 kPa and 217 kPa, respectively. The variation in the

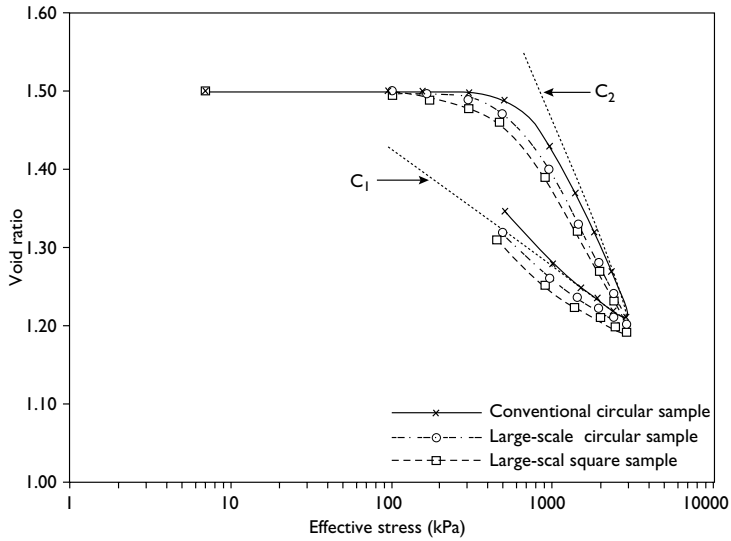

Figure 7.5 Void ratio-effective stress relationships.

vertical swelling pressure is mainly due to the presence of soil discontinuities, which were numerous in the large-scale samples having large cross-sectional areas. The fissures, joints, and cracks in the clay consumed a significant portion of the movement during swelling thereby decreasing the observed values by 35% and 60% for the two large-scale samples.

The constant volume test procedure gives an accurate estimate of the vertical swelling pressure because the only factor that affects its performance is the complete confinement of the sample that is related to mold rigidity. The influence of apparatus deformability is minimal since infinitesimal soil deformations due to swelling are simultaneously cancelled by the applied loads (El-Sohby *et al*., 1989). Using laboratory data from a number of test methods, Abduljauwad *et al*. (1998) predicted the heave of structures on expansive soils. Estimates based on the constant volume test best matched actual field measurements. The observed reductions in vertical swelling pressure are attributed to the high wall contact areas of the large-scale samples (Table 7.2).

The movement of water through an initially unsaturated soil takes place under a hydraulic gradient set up by negative pore water pressure within the soil relative to free water, that is, soil suction (Fredlund and Rahardjo, 1993). Evidently, water movement and the resulting development of vertical swelling pressure in the soil are time dependent phenomena. The initial straight-line portion of Figure 7.5 was used to determine the development of the vertical swelling pressure as a function of time. Figure 7.6 plots the vertical swelling pressure versus time for the three sample geometries. Vertical swelling pressure curves were S-shaped exhibiting initial, primary, and secondary swelling. The low swelling rate during the initial stage is attributed to the low unsaturated hydraulic conductivity of the samples. Once water mobility was initiated, the high water adsorptive forces on clay particle surfaces were readily wetted thereby resulting in a high rate of primary swelling. The gradual reduction

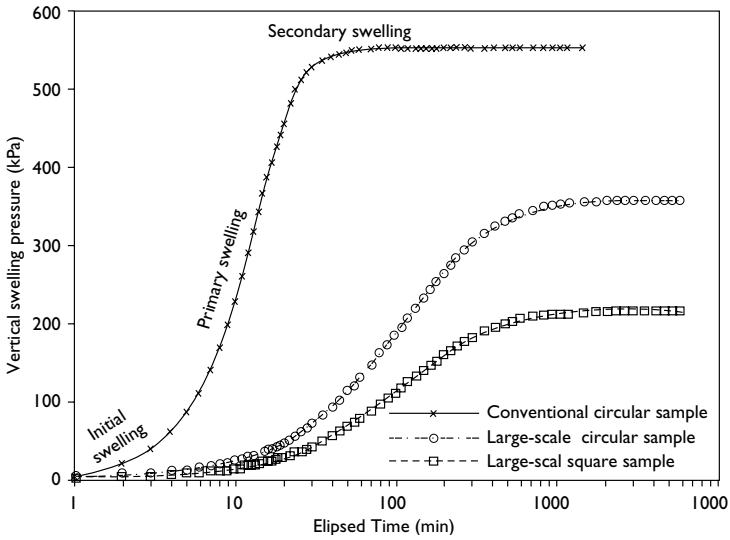

Figure 7.6 Development of vertical swelling pressure with time.

in the swelling rate during the primary and secondary stages and the eventual cessation of the vertical swelling pressure in the latter stage is attributed to increasing sample saturation due to water migration. A higher degree of saturation is associated with a lower soil suction and therefore with a lower soil affinity for water adsorption.

The development of vertical swelling pressure and the rate of water mobility through the various samples strongly depended on the in situ soil structure and the geometry of the molds. In comparison to the conventional circular sample, the cross-sectional areas of the large-scale circular and square samples were more than 18 times and more than 23 times, respectively (Table 7.2). This means that numerous soil fissures were captured in the large-scale samples and water initially moved favorably into these paths of least resistance. However, the clay minerals expanded into these void spaces thereby closing the flow channels; subsequent water flow occurred through the regular soil matrix. This internal assimilation of clay expansion in both of the large-scale samples resulted in slower pressure development during initial swelling when compared with the conventional circular sample (Figure 7.6). Further, the large-scale samples took about 5 hours to saturate completely whereas the conventional circular sample hydrated within 30 minutes of water flooding. This is attributed to the more than 4 times greater sample height in the large-scale samples compared to the conventional circular sample; water traversed much longer paths in the former samples. The same trend was observed for the completion of the secondary swelling stage. The large-scale samples came to equilibrium in about two days whereas the conventional sample stabilized in only 90 minutes after the initial water inundation.

When clay minerals hydrate, water is adsorbed between the stacked clay particles causing the latter to push in the direction normal to the layering. The vertical push is restrained by the top and bottom plates whereas the lateral thrust is confined by the sides of the odometer molds. Figure 7.7 gives the swelling pressure of the clay measured by the load cell and

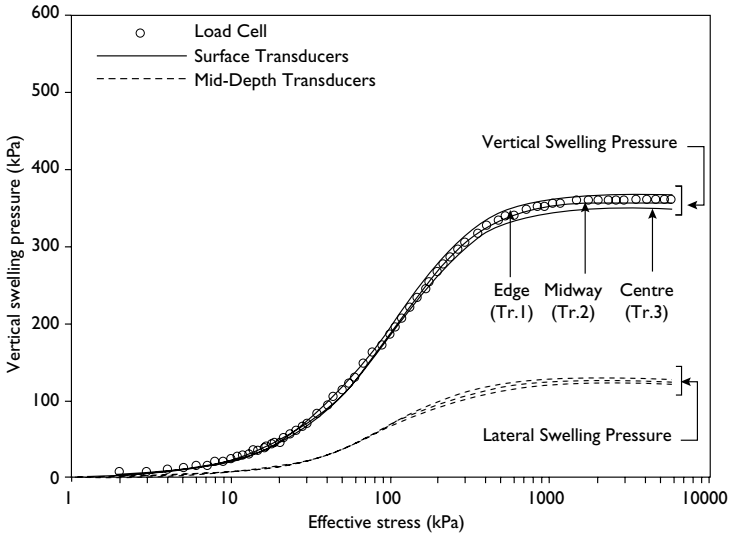

Figure 7.7 Development of swelling pressure with time in large-scale circular sample.

the pressure transducers in the large-scale circular sample. The swelling pressure curve obtained from the load cell closely matched the average vertical pressure measured by the three surface transducers. The figure shows negligible variation in the lateral swelling pressure recorded by the three mid-depth transducers. The average lateral swelling pressure was 125 kPa, which equated to about one-third of the vertical swelling pressure. This is attributed to the fact that layering in Al-Qatif clay is predominantly horizontal with localized randomness in soil particle orientation (Azam, 1997). By restraining the preferred vertical movement during the test, the sample redistributed part of the expansion in the lateral direction (Edil and Alanazy, 1992). These results were consistent with the data reported by Ofer (1981) using various types of expansive soils and testing techniques.

Figure 7.8 records the swelling pressure of Al-Qatif clay measured by the load cell and the pressure transducers in the large-scale square sample. Similar to the large-scale circular sample, the swelling pressure curve obtained from the load cell approximated the average vertical swelling pressure measured by the four surface transducers. Again, the variation in the lateral swelling pressure measured by the two mid-depth transducers was marginal. The average lateral swelling pressure that amounted to 74 kPa was almost one-third of the vertical swelling pressure.

The influence of sample shape is elucidated by comparing the results of the two large-scale samples. The vertical swelling pressure was reduced by 40% when the sample section was changed from circular to square. This was mainly due to increased resistance offered by the square mold to the expanding soil by virtue of a higher wall contact area (Table 7.2) despite a constant surface roughness of both stainless steel molds. Further, the lower mold rigidity of the square section (with jointed walls) in contrast to the circular section (cut from a cylindrical pipe) partly contributed to a lower vertical swelling pressure. Figure 7.8 indicates that the vertical swelling pressure at the edge (Transducer No. 1) was always higher than that at

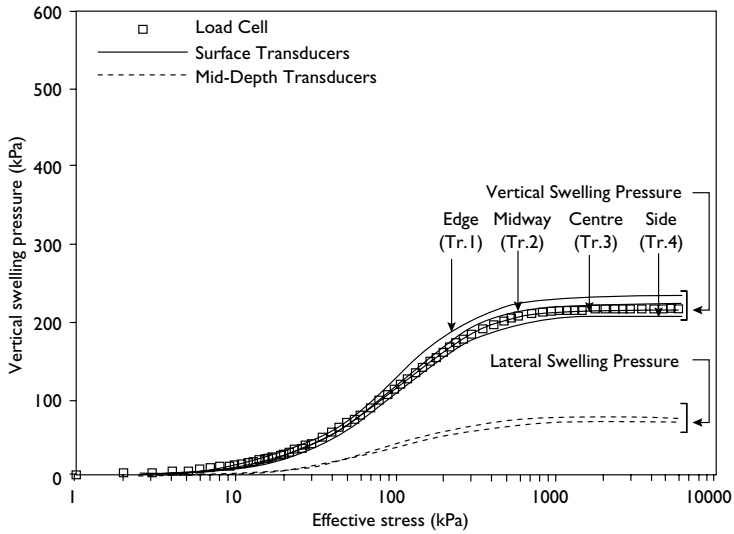

Figure 7.8 Development of swelling pressure with time in large-scale square sample.

the side (Transducer No. 4) in the large-scale square sample. This is due to the greater resistance offered by the edge that leads to a local stress concentration.

Figure 7.9 gives the diagonal variation of vertical swelling pressure in the large-scale circular and square samples. The vertical swelling pressure recorded by the surface transducers was at a maximum at the edge and linearly decreased to a minimum at the center. This trend was identical for both of the large-scale samples because of their complete lateral confinement in the molds. The observed trend is analogous to the distribution of contact pressure of rigid footings on clays and can be confirmed using the theory of elasticity. Saada and Townsend (1981) observed similar variations in the vertical normal stresses and shearing stresses while studying the direct shear apparatus. Given an initially leveled sample surface, the nonuniform vertical swelling pressure distribution may be partially related to the inhomogeneity of Al-Qatif clay and to possible sample disturbances during retrieval, transportation, and transducer installation.

Table 7.3 summarizes the volume change characteristics of Al-Qatif clay in different sample geometries. The compression index (C_c) and the swelling index (C_s) were obtained from test data depicted in Figure 7.5. The C_c of Al-Qatif clay in the conventional circular

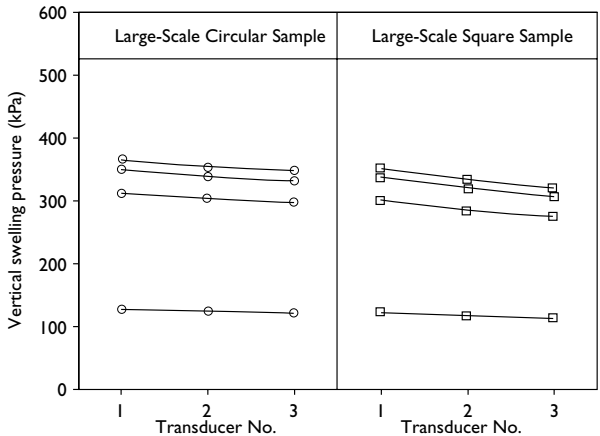

Figure 7.9 Diagonal variation of vertical swelling pressure in large-scale samples.

Table 7.3 Summary of volume change characteristics of Al-Qatif clay

Parameter	*Conventional sample (Circular)*	*Large-scale samples*	
		Circular	*Square*
Vertical swelling pressure, P_{vs} (kPa)	55	360	217
Lateral swelling pressure (kPa)	—	125	74
Compression index, C_c	0.54	0.41	0.36
Swelling index, C_s	0.16	0.13	0.12
Estimated heave, ΔH (mm)	47.6	28.9	16.2

sample was 0.54, which is less than half of what was obtained by Azam (2003) using an identical circular ring in the free swell odometer test. This overestimation of C_c in the reported method was attributed to sample expansion preceding compression. Enlarged pore spaces with an associated reduced tortuousity were filled with water that was easily expelled under applied loading. The constant volume method used in this study better estimated C_c because soil conditions such as void ratio and to a great extent tortuousity remained unchanged during swelling.

The variation in C_c and C_s among various samples is associated with the wall contact area (Table 7.2). A large wall contact area offered a high mold resistance to the consolidating or the swelling specimen. Under a given load, a smaller change in sample void ratio was observed in the large-scale molds compared to those in the conventional ring. The C_s was about one-third of the C_c for all of the samples. This relatively higher ratio of the two indices is attributed to changes in soil structure due to water addition; soil discontinuities were filled with expanded clay platelets. The soil rebounded almost elastically when unloaded because the preceding loading could only remove the pore water and not the adsorbed clay water. Finally, heave (ΔH) in the surface layer of Al-Qatif clay was predicted using the following equation (Johnson and Snethen, 1978):

$$\Delta H = H \frac{C_s}{1 + e_0} \log \frac{p_{vs}}{\sigma_{vf} - u_{wf}} \tag{7.1}$$

where, H was the thickness of the swelling soil, p_{vs} was the vertical swelling pressure, σ_{vf} was the total vertical overburden pressure, and u_{wf} was the final pore water pressure. The estimated heave depicted in Table 7.3 strongly depends on the measured swelling pressure.

The selection of sample size and shape for the determination of swelling and consolidation behavior depends on the risk associated with a project and on the type of construction for which the data is required. For low risk projects, a conservative engineering design is usually based on conventional odometer test results despite overestimation. Site-specific correlations sensitive to local geology, climate, environment, and topography must be established to provide a sound design basis in high risk projects. Retrieval of high quality undisturbed samples and the use of test equipment and techniques such as those used in this study are the prerequisites of mimicking actual field conditions.

Structures on expansive clays are designed to resist the upward movement due to swelling pressure and settlement due to consolidation. Contrary to rigid construction, a flexible structural design accommodates such movements of the supporting soil. This study highlighted that an important design aspect is the sideways soil movement under lateral thrust. The rate and amount of vertical and lateral swelling pressure are key design inputs while dealing with expansive soils. The conventional circular ring grossly overestimates swelling pressure because of a small sample size that may disregard important soil features.

The large-scale odometer is useful in understanding the swelling and consolidation behavior of expansive soils in the Arabian Gulf coastal region. This study illustrated that the large-scale samples effectively capture soil discontinuities of Al-Qatif clay. Results of the large-scale circular sample are directly applicable to the design of isolated column footings, piles, and piers of circular cross sections. Likewise, the data obtained from the large-scale square sample are useful in designing isolated column footings, raft foundations, and slabs on grade with square and rectangular cross sections.

Concluding remarks

Knowledge of the potential volume change characteristics in soils at the outset of any engineering construction project is obligatory because of their relationships to heave and lateral thrust due to expansion as well as settlement due to compression. This study investigated the swelling and consolidation behavior of undisturbed field samples of Al-Qatif clay using the constant volume test method. Large-scale circular and square samples were tested in a highly instrumented large-scale odometer fabricated at KFUPM.

The major findings of this investigation can be summarized as follows: Parent geological materials, hot and arid climate, alkaline environment, and flat topography influenced the development of expansive minerals in the clay deposits of the Arabian Gulf coastal region. Al-Qatif clay is a typical expansive soil usually encountered in the area. Soil structure governs the volume change behavior of this over-consolidated clay deposit. Discontinuities such as fissures and joints in the desiccated surface layer partly consume the expansive movement of the clay when the water content is increased. Large-scale samples effectively capture soil fissuring thereby representing actual field conditions. Lateral confinement, wall contact area, and mold shape significantly affect the determination of swelling and consolidation in the odometer. The vertical swelling pressure of the clay measured 555 kPa in the conventional odometer ring. The large-scale circular and square samples recorded 35% and 60% reduced vertical swelling pressures, respectively. Irrespective of sample geometry, the lateral swelling pressure equated to about one-third of the vertical swelling pressure. Likewise, the swelling index was one-third of the compression index for the investigated soil.

Acknowledgments

The author acknowledges the support of KFUPM for providing laboratory facilities. Thanks go to Mrs Shehla Farah and also to Ms Jill M. Baldwin for her invaluable help during final stages of the manuscript write-up.

References

Abduljauwad, S.N. (1994). Swelling behavior of calcareous clays from the Eastern Province of Saudi Arabia. *Quarterly Journal of Engineering Geology*. 27: 333–351.

Abduljauwad, S.N., Sulaimani, G.J., Basunbal, I.A., and Al-Buraim, I. (1998). Laboratory and field studies of response of structures to heave of expansive clay. *Geotechnique*. 48(1): 103–121.

Al-Amoudi, O.S.B. and Abduljauwad, S.N. (1995). Compressibility and collapse potential of an arid, saline sabkha soil. *Engineering Geology*. 39(3): 185–202.

Al-Sayyari, S.J. and Zotl, J.G. (1978). *Quaternary Period in Saudi Arabia*. Springer-Verlag, Wien, Austria.

Azam, S. (1997). *Effect of Gypsum-Anhydrite on the Behavior of Expansive Clays*. MSc Thesis, King Fahd University of Petroleum and Minerals, Dhahran, Saudi Arabia.

Azam, S. (2003). Influence of mineralogy on swelling and consolidation of soils in eastern Saudi Arabia. *Canadian Geotechnical Journal*. 40(5): 964–975.

Azam, S. and Al-Shayea, N.A. (1999). Clayey behavior of calcareous soils. *Proceedings, 2nd International Conference on Engineering for Calcareous Sediments*, Bahrain. 1: 199–208.

Chen, F.H. (1988). *Foundation on Expansive Soils*. Elsevier Scientific Publishing Company, Amsterdam, The Netherlands.

Edil, T.B. and Alanazy, A.S. (1992). Lateral swelling pressures. *Proceedings, 7th International Conference on Expansive Soils*, Dallas, Texas, United States of America. 1: 227–232.

El-Sohby, M.A., Mazen, S.O., and Abou-Taha, M.M. (1989). Effect of apparatus deformability on swelling pressure. *Proceedings, 12th International Conference on Soil Mechanics and Foundation Engineering*, Rio de Janeiro, Brazil. 1: 589–592.

Fookes, P.G. (1978). Middle East-inherent problems. *Quarterly Journal of Engineering Geology*. 11: 33–39.

Fredlund, D.G. and Rahardjo, H. (1993). *Soil Mechanics for Unsaturated Soils*. John Wiley & Sons, Inc. New York, United States of America.

Johnson, L.D. and Snethen, D.R. (1978). Prediction of potential heave of swelling soils. *Geotechnical Testing Journal*. 1(3): 117–124.

Mitchell, J.K. (1993). *Fundamentals of Soil Behavior*. 2nd edn, John Wiley & Sons, Inc. New York, United States of America.

Ofer, Z. (1981). Laboratory instrument for measuring lateral soil pressure and swelling pressure. *Geotechnical Testing Journal*. 4(4): 177–182.

Potter, P.E., Maynard, J.B., and Pryor, W.A. (1980). *Sedimentology of Shale*, Springer, New York, United States of America.

Saada, A.S. and Townsend, F.C. (1981). State of the art: laboratory strength testing of soils. *Laboratory Shear Strength of Soils*. ASTM STP 740: 7–77.

Saint-Marc, P. (1978). *Arabian Peninsula: Phanerozoic Geology of the World II: The Mesozoic*. Elsevier Scientific Publishing Company, Amsterdam, The Netherlands.

Slater, D.E. (1983). Potential expansive soils in Arabian Peninsula. *ASCE Journal of Geotechnical Engineering*. 109(5): 744–746.

Van Olphen, H. (1977). *An Introduction to Clay Colloid Chemistry*. Wiley-Interscience, New York, United States of America.

Chapter 8

Water sorption and dilatation of bentonites and montmorillonite-rich clays

Radek Hanus,[1] *Irena Kolaříková,*[1] *and Richard Přikryl*[1]

Summary

Humidity sorption and dilatation characteristics of two different genetic types of smectite-rich clays were studied. Two distinct stages observed during the desorption experiments correspond to the release of adsorbed water and the loss of absorbed water. Absorption experiments revealed the differences in the length of C-D interval (i.e. the amount of absorbed humidity in the samples mainly in the clay particle interlayer) in the absorption curve, which can be explained by variable contents of clay minerals. Dilatation experiments confirmed the correlation between the ability to dilate (i.e. swell) and the smectite content.

Introduction

Sorption is a characteristic behavior of materials showing high specific surface and cation exchange like zeolites or some kinds of clays. Sorption of water and associated physical swelling is a characteristic property of clays, namely of smectite group minerals (e.g. Pimentel, 2003). Previous studies of water humidity sorption (Bogoslovskaya *et al*., 1987; Hunger *et al*., 1997; Siriwardane *et al*., 2003) were focused on the behavior of synthetic zeolites (mainly clinoptilolite). Studies on swelling of water-saturated clays are common in geotechnics (e.g. Komine, 2004; Komine and Ogata, 2004). Clay dilatation in the presence of water humidity has not been studied before.

The aim of the studies reported in this chapter was to determine the differences in behavior between bentonites and montmorillonite-rich sedimentary clays during desorption–absorption cycles and dilatation experiments.

Methodology

Materials

Humidity sorption and dilatation experiments were conducted on samples coming from six Czech bentonite s.s. deposits – in situ weathered pyroclastic rocks (Rokle deposit – sample Ro,

[1] Charles University in Prague, Faculty of Science, Institute of Geochemistry, Mineralogy, and Mineral Resources Albertov 6, Prague 2, 128 43 Czech Republic. E-mail: kakt@centrum.cz, jaro@natur.cuni.cz, prikryl@natur.cuni.cz

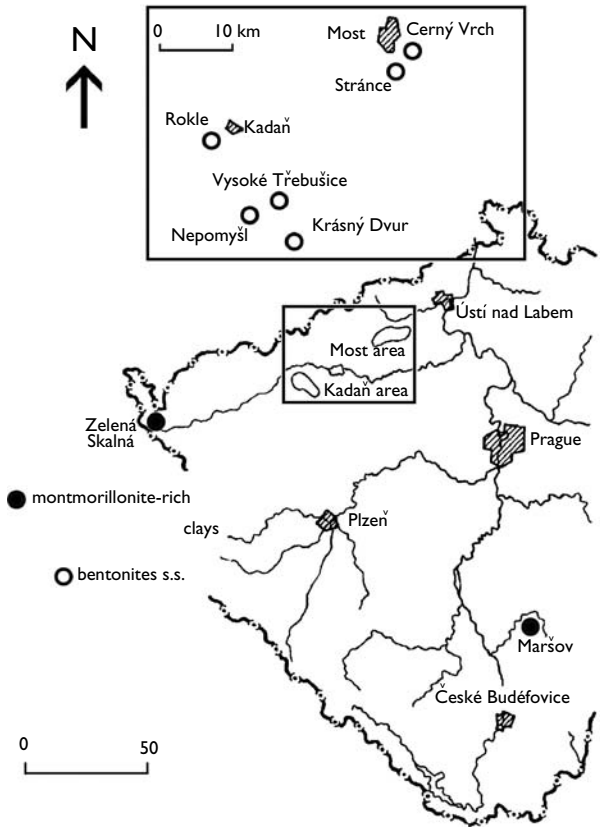

Figure 8.1 Geographical location of major bentonite and montmorillonitic clay deposits in the Czech Republic.

Černý vrch deposit – sample Ce, Nepomyšl deposit – sample Ne, Krásný Dvůr deposit – sample KD, Vysoké Třebušice deposit – borehole sample Tr, and Stránce deposit – sample St) (Figure 8.1), which are related to the Tertiary alkaline volcanism (Franče, 1992). Czech bentonites were formed by devitrification and chemical alteration of igneous rocks (tuffs or volcanic ash). This process occurs at the position of the original volcanic eruption and is not accompanied by any significant transport of weathered material to another sedimentary basin.

Samples from Maršov deposit (sample Ma) and Zelená deposit near Skalná (sample Sk) represent a different genetic type of smectite-rich clay material (see Figure 8.1). Transport and deposition at a place different from the place of their origin play a key role in formation of these deposits.

Mineralogical composition of studied clays was determined by X-ray diffraction. Analysis of smectites was facilitated by preparation of oriented and glycolated samples.

Table 8.1 Major crystalline phases in Czech bentonites and montmorillonite-rich clays (bulk samples)

Phases	*Locality*							
	Ro	*Ce*	*Ne*	*KD*	*Tr*	*St*	*Sk*	*Ma*
Smectite	+	+	+	+	+	+	+	+
Kaolinite	+	+	+	+	+		+	+
Illite	+	+	+	+	+	+	+	+
Quartz		+		+	+		+	+
Calcite			+					+
Feldspar								+
Fe oxihydroxides	+	+					+	+

Semiquantitative mineralogy of selected samples was determined using the CQPA (Chemical Quantitative Phase Analyses) recalculation program (Klika and Weiss, 1993), XRD, and chemical analyses data.

The presence of iron oxohydroxides was determined using infrared spectrometry with Fourier transform. Phases were identified by the comparison with standard spectra in spectral libraries (Institute of Chemical Technology in Prague). Qualitative mineralogical data are presented in Table 8.1.

Control measurement was conducted on two standards – MX 80 bentonite (containing montmorillonite with Na^+ exchangeable cation) and STx-1 bentonite (rich in montmorillonite with Ca^{2+} and Mg^{2+} exchangeable cations). Before experiments, particles above 0.5 cm were removed from homogenous bulk clay samples. Samples were dried in the circulated atmosphere (40°C) for 72 hours.

Equipment

Humidity sorption and dilatation experiments were conducted at the Institute of Physical Chemistry of Jaroslav Heyrovský, Academy of Sciences of the Czech Republic. The apparatus (Figure 8.2), constructed exclusively for this experiments, consisted of: source of N_2, device for mixing nitrogen and humidity, valve, U-tube with clay sample, cathetometer, hygrometer, electric vertical resistance furnace employed during desorption experiment, and water bath employed during absorption and dilatation measurements.

Desorption experiments

Samples (0.5 g) were placed in the glass U-tube and covered with a glass grater containing a reference point and heated to 115°C (2°C/min) using a heating device. The U-tube containing the sample was subsequently saturated with dry nitrogen (flow rate 40 ml/min).

Desorption parameter was calculated according to the following formula:

$$m_D = F.\int_0^{t_k} g dt \tag{8.1}$$

where m_D is desorbed water humidity, F is flow of N_2 (ml/min), t is time (min), t_k is const. time (min), and g is absolute humidity (g/m^3).

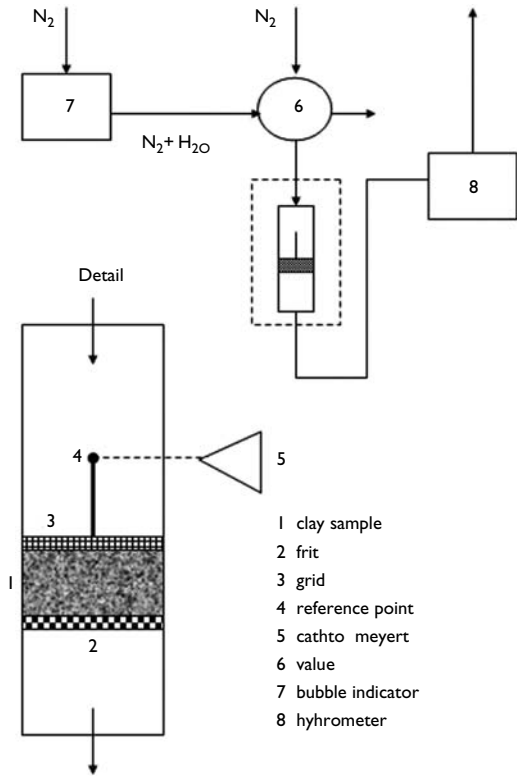

Figure 8.2 Analytical apparatus used for desorption, absorption, and dilatation measurements.

Absorption experiments

Absorption experiments followed the desorption. The U-tube containing dried clay sample was placed in the 30°C aqueous bath to control the temperature of the system. The sample was then flooded with humidified nitrogen at a flow rate F = 40 ml/min for 100 min. Residual humidity of gas flow coming from the sample was measured by a Sensorica hygrometer every 15 seconds. The absorption parameter was calculated according to the following formula:

$$m_A = F.(g_{\max}.t_k - \int_0^{t_k} g dt) \tag{8.2}$$

where g is absolute humidity (g/m^3), $g_{\max}$ is maximal absolute humidity (g/m^3), m_A is absorbed water (mg), F is flow of N_2 (ml/min), t is time (min), and t_k is const. time (min).

Dilatation experiments

During dilatation measurements, swelling ability of clay material was evaluated. This parameter was measured simultaneously with absorption experiment. When moistured, the clay sample placed in the U-tube swelled. The degree of swelling was read with the help of cathetometer focused on the reference point.

Results and discussion

Desorption

During desorption, humidity of the sample gradually decreased until reaching point A (Figure 8.3). Two distinct stages on the curve of released humidity correspond to the adsorbed water (stage I) and to the absorbed water (stage II). When reaching point A, the adsorbed and absorbed waters (clay minerals interlayer water) were completely replaced by nitrogen. Point A thus represents the function of specific surface of the particles that is occupied by humidity.

Czech bentonites s.s. and sedimentary smectite-rich clays showed desorption behavior (Figures 8.4 and 8.5) similar to Ca-Mg montmorillonite standard (STx-1). The only exception was recorded for one bentonite s.s. sample (from Krásný Dvůr deposit) and for one sedimentary smectite-rich clay (from Maršov deposit). As these two clays also contain Ca-Mg montmorillonite, this behavior remains unclear and needs further study.

Absorption

The water humidity absorption curve reflects two different features when plotted against time. The length of C-D interval is proportional to the amount of absorbed humidity in the

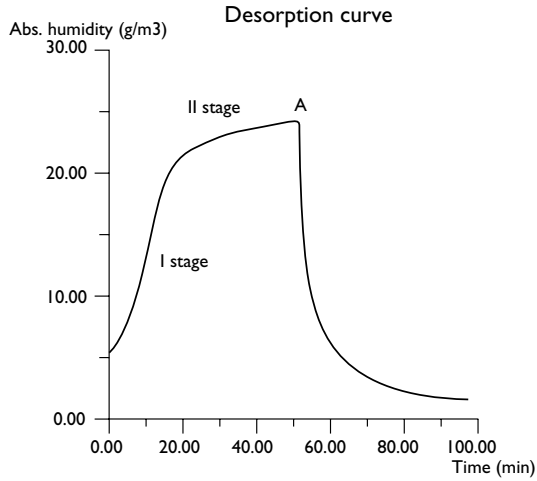

Figure 8.3 Desorption curve of smectite-rich clay material.

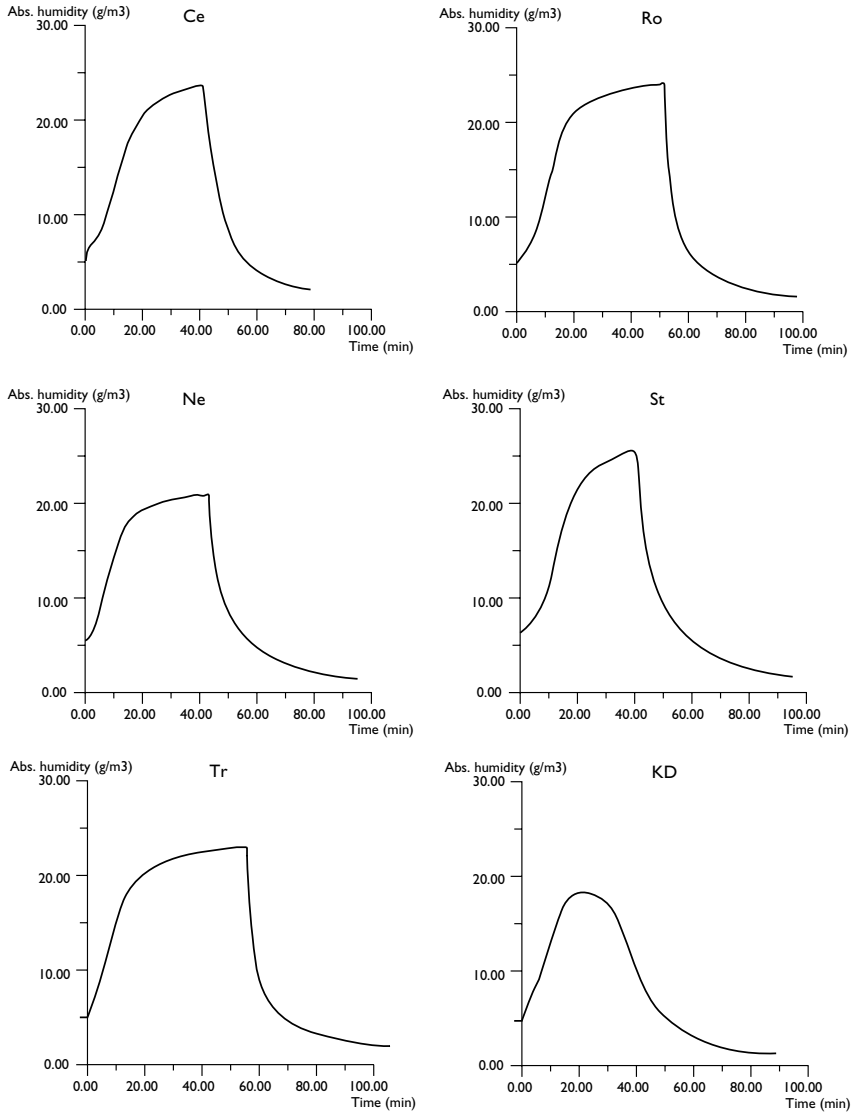

Figure 8.4 Desorption curves of Czech bentonites (Černý vrch – Ce, Rokle – Ro, Nepomyšl – Ne, Stránce – St, Třebušice – Tr, and Krásný Dvůr – KD deposits).

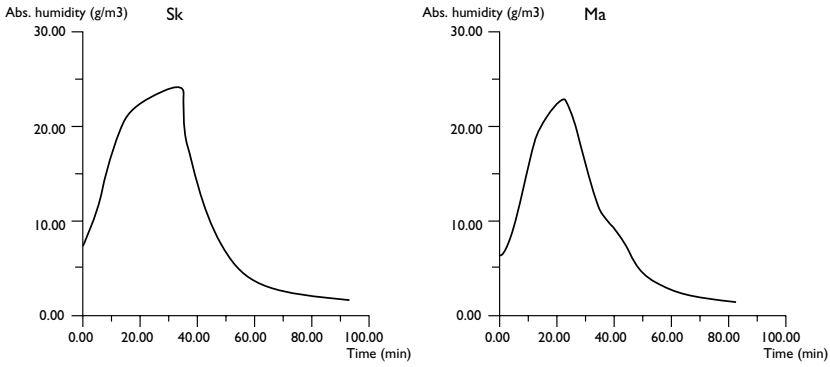

Figure 8.5 Desorption curves of Czech smectite-rich clays (Skalná – Sk and Maršov – Ma deposits).

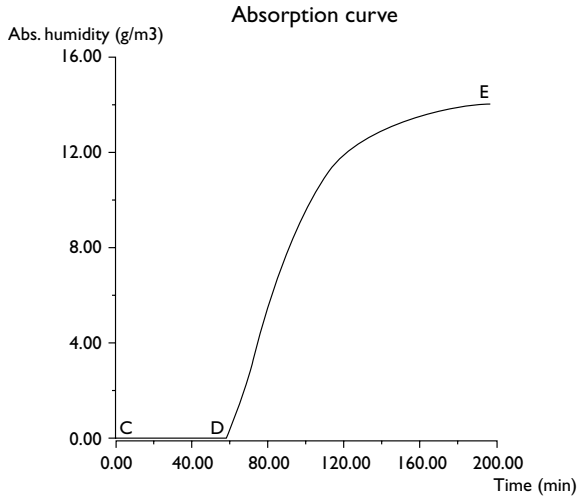

Figure 8.6 Absorption curve of smectite-rich clay material.

samples mainly to the clay particle interlayer and forming hydrate shells (Figure 8.6). After reaching point D, the humidity reaches maximal value (point E) that is equal to the input value. Absorption curves of Czech clays are plotted in Figures 8.7 and 8.8. Absorption curves of standard (Ca-Mg montmorillonite STx-1) and of studied samples showed similar trends. The difference in the length of C-D interval is explained by variable content of clay minerals, mainly smectites.

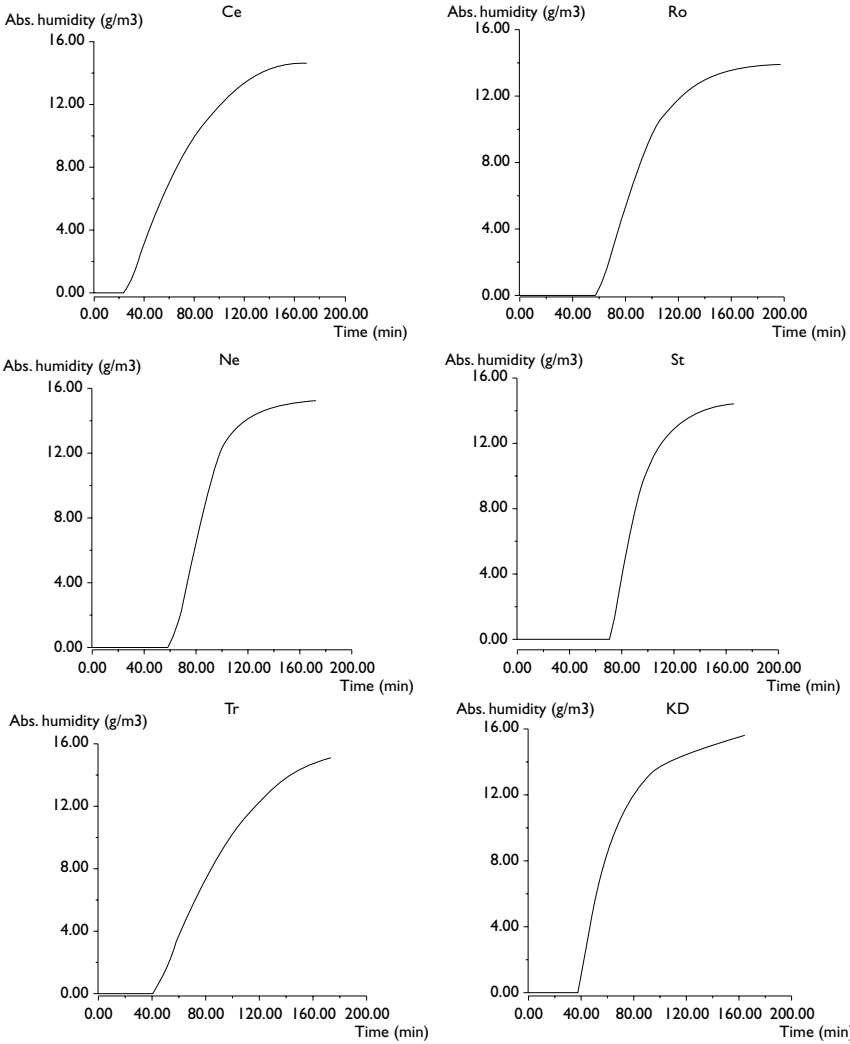

Figure 8.7 Absorption curves of Czech bentonites (Černý vrch – Ce, Rokle – Ro, Nepomyšl – Ne, Stránce – St, Třebušice – Tr, and Krásný Dvůr – KD deposits).

Dilatation

Dilatation experiments evaluated the swelling ability of studied clay samples (Figures 8.9–8.11). Dilatation curves showed a nonlinear increase with time that corresponded to the water humidity from the passing gas (Figure 8.8). The ability to dilate depends on the water humidity sorption to the surface and into the interlayer of clay minerals. The maximum

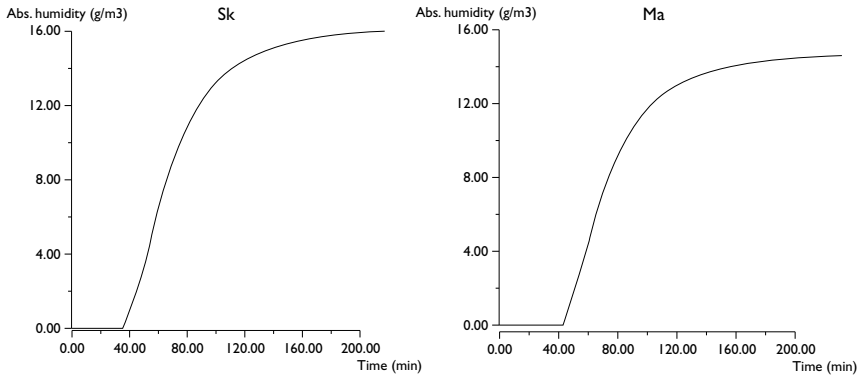

Figure 8.8 Absorption curves of Czech smectite-rich clays (Skalná – Sk and Maršov – Ma deposits).

dilatation at point B was reached when the interlayer of clay minerals was totally filled with hydrate shells.

Correlation of experimental data with other parameters

The principal parameters of desorption, absorption, and dilatation experiments (Table 8.2) were further evaluated in order to find possible explanations for the samples' behavior. The highest correlation (0.90213) was found for dilatation and smectite content. This relationship is, however, more complex due to diverse swelling capacity of minerals from the smectite group.

The ability to dilate (swell) is significantly lower for bentonites composed of montmorillonite with Ca^{2+} (Mg^{2+}) exchangeable cations than for bentonites containing montmorillonite with Na^{+} exchangeable cation. The difference can be explained by the following:

1 The different abilities to form shells of water molecules for Na^{+} and Ca^{2+} (Mg^{2+}), and consequently the different arrangements of cations and water molecules in the structure of the interlayer (Weiss *et al*., 1997).
2 The different negative charges for montmorillonite with Ca^{2+} (Mg^{2+}) exchangeable cations and for montmorillonite with Na^{+} exchangeable cation. Swelling ability of dioctahedral smectite increases with decreasing octahedral negative charge (Kawano and Tomita, 1991).

Low dilatation values of Krásný Dvůr bentonites are probably caused by the presence of mixed-layer structures in this clay material. Illite-smectite interlayering deteriorates the ability to dilate (Hanus *et al*., 2004) and decreases swelling pressure (Pusch and Kasbohm, 2002).

Absorption experiments confirmed the anticipated correlation between the smectite content and C-D interval in the absorption curve (Table 8.2). Sedimentary clays (Skalná, Maršov) showed higher values (31.79 and 42.80 g/cm^3) that can be interpreted as a result of water sorption to organic complexes of iron (Pechenyuk *et al*., 2003).

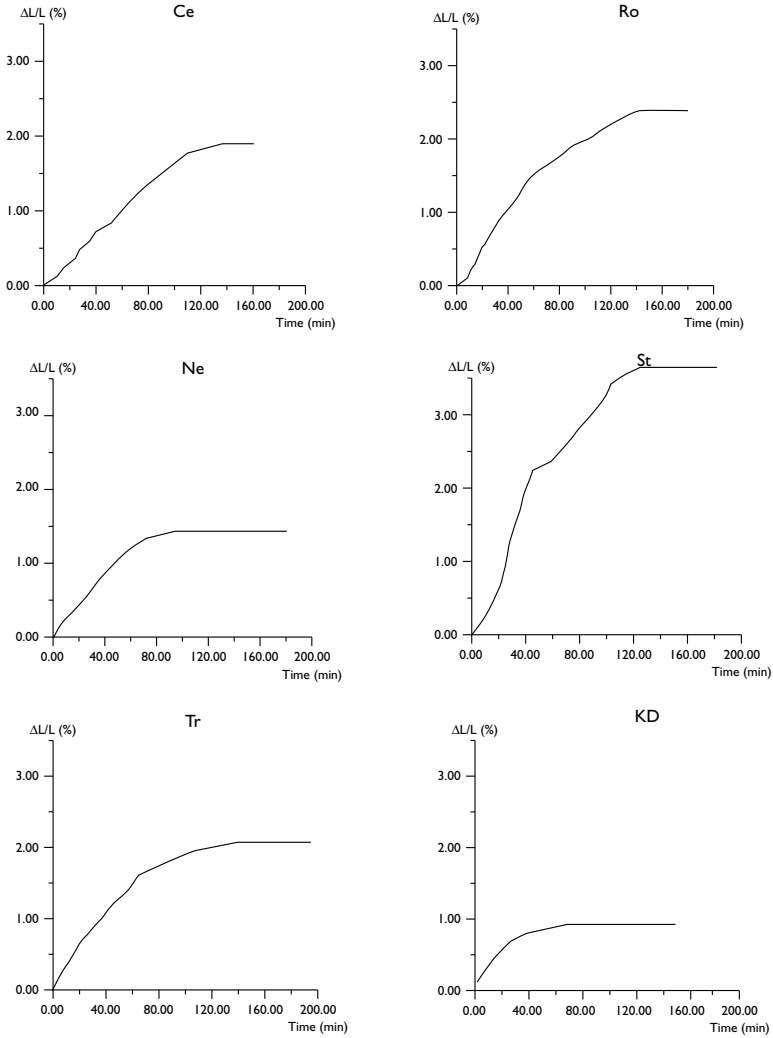

Figure 8.9 Dilatation curves of Czech bentonites (Černý vrch – Ce, Rokle – Ro, Nepomyšl – Ne, Stránce – St, Třebušice – Tr, and Krásný Dvůr – KD deposits).

Conclusions

The behavior of clay materials in the presence of water humidity can be estimated using water sorption and dilatation measurements. Measured parameters satisfactorily correlated to the smectite content (regression coefficient R-squared = 0.90). Experimental studies confirmed

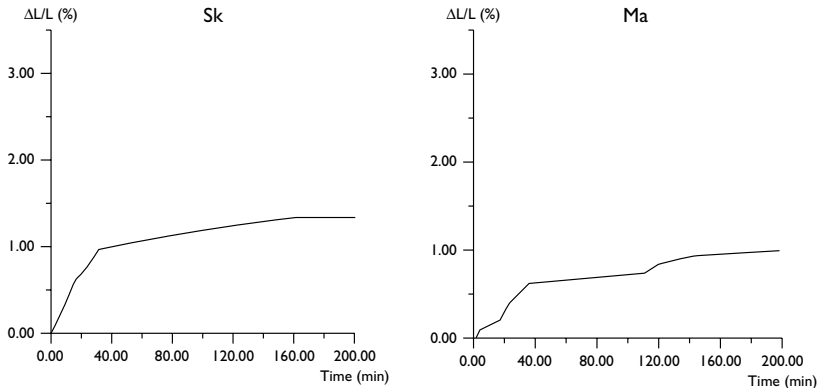

Figure 8.10 Dilatation curves of Czech smectite-rich clays (Skalná – Sk and Maršov – Ma deposits).

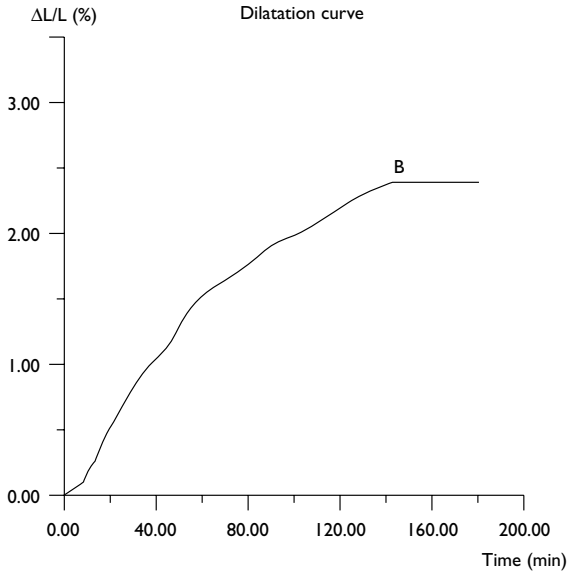

Figure 8.11 Dilatation curves of smectite-rich clay material.

the anticipated decrease in dilatation ability of Czech sedimentary montmorillonite-rich clays that can be explained by lower swelling component content (smectite group minerals). Different genetic types revealed different behavior during desorption/absorption cycles. Higher values of absorption, desorption, and dilatation were recorded for bentonites with

Table 8.2. Summary of principal parameters obtained from desorption, absorption, and dilatation experiments

Locality/sample	*Desorption (g/cm³) (point A)*	*Dilatation (%) (point B)*	*Absorption (g/cm³) (C-D interval)*
Rokle (Ro)	24.2	2.4	58.33
Černý vrch (Ce)	23.7	1.8	23.53
Nepomyšl (Ne)	21.1	1.5	38.55
Krásný Dvůr (KD)	18.6	1.0	36.54
Třebušice (Tr)	21.4	1.8	59.15
Stránce (St)	25.7	3.3	70.07
Skalná (Sk)	23.7	1.2	31.79
Maršov (Ma)	22.7	1.1	42.80
Ca-Mg montmorillonite (STx-1)	26.8	3.2	95.02

several exceptions, which can be interpreted as a result of illite–smectite interlayering and water sorption to organic complexes of iron.

Acknowledgments

Financial support was provided by a grant from GAČR No. 104/02/1464. Special thanks are given to Dr Libor Brabec (Institute of Physical Chemistry of Jaroslav Heyrovský, Academy of Sciences of the Czech Republic) for his assistance in sorption theory and helpful discussion. RAWRA kindly allowed publication of results obtained during the project "Verification of substitution of bentonites by montmorillonitic clays" (contract No. 10/2002/Wol).

References

Bogoslovskaya, N.S., Ustinova, E.A., and Seballo, A.A., 1987. Dynamics of water desorption from a zeolite by a heated stream of inert gas. *Journal of Applied Chemistry of the USSR*, 60 (12): 2479–2483.

Franče, J., 1992. Bentonites in the eastern part of the Doupovské hory Mts. *Sbor. Geol. Věd, ložisk – geol., miner*. 30, 43–90 (In Czech with English summary).

Hanus, R., Kolaříková, I., Brabec, L., Kočiřík, M., Přikryl, R., Jelínek, E., and Zikánová, A., 2005. Simultaneous sorption and dilatation measurements on raw smectite-rich materials. *Chemical Papers* (In Czech with English summary), 99, 246–249.

Hunger, B., Matysik, S., Heuchel, M., Geidel, E., and Toufar, H., 1997. Adsorption of water on zeolites of different types. *Journal of Thermal Analysis*, 49 (1): 553–565.

Kawano, M. and Tomita, K., 1991. X-ray powder diffraction studies on the rehydration properties of beidelite. *Clays and Clay Minerals*, 39: 77–83.

Klika, Z. and Weiss, Z., 1993. CQPA, Program for Chemical Quantitative Phase Analysis, Central Analytical Laboratory, Technical University of Mining and Metallurgy, Ostrava.

Komine, H., 2004. Simplified evaluation for swelling characteristics of bentonites. *Engineering Geology*, 71: 265–279.

Komine, H. and Ogata, N., 2004. Predicting swelling characteristics of bentonites. *Journal of Geotechnical and Geoenvironmental Engineering*, 130 (8): 818–829.

Pechenyuk, S.I., Mikhailova, N.L. and Kuzmich, L.F., 2003. Physicochemical study of iron (III), chromium (III) and indium oxohydroxide xerogels. *Russian journal of inorganic chemistry*, 48 (8): 1136–1146.

Pimentel, E., 2003. Swelling behaviour of sedimentary rocks under consideration of micromechanical aspects and its consequences on structure design. In Natan, O., Fecker, E. and Pimentel, E. (eds), *Geotechnical Measurements and Modelling*. Swets & Zeitlinger, Lisse, pp. 367–374.

Pusch, R. and Kasbohm, J., 2002. Alteration of MX-80 by hydrothermal treatment under high salt content conditions. *Technical report TR-02–06*, SKB, Stockholm.

Siriwardane, R.V., Shen, M.S. and Fisher, E.P., 2003. Adsorption of CO_2, N_2, and O_2 on natural zeolites. *Energy and Fuels*, 17 (3): 571–576.

Weiss, Z., Chmielová, M., Buchal, A., Bílková, L., Rieder, M., 1997. Dehydration and rehydration of montmorillonite from Ivančice (Czech Republic). *Geologica Carpathica* 6 (2): 91–96.

Part 3

Swelling potential measurement

Chapter 9

ESEM–DIA method to estimate swelling–shrinkage of raw and cation-saturated bentonite

German Montes-Hernandez[1]

Summary

Swelling clays have been proposed as engineered barriers in geological disposal systems for waste because these materials build a better impermeable zone by swelling. However, swelling potential of soils is also considered as a most prevalent cause of damage to buildings and constructions. For these reasons, it is fundamental to investigate the physical–chemical and mechanical behavior of swelling clays. In the current study, the swelling–shrinkage potential (aggregates scale) was estimated by using an environmental scanning electron microscope (ESEM) coupled with a digital images analysis (DIA) program (Visilog). The isolated aggregates of raw and cation-exchanged bentonite were directly observed at different relative humidities in an ESEM chamber. "Visilog" software was used to estimate the percent augmentation of the aggregate surface as a function of relative humidity. This estimation allows for the calculation of the swelling–shrinkage potential (%) of bentonite. The results showed that ESEM–DIA coupling can be a powerful method for estimating the swelling–shrinkage potential of expansive clays. This potential is governed by the relative humidity and by the nature of the interlayer cation.

Introduction

The industrial and environmental uses of clays are expanding every year. For example, it is estimated that about 8 million tons of the bentonites were used in 1992 throughout the world (Murray, 2000). One of the principal applications for bentonite is in drilling muds. However, it is also widely used as a suspending and stabilizing agent, and as an adsorbent or clarifying agent in many industries. Recently, the swelling clays have been proposed as engineered barriers in the geological disposal systems for waste because these materials build up a better impermeable zone around wastes by swelling (Pusch, 1992; Al-Tabbaa and Aravinthan, 1998). Unfortunately, the swelling soils are also one of the nation's most prevalent causes of damage to buildings and construction. The losses include severe structural damage, cracked driveways, sidewalks, and basement floors, heaving of roads and highway structures, condemnation of buildings, and disruption of pipelines and sewer lines (Al Rawa *et al*., 1998;

[1] UMR 7517 ULP-CNRS, CGS, 1 rue Blessig, F-67084 Strasbourg, France, Fax: (33) 390240402; e-mail address: montes@illite.u-strasbg.fr; german_montes@hotmail.com

Al Rawas, 1999). For these reasons, the estimation of the swelling–shrinkage potential of expansive clays in the laboratory is very important.

The methods available for the estimation of the swelling–shrinkage potential are grouped into two categories: physico-chemical and mechanical methods. The common analytical techniques used in physico-chemical methods are the X-ray diffusion at small angles, X-ray diffraction, Scanning Transmission Electron Microscopy (STEM), and imbibition. On the other hand, the classic experimental techniques used in the mechanical methods are the consolidometer test and the soil suction test (Parcevaux, 1980; Waddah *et al*., 1999; Komine and Ogata 1994).

In the study reported in this chapter, the swelling–shrinkage potential (aggregates scale) was estimated by using an ESEM coupled with a DIA program (Visilog). The isolated aggregates of raw and cation-exchanged bentonite were directly observed at different relative humidities in an ESEM chamber. "Visilog" software was used to estimate the percent augmentation of the aggregate surface as a function of relative humidity. This estimation allows the calculation of the swelling–shrinkage potential (%) of bentonite (Montes-H, 2002; Montes-H *et al*., 2003a,b; Montes-H, 2005).

Material and methods

MX80 bentonite

MX80 bentonite contains Na/Ca-montmorillonite (80%), quartz (6%), K-feldspars (2%), plagioclases (4%), carbonates (4%), mica (3%), and other minerals (1%) (Sauzeat *et al*., 2001). Bulk sample is composed by 86.1% of particles in a size range less than 2 μm, 8.8% in the 2–50 μm range, and 5.1% for sizes larger than 50 μm (Neaman *et al*., 2003). The specific surface area of the bulk sample was estimated at 33 m^2/g ($\pm$ 1 m^2/g) by applying the Brunauer-Emmet-Teller (BET) equation and by using 16.3 $Å^2$ for a cross-sectional area of molecular nitrogen. For this estimation, a Sorptmatic 1990 instrument was used.

Sample preparation

The bulk samples of MX80 bentonite were treated separately with two concentrated solutions (1-N concentration) of sodium and calcium chlorides, both salts with the same ionic force (I = 2). Twenty grams of MX80 bentonite were dispersed into 1 L of salt solution (1N) at 60°C. This suspension was vigorously stirred with magnetic agitation for 1 hour at 60°C. Then, the cation-saturated clay was separated by centrifugation (15 minutes at 13000 rpm) and decanting the supernatant solutions. This process was repeated three times. The cation-saturated bentonite was then washed 3 to 4 times with distilled water until the $AgNO_3$ test for chloride was negative. This method was used by Seung Yeop Lee and Soo Jin Kim (2002) and Giora Rytwo (1996). The cation-saturated bentonite was subsequently dried for 48 hours at 60°C and finally ground for two minutes. Finally, the raw and cation-saturated bentonite were dried for 24 hours at 110°C and placed in the plastic desiccators (2 l) in order to keep constant the hydration state of samples by using silica gel.

ESEM

For all environmental scanning electron microscope investigations, an XL30 ESEM LaB6 (FEI and Philips) was used, with a gaseous secondary electron detector (GSED) to produce a surface image. This microscope was also equipped with a "cooling stage" to control the sample temperature. Each sample was submitted to a hydration and then respectively dehydration cycle, with progressively increasing and decreasing the relative humidity. This procedure consisted of three stages: In the drying stage, the chamber pressure and sample temperature were respectively fixed at 2.3 Torr and 50°C. In this case, the relative humidity of surrounding sample was 2.5% according to the water phase diagram. The sample was maintained at these "reference conditions" for about 15 minutes, and an image of an aggregate of interest was chosen and stored in the hard disk of the control PC.

Swelling was achieved at constant sample temperature of 9°C. Then the progressive sample hydration was performed by increasing the chamber pressure until water over-saturation of the sample was achieved. The water over-saturation of aggregates was observed between 80% and 95% relative humidity. The pressures shown in Table 9.1 were used to keep a constant relative humidity of surrounding sample in the ESEM chamber. In each step of chamber pressure an image of interest was taken after 5 minutes. This time was considered as equilibrium time and was previously estimated by kinetic manipulations.

Shrinkage was done inversely from that of swelling. Here the chamber pressure was progressively decreased until the reference conditions were reached (see Table 9.1). The sample temperature was always kept at 9°C.

DIA

Digital image analysis consisted of isolating an area of interest by Visilog 5.3 software. In this study the area of interest was always an aggregate. Generally, the ESEM images have a sufficient density contrast to isolate the area of interest by applying a simple gray level threshold. To minimize the experimental error of the surface measure, the same procedure, that is, the DIA, was applied manually five times. In addition, each analysis was visually controlled by the reconstitution of a binary image (Figure 9.1). The ESEM images of the test section occupied about 1424 × 968 pixels, and in all measurements the same gray level range "0–256" was considered.

Table 9.1 Pressures used to control the constant relative humidity of surrounding sample in the ESEM-chamber

Swelling	*Chamber pressure (Torr)*	*Relative humidity RH (%)*	*Shrinkage*
● ↓	2.6	30	↑
	3.4	40	
	4.3	50	
	5.2	60	
	6.0	70	
	6.4	75	
	6.9	80	●

Note
Constant temperature of sample = 9°C.

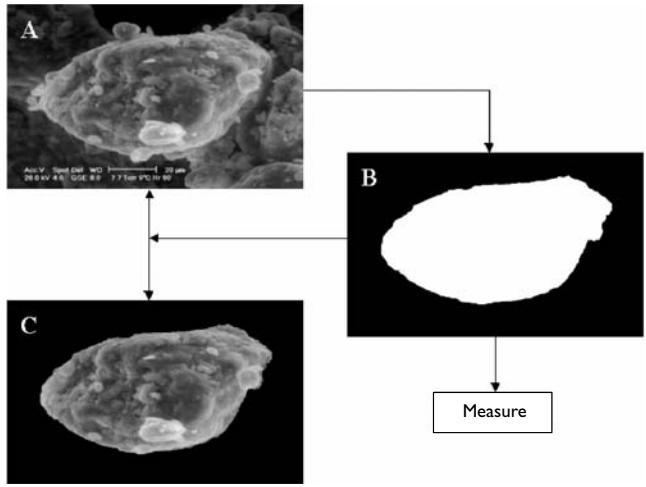

Figure 9.1 Digital image analysis methodology. (A) ESEM image; (B) Image binarization and isolation of the surface "aggregate" of interest; (C) Image reconstitution and control verification.

Source: Montes-H *et al.*, 2003a.

Results and discussion

The experimental swelling–shrinkage data were derived from DIA "bi-dimensional analysis." The results were shown as surface augmentation and/or diminution as function of relative humidity (isotherms). The swelling–shrinkage percentage was then estimated by:

$$S = \frac{S_e - S_i}{S_i} 100 \qquad [9.1]$$

where S_e represents the surface area at an "RH" equilibrium-state (μm^2) and S_i represents the initial surface area of the dry sample (μm^2). The experimental isotherms of swelling–shrinkage potential of bentonite (aggregate scale) are shown in Figure 9.2.

The average standard deviation obtained after five repeated surface area measurements was considered as an estimate of the absolute error on swelling–shrinkage:

$$E = \frac{s(\overline{q})}{S_i}(200 + S) \qquad [9.2]$$

where $s(\overline{q})$ is the average standard deviation, S_i is the initial surface, and S is the swelling–shrinkage percentage.The absolute error remained relatively low. However, the error was always more significant at low relative humidity (Figure 9.3).

The swelling–shrinkage isotherms at 9°C are shown in the Figure 9.2. It is clear that the swelling–shrinkage potential was governed by the relative humidity and by the nature of interlayer cation. For example, globally the Na-saturated bentonite presented an excellent

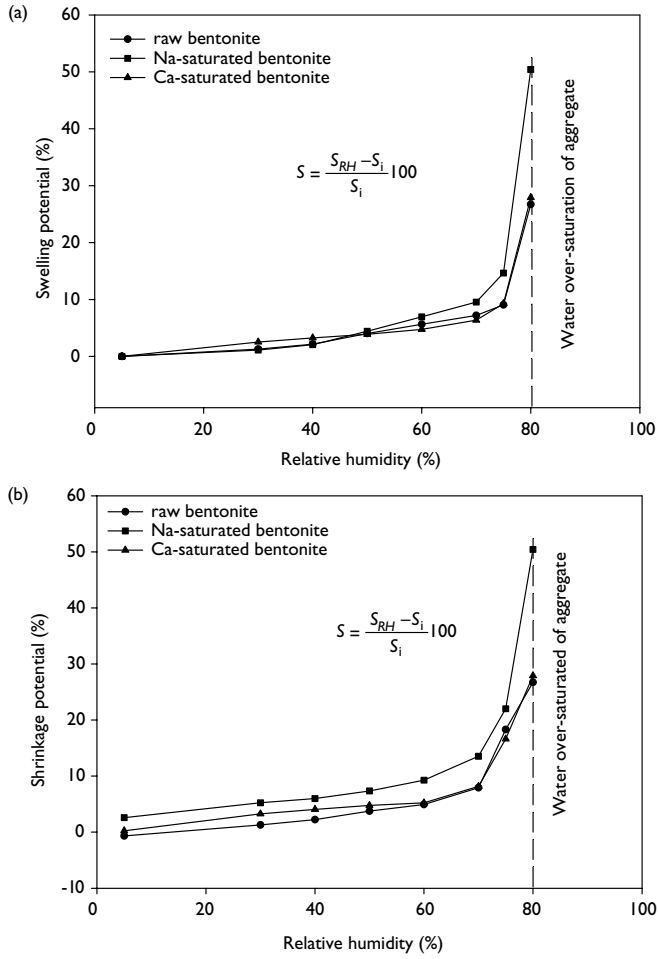

Figure 9.2 (a) Swelling potential isotherms of raw and cation-saturated bentonite by ESEM–DIA and (b) Shrinkage potential isotherms of raw and cation-saturated bentonite by ESEM–DIA.

Source: Montes-H, 2002 and 2005.

capacity to swell while the Ca-saturated bentonite swelled less significantly at high relative humidities (>0.5). The raw bentonite presented a swelling–shrinkage intermediary potential because of the montmorillonite with mixed "Na-Ca" interlayer filling.

A Cartesian correlation between the amount of adsorbed water and the swelling potential showed a nonlinear correlation (Figure 9.4). For this reason, a swelling to amount of adsorbed water ratio was calculated for low, medium, and high relative humidity (30%, 50%,

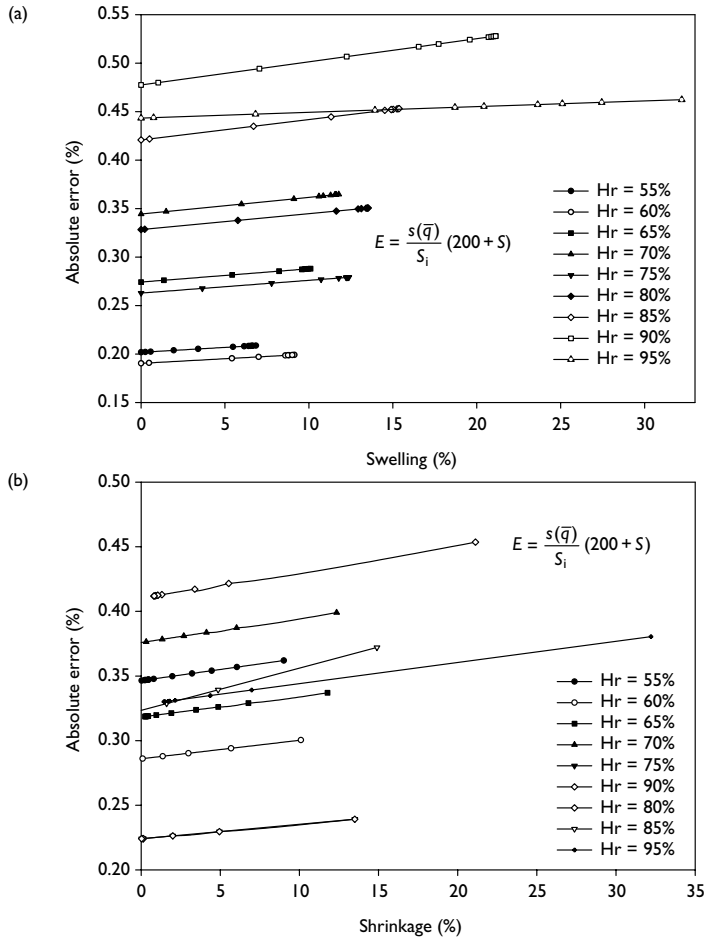

Figure 9.3 Absolute error behavior. (a) Swelling; (b) Shrinkage.
Source: Montes-H *et al.*, 2003a.

and 75% respectively) (Table 9.2). This basic approach must be considered with care because the measurements of the amount of adsorbed water and swelling potential were estimated separately by different analytical methods with different scales.

The swelling–shrinkage isotherms presented a hysteresis phenomenon similar to the water vapour adsorption–desorption isotherms, that is, a hysteresis loop with the branches approximately parallel to one another (Figure 9.5); because the samples retained a certain amount of water at low relative humidity, which can not be removed except by drying at

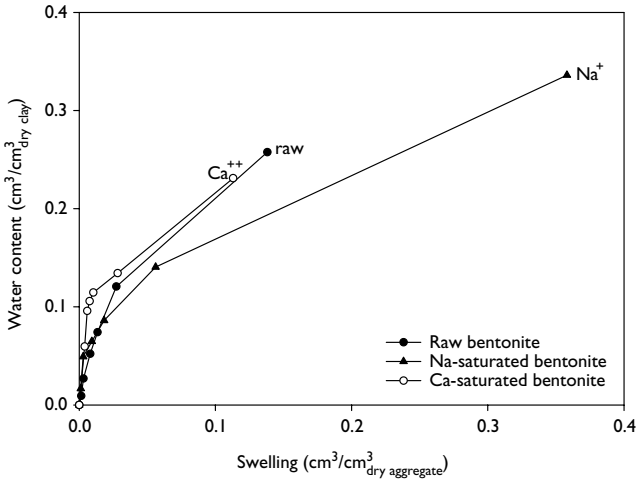

Figure 9.4 Amount of adsorbed water and swelling potential correlation for raw and cation-saturated bentonite.

Source: Montes-H 2002 and 2005.

Note

The swelling potential was considered as equidimensional to aggregate scale.

Table 9.2 The swelling-to-amount of adsorbed water ratio for low, medium, and high relative humidity

Sample	*Low (HR = 30%)*	*Medium (HR = 50%)*	*High (HR = 75%)*
MX80 raw	0.1605	0.1558	0.2260
MX80-Na	0.0715	0.1442	0.3996
MX80-Ca	0.0681	0.0730	0.2106

Source: (Montes-H 2005).

room temperature. In addition, the experimental system (ESEM–DIA) could have induced other causes of hysteresis such as the irreversible deformation produced by water over-saturation in the aggregates (Figure 9.6).

Conclusions

Our studies showed that the coupling of ESEM with DIA is a powerful method for estimating the swelling–shrinkage potential of expansive clays. The main advantage of this method is the rapidity with which one obtains the qualitative and quantitative results. However, this method allows only the estimation of the free swelling–shrinkage potential in the sample

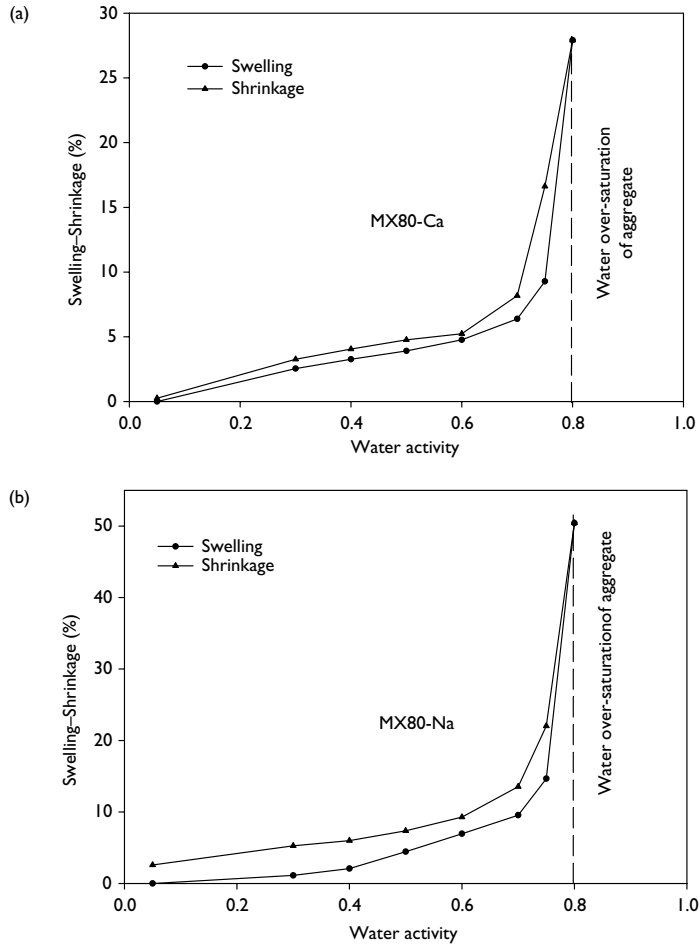

Figure 9.5 Hysteresis phenomena between swelling–shrinkage. (a) Ca-saturated bentonite "MX80-Ca"; (b) Na-saturated bentonite "MX80-Na".

Source: Montes-H *et al.*, 2003b.

Note
Water activity = Relative humidity/100.

chamber. Swelling potential is governed by the relative humidity and by the nature of the interlayer cation. For example, globally the Na-saturated bentonite presents an excellent capacity to swell while the Ca-saturated bentonite swells less significantly at high relative humidities (>0.5). The raw bentonite presents a swelling–shrinkage intermediary potential because of the montmorillonite with mixed "Na-Ca" interlayer filling.

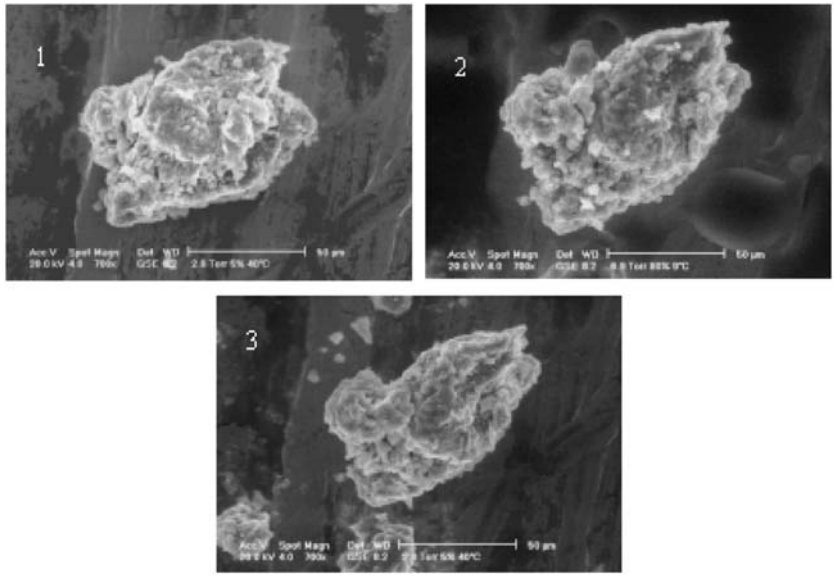

Figure 9.6 Aggregate deformation after water over-saturation. Example of Mg-saturated bentonite. (1) Initial state (*Relative humidity* = 5%); (2) Water over-saturation beginning (*Relative humidity* = 80%); (3) After water over-saturation (*Relative Humidity* = 75%).

Source: Montes-H *et al.*, 2003b.

Acknowledgments

The authors are grateful to National Council of Science and Technology (CONACYT), Mexico, and Louis Pasteur University (ULP), France, for providing a financial grant for this work.

References

Al-Rawas, A.A. (1999). The factors controlling characteristics of expansive soils and rocks in northern Oman. *Engineering Geology*, 53, 327–350.

Al-Rawas, A.A., Ingeborg Guba, and McGown, A. (1998). Geological and engineering characteristics of expansive soils and rocks in northern Oman. *Engineering Geology*, 50, 267–281.

Al-Tabbaa, A. and Aravinthan, T. (1998). Natural clay-shredded tire mixture as landfill barrier materials. *Waste Management*, 18, 9–16.

Komine, H. and Ogata, N. (1994). Experimental study of swelling characteristies of compacted pentonite. *Canadian Geotechnical Journal*, 31, 478–490.

Montes-H.G. (2002). Etude experimentale de la sorption d'eau et du gonflement des argiles par microscopie électronique à balayage environnementale (ESEM) et analyse digitale d'images. PhD Thesis, Louis Pasteur University, Strasbourg I, France, p. 161.

Montes-H.G., (2005). Swelling-Shrinkage measurements of bentonite using coupled environmental scanning electron microscopy and digital image analysis. *Journal of Colloid and Interface Science*, 284, 271–277.

Montes-H.G., Duplay J., Martinez L., and Mendoza C., (2003a). Swelling-shrinkage kinetics of MX80 bentonite. *Applied Clay Science*, 22, 279–293.

Montes-H.G., Duplay J., Martinez L., Geraud Y. and Rousset-Tournier B., (2003b). Influence of interlayer cations on the water sorption and swelling-shrinkage of MX80 bentonite. *Applied Clay Science*, 23, 309–321.

Murray, H.H. (2000). Traditional and new applications for kaolin, smectite and palygorskite: a general overview. *Applied Clay Science*, 17, 207–221.

Neaman, A., Pelletier, M., and Villieras, F., (2003). The effects of exchanged cations, compression, heating and hydration on the textural properties of bulk bentonite and its corresponding purified montmorillonite. *Applied Clay Science*, 22, 153–168.

Parcevaux, P. (1980). Etude microscopique et macroscopique du gonflement des sols argileux. PhD Thesis, Pierre et Marie Curie University, Paris VI, 1980, p. 266

Pusch, R. (1992). Use of bentonite for isolation of radioactive waste products. *Clay Minerals*, 27, 353–361.

Rytwo, G. (1996). Exchange reactions in the Ca-Mg-Na-Montmorillonite system. *Clays Clay Minerals*, 44 (2), 276–285.

Sauzeat, E., Guillaume, D., Neaman, A., Dubessy, J., François, M., Pfeiffert, C., Pelletier, M., Ruch, R., Barres, O., Yvon, J., Villéras, F. et Cathelineau, M. (2001). Caractérisation minéralogique, cristallochimique et textutale de l'argile MX80. Technical Rapport ANDRA No. CRP0ENG 01-001, p. 82.

Seung Yeop Lee and Soo Jin Kim (2002). Delamination behavior of silicate layer by adsorption of cation surfactants. *Journal of Colloid and Interface Science*, 248, 231–238.

Waddah S. Abdullah, Khalid A. Alshibli, and Mohammed S. Al-Zou'bi (1999). Influence of pore water chemistry on the swelling behavior of compacted clays. *Applied Clay Science* 15, 447–462.

Chapter 10

Effect of remolding techniques on soil swelling and shear strength properties

Mousa F. Attom,[1] *Majed M. Abu-Zreig,*[2] *and Mohammed Taleb Obaidat*[3]

Summary

This chapter presents the results of the effect of remolding methods on soil swell pressure, unconfined compressive strength, and swell potential of three types of undisturbed and disturbed soil samples. Disturbed soil specimens were prepared using dynamic remolding, static remolding, and kneading remolding. Swell potential, swelling pressure, and unconfined compression tests were conducted on identical samples remolded by different methods having similar initial conditions to the undisturbed samples. Another set of experiments was also conducted to examine the influence of initial water content on soil swell pressure and unconfined compressive strength under different remolding techniques. Results indicated that the undisturbed samples have the highest swell pressure and swell potential values followed by dynamic remolding, while kneading remolding gave the lowest values for the three types of soil. For the same types of soils, it has been found that the swell pressures of the undisturbed samples were a factor of 1.5, 1.96, and 3.07 higher than that for the dynamic, static, and kneading remolding, respectively. Similar trends were obtained with regard to unconfined compressive strength and swell potential. The unconfined compressive strengths of the undisturbed samples were a factor of 1.35, 1.6, and 2.53 higher than soil strength obtained by dynamic, static, and kneading remolding, respectively.

Introduction

Evaluation of soil physical properties is considered as the first and the most vital step in civil engineering work. Disturbed and undisturbed samples are usually obtained and tested as part of the design of many engineering projects such as foundations, slope stability, retaining structures, and highways. However, laboratory results obtained from disturbed and undisturbed samples are highly variable and may not represent the actual soil behavior as field conditions. Undisturbed samples are obtained from the field keeping soil structure unchanged, whereas disturbed samples are obtained in batches without any consideration to soil structure. Although applications of laboratory testing to field conditions are

[1] Department of Civil Engineering, Jordan University of Science and Technology, Irbid – Jordan.
[2] Department of Agricultural Engineering, Jordan University of Science and Technology, Irbid – Jordan.
[3] Department of Civil Engineering, Jordan University of Science and Technology (J.U.S.T.), Irbid – Jordan, Phone: 00–962–2–250222; 00–962–2–295111 Ext. 2125 or 2139, Fax: 00–962–2-250222; 00–962–2– 295018, e-mail: mobaidat@just.edu.just (corresponding author).

questionable, results obtained from undisturbed soil samples can be the closest to the in situ behavior of soil with similar loading and field conditions. However, due to sampling, transportation, and trimming, significant changes to the structure of soil specimens might occur. These changes in soil structure may cause soil specimens to behave in a way similar to that of disturbed or remolded samples.

Much work has been done on the effect of disturbance on soil properties and the changes to soil structure associated with it (Schmertmann, 1955; Ladd and Lambe, 1963; Skempton and Sowa, 1963; Murray, 2000; Neaman *et al.*, 2003; Montes-H, 2005). Remolded samples are considered as disturbed samples prepared in the laboratory. Most of the clay deposits showed a reduction in strength when they remolded in comparison to the undisturbed condition. The strength reduction of saturated clay is expressed in the term of sensitivity which is the ratio of $S_{u(undisturbed)}$ to the $S_{u(remolded)}$ (Das, 1983). This can be explained by the breakdown of the natural original structure of the soil and thixotropy phenomenon. The strength of undisturbed samples of clay increases as a result of a long time-dependent process. Remolding samples soften due to disturbance and will regain their original strength when allowed to rest for a long time (Seed and Chan, 1959). Other clayey soils regain only a partial portion of their original strength. Lambe (1979) mentioned that for Kawasaki clay the laboratory measured stress was almost one-third of that for perfect undisturbed samples. The undrained unconfined compressive strength for disturbed sample was around 40% of the in situ value.

Evaluation of soil characteristics under laboratory experiments is not only affected by the status of the sample, disturbed or remolded, but also by the initial conditions and method of preparation (Rao *et al.*, 1989; Basma *et al.*, 1994). In fact, the engineering properties of clay soil including swell potential and unconfined compressive strength are highly affected by method of drying under laboratory conditions (Basma *et al.*, 1994). Evaluation of soil swell pressure and swell potential requires remolding of undisturbed soil samples before experimentation. Soil samples can be remolded by different methods such as dynamic, static, and kneading remolding. The standard procedure of remolding methods can be found in the American Standard for Testing and Materials (ASTM). Many researchers indicated that remolding methods have major effects on the measurements of soil properties under laboratory conditions (Ogwa, 1995; Attom, 1997). Ogwa (1995) reported that the duration of the remolding process significantly affected soil plastic and liquid limits. Attom (1997) showed that the level of compaction during remolding has a major impact on soil swelling, unconfined shear strength, and permeability.

The main objective of this chapter was to study the influence of remolding method on the evaluation of soil swell pressure, swell potential, and unconfined compressive strength of disturbed samples in comparison with undisturbed soils.

Experimental

Three types of soils were selected from the northern part of Jordan, with a wide range of clay contents. The physical properties of these soils including gradation, plastic and liquid limits, specific gravity, maximum dry unit weight, and optimum water content were obtained in accordance with ASTM (Table 10.1). Disturbed and undisturbed soil samples were obtained from the same locations and tested in the Soil Mechanics Laboratory at Jordan University of Science and Technology. The physical properties of undisturbed soil samples are also shown in Table 10.1.

Table 10.1 Physical properties of soils used in study

Properties	*Unit*	*Soil-1*	*Soil-2*	*Soil-3*
Gradation				
Sand (2 mm–75 μm)	%	13	20	22
Silt (75 μm–2 μm)	%	16	21	28
Clay (less than 2 μm)	%	70	56	45
Consistancy limits				
Liquid limit	%	71	63	43
Plastic limit	%	32	37	24
Plastic index	%	39	26	19
Clay activity	Unitless	0.56	0.46	0.42
Compaction				
Optimum water content	%	31	26	23
Maximum dry density	kN/m^3	13.2	13.9	14.6
Specific gravity	Unitless	2.67	2.65	2.65
Physical properties of undisturbed soil samples				
Initial dry density	kN/m^3	14.1	14.6	15.1
Initial water content	%	24	22	20
Unified soil classification		CH	MH	CL

Remolded specimens were prepared for both unconfined compression and swelling tests using three types of remolding techniques: dynamic, static, and kneading remolding. The initial conditions of the disturbed samples were kept identical to the undisturbed samples, as shown in Table 10.2. Soil samples remolded by the dynamic method were prepared using the standard mold of the proctor density test modified procedure. Static and kneading remolded samples were directly prepared using the corresponding standard mold for each test.

Sample preparation for unconfined compression test

For dynamic remolding, soil specimens were prepared using the modified compaction test mold at 5 layers, 25 blows for each layer. To achieve a similar initial water content and density to the undisturbed sample, a predetermined amount of water was mixed thoroughly with the soil and compacted in the proctor test mold. After that a standard unconfined compression mold was pushed into the compacted soils. Soil specimens were then extruded from the unconfined compression mold by using a soil ejector device and wrapped carefully in a plastic cover to prevent any moisture loss.

For the static and kneading remolding, soil samples with similar initial conditions to the undisturbed soil were prepared by using the standard unconfined compression mold. Soil specimens were then extracted from the standard unconfined compression test mold using the ejector device and wrapped carefully with a plastic cover. The unconfined compressive test was conducted in accordance with ASTM D-2166 standard procedure.

Sample preparation for swelling test

In this test, the disturbed soil was compacted in accordance with the modified compaction test (ASTM D-1557) at an initial density and water content similar to that of undisturbed

Table 10.2 Detailed testing program

Soil series	*Type of test*	*Condition of experimental test*						
		Undisturbed	*Remolding with soil initial properties identical to undisturbed sample*			*Remolding at 13 kN/m³ with various initial water content*		
			Dynamic remolding	*Static remolding*	*Kneading remolding*	*Dynamic remolding*	*Static remolding*	*Kneading remolding*
Soil-1	Unconfined compression	*	*	*	*	4 water contents	4 water contents	* 4 water contents
	Swelling pressure	*	*	*	*	* 5 water contents	* 5 water contents	* 5 water contents
	Swell potential	*	*	*	*	No test	No test	No test
Soil-2	Unconfined compression	*	*	*	*	* 4 water contents	* 4 water contents	* 4 water contents
	Swelling pressure	*	*	*	*	* 5 water contents	* 5 water contents	* 5 water contents
	Swell potential	*	*	*	*	No test	No test	No test
Soil-3	Unconfined compression	*	*	*	*	* 4 water contents	* 4 water contents	* 4 water contents
	Swelling pressure	*	*	*	*	* 5 water contents	* 5 water contents	* 5 water contents
	Swell potential	*	*	*	*	No test	No test	No test

Note
* Tested.

samples. After compaction, soil specimens were obtained by pushing the consolidometer ring inside the compaction mold to extrude the sample. The sample was then trimmed inside the consolidometer ring and wrapped immediately to prevent any moisture loss. For static and kneading remolding soil samples were prepared using a standard consolidometer ring. The soil specimens inside the ring were wrapped carefully with a plastic cover to prevent moisture losses and tested in accordance to ASTM D-4546.

Other sets of unconfined compression and swelling experiments were conducted using remolded soil samples at 13 kN/m^3 initial dry density. In those tests the initial water contents of soil samples were varied from 10% to 30%. All samples were tested in accordance with ASTM standard procedures. The testing program for this study is shown in Table 10.2.

Unconfined compression test

Both undisturbed and remolded specimens for this test were subjected to a strain rate of 1.5 mm/min. Deformations due to the applied load were recorded at different levels of loading using a convenient increment. The 16% strain or peak stress in the stress–strain relation, whichever occurred first, was defined as the undrained unconfined compressive strength of the soil.

Zero swell test

Zero swell tests were conducted in this study to evaluate the swelling pressure as affected by types of remolding. Swelling pressure according to this test was defined as the final pressure that prevents a soil sample from expansion. Soil specimens were placed in the standard consolidation cell after being extruded from the compaction mold and water was added. With an initial seating load of 6.9 kPa, soil expansion due to the addition of water would be ceased by applying small convenient load increments throughout the swelling process until no further swelling occurred. The swelling pressure was defined as the total weight of all load increments that prevented soil expansion, divided by the cross-sectional area of the specimen.

Swell potential test

Both undisturbed and remolded samples were subjected to swell potential test. A standard one-dimensional consolidometer device was used for this test. The swell potential was defined as the swell percent of saturated soil sample under an applied pressure of 7 kN/m^3 on the tested sample. The ratio of the maximum swell height of a soil sample to the initial height of the sample was defined as the swell potential of the soil.

Results and discussion

The compaction curves and particle size distributions of soils used in this study are shown in Figures 10.1 and 10.2 respectively. Soil-1 had the lowest dry unit weight of 13.2 kN/m^3 and consequently the highest plasticity index of 39 (Table 10.1). Soil-3 had the highest dry unit weight of 14.6 kN/m^3 and the lowest plasticity index of 19%. Consequently the clay content decreased from 70% for Soil-1 to only 45% for Soil-3.

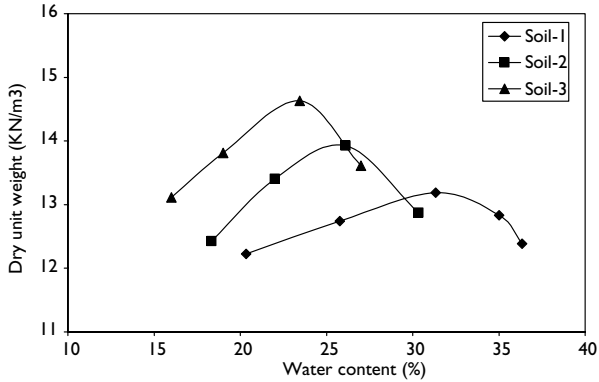

Figure 10.1 Compaction curves for the three soils used.

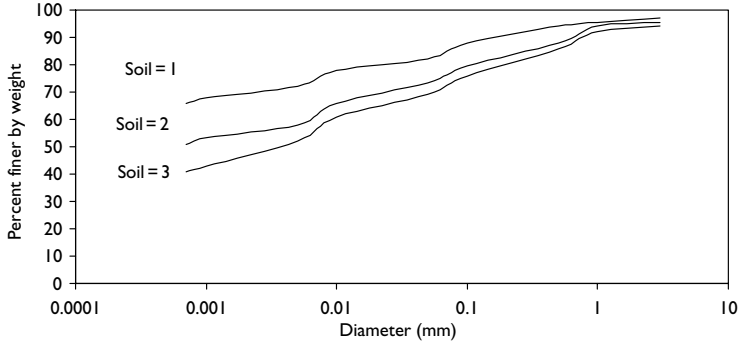

Figure 10.2 Particle size distribution curves for the soils used.

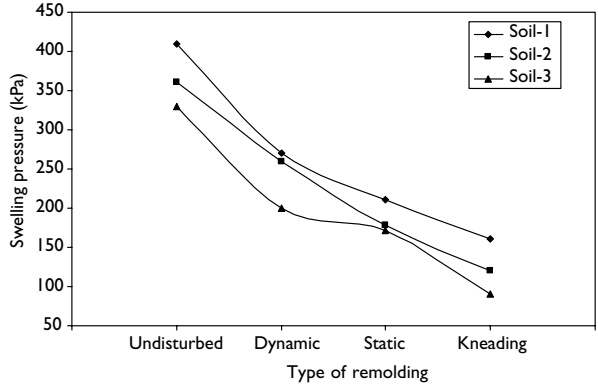

Figure 10.3 Comparison between undisturbed samples and three remolding techniques in evaluating swelling pressure.

The effects of type of remolding in comparison to undisturbed soil on swelling pressure, unconfined compression strength, and final swell percent for all soils are shown in Figures 10.3, 10.4, and 10.5, respectively. Figures 10.6 through 10.8 show the influence of initial water content on the swelling pressure of the Soils 1, 2, and 3 for various types of remolding. The corresponding results for the unconfined compression strength as affected by the initial water content and remolding techniques are shown in Figures 10.9, 10.10, and 10.11 for Soils 1, 2, and 3, respectively.

Results indicated that undisturbed soil samples had the highest swell pressure, unconfined compression strength, and swell percent for all soils compared to disturbed soil samples

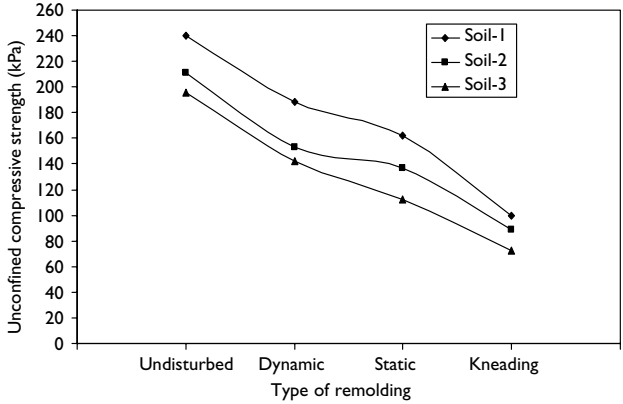

Figure 10.4 Comparison between undisturbed samples and three remolding techniques in evaluating unconfined compressive strength.

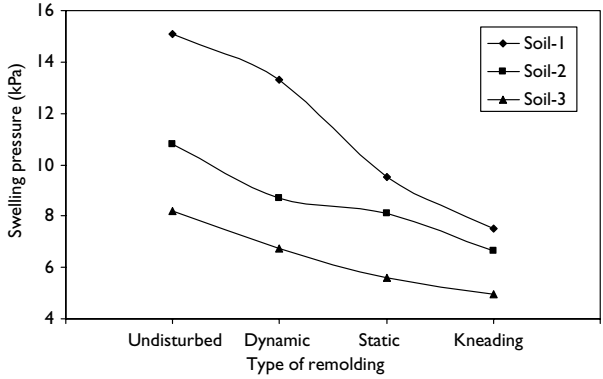

Figure 10.5 Comparison between undisturbed samples and three remolding techniques in evaluating swelling potential.

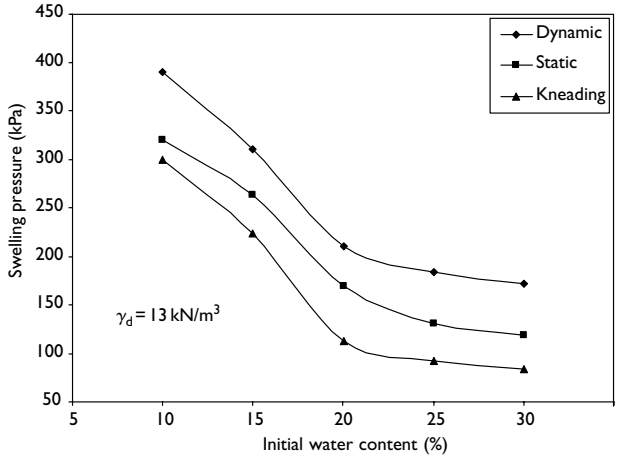

Figure 10.6 The effect of initial water content on swelling pressure as remolded by three methods for Soil-1.

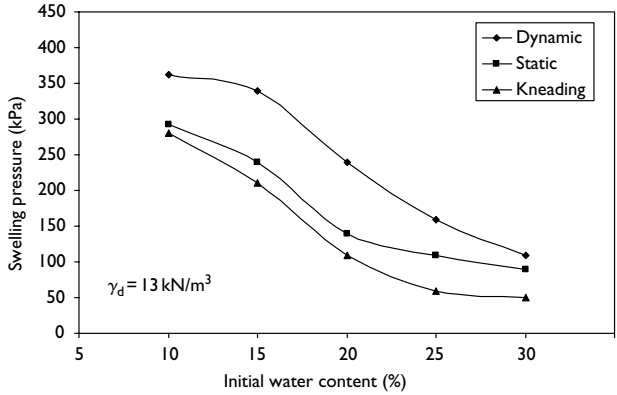

Figure 10.7 The effect of initial water content on swelling pressure as remolded by three methods for Soil-2.

(Figures 10.3 through 10.5). Among samples, dynamic remolding gave the highest swell pressure, compression strength, and swell percent and seemed to decrease steadily for static remolding followed by kneading remolding. The reason behind that can be explained due to the fact that the soil particles in the undisturbed condition had been sediment and formed for a very long period of time. This long time allowed the soil particles to rest, to be

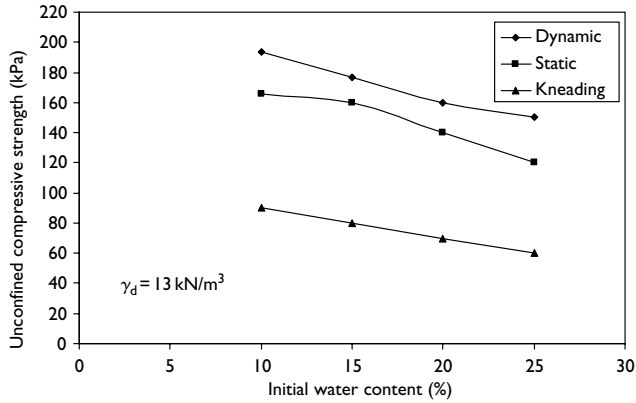

Figure 10.8 The effect of initial water content on swelling pressure as remolded by three methods for Soil-3.

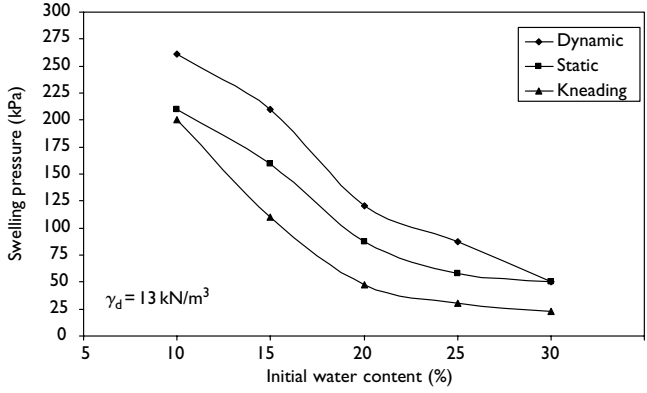

Figure 10.9 The effect of initial water content on unconfined compressive strength as remolded by three methods for Soil-1.

cemented and to harden, resulting in a higher strength. This phenomenon is called thixotropy. In the undisturbed samples, the soil particles were very close together due to the slow rate of sedimentation and compaction. The compacted structure of the undisturbed soil resulted in higher swell pressure and swell potential. The impact of remolding technique on soil behavior appeared to be much more important than soil type (Figures 10.3 through 10.6).

The average swell pressure for undisturbed samples for all soils was 3.5 kg/cm^2 and decreased to 2.2, 1.7, and 1.1 kg/cm^2 for dynamic, static, and kneading remolding, respectively. The corresponding figures for the unconfined compression strength were

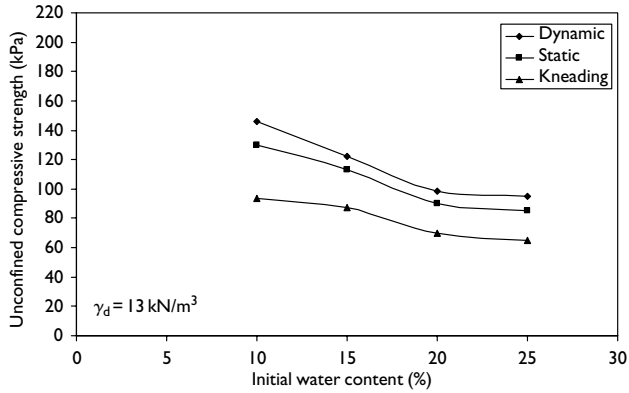

Figure 10.10 The effect of initial water content on unconfined compressive strength as remolded by three methods for Soil-2.

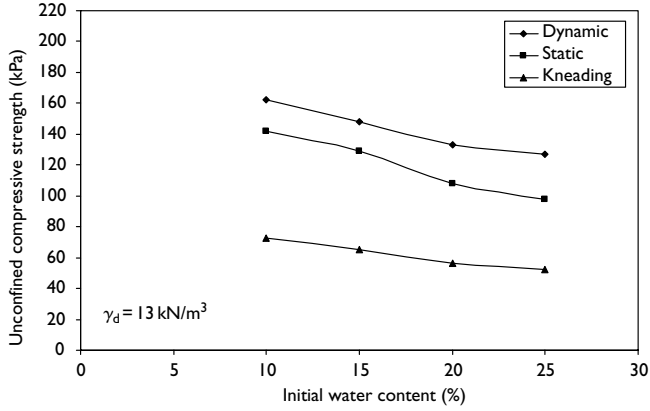

Figure 10.11 The effect of initial water content on unconfined compressive strength as remolded by three methods for Soil-3.

210, 160, 120, and 80 kPa for undisturbed, dynamic, static, and kneading remolded samples, respectively. This is due to the destruction of the cemented compacted structure of the soil during remolding preparation. The swell percent of soils followed a similar trend. The percentage of swell for undisturbed sample for Soil-1 was 15% compared to only 6% for kneading remolding.

Irrespective of remolding techniques, Soil-1 had the highest swell pressure, unconfined compressive strength, and swell percent among all the soils. However, the effect of soil type was much smaller than remolding techniques except in the case of final swell percent.

Table 10.3 Ratios of swelling pressure, unconfined compression strength, and final swell percent of undisturbed soil samples to values evaluated with various remolding methods

Type of soil test	*Remolding method*		
	Dynamic	*Static*	*Kneading*
Unconfined compression strength	1.35 ± (0.05)	1.60 ± (0.11)	2.53 ± (0.14)
Final swell percent	1.16 ± (0.04)	1.42 ± (0.07)	1.72 ± (0.19)
Swelling pressure	1.51± (0.09)	1.96 ± (0.02)	3.07 ± (0.039)

The swell was 15%, 11%, and 8% for Soils 1, 2, and 3, respectively. The corresponding decrease in swell with respect to remolding type for Soil-1 was 15%, 13%, 9.5%, and 7% for undisturbed, dynamic, static, and kneading remolded samples, respectively.

The overall effect of remolded techniques compared to undisturbed soils is shown in Table 10.3. This table summarizes the rate of swell pressure, unconfined compression strength, and swell percent of the undisturbed samples to the samples remolded by different techniques. Results indicated that swelling pressure of undisturbed samples was almost 150%, 200%, and 300% of disturbed soils remolded by dynamic, static, and kneading, respectively. The corresponding results for the unconfined compressive strength were 135%, 160%, and 250%.

The impact of initial water content on swelling pressure and unconfined compression strength is very clear from Figures 10.6 through 10.10. An increase in the initial water content resulted in a major decrease in the swelling pressure and unconfined compression strength of soils. The values of swell pressure and unconfined compressive strength were always higher in the case of dynamic remolding followed by static and kneading remolding techniques, respectively, for all water contents. The soil particles which are in flocculated condition came closer together in the case of dynamic remolding than in the cases of static and kneading techniques. The average swell pressure for all soil samples at 10% water content was 3.5 compared to only 1 at 30% water content. In the case of unconfined compression strength at 10% water content, the values decreased from 200 kPa for dynamic remolding in Soil-1 to about 160 kPa at 25% water content. The figures also show that the relative decrease in swell pressure and unconfined compression strength were much higher at smaller water contents below 20% compared to higher ones (Figures 10.6 through 10.10). In the case of dynamic remolding in Soil-1, the swelling pressure decreased by 75% when the water content increased from 10% to 20%. However, the relative decrease in swelling pressure was only 10% when the water content increased to 30%.

Conclusions

The evaluation of swelling pressure, swell potential, and unconfined compressive strength was affected by the method of remolding. Undisturbed samples gave higher values of swelling pressure, swell potential and unconfined compressive strength than remolded samples. Dynamic remolding had the highest values of swelling and unconfined compressive strength followed by static and kneading remolding respectively. The initial water content affected both the swelling pressure and the unconfined compressive strength. The swelling

pressure of undisturbed samples was almost 1.5, 2, and 3 times that of disturbed soil by dynamic, static, and kneading remolding respectively. The unconfined compressive strengths of undisturbed samples were higher by a factor of 1.35, 1.6, and 2.5 in comparison to soil samples remolded by dynamic, static, and kneading processes.

References

ASTM D1266 Standard Test Method for Unconfined Compressive Strength of Cohesive Soils, Annual Book of ASTM Standards, 1985, Sec. 4, Vol. 04.08, Soil and Rock; Building Stones, American Society for Testing and Materials, Philadelphia.

ASTM D1557 Standard Test Method for Moisture–Density Relation for Soil and Soil Aggregate, Annual Book of ASTM Standards, 1985, Sec. 4, Vol. 04.08, Soil and Rock; Building Stones, American Society for Testing and Materials, Philadelphia.

Attom, M. Fayiz, 1997. The effect of compaction energy level on some engineering properties, *Applied Clay Science*, No. 12, pp. 61–72.

Basma, Adnan A., Al-Homoud, Azem S., and Al-Tabari, Emad Y., 1994, Effects of methods of drying on engineering behavior of clay, *Applied Clay Science*, Vol. 9, pp. 151–164.

Das, B.M., 1983. *Advanced Soil Mechanics*, Hemisphere Publishing Corporation, McGraw-Hill Book Company, New York, 511 pages.

Ladd, C.C. and Lambe, T.W., 1963. The Strength of "Undisturbed" Clay Determined from Undrained Tests, ASTM-NRC Symposium, Ottawa.

Lambe, T. Wiliams and Whitman, Robert V.1, 1979. *Soil Mechanics*, SI version, John Willey & Sons, Inc., New York, 553 pages.

Montes-H G., 2005. Swelling-Shrinkage measurements of bentonite using coupled environmental scanning electron microscopy and digital image analysis. *Journal of Colloid and Interface Science*, Vol. 284, pp. 271–277.

Murray H.H., 2000. Traditional and new applications for kaolin, smectite and palygorskite: a general overview. *Applied Clay Science* Vol. 17, pp. 207–221.

Neaman A., Pelletier M., and Villieras F., 2003. The effects of exchanged cations, compression, heating and hydration on the textural properties of bulk bentonite and its corresponding purified montmorillonite. *Applied Clay Science*, Vol. 22, pp. 153–168.

Ogawa, Fumiko and Kobayashi, Masaki, 1995. Influence of remolding on the liquid and plastic limits of soil, *Soils and Foundations*, Vol. 35, No. 4, pp. 115–121.

Rao, S.M., Sridharan, A., and Chandrakaran, S., 1989. Influence of drying on the liquid limit behavior of the marine clay. *Geotechnique*, Vol. 39, No. 4, pp. 715–719.

Schmertmann, J.M., 1955. The undisturbed consolidation of the clay, *Transaction of the American Society of Civil Engineers*, Vol. 120, p. 1201.

Seed, H.B. and C.K. Chan. 1959. Thixotropic characteristics of compacted clays, *Transactions of the American Society of Civil Engineers* ASCE, Vol. 124, pp. 894–916.

Skempton, A.W. and Sowa, V.A., 1963. The behavior of saturated clays during sampling and testing, *Geotechnique*, Vol. 13, No. 4, pp. 269–290.

Chapter 11

Swelling rate of expansive clay soils

Roslan Hashim[1] *and Agus Setyo Muntohar*[2]

Summary

The study of engineered expansive soils attracts the attention of researchers since this type of mixed soil is increasingly used in many geotechnical and geoenvironmental applications. This chapter studies properties such as swell and swelling pressure, rate of swell, and water adsorption. Kaolin–bentonite mix and sand–bentonite mix specimens were statically compacted and tested in a conventional oedometer apparatus for swelling determination. The results of the study showed that the mechanism of swelling followed three distinct stages: intervoid, primary, and secondary swelling. Swelling occurred since the soils adsorbed water. The rate of swelling and maximum swelling were successfully determined using a hyperbolic equation.

Introduction

Expansive soils are found in many parts of the world, especially in arid or semiarid regions, and temperate climate zones. Although expansive soils have been recognized as problematic soils, in underdeveloped countries this is often not true. Severe damage of structures, such as foundation and floor crack, roadway distress, has been reported in many countries (Daniel and Wu, 1993; Alawaji, 1999). In the 1980s, researchers turned to the study of expansive soils for other engineering purposes.

Yong *et al*. (1986) utilized expansive clay as back filling (buffer) materials for high-level nuclear waste. Other applications, such as soil barriers, landfill liners, and vertical barrier walls, have been investigated as well (Daniel and Wu, 1993; Alawaji, 1999). Furthermore, expansive soils sometimes need to be engineered to give the desired properties. The materials are often designed to give soil mixtures with properties between expansive clay fraction (commonly bentonite) and non-swelling expansive soils fraction (commonly kaolin and sand).

Previous researchers have studied swelling behavior, mechanics of swelling, and compressibility of expansive soil mixtures (Komine and Ogata, 1994; Alawaji, 1999). They assessed the effect of factors affecting swelling and compressibility of expansive soils such as initial water content and initial dry density. Sridharan and Nagaraj (1999) denoted that plastic clay

[1] Department of Civil Engineering, University of Malaya, Kuala Lumpur, Malaysia. 50603.
[2] Department of Civil Engineering, Muhammadiyah University of Yogyakarta, Yogyakarta, Indonesia. 55253. Jl. Ringroad Selatan, Taman Tirto. Tel. +62 274 387 656, Fax. +62 274 387 646, email: muntohar@umy.ac.id

under zero confining pressure will imbibe water until the water absorption capacity becomes zero and reaches an equilibrium condition. The magnitude of water adsorption will depend upon the equilibrium suction pressure in the sample, which will depend on the height of the sample above the water source. The swelling of expansive soil is strongly related to the variation in water content. It will be swelling as the water content increases. The soil–water characteristics curve is commonly used for describing the relationship between soil suction and volumetric or gravimetric water content (Alonso *et al*., 1999; Miao *et al*., 2002). However, the rate of swelling and the variation in water adsorption during swelling also has to be taken into account.

Engineered expansive soils are increasingly used in many geotechnical and geoenvironmental applications. A further understanding of the swelling mechanism and properties of this type of soil will lead to an increased confidence level. This chapter presents the results of a swelling study with mixed clay soils and also establishes a correlation for water adsorption during swelling.

Materials and methods

The soils used in this study were commercial bentonite clay, kaolin, and fine sand (Figure 11.1, Table 11.1). These soils were mixed between bentonite–kaolin and bentonite – sand to produce various specimens. Percentage of bentonite by weight was varied from 5%, 10%, 20%, and 30% for kaolin–bentonite mixtures and 10%, 30%, and 50% for sand–bentonite mixtures. The index properties of these soil samples are presented in Table 11.2 and the plasticity and potential expansiveness of soil–bentonite mixtures are illustrated in Figure 11.2.

Kaolin is predominantly comprised of silt (75.6%), whereas bentonite consists of clay (73.2%). The sand used was comprised of 35.6% coarse, 23.6% medium, and 12.3% fine size. Uniformity coefficient (Cu) and coefficient of curvature (Cc) were 9.08 and 1.19

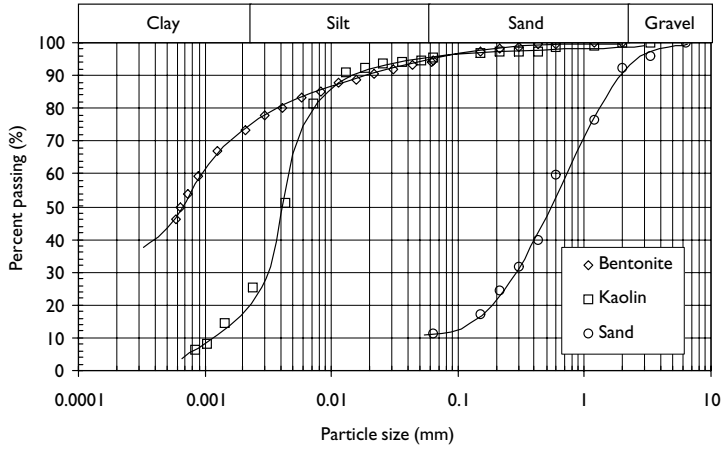

Figure 11.1 Particle size distribution of soils.

Table 11.1 Physical properties of the soil used

Soils description	*Sand (%)*	*Silt (%)*	*Clay (%)*	D_{50} *(μm)*	*LL (%)*	*PL (%)*	*LS (%)*	*Activity, PI/CF*
Bentonite[a]	5.4	2.4	73.2	0.62	307.3	45.4	17.4	3.6
Kaolin	4.3	75.6	19.9	4.1	72.3	39.8	6.6	1.6
Sand[b]	71.5	4.0	0.0	820	NP	—	—	—

Notes
NP: Non-plastic, LL: Liquid limit, PL: Plastic limit, LS: Linear shrinkage, PI: Plasticity index, CF: Clay fraction.
a Wyoming bentonite.
b Mining sand (24.5% gravel).

Table 11.2 Index properties of soil samples

Soils description	*Soil code*	*CF (%)*	*LL (%)*	*PL (%)*	*PI (%)*	*LS (%)*
Kaolin–bentonite mixtures						
5% Bentonite	KB1	26.9	76.9	39.4	37.5	7.7
10% Bentonite	KB2	30.0	89.7	42.2	47.5	12.3
20% Bentonite	KB3	32.5	106.8	44.4	62.4	13.8
30% Bentonite	KB4	39.0	121.5	43.1	78.4	14.0
Sand–bentonite mixtures						
10% Bentonite	SB1	4.0	42.9	21.1	21.8	2.4
30% Bentonite	SB2	21.7	85.1	27.2	57.9	4.3
50% Bentonite	SB3	47.0	138.3	43.2	95.1	8.8

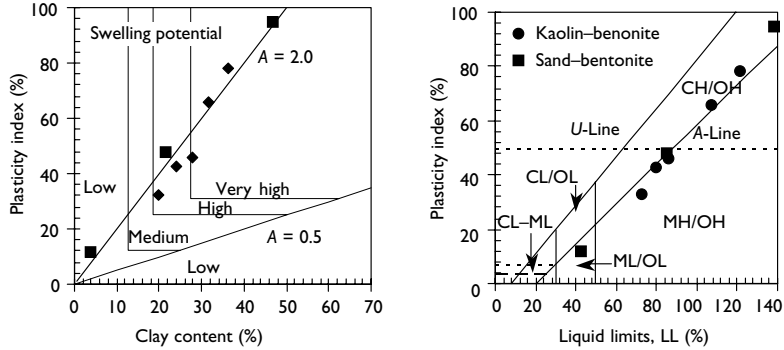

Figure 11.2 Potential expansiveness and plasticity chart of soil–bentonite mixtures.

respectively. Furthermore, the sand was classified as well-graded with gravel (SW). Muntohar and Hashim (2002) reported that the clay fraction in the kaolin–bentonite and sand–bentonite mixtures increased almost linearly with increasing bentonite content.

A conventional oedometer apparatus was used for determination of the swelling and compressibility of soil mixtures. Required quantities of soil mixtures, at optimum moisture

content, were transferred to a consolidation ring of 50 mm internal diameter and 20 mm height. All the soil mixtures were compacted statically to their maximum dry density. The specimen was positioned in the loading frame with a seating load of 3.89 kPa. The soil samples were then inundated with distilled water and allowed to swell until they reached equilibrium swelling values. At this point a standard consolidation test was conducted by applying incremental loads starting with 7 kPa and ending with 1600 kPa. The pressure required to revert the specimen to its initial height was determined as the swelling pressure.

Results and discussion

Swelling mechanism

The swell potential, in this study, was defined as the percentage swell of a laterally confined sample, which has soaked under a surcharge pressure of 3.89 kPa after being compacted to maximum density at optimum moisture content according to the compaction test. The results obtained are presented in Figure 11.3 in the form of percentage of swell versus time with varying percentage of bentonite content. The swell was expressed as a percentage increase in sample height. It was observed that for all the mixtures, an increase in swelling with log time was slow initially, increased steeply, and then reached an asymptotic value. The time required to reach an asymptotic value varied considerably, depending upon the percentage of bentonite and the type and amount of non-swelling fraction. The maximum amount of swelling generally increased with increasing bentonite content. Even at the same percentage of bentonite, considerable differences existed in the nature of the time–swell relationship. At low bentonite content, the rate of swelling was very slow with sand but increased gradually with a decrease in the particle size of the non-swelling fraction.

Figure 11.4 replots the time–swell relationship as percentage of the maximum swell. Here, the percent swell at a particular time was calculated as the ratio of amount of swell of the mixture at that time to the total swell and was denoted as a percentage. For sand–bentonite

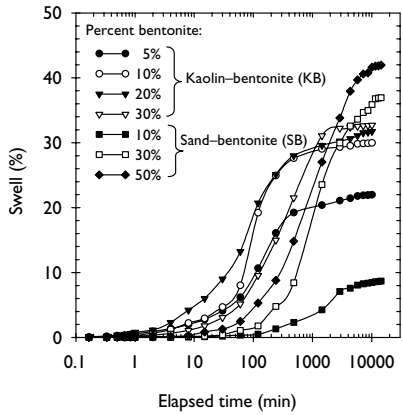

Figure 11.3 Swelling behavior (as percent of initial height) of soil–bentonite mixtures.

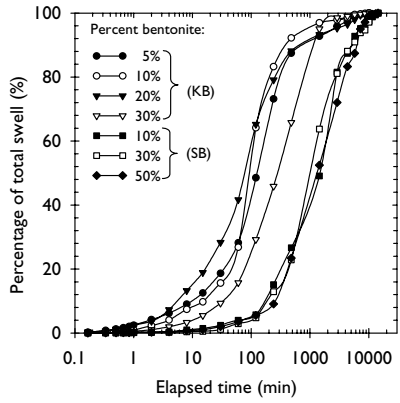

Figure 11.4 Swelling behavior (as percent of total swell) of soil–bentonite mixtures.

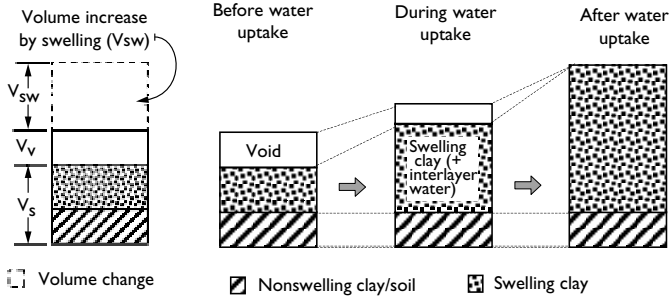

Figure 11.5 The model of swelling deformation of compacted expansive clay.

mixtures, the rate of swelling was very slow and followed a similar swell path. On the other hand, it was observed that swelling was almost complete within 1440 minutes (i.e. 24 h) for kaolin mixtures for all percentages of bentonite.

Dakshanamurthy (1978) noted two stages of swelling. In the first stage, hydration of dry clay particles, water is adsorbed in successive monolayers on the surface of montmorillonite clay. This is referred to as interlayer or intercrystalline swelling. The second phase of swelling is due to double-layer repulsion. Large volume changes accompany this stage of swelling. The sequence is illustrated in Figure 11.5. Initial swelling was generally less than 10% of the total swelling. This was essentially due to swelling of the bentonite clay particles within the voids of the coarser non-swelling fraction.

Primary swelling developed when the void could no longer accommodate further clay particle swelling. It occurred at a faster rate. After primary swelling was completed, slow continuous swelling occured. It was observed that the end of primary swelling of

kaolin–bentonite mixtures varied between 200 and 1000 minutes. In general, the increased time needed for completion of the primary swelling was associated with an increase in bentonite content. This was not observed in sand–bentonite mixtures. Furthermore, the swelling mechanism of compacted expansive clay can be illustrated by the model given in Figure 11.5. The volume of swelling clay particles, such as montmorillonite, increased by absorbing water into the interlayer of montmorillonite. The void in the compacted expansive clay was filled by this volume.

Rate of swelling and maximum swelling

Basma and Tuncer (1991) defined the rate of swelling as the time to 50% swell, t_{50s} (i.e. the time to half the full swell). This definition was adopted from theory for determination of rate of consolidation. However, it should be noted that the mechanics of swell and consolidation are totally different. Daksanamurthy (1978) proposed a hyperbolic equation to predict swelling of expansive soils as given in Equation 11.1:

$$\varepsilon = \frac{t}{(a + bt)} \tag{11.1}$$

where,

ε = axial swelling
t = time
a and b are appropriate constants.

The constants, a and b, can be obtained by means of linearizing the nonlinear curve. Typical plots of percentage vertical swelling, ε, versus time, t (Figure 11.6a), have been transformed into plots of t/ε versus t. It should be noted here that in the transformed plots in Figure 11.6b, the coordinates on both the axes have been divided by a constant time, t_0,

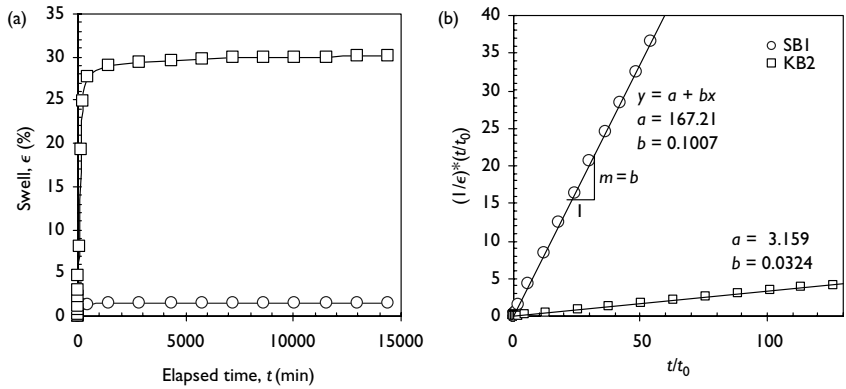

Figure 11.6 Determination of the coefficients rate of swelling.

Table 11.3 Swelling properties of expansive soils

Parameters	*Soils*						
	KB1	*KB2*	*KB3*	*KB4*	*SB1*	*SB2*	*SB3*
Coefficient rate of swell, m_s	0.0448	0.0324	0.0317	0.0293	0.1007	0.0244	0.0206
Measured swell (%)	21.92	29.96	31.75	32.65	8.68	36.96	41.96
Maximum swell (%)[a]	22.22	30.82	31.57	34.37	9.93	40.93	48.63
Error (%)	1.37	2.87	0.57	5.27	14.40	10.74	15.90

Notes
a Predicted using Equation 11.2

$$\text{Error} = \left| \frac{(\text{Maximum swell} - \text{Measured swell})}{\text{Measured swell}} \right| 100\%.$$

in order to make them dimensionless. The constants, *a* and *b*, are defined from the straight-line. Herein, *b* is the slope of the swelling path. Moreover, the rate of swelling can be known by the value of the slope, *b*, which shows the flow of swelling path. Therefore, b is then defined as coefficient of the rate of swelling. A steeper slope is a sign that the rate of swelling is smaller. The rate of swelling of SB1 soil was faster than KB1 soil (Figure 11.6b). The coefficients of the rate of swelling for each tested specimens, m_s, are presented in Table 11.3.

The maximum swelling can be also predicted using a hyperbolic equation, which is obtained from the asymptotic line of a hyperbola. It can be calculated using:

$$\varepsilon_{max} = \lim_{t \to \infty} \varepsilon(t) = \lim_{t \to \infty} \left(\frac{1}{a/t + b} \right) = \frac{1}{b} \tag{11.2}$$

Typical data presented in Table 11.3, basically, shows good agreement between the maximum swelling predicted and the maximum swelling measured over a period of 10 days. However, the observation period is inadequate to produce the maximum swelling, especially for sand–bentonite mixtures samples which show large discrepancies (i.e. errors). Meanwhile, several researchers have stated that the hyperbolic relationship is accurate for predicting maximum swelling (Dakshanamurthy, 1978; Al-Mukhtar *et al*., 1999; Waddah *et al*., 1999).

Water absorption during swell

After uptake, the compacted expansive clay can swell at a constant vertical pressure as in the swelling deformation test. Komine and Ogata (1994) found that the volume of compacted clay increased as the volume of swelling clay particles increased until the swelling pressure of the clay particles equaled the vertical pressure. Furthermore, they explained that the volume of swollen clay particles such as montmorillonite increased by absorbing water into the inter-layers of montmorillonite. The voids in the compacted expansive clay were thought to be filled by this volume increase. This did not increase the volume of the compacted expansive clays.

Based on the previous discussion and using a basic relationship on unit weight, void ratio, moisture content, and specific gravity, the water adsorption at a given time during

swell can be determined as follows:

$$\varepsilon = \frac{\Delta e}{1 + e_0} = \frac{V_v / V_s}{1 + e_0} \tag{11.3}$$

where,

$$V_v = V_w = w\, G_s \tag{11.4}$$

$$V_s = \frac{G_s \gamma_w}{\gamma_s} \tag{11.5}$$

Substituting Equations 11.4 and 11.5 into Equation 11.3, the approximate water adsorption (w_a) is given by:

$$w_a = \varepsilon (1 + e_0) \frac{\gamma_s}{\gamma_w} \tag{11.6}$$

where,

e_0 = initial void ratio of specimen
γ_s = density of soil particles (mg/m^3).
γ_w = water density (= 1 mg/m^3).

Figure 11.7a shows that the adsorbed water increased due to elapsed time. It was linearly correlated with the swelling (Figure 11.7b).

Swelling pressure

Swell pressure is defined here as the pressure required to compress a specimen which has been soaked and completely swollen under seating pressure, back to its original configuration (i.e. before swelling). The swell pressure was measured by the pre-swelled method.

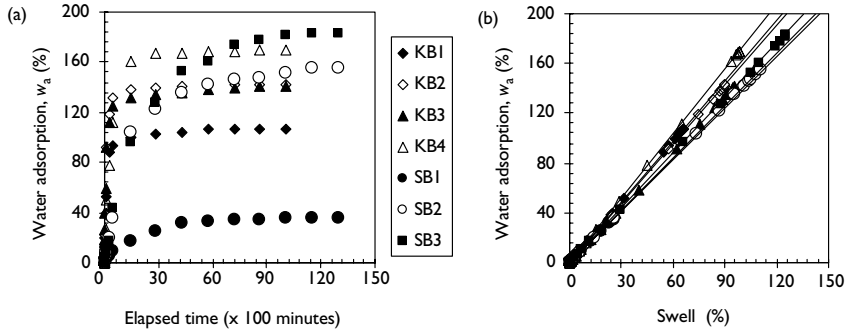

Figure 11.7 Water adsorption during swelling.

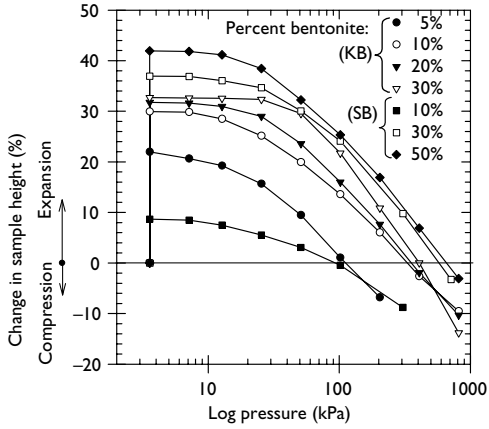

Figure 11.8 Percent change in sample height versus loading applied pressure.

However, there is experimental evidence that different methods give similar results (El-Sohby and Rabba, 1981; Borgesson, 1989) especially at high density.

Figure 11.8 shows the change in sample height (%) and pressure (kPa) curves for soil–bentonite mixtures. This was determined using the oedometer test. Two essential values can be obtained from these results: the compressibility and the swelling pressure of compacted soil. The study showed that the swell pressure increased with increasing bentonite content. Sand–bentonite mixtures exhibited greater swelling pressure than other mixtures. It was perhaps caused by the greater initial dry density and the lower water content when the specimen was compacted. This was in agreement with El-Sohby and Rabba (1981)

Mathew and Rao (1997) indicated that by increasing the valence of exchangeable cations in homoionized clay, the overall compression in the system was reduced and the preconsolidation pressure (p_c) was increased. The equilibrium void ratio at any applied pressure is a direct function of the repulsive forces arising from the interaction of adjacent diffuse double layers and pore fluid. As the valence of exchangeable cations in the clay increased, there was a reduction in the diffuse double-layer thickness and in the magnitude of the repulsive forces. This resulted in a lower equilibrium void ratio at any given pressure until higher pressures were reached (Sridharan and Choudhury, 2002).

Conclusions

The swelling and swelling pressure of bentonite-mixed kaolin and sand increased with an increase in bentonite content. Apart from the mineralogical and clay content, the amount and size of the non-swelling fraction played a role in governing the swelling and compression behavior. The swelling of soils occurred in three distinct stages: intervoid swelling (i.e. initial), primary swelling, and secondary swelling. The volume change occurred since the compacted soil adsorbed water. This was linearly correlated with swelling. The rate of swell and maximum swelling could be estimated by using a hyperbolic equation. The rate of swell was

termed as the coefficient rate of swell (m_s) which was obtained from the constants of the hyperbolic equation.

Acknowledgments

The authors gratefully appreciated the funding provided by the Ministry of Science, Technology and Environmental (MOSTE) Malaysia through IRPA No. 02-02-03-1001, and Fundamental and Short Term Research Vot-F 0153/2002B.

References

Alawaji, H.A., 1999, "Swell and compressibility characteristics of sand–bentonite mixtures inundated with liquids," *Applied Clay Science*, Vol. 15, No. 3–4, pp. 411–430.

Al-Mukhtar, M., Touray, J.C., and Bergaya, F., 1999, "Une argile modèle pour l'étude du gonflement des sols argileux: la laponite-Na de synthèse," *Sciences de la terre et des planètes*, Vol. 329, pp. 239–242.

Alonso, E.E., Vaunat, J., and Gens, A., 1999, "Modeling the mechanical behavior of expansive clays," *Engineering Geology*, Vol. 54, pp. 173–183.

Basma, A.A. and Tuncer, E.R., 1991. "Effect of lime on volume change and compressibility of expansive clays," *Transportation Research Record*, 1295, pp. 52–61.

Borgesson, L., 1989, "Laboratory testing and computer simulation of clay barrier behavior," Proceedings of the Ninth International Clay Conference, AIPEA, Strasbourg, pp. 117–126.

Dakshanamuthy, V., 1978, "A new method to predict swelling using a hyperbolic equation," *Geotechnical Engineering*, Vol. 9, pp. 79–87.

Daniel, D.E. and Wu, Y.K., 1993, "Compacted clay liners and covers for arid sites," *Journal of Geotechnical Engineering, ASCE*, Vol. 119, No. 2, pp. 223–237.

El-Sohby, M.A. and Rabba, E.A., 1981, "Some factors affecting swelling of clayey soils," *Geotechnical Engineering*, Vol. 12, pp. 19–39.

Komine, H. and Ogata, N., 1994, "Experimental study of swelling characteristics of compacted bentonite." *Canadian Geotechnical Journal*, 31, 478–490.

Mathew, P.K. and Rao, S.N., 1997, "Influence of cations on compressibility behavior of a marine clay," Technical Note, *Journal of Geotechnical and Geoenvironmental Engineering, ASCE*, Vol. 123, No. 11, pp. 1071–1073.

Miao, L., Liu, S., and Lai, Y., 2002, "Research of soil-water characteristics and shear strength features of Nanyang expansive soil," *Engineering Geology*, Vol. 65, pp. 261–267.

Muntohar, A.S. and Hashim, R., 2002, "Properties of engineered expansive soils," Proceedings of the First Technical Postgraduate Symposium, University of Malaya, 16–17 October 2002, pp. 272–276.

Sridharan, A. and Choudhury, D., 2002, "Swelling pressure of sodium montmorillonites," *Géotechnique*, Vol. 52, No. 6, pp. 459–462.

Sridharan, A. and Nagaraj, H.B., 1999, "Absorption water content and liquid limit of soils," *Geotechnical Testing Journal*, Vol. 22, No. 2, pp. 121–127.

Waddah, S.A., Khalid, A.A., and Al-Zou'bi, S.M., 1999, "Influence of pore water chemistry on the swelling behavior of compacted clays," *Applied Clay Science*, Vol. 5, pp. 447–462.

Yong, R.N., Boonsinsuk, P., and Wong, G., 1986, "Formulation of backfill material for a nuclear fuel waste disposal vault," *Canadian Geotechnical Journal*, Vol. 23, pp. 216–228.

Chapter 12

Swelling behavior of Ankara Clay

Predictive techniques, damage details, and swelling maps

Zeynal Abiddin Erguler[1] *and Resat Ulusay*[1]

Summary

The specific objectives of the research reported in this chapter were to investigate the effect of disturbance on the swelling behavior of Ankara Clay, to estimate the depth of the active zone, to develop a simple technique based on water content of soil–water mixture for predicting degree of swelling, to propose predictive models for swelling pressure and percent swell using index properties of the clay, to make a synthesis of observed damage details, and to construct swell pressure and percent swell maps. The latter would provide information on the swelling potential of the clay for engineers, city planners, and local authorities. The basis for site selection and climatic and geological conditions, were discussed. The physical and mineralogical properties were obtained, and laboratory-swelling tests were conducted for direct estimation of swell potential. A simple laboratory test method to predict swelling potential was also suggested. The data obtained was statistically analyzed, to determine if any single property or a group of properties could be used for prediction of swelling potential. Finally, details of damage to structures in the light of environmental conditions, site observations, and laboratory-derived data were discussed, and swelling potential maps for the metropolitan area were constructed.

Introduction

Expansive clay soils swell when wetted and shrink when they dry out, hence giving rise to ground movement. Depending on its severity, this can cause structural damage to low-rise buildings. Upon expansion, the soil exerts an upward pressure on foundations and structures founded on it. If this pressure is greater than the foundation pressure, then uplift or differential uplift can occur causing walls, beams, and columns to crack (Basma *et al*., 1995). Assessing the swelling pressure and amount of swelling is an important stage in designing foundations on expansive soils. These soils, particularly those located in arid and semi-arid climate regions, represent a problem and occur extensively throughout the world. There are several factors which influence the swelling potential of clay soils including the amount and type of clay minerals, the cation exchange capacities of clay minerals, availability of moisture, and the initial water content. Among the three major structural groups of clay minerals, the smectite group, consisting mainly of montmorillonites, constitutes the most highly expansive soils.

[1] Department of Geological Engineering, Applied Geology Division, Hacettepe University, 06532 Beytepe, Ankara, Turkey; email: zerguler@hacettepe.edu.tr; resat@hacettepe.edu.tr

Numerous expansive soil problems and related damage have been reported (Mohan *et al*., 1973; Popescu, 1979; Chen, 1988; Basma, 1991; Abduljauwad and Al-Suleimani, 1993; Bell and Maud, 1995; Popa, 1997; Al-Rawas, 1999; Derriche and Iguechtal, 2000; Meisina, 2002; Shi *et al*., 2002). Although a limited number of these studies concentrated on developing equations that could be used to predict the swelling potential of expansive clays from their index properties (Chen, 1988; Abduljauwad, 1993; Al-Homoud and Al-Suleiman, 1997; Li and Du, 1997; Bonner and Shakoor, 1998; Al-Rawas, 1999), they provided helpful information for practicing engineers. In addition, a small number of studies have been conducted on swelling/shrinking soils mapping and hazard assessment (Ramana, 1993; Basma *et al*., 1995; Oteo *et al*., 1995; USGS, 2000; Meisina, 2002).

Ankara Clay, can be found in abundance in central, western, and southern parts of Ankara, the capital of Turkey (Birand, 1963; Ordemir *et al*., 1977; Cokca, 1991). During the past decades, rapid expansion of the city and the growth of population due to migration from different parts of Anatolia led to the construction of various structures, particularly low-cost one-storey buildings in the suburbs. This situation resulted in an increase in the length of the street network and buried utility lines. The existence of expansive soils in the Ankara metropolitan area has caused structural damages on light buildings, asphalt pavement, and buried utility lines. City planners and engineers did not appear to pay attention to the problems associated with Ankara Clay during site selection and construction of low-rise and low-cost buildings. There has been limited research effort directed at the swelling properties of Ankara Clay (Birand, 1963; Ordemir *et al*., 1965; Doruk, 1968; Omay, 1970; Uner, 1977; Furtun, 1989; Cokca, 1991). These studies were mainly concentrated on the swelling parameters of the clay, and were done on a small number of samples from a very limited area of the city.

Due to the lack of detailed information on swelling characteristics of expansive Ankara Clay in the southwestern part of the city, where swelling-induced damage to structures was observed, a comprehensive research program was needed. The specific objectives of the research reported in this chapter were to investigate the effect of disturbance on the swelling behavior of Ankara Clay, to estimate the depth of the active zone, to develop a simple technique based on water content of soil–water mixture for predicting degree of swelling, to propose predictive models for swelling pressure and percent swell using index properties of the clay, to make a synthesis of observed damage details, and to construct swell pressure and percent swell maps. The latter would provide information on the swelling potential of the clay for engineers, city planners, and local authorities. The basis for site selection and climatic and geological conditions were discussed. The physical and mineralogical properties were obtained, and laboratory-swelling tests were conducted for direct estimation of swell potential. A simple laboratory test method to predict swelling potential was also suggested. The data obtained was statistically analyzed, to determine if any single property or a group of properties could be used for prediction of swelling potential. Finally, details of damage to structures in the light of environmental conditions, site observations, and laboratory-derived data were discussed, and swelling potential maps for the metropolitan area were constructed.

Site selection criteria and site description

For the selection of the site in the metropolitan area of Ankara with expansive soil formation, available data from previous geological maps, mineralogical and geotechnical studies, and site visits to ascertain the extent of structural damage associated with the soil swelling were

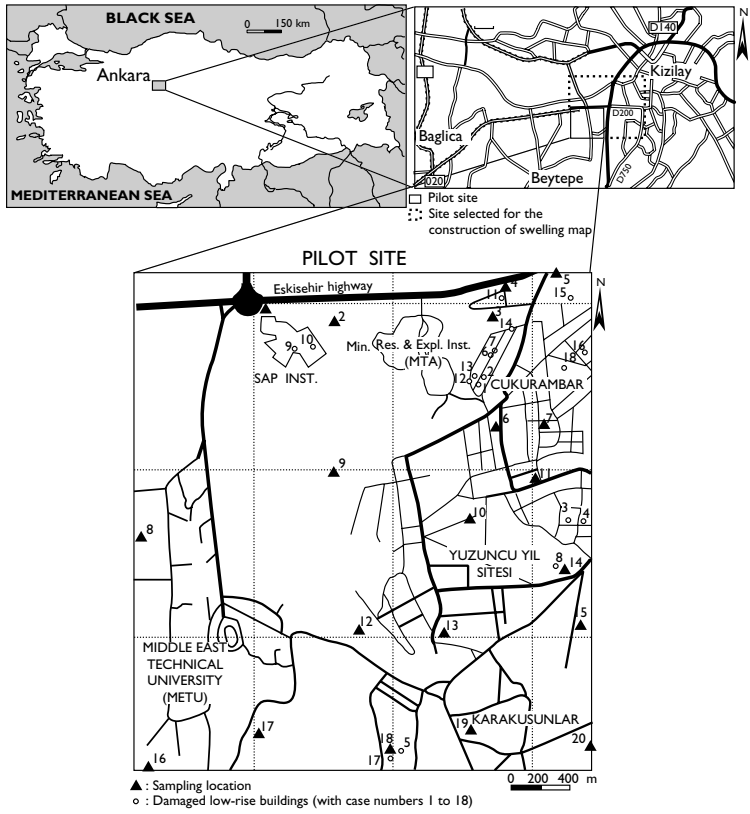

Figure 12.1 Location map of Ankara city with boundaries of the pilot study site and the site selected for construction of swelling maps, and the detailed map of the pilot site showing the main streets and districts, sampling locations and damaged light structures selected as case examples.

evaluated. It was also considered to be important that the soil must have a clay content that was representative of the natural soil deposits of Ankara Clay. On the basis of these criteria, a pilot site of 16 km^2 in the southwestern part of the Ankara metropolitan area was selected (Figure 12.1). Low-rise residential buildings constructed with limited budgets were common in this area. However, due to rapid growth of the city toward this district, some of the single-storey buildings were abandoned and construction of high-rise apartment blocks at the site rapidly increased (Figure 12.2a). This situation provided an opportunity to clearly observe the clay on the faces of foundation cuts (Figure 12.2b).

The study area had a flat topography. Natural slopes varied between 0% and 8% in its north and central parts, while southern slopes were between 8% and 30%. The damaged low-rise buildings were founded on flat areas where the drainage system was not effective.

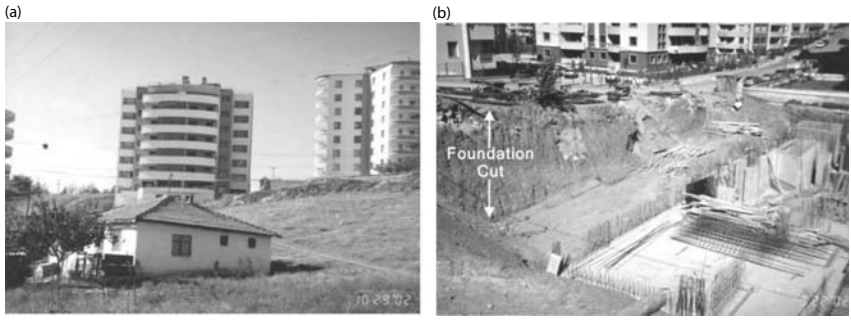

Figure 12.2 (a) A view of a low-rise house and recently constructed multi-storey apartment blocks, and (b) a vertical foundation cut in Ankara Clay.

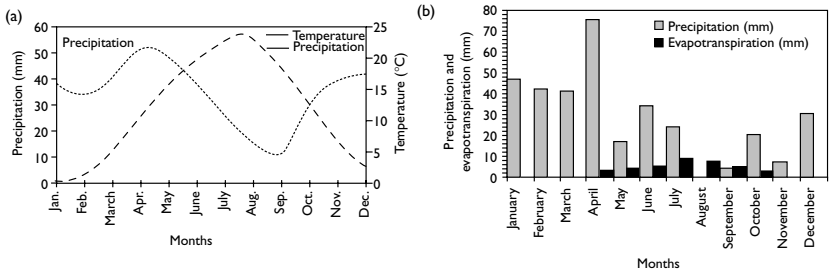

Figure 12.3 (a) Mean monthly temperatures and precipitation between 1980 and 2000, and (b) comparison of mean monthly precipitation and evapotranspiration in the year 2000 for Ankara and close vicinity

Therefore, after rains poor surface drainage resulted in accumulation of water on ponding in these areas. This provided a source of moisture for the expansive soil to absorb and swell.

Climatic conditions

Ankara is situated in Central Anatolia at 38° 43′–40° 41′ latitude north and 30° 51′–34° 05′ longitude east. Heights in the region varied between 848 and 1000 m above sea level and presented a flat topography, surrounded by highlands. The climate of the region was semi-arid, which was represented by hot and dry summers, and cold and rainy–snowy winters. Based on the records between 1980 and 2000 from the meteorological station of Ankara, mean annual temperature for the city was 11.6°C. Mean monthly temperatures throughout this 20-year period ranged from 0 to 23.5°C. Intense precipitation was concentrated between December and April (Figure 12.3a). In the rainy season, the humidity level rose up to 84%. The dry season was between June and September, and evapotranspiration exceeded

precipitation in August and September. Figure 12.3b shows the evapotranspiration–precipitation histogram for the year 2000 when the sampling for this study was carried out. As can be seen, in addition to the soil type, both the climatic conditions in the region and drainage characteristics of the selected site seemed to be suitable factors for soil swelling.

Geological setting and Ankara Clay

The geological units in the Ankara region include sedimentary, metamorphic, and igneous rocks ranging from Paleozoic to Quaternary in age. The simplified geological map of Ankara city is shown in Figure 12.4. The Mesozoic and Paleozoic aged rocks form the basement rocks and consist of limestones, greywackes, spilites, and metamorphic rocks. Volcanic and volcano-sedimentary rocks of Miocene age overlie the basement rocks. Several lakes, which developed on eroded surfaces in Miocene time survived, but disappeared as the epirogenic movements in Middle Pliocene affected the region (Erol, 1973). The sediments of Late Pliocene, which filled the basins, were uplifted again and as a result of this process, they were carved into plains and valleys. The alluvial materials, which included various sediments of Quaternary age accumulated in the valleys.

The fluvial clastics of Late Pliocene age and Quaternary alluvial deposits are the soil grounds in Ankara city and formed the Ankara Basin. The sedimentary fill of the basin mainly consisted of debris-flow conglomerate, wedge to through cross-bedded conglomerate-sandstone and finer reddish-brown clastics deposited in alluvial fan, braid plain, and flood plain respectively (Kocyigit and Turkmenoglu, 1991). Finer reddish-brown clastics are referred in geotechnical studies as "Ankara Clay" (Ordemir *et al*., 1965).

Ankara Clay is a preconsolidated, stiff, and fissured clay (Figure 12.5), composed mainly of clay sized material. However, occasional sandy and gravely layers are also observed

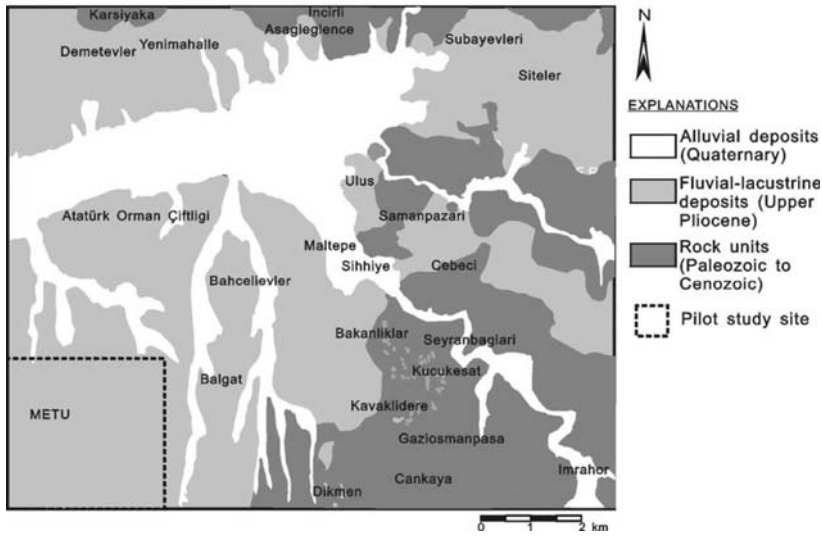

Figure 12.4 Simplified geological map of Ankara city (modified from Kasapoglu, 1980).

Figure 12.5 A view of the fissures in Ankara Clay.

within the clay in variable thicknesses, and locally at shallow depths very thin lime levels, lime nodules, and lime concretions with no lateral continuity. Aras (1991) stated that andesitic rock fragments and their weathering products in the sand fraction of the brownish clay indicate that the andesitic rocks surrounding the city from its north and east are the major source rocks for this clay. The thickness of this clayey sequence changed locally, but it exceeded 200 m (Erol, 1973).

Both the pilot site and a very large district in the metropolitan area selected for a study of the swelling characteristics of the clay and for the construction of swelling maps, respectively, were the areas where Ankara Clay was observed with its typical characteristics. In these areas, the clay consisted of a small number of sand and gravel lenses, and generally was free from lime nodules. Vertical cuts about 5–6 m in depth maintained their stability throughout construction periods (Figure 12.2b).

Mineralogical and physicochemical properties

The study site was divided into sub-areas (Figure 12.1). Sampling was carried out in each sub-area. But due to rapid urbanization of the site, sampling from each sub-area could not be possible. However, both disturbed and undisturbed samples were collected from 20 locations shown in Figure 12.1 at depths between 1 and 2 m by considering very shallow foundations of the low-rise buildings. In addition, extra-undisturbed samples were taken from different depths at some sampling locations to determine the depth of the active zone and for preliminary assessment of swelling anisotropy.

Mineralogical and chemical properties of the soil

Knowledge of the mineralogy of soils is very important in order to determine whether the soil contains active clay minerals. The primary method for identifying and analyzing clay minerals is X-ray diffraction. X-ray diffraction analysis was conducted on 20 soil samples using a Philips PW-1140 model diffractometer with a goniometer speed of 2°/min. An external standard method suggested by Gundogdu (1982) was used as a guide for quantitative

Table 12.1 Summary of semi-quantitative whole soil mineralogy and clay mineralogy of the samples from Ankara Clay based on XRD

Clay and non-clay minerals (%)				*Clay minerals (%)*		
Calcite	*Quartz*	*Feldspar*	*Clay*	*Smectite*	*Illite*	*Kaolinite*
5.1–37.4 (12.6)	8.0–24.1 (14.9)	1.3–25.0 (6.6)	36.0–85.5 (65.9)	14.7–54.8 (33.8)	3.6–28.9 (15.8)	7.3–26.6 (16.3)

Note
The numbers in parentheses are the mean values.

Table 12.2 Chemical analysis for the samples from Ankara Clay

Oxides	*Percentage oxides*
SiO_2	37.88–63.34
Al_2O_3	8.22–16.33
Fe_2O_3	3.51–7.06
MnO	0.07–0.13
MgO	1.69–3.60
CaO	3.80–24.30
Na_2O	0.19–1.07
K_2O	0.87–2.17
TiO_2	0.41–1.03
LOI	7.61–22.59

Note
LOI: loss on ignition.

estimates of the minerals. Table 12.1 shows a summary of types and percentages of minerals present in the investigated samples. The results indicated that non-clay minerals present were quartz, feldspars, and calcite. Clay minerals were smectite, illite, and kaolinite. Of the minerals, clay was dominant in the samples with a range of 36–85% and the smectite group mineral montmorillonite was the chief clay mineral.

The physicochemical properties of clay porewater directly affect many engineering properties of a soil such as swelling (Sherard *et al*., 1972; Nawari and Schetelig, 1991). A chemical study, therefore, was carried out to determine the type and percentage of the oxides present in the samples using X-RF spectrometer. High percentages of SiO_2, Al_2O_3, Fe_2O_3, MgO, and CaO indicated the presence of smectite (Abduljauwad, 1993). The results of the chemical analysis given in Table 12.2 suggested that the swelling potential of the soils was likely to be high and were confirmed by those from the XRD analysis. A slightly elevated percentage of CaO was probably due to the presence of lime concentrations at shallow depths.

Physical and index properties

Laboratory tests to determine the physical properties of the soil were carried out in accordance with the procedures suggested by ASTM (1994). They involved determinations

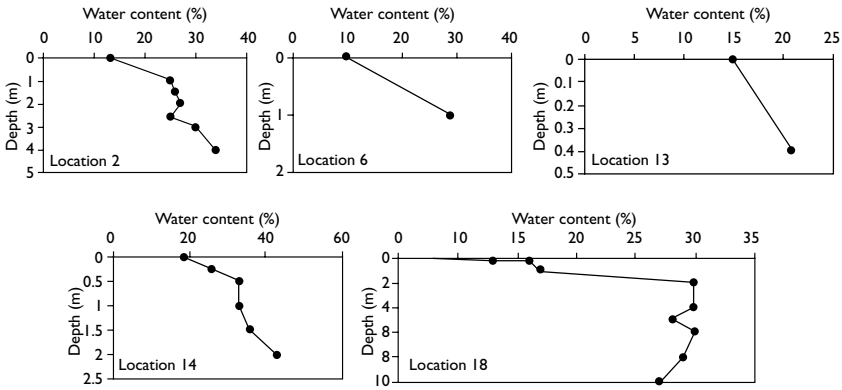

Figure 12.6 The variation of natural water content with depth at different sampling locations.

of natural water content, unit weight and dry density, and grain size distribution analyses and Atterberg limits in conjunction with activity and soil classification. The results indicated that the initial water content varied between 14% and 44% with a mean of 28.2%, and initial water content of all samples were greater than their shrinkage limits. This situation suggested that these samples at their natural water contents were subjected to swelling, and consequently, it was considered that in the case of swelling tests on samples at initial water content, a considerable amount of swelling cannot be observed. This was taken into consideration during the swelling tests.

The meteorological records previously mentioned and site observations suggested that maximum drying of the soil occurred in September 2000. In order to determine the depth of the active zone a total of 27 additional samples from different depths at five locations were obtained and their water contents were determined. Figure 12.6 indicated that the depth of the active zone was about 2 m at locations 2, 14, and 18. It could not be identified at two other locations due to considerably shallow sampling depths.

The determinations on undisturbed samples suggested bulk and dry unit weights of the clay ranging between 14.9 and 19.6 kN/m^3, and 13.4 and 18.3 kN/m^3, respectively. The specific gravity of the soil was found to be 2.60.

A summary of the Atterberg limits, grain-size characteristics, and activity of the soil is given in Table 12.3. Grain-size analyses indicated that clay-size particles were dominant. A notable proportion of silt also existed. In addition, the soil contained variable quantities of sand and small gravel. While the amount of sand and gravel was very low at the northern and central parts of the site, it gradually increased toward the basin margin at the south.

The relationship between the clay content and Atterberg limits shown in Figure 12.7a suggested that the higher the clay content, the higher is the Atterberg limits, and natural water contents are higher than shrinkage limits. The large differences observed between the values of natural water content and the liquid limit clearly demonstrated the state of intense desiccation of the clay. The natural water contents generally around the plastic limit indicated that swelling controlled the soil behavior at the time of sampling.

Table 12.3 Physical properties of the soil samples extracted from Ankara Clay

Grain size (%)				*Atterberg limits (%)*				*Activity*
Gravel	*Sand*	*Silt*	*Clay*	*LL*	*PL*	*PI*	*SL*	
1.2–23.9 (11.8)	5.9–32.2 (17.5)	9–63.3 (32.1)	11.0–75.0 (38.7)	44–103 (64.1)	25–45 (33.6)	17–67 (30.9)	9–27 (17.6)	0.49–1.83 (0.94)

Notes
LL: liquid limit;
PL: plastic limit;
PI: plasticity index;
SL: shrinkage limit.
The numbers in parentheses are the mean values.

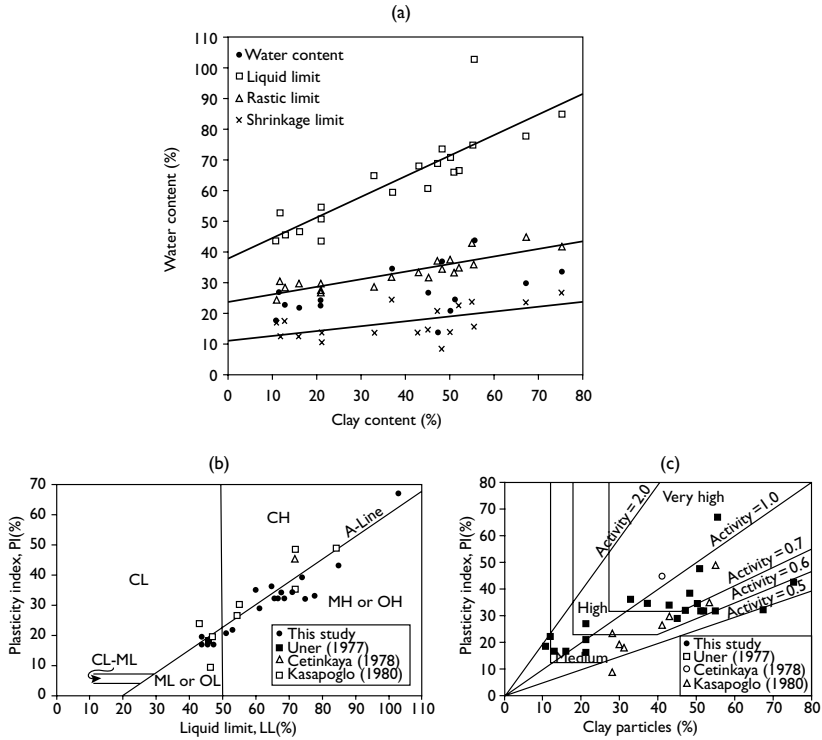

Figure 12.7 (a) Clay content, Atterberg limits and natural water content of Ankara Clay samples, and distribution of the samples on (b) plasticity chart and (c) swell potential chart proposed by Van der Merve (1964).

Based on the Unified Soil Classification System, the majority of the soil samples were classified as inorganic clays of high plasticity (CH), and highly compressible inorganic silt and organic clays (MH) (Figure 12.7b). Moreover, as indicated in Figure 12.7c, which also involved data from previous studies carried out on this clay, Ankara Clay had high to very high swell potential.

Laboratory assessment of swelling potential

Swelling potential of the soil samples from 20 locations in the study site were assessed in two stages. In the first stage, indirect measurements were carried out such as the free swell (FS) (Holtz and Gibbs, 1956), modified free swell index (MFSI) (Sivapullah *et al*., 1987), and methylene blue absorption tests (AFNOR 1980). In addition, a simple and practical test called w_{max24}, developed by the authors, was also conducted indirectly to assess the swelling potential of the soil. In the second series of experiments, the magnitude of swell was obtained by conducting swell tests in accordance with the procedure suggested by ASTM (1994) using an oedometer. The results obtained from these tests are given in Table 12.4.

Indirect measurements

The values of FS of the clay given in Table 12.4 indicated high and very high swelling potential. Higher values of FS were obtained on the samples collected from the central,

Table 12.4 Indirect and direct measurements of swelling potential

Location no.	w_{max24} *(%)*	*FS (%)*	*MFSI*	*Swelling pressure (kPa)*		*Swelling percent (%)*	
				(SWUD)	*(SWR)*	*(SPUD)*	*(SPR)*
1	125	102.5	3.51	820	1580	30.6	43.0
2	95	105.0	3.32	520	860	16.5	17.7
3	75	87.5	2.60	420	590	12.9	14.5
4	73	90.0	3.16	200	290	14.7	16.9
5	81	80.0	2.58	290	410	14.5	16.5
6	97	93.0	3.63	700	1000	24.8	30.0
7	33	37.5	2.05	10	14	0.6	0.8
8	110	115.0	3.21	1310	1260	22.6	22.0
9	61	65.0	2.27	60	90	6.5	4.6
10	71	87.5	3.11	120	280	13.7	10.3
11	77	80.0	3.02	280	400	12.2	13.9
12	75	70.0	2.47	100	290	5.3	8.7
13	58	105.0	3.05	120	260	12.0	25.4
14	103	90.0	3.42	720	960	29.8	33.1
15	48	35.0	2.37	20	60	2.5	3.3
16	50	45.0	2.96	190	200	9.2	10.8
17	63	45.0	2.36	90	100	5.2	5.6
18	81	82.5	3.22	290	250	10.2	10.8
19	63	75.0	3.49	80	120	10.9	11.0
20	50	47.5	2.59	20	30	2.0	3.3

Notes
W_{max24}, Water content at 24 hours (%); FS: Free swell (%); MFSI: Modified free swell index; SWUD and SWR: Swelling pressure of the undisturbed and remoulded samples, respectively; SPUD and SPR: Swelling percent of the undisturbed and remoulded samples, respectively.

western, and northern parts of the site where damage to light structures was more evident. Based on the MFSI classification (Sivapullah *et al*., 1987), the soil investigated had moderate swelling potential.

Methylene blue values (MBV) and cation exchange capacities (CEC) of the samples varied between 4 and 14.8 g/100 g (mean = 7.6 g/100 g), and 9.12 and 33.74 meq/100 g (mean = 17.4 meq/100 g). These results were reasonable if the clay mineralogy of Ankara Clay is considered. Since montmorillonite was the chief mineral in almost 100% of the samples, it caused high values of CEC. Based on the tentative classification for swelling potential proposed by Cokca and Birand (1993), 60% of the samples had high to very high swelling potential.

FS suffers from certain limitations as discussed by Sridharan *et al*. (1985; after Sivapullah *et al*., 1987). On the other hand, the amount of the soil used in the MFSI tests is a limited 10 g, the sample in powder form does not represent its natural state, and errors in readings between 0.28 and 0.50 cm^3 due to pouring of the sample into the cylinder are possible. Due to these difficulties and limitations, a simple and more practical way to indirectly estimate swelling potential of expansive soils seemed to be needed. Irrespective of the internal processes and mechanism of clay mineral swelling, the change in water content of a soil plays a major role in determining the degree of swelling. When water is introduced in the environment, clay soils both absorb and adsorb water more than sandy and gravelly soils. Absorbed water cannot escape easily from the environment in a short period. Therefore, it is logical that the water content of a clay soil should determine its potential for further expansion, and consequently an increase in water content of the clay soil inundated in water will result in an increase in the magnitude of its swelling. By considering this idea, a simple test, called w_{max24}, was suggested by Erguler and Ulusay (2003). In this test, special sample preparation was not required and the disturbed or undisturbed samples could be used. In the test, about 400 g soil sample is transferred into a 200 or 300 ml jar and then distilled water is added to the soil. The mixture is stirred with a glass or metal rod for about 5–6 minutes until a viscous material is obtained (Figure 12.8a). Then the mixture is left in the jar for 24 hours. After 24 hours, the jar is laid down on its side for about 15–20 minutes to remove the water accumulated at the surface of the soil, and finally water content of the soil is determined by transferring about 25–30 g of soil sample from the jar into the container (Figure 12.8b). Then w_{max24} is calculated from the following expression.

$$w_{max24}(\%) = \frac{w_1 - w_2}{w_2 - w_0} \times 100 \tag{12.1}$$

where, w_1: weight of the wet sample and the container (g) after 24 hours of waiting, w_2: weight of the oven-dried sample and the container (g), and w_0: weight of the container (g). The results of w_{max24} tests are given in Table 12.4. The relationships between w_{max24} and swelling parameters are discussed in the following section.

Swelling tests

Swelling pressure and swelling percent for the samples were directly measured using the conventional one-dimensional oedometer. After a series of oedometer tests according to the ASTM (1994) test method B for the samples at their natural water content, a remarkable swell pressure could not be recorded. However, this situation resulted in a question of how

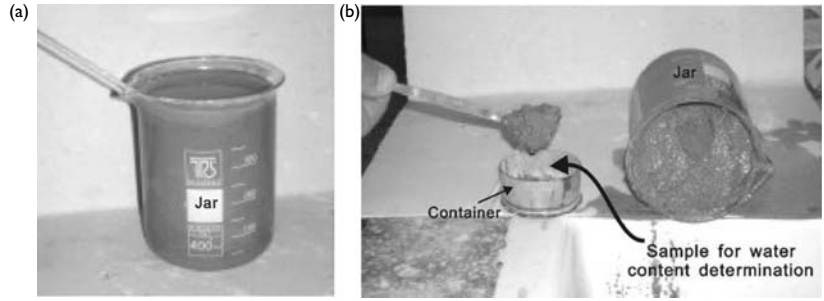

Figure 12.8 Photographs showing the steps followed in w_{max24} test: (a) mixture of soil sample and distilled water, and (b) the jar and the sample laid down to remove the water accumulated on the surface of the soil and sampling for water content determination.

the damage to structures found in this clay could be related to its expansive nature, if the clay shows a slight response during the swell test. It was reported that damages to structures on desiccated clays would be highly severe and substantial increase in the swell pressure would occur as the water content of the clay specimens decreased (Chen, 1988; Day, 1998). On the other hand, tests on desiccated clay samples from California carried out by Day (1998) to simulate field conditions suggested that a substantial increase in the swell pressure occurred as the water content of the clay specimens decreased. As previously mentioned, the natural water content of Ankara clay is lower than its shrinkage limit through a depth of approximately 2 m in dry seasons. The swelling tests were therefore also carried out on 20 desiccated samples. Typical "time-vertical displacement" and "pressure-vertical displacement" curves of a specimen are depicted in Figure 12.9a. The test results are given in Table 12.4. Except for a few specimens, swelling pressures were greater than 200 kPa with a mean value of 450 kPa. Higher swelling pressures were obtained from the samples representing western and northern parts of the site where damages to light buildings were more evident.

It is known that under natural undisturbed conditions, some clays exhibit a certain level of swelling shrinkage, but their swelling degrees are low. When disturbed and compacted, their natural structures are destroyed and cementing bonds are broken, the water content decreases, and swelling-shrinkage indices increase (Li and Du, 1997; Du *et al*., 1999). Some of the roads and low-rise buildings at the study area were constructed on the fill materials consisting of remoulded Ankara Clay. By considering these, specimens identical to those of undisturbed soil, samples were prepared from disturbed bag samples and swelling tests were conducted on these. It was clear from the comparison of the test results in Table 12.4, Figures 12.9a and 12.9b that both swelling pressure and swelling percent increased when the soil was remoulded and compacted. The breakdown of the cementing bonds and the change in the fabric were the main factors influencing the change in swelling ability and swelling pressure of the compacted expansive soil.

The natural water content of the clay was lower than its shrinkage limit at depths between 0 and 2 m in dry seasons. However, it gradually increased with depth beyond 2 m. This increase suggested that swelling pressure and swelling percent will decrease until to a certain depth and tend to approach zero at depths greater than 2 m. Therefore, the variation

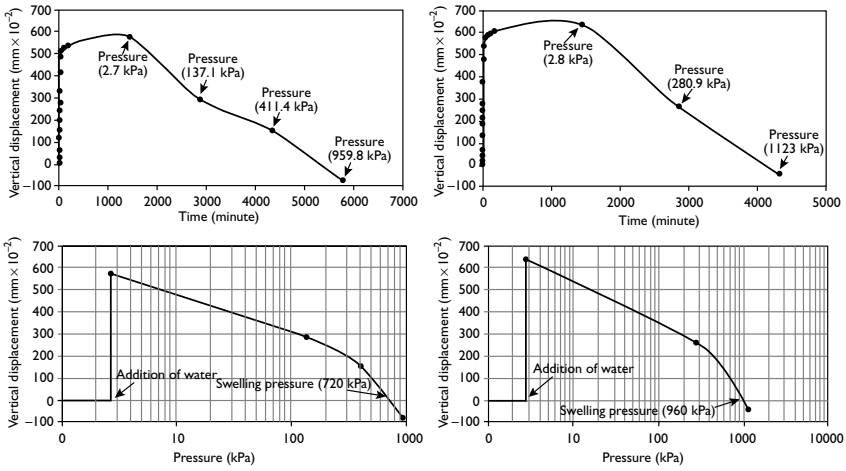

Figure 12.9 Typical "time-vertical displacement" and "pressure-vertical displacement" curves for undisturbed (a) and remoulded (b) specimens from location 14 in the study site.

of swell parameters with water content was also investigated on a limited number of the samples from three locations due to difficulties during sampling, particularly in dry season. These samples were prepared with different water contents in the laboratory and swelling pressure of each specimen was determined. Figure 12.10 suggests that a sharp decrease in swelling pressure depended on an increase in the water content. Thus it was clear that swelling pressure of Ankara Clay tended to die out at water contents greater than 30%. It could be concluded that the natural water content of the soil will possibly increase at 2–3 m below the surface, and the problems due to swelling would not be expected beyond this depth.

Swell anisotropy

A study by Fourie (1989) on laboratory evaluation of swelling pressure suggested that the measured lateral swelling pressure was significantly greater than its vertical equivalent. A few studies (Uner, 1977; Cetinkaya, 1978) were conducted on the swell anisotropy of Ankara Clay on a limited number of samples taken from a university campus area. In the current study, samples from locations numbered 1 and 13 (Figure 12.1) were taken to perform additional assessments on the swell anisotropy of Ankara Clay in conjunction with the results from the previous work. The test results showed that swelling percent in the horizontal direction (SP_{hor}) for both samples were greater than those from the vertical direction. Comparison of the swell pressure values determined in both directions for the samples from this (location 1: SW_{hor} = 1200 kPa, and SW_{ver} = 820 kPa; location 13: SW_{hor} = 330 kPa, and SW_{ver} = 120 kPa) and previous studies suggested that the swell pressures in the horizontal direction were considerably higher (Figure 12.11). This clay had a tendency to

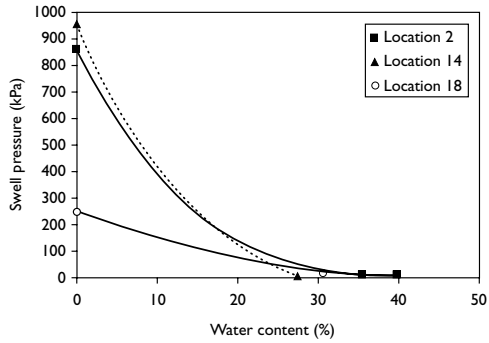

Figure 12.10 Swell pressure versus water content of the samples from three different locations.

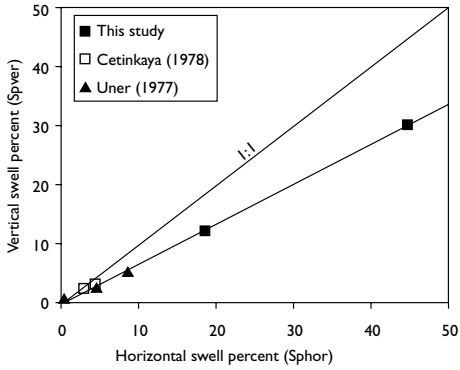

Figure 12.11 Swell percent in horizontal direction (SP_{hor}) versus swell percent in vertical direction (SP_{ver}) of Ankara Clay samples.

show more anisotropical behavior with respect to swelling, as the effects of fissures and preconsolidation due to desiccation increased at very shallow depths.

Prediction of swelling behavior from other soil parameters

Methods of predicting volume changes in soils are primarily oedometer tests and empirical methods. Since the laboratory-swelling test is a difficult and an expensive process for practicing engineers and small builders, empirical methods that make use of the swelling potential, as determined from index and/or physical properties such as liquid limit, have increasing popularity. The empirical equations appearing in the literature are generally related to predicting of free swell and swell percent from index and/or basic physical

properties of the soils (Van der Merve, 1964; Weston, 1980; Abduljauwad, 1993; Ramana, 1993; Basma *et al*., 1995; Al-Homoud and Al-Suleiman, 1997; Booner and Shakoor, 1998). There is only one empirical equation for Ankara Clay to predict its swelling pressure. It involves natural water content, dry unit weight, and liquid limit (Furtun, 1989). However, it is based on limited test data and the samples were from 1.5 to 4 m.

In the study reported in this chapter, the swelling pressure, and swelling percentage from 12 physical and index soil properties were predicted via simple and multiple regression analyses using data both from undisturbed and disturbed samples. The simple regression analyses (Table 12.5) indicated that the correlations between the soil properties and swelling parameters determined from the remoulded samples were higher than those obtained for undisturbed samples. It was also noted that w_{max24}, natural water content, MBV, liquid limit, and plasticity index played a more significant role in predicting the swell of the soil when compared to others.

In order to take into account combined effects of the soil properties on swelling parameters and to obtain predictive equations with higher coefficients of correlation than those obtained from simple regression, multiple regression analyses were carried out. In the selection of independent variables, particularly the soil properties exhibiting statistically significant correlations with swelling parameters at 95% confidence level were considered, and 48 regression models with coefficients of correlation ranging between 0.95 and 0.66 were obtained. Table 12.6 suggests that w_{max24}, liquid limit, and MBV, which can be easily and cheaply determined, are good predictors for the estimation of swelling pressure and swelling percent. Figure 12.12 shows predicted versus observed values of swelling parameters of the soil based on four predictive equations selected from Table 12.6. The margins of error as indicated by the distance of data from 1 : 1 line in Figure 12.12 were generally small. This suggested that the empirical equations predict the swelling parameters of Ankara Clay with a good degree of accuracy. In addition, these predictions have considerably higher coefficients of correlation when compared to those obtained from simple regression analyses. Therefore, some of these predictive equations could be used in the construction of the swelling maps for Ankara City.

Assessment of damage observations

The selected pilot site was one of the typical areas where a significant number of light, one-storey residential houses were constructed on low budgets. Due to low cost of housing, only limited measures were economically justifiable to restore the structural integrity of the houses. Consequently, most of these houses were left, and a rapid construction of high-rise apartment blocks was initiated at the site (Figure 12.2a). For this reason, 16 damaged one-storey and one or two-storey light buildings and 1 garden wall (Figure 12.1) were selected as typical case examples for the assessment of the effects of soil swelling on structural damage.

The internal and external hollow brick walls of the houses investigated were built on unreinforced concrete floor slabs with a thickness of 20–35 cm, directly constructed on the ground or extended to a depth of a maximum of 0.5 m below the ground surface located in the active zone. Most of them were built on flat topography, which offered poor drainage conditions, and underwent large absolute and differential movements on subsoils of moderate to high swelling potential. Based on the observations and information from the local people, problems occurred after the summer season in which the water content of the soil was minimum, and thus any increase in moisture caused swelling of the soil. In addition,

Table 12.5 Empirical equations which are statistically significant for predicting swelling parameters of Ankara Clay from its index and physical properties[a]

Parameters (x)	*SWUD (y)*	*SWR (y)*	*SPUD (y)*	*SPR (y)*	*FS (y)*	*MFSI (y)*
LL	$y = 14.87x - 635.4$ ($r = 0.66$)	$y = 23.9x - 1080.4$ ($r = 0.81$)	$y = 0.45x - 16.06$ ($r = 0.78$)	$y = 0.60x - 23.14$ ($r = 0.82$)	$y = 1.05x + 9.52$ ($r = 0.66$)	$y = 0.016x + 1.84$ ($r = 0.54$)
PL	$y = 35.7x - 878.1$ ($r = 0.56$)	$y = 46.9x - 1121.4$ ($r = 0.57$)	$y = 1.015x - 21.22$ ($r = 0.63$)	$y = 1.238x - 26.41$ ($r = 0.61$)	$y = 0.8787x^{1.26}$ ($r = 0.55$)	No correlation
PI	$y = 0.067x^{2.31}$ ($r = 0.61$)	$y = 30.2x - 481.3$ ($r = 0.78$)	$y = 0.55x - 4.303$ ($r = 0.74$)	$y = 0.76x - 8.23$ ($r = 0.79$)	$y = 7.53x^{0.673}$ ($r = 0.65$)	$y = 0.022x + 2.22$ ($r = 0.55$)
Clay percent	$y = 1.06x^{1.44}$ ($r = 0.66$)	$y = 14.9x - 124.9$ ($r = 0.64$)	$y = 0.312x + 0.7546$ ($r = 0.69$)	$y = 0.38x + 0.28$ ($r = 0.67$)	$y = 19.58x^{0.374}$ ($r = 0.63$)	$y = 1.74x^{0.144}$ ($r = 0.52$)
Clay	$y = 5.18 \times 10^{-4}x^{3.04}$ ($r = 0.50$)	$y = 19.3x - 818.3$ ($r = 0.56$)	$y = 0.39x - 13.16$ ($r = 0.59$)	$y = 0.49x - 17.00$ ($r = 0.58$)	$y = 0.85x^{1.06}$ ($r = 0.64$)	No correlation
FS	$y = 4 \times 10^{-4}x^{2.99}$ ($r = 0.82$)	$y = 8.52e^{0.044x}$ ($r = 0.85$)	$y = 0.000495x^{2.29}$ ($r = 0.85$)	$y = 0.00081x^{2.218}$ ($r = 0.85$)		$y = 0.677x^{0.338}$ ($r = 0.73$)
MFSI	$y = 0.35x^{5.8}$ ($r = 0.73$)	$y = 0.77x^{5.47}$ ($r = 0.73$)	$y = 0.059x^{4.77}$ ($r = 0.82$)	$y = 0.078x^{4.67}$ ($r = 0.83$)	$y = 13.6x^{1.58}$ ($r = 0.73$)	
MBV	$y = 0.53x^{2.91}$ ($r = 0.74$)	$y = 142.9x - 634.5$ ($r = 0.85$)	$y = 2.63x - 7.19$ ($r = 0.81$)	$y = 3.41x - 10.83$ ($r = 0.83$)	$y = 6.88x + 24.54$ ($r = 0.76$)	$y = 0.11x + 2.06$ ($r = 0.63$)
CEC	$y = 0.046x^{2.92}$ ($r = 0.74$)	$y = 62.6x - 637.9$ ($r = 0.85$)	$y = 1.15x - 7.19$ ($r = 0.81$)	$y = 1.49x - 10.83$ ($r = 0.83$)	$y = 6.56x^{0.85}$ ($r = 0.79$)	$y = 0.048x + 2.075$ ($r = 0.63$)
w_{max24}	$y = 1.65 \times 10^{-5}x^{3.78}$ ($r = 0.92$)	$y = 4.5x10^{-5}x^{3.64}$ ($r = 0.93$)	$y = 0.34x - 12.48$ ($r = 0.90$)	$y = 0.00022x^{2.53}$ ($r = 0.86$)	$y = 1.3956x^{0.93}$ ($r = 0.82$)	$y = 0.602x^{0.37}$ ($r = 0.70$)
w_n	$y = 0.00178x^{3.46}$ ($r = 0.72$)	$y = 0.00194x^{3.56}$ ($r = 0.78$)	$y = 0.00061x^{2.917}$ ($r = 0.82$)	$y = 0.00058x^{2.978}$ ($r = 0.87$)	$y = 3.146x^{0.95}$ ($r = 0.72$)	$y = 0.689x^{0.433}$ ($r = 0.71$)
Smectite	$y = 0.26x^{1.862}$ ($r = 0.49$)	$y = 23.7x – 348.7$ ($r = 0.57$)	$y = 0.3746x + 0.188$ ($r = 0.47$)	$y = 0.5659x – 3.99$ ($r = 0.55$)	$y = 1.109x + 3943$ ($r = 0.49$)	No correlation

Note

a Statistically significant at $p = 0.05$ level based on F-test statistics.

Table 12.6 Predictive equations for estimation swelling parameters from multiple regression analysis developed in this study

Equation no.	*Empirical equation*	*Coefficient of correlation (r)*
1	SWR = −1660.3 + 35.1 MBV + 440.9 γ_d + 3.6 LL + 12.4 w_{max24}	0.96
2	SWR = −1084.2 + 2.9 LL + 6.0 Sm + 15.4 w_{max24}	0.95
3	SWR = −1054.6 + 1.7 LL + 5.8 Sm + 13.9 w_{max24} + 22.5 MBV	0.95
4	SWR = −1043.9 + 16.4 w_{max24} + 8.1 Sm	0.95
5	SWR = −1617.9 + 5.86 LL + 14.82 w_{max24} + 378.4 γ_d	0.95
6	SWR = −1050.9 + 24.1 MBV + 5.5 LL + 13.0 w_{max24}	0.94
7	SWR = −906.6 + 39.5 MBV + 14.2 w_{max24}	0.94
8	SWR = −1082.5 + 6.9 LL + 14.7 w_{max24}	0.94
9	SWUD = −1739.24 + 17.57 MBV + 795.2γ_d + 12 w_{max24}–3.3LL	0.93
10	SWUD = −1755.5 + 7.7 MBV + 748.1γ_d + 11.4 w_{max24}	0.93
11	SWUD = −1741 + 739.9γ_d + 12.1 w_{max24}	0.93
12	SPUD = − 16.09 + 0.18 LL−0.06 Sm + 0.27 w_{max24}	0.92
13	SPUD = − 15.77 + 0.16 LL−0.06 Sm + 0.24 MBV + 0.25 w_{max24}	0.92
14	SPUD = − 15.81 + 0.12 LL + 0.22 MBV + 0.26 w_{max24}	0.92
15	SPUD = − 16.10 + 0.13 LL + 0.27 w_{max24}	0.92
16	SPUD = − 14.54 + 0.20 MBV−0.91γ_d + 0.12 LL + 0.26 w_{max24}	0.92
17	SPUD = − 13.64 + 0.06 Sm + 0.33 w_{max24}	0.91
18	SPUD = − 13.93 + 0.57 MBV + 0.86γ_d + 0.28 w_{max24}	0.91
19	SPR = −63.3 + 0.41LL + 12.04γ_d + 0.52 PL–0.25Clay + 0.9w_n	0.90
20	SWR = −5160.5 + 29.4 LL + 1766.4γ_d + 30.5 PL–26.2Clay + 34wn	0.90
21	SPR = −33.87 + 0.34 LL + 3.36 γ_d + 0.77 wn	0.89
22	SPR = −21.72 + 0.26 LL–0.0014 Sm + 1.1 MBV + 0.16 w_{max24}	0.89
23	SPR = −21.72 + 0.26 LL + 1.1 MBV + 0.16 w_{max24}	0.89
24	SPR = −21.72 + 1.11 MBV + 0.26 LL−0.00014 Sm + 0.16 w_{max24}	0.89
25	SPR = −9.69 + 0.88 MBV + 0.29 LL–8.71γ_d + 0.17 W_{max24}	0.89
26	SPR = −8.62 + 0.351LL + 0.23 w_{max24}–10.3 γ_d	0.89
27	SPR = −23.18 + 0.32 LL + 0.01 Sm + 0.24 w_{max24}	0.88
28	SPR = −23.17 + 0.32 LL + 0.24 w_{max24}	0.88
29	SPUD = −59.07 + 0.71 LL + 16.76γ_d−0.49PI +0.18 Clay + 0.79 wn	0.87
30	SWUD = −638.2−2.3 LL + 3.38 Sm + 13.3 w_{max24}	0.87
31	SWUD = −642.3−2.1 LL + 3.4 Sm + 13.5 w_{max24}–3.2MBV	0.87
32	SWUD = −637−1.93 MBV + 13 w_{max24}	0.87
33	SPR = −20.52 + 2.01 MBV + 0.32 LL	0.87
34	SWUD = −638.163−2.3 LL + 3.38 Sm + 13.3 w_{max24}	0.87
35	SWUD = −637.2 + 12.8 w_{max24} + 0.012 LL	0.86
36	SWUD = −640.2−2.3MBV + 0.1 LL + 13 w_{max24}	0.86
37	SPUD = −34.28 + 0.23 LL + 9.45γ_d + 0.62 wn	0.86
38	SPUD = − 13.90 + 1.66 MBV + 0.22 LL	0.85
39	SPR = −18.78 + 0.23 Sm + 0.35 w_{max24}	0.85
40	SWR = −2222.6 + 13 LL + 732.1γ_d + 3.6PI + 20.8 wn	0.84
41	SWR = −2272.7 + 21.4 wn + 15.4 LL + 724.9γ_d	0.84
42	SWR = −2831.9 + 35.6 LL + 809.4γ_d + 9.05PL− 14.6Clay	0.84
43	SWR = −2537.1 + 35.2 LL + 762.8+$_d$− 11.9Clay	0.84
44	SWR = −1325.5 + 25.1 LL + 1.7PL−4.4Clay + 9.98 wn	0.82
45	SWR = −1284.5 + 25.2 LL−4 Clay + 9.8 wn	0.82
46	SPR = −21.8 + 0.62 LL−0.08 PL	0.82
47	SWR = −923.4 + 26.5 LL−9.8 PL	0.81
48	SPUD = −18.13 + 0.4 LL + 0.13 PL	0.79

Notes

SWUD: Swelling pressure of undisturbed sample (kPa).
SWR: Swelling pressure of remolded sample (kPa).
SPUD: Swelling percent of undisturbed sample (%).
SPR: Swelling percent of remolded sample (%).
MBV: Methylene blue value (g/100 g).
W_{max24}: Water content at 24 hours (%).
Sm: Percent of smectite.
Clay: Percent of clay fraction.
LL: Liquid limit (%).
PI: Plasticity index (%).
PL: Plastic limit (%).
γ_d: Dry unit weight (g/cm^3).
W_n: Natural water content (%).

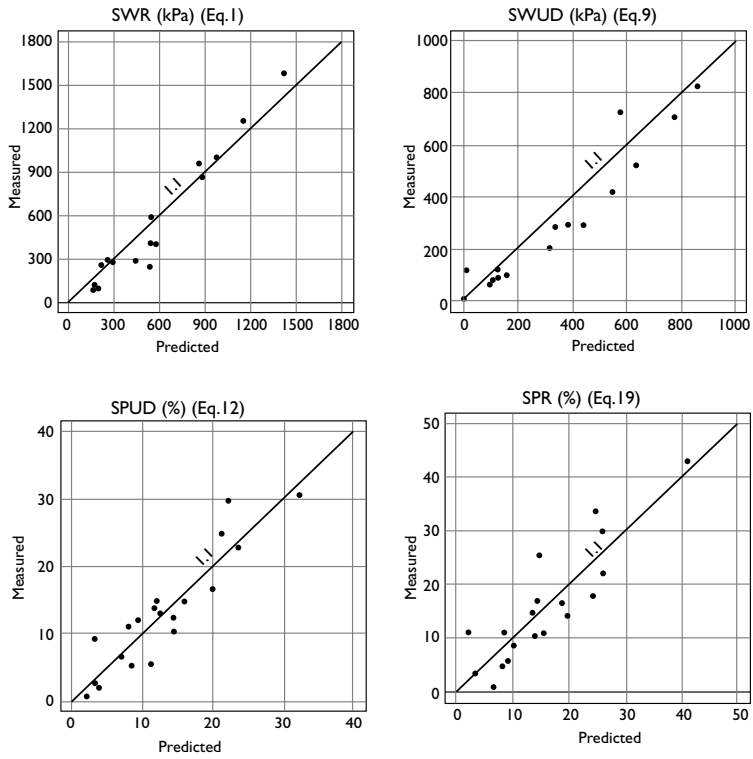

Figure 12.12 Predicted versus observed values of swelling parameters of Ankara Clay (SWUD and SWR are swelling pressure, and SPUD and SPR are the swelling percent of undisturbed and remoulded samples, respectively).

ponds of accumulated water were also observed around some of the damaged houses during rainy seasons. The cracks, which developed in the external walls, were generally diagonal at about 45°, occurring above and below windows and above doorways (Figures 12.13a and 12.13b). They widened with time reaching a few centimetre to 10 cm. Apart from filling the cracks in the walls with mortar or cement as shown in Figure 12.13b, no serious precautions were taken. An excavation of 1 or 1.5 m for house basement resulted in a net unloading of the subsoil, which was conducive of large, non-uniform expansion of subsoils and differential heaving of shallow foundations. Diagonal shear cracks, which begin in the corner of windows and doors, as well as horizontal traction cracks situated on the top of peripheral walls resulted due to a differential heaving of the soil profile as seen in Figures 12.13a and 12.13b. Door and window frames were frequently distorted by movement of the internal walls (Figure 12.13c). In one case, where the slab joints were not at the same level, slight doming of the floor slab occurred as can be seen in Figure 12.13d. This was probably caused by greater loss of soil moisture from the perimeter of the building due to evaporation so that the soil beneath the center of the floor slab had a higher water content.

Garden walls (Figure 12.14a) and roadways (Figure 12.14b) were also subjected to cracking by volume changes, which occurred in the subsoils beneath. A severely damaged asphalt pavement shown in Figure 12.14b was due to poor drainage systems, which resulted in water seeping into the soil underneath the pavement. In addition to this, heavy traffic also resulted in undulations with great amplitudes on the roadways in conjunction with expansion of the soil as seen in Figure 12.14b.

By considering the dimensions of the damaged light buildings, and the unit weight of the concrete and bricks, dead load, and load imposed by the roof and slab, the calculated pressures transferred onto the soil from buildings ranged between 10.6 and 49.5 kPa. This range was

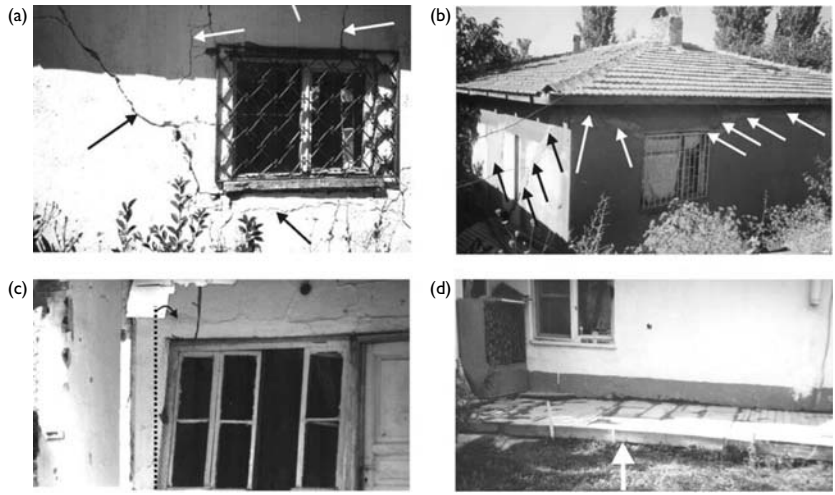

Figure 12.13 Typical views of the damaged low-rise buildings at the study site: (a) shear diagonal cracks in exterior walls as a result of upward soil expansions (case no.5), (b) diagonal cracks filled by cement (case no.18), (c) distorted window frame due to the movement of the walls (case no.13), and (d) slight doming of a floor slab due to heave (case no.10).

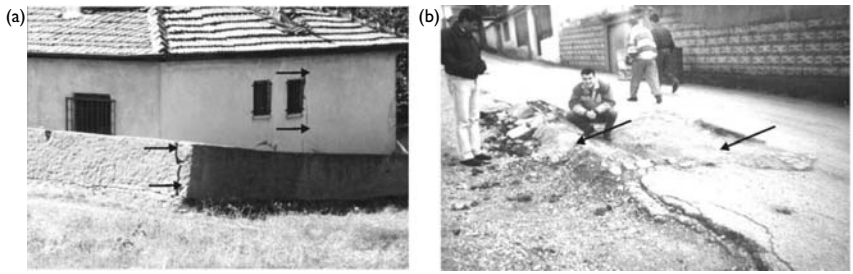

Figure 12.14 (a) Damaged garden wall due to differential heave of the clay, and (b) excessive heave and cracking of the asphalt pavement caused by reactive soil.

considerably smaller than the swelling pressures caused by the soil experimentally determined in the laboratory (see Table 12.4). Foundations of modern multi-storey apartment blocks constructed on the site extended to depths 5–7 m beyond the active zone. They were heavy enough to counter swelling pressures. Therefore, no structural damage to these buildings was observed.

Swelling map

Maps showing the areal distribution of low to very high expansive soils in the Ankara metropolitan area are considered to be a useful tool for city planners and engineers in their efforts to achieve better land use planning, and for assessment of environmental problems. Preparation of such maps based on swelling pressure and/or swelling percent, which are determined through expensive laboratory tests, takes a long time particularly for large areas. Therefore, the use of predictive equations for the estimation of swelling parameters as the inputs of these maps seems to be more practical. By considering this and the absence of such maps for the Ankara metropolitan area, swelling maps were prepared in two phases. The swelling map prepared for pilot site in phase 1, using the laboratory derived swelling parameters and remoulded samples indicated that the soils in the northern, western, and partly central parts of the site exhibited higher swelling pressures and swelling percentage (Figures 12.15a and 12.15b). The locations of the damaged low-rise buildings shown on the maps also confirmed this distribution.

In phase 2, swelling maps for a large district involving both the pilot site and the central part of the metropolitan area were constructed. In this district, Ankara Clay preserved its typical characteristics and the urbanization was very dense. However, except in the investigated pilot site, swelling parameters for the whole district were not available. For this reason, the predictive equations in Table 12.6 (Equations 47 and 46 for swelling pressure and swelling percentage, respectively) and the common available index properties of the clay such as liquid limit and plastic limit from previous studies in Ankara (Doruk 1968;

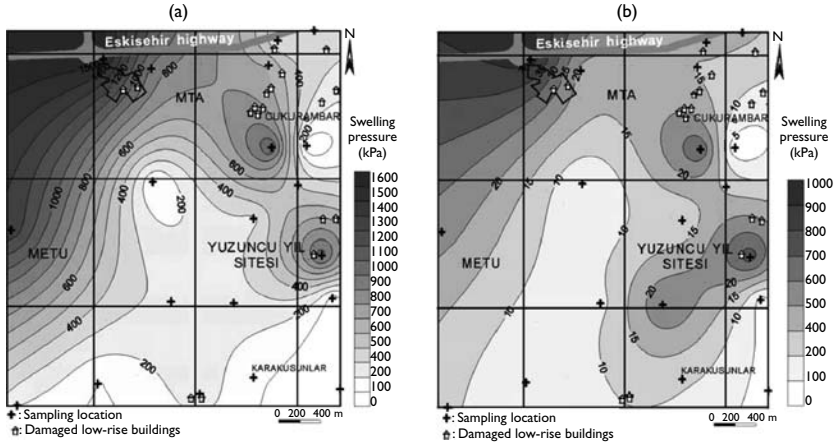

Figure 12.15 (a) Swelling pressure and (b) swelling percentage maps of the pilot site based on laboratory measured values from remoulded samples.

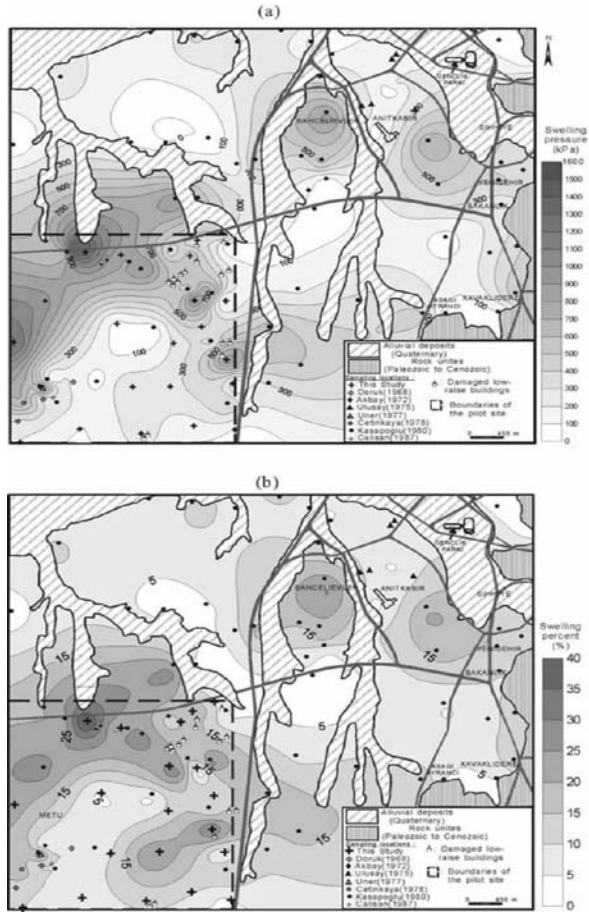

Figure 12.16 (a) Swelling pressure and (b) swelling percentage maps based on predictive equations 47 and 46, respectively, for the SW and central parts of the Ankara metropolitan area.

Akbay 1972; Ulusay 1975; Uner 1977; Cetinkaya 1978; Kasapoglu 1980; Calisan 1987) were employed to construct swelling pressure and swelling percentage maps (Figure 12.16). It was noted that although moderate swelling pressures were estimated in some districts out of the pilot site (Figure 12.16a), no structural damage had occurred due to the absence of low-rise building in these densely urbanized districts.

Concluding remarks

Ankara Clay with very high liquid limits had high to very high activity and exhibited high swelling pressure, which resulted in damage to light structures. The depth of the active zone

was very shallow and extended to about 2 m below the ground surface. Swell pressure of soil considerably increased when the water content was less than 30%. The use of remoulded and desiccated samples provided a better approach in swelling tests for achieving more reliable swelling parameters. Based on the limited data, it could be concluded that the soil seemed to be anisotropic with respect to swelling. However, further studies on this phenomenon are needed. The swelling pressures obtained from the remoulded samples correlated with mineralogical and index properties when comparing swelling percentage and swell indices such as FS and MFSI. Therefore, the swell pressure is a better parameter for quantifying swell potential.

The empirical equations based on two or more index and/or physical properties were better predictors than those including single parameter. Particularly w_{max24}, liquid limit and MBV can be used to predict swelling parameters more precisely. Distribution of the low-rise buildings with some damage due to swelling was highly consistent with the locations of the samples having higher swelling pressures. Soil heave was the main cause of the damage to light structures at the study site due to the highly expansive nature of the soil, flat topography resulting in poor drainage, semi-arid climate, poor construction methods, and ineffective precautions. It was also noted that the pressure on the soil caused by the light structures was very low when compared to the swelling pressure caused by the soil.

The swelling maps constructed by using the predictive equations were generally in good agreement with those constructed from measured values. It is hoped that these maps will be useful tools for planners and engineers in their efforts to achieve better land use planning and to assess suitable remedial measures. The low-rise buildings at the southwestern part of Ankara metropolitan area were associated with low cost margins, and extensive site investigations and effective remedial measures before and after their construction were not considered due to economic reasons. On the other hand, these buildings were rapidly giving way to heavy, high-rise apartment blocks with deep foundations, and consequently such buildings will probably disappear in the near future in this region of the city. However, certain precautions such as reinforced deep strip footings or rafts, as foundations at an adequate depth, particularly below the active zone, should be considered at the site. Installation of sub-surface drains to eliminate ponding, protective gravelly isolations around the shallow-seated buried utility lines such as water pipes and sewage network, soil treatment, if necessary, and caution when planting trees close to the structures are also suitable remedies to minimize or overcome the effects of heave.

References

Abduljauwad, S.N., 1993. Study on the performance of calcareous expansive clay. *Bulletin of the Association of Engineering Geologists*, 30(4), 481–498.

Abduljauwad, S.N. and Al-Suleimani, G.J., 1993. Determination of swell potential of Al-Qalif clay. *Geotechnical Testing Journal of ASTM*, 16(4), 469–484.

AFNOR (L'Association Francaise De Normalisation), 1980. Essai au bleu de methylene. 18–592, AFNOR 80181, Paris La Defence.

Akbay, U., 1972. The influence of saturation on volume change characteristics of Ankara Clay under various surcharge pressures. MSc Thesis, Civil Engineering Department, Middle East Technical University, Ankara, Turkey.

Al-Homoud, A.S. and Al-Suleiman, T.I., 1997. Loss in serviceability of pavements due to expansive clay subgrades. *Environmental and Engineering Geoscience*, III(1), 277–294.

Al-Rawas, A.A., 1999. The factors controlling the expansive nature of the soils and rocks of northern Oman. *Engineering Geology*, 53, 327–350.

Aras, I.A., 1991. Clay mineralogy and sedimentological features of the Late Pliocene sediments in Ankara area. MSc Thesis, Department of Geological Engineering, Middle East Technical University, Ankara, Turkey.

ASTM, 1994. Annual Book of ASTM Standards-Soil and Rock, Building Stones, Section 4, Construction, V. 04.08, ASTM Publication.

Basma, A.A., 1991. Estimating uplift of foundations due to expansion: A case history. *Geotechnical Engineering*, 22, 217–231.

Basma, A.A., Al-Hamoud, A.S., and Husein, A., 1995. Laboratory assessment of swelling pressure of expansive soils. *Applied Clay Science*, 9, 355–368.

Bell, F.G. and Maud, R.R., 1995. Expansive clays and construction, especially of low-rise structures: A viewpoint from Natal, South Africa. *Environmental and Engineering Geoscience*, I(1), 41–59.

Birand, A.A., 1963. Study of the characteristics of Ankara Clays showing swelling properties. MSc Thesis, Department of Civil Engineering, Middle East Technical University, Ankara, Turkey.

Bonner, C. and Shakoor, A., 1998. Predicting the swelling potential of a bentonitic clay from initial water content and dry density values. Proceedings of the 8th International IAEG Congress, Vancouver, Canada, Vol. I, 925–935.

Calisan, O.F., 1987. A study on volume change behavior of silt added METU Clay. MSc Thesis, Department of Civil Engineering, Middle East Technical University, Ankara, Turkey.

Cetinkaya, A.S., 1978. Preconsolidation pressure and its effects on some properties of METU campus clay. MSc Thesis, Department of Civil Engineering, Middle East Technical University, Ankara, Turkey.

Chen, F.H., 1988. *Foundations on Expansive Soils*. Elsevier Science Publishers, Amsterdam, The Netherlands.

Cokca, E., 1991. Swelling potential of expansive soils with a critical appraisal of the identification of swelling of Ankara soils by methylene blue tests. PhD Thesis, Department of Civil Engineering, Middle East Technical University, Ankara, Turkey.

Cokca, E. and Birand, A.A., 1993. Prediction of swelling potential of Ankara soils by methylene blue test. *Doga Turkish Journal of Engineering and Environmental Sciences*, 17, 57–63.

Day, R.W., 1998. Swelling behavior of desiccated clay. *Environmental and Engineering Geoscience*, IV(1), 124–129.

Derriche, Z. and Iguechtal, L., 2000. Damage due to swelling soils in the region of In-Amenas: Algeria. Proceedings of GeoEng 2000, An International Conference on Geotechnical and Geological Engineering, Melbourne, Australia (on CD).

Doruk, M., 1968. Swelling properties of clays on the METU Campus. MSc Thesis, Department of Civil Engineering, Middle East Technical University, Ankara, Turkey.

Du, Y., Li, S., and Hayashi, S., 1999. Swelling-shrinkage properties and soil improvement of compacted expansive soil, Ning-Liang Highway, China. *Engineering Geology*, 53, 351–358.

Erguler, Z.A. and Ulusay, R., 2003. A simple test and predictive models for assessing swell potential of Ankara (Turkey) Clay, *Engineering Geology*, 67, 331–352.

Erol, O., 1973. Ankara sehri cevresinin jeomorfolojik ana birimleri. *AUDTCF Yayinları* No. 240, 29 p (in Turkish).

Fourie, A.B., 1989. Laboratory evaluation of lateral swelling pressure. *Journal of Geotechnical Engineering ASCE* 115(10), 1481–1486.

Furtun, U., 1989. An investigation on Ankara soils with regard to swelling. MSc Thesis, Department of Civil Engineering, Middle East Technical University, Ankara, Turkey.

Gundogdu, M.N.G., 1982, Geological, mineralogical and geochemical investigation of the Neogene agend Bigadic sedimentary basin. PhD Thesis, Department of Geological Engineering, Hacettepe University, Ankara, Turkey (in Turkish).

Holtz, W.G. and Gibbs, H., 1956. Engineering properties of expansive clays. *Transactions of the American Society of Civil Engineers*, 121, 641–677.

Kasapoglu, K.E., 1980. Ankara kenti zeminlerinin jeo-muhendislik ozellikleri. Associate Professorship Thesis, Department of Geological Engineering, Hacettepe University, Ankara, Turkey.

Kocyigit, A. and Turkmenoglu, A., 1991. Geology and mineralogy of the so-called Ankara Clay formation: A geologic approach to the Ankara Clay problem. Proceedings of the 5th National Symposium on Clay, Eskisehir, Turkey, 112–125.

Li, S. and Du, Y., 1997. On the swelling–shrinkage properties and mechanisms of compacted expansive soil. Proceedings of the 30th International Geological Congress, China, Vol. 23, 253–259.

Meisina, C., 2002. Swelling/shrinkage hazard assessment applications in Italy, Proceedings of the 9th Congress of International Association for Engineering Geology and Environment, Durban, South Africa, 625–635.

Mohan, D., Jain, G.S., and Sharma, D., 1973, Foundation practice in expansive soils in India. Proceedings of the 3rd International Conference on Expansive Soils, Haifa, Israel, 125–132.

Nawari, O. and Schetelig, K., 1991. Geotechnical study on Kordofan tropical black soils, Sudan Republic. *Engineering Geology*, 31, 1–26.

Omay, B., 1970. Swelling clays on METU Campus. MSc Thesis, Department of Civil Engineering, Middle East Technical University, Ankara, Turkey.

Ordemir, I., Alyanak, I., and Birand, A.A., 1965. Report on Ankara Clay. METU Publication No.12.

Ordemir, I., Soydemir, C., and Birand, A.A., 1977. Swelling problems of Ankara clays. Proceedings of the 9th International Conference on Soil Mechanics and Foundation Engineering, Tokyo, Japan, Vol. 1, 243–247.

Oteo, C.S., Salinas, J.L, Ayala, F.J, and Ferrer, M., 1995. Risk map for swelling of soils in Spain: results. Proceedings of the 1st International Conference on Unsaturated Soils, Paris, Vol. 34, 915–920.

Popa, A., 1997. Shrinkage–swelling phenomena effects on building. Proceedings of the International Symposium on Engineering Geology and the Environment, Athens, Greece, 327–329.

Popescu, M.E., 1979. Engineering problems associated with expansive clays from Romania. *Engineering Geology*, 14, 43–53.

Ramana, K.V., 1993. Humid tropical expansive soils of Trinidad: Their geotechnical properties and areal distribution. *Engineering Geology*, 34, 27–44.

Sherard, J.L., Decker, R.S., and Ryker, N.L., 1972. Piping in earth dams of dispersive clay. Proceedings of ASCE Speciality Conference on Performance of Earth and Earth-Supported Structures, Vol. 1, 589–626.

Shi, B., Jiang, H., Liu, Z., and Fang, H.Y., 2002. Engineering geological characteristics of expansive soils in China, *Engineering Geology*, 67, 63–71.

Sivapullaiah, P.V., Sitharam, T.G., and Rao, K.S.S., 1987. Modified free swell index for clays. *Geotechnical Testing Journal of ASTM*, 10(2), 80–85.

Ulusay, R., 1975. Clays in Ankara city and their engineering properties. *Yerbilimleri* (Earthsciences), 1, 67–72 (in Turkish).

Uner, A.K., 1977. A comparison of engineering properties of two soil types in the Ankara region. MSc Thesis, Department of Civil Engineering, Middle East Technical University, Ankara, Turkey.

USGS, 2000. Swelling clays map of the conterminous U.S. US Geological Survey (http://www.webbwebs.com/surevoid/surevoid_web/soil . . . /intro1.htm, 14.04.2000)

Van der Merve, D.H., 1964. The prediction of heave from the plasticity index and the percentage clay fraction. *The Civil Engineer* (South African Institution of Civil Engineer), 6, 103–107.

Weston, D.J., 1980. Expansive road treatment for Southern Africa. Proceedings of the 4th International Conference on Expansive Soils, Denver, Vol. 1, 339–360.

Chapter 13

Prediction of swelling characteristics with free swell index

Bhyravajjula R. Phanikumar[1]

Summary

The aim of this chapter was to report studies on swelling characteristics that could be predicted with free swell index as a parameter. An extensive laboratory program was conducted to develop correlations for swell potential and swelling pressure. Relationships for swell potential and swelling pressure of remolded and compacted expansive soils in terms of free swell index and placement conditions as developed by the author were presented.

Introduction

Troubles posed by expansive soils have been recorded all over the world. They have been found to cause detrimental damage to structures founded on them because of their innate potential to react to changes in moisture regime. They undergo severe volume changes corresponding to changes in moisture content. Expansive soils *swell* or increase in their volume by imbibing or absorbing water in rainy or wet seasons and *shrink* or decrease in their volume when water evaporates from them during summer or dry seasons (Holtz and Gibbs, 1956; Johnson and Snethen, 1978; Chen, 1988). Furthermore, upon wetting during a monsoon, expansive soils can exhibit swell or reduction in volume depending upon the stress and suction history of the soil (Sharma, 1998; Sharma and Wheeler, 2000; Gallipoli *et al*., 2003; Wheeler *et al*., 2003). The alternate swelling and shrinkage of such soils in different seasons result in severe cracking of civil engineering structures. As the lightly loaded structures cannot counteract the swelling pressure caused by expansive soils, they are subjected to severe cracking (Technical Manual, 1983; Chen, 1988). The types of structures that are damaged are foundations, retaining walls, pavements, airports, sidewalks, canal beds, and linings (Chen, 1988; Wray, 1980). The types of problems that have caused the damage are diagonal cracks above doors and windows, pavement cracking, and heaving of floors (Technical Manual, 1983).

The cost of repair to damage caused by expansive soils to civil engineering structures per annum is estimated at $300 million in the UK, $1000 million in the USA and many billions of dollars worldwide (Gourley *et al*., 1993). The cost of repair has been found to increase

[1] Dept of Civil Engineering, GMR Institute of Technology, Rajam 532127, Andhra Pradesh, India; e-mail: phanikumar_29@yahoo.com

with every passing year. While it was estimated at $2.3 billion in 1973 in USA itself, it reached $7 billion in USA by 1980. It is reported that the annual cost of repair at present is placed at $10 billion in USA, exceeding the annual cost of repair to damage by tornadoes, floods, earthquakes, and hurricanes put together. The problems posed by expansive soils have been counteracted by various techniques such as chemical treatment using lime, cement and calcium chloride, and also by different innovative foundation techniques such as belled piers (Chen, 1988).

The prime factors for this basic tendency for expansion in these soils are the presence of the mineral montmorillonite, the soil being dry or unsaturated, and the presence of suction. Of all the three important types of clay minerals, namely, montmorillonite, kaolinite, and illite, it is the mineral montmorillonite that contributes most to swelling in expansive soils. It has an expanding lattice structure. The building blocks of the mineral get separated when these soils absorb water and, thereby, cause expansion or volume increase. Second, the soil must be dry or in an unsaturated condition to be able to absorb water and swell. A completely saturated soil does not show any volumetric increase because it cannot imbibe any water. Third, the soil must have some amount of suction, or negative pore pressure, which represents the affinity that a soil has for water. A dry or unsaturated soil has greater affinity for water and, therefore, shows a greater volume increase on absorption of water, whereas, a saturated soil has no affinity for water and consequently does not swell.

The aim of this chapter was to report studies on swelling characteristics that could be predicted with free swell index as a parameter. An extensive laboratory program was conducted to develop correlations for swell potential and swelling pressure. Relationships for swell potential and swelling pressure of remolded and compacted expansive soils in terms of free swell index and placement conditions as developed by the author were presented.

Identification of expansive soils

To be able to counteract the problems posed by expansive soils, it is necessary to identify them first. A successful design and construction of foundations on expansive soils requires a good understanding of swelling characteristics, namely, free swell index, swell potential, and swelling pressure. Expansive clays are identified by mineralogy, by direct measurement of swelling characteristics (swell potential and swelling pressure), and by indirect correlations of swelling characteristics with simple index properties.

Mineralogical composition

The degree of volume change experienced by an expansive soil depends, to a great extent, on its mineralogical composition. The three basic groups of clay minerals are montmorillonite, illite, and kaolinite. Expansive soils are usually composed of these clay minerals. The presence of montmorillonite, which has an expanding lattice contributes most to swelling, while that of illite contributes a little less (Shreiner, 1987). Kaolinites, on the other hand, are non-expansive.

The various techniques (Chen, 1988) employed to determine the mineralogical compositions are X-Ray Diffraction, Differential Thermal Analysis (DTA), Dye Adsorption Technique, Chemical Analysis, and Electron Microscope Resolution (EMR). As these techniques require highly sophisticated equipment, most of the laboratories cannot afford them.

Direct measurement of swelling characteristics

The best and the easiest way of identifying expansive soils is to directly measure swelling characteristics, namely, swell potential and swelling pressure by performing one-dimensional swell-consolidation tests in an oedometer. In this test, the sample is first allowed to swell completely (for the determination of full swell potential) and then consolidated under applied pressures (for the determination of swelling pressure).

Swell potential (S) of a soil is defined as the ratio of increase in thickness (ΔH) to the original thickness (H) of the soil sample compacted at optimum moisture content in a consolidation ring and soaked under a token surcharge of 6.9 kPa (Seed *et al*., 1962). It is expressed as:

$$S = (\Delta H/H) \times 100 \tag{13.1}$$

Swelling pressure (σ_{sp}), as determined by free swell method, is defined as the pressure that is required to recompress a completely swollen soil sample to its original unloaded volume or volume under a small token surcharge of about 10 kPa (Jennings, 1963). It is obtained from e-log p curve as the pressure corresponding to the initial void ratio.

Indirect correlations of swelling characteristics with index properties and placement conditions

The degree of expansiveness or swelling of an expansive soil can be estimated by predicting swelling characteristics from its index properties. Simple index properties such as Atterberg limits, clay content and activity are used as parameters for developing correlations for swelling characteristics. As the scope of this chapter is limited, correlations with only a few index properties are discussed here. Some correlations with placement conditions are also dealt with because swelling characteristics depend also on placement conditions such as water content and dry unit weight.

Correlations for swelling characteristics with index properties

In a previous research Seed *et al*. (1962), Ranganatham and Satyanarayana (1965), and Bandyopadhyay (1981) proposed relationships for swell potential of remolded natural expansive soils using index properties such as plasticity index (numerical difference between liquid and plastic limits), clay content, activity, and shrinkage index (difference between liquid and shrinkage limits) which have only an indirect bearing on the degree of swelling. Activity (Skempton, 1953) is defined as the ratio of plasticity index to the percentage of the soil fraction less than 2 μm. The definition of activity was later modified (Seed *et al*., 1962) as:

$$\text{Activity} = (\text{Plasticity index}) / (\%\text{clay fraction} < 2\ \mu\text{m} - 5) \tag{13.2}$$

A soil with activity of less than 0.75 is termed as inactive, which means that it indicates a low potential for volume change. A soil with activity of more than 1.25 is termed as active, indicating a high potential for volume change. The values in between indicate medium potential and soils possessing medium values are classified as normal.

Table 13.1 Shrinkage factors as a guide to potential expansion

Shrinkage limit (%)	*Linear shrinkage (%)*	*Probable swell (%)*	*Degree of expansion*
<10	>8	>1.5	Critical
10–12	5–8	0.5–1.5	Marginal
>12	<5	<0.5	Non-critical

Source: Altmeyer (1955).

Table 13.2 Data for estimating probable volume change

Colloidal content	*Plasticity index (%)*	*Shrinkage limit (%)*	*Probable volume change (%)*	*Degree of expansion*
>28	>35	<11	>30	Very high
20–31	25–41	7–12	20–30	High
13–23	15–28	10–16	10–20	Medium
<15	<18	>15	<10	Low

Source: Holtz (1959).

Altmeyer (1955) characterized the degree of expansion of a soil based on its shrinkage limit and linear shrinkage as shown in Table 13.1. Linear shrinkage is defined as the ratio of decrease in linear dimension of a specimen to its initial dimension, expressed as a percentage and is given by the nearest whole number.

Holtz and Gibbs (1956) proposed some identification criteria based on the probable volume change in expansive soils, which is the percentage change in the thickness of the sample from oedometer swell under a surcharge of 6.9 kPa or 1 psi from the air dry condition to saturation. Considering some important soil properties (Table 13.2), the probable expansion is calculated.

Seed *et al*. (1962) proposed a linear relationship between swell potential (S) and plasticity index (PI) as:

$$S = 2.16 \times 10^{-3} (\mathrm{PI})^{2.44} \tag{13.3}$$

where swell potential is the ratio of the increase in thickness to the original thickness of the soil sample in a consolidation ring, compacted at optimum moisture content, and soaked in water under a surcharge of 6.9 kPa (1 psi). This is expressed as a percentage. Seed *et al*. (1962) gave another expression for swell potential (S) in terms of activity (A) and clay content (C) as:

$$S = 3.6 \times 10^{-5} (A^{2.44}) (C^{3.44}) \tag{13.4}$$

Chen (1988) proposed a relationship for the percentage swell (S) of undisturbed soils in terms of plasticity index (PI) in the form:

$$S = B \times \mathrm{e}^{A(\mathrm{PI})} \tag{13.5}$$

where A and B are constants equal to 0.0838 and 0.2558 respectively. For the development of this correlation, the surcharge pressure used was 6.9 kPa. The water content varied between 15% and 20% and the dry density between 16 and 17.6 kN/m^3.

Williams and Donaldson (1980) classified the degree of expansiveness considering plasticity index of the whole sample, PI_{ws}, which is given as:

$$PI_{ws} = \text{PI of soil passing 425 } \mu\text{m sieve} \times (\text{mass of soil passing 425 } \mu\text{m sieve/mass of whole sample}) \quad (13.6)$$

The classification of the degree of expansiveness based on PI_{ws} is shown in Table 13.3.
Holtz and Gibbs developed a simple test called the free swell test for the determination of swell potential of a soil. The test is performed by pouring 10 cc of soil passing 425 μm sieve into a graduated cylindrical glass jar of 100 ml capacity filled with water. The swollen volume of the soil is observed after 24 hours. The free swell is expressed as a percentage increase in the volume to the original volume of the soil. Soils having a free swell of 100% or more damage lightly loaded structures and those having a free swell of less than 50% do not pose serious problems to structures.

Mohan and Goel (1959) suggested a more convenient method, wherein 10 g of oven-dried soil passing 425 μm sieve are poured separately into two graduated cylindrical jars of 10 ml capacity, one containing distilled water and the other kerosene. After allowing both the jars to stand for 24 hours, the final volumes of the soil in the two cylinders are noted. The differential free swell, which is later re-designated as free swell index (FSI) expressed as a percentage, is given as:

$$FSI = \left(\frac{\text{Final volume of soil in water} - \text{Final volume of soil in kerosene}}{\text{Final volume of soil in kerosene}}\right) \times 100 \quad (13.7)$$

The classification of degree of expansiveness based on FSI is shown in Table 13.4.

Table 13.3 Degree of expansiveness based on plasticity index of whole sample

PI of whole sample	*Degree of expansiveness*
>32	Very high
24–32	High
12–24	Medium
<12	Low

Source: Williams and Donaldson (1980).

Table 13.4 Degree of expansion based on free swell index, FSI

Liquid limit (%)	*Plasticity index (%)*	*Free swell index (%), FSI*	*Degree of expansion*	*Degree of severity*
70–90	>32	>200	Very high	Severe
50–70	23–32	100–200	High	Critical
35–50	12–23	50–100	Medium	Marginal
20–35	<12	<50	Low	Non critical

Source: Mohan and Goel (1959).

Correlations for swelling characteristics with placement conditions

Placement conditions, which include surcharge, water content, and dry density of the soil, govern the volume change behavior of a soil. Swell potential and swelling pressure depend on the above placement conditions apart from index properties and clay content. The higher the initial dry unit weight, the greater will be the swell potential and swelling pressure. Both swell potential and swelling pressure decrease with increasing initial water content. An increase in surcharge pressure obviously reduces the amount of swell potential. But, various opinions prevail about the effect of surcharge pressure on swelling pressure. According to Satyanarayana (1966), swelling pressure is dependent on initial surcharge, but Chen (1988) observed that it is independent of initial surcharge. Having a direct influence on the values of swell potential and swelling pressure, the placement conditions are important parameters for predicting swelling characteristics.

Some researchers, (Komornik and David, 1969; Vijayvergiya and Ghazzaly, 1973; Nayak and Christensen, 1974) based on experimental data, proposed relationships for swell potential and swelling pressure involving both placement conditions and index properties. Komornik and David (1969) proposed the following correlation for swelling pressure of undisturbed clays:

$$\log p_s = -2.132 + 0.0208\, w_L + 0.00665\, \gamma_d - 0.0269\, w_i \tag{13.8}$$

where p_s is the swelling pressure in kg/cm^2, w_L is the liquid limit of the soil, γ_d is the initial dry density in kg/m^3 and w_i is the initial water content.

Vijayvergiya and Ghazzaly (1973) proposed the following correlations for swell potential and swelling pressure of undisturbed samples tested under a surcharge of 10 kPa.

$$\log S = 1/19.5\,(\gamma_d + 0.65\, w_L - 130.5) \tag{13.9}$$

where S is the percent swell, γ_d is the dry density of the soil in lb/ft^3, w_L is the liquid limit (%) and w_i is the natural water content (%).

$$\log p_s = 1/19.5\,(\gamma_d + 0.65\, w_L - 139.5) \tag{13.10}$$

where p_s is the swelling pressure in tons/ft^2.

Nayak and Christensen (1974) gave statistical relationships for swell potential and swelling pressure as,

$$S = (2.29 \times 10^{-2})\,(I_P)^{1.45} \times C/w_i + 6.39 \tag{13.11}$$

$$\text{and } p_s = 2.50 \times 10^{-1}\,(I_P)^{1.12} \times C^2/w_i^2 + 25 \tag{13.12}$$

where S is the percent swell, p_s is the swelling pressure (kN/m^2), I_P is the plasticity index, C is the clay content, and w_i is the initial water content (%).

Importance of free swell index (FSI) and developed correlations

The FSI can be considered as a property of an expansive soil. It reflects the potential for expansion of the soil. The FSI test is carried out on oven-dried soil passing 425 μm sieve.

It is defined as the ratio of the difference in volumes of soil in water and kerosene to the volume of soil in kerosene (Holtz and Gibbs, 1956). It is expressed as:

$$\text{FSI} = \left(\frac{\text{Final volume of soil in water} - \text{Final volume of soil in kerosene}}{\text{Final volume of soil in kerosene}} \right) \times 100 \tag{13.13}$$

Soils having FSI $>$ 200, FSI between 100 and 200, FSI between 50 and 100 and FSI $<$ 50 are respectively characterized as having a degree of expansion described as "very high," "high," "medium," and "low" (Mohan, 1977). The author of this chapter considered that swelling characteristics could be predicted with free swell index as a parameter instead of other index properties. An extensive laboratory program was conducted to develop correlations for swell potential and swelling pressure (Phanikumar, 1997). Relationships for swell potential and swelling pressure of remolded and compacted expansive soils in terms of free swell index and placement conditions as developed by the author are presented in this chapter. The relationships are based on experimental data determined on soil samples from ten different sources. All the soils are CH soils (clays of high plasticity) and had FSI values more of than 100%.

Test details and variables

Swell potential and swelling pressure were determined by swell-consolidation method, in which the sample is freely allowed to swell by inundation. Swell potential and swelling pressure were determined at the following placement conditions:

Initial water content, w_i (%): 0, 5, 10, 15, and 20
Initial dry unit weight, γ_{di} (kN/m^3): 10, 12, 14, 16, and 18
Initial surcharge, q_i(kPa): 5, 50, 100, 150, and 200

In total, 1250 swell-consolidation tests were performed.

Sample preparation and test procedure

The expansive soil was first air dried and pulverized to pass through 4.75 mm. It was then oven dried at a constant temperature of 105°C to reduce the water content to 14% so that the maximum value of swell potential would be obtained. The sample was allowed to cool down to the room temperature. The required weight of the oven-dried sample was mixed with the required amount of distilled water (based on the weight of the oven-dry soil) and the wet sample was statically compacted in four layers, each of 5 mm thickness in the consolidation ring of thickness 20 mm and diameter 60 mm, to the desired placement water content and dry unit weight. A thin layer of silicon grease was applied to the walls of oedometer to reduce friction between the sample and the oedometer wall. A filter paper and a porous stone were placed at each end of the sample. This unit was placed in the oedometer and the loading pad positioned centrally on the top porous stone. The required initial surcharge pressure was applied on the specimen after setting the dial gauge reading (initial reading) to zero. Swell potential and swelling pressure were determined by free inundation method in which

the sample is completely inundated with water and allowed to swell freely under the applied surcharge. Dial gauge readings were taken up to equilibrium swell (no further change in the dial gauge reading). The increase in the thickness (ΔH) of the sample was noted after equilibrium swell. The sample was consolidated under increased applied pressures till the dial gauge reading was less than the initial reading. Swell potential (Seed *et al*., 1962) was determined as $S = [(\Delta H/H) \times 100]$, and swelling pressure from the e-log p curve as the pressure corresponding to the initial void ratio (Jennings, 1963).

Results

Figure 13.1 shows a typical example of e-log p curves for the soil (from a source called Waddilanka) compacted at an initial water content (w_i) of 10% and at a dry unit weight (γ_{di}) of 16 kN/m^3 and subjected to different initial surcharge pressures (q_i). As the initial surcharge increased, swell potential decreased as indicated by the decreasing void ratio. However, the swelling pressure was not influenced by the initial surcharge. This is in accordance with the observations made by Chen (1988). The swelling pressure was nearly the same for all the samples (Figure 13.1) irrespective of the initial surcharge, because swelling pressure is the pressure required to bring back a fully swollen soil sample to its initial void ratio (as per the free inundation method). Therefore, the total amount of pressure required to bring back the swollen sample to the initial volume (or void ratio) remains unchanged.

The results indicated that, for a given water content, swell potential increased with increasing dry unit weight. Increasing dry unit weight resulted in greater potential swelling. The results also showed that swell potential decreased with increasing water content for a given initial dry unit weight. With an increase in the initial water content the amount of uptake of water by the soil would be less resulting in a lower swell potential. Swelling

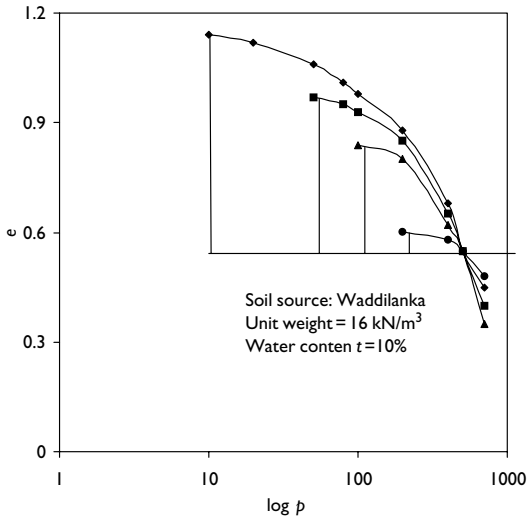

Figure 13.1 Effect of surcharge on swell potential and swelling pressure.

pressure also decreased with increasing water content. As the amount of swelling decreased with increasing water content, the pressure required to nullify the amount of swelling would also decrease.

Correlations developed

Relationships for swell potential ($S\%$) and swelling pressure (p_s) have been developed in terms of the placement conditions and FSI by performing multiple linear regression analysis on the entire experimental data, with the following results:

$$S\% = a_1\gamma_{di} - b_1 w_i - c_1 q_i + d_1(\text{FSI}) - K_1 \text{ and} \tag{13.14}$$

$$\log p_s = a_2\gamma_{di} - b_2 w_i + d_2(\text{FSI}) - K_2 \tag{13.15}$$

The constants or the regression coefficients for the above equations are,

$$a_1 = 4.24; b_1 = 0.47; c_1 = 0.14; d_1 = 0.06; \text{and } K_1 = 55 \text{ and}$$

$$a_2 = 0.30; b_2 = 0.02; d_2 = 0.005; \text{and } K_2 = 3$$

Since the initial surcharge pressure (q_i) had no effect on the swelling pressure as shown in Figure 13.1, it was not included in the analysis. The standard errors for the regression coefficients a_1, b_1, c_1, and d_1 are 9.69, 3.22, 1.76, and 1.15 respectively. The standard deviation is 4.69. Similarly, the standard errors for the regression coefficients a_2, b_2, and d_2 are 4.82, 1.24, and 0.62 respectively. The standard deviation is 8.77. This means that most of the values of the predicted swell potential and swelling pressure do not show much deviation from the mean of the measured values. Hence, the linear model proposed for the prediction of swell potential and swelling pressure from FSI and placement conditions is a successful model.

Validation of relationships developed

Figure 13.2 shows the measured values of swell potential at water contents $w = 5\%$ and $w = 10\%$ of all the soils tested in comparison with those predicted from the equation proposed by the author (series 1 and 3) and by Nayak and Christensen as shown in series 2 and 4. Each series in the figure shows the measured and predicted values for all the 10 soils. The measured swell potential tallied closely with the swell potential predicted from the equation proposed by the author (Equation 13.14). For other water contents also the measured and predicted values tallied. However, the equation proposed by Nayak and Christensen (1974) shows significant difference between measured and predicted values of swell potential (series 2 and 4). The predicted values are much higher than the measured ones. The values predicted from the equation proposed by Vijayvergiya and Ghazzaly (1973) are too high to be plotted alongside those shown in Figure 13.2.

Figure 13.3 shows the measured values of swelling pressure at water content $w = 10\%$ of all the soils tested in comparison with those predicted from the equation proposed by the author (series 1) and from the equations proposed by Nayak and Christensen, and Komornik and David (series 2 and 3). The values predicted from the equation proposed by Vijayvergiya and Ghazzaly (1973) are also too high to be plotted alongside those shown in Figure 13.3. The swelling pressure predicted from the equation proposed by the author (Equation 13.15) showed

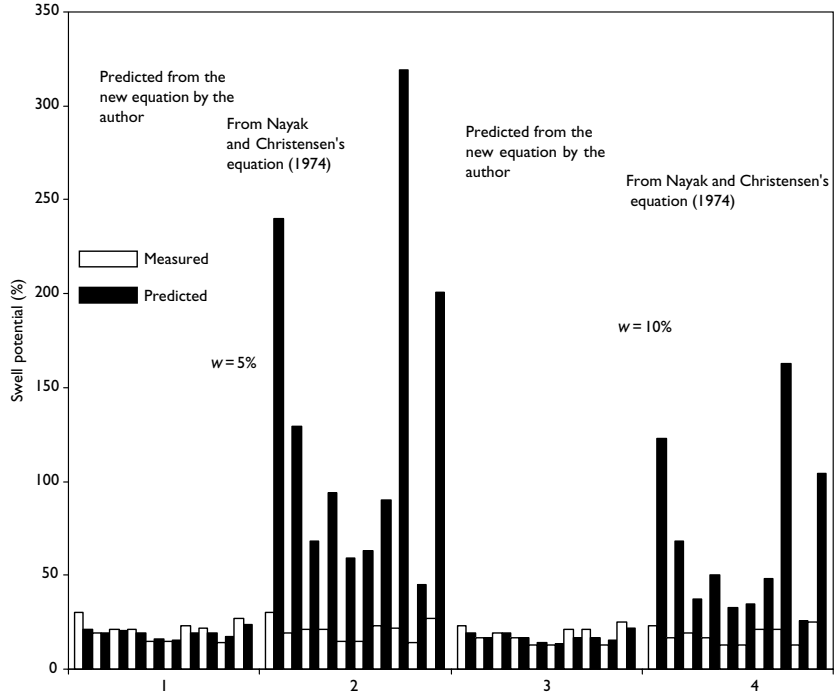

Figure 13.2 Swell potential values for $w = 5\%$ and $w = 10\%$ measured and predicted for all the 10 soils tested.

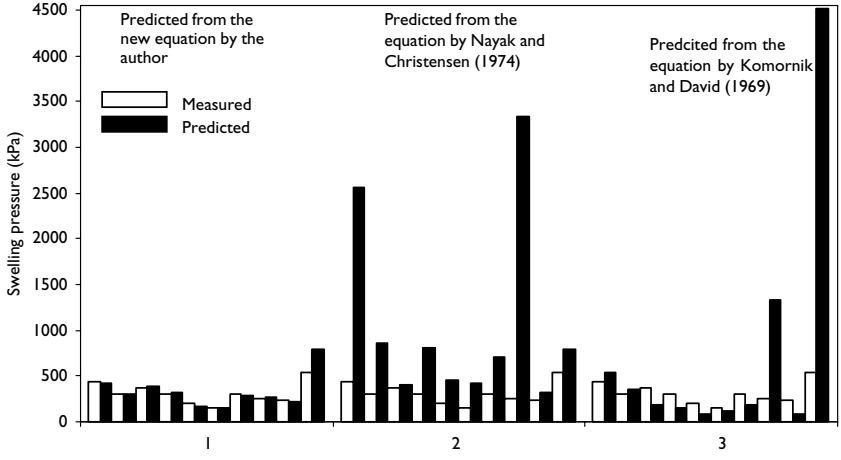

Figure 13.3 Swelling pressure values for $w = 10\%$ measured and predicted for all the 10 soils tested.

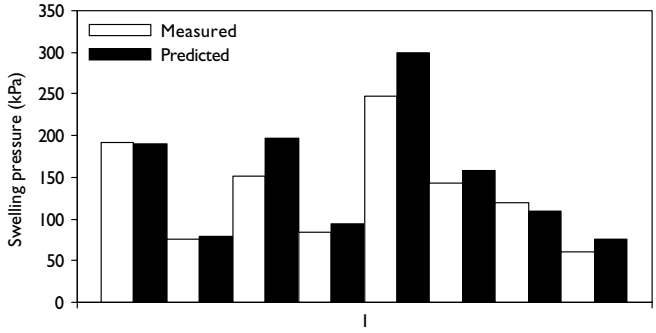

Figure 13.4 Swelling pressure of soils from other sources predicted by the new proposed equation.

a good relationship with that measured. The values predicted from the equation proposed by Nayak and Christensen were much higher than the measured values for all the soils. Komornik and David (1969) did not consider the initial surcharge pressure, while Nayak and Christensen (1974) considered only initial water content and Vijayvergiya and Ghazzaly (1973) only dry unit weight among the placement conditions. Apart from this inadequacy of not considering all the placement conditions together, these expressions included plasticity index, clay content and liquid limit, which do not directly reflect the swelling nature of expansive soils. The new proposed equation, however, considers the placement conditions together and also includes FSI, which directly reflects the swelling characteristics. Hence, the predicted values are close to the measured ones. Figure 13.4 compares the measured and predicted values of swelling pressure for soils from other sources (see Komornik and David, 1969) using the new proposed equation. The figure shows that the new equation predicts the swelling pressure values for the other soils very well. From the close agreement between the measured and predicted values of swelling pressure of soils from other sources also, it can be said that the proposed equations could be used for the prediction of swell potential and swelling pressure for a wide range of remolded and compacted expansive soils all over the world.

References

Altmeyer, W.T., 1988. "Discussion of engineering properties of expansive clays," *Proceedings of ASCE*, Vol. 81, separate No. 658.

Bandyopadhyay, S.S., 1981. "Prediction of swelling potential for natural soils," *Proceedings of ASCE, Journal of Geotechnical Engineering Division*, Vol. 107, No. GT 1, 658–661.

Chen, F.H., 1988. *Foundations on Expansive Soils*, Elsevier Scientific Publishing Co., Amsterdam.

Gallipoli, D., Gens, A., Sharma, R., and Vaunat, J., 2003. "An elasto-plastic model for unsaturated soil incorporating the effects of suction and degree of saturation on mechanical behaviour," *Geotechnique*, 53, No. 1, 123–135.

Gourley, C.S., Newill, D., and Schreiner, H. D., 1993. Expansive soils: TRL's research strategy. Proceedings of 1st International Symposium on Engineering Characteristics of Arid Soils, London.

Holtz, W.G. and Gibbs, H.J., 1956. "Engineering properties of expansive clays," *Transactions of ASCE*, Vol. 121, 641–677.

Jennings, J.E., 1963. Discussion on "The heaving of buildings and associated economic consequences with particular reference to orange free state gold fields," *The Civil Engineers, S. A.* Vol. 5, 122.

Johnson, L.D. and Snethen, D.R., 1978. "Prediction of potential heave of swelling soil." *Geotechnical Testing Journal*, Vol. 1, No. 3, 117–124.

Komornik, J. and David, A., 1969. "Prediction of swelling potential for compacted clays," *Journal of the Soil Mechanics and Foundation Engineering Division, ASCE*, Vol. 95, No. 1, 209–225.

Mohan, D., 1977. Engineering of expansive soils, Inaugural address. Proceedings of the 1st National Symposium on Expansive Soils, HBTI, Kanpur, India.

Mohan, D. and Goel., R.K., 1959. "Swelling pressures and volume expansions on Indian black cotton soils," *Journal of the Institute of Engineers* (India), Vol. XL, No. 2, pt 1, 58–62.

Nayak, N.V. and Chiristensen, R.W., 1974. "Swelling characteristics of compacted expansive soils," *Clays and Clay Minerals*, Vol. 19, No. 4, 251–261.

Phanikumar, B. R., 1997. A study of swelling characteristics of and granular pile-anchor foundation system in expansive soils, PhD Thesis submitted to JN Technological University, Hyderabad, India.

Ranganatham, B.V. and Satyanarayana, B. 1965. A rational method of predicting swelling potential for compacted expansive clays. Proceedings of 6th International Conference Social Mechanics and Foundation Engineering, Canada, Vol.1, pp. 92–96.

Satyanarayana, B., 1966. Swelling pressure and related mechanical properties of black cotton soils, PhD Thesis, I. I. Sc., Bangalore, India.

Seed, H.B., Woodward, R.J., and Lundgren, R., 1962. "Prediction of swelling potential for compacted clays," *Journal of Social Mechanics and Foundation Engineering Soil Division, ASCE*, Vol. 88, No. SM3, Part I, Proceedings of *3169*, 53–87.

Sharma, R.S., 1998. Mechanical behaviour of unsaturated highly expansive clays, DPhil Thesis, University of Oxford, UK.

Sharma, R.S. and Wheeler, S.J., 2000. Behaviour of an unsaturated highly expansive clay during wetting/drying cycles. Proceedings of International Conference on Unsaturated Soils (UNSAT-ASIA), Singapore, 721–726.

Shreiner, H.D., 1987. "State-of-the-art review of expansive soils for TRRL", Imperial College, London, England.

Skempton, A.W., 1953. The colloidal activity of clays. Proceedings of 3rd International Conference on Soil Mechanics and Foundation Engineering, Zurich, Vol. 1, 57–61.

Technical Manual, TM 5-818-7., 1983. Department of the Army, USA.

Vijayavergiya, V.N. and Ghazzaly, O.I., 1973. "Prediction of swelling potential for natural clays," Proceedings of 3rd International Conference on Expansive Soils, Haifa, Israel, Vol. 1, 227–236.

Wheeler, S.J., Sharma, R.S. and Buisson, M.S.R., 2003. "Coupling of hydraulic hysteresis and stress–strain behaviour in unsaturated soils," *Geotechnique*, Vol. 53, No. 1, 41–54.

Williams, A.A.B. and Donaldson, G.W., 1980. Building on expansive soils in South Africa, 1976–1980, Proceedings of 4th International Conference on Expansive Soils, ASCE Publication, Vol. 2.

Wray, W.K., 1980. Analysis of stiffened slabs on ground over expansive soil, Proceedings of the 4th International Conference on Expansive Soils, American Society of Civil Engineers, Vol. 1, Denver, Colorado.

Part 4

Advanced techniques for swelling potential assessment

Chapter 14

Remote sensing of expansive soils

Use of hyperspectral methodology for clay mapping and hazard assessment

Sabine Chabrillat[1] *and Alexander F.H. Goetz*[2]

Summary

Hyperspectral remote sensing technology has the potential for direct identification of constituent minerals in soils. The question arises whether this technology could become a useful tool for identifying and evaluating expansive soils. This chapter reports on the use of high spectral resolution optical remote sensing to detect and map swelling clays, in the context of a rapidly growing urban area severely affected with swelling soil problems. The results showed that such optical remote sensing methods, coupled with reduced field and laboratory analyses, can offer practical help to civic planners, as long as the swelling soils are adequately exposed.

Introduction

Expansive clays and clay-shales cause billions of dollars of damage world-wide every year, more than all other natural hazards combined (Jones and Holtz, 1973). Chen (1988) showed the distribution of reported instances of heaving, indicating that the problem of expansive soil is widespread throughout the five continents. The potentially expansive soils are confined to the semi-arid regions of the tropical and temperate climate zones where the annual evapotranspiration exceeds the precipitation. Current engineering and geologic practices for characterization of expansive clays involve time-consuming and expensive standard engineering tests for determination of swelling potential, and *x*-ray diffraction analyses for mineralogical identification. Remote sensing methods are of interest because of the potential for rapid and inexpensive regional and local mapping. Hyperspectral remote sensing technology has the potential for direct identification of constituent minerals in soils (Hunt and Salisbury, 1970; Hunt, 1977; Clark *et al*., 1990). The question arises whether this technology could become a useful tool for identifying and evaluating expansive soils. This study reports on the first attempt to use high spectral resolution optical remote sensing to detect and map swelling clays.

[1] GeoForschungsZentrum (GFZ) Potsdam Dept 1: Geodesy and Remote Sensing; Section; 1.4: Remote Sensing; Telegrafenberg; D-14473 Potsdam, Germany; Tel: +49–(0)331–288–1108; Fax: +49–(0)331–288–1192; email: chabri@gfz-potsdam.de (corresponding author)

[2] Center for the Study of Earth from Space/CIRES and Department of Geological Sciences; University of Colorado; Boulder, CO 80309 USA; Tel: +1-303-492-5087; Fax: +1-303-492-5070; email: goetz@cses.colorado.edu

Hyperspectral imagery

Remote sensing (i.e. the observation of a target by a device separated from it by some distance thus without physical contact) of the surface of the Earth from an aircraft and from a spacecraft provides information not easily acquired by surface observations. Until recently, the main limitation of remote sensing was that surface information lacked detail due to the broad bandwidth of available sensors. Work in the laboratory and at the telescope over the past few decades has amply demonstrated the utility of spectroscopy for determining the composition of the surface materials of the Earth and other planetary bodies. Recent advances in several key sensor technologies now make it possible to combine the power of spectroscopy with the advantages of imaging to acquire spectroscopic information over large areas. This new approach to remote sensing is called *imaging spectroscopy* or *hyperspectral imagery*.

The concept underlying imaging spectroscopy is illustrated in Figure 14.1. It consists of acquiring images in many (>100) narrow contiguous spectral bands (Goetz *et al*., 1985), thus providing a continuous spectrum for each pixel, unlike multispectral systems that acquire images in a few (<10) wide spectral bands. Conventional sensors (e.g. Landsat MSS and TM, and SPOT) acquire information in a few separate spectral bands of various widths (typically in the order of 0.1–0.2 μm), thus under-sampling to a large extent the reflectance characteristics of the surface (Goetz and Rowan, 1981). Hyperspectral images acquire information in spectral bandwidths typically in the order of 10–20 nm, which is sufficient for analysis of the composition of each picture element (*pixel*) in the image. Figure 14.2 shows the spectral reflectance of characteristic Earth surface materials, along with nominal band-passes for operational optical sensors. This figure illustrates the need for high spectral resolution to allow direct identification of the materials from the remote sensing data. The absorption features observed in the spectra are characteristics of:

- Water content at ~1.4 and 1.9 μm. Those spectral absorptions, observed in most of the spectra, are caused by H_2O and OH^-.
- Iron content (goethite spectrum) at ~0.5, 0.65, and 0.9–1 μm. These spectral features are caused by Fe^{3+} ion electronic transitions within the crystal lattice.
- Chlorophyll content (grass spectrum) at 0.45, 0.7 μm.

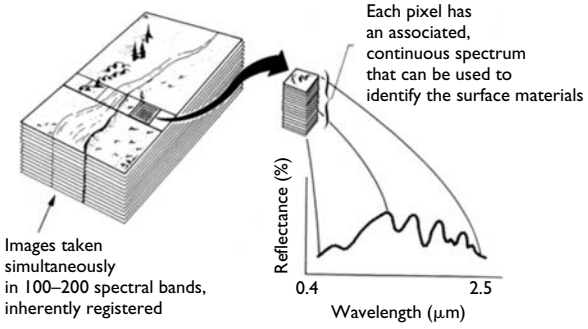

Figure 14.1 The concept of imaging spectroscopy or hyperspectral imagery (from Vane *et al*., 1993).

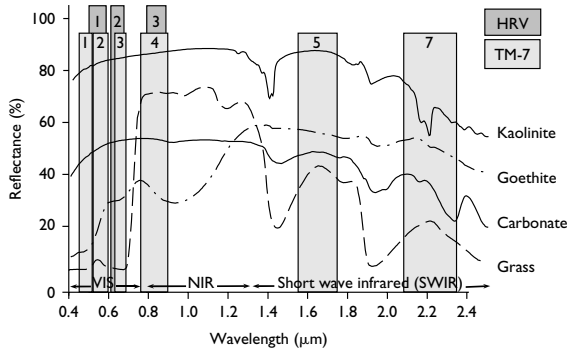

Figure 14.2 Characteristic reflectance spectra of kaolinite, goethite, green grass, and carbonate, superimposed over HRV and Landsat-TM7 bands.

- Clay minerals and carbonate content (kaolinite and carbonate spectrum) vibrational transitions at ~2.2 and 2.3 μm respectively. These spectral features are caused by Al-OH and C-O respectively.

Hyperspectral imagery enables us to spectrally identify minerals, rocks, or soils at the surface since it can provide laboratory-like reflectance spectroscopy at the remote sensing scale. The usefulness of imaging spectrometry for geological applications has been demonstrated in many cases. The Airborne Visible/Infrared Imaging Spectrometer (AVIRIS), developed by NASA at the Jet Propulsion Laboratory, USA (e.g. Vane *et al*., 1993; Green *et al*., 1998) has been flying since 1987. Spectra from AVIRIS have been used to identify individual minerals such as alunite, calcite, dolomite, kaolinite, and muscovite (e.g. Kruse, 1988), ammonium minerals (Baugh *et al*., 1998), and crustal/mantle rocks (Mustard and Pieters, 1987). It has also enabled the mapping of units and subunits of carbonate, clay, and iron oxide minerals in sedimentary rocks (e.g. Clark *et al*., 1992). The best results have been obtained from areas where the rock surfaces are well exposed, little weathered, and the minerals occur in largely pure concentrations. The main limits to successful mapping are the mixing at the sub-pixel scale, and the degree of exposure of the target at the surface. Those limits have been pushed forward in recent years by the development of new processing algorithms such as the spectral mixture analysis (Adams *et al*., 1993), and the improvement of the signal-to-noise ratio (SNR) of the instruments along with better spectral and spatial resolution. The SNR of AVIRIS has evolved from less than ~50 in 1987 to more than 1000 in the visible and ~400 around 2200 nm in 1998 (Green *et al*., 1998). As a result, hyperspectral imagery has been used lately as a new tool for environmental hazard applications, in studies such as the Environmental Protection Agency (EPA) abandoned mine lands imaging spectroscopy project (e.g. Hauff *et al*., 1999; Rockwell *et al*., 1999), or here for swelling soils mapping. The airborne hyperspectral sensors used in this study, the AVIRIS and the HyMap (Cocks *et al*., 1998), are advanced high-quality scanners that represent the highest performance hyperspectral systems available today, and are the precursors of what could be available soon from space.

Expansive soils in Front Range Urban Corridor in Colorado

In the United States, from the Gulf of Mexico to the Canadian border and from Nebraska to the Pacific Coast, the abundance of montmorillonite is common in both clays and claystone shales. The reported problem locations are mostly in the regionally abundant montmorillonite areas (Figure 14.3). In the United States, Colorado is experiencing the greatest swelling soil problem, as represented by the current situation in the Denver Metropolitan Area. This area is underlain by Cretaceous clay-shales, including the Pierre Shale (Hart, 1974). The sedimentary strata are generally flat lying, except near the foothills of the Rocky Mountains where they have been uplifted into steeply dipping strata. Thompson (1992) showed that damage to residential development was substantially more extensive and severe in this outcrop belt than in areas underlain by relatively flat-lying claystone. These conditions underlie several cities along the Front Range Urban Corridor in Colorado that extends from the Wyoming border to Pueblo. This corridor is expected to provide land for much of the housing to be built to support the substantial increase in Colorado's population expected in the next 25 years (Noe and Dodson, 1995, 1999; Gill *et al*., 1996).

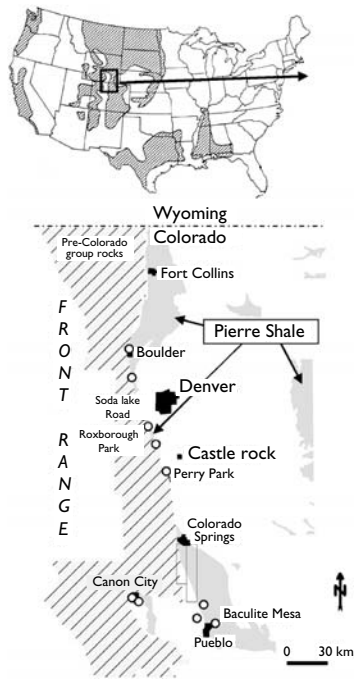

Figure 14.3 Geologic context of the Colorado Front Range Urban Corridor and sampling locations (above). General abundance of montmorillonite in near outcrop bedrock formations in the United States (Modified from Tourtelot, 1973); (below) location of the Pierre Shale (Hart, 1974) with location of field sampling (circles) and AVIRIS images south of Colorado Springs.

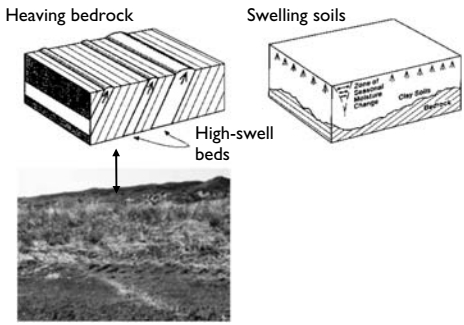

Figure 14.4 Block diagrams of heaving bedrock and expansive soils (from Noe and Dodson, 1999); Steeply dipping shale outcrop near Roxborough Park. The dark soils are composed of silty claystone, I/S layers, and the yellow stripe is a bentonite bed.

Figure 14.3 indicates one of the most expansive bedrock formations in the Front Range area, the Pierre Shale, and shows the geological setting of the study area. A high incidence of damage to roads, utilities, and lightly loaded residential and commercial structures has occurred along the Colorado Front Range Piedmont where steeply dipping beds of expansive claystone bedrock are encountered at shallow depth. Uneven ground deformations can occur in such areas, resulting in the growth of elongate heave features that are the causes of extensive damage in some neighborhoods. The heave features have been associated with differential swell caused by the occurrence of thin bentonite beds (10–30 cm thick), consisting of nearly pure smectite with very high swelling potential, surrounded by mixed-layer illite/smectite (I/S) soils that have a lower swelling potential (Gill *et al*., 1996). Figure 14.4 illustrates the differential swell hazard associated with steeply dipping layers. The adjoining picture shows one of these thin bentonite beds exposed at the surface. To differentiate the geological hazard responsible for this type of deformation from the general expansive soils problem, it has been termed heaving bedrock (Noe, 1997). Heaving bedrock hazard is expected to occur in very localized areas associated with the coincidence of steeply dipping layers of sedimentary bedrock having dip angles of greater than 30°, and zones of expansive bedrock that swell in volume when excess moisture is introduced.

The heaving bedrock hazard area is approximately 1.5–3.2 km wide along the Front Range Piedmont. The Piedmont area corresponds to flat-to-moderate relief area extending eastward from the base of the Front Range, and exposed bedrock formations in a series of hogback ridges, valleys, and benchlands. The great majority of expansive clay samples collected in this region is clay-shale consisting predominantly of mixed-layer I/S with frequent thin bentonite beds. It is classified as having moderate to very high swell potential. In most cases, expansive clay soils are exposed at the surface, and directly related to the claystone bedrock encountered at the near-surface or at shallow depth in the region. For remote sensing purposes, good exposures of expansive clays along the Front Range Urban Corridor are limited in size and are sparse. Most of the region is covered with vegetation, forests, or grass, especially in the northern and Denver areas. However, south of Colorado Springs and around Pueblo and Canon City, exposures are more common and partially covered with

desert-type vegetation. Also, another problem for the identification and mapping of expansive soils in Colorado from afar is that outcrops are of variable mineralogy at a small scale (<1 m) near the mountain front where steeply dipping beds occur.

Background

Basic physics of spectroscopy

When light interacts with a mineral or rock, light of certain wavelengths is preferentially absorbed while at other wavelengths it is transmitted in the substance. The quantity of interest, reflectance, is defined as the ratio of the intensity of light reflected from a sample to the intensity of light incident on it. Reflectance is measured with spectrometers, which separate light reflected from a source into various wavelengths. The light from the source interacts with the sample and the intensity of reflected light at various wavelengths is measured by a detector, relative to a reference standard of known reflectance. Thus a continuous reflectance spectrum of the sample is obtained in the wavelength region measured.

Reflectance spectra have been used for many years to obtain compositional information of the Earth's surface. Similarly, it has been shown that spectral reflectance in the visible and near-infrared (NIR) offers a rapid and inexpensive technique for determining the mineralogy of samples and obtaining information on chemical composition. Electronic transition and charge transfer processes (e.g. changes in energy states of electrons bound to atoms or molecules) associated with transition metal ions such as Fe, Ti, Cr, etc. determine the position of diagnostic absorption features in the visible and NIR wavelength region of the spectra of minerals (Burns, 1993). In addition, vibrational processes in H_2O and OH^-, associated with small displacements of the atoms about their resting positions, produce fundamental, overtone, and combination absorptions (Hunt and Salisbury, 1970; Hunt, 1977). Electronic transitions produce broad absorption features that require higher energy levels than do vibrational processes, and therefore take place at shorter wavelengths (Hunt, 1980; Goetz, 1991). The position, shape, depth, and width of the absorption features are controlled by the particular crystal structure in which the absorbing species is contained and by the chemical structure of the mineral. Thus, variables characterizing absorption features can be directly related to the composition and mineralogy of the sample.

Spectroscopic indicators of clay minerals

Previous research on synthetic monomineralic clay-water systems shows that expansive potential varies directly with the amount of smectite, or montmorillonite, present in a soil (Seed *et al*., 1962), and inversely with both the valence of the exchangeable cations and the concentration of electrolytes in the pore fluid (Mitchell, 1993). Spectroscopic indicators are of great interest because reflectance spectra show absorption bands in the visible and NIR spectral region, which permit identification of smectites in natural soils. Laboratory reflectance spectra of kaolinite, illite, and montmorillonite from the US Geological Survey (USGS) spectral library (Clark *et al*., 1990) are shown in Figure 14.5. The strong absorption bands at 1400 and 1900 nm are due to bound water, typical of montmorillonite, while strong OH bands at 1400 and 2200 nm are typical of kaolinite (Hunt and Salisbury, 1970). The presence of a 1900 nm band is also key to the swelling potential as it indicates molecular water in the sample (2:1 layer clay, montmorillonite, or illite), whereas its absence but the

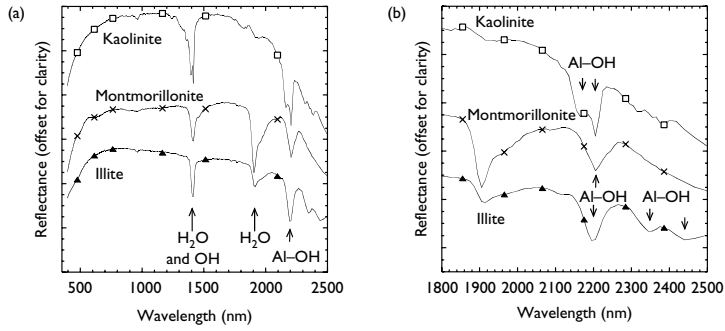

Figure 14.5 Reflectance spectra from the USGS spectral library (Clark *et al*., 1990): Montmorillonite (SWy-1), Illite (IL101), and Kaolinite (Kga-1). (a) In the visible-NIR, (b) in 1800–2500 nm.

presence of a 1400 nm band indicates that only OH is present (kaolinite, 1:1 layer clay) (Kariuki, 1999; Chabrillat *et al*., 2004).

The Al–OH overtone-combination absorption band around 2200–2300 nm is diagnostic of all clays. The Short Wave Infrared (SWIR) part of the spectrum, 1000–2500 nm, and particularly the region 1900–2500 nm, are the most useful part of the spectrum for the identification of clays. Kaolinite shows doublet absorption bands at 1400 and 2200 nm that are characteristic of the mineral. The doublet bands consist of a broad absorption with a sharper, deeper band at slightly longer wavelength: 1395 and 1415 nm for the OH stretch overtones and 2163 and 2208.5 nm for the combination Al–OH bend plus OH stretch. Montmorillonite and illite have similar absorption bands that do not show fine structure. Montmorillonite shows a single well-defined absorption band around 2200 nm, due to the combination Al–OH bend and OH stretch. Illite, unlike montmorillonite, shows additional absorption bands at 2340 and 2450 nm. The one at 2450 nm is poorly defined.

Reflectance spectra of montmorillonites exhibit shifts in the 2200 nm absorption band, from ~2204 to 2214 nm. There is an argument in the literature whether this shift could be correlated with an increasing Ca content, or decreasing Na content. If so, the position of the 2200 nm absorption band could be useful for the evaluation of swelling potential, because sodium-rich montmorillonites swell more than calcium-rich montmorillonites. The shift in the 2200 nm absorption band has been attributed to interaction with the interlayer cation field (e.g. Ryskin, 1974) although this interpretation has been disputed (Farmer, 1974). Clark *et al*. (1990) observed an apparent trend among a few samples that shows a shift in the 2200 nm band to a longward position with increasing Ca content. On the other hand, Post and Noble (1993) showed that decreasing Al_2O_3 content in smectite minerals shifts the 2200 nm absorption feature toward longer wavelengths. We conclude that the position of the 2200 nm absorption band should not be used for the evaluation of swelling potential (Chabrillat *et al*., 2004).

Remote sensing methods have the potential for rapid and inexpensive regional and local mapping. This chapter reports on the first attempt to use high spectral resolution optical remote sensing to detect and map swelling clays.

Methodology

Field and laboratory analyses

The development of reflectance spectroscopy for identifying and characterizing expansive soils required the correlation of clay mineralogy with swelling potential indices determined from engineering tests, and the expansion of existing correlations of reflectance spectra with clay mineralogy determined by X-ray diffraction. A suite of 182 samples was collected in 1997–98 from several locations shown in Figure 14.3 from Boulder to Pueblo and Canon City. On each sample, mineralogy and swelling potential were determined from standard laboratory analyses, and reflectance spectra were acquired. Semi-quantitative mineralogy and mixed-layer illite–smectite expandability were determined from X-ray diffraction patterns acquired on oriented samples (Chabrillat *et al*., 2004). Swelling potential was determined from geotechnical index tests (Olsen *et al*., 2000), including the Atterberg limits, grain size analyses, and one-dimensional swell tests. Bi-directional reflectance spectra were acquired in the laboratory in the visible-NIR and short wave infrared (SWIR) region with a FieldSpec® FR spectroradiometer (ASD, 1995) reproducing solar geometry conditions, off-nadir tungsten illumination (incidence 30°, emergence = 0°). Spectral resolution is 3–4 nm in the 350–1000 nm region (spectral sampling 1.4 nm), and 10–12 nm in the 1000–2500 nm (spectral sampling 2 nm). The entire spectrum is resampled at 1 nm for display purposes.

Figure 14.6 presents the suction versus water content data obtained on the 182 samples together with McKeen's swell potential categories, and summarizes our results. In this figure we added the schematic mineralogical composition determined with XRD, which was associated with the samples in each category, along with characteristic spectral signatures around 2200 nm of field samples in each swelling potential category. This figure shows that the samples are widely distributed throughout all McKeen's categories, and that this is correlated with mineralogical changes. The clays smectite, illite, and kaolinite can be identified spectroscopically throughout the suite of samples, in mixed proportions, based on their characteristic H_2O and OH overtone combination absorptions in the spectral region 1800–2500 nm (Chabrillat *et al*., 2001, 2004; Goetz *et al*., 2001). The results from the laboratory analyses are summarized in the following paragraph.

From spectral reflectance we are able to discriminate among smectite and mixed layers I/S samples. Smectite has a characteristic well-marked, single absorption feature centered at ~2200 nm, followed by a steep drop in reflectance. Reflectance at ~2400 nm is lower than reflectance at ~2200 nm. Mixed layers I/S samples have a similar absorption feature centered at ~2200 nm, usually less deep, with an additional absorption feature at 2340 nm, and higher reflectance at ~2400 nm than at ~2200 nm. The last point can help the identification of minor amounts of illite in the sample when the absorption band at 2340 nm is barely noticeable or appears as a shoulder. The additional absorption band at 2340 nm provides a measure of the illite content. The more smectite (the less illite), the higher the swell potential.

Kaolinite is detected spectrally if above 10% in clay fraction in the sample with the appearance of an asymmetric absorption band at 2200 nm, caused by the characteristic doublet feature. Spectral identification of a significant amount of kaolinite (>10–15%) is indicative of low swelling potential.

Along with clay identification, the presence of a 1900 nm absorption band is key to swelling potential, since it indicates molecular water in the sample (2:1 layer clays,

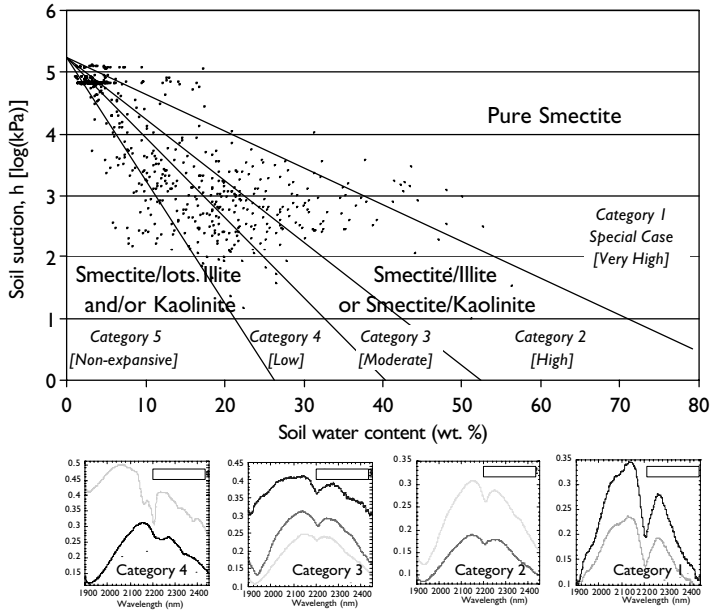

Figure 14.6 Suction versus water content data for 182 samples together with McKeen (1992) classification categories. The schematic mineralogical composition associated with samples is added for each category. The spectra shown on the bottom of the figure are associated with field samples in each of McKeen category of swelling potential.

montmorillonite, illite). The deeper the 1900 nm absorption band, the more swelling. When a deep 1900 nm band co-exists with kaolinite mineralogical identification (doublet at 2200 nm), the swell potential interpretation is suspect.

Quantitative analyses were performed aiming at relating the spectral features with the swell potential and/or mineralogy of the samples. Olsen *et al*. (2000) showed that the percent total smectite provides a useful index of the swelling potential concept defined by Seed *et al*. (1962), Chen (1988), and McKeen (1992), with correlation coefficients in the range of 0.6–0.75. Chabrillat *et al*. (2004) and Goetz *et al*. (2001), showed using multi-dimensional statistical analyses, that laboratory spectral reflectance in the short-wave infrared correlates well with the percent smectite of the samples in clay fraction and with swelling potential indices, with correlation coefficients as high as 0.8–0.9. However, such models are presently limited, and more detailed studies are needed before they could be used in practice. Refined models linking reflectance with swell potential are currently being developed.

Additionally, field analyses were conducted in order to study the transferability of the results from the laboratory to the outdoor conditions. Reflectance spectra were acquired in the field with the FieldSpec® FR spectroradiometer, over different exposures of expansive clays associated with sampling locations and/or remote sensing data. Smectite, illite, and

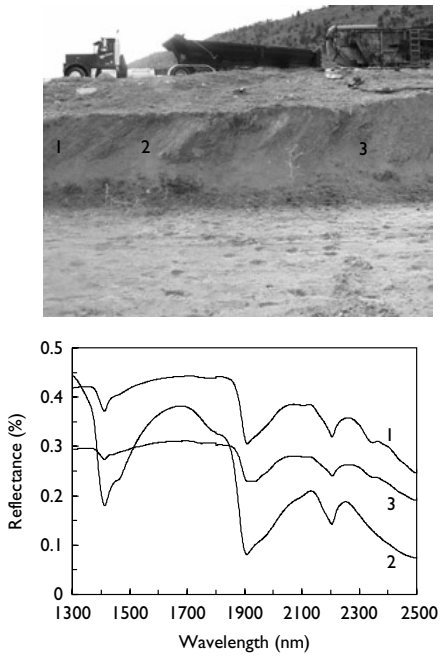

Figure 14.7 Reflectance spectra acquired in the field over a vertical exposure of steeply dipping beds of expansive clays west of Denver (Soda Lake Rd). The location of the spectra over the exposure is marked in the associated picture: 1 – Grey shale, 2 – Bentonite bed, 3 – Grey shale.

kaolinite are identifiable spectroscopically in the field as well, and the spectral discrimination between pure smectite and illite–smectite layers is possible, as shown in Figure 14.7. From their spectral signature (spectra 1 and 3), the grey shales are associated with mixed-layer illite–smectite and this is confirmed by the XRD analyses of field samples from these layers, unlike the bentonite beds that are associated with a characteristic smectite spectral feature (spectrum 2). Those spectra are representative of what could be measured in other outcrops with an equivalent mineralogy, such as the Perry Park area. Note that the spectra shown in Figure 14.7 were acquired with the ASD (analytical spectral device) high-intensity reflectance probe™ that has a quartz halogen light source. Indeed, the 1400 and 1900 nm water absorption bands are masked by the atmospheric water vapor absorption bands when spectral measurements are acquired with the sun as the light source. The 1900 nm band, discriminative for clays, cannot be used for remote sensing measurements.

Nevertheless, using the spectral region 2000–2500 nm alone it is possible to discriminate among smectite, illite, and kaolinite, having decreasing swell potential, from characteristic absorption features already identified both in the laboratory and in the field. Therefore, identification and mapping of expansive clay shales along the Front Range Urban Corridor is a reasonable objective, provided that the clays are exposed at the surface, and that exposures are large enough with respect to the sensor capabilities.

Remote sensing acquisition

AVIRIS and HyMap hyperspectral images were acquired along the Colorado Front Range Urban Corridor in the Fall 1998 and 1999 (Table 14.1). The overflights were requested for late summer when the amount of green vegetation cover is at a near minimum.

The AVIRIS (Figure 14.8) is a NASA research instrument operated by the Jet Propulsion Laboratory (JPL) in Pasadena, California. It measures upwelling radiance through 224 contiguous spectral channels at 10 nm intervals, from 400 to 2500 nm. AVIRIS spectral images are traditionally acquired in high altitude mode, from the Q-bay of a NASA ER-2 aircraft (Figure 14.9) from an altitude of 20 km. In October 1998, for the first low altitude experiment (Green *et al*., 1999a), it was mounted on-board a NOAA Twin-Otter aircraft flying at an altitude of 3.8 km. A detailed description of AVIRIS characteristics, operations, and applications can be found in Green *et al*. (1998). In 1998, AVIRIS was radiometrically calibrated to better than 96% accuracy (Green *et al*., 1999b). Six flight lines were acquired from high altitude both in 1998 and 1999 for a total each year of ~300 km length. Due to the mean ~1.7 km surface elevation in the area covered, the AVIRIS pixel size is ~17 m × 17 m, and the swath width is ~10 km. During the low altitude overflight in 1998, AVIRIS produced a pixel size of ~2 m × 2 m and a swath width of ~1.2 km. AVIRIS data were distributed by the JPL a few months after the overflights in at-sensor radiance, radiometrically calibrated, georectified in 1998, and non-georectified in 1999.

The HyMap™ hyperspectral scanner (Figure 14.10), manufactured by Integrated Spectronics Pty Ltd, is operated by HyVista Corporation (http://www.hyvista.com). The HyMap images were acquired in September 1999 during the 1999 USA HyMap Group Shoot (Kruse *et al*., 1999). The HyMap provides 126 bands across the reflective solar wavelength region of 440–2470 nm with contiguous spectral coverage (except in the atmospheric water vapor bands) and bandwidths between 13 and 17 nm. The sensor operates on a 3-axis gyro-stabilized platform to minimize image distortion due to aircraft motion. The system can be rapidly adapted to any aircraft with a standard aerial camera port and is transported between international survey sites by airfreight. During the 1999 USA campaign, the HyMap was mounted aboard a Cessna 402 and flown at variable altitudes to achieve a

Table 14.1 AVIRIS and HyMap hyperspectral data acquired along the Colorado Front Range Urban Corridor

Date	*Instrument*	*Overflight altitude (km)*	*Pixel size (m)*	*Swath width (km)*	*Acquisitions (cloud free)*
September 30, 1997	AVIRIS	20	17	10	Colorado Springs[a]
September 10, 1998	AVIRIS	20	17	10	Pueblo, Golden, Boulder
October 21, 1998	AVIRIS	~4	2	1.2	Boulder, Golden
September 16, 1999	HyMap	~3.6	4	2.3	Boulder, Golden, Perry Park
September 30, 1999	AVIRIS	20	17	10	Canon City, Pueblo, Perry Park, Golden, Boulder
October 1, 1999	HyMap	Low altitude	4	2.3	Pueblo

Note
a USGS data.

Figure 14.8 View of AVIRIS hyperspectral sensor inside the Twin-Otter aircraft http://aviris.jpl.nasa.gov).

Figure 14.9 View of the NASA Lockheed ER-2 high altitude research aircraft in flight (NASA Dryden flight research center photo collection, http://dfrc.nasa.gov).

4 m × 4 m pixel size, thus providing images of ~2.3 km width. Several flight lines were acquired over different sites. Two overflight days were necessary to obtain cloud-free images. HyMap data were distributed by Analytical Imaging and Geophysics (AIG) (http://www.aigllc.com) two weeks after the overflights, both in radiance and reflectance, radiometrically calibrated and georectified.

Figure 14.11 shows calculated SNR for the AVIRIS and the HyMap for a 50% reflectance target and similar solar zenith angle, AVIRIS: 23.5°, HyMap: 30° (Cocks *et al*., 1998; Green and Pavri, 2000; Green, 2002). The SNR shown for AVIRIS was calculated from the 1999 in-flight calibration experiment, and range from 1000:1 in the visible portion of the spectrum, to a peak of ~500:1 around the 2100–2200 nm spectral region. The

Figure 14.10 View of HyMap™ hyperspectral scanner (http://www.hyvista.com/hymap.html).

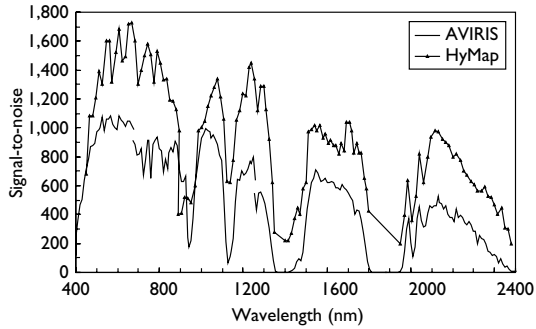

Figure 14.11 Comparison of calculated Signal-to-noise ratio for the AVIRIS and the HyMap.

Source: The AVIRIS performances are from 1999 in-flight calculations (Green, R.O., 2002), the HyMap performances are from ground measurements (Cocks *et al*., 1998).

SNR shown for HyMap was calculated from ground measurements. HyMap SNR in the SWIR 2 region is approximately twice as good as AVIRIS. Cocks *et al*. (1998), after a sensitivity analysis, concluded that the ground-based measurements of HyMap SNR are a very good indicator of the sensor's in-flight performance. On this basis, we assume that the HyMap in-flight SNR around 2200 nm should be at least ~600:1, and no better than 800:1.

Image processing

Hyperspectral images require specialized data processing to take into account both the spatial and spectral dimension of the data. For this reason, hyperspectral images are often called

data cubes, since they are considered to have three dimensions: x is the number of columns, y the number of rows, and z is the number of spectral channels.

In order to derive surface reflectance from the raw data (at-sensor radiance), they must be corrected for solar irradiance and atmospheric effects such as two-way transmission multiple scattering and path radiance. Radiative transfer algorithms were used to derive reflectance from radiance. AVIRIS and HyMap data were atmospherically corrected using the ATREM (atmospheric removal) algorithm (Gao *et al*., 1993), version 3.0 and 3.1. To correct the artifacts introduced by the modeled solar irradiance, two different approaches were used, ground correction and a semi-empirical approach. AVIRIS data were ground-corrected using spectral surface measurements acquired on the day and at the time of the overflights from an almost bare field calibration target within the scene. For HyMap data, we used the reflectance data distributed by AIG, where after the ATREM correction, they used the Empirical Flat Field Optimal Reflectance Transformation (EFFORT) (Boardman and Huntington, 1997). This semi-empirical approach makes the assumption that the residual spectral artifacts in the derived reflectance from ATREM are only associated with systematic errors in the model or in the spectral and radiometric calibration of the sensor. As a result, the reflectances obtained independently from both sensors over a similar ground field-of-view are highly coherent, and coincide within 0.02–0.08 in reflectance (Chabrillat *et al*., 2002).

To detect and map expansive soils along the Colorado Front Range, we applied the same processing methodology, on both AVIRIS and HyMap images. The advantage of this methodology is that no a priori knowledge of the area or fieldwork is required. Also, only the 2000–2450 nm spectral region of the spectrum (43 spectral channels for AVIRIS, 28 for HyMap) was used, since characteristic clay spectral signatures are in this region. The software package ENVI (RSI, 2000) was used to process the images. A minimum noise fraction (MNF) transform was performed. The Pixel Purity Index (PPI) method was used to find the most spectrally pure (extreme) pixels. The extreme pixels were visualized in the data cloud from the 10 first MNF bands. One of the clusters was identified as the clay cluster, since associated spectra showed characterictic clay features around 2200 nm, such as kaolinite, smectite, and possibly illite. Extreme clay pixels (endmembers) were then extracted from the clay cluster. The Spectral Angle Mapper (SAM) and Mixture Tuned Matched Filtering (MTMF) algorithms were used to locate and map expansive clays outcrops. The SAM analysis provides distribution maps, and the MTMF analysis provides abundance maps for each selected endmember. A more detailed description of the methodology and processing used is to be found in Chabrillat *et al*. (2002).

Results and discussion

The focus here will be on two examples, Colorado Springs and Perry Park. The Colorado Springs area is representative of the situation in southern Colorado where vegetation is sparse and soils well exposed. Data over Colorado Springs were acquired with the AVIRIS sensor flying at 20 km high, thus producing a pixel size of ~17 m. The results from the Colorado Springs images are representative of what can be expected for a regional analysis in a semi-arid area. Interested readers can find the results from another typical regional mapping associated with the Pueblo area, in Chabrillat *et al*. (2001). Perry Park, shown as a second example, is representative of the situation in northern Colorado with small sparse outcrops and heavy vegetation cover, and is close to the mountain front with variable

mineralogy and many steeply dipping bentonite beds. The images over Perry Park are from the HyMap sensor flying at ~3.6 km high (above sea level). The resulting pixel size is ~4 m. This analysis represents the results that can be expected for a local mapping over a highly vegetated region.

Regional mapping

Figure 14.12 presents the results obtained from AVIRIS-high altitude scenes south of Colorado Springs (Fort Carson area). The area covered by these scenes is located in Figure 14.3. Note that when we processed the images, we did not have any field knowledge from the area. Figure 14.12a shows the AVIRIS image covering an area of ~20 km × 37 km. Figure 14.12b shows the clay map created from the SAM algorithm, and Figure 14.12c shows the three AVIRIS spectra associated with the endmembers. The image (Figure 14.12a) is comprised of 2 parallel adjacent flight lines, 4 scenes for the eastern line, and 3 for the western line. The scenes in each flight line were mosaicked together, and the western flight line was registered to the eastern one using ground control points. These AVIRIS scenes were acquired in 1997 for the

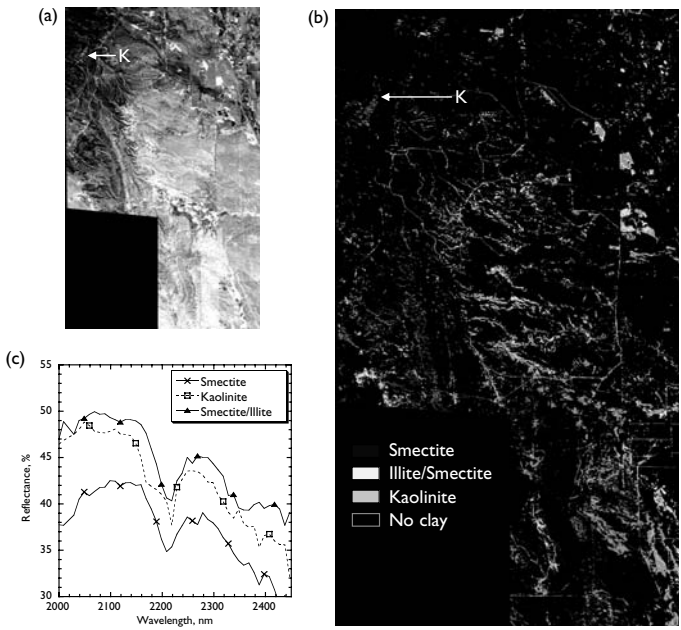

Figure 14.12 Results obtained from the AVIRIS high altitude images south of Colorado Springs. (a) Image at 0.65 microns (1168 × 2050 pixels) covering an area of ~20 × 37 km, (b) clay map produced from the combination of the three SAM distribution maps associated with the three endmembers shown in (c). The grey-coded scale is interpreted from top to bottom in terms of decreasing swell potential, and (c) endmembers spectra. The K letter locates the picture shown in Figure 14.13.

US Geological Survey (Livo, 1998). The three endmembers, identified from the shape of the spectra in Figure 14.12c, are interpreted as smectite (single deep band at ~2200 nm), kaolinite (doublet band), and illite/smectite layers (additional band at ~2340 nm). Figure 14.12b shows the distribution map of the three endmembers, resulting from the combination of three SAM images where: the pixels showing a high spectral similarity with the endmember smectite are coded in white, the pixels showing a high spectral similarity with the endmember kaolinite are coded in dark grey, and the pixels showing a high spectral similarity with the endmember illite/smectite are coded in light grey. The black background is associated with areas where no clay materials were identified at the surface.

The image presented in Figure 14.12b represents a map of clay materials exposed, and can be interpreted in terms of increasing swell potential, from kaolinite (dark grey areas) to illite/smectite layers (light grey areas), to more smectite-rich materials (white areas). The patchy pattern of clay exposures among the black background is associated with the scattered nature of clay occurrences. It is interpreted to come from the predominance of non-clay materials at the surface, where the presence of vegetation cover (trees, grass) or non-expansive Quaternary-age alluvial deposits is also typical in this region. The mountainous western slopes, composed of pre-Colorado group rocks, exhibit a relatively homogeneous clay signature interpreted to be kaolinite. From the knowledge gained with the laboratory analyses, the associated areas are interpreted as being none to very-low swelling.

Geologically, this area contains Precambrian-age granite and diorite and Pennsylvanian- and Permian-age sandstone from the Fountain Formation (Scott and Wobus, 1973), which are known to contain kaolinitic clays. These rocks were considered non-expansive by Hart (1974) because they generally lack smectite. Field checking done later in this region has shown, for example, that an area identified as kaolinite and located in Figure 14.12 with the K letter was associated with well-exposed reddish sandstones (Figure 14.13). Laboratory spectra obtained from associated field samples showed a very strong kaolinite feature, substantiating the remote sensing identification. The eastern part of the image, a more level area, contains bands of two clay signatures interpreted to be smectite and mixed-layers I/S, and thus could be interpreted as having moderate (light grey areas) to high (white areas) swell potential. These appear to correspond with bands of steeply to gently dipping Pierre Shale that were mapped by Hart (1974). Hart recognizes bands of moderately to highly swelling claystone that contain different amounts of smectite. This coincides with the interpretation from the AVIRIS results.

The analysis of the high altitude AVIRIS data south of Colorado Springs, over an unknown area in terms of exposures of swelling clays, showed that there are some clay exposures in the image. The limitation to remote sensing mapping is the lack of exposure, but in southern Colorado the vegetation cover is significantly sparser than more in the north (Denver area). The remote sensing data allowed identification of the clay exposures among the other components in the image despite the mixing at the sub-pixel scale. The map of exposed clay material showed that spectral discrimination and identification of variable clay mineralogy, related to variable swelling potential, is possible. These results also showed that, without a priori knowledge, an accurate map of the clay mineralogy could be created that matched well with the very sparse swelling potential maps available for the region, obtained from time-intensive field work and interpretation of geological maps. The interpretation of the AVIRIS results in terms of type of clay content and swelling potential hazard is consistent with observations from the literature and field knowledge from the area. The map presented in Figure 14.12b, computed in a few months, could be directly integrated into a city-planning

Figure 14.13 Outcrop associated with an area identified as kaolinite in the Colorado Springs AVIRIS clay mapping (K letter in Figure 14.12a,b.)

management and serve as a tool to identify areas with variable swelling clay hazard. This example is representative of the results that can be expected from a clay-rich area in a semi-arid region.

Local mapping

Figure 14.14 presents the results obtained from the HyMap scenes acquired in 1999 over Perry Park. This area is very close to the mountain front, and characterized by heavy vegetation cover of forests and grass, and very steeply dipping beds (~70°). Figure 14.14a shows the Hymap image covering an area of ~1 km^2. Only a small part of the HyMap flight-line, the most interesting in terms of clay materials exposed, is shown here. Figure 14.14b shows the clay map resulting from the image processing, and Figure 14.14c shows the three endmembers spectra, selected from the extreme corners of the clay cluster from the whole HyMap image. The endmembers, from their spectroscopic signature, were interpreted to be associated with smectite, kaolinite, and illite/smectite. Figure 14.14b shows the abundance maps obtained with the matched filtering algorithm for the three endmembers, represented as one single grey-scale coded(RGB) image. Each abundance map from each endmember ranges from 0% (black background), meaning that the spectrum of the associated pixel does not match with the endmember one, to 100%, meaning a perfect match between the image spectrum and the endmember spectrum. White is associated with smectite, dark grey with kaolinite, and light grey with illite/smectite. In the resulting image combining the three abundance maps (Figure 14.14b), the black background is associated with areas where no clay materials were identified at the surface. Variations from white to light grey are associated with mixtures of smectite and I/S layers (no kaolinite). The darker a light grey pixel is, the higher the concentration of illite.

The image presented in Figure 14.14b represents a map of clay materials exposed, and can be interpreted in terms of variable swell potential. Dark grey pixels are associated with kaolinite-like spectral signatures, and are interpreted as having very low to none swelling potential. The kaolinite endmember was associated with boulders falling from a cliff that showed a strong kaolinite feature in their field spectra. The area associated with the smectite endmember (S letter in Figure 14.14) was later located in the field and is showed in Figure 14.15. It was exposed soils around a house under construction. The field samples collected around this house showed a pure smectite feature in their spectra, confirming the remote sensing identification. Note that the clay materials exposed in this area are very sparse and small in size, which agrees with our fieldcheck. Also, many areas rich in smectite

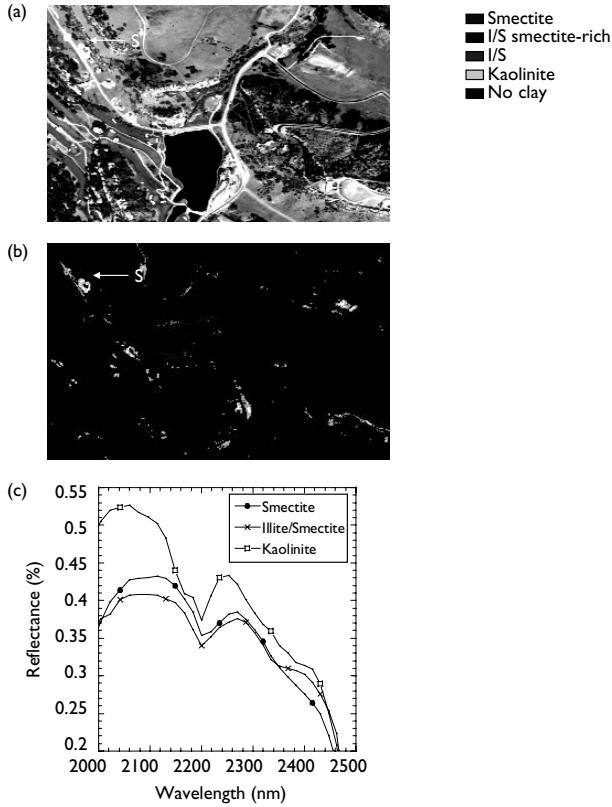

Figure 14.14 Results obtained from the HyMap images over the Perry Park area. (a) Image at 0.6 microns (310 × 230 pixels) covering an area of ~1.2 × 0.9 km, (b) clay map produced from the RGB image of the three MTMF abundance maps associated with the three endmembers shown in (c) The grey-coded scale is interpreted from top to bottom in terms of decreasing swell potential and (c) endmembers spectra. The S letter locates the smectite endmember, whose picture is shown in Figure 14.15.

were detected. The areas mapped in white in Figure 14.14b are interpreted as having the highest swelling hazard. This is in agreement with the fact that Perry Park is known for its smectite-rich claystone exposures, along with the occurrence in the mixed smectite/illite layers of several thin bentonite beds with very high swelling potential. The clay abundance map created from the HyMap data is interpreted in terms of variable clay mineralogy, and thus as having variable swelling potential, from the non-swelling kaolinite-rich areas (coded in dark grey), to low swelling potential (illite-rich areas coded in light grey), to moderate and high swelling areas (coded in very light grey and white).

Figure 14.15 Outcrop associated with the smectite endmember in Perry Park HyMap images (S letter in Figure 14.14a,b).

The clay map developed for the Perry Park area with HyMap data was a challenge since this area is very heterogeneous, and there are very few outcrops that are very small in size. The results show that we were able to detect and map the clay materials exposed, even with sub-pixel outcrops. The areas field-checked are accurately represented in the map. Also, as shown previously with AVIRIS data over southern Colorado Springs, the remote sensing advantage provided a global view of the area and enabled the discovery of unknown clay exposures. It also showed that the slightly degraded spectral resolution of HyMap versus AVIRIS over the spectral range analyzed (but with a slightly higher SNR) did not prevent the detection of characteristic clay spectral features. The map created from the HyMap data (Figure 14.14b) represents the results that can be expected for local mapping in a temperate clay-rich area where vegetation cover is high.

In closing, the remote sensing of expansive clays allowed a successful mapping in different areas depending on the quality of exposures and variable mireralogy. The main limitations for the expansive clay soils detection were in case of a heavy vegetation cover (forest or green grass), and when the reflectance of the soils is approximately 10% or less.

Conclusions

This chapter examined the potential of remote sensing and in particular high spectral resolution (hyperspectral) imagery for the detection and mapping of expansive clays in the Front Range Urban Corridor in Colorado, USA. The study covered analyses at specific sites with high spatial resolution data ($<$5 m), and on a regional basis with slightly lower spatial resolution (20 m). The airborne hyperspectral sensors used in this study, the AVIRIS and the HyMap, were advanced high-quality scanners that represented the highest performance hyperspectral systems available today, and were the precursors of what could be available soon from space. Both sensors provided laboratory-like reflectance spectroscopy at the remote sensing scale.

Preliminary laboratory and field analyses showed that near-infrared reflectance spectroscopy can be used to discriminate among pure smectite and mixed-layers illite/smectite samples, associated with decreasing swelling potential, based on characteristic absorption bands in the 1900–2400 nm spectral region.

The analysis of the hyperspectral images showed that it is possible, using different algorithms, to detect the expansive clays exposed at the surface, along with other components in the images, and in the presence of significant vegetation cover. Mapping was successful in different areas depending on the quality of exposures and variable mineralogy. The best results for regional mapping were obtained with AVIRIS high altitude data over large areas in southern Colorado where there was little vegetation cover and outcrops were plentiful.

The best results for local mapping over specific sites with variable mineralogy and landscape at a fine scale were obtained with HyMap data, with the highest spatial resolution (<5 m). In these areas, spectral discrimination and identification of variable clay mineralogy (smectite, illite/smectite, kaolinite) related to variable swelling potential was possible. Field checks have shown that the maps of clay type derived from the imagery and interpretation in terms of swell hazard are accurate.

The geological context of the Colorado Front Range area, with locally variable mineralogy at a very fine spatial scale due to steeply dipping layer, represented a particular geological setting which might not be representative of the swelling soils affected areas throughout the world. Nevertheless, hyperspectral imagery was able to identify the swelling clays in this semi-arid area. Therefore, global surveys at moderate spatial resolution (20–30 m) could be useful for detecting clay exposures, and guide future work, although local surveys at higher spatial resolution (<5 m) might be necessary for a more precise mapping or when only a scattered handful of pixels in the scene show as clays, for example in a more populated area.

In closing, this study was the first evaluation of hyperspectral imagery for the detection and mapping of expansive clays, in the context of a rapidly growing urban area severely affected with swelling soils problems. The results showed that such optical remote sensing methods, coupled with reduced field and laboratory analyses, can offer practical help to civic planners, as long as the swelling soils are adequately exposed.

Acknowledgments

This work was performed under NASA/JPL contract No. 960983. We are indebted to Hal Olsen and Lisa Krosley of the Colorado School of Mines, and Dave Noe of the Colorado Geological Survey, for their participation in the entire swelling soil mapping project. Eric Livo of the US Geological Survey provided the calibrated AVIRIS Colorado Springs dataset. We wish to thank the Jet Propulsion Laboratory AVIRIS team for the acquisition and support for the AVIRIS data, and the HyMap/AIG team for their support and acquisition of the HyMap data.

References

Adams, J.B., Smith, M.O., and Gillespie, A.R. (1993), Imaging spectroscopy: Interpretation based on spectral mixture analysis. In: C.M. Pieters and P.A.J. Englert (Eds), *Remote Geochemical Analyses: Elemental and Mineralogical Composition*. Cambridge University Press, Cambridge, UK, pp. 145–166.

ASD (1995), *Analytical Spectral Devices (ASD): Technical Guide*, Portable spectroradiometers, Analytical Spectral Devices, Inc., Boulder, CO, USA, p. 40.

Baugh, W.M., Kruse, F.A., and Atkinson, W.W.Jr (1998), Quantitative geochemical mapping of ammonium minerals in the southern Cedar Mountains, Nevada, using the airborne visible/infrared imaging spectrometer (AVIRIS), *Remote Sensing of Environment* 65: 292–308.

Boardman, J.W. and Huntington, J.F. (1997), Mineralogic and geochemical mapping at Virginia City, Nevada, using 1995 AVIRIS data. Proceedings of the 12th International Conference on Applied Geologic Remote Sensing, Denver, Colorado, 17–19 November 1997. ERIM, Ann Arbor, MI, vol. 1, pp. 191–198.

Burns, R.G. (1993), *Mineralogical Applications to Crystal Field Theory*, 2nd edn, Cambridge University Press, 551 pp.

Chabrillat, S., Goetz, A.F.H., Olsen, H.W., and Krosley L. (2001), Field and imaging spectrometry for identification and mapping of expansive soils, In: F.D. van der Meer and S.M. de Jong (Eds), *Imaging Spectrometry: Basic principles and Prospective Applications*, Kluwer Academic Publication, Dordrecht, The Netherlands, pp. 87–109.

Chabrillat, S., Goetz, A.F.H., Olsen, H.W., and Krosley L. (2002), Use of hyperspectral images in the identification and mapping of expansive clay soils and the role of spatial resolution, *Remote Sensing of Environment*, 82(2–3): 431–445.

Chabrillat, S., Goetz, A.F.H., Krosley L., Olsen, H.W., and Noe, D.C. (2004), Near-infrared spectra of expansive clay soils and their relationships with mineralogy and swelling potential, *Clays and Clay Minerals*, accepted major corrections.

Chen, F.H. (1988), *Foundations on Expansive Soils*, 2nd ed., Elsevier, Amsterdam, p. 463

Clark, R.N., King, T.V.V., Klejwa, M., and Swayze, G.A. (1990), High spectral resolution reflectance spectroscopy of minerals, *Journal of Geophysics Research*, 95(B8), 12: 653–680.

Clark, R.N., Swayze, G., and Gallagher, A. (1992), Mapping the mineralogy and lithology of Canyonlands, Utah with imaging spectrometer data and multiple spectral feature mapping algorithm. Summaries of the 3rd Annual JPL Airborne Geoscience Workshop, Pasadena, CA, 1–5 June 1992. JPL Publication 92–14, Jet Propulsion Laboratory, Pasadena, CA, vol. 1, pp. 11–13.

Cocks, T., Jenssen, R., Steward, A., Wilson, I., and Shields, T. (1998), The HyMap^{TM} airborne hyperspectral sensor: The system, calibration and performance. Proceedings of the 1st European Association of Remote Sensing Laboratories (EARSeL) Workshop on Imaging Spectroscopy, University of Zurich, Switzerland, 6–8 October 1998. EARSeL, Paris, pp. 37–42.

Farmer, V.C. (1974), The layer silicates. In V.C. Farmer (Eds), *The Infrared Spectra of Minerals*, Mineralogical Society, London, pp. 331–364.

Gao, B.-C., Goetz, A.F.H., and Wiscombe, W.J. (1993), Cirrus cloud detection from airborne imaging spectrometer data using the 1.38 μm water vapor band, *Geophysics Research Letters*, 20: 301–304.

Gill, J.D., West, M.W., Noe, D.C., Olsen, H.W., and McCarty, D.K. (1996), Geologic control of severe expansive clay damage to a subdivision in the Pierre Shale, Southwest Denver metropolitan area, Colorado, *Clays and Clay minerals*, 44(4): 530–539.

Goetz, A.F.H. (1991), Imaging spectrometry for studying Earth, Air, Fire, and Water, EARSeL, *Advances in Remote Sensing*, 1: 3–15.

Goetz, A.F.H. and Rowan, L.C. (1981), Geologic remote sensing, *Science*, 211: 781–791.

Goetz, A.F.H., Vane, G., Solomon, J.E., and Rock, B.N. (1985), Imaging spectrometry for Earth remote sensing, *Science*, 228: 1147–1153.

Goetz, A.F.H., Chabrillat, S., and Lu, Z. (2001), Field reflectance spectrometry for detection of swelling clays at construction sites, *Field Analytical Chemistry and Technology*, 5(3): 143–155.

Green, R.O. (2002), Personal Communication.

Green, R.O. and Pavri, B.E. (2000), AVIRIS in-flight calibration experiment, sensitivity analysis, and intraflight stability. Proceedings of the 9th JPL Airborne Earth Science Workshop, Jet Propulsion Laboratory, Pasadena, CA, 23–25 February 2000. JPL Publication 00–18, pp. 207–221.

Green, R.O., Eastwood, M.L., Sarture, C.M., Chrien, T.G., Aronsson, M., Chippendale, B.J., Faust, J.A., Pavri, B.E., Chovit, C.J., Solis, M., Olah, M., and Williams, O. (1998), Imaging spectroscopy and the airborne visible/infrared imaging spectrometer (AVIRIS). *Remote Sensing of Environment*, 65: 227–248.

Green, R.O., Chrien, T.G., Sarture, C.M., Eastwood, M.L., Chippendale, B.J., Kurzweil, C., Chovit, C.J., and Faust, J.A. (1999a), Operation, calibration, georectification, and reflectance inversion of NASA's airborne visible/infrared imaging spectrometer (AVIRIS) four- and two-meter data acquired from a low-altitude platform. Summaries of the 8th JPL Airborne Earth Science Workshop, Jet Propulsion Laboratory, Pasadena, USA, 9–11 February 1999, JPL Publication 99–17, pp. 177–188.

Green, R.O., Pavri, B.E., Faust, J.A., and Williams, O. (1999b), AVIRIS radiometric laboratory calibration, inflight validation and a focused sensitivity analysis in 1998. Summaries of the 8th JPL Airborne Earth Science Workshop, Jet Propulsion Laboratory, Pasadena, USA, 9–11 February 1999, JPL Publication 99–17, pp. 161–176.

Hart, S.S. (1974), Potentially swelling soil and rock in the front range urban corridor, Colorado. Environmental Geology 7, Colorado Geological Survey, Denver, CO, 23 p. 4 maps, scale 1 : 100000.

Hauff, P.L., Lindsay, N., Peters, D., Borstad, G., Peppin, W., Costik, L., and Glanzman, R. (1999), Hyperspectral evaluation of mine waste and abandoned mine lands, NASA and EPA sponsored projects in Idaho. Summaries of the 8th JPL Airborne Earth Science Workshop, Jet Propulsion Laboratory, Pasadena, USA, 9–11 February 1999, JPL Publication 99–17, pp. 229–238.

Hunt, G.R. (1977), Spectral signatures of particulate minerals in the visible and near-infrared. *Geophysics*, 42: 501–513.

Hunt, G.R. (1980), *Electromagnetic radiation: the communication link in remote sensing*, In: B. Siegal and A. Gillespie (Eds), *Remote Sensing in Geology*, John Wiley & Sons, New York, 702 p.

Hunt, G.R. and Salisbury, J.W. (1970), Visible and near-infrared reflectance spectra of minerals and rocks, I: Silicate minerals. *Modern Geology*, 1: 219–228.

Jones, D.E. and Holtz, W.G. (1973), Expansive soils – The hidden disaster. *Civil Engineering, ASCE*, 43(8): 49–51.

Kariuki, P.C. (1999), Analysis of the effectiveness of spectrometry in detecting the swelling clay minerals in soils, M.S. thesis, International Institute for Aerospace Survey and Earth Sciences, Enschede, The Netherlands, 96 p.

Kruse, F.A. (1988), Use of Airborne Imaging Spectrometer data to map minerals associated with hydrothermally altered rocks in the northern Grapevine Mountains, Nevada and California, *Remote Sensing, Environment* 24: 31–51.

Kruse, F.A., Boardman, J.W., Lefkoff, A.B., Young, J.M., Kierein-Young, K.S., Cocks, T.D., Jenssen, R. and Cocks, P.A. (1999), The 1999 USA HyMap group shoot. Proceedings of the International Symposium on Spectral Sensing Research (ISSSR'99), Las Vegas, NV, 31 October 31–4 November 1999. ISSSR, Alexandria, VA, pp. 351–359.

Livo, K.E. (1998), Personal Communication.

McKeen, R.G. (1992), A model for predicting expansive soil behavior. Proceedings of the 7th International Conference on Expansive Soils, Dallas, TX, 3–5 August 1992. pp. 1–6.

Mitchell, J.K. (1993), *Fundamentals of Soil Behavior*, John Wiley and Sons, New York, 437 p.

Mustard, J.F. and Pieters, C.M. (1987), Abundance and distribution of ultramafic microbreccia in Moses Rock dike: Quantitative application of mapping spectroscopy. *Journal, Geophysics Research*, 92: E617–E626.

Noe, D.C. (1997), Heaving-bedrock hazards, mitigation, and land-use policy: Front Range Piedmont, Colorado. *Environmental Geosciences*, 4(2): 48–57.

Noe, D.C. and Dodson, M.D. (1995), The dipping bedrock overlay district (DBOD): An area of potential heaving bedrock hazards associated with expansive, steeply dipping bedrock in Douglas County, Colorado. Colorado Geological Survey Open-File Report 95–5, Colorado Geological Survey, Denver, CO, 32 p. 1 plate, scale 1 : 50000.

Noe, D.C. and Dodson, M.D. (1999), Heaving bedrock hazards associated with expansive, steeply dipping bedrock in Douglas County, Colorado. Colorado Geological Survey Special Publication 42, Colorado Geological Survey, Denver, CO, 80 p. 2 plates, scale 1 : 24000.

Olsen, H.W., Krosley, L., Nelson, K., Chabrillat, S., Goetz, A.F.H., and Noe, D.C. (2000), Mineralogy-swelling potential relationships for expansive shales. In: C.D. Shackelford, S.L. Houston, and N.-Y. Chang (Eds), *Geotechnical Special Publication No. 99, Advances in Unsaturated Geotechnics*. ASCE, Reston, VA, pp. 361–378.

Post, J.L. and Noble, P.N. (1993), The near-infrared combination band frequencies of dioctahedral smectites, micas, and illites, *Clays and Clay minerals*, 41(6): 639–644.

Rockwell, B.W., Clark, R.N., Livo, K.E., McDougal, R.R., Kokaly, R.F., and Vance, J.S. (1999), Preliminary materials mapping in the Park City region for the Utah USGS-EPA imaging spectroscopy project using both high and low altitude AVIRIS data. Summaries of the 8th JPL Airborne Earth Science Workshop, Jet Propulsion Laboratory, Pasadena, USA, 9–11 February 1999, JPL Publication 99–17, pp. 365–376.

RSI (2000), ENVI User's Guide, The Environment for Visualizing Images, Version 3.2. Research Systems, Inc., 2995 Wilderness Place, Boulder, CO, 80301, USA, 930 pp.

Ryskin, Y.I., (1974), The vibrations of protons in minerals: Hydroxyl, water and ammonium, in V.C. Farmer (Ed.), *The Infrared Spectra of Minerals*, Mineralogical Society, London, pp. 137–183.

Scott, G.R. and Wobus, R.A. (1973), Reconnaissance geologic map of Colorado Springs and vicinity, Colorado. US Geological Survey map MF-482, scale 1 : 62,500.

Seed, H.B., Woodard, R.J., and Lundgren, R. (1962), Prediction of swelling potential for compacted clays. *Journal of American Society of Civil Engineers*, Soil Mechanics and Foundations Division, 88(SM3): 53–87.

Thompson, R.W. (1992), Swell testing as a predictor of structural performance. Proceedings of the 7th International Conference on Expansive Soils, Dallas, USA, 3–5 August 1992, pp. 84–88.

Tourtelot, H.A. (1973), Geologic origin and distribution of swelling clays. Proceedings of the Workshop on Expansive Clays and Shales in Highway Design and Construction, Denver, CO, 13–15 December 1972. Federal Highway Administration (FHWA), Denver, CO, vol. 1, pp. 44–69.

Vane, G., Duval, J.E. and Wellman, J.B. (1993), Imaging spectroscopy of the Earth and other solar system bodies. In: C.M. Pieters and P.A.J. Englert (Eds), *Remote Geochemical Analyses: Elemental and Mineralogical Composition*. Cambridge University Press, Cambridge, UK, pp. 121–144.

Chapter 15

Spectroscopy as a tool for studying swelling soils

Patrick Chege Kariuki,[1] *Keith Shepherd,*[2] *and Freek van der Meer*[3]

Summary

This chapter describes the development of spectroscopy from an experimental research instrument toward an operational mapping tool. Integrating spectral based methods with well-established physicochemical methods such as the Atterberg limits, cation exchange capacity (CEC), and coefficient of linear extensibility (COLE), will bring about a better understanding of expansive soils and result in a better classification. Proper calibrations based on a limited number of samples will enable a user to classify soils of unknown swell potential. Such an approach provides a tool for generalizing results of soil assessments conducted at limited sites, and thereby increases the efficiency of expensive and time-consuming studies. The rapid nature of the measurement allows soil variability to be more adequately sampled than with conventional approaches. The spatial characterization of the soil surface in the field provides a coherent framework for linking soil information with remote sensing information for improved spatial prediction of swelling.

Introduction

Swelling of soils, which is caused by the chemical attraction of water molecules into the clay structure, is dependent on type and amount of clay particles. Smectite, illite, and kaolinite, (here listed in order of decreasing swelling potential) are the most important indicators.

Many engineering methods at quantifying soil swelling involve time consuming and expensive laboratory measurements. There has been a continued search for cheaper and faster techniques. Spectroscopy (i.e. laboratory, field, or imaging) offers a rapid and inexpensive complimentary if not alternative method since clay minerals and clay soils have unique spectral properties. Determination of their presence and abundance has been the basis of many direct and indirect methods due to their influence on the soil physicochemical properties such as plasticity. In indirect methods, thresholds have been established within which soils are described as dominated by one or the other of these three influential minerals (Skempton, 1953; Pearring, 1963; Holt, 1969; McKeen and Hamberg, 1981; Hamberg, 1985; Nelson and Miller, 1992).

[1] International Livestock Research Institute (ILRI) PO Box 30709, Nairobi, Kenya; email: pkariuki@cgiar.org
[2] World Agroforestry Centre (ICRAF) PO Box 30677, Nairobi, Kenya; email: K.Shepherd@cgiar.org Tel: +254 2 524174.
[3] Delft University of Technology Faculty of Civil Engineering and Geosciences, Centre for Technical Geosciences Mijnbouwstraat 120 2628 RX Delft, The Netherlands; email: vdmeer@itc.nl

Direct quantitative measuring methods include X-ray diffraction (XRD), differential thermal analysis (DTA), and scanning electron microscope (SEM). They are rarely used due to cost. Spectroscopy offers a quick and non-destructive method of identifying minerals on the basis of mineralogical differences found in the Short Wave Infrared (SWIR) (Kruse *et al*., 1991; Goetz *et al.*, 2001). Other studies have reported applications of spectroscopy to estimate associated properties (Zhang *et al.*, 1992; Chang *et al.*, 2001; Ben Dor *et al.*, 2002; Kariuki *et al.*, 2003) and recent work has shown potential application of airborne spectroscopy (Muller and Decamps, 2000; Chabrillat *et al.*, 2002). Rowan and Mars (2002) quantified Al-OH, Mg-OH, and Fe-OH, three key components of minerals in expansive soils using Advanced Spaceborne Thermal Emission and Reflection Radiometer (ASTER) imaging. Launching of spaceborne hyperspectral imaging systems, such as the Hyperion (Pearlman *et al.*, 2001) opens new avenues for applicability of spectroscopy to solve world problems as is the case with swelling potential. The increased spatial resolution of satellites also makes their application in swelling soil identification more feasible based on the surface manifestations of these soils in terms of micro topography.

This chapter describes the development of spectroscopy from an experimental research instrument toward an operational mapping tool. Integrating spectral based methods with well-established physicochemical methods such as the Atterberg limits, CEC, and COLE, will bring about a better understanding of expansive soils and result in better classification.

Swelling process

Swelling is restricted to soils containing clay minerals, which are susceptible to penetration of their chemical structure by water molecules (Carter and Bentley, 1991). It has been attributed to osmotic pressures generated by chemical potential gradients between free water and water in diffuse double layers (DDL) forming around the clay mineral surfaces (Parker *et al.*, 1977). The DDLs are a result of electrostatic attraction of positive ions in the pores by the negatively charged clay particle surfaces whose overlapping generate interparticle repulsive forces that bring about swelling (Bohn *et al.*, 1985). Thus fundamentally, soil swelling is an intrinsic property of the clay mineralogy (Seed *et al.*, 1963). It is on this basis that many of the soil swelling potential indices have been developed.

The clay minerals are layer alumino silicates, also called crystalline phyllo-silicates (Jackson *et al.*, 1986), in which atomic sheets of silicon tetrahedra are bound by sheets of aluminium octahedra. The most abundant clay minerals in soils are the kaolins having a 1 : 1 (silica : aluminium) layered structure, and the smectites and illites both having a 2 : 1 (silica : aluminium) layered structure. Other less abundant clay minerals include chlorite and vermiculite. The grouping of the clay mineral according to these three major groups is convenient, since members of the same group have similar engineering properties (Mitchell, 1993).

The members of the kaolinite group are 1 : 1 (silica : aluminium) layer silicates whose theoretical composition of the diotahedral subgroup is $Al_2Si_2O_5\,(OH)_4$ (Gillott, 1968). The mineral species are kaolinite, nacrite, dickite, halloysite, and anauxite. The layers have little charge unbalance and sheets are held together by hydroxyl bonds. Kaolinite does not usually experience isomorphous substitution which makes them less subject to swelling characteristics (Thomas, 1994). Their formation is favored when aluminium is abundant and silica is scarce because of the 1 : 1 (silica : aluminum) structure as opposed to the 2 : 1 structure of the three layer minerals. Formation at the expense of primary minerals is favored by acid

conditions under weathering and develops where precipitation is relatively high with good drainage.

The smectites are 2 : 1 (silica : aluminum) layer silicates with a layer charge of 0.25–0.6 per formula unit which due to their 2 : 1 (silica : aluminum) structure form where silica is abundant. There is considerable range in composition and there are both dioctahedral and trioctahedral members. Montmorillonite, beidellite, and notronite are important dioctahedral members while saponite, hectorite, and sauconite make up the trioctahedral membership (Gillott, 1968). They experience a variety of isomorphous substitutions in the octahedral layers and thus have a range of chemical compositions. The negative charge leads to a readiness to exchange cations and water layers, and this in turn contributes to their well-known capacity to swell and shrink. Water and other polar molecules can enter between the unit layers, causing the lattice to expand in the c-direction. Conditions favoring their formation include high pH, high electrolyte content, and the presence of more Mg^{2+} and Ca^{2+} than Na^{+} and K^{+}. They mainly form in areas with poor drainage. Illite forms under conditions leading to the formation of smectites but the presence of potassium is essential for their formation.

Influence of clay minerals on swell potential of soil

The structure of the clay minerals influences the physical and chemical character of the soil (Yong and Warkentin, 1966; Grim, 1968; Selby, 1993) such as CEC, that is a result of isomorphous substitution. Isomorphous substitution is the process by which Al^{+3} is replaced by divalent cations such as Mg^{+2} or Fe^{+2} in clay minerals. These minerals are disordered leading to low structural stability, and large surface area. Atoms are joined to other atoms on only one side leading to unbalance, to satisfy which surface atoms attract water molecules. The absorbed water lubricates movement of one clay plate over another and promotes plasticity in soil. The net negative charge gives such minerals the property of absorbing certain anions and cations and retaining them in an exchangeable state, which makes CEC important in swell potential estimations.

However, despite this simplification, swelling is a result of more complicated processes taking place in the course of interaction between water and the lattice structure of a clay soil that develops from the hydration of clay mineral platelets and exchangeable cations.

Spectroscopy and swelling potential mapping

Reflectance spectroscopy is the study of light as a function of the wavelength that has been reflected or absorbed by a material. It is a rapidly growing science that can be used to derive significant information about mineralogy and with little or no sample preparation. In many cases spectroscopy is very sensitive to subtle changes in crystal structure and chemistry, a characteristic that has more recently been recognized as a powerful means of studying the structure and composition of materials (Hunt, 1982; Clark, 1999).

Reflectance spectroscopy of a material is defined by its reflectance, or absorbance, as a function of wavelength. Fundamental features occur at energy levels that allow molecules to rise to higher vibrational states (Hunt, 1982; Clark, 1999). For example, soil clay minerals have very distinct spectral signatures in the short-wave infrared region because of strong absorption of the overtones of OH^{-} and combinations of fundamental features of, H_2O and CO_2 (Hunt, 1982; Clark, 1999). This when coupled to chemometrics has led to increased use

of spectroscopy as a tool to quantify functional groups present in a material through characterization of the spectra based on known diagnostic reflectance or absorption of specific wavelengths (Clark, 1999).

Absorption process

Photons entering an absorbing medium are absorbed in accordance to Beer–Lambert Law, where the concentration (c) and absorption coefficients (k) of the material determine the level of absorption (Svanberg, 2001). Absorption is therefore a function of the type and arrangement of atoms within the crystal lattice of the material and directly influences the appearance of the spectrum, more so the intensities and shape of the absorption features (Schmidt, 2003). Thus for absorption spectra, the intensity of the emerging energy (I) can be expressed in terms of the incident energy (I_0) and in Beer Lambert law is given as:

$$\log_{10}(I_0/I) = \log_{10}(1/T) = kcl = \mathrm{A} \tag{15.1}$$

where A is absorbance; k proportionality constant called molecular absorption (extinction) coefficient characteristic of the absorbing media, c is the concentration of absorbing molecules, and l the path length of the irradiating energy through the sample. The absorbance is therefore directly proportional to the concentration of the absorbing material and a linear relationship exists between absorbance and concentration, provided Beers law is upheld.

In spectroscopy, reflectance (R) is analogous to transmittance and Equation 15.1 can be expressed as:

$$\log_{10}(1/R) = kcl = A \tag{15.2}$$

This is more commonly expressed as

$$A = \log_{10}(1/R) \tag{15.3}$$

This has the advantage of a near linear relation between the concentration of the absorbing component and its contribution to $\mathrm{Log}_{10}(1/R)$ at the wavelength absorbed (Hruschka, 1987). The parameters of these absorption features namely: position, shape, depth, width, and asymmetry are therefore good indicators of the concentration of the absorbing material.

Reflectance process

Mathematical models for the analysis of reflectance spectra have been presented by many workers. One such model developed by Hapke (1981) has been applied successfully in many studies (Clark, 1983; Mustard and Pieters, 1987; van der Meer, 1995). In the model, diffuse reflectance, r, of a particulate medium is related to mean single-scattering albedo, $\acute{w}$, of an individual particle through the Kubelka–Munk (1948) equation:

$$\sqrt{(1 - w)} = (1 - r)/(1 + r) \tag{15.4}$$

which can be rearranged to give

$$w = 4r/(1 + r)^2 \tag{15.5}$$

where r and w are functions of wavelength. For a material having a measured reflectance spectrum, $r(\lambda)$, the single scattering albedo spectrum can be derived directly from Equation (15.5). The mean single-scattering albedo, $w(\lambda)$, of a multi-component particulate mixture is the linear combination of their single scattering albedos, weighted by their effective cross-sectional area:

$$w(\lambda) = \frac{\sum M_i w_i(\lambda)\}/\{\rho_i d_i\}}{\sum M_i/\{\rho_i d_i\}} \tag{15.6}$$

where i refers to the ith component in the mixture, M is the mass fraction, ρ is the particle density, and d is the effective particle diameter. This equation assumes the particles to be homogeneously distributed and none of the particle coating the other. By inverting Equation 15.5, the reflectance of the resulting mixture can be obtained as:

$$r(\lambda) = \frac{1 - \sqrt{(1 - w(\lambda))}}{1 + \sqrt{(1 - w(\lambda))}} \tag{15.7}$$

Further development of this model to incorporate the phase and the backscattering functions of the surface adds unknowns to the equation and has been found to only add a few percentages in the derived reflectance level (van der Meer, 1995). This model is thus adequate and is commonly used to assess quantitative mixtures. This characterization of reflectance is widely used to study material properties.

Spectral data interpretations

The resulting spectra can be characterized in terms of the absorption feature parameters (in absorbance) and optical density (in reflectance) among other established properties. Absorption features are characterized in terms of position, depth, width, and asymmetry (Figure 15.1).

Where, position is the wavelength of minimum reflectance width, W, is given by;

$$W = \frac{\text{Area}_{\text{left}} + \text{Area}_{\text{right}}}{2D} \tag{15.8}$$

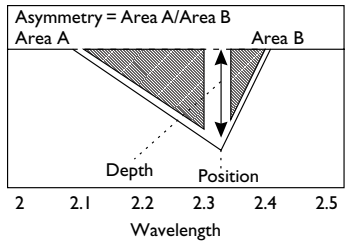

Figure 15.1 Absorption feature parameters.

D = the depth of the feature relative to the hull (Green and Graig, 1985) and area is the summation of the $\text{Area}_{\text{left}}$ and $\text{Area}_{\text{right}}$ of the line through the center of the absorption feature. Asymmetry, S, is the ratio of the $\text{Area}_{\text{left}}$ to $\text{Area}_{\text{right}}$ of the absorption center,

$$S = \text{Area}_{\text{left}}/\text{Area}_{\text{right}} \tag{15.9}$$

Optical density $\log_{10}$ $(1\backslash R)$ is used to provide quantitative information on the functional groups based on the analysis of the whole spectrum because of the almost linear relationship between the concentration of the absorbent and its contribution to the $\log_{10}$ $(1\backslash R)$ value. Other methods used in data interpretations include manipulations into the 1st and 2nd derivatives.

Obtained parameters can then be related to various properties of the absorbing material through regression analysis with known compositional information in a method popularly known as Near Infrared Reflectance spectroscopy (NIRS). This is then used to develop a spectral library with which to characterize similar materials of known spectral characteristics but unknown concentration of the functional groups.

In developing the spectral libraries, the first step is to widely sample the material in question from a target area and scan the samples through the spectrometer. In the case of soils the properties or attributes of functional capacity are measured and can include laboratory measurements (e.g. clay content, cation exchange capacity, Atterberg limits etc.) or field measurements. Calibrations should be made between the attributes and the reflectance spectra which if on the basis of cross-validation, calibrations are found to be insufficiently accurate for user requirements, the calibration sample size can be increased (Shepherd and Walsh, 2002).

Prior to follow up statistical analysis, the raw spectral reflectance data is pre-processed to reduce data through such methods like reflectance spectra resampling, principal component analysis, and factor analysis among other data reduction methods.

The calibrations are tested by predicting the soil variables on validation data sets and prediction success is evaluated on predicted and actual observations using the coefficient of determination (r^2) and root mean square error (RMSE).

Clay minerals spectral properties

There are three major absorption features that characterize the reflectance spectra of clay minerals in the SWIR region. These are overtones and combinations of fundamental features that occur at longer wavelengths due to vibrational processes in hydroxyl (OH), and water (H_2O). The H_2O and OH produce diagnostic absorptions in the spectra of these minerals where overtones of water are seen in spectra of smectites (the water-bearing mineral in the group) with the first overtone of the OH stretch occurring at 1400 nm and that due to the combinations of the H–O–H bend with the OH stretch near 1900 nm. The combination of fundamental OH stretching ($\underline{n}$) and bending (δ) modes occur between 2,200 and 2,300 nm and is also diagnostic of the clay minerals (Clark, 1999). Farmer (1974) assigned them as 2,160–2,170 nm, 2,210–2,240 nm, and, 2,300 nm ($\nu_{\text{Al–OH–Al}} + \delta_{\text{Al–OH–Al}}$), ($\nu_{\text{Al–OH–Fe}} + \delta_{\text{Al–OH–Fe}}$), and ($\nu_{\text{Mg–OH–Mg}} + \delta_{\text{Mg–OH–Mg}}$,) respectively. The positions vary among the minerals, depending on the details of their composition and associated atomic bonding characteristics.

Crowley and Vergo (1988) observed the 2200 nm OH band to occur near 2,220 nm in illites, closer to 2,200 nm in smectites, and near 2,199 nm in kaolinite, which they attributed to ratios between the three basic metal cations of Al, Fe, and Mg. Chemical bonding of these

cations (Al, Mg, and Fe) to the molecules (OH and H_2O) result in predictable wavelength positions which can be used to identify the specific molecular bonds and the mineral species (Alonzo, 2002). Manifestation of these characteristics is the key to identification of the minerals in natural materials such as rocks or soils.

At high resolution, kaolinite shows diagnostic doublets at 2,200 and 1,400 nm whose strength has been attributed to higher fraction of octahedral (1 : 1 Al–OH : SiO_4) to tetrahedral structure relative to (2 : 1 tetrahedral : octahedral) in the other clay minerals. The spectrum of smectite is typical for a water-rich mineral with strong absorption bands, near 1,400 and 1,900 nm and an additional weaker band near 2200 nm that is usually broad due to the presence of structural water. In the absence of free water the feature at 1900 nm is sharp and intense and shifts to lower wavelengths and is diagnostic (Hauff, 2000). Illite, like smectites, does not show fine structure at the hydroxyl positions but diagnostically shows additional bands near 2,350 and 2,450 nm.

Very strong molecular water bands are therefore indicative of bound water typical of smectites while strong hydroxyl bands are typical of kaolinite (Hunt and Salisbury, 1970). Broader and low absorption intensities of both are indicative of illite which has the hydroxyls more randomly distributed in the octahedral sites (Mathews *et al.*, 1973). Table 15.1 gives a generalized description of the important absorption features in these minerals and their molecular assignments.

Figure 15.2 gives an illustration of observed changes in the absorption features with changing contents of kaolinite and smectite in laboratory obtained spectra (Kariuki 2004) where abundant kaolinite shows three unique diagnostic features at 1,395, 2,170, and 2,384 nm up to 40%. It is evident that the strength of the doublets in terms of sharpness and intensity decrease with decreasing kaolinite. The molecular water absorption feature on the other hand is seen to increase both in depth and sharpness from the generally broad feature at 100% kaolinite, to a relatively sharp feature at 100% smectite. This provides quantitative evidence of the mineral contents based on Hapke (1981) theory and is significant to interpretations.

Figure 15.3 shows the absorption parameters as a function of weight percentage of smectite in mixtures where depth intensity of the molecular water feature (1,900 nm) increase and asymmetry and depth of the hydroxyl positions (1,400 and 2,200 nm) decrease, with smectite. This probably reflects a decrease in Al–OH relative to Mg–OH/Fe–OH. Duke (1994) found the wavelength of the Al–OH to shift from 2217 to 2,199 nm, corresponding to an increase in octahedral aluminum (Al) from 3.3 to 3.7 atoms, relative to Fe and Mg

Table 15.1 Major clay mineral related absorption feature positions

Major feature positions (nm)	*Molecule*	*Clay mineral*
1,400	OH and H_2O	Kaolinite/smectites/illites
1,900	H_2O	Smectites/illites
2,170	Al–OH	Kaolinite
2,200	Al–OH	Kaolinite/smectites/illites
2,290	Fe–OH	Smectite (notronite)
2,300	Mg–OH	Smectite (hectorite)
2,340	Fe–OH/Mg–OH	Illite
2,384	Fe–OH	Kaolinite

Source: Hauff, 2000.

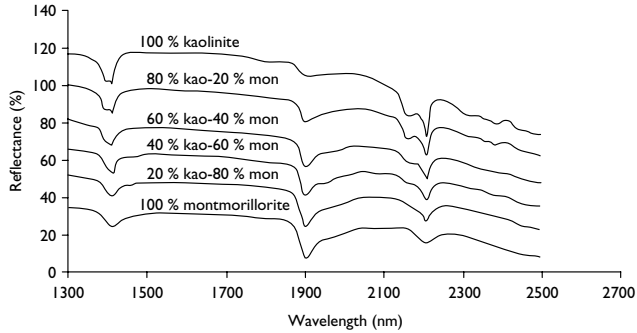

Figure 15.2 Calculated reflectance spectral of mineral mixtures of kaolinite and montmorillonite (20 μm) notice changes in 2,200 nm shape.

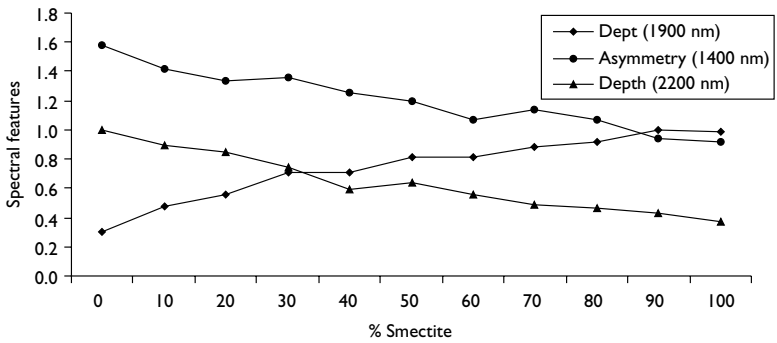

Figure 15.3 Changes in absorption feature parameters with smectite content.

per 22 oxygen. Kruse *et al*. (1991) successfully used this approach to obtain quantitative estimates of kaolinite and smectite in clay soils. Shift in position has also been described to be characteristic of cation substitution at the exchangeable sites (Van der Meer, 1995).

Derivatives have, in addition, been widely used to resolve compositional information based on presumed capability to remove baseline effects and thus separate subtle spectral differences in overlapping features (Escadafal, 1994). In kaolinite/smectite mixtures, 1st and the 2nd derivatives have been observed to enhance the water and hydroxyl peaks to different magnitude (Kariuki *et al.*, 2004). Absorption peaks are stronger at the molecular water features in abundant smectite and in hydroxyl in abundant kaolinite. Figure 15.4 illustrates this in the 1st derivative for both theoretical and physical quantitative mixtures at 50% quantities of each.

Soil spectral properties

Soil reflectance provides information on the properties and state of the soil (Irons *et al*., 1989). It is a cumulative property that derives from spectral behavior of a heterogeneous

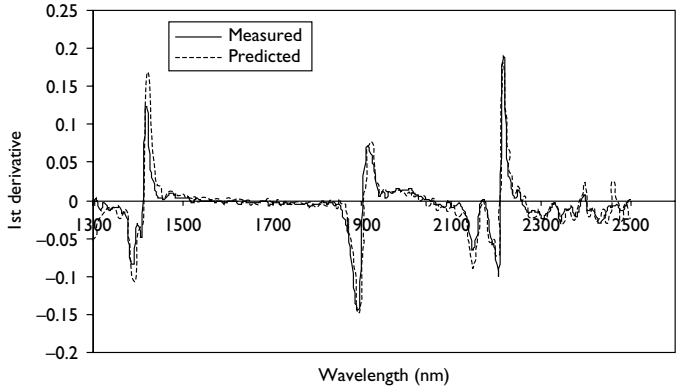

Figure 15.4 Calculated and measured derivative peaks of 50% kaolinite/smectite mix.

combination and is determined by a combination of inherent spectral behavior of minerals, organic matter, and soil water (Mulders, 1987; Van der Meer 1995). Unsatisfied valences on the surfaces and at the broken edges of clay mineral particles in the soil where the exposed oxygen's and the hydroxyls of silica and aluminum sheets act as negatively charged sites, attract hydrogen ions and other cations. The hydroxyl groups formed at the edges of the clay particles cause absorption features in soil spectra and is dependent on the atomic structure causing it (Irons *et al.*, 1989). The resulting absorption is dependent on the clay mineral type since, the position of absorption features caused by cations are not diagnostic of the cation itself, but rather of the crystal lattice in which the ion is embedded (Goetz, 1989). This enables assignment of a soil to a dominant clay mineral and its related properties.

The presence of a doublet at 2,200 nm and unique presence of 2,160–2,170 nm and 2,384 nm features in combination is diagnostic of dominant kaolinite in a soil. The position of the water feature (1,900 nm) in dry soils also gives characteristic differences in smectite/kaolinite rich soil. Asymmetries (1,400 and 2,200 nm) also give an indication of differences in the soil clay mineralogy (Van der Meer, 1999) where kaolinitic soils give higher asymmetries relative to smectite. Hauff (2000) described asymmetries in general to indicate order in structural sites and asymmetry to the right at 2,200 nm to show an increment in smectite and to the left as due to the doublets in kaolinite. Kaolinite rich soils have been found to generally give higher asymmetries at the hydroxyl (2,200 and 1,400 nm) sites attributable to the characteristic doublets emanating from structural order at the two sites. This combined with presence of 2,384 nm are diagnostic of low swelling potential (Kariuki *et al.*, 2004).

Two depths (1,900 and 2,200 nm) intensities provide another source of information to clay mineral differences with that at 1,900 nm increasing in intensity with smectite contents in dry soil and that at 2,200 nm intense in kaolinite rich soils (Figure 15.5). Alonso *et al.* (2002) described the strength of the later to vary with quantitative differences in Al, Fe, and Mg in octahedral sites where abundant Al^{3+} leads to much more developed structure as is the case in kaolinite.

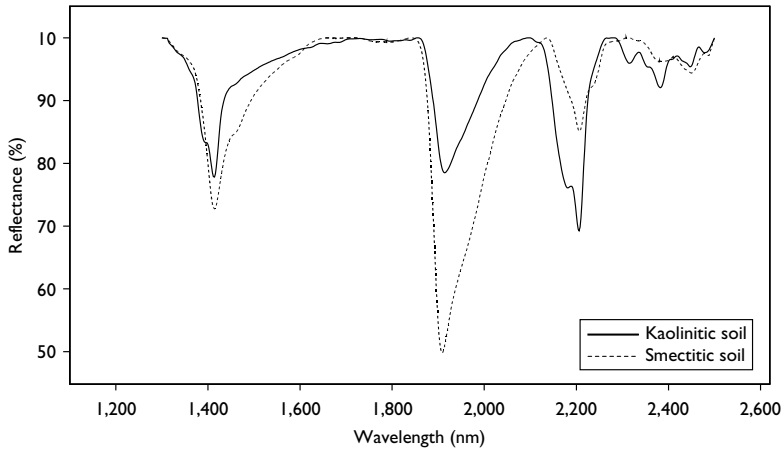

Figure 15.5 Illustration of absorption feature parameters in soils rich in kaolinite/smectite.

Soil spectra and related physicochemical properties

Recent research has demonstrated the ability of reflectance spectroscopy to provide rapid prediction of soil physical, chemical, and biological properties in the laboratory (Ben-Dor and Banin, 1995; Janik *et al.*, 1998; Reeves *et al.*, 1999). There has also been some success with reflectance spectroscopy for sensing of soil properties in the field (Sudduth and Hummel, 1993), and for the discrimination of major soil types from satellite multispectral and aircraft hyperspectral data (Baumgardner *et al.*, 1985; Coleman *et al.*, 1993; Palacios-Orueta *et al.*, 1999). Despite these indications of the potential of the technique, much still needs to be done to encourage application of reflectance spectroscopy for nondestructive assessment of soils (Janik *et al.*, 1998; Myer, 1998) and to build soil spectral libraries to include diversity of soils with information on physical, chemical, and biological properties.

Conventional soil swelling determination

One setback in the characterization of swelling potential of soils has been the lack of a standard definition of swell potential (Nelson and Miller, 1992) thus, whereas Holtz (1959) referred to swell potential as the volume change of air-dried undisturbed sample, Seed *et al.* (1962) defined it as the change in volume of a remolded sample. It is therefore not to be unexpected that disparities occur in classifications when these indices are applied, making it difficult to use one method to conclusively state the nature of the expansiveness of a soil and thus relate one region to another.

Many examples abound where either of the indices have been described to best represent the swelling potential. McCormack and Wilding (1975) described clay content to be as reliable in predicting swelling potential as the Atterberg limits in soils dominated by illite, but (Ross, 1978), found it to be less certain relative to the specific surface area (SSA). Yule and Ritchie (1980) and Gray and Allbrook (2002) on their part found no relationship

between clay percentage and soil swelling. Gill and Reaves (1957) described CEC, saturation moisture, and Plasticity index (PI) as some of the most representative properties in the estimation of swelling whereas Snethen *et al.* (1977) having evaluated seventeen swelling indices concluded Liquid limit (LL) and PI as best indicators of swell potential. Parker *et al.* (1977) established swell index (Lambe, 1960) and PI as superior to other indices whereas Schafer and Singer (1976) concluded clay type rather than content as more important. Among all these indices however, smectite content has been described as the most important and consistent soil property that significantly correlates with laboratory-measured shrink–swell potential (Karathanasis Hajek, 1985; Thomas *et al.*, 2000).

This has led to the general conclusion that no one method estimates swell potential accurately for all soils and there is therefore the need to use a combination of these methods for better results. Several classification schemes have taken cognition of this fact (Pearring, 1963; Holt, 1969; McKeen and Hamberg, 1981; Thomas *et al.*, 2000). Spectroscopy therefore significantly adds value to such combinations based on its ability to qualitatively determine smectite presence in soils.

Spectral data integration into swelling potential mapping

The previously described swelling indices can help establish the relationships between soil spectra and swelling potential for a region of interest and build such into a spectral library that could result in the estimation of swelling potential of soils in the region based only on the spectral data. Some results have shown very small calibration sample sizes to provide adequate predictive performance for such indices from spectral data as was the case with CEC, where Shepherd and Walsh (2002) used 34 soils to predict abnormal cases for 647 library soils with a predictive efficiency of 86%. Combinations of such indices through reduction methods such as factor analysis (Figure 15.6) give weighted parameters which can help establish more representative libraries (Kariuki and Meer, 2003).

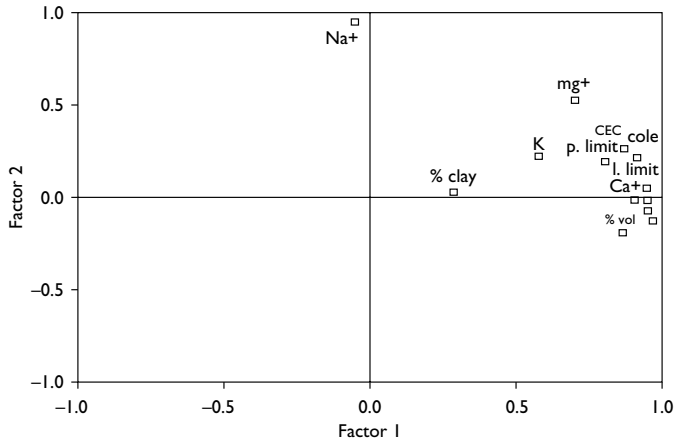

Figure 15.6 Common factor scores of the engineering indices.

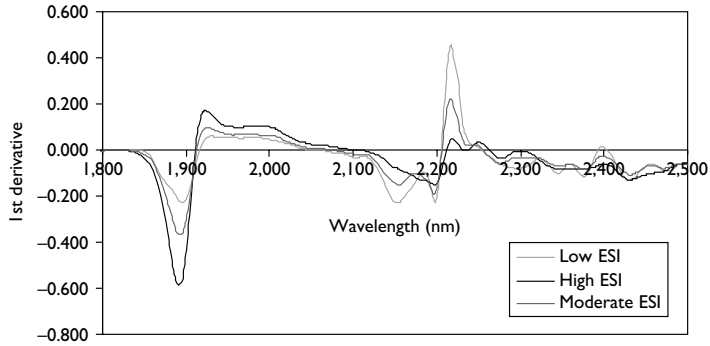

Figure 15.7 1st derivative spectrum of representative samples of the three ESI classes.

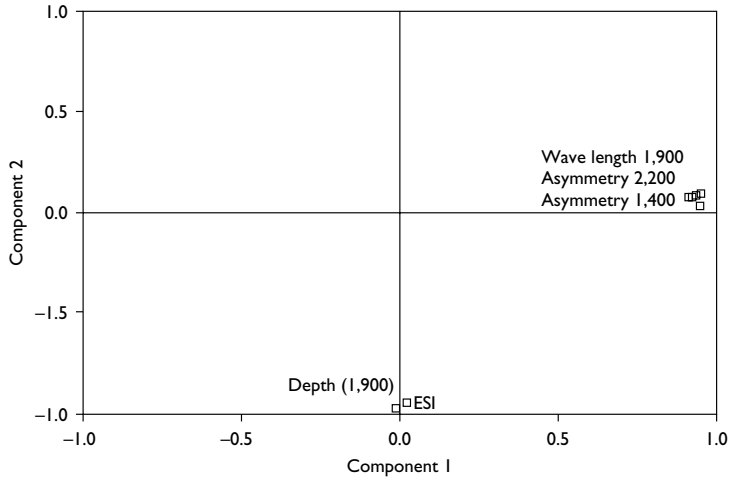

Figure 15.8 Results of principal component analysis on soil samples spectra.

Figure 15.7 gives the differences in peak intensities for the first derivative of the soils used in the above data reduction process where an Expansive Swell Index (ESI) was established and used to group soils into three swelling potential groups. It shows soil with high ESI to show the bound water peak (1,800–2,000 nm) intense relative to those with moderate and low ESI values as was the case with kaolinite and smectite mixtures (Figure 15.4).

Figure 15.8 shows principal components analysis of the soil spectra absorption feature parameters and the ESI. There are high loadings from asymmetries (1,400 and 2,200 nm) and the wavelength position at 1,900 nm in the first component which could be assigned to order in functional group related to abundant kaolinite and low swelling. The second

component shows high loading from ESI and 1,900 nm depth and can thus be assigned to swelling and thus smectite increase. Loadings for a soil in the two can thus be used as a measure of its potential suitability in terms of swell potential. By building libraries with such an index and spectral parameters, soils of unknown swell potential but known spectral parameters can be assigned to a swelling potential class based on the spectral information alone.

However, where diagnostic performance is less than desired, combining additional screening tests based on other information, such as land use, topography, or satellite imagery can help increase the predictive potential from such data. Calibrations could also be improved by restricting geographical extent (Sudduth and Hummel, 1996).

Conventional remote sensing

Surface spatial characteristic patterns associated with swelling soils (gilgai), provide another source of information (Figure 15.9) on presence of these soils through the analysis of satellite imagery. Several methods used for quantitative analysis of such patterns in order to extract the relevant information (Webster, 1977) can be used on these images. They include micro-relief factor, specific micro-relief factor, slope variation, structural homogeneity, avoidance factor, and cell length (Russell and Moore, 1972). These factors are critical in relating corresponding properties in geographically separated areas and make identification of gilgai in satellite image very significant in mapping of swelling soils.

Determination of the structural homogeneity factor (K) that measures the tendency of repeatability, forms an ideal method for gilgai in the given image, based on their well-recognized repeatability of lows and highs.

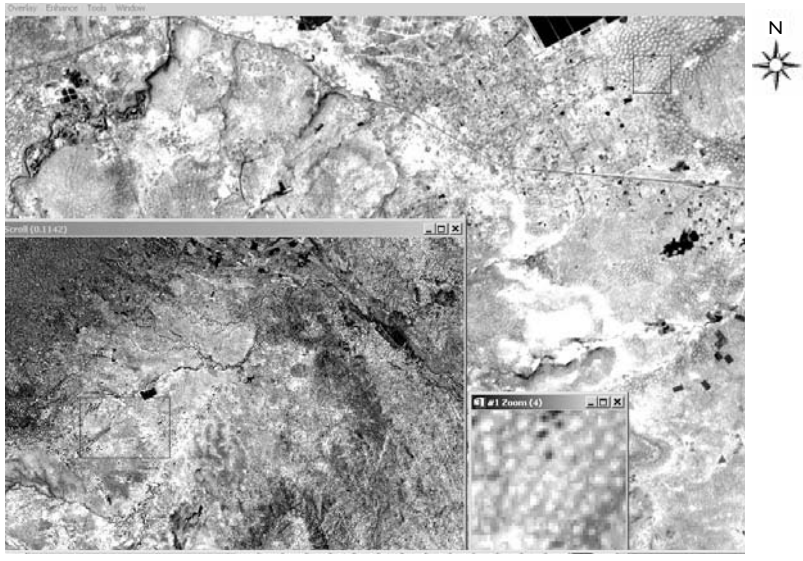

Figure 15.9 Image showing the individual mounds that could be used to estimate the various factors.

Table 15.2 Micro-relief parameter

Polygon	*Range*	*K*	*Rank*
1	3–6	0.17	1
2	10–11	0.13	4
3	6–10	0.15	2
4	8–11	0.13	4
5	7–9	0.13	4
6	8–13	0.14	3

Source: Russell and Moore, 1972.

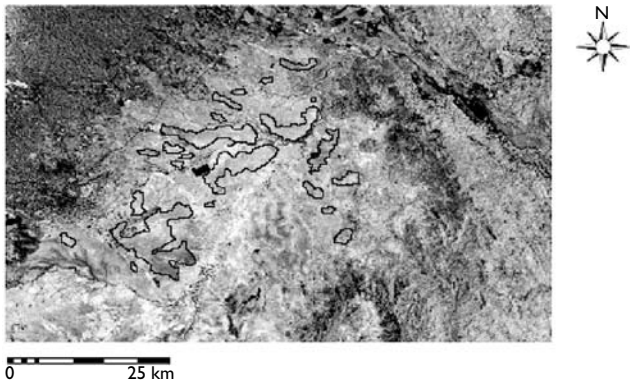

Figure 15.10 Gilgai topography spatial distribution (red polygons).

Table 15.2 gives the results of *K* analysis of established polygons of gilgai structures in the image (Figure 15.10) where they show generally moderate values signifying a uniform distribution of the features in the area. This could form a relative case for an area with similar patterns but with little ground surveys done and thus provides a tool for recognition of swelling soils in inaccessible areas based on the synoptic nature of satellite image. Combining such information with the soil or topographic nature of an area can further improve the derived conclusions (Figure 15.11). In the figure, the red colour consists of vertisols and are on the lowlands in terms of topographic position, known for their swelling nature whereas the other areas consist of mainly nitisols (blue and forest green) that form the surrounding highlands, thus allowing for a wider area diagnosis.

Discussion

There is generally strong correlation between swelling potential and spectral parameters with known relationships to clay mineralogy which shows a common dependency on clay mineralogy properties. The fact that spectroscopy provides information on bound water and hydroxyl in clay minerals, seen in the negative relationship between ESI and lattice hydroxyl parameters (1,400 nm; 2,160–2,220 nm) and the positive correlations with bound water parameters (1,870–1,880 nm) makes its use in engineering ideal.

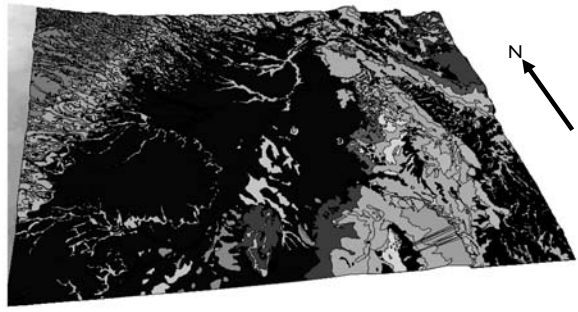

Figure 15.11 Perspective view of DEM wrapped with the soil distribution map of image area.

Sensitivity of spectroscopy to soil differences is evident from derivatives where subtle differences in the positions and intensity of spectral peaks show the quantitative mineralogical differences. The fact that the significant spectral parameters provide information on what Kariuki *et al.* (2003) described as changes in surface area among the dominant clay minerals and whose order of increase was given as smectites > illite > kaolinite by Ben Dor *et al.* (1999) is further proof of the suitability of the method. Chabrillat *et al.* (2001) found the water spectral features useful for identification of swelling soils whereas several other studies have found such data to be good predictors of swelling indices to levels where measured versus predicted give very significant values (Dalal and Henry, 1986; Shepherd and Markus, 2002).

High spatial resolution satellite images are also useful for soil swell mapping based on unique topographic differences in the form of gilgai described by Newman (1983) as "chimney" structures. This is so mainly due to what Driese *et al.* (2000) established as significant differences in the soil physical–chemical properties between the micro-highs and micro-lows where the wetter soil conditions in micro-lows give greater depths of leaching while micro-highs behave as evaporative "wicks" that draw moisture and soluble phases toward the soil surface resulting in precipitation of carbonates. This is what makes them good targets for capture from satellite imagery bearing in mind that they can range between 20 and 50 m in diameter. The uneven vegetation growth between the micro-high and micro-low (Macdonald *et al.*, 1999) provides another good distinguishing characteristic observable from a satellite image.

Conclusions

Spectroscopy is developing from an experimental research instrument into an operational mapping tool. Proper calibrations based on a limited number of samples will enable a user to classify soils of unknown swell potential. Such an approach will provide a tool for generalizing results of soil assessments conducted at limited sites, and thereby increasing the efficiency of expensive and time-consuming studies. The rapid nature of the measurement will allow soil variability to be more adequately sampled than with conventional approaches. The spatial characterization of the soil surface in the field provides a coherent framework

for linking soil information with remote sensing information for improved spatial prediction of swelling. Thus even though remote sensing of soil properties directly from space platforms is hampered by problems such as atmospheric interference and variation in soil moisture, other important uses can be derived.

Empirical relationships may yield unreliable predictions of swelling. Additional geological and experimental information is necessary to validate any empirical relationship when it is used in an unfamiliar situation. The future should therefore be to explore approaches that integrate the various methods such as combining soil spectral libraries, geo-referenced information (e.g. digital terrain models), and field observations together with information from hyper-spectral remote sensing imagery to derive swelling potential maps.

References

Alonso, S.M., Rustard, J.R., and Goetz, A.F.H., 2002, Ab initio quantum mechanical modelling of infrared vibrational frequencies of the OH group in dioctahedral phyllosilicates, Part II, main physical factors governing the OH vibrations, *American Mineralogist*, 87, 1224–1234.

Baumgardner, M.F., Stoner, E.R., Silva, L.F., and Biehl, L.L., 1985, Reflectance Properties of Soils. In *Advances of Agronomy*, edited by N. Brady (New York: Academic Press), pp. 1–44.

Ben-Dor, E., and Banin, A., 1995, Near infrared analysis (NIRA) as a rapid method to simultaneously evaluate several soil properties, *Soil Science Society of America Journal*, 59, 364–372.

Ben-Dor E., Irons, J.R., and Epema, G.F., 1999, Soil reflectance. In *Remote Sensing for the Earth Science, Manual of Remote Sensing* 3rd edition, edited by A.N. Rencz (New York: John Wiley & Sons), pp. 111–188.

Ben-Dor, E., Patkin, K., Banin, A., and Karnieli, A., 2002, Mapping of several soil properties using DAIS-7915 hyperspectral scanner data: a case study over clayey soils in Israel, *International Journal of Remote Sensing*, 23(6), 1043–1062.

Carter M. and Bentley S.P., 1991, *Correlations of Soil Properties*, (London: Pentech Press, UK).

Chabrillat, S., Goetz, A.F.H., Olsen H.W., and Krosley, L., 2001, Field and imaging spectrometry for identification and mapping of expansive soils. In *Imaging Spectrometry: Basic Principles and Prospective Applications*, edited by F.D. van der Meer and S.M. de Jong (Dordrecht: Kluwer Academic Publishers), pp. 87–109.

Chabrillat, S., Goetz, A.F.H., Krosley, L., and Olsen, H.W., 2002, Use of hyperspectral images in the identification and mapping of expansive clay soils and the role of spatial resolution, *Remote Sensing of Environment*, 82, 431–445.

Chang, C.W., Laird, D.A., Mausbach, M.J. and Hurburgh C.R. Jr, 2001, Near infrared reflectance spectroscopy-principal components regression analysis of soil properties, *Soil Science Society of America Journal*, 65, 480–490.

Clark, R.N., 1983, Spectral properties of mixtures of montmorillonite and dark carbon grains: implications for remote sensing minerals containing chemically and physically adsorbed water, *Journal of Geophysics Research*, 88, 10635–10644.

Clark R.N., 1999, Spectroscopy of Rocks and Minerals, and Principles of Spectroscopy, Remote Sensing for the Earth Science, manual of remote sensing 3rd edition, edited by A.N. Rencz (New York: John Wiley & Sons), pp. 111–188.

Coleman, T.L., Agbu, P.A., and Montgomery, O.L., 1993, Spectral differentiation of surface soils and soil properties: Is it possible from space platforms? *Soil Science*, 155, 283–293.

Crowley, J.K. and Vergo, N., 1988, Near-infrared reflectance spectra of mixtures of kaolin group minerals: use in clay studies, *Clays and Clay Minerals*, 36, 310–316.

Dalal, R.C. and Henry, R.J., 1986, Simultaneous determination of moisture, organic carbon, and total nitrogen by near infrared reflectance, *Soil Science Society of America Journal*, 50, 120–123.

Driese, S.G., Mora, C.I., Stiles, C.A., Joeckel, R.M., and Nordt, L.C., 2000, Mass-balance reconstruction of a modern Vertisol: implications for interpreting the geochemistry and burial alteration of paleo-Vertisols, *Geoderma*, 95(3–4), 179–204.

Duke, E.F., 1994, Near infrared spectra of muscovite, Tschermak substitution, and metamorphic reaction progress: implications for remote sensing, *Geology*, 22, 621–624.

Escadafal, R., 1994, Soil spectral properties and their relationships with environmental parameters – examples from arid regions. In *Imaging Spectrometry – A Tool For Environmental Observations*, edited by J. Hill and J. Megier (Dordrecht: Kluwer Academic Publishers), pp. 71–87.

Farmer, V.C., 1974, The layer silicates. In The Infra-Red Spectra of Minerals, edited by V.C. Farmer, (London: Mineralogical Society), pp. 331–364

Gill, W.R. and Reaves, C.A., 1957, Relationships of Atterberg limits and cation-exchange capacity to some physical properties of soil, *Soil Science Society of American Proceedings* 21, 491–494.

Gillott, J.E., 1968, *Clay in Engineering Geology* (Amsterdam, London and New York: Elsevier Publishing Company).

Goetz, A.F.H., 1989. Spectral Remote Sensing in Geology In: G. Asrar (Editor), Theory and Applications of Optical Remote Sensing. (New York: John Wiley & Sons), pp. 491–526.

Goetz, A.F.H., Chabrillat, S., and Lu, Z., 2001, Field reflectance spectrometry for detection of swelling clays at construction sites, *Field Analytical Chemistry and Technology*, 5(3), 143–155.

Gray, C.W. and Allbrook, R., 2002, Relationships between shrinkage indices and soil properties in some New Zealand soils, *Geoderma*, 108 (3–4), 287–299.

Green, A.A. and Graig, M.D. 1985, *Analysis of Aircraft Spectrometer Data with Logarithmic Residuals* (NASA-JPL Publication 85–41), pp. 111–119.

Hamberg, D.J., 1985, A simplified method for predicting heave in expansive soils, MS thesis, Colorado State University, Fort Collins, CO.

Hapke, B.W., 1981, Bidirectional reflectance spectroscopy I. Theory, *Journal of Geophysical Research*, 86, 3039–3054.

Hauff, P.L., 2000, *Manual of Applied Reflectance Spectroscopy With Emphasis on Data Collection and Data Interpretation Using the PIMA-II Spectrometer. Users Manual* (Arvada, CO: Spectral international inc.)

Holt, J.H., 1969, A study of physico-chemical, mineralogical and engineering index properties of fine grained soils in relation to their expansive characteristics. PhD Dissertation, Texas A&M University, College Station, TX.

Holtz, W.G., 1959, Expansive clays-properties and problems. Quart, *Colorado School of Mines*, 54(4), 89–117.

Hruschka, W.R., 1987, Data analysis: wavelengths selection methods. In *Near Infrared Technology in the Agricultural and Food Industries*, edited by P. Williams, and K. Norris (St. Paul, MN: American Association of Cereals Chemists) pp. 35–55.

Hunt, G.R., 1982, Spectroscopic properties of rocks and minerals. In *Handbook of Physical properties of Rocks*, Volume I, edited by R. S. Carmichael (Boca Raton: CRC press), pp. 295–385.

Hunt, G.R. and Salisbury, J.W., 1970, Visible and near infrared spectra of minerals and rocks. I. *Silicate minerals, Modern Geology*, 1, 283–300.

Irons, J.R., Weismiller, R.A., and Petersen, G.W., 1989, Soil reflectance. In *Theory and Applications of Optical Remote Sensing*, edited by G. Asrar (New York: John Wiley & Sons).

Janik, L.J., Merry, R.H., and Skjemstad, J.O., 1998. Can mid infrared diffuse reflectance analysis replace soil extractions? *Australian Journal of Experimental Agriculture*, 38, 681–696.

Karathanasis, A.D. and Hajek, B.F., 1985, Shrink-swell potential of montmorillonitic soils in udic moisture regimes, *Soil Science Society of America Journal* 49, 159–166.

Kariuki, P.C., 2004. Spectroscopy and Swelling Soils an Integrated approach. PhD Dissertation, Delft University of Technology, Delft.

Kariuki, P.C., Van der Meer, F.D., and Verhoef, P.N.W., 2003, Cation exchange capacity determination from spectroscopy, *International Journal of Remote Sensing*, 24(1), 161–167.

Kariuki P.C., Woldai, T., and Van der Meer, F., 2004, Effectiveness of spectroscopy in identification of swelling indicator clay minerals, *International Journal of Remote Sensing*, 25(2), 455–469.

Kruse, F.A., Thiry, M., and Hauff P.L., 1991, Spectral identification (1.2–2.5 μm) and characterization of Paris basin kaolinite/smectite clays using a field spectrometer. Proceedings of 5th International Colloquium on Physical Measurements and Signatures in Remote Sensing, Courchevel, France, 14–18 January 1991 ESA SP-319 (Noordwijk: ESA), pp. 181–184.

Kubelka, P. and Munk, F., 1948, New contributions to the optics of intensely light scattering materials, *Journal of Optic Society of America*, 38, 448–457.

Lambe, T.W., 1960, The character and identification of expansive soils, Federal Housing Administration. Report No. 701. US Government Printing Office, Washington, DC.

Macdonald, B.C.T., Melville, M.D., and White, I., 1999, The distribution of soluble cations within chenopod-patterned ground, arid western New South Wales, Australia, *Catena*, 37, 89–105.

McCormack, D.E. and Wilding, L.P., 1975, Soil properties influencing swelling in Canfield and Geeburg soils, *Soil Science Society of America Journal*, 39, 496–502.

McKeen, R.G. and Hamberg, D.J., 1981, Characterization of expansive soils. Transportation. Research. Record. 790, Transportation. Research. Board, USA.

Mathews, H.L., Cunningham, R.L., and Peterson, G.W., 1973, Spectral reflectance of selected Pennsylvania soils. *Soil Science Society of America Journal*, 37, 421–424.

Mitchell, J.K., 1993, *Fundamentals of Soil Behaviour* (New York: John Wiley & Sons, Inc.).

Mulders, M.A., 1987, Remote sensing in Soil Science. In *Developments in Soil Science 15* (Amsterdam: Elsevier Publishers).

Muller, E., and Decamps, H., 2000, Modelling soil moisture reflectance, *Remote Sensing of Environment*, 76, 173–180.

Mustard, J.F. and Pieters, C.M., 1987, Quantitative abundance estimates from bi-directional reflectance measurements, *Journal of Geophysical Research*, 92, 617–626.

Nelson, J.D. and Miller, D.J., 1992, *Expansive Soils: Problem and Practice in Foundation and Pavement Engineering* (New York: John Wiley & Sons).

Newman, A.L., 1983, Vertisols in Texas, *Soil Survey Horizons*, 24, 8–20.

Palacios-Orueta, A., Pinzon, J.E., Ustin, S.L., and Roberts, D.A., 1999, Remote sensing of soils in the Santa Monica mountains: II. Hierarchical foreground and background analysis, *Remote Sensing of Environment*, 68, 138–151.

Parker, J.C., Amos, D.F., and Kaster, D.L., 1977, An evaluation of several methods of estimating soil volume change. *Soil Science Society of America Journal*, 41, 1059–1064.

Pearlman, J., Carman, S., Segal, C., Jarecke, P., Barry, P.S., Browne W., 2001, Overview of the Hyperion Imaging Spectrometer for the NASA EO-1Mission, *IGARSS Special Session* 40, SS40MO, Paper 1775, 2001.

Pearring, J.R., 1963, A study of basic mineralogical, physical–chemical, and engineering index properties of laterite soils. PhD Dissertation, Texas A&M University Texas, College Station, TX, USA.

Reeves, J.B., McCarty, G.W., and Mesinger, J.J., 1999, Near infrared reflectance spectroscopy for the analysis of agricultural soils, *Journal of Near Infrared Spectroscopy*, 7, 179–193.

Ross, G.J., 1978, Relationships of specific surface area and clay content to shrink-swell potential of soils having different clay mineralogical compositions, *Canada Journal of Soil Science*, 58, 159–166.

Rowan, L.C. and Mars, J.C., 2002, Lithologic mapping in the mountain pass, California area using advanced spaceborne thermal emission and reflection radiometer (ASTER) data. *Remote Sensing of Environment*, 84(3), 350–366.

Russell, J.S. and Moore, A.W., 1972, Some parameters of gilgai micro relief, *Soil Science*, 114(2), 82–87.

Schafer, W.M. and Singer J.M. 1976, A new method of measuring shrink–swell potential using soil pastes, *Soil Society of America Journal*, 40, 805–806.

Seed, H.B., Woodward, R.J., Jr, and Lundgren, R., 1962, Prediction of swelling potential for compacted clays. *Journal of Soil Mechanics Foundation Division, American Society of Civil Engineers*. 88(SM3), 53–87.

Seed, H.B., Woodward, R.J., and Lundgren, R. 1963, Prediction of swelling potential for compacted clays. *Transactions of American Society of Civil Engineers*, 128(1), 1443–1477.

Shepherd, K.D. and Markus G.W. 2002, Development of reflectance spectral libraries for characterization of soil properties. *Soil Science Society of America Journal*, 66, 988–998.

Shepherd, K.D. and Walsh, M.G., 2002, Development of reflectance spectral libraries for characterization of soil properties, *Soil Science Society of America Journal*, 66, 988–998.

Skempton, A.W., 1953, The colloidal activity of clay. In Proceedings of the 3rd International Conference on Soil Mechanics and Foundation Engineering, London, vol. I, pp. 57–61.

Snethen, D.R., Johnson, L.D., and Patrick, D.M., 1977, An evaluation of expedient methodology for identification of potentially expansive soils. Soil and Pavements Laboratory, US Army Engineering Waterway Experiment Station, Vicksburg, MS, Rep. No. FHWA-RE-77-94, NTIS PB-289-164.

Sudduth, K.A. and Hummel, J.W., 1996, Geographic operating range evaluation of a NIR soil sensor, *Transactions of American Society of Agricultural Engineers* 39, 1599–1604.

Svanberg, S., 2001, *Atomic and Molecular Spectroscopy*: *Basic Aspects and Practical Applications*, 3rd edn (Berlin: Springer).

Thomas, M.F., 1994, *Geomorphology In The Tropics*: *A Study Of Weathering Denudation In Low Latitudes* (New York: John Wiley & Sons).

Thomas, P.J., Baker, J.C., and Zelazny, L.W., 2000, An expansive soil index for predicting shrink-swell potential, *Soil Science Society of America Journal*, 64, 268–274.

Van der Meer, F.D., 1995, Spectral reflectance of carbonates mineral mixtures and bidirectional reflectance theory: quantitative analysis techniques for application in remote sensing, *Remote Sensing Reviews*, 13, 67–94.

Van der Meer, F.D., 1999, Can we map swelling clays with remote sensing? *International Journal of Applied Earth Observation and Geoinformation*, 1(1), 27–35.

Webster, R., 1977, Spectral analysis of gilgai soil. *Australian Journal of Soil Research*, 15, 191–204.

Yule, D.F. and Ritchie, J.T., 1980, Soil shrinkage relationships of Texas vertisols: small cores, *Soil Science Society of America Journal*, 44, 1285–1291.

Zhang, R., Warrick A.W., and Myers D.E., 1992, Improvement of the prediction of soil particle size fractions using spectral properties, *Geoderma*, 52, 223–234.

Chapter 16

Finite element analysis of piers in expansive soils

Yahia E.-A. Mohamedzein[1]

Summary

The objective of this chapter was to present a model for finite element analysis of piers in expansive soils. First, a brief review of the methods for analysis and design of piers in expansive soils was given. Then, detailed formulation of the finite element model was presented. Finally, parametric studies were performed to give an insight into the behavior of piers.

Introduction

Foundations for support of structures on expansive soils can be shallow or deep. The choice of a system depends on many factors such as the thickness and degree of expansiveness of the soil, structural loads, and type of structure, environmental conditions, climate, budget, risk level, and experience of local contactors. The ideal situations for use of shallow foundations are soils with low to moderate swelling potential with the resulting amount of differential heave less than 1.25 cm (0.5 in.) for individual footing and less than 10 cm (4 in.) for heavy mat foundation, depth of the active zone is very shallow (less than 2 m), and lightly loaded buildings and residence (Army Manual TM5, 1983; Dhowian *et al.*, 1988; Nelson and Miller, 1992; Kariuki and van der Meer, 2003; Kariuki *et al.*, 2004).

Ideal situations for deep foundations (mainly piers or drilled piles) are soils with moderate to high swelling potential, soils for which the swelling zone is too thick, in cold climatic regions where buildings are constructed with basement, soils where depth to the bedrock or dense soil is few meters below the ground, heavy loaded structures, and availability of experienced contractors for installation of piers (Army Manual TM5, 1983; BRE and CBRI, 1986; Dhowian *et al.*, 1988; Nelson and Miller, 1992).

Deep foundations are usually classified into two types depending on the method of construction: driven and drilled piles. Drilled piles are formed in situ by specialized drilling machines. Piers are drilled piles with a relatively large diameter compared to driven piles. Piers are usually more suitable for expansive soils than other types of piles because of the difficulties in driving piles in the usually very stiff or hard desiccated expansive soils, and since pile caps that will be used for a group of piles will increase the uplift forces on the piles. Thus engineers tend to use one pier with a large diameter to support one column.

[1] Department of Civil and Architectural Engineering, College of Engineering, Sultan Qaboos University, PO Box 33 Al-Khod 123, Sultanate of Oman, Tel: 968 24415 331 (ext. 2577), Fax: 968 24413 416, Email: yahiaz@squ.edu.om

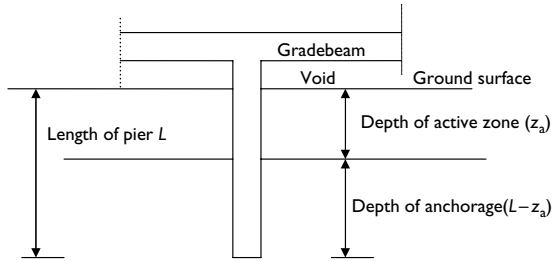

Figure 16.1 Pier–Grade beam configuration.

The design philosophy behind using piers to support structures in expansive soils is to isolate the structure from expansive soil movement (Dhowian *et al.*, 1988; Nelson and Miller, 1992). The pier is installed through the active zone to bear on the stable soil or rock below. The pier can be a straight shaft or a belled pier (i.e. a pier with an enlarged base). Belled piers have an enlarged base at least three times the shaft diameter to allow for inspection of the bottom of the pier. Grade beams spanning between piers are designed to support structural loads and to transfer them to the piers. Grade beams are isolated from the underlying soil with a void space (Figure 16.1).

The objective of this chapter was to present a model for finite element analysis of piers in expansive soils. First, a brief review of the methods for analysis and design of piers in expansive soils was given. Then, detailed formulation of the finite element model was presented. Finally, parametric studies were performed to give an insight into the behavior of piers.

Analysis and design of piers in expansive soils

Piers in expansive soils should be designed to resist the applied load from the structure and the uplift forces caused by swelling of the expansive soil in the active zone. The resulting deformations from the loads should be within the tolerable limits. The design process involves the determination of pier length and diameter, pier axial compression capacity, pier uplift capacity, pier settlement and/or heave, and stresses and strains within the pier.

A variety of approaches can be used for the analysis and design of piers in expansive soils with different levels of success including empirical and analytical methods, full-scale field or laboratory model tests, and numerical methods specially the finite element method.

Empirical methods are based on experience with construction of piers in a particular site or a region and therefore should be used only as guidelines for preliminary design. The empirical methods give only the pier length and diameter. Johnson (1979) recommended an equation for minimum length of a pier in expansive soil. Holland and Richard (1984) recommended that in areas of deep water table, piles should be founded, at least, at twice the active zone or on stable soil or bedrock. David and Komornik (1980) suggested that the depth of the embedment of the pier should be 1.5 times the depth where the swelling pressure is equal to the overburden pressure. The analytical methods give the compression and uplift capacities as well as the pier length and diameter. Some analytical methods that

are based on elastic theory can be used to obtain the pier settlement and the stresses in the pier. Two different approaches are usually used for analysis and design of piers in expansive soils: limit equilibrium and elastic methods (Nelson and Miller, 1992). The limit equilibrium methods are semi-empirical methods and were advanced by Chen (1988) and O'Neil (1988). As their name implies, the limit equilibrium methods consider the state of equilibrium just before failure. They assume that the system moves as a rigid body without deformations. In contrast the elastic methods consider the deformation of the pier and the surrounding soil and were proposed by Poulos and Davis (1980).

Full-scale field and model laboratory tests were performed to gain insight into the behavior of piers in expansive soils. These tests can give all the parameters required for design and construction of piers. A number of field and laboratory experiments have been reported in the literature (e.g. O'Neil and Poormoayed, 1980; Blight 1984; BRE and CBRI, 1986; Simons, 1991; Abdel-Halim and Al-Qasem, 1995; Osman and Elsharief, 1999; Chapel and Nelson, 2000; Crilly and Driscoll, 2000).

Finite element analysis of piers in expansive soils

The finite element method is a powerful analytical technique that can be used effectively to analyze the soil-pier system in expansive soils. Ellison *et al.* (1971) used the finite element method to study the load deformation mechanism of piers in London clay. The axisymmetric stress condition was assumed. The pile was assumed linear elastic and a trilinear elastic stress–strain relationship was assumed for the soil.

Amir and Sokolov (1976) used the finite element method to study the behavior of piers in expansive soils. The conditions of axisymmetric stress for a single pier was assumed and the soil was modeled as linear elastic. Environmental effects were represented by a sinusoidal moisture flux function. They concluded that volume changes of the soil caused all piers to move, but displacements were smaller for deeper piers and piers with heads laterally fixed. Bells and isolation sleeves showed only a minor effect. In contrast to shallow foundations where an impervious peripheral membrane is beneficial, such precaution measure may increase the displacement of the pier.

Justo *et al.* (1984) presented a three-dimensional finite element method to find the stresses and strains in piles in expansive soils. In their method the stress path followed by the soil elements during the loading and wetting processes were taken into account. The soil is assumed isotropic, nonlinear, and non-homogeneous. The nonlinearity and non-homogeneity were modeled through the dependence of the initial swelling constraint modulus upon vertical stress. They concluded that stress path has a large influence in the calculated heave and tension in the pier. They found that the parameters with more influence in the pier behavior were the amount of free ground heave, net applied pressure for belled piers, an increase in Poisson's ratio above 0.3, the constrained modulus as obtained from oedometer test, and the placement of a soft soil between the pier shaft and the soil.

Lytton (1977) suggested a finite element model for calculating the stresses and displacements in a pile founded in expansive soil. This method assumed the soil to behave elastically.

Finite element formulation of a pier in expansive soil

The finite element formulation is described in detail elsewhere (Bathe, 1996). Only the formulation relevant to piles in expansive soils is presented in this section. The swelling-induced

forces can be obtained following the formulation presented by Lytton (1977). The equilibrium equations for a soil element undergoing volume change are:

$$[F] = \int\int\int Vol\,[B]^T[C][\varepsilon]dv \tag{16.1}$$

where

$[F]$ = nodal forces induced by expansion of the soil;
$[B]$ = strain–displacement matrix;
$[C]$ = stress–strain matrix;
$[\varepsilon]$ = swelling-induced strains.

Also

$$[\sigma] = [C][\varepsilon] \tag{16.2}$$

where

$[\sigma]$ = stress vector.

Lytton (1977) suggested the swelling-induced strains to be related to the change in moisture content. However, heave can be better evaluated in terms of soil suction because soil suction is a fundamental factor in controlling mechanical properties of partially saturated soils. Unlike the change in moisture content which is an environmental factor, the soil suction is related to both the intrinsic and extrinsic properties of an expansive soil. Several methods have been proposed for prediction of swell potential and magnitude of heave based on soil suction measurements (Mckeen, 1980; Mitchell and Avalle, 1984; Snethen and Huang, 1992). In these methods, swell is related to change in soil suction through a volume change parameter which is an intrinsic property of the soil. Mckeen's method is one of the methods in which the total heave is related to soil suction change by a parameter called suction compression index. In one-dimensional form, Mckeen's equation can be written as:

$$\frac{\Delta H}{H} = \alpha_s \log \frac{\Psi_f}{\Psi_0} \tag{16.3}$$

where

$\Delta H/H$ = swelling-Induced strains = ε;
α_s = suction compression index;
Ψ_0, Ψ_f = initial and final suctions, respectively.

The swelling-induced strain vector [ε] in three dimensions can be obtained from the following equation:

$$[\varepsilon] = \begin{bmatrix} \alpha_{s1} \\ \alpha_{s2} \\ \alpha_{s3} \end{bmatrix} \log \frac{\Psi_f}{\Psi_0} \tag{16.4}$$

where α_{s1}, α_{s2}, and α_{s3} are the suction compression indices in the *x, y*, and *z* directions for the three dimensions stress condition, respectively.

Equations 16.3 and 16.4 show that the heave strain can be related to soil suction. The suction compression indices (α_s) can also be related to the change in moisture content since the change in moisture content has a well-defined relation to the change in soil suction. Mohamedzein *et al.* (1999) implemented Equation 16.4 in a computer program developed to compute the soil heave. The suction compression indices in the three dimensions are assumed to be equal to the suction compression index obtained from one-dimensional consolidation (i.e. $\alpha_{s1} = \alpha_{s2} = \alpha_{s3} = \alpha_s$) where ($\alpha_s$) can be obtained from the results of one-dimensional swelling tests by measuring the amount of swelling, and change in suction as:

$$\alpha_s \frac{\%\text{swell}}{\log(\Psi_f/\Psi_0)} \tag{16.5}$$

where the percentage swell can be measured in a one-dimensional consolidation swelling test for given initial suction (Ψ_0) and final suction (Ψ_f). The change in soil suction can be measured by different methods as outlined by Nelson and Miller (1992).

The assumption of equal (α_s) in all directions (i.e. isotropic soil) is a simplifying assumption and is consistent with the isotropic stress–strain relationship used in this study. The values of (α_s) from a one-dimensional consolidation test are greater than the actual values of (α_s) for three-dimensional conditions; thus, the given assumption will give conservative results (i.e. overestimates swelling under three-dimensional conditions). Further (α_s) is considered to be constant over a given change in suction from Ψ_0 and Ψ_f. This is believed to be a reasonable assumption as long as ($\Psi_0 - \Psi_f$) is kept as small as possible.

Displacement based finite element formulation for soil–structure interaction

The displacement-based finite element formulation for soil–structure interaction was implemented in a computer subprogram by Mohamedzein *et al.* (1999). The subprograms were linked to a soil–structure program developed by Mohamedzein (1989). Major changes to the program code were the addition of new subroutines for calculation of the displacements in the soil and pile due to an increase or change in soil suction following the procedure outlined in the previous section. A subroutine for generation of an automated mesh was developed. Figure 16.2 shows a typical finite element mesh for a single pier. The dimensions of the mesh are given in terms of pier length, pier diameter, and the thickness of expansive layer from the ground surface. The lateral extent of the mesh is solely controlled by the pier diameter. The mesh extends 5.5*D* (where *D* is the diameter). The vertical extent of the mesh is controlled by the pier length and the thickness of the expansive layer. The pier is divided into ten 8-noded isoparametric elements. The soil media is represented by ninety-five 8-noded isoparametric elements. The boundary conditions are shown in the figure. The rollers on the left vertical face of the mesh are intended to simulate the condition of symmetry. Slip between the soil and the pier is accounted for by using interface elements. The formulation of the interface element was derived on the basis of relative nodal displacement of the solid elements surrounding the interface element and slip mode of interface was considered with special selection to the values of normal and tangential stiffness (Desai *et al.*, 1984; Nour Eldayem, 1999). The soil was modeled as non-linear elastic by using the

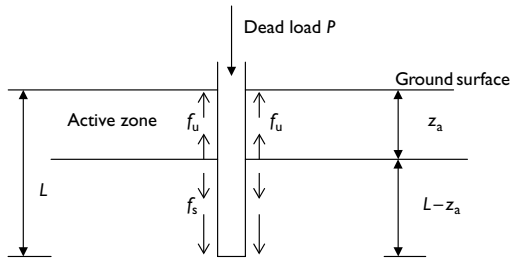

Figure 16.2 Loads acting on the pier.

Duncan–Chang model or modified Duncan–Chang model (Duncan *et al.*, 1978). The pier material is assumed linear elastic.

The program simulates the actual sequences of events that the piers are subjected to during and after construction. These sequences are non-loaded pier after installation, gradual application of load from structure, (under this load the pier will move downward), and swelling due to saturation of soil sometimes after end of construction. Due to swelling the pier will move upward.

Parametric study

Many examples were analyzed to illustrate the use of the finite element method and to gain some insight in the effect of important factors on the pier-soil response in an expansive soil. Elfao site in Sudan which has the properties shown in Table 16.1. The soil parameters required for the analysis are listed in Table 16.2 and Table 16.3. Table 16.2 lists the values of suction compression index (α_s) with depth. The values were obtained from Equation 16.5 using the results of one-dimensional swelling tests and the change in suction (Mohamedzein *et al.*, 1999). Table 16.3 contains the parameters for the Modified Duncan–Chang nonlinear elastic model. The parameters were obtained from the data base provided by Duncan *et al.* (1978).

The effect of pier length for constant pier diameter is studied using the program. Different pier lengths were used to find resultant heave when different axial loads are applied to the piers. Heave versus load for different pier lengths are shown in Figure 16.3. The figure indicates that the upward vertical movement of the pier increases when the applied axial load decreases and the pier length decreases. So by increasing the pier length we minimize the vertical movement of piers in expansive soil. The figure also shows that increasing pier length is more effective in decreasing heave than increasing the axial load. The effect of axial load in reducing heave is similar for each length of pier. A combination of length of 4 m and an axial load greater than 90 kN are required to reduce heave to a negligible amount in this site. Design charts similar to those of Figure 16.3 can be developed for a specific site using the program if the necessary soil parameters and pier diameter are known.

Figure 16.4 shows the results of the pier heave obtained by the computer program for a pier of length 6 m subjected to an axial load of 60 kN. As the pier diameter increases the downward movement under the applied load decreases. This indicates that for small

Table 16.1 Properties of black cotton soils from Sudan (Osman and Elsharief, 1999)

Property	*Value*	
	Site 1 (Wad Medani)	*Site 2 (ElFao)*
Soil description	Brown to dark brown highly plastic clay with calcareous concretion (CH)	Dark grey to dark brown highly plastic clay with calcareous concretions (CH)
Liquid limit	63–70	64–71
Plasticity index	29–35	33–37
Unit weight (kN/m^3)	16.7–19.4	19.5–20.2
Percentage of particles $<2\,\mu$m (%)	47–65	46–58
Swelling pressure (kN/m^2)	156–337	382–701

Table 16.2 The percentage swell and the suction indices for ElFao Soil (Mohamedzein *et al.*, 1999)

Depth (m)	*Swelling (%)*	*Suction index (α_s)*
1	10.3	0.0453
2	6.1	0.022
3	5.05	0.058

Table 16.3 Parameters for Duncan–Chang Model (Mohamedzein *et al.*, 1999)

Parameter	*Value*
Cohesion intercept, c (kN/m^2)	67.57
Frictional angle parameter ϕ, $\Lambda\phi$ ($\Lambda\phi$ in parentheses)	1.0(0.0)
Modulus number, K	65.0
Modulus exponent, n	0.14
Failure ratio R_f	0.77
Bulk modulus number k_b	25.0
Bulk modulus exponent, m	1.05
Dry unit weight, γ (kN/m^3)	15.11
Earth pressure coefficient k_0 1.05	0.75

diameter piers the downward movement is more significant than the upward (heave) movement. For large diameter piers (i.e. $d > 0.4$ m), the heave is dominant. The net vertical movement depends on whether slip is allowed at interface or not. The slip reduces the net vertical movement for piers with a large diameter. For example, for a diameter of 0.6 m the net vertical movement is approaching zero if slip is allowed, whereas it is about 6.5 for a no-slip case.

The distribution of axial stresses in a pier of length of 6 m due to heave and axial load for different pier diameters are shown in Figure 16.5 for the case of slip at the interface. The figure shows that all the stresses exerted on the pier are tensile stresses. These tensile stresses are decreasing as the pier diameter increases and the maximum axial tensile stress

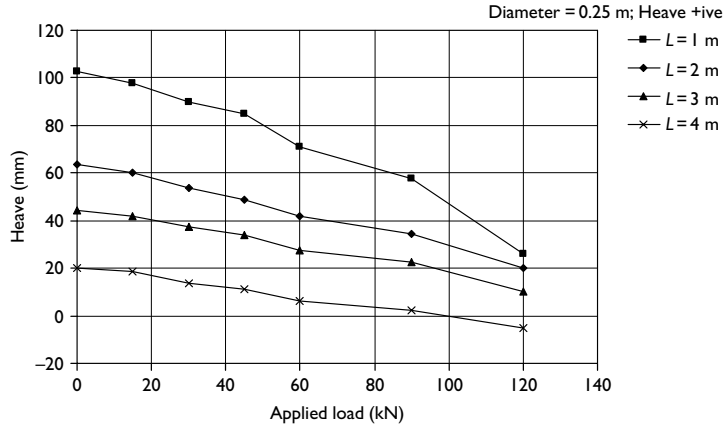

Figure 16.3 Effect of the pier length on movement (Reproduced from Mohamedzein *et al.*, 1999).

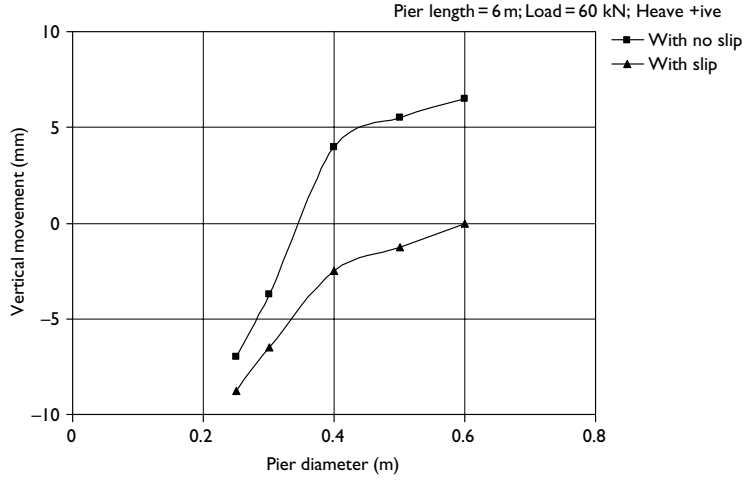

Figure 16.4 Effect of the pier diameter on movement.

is occurring at the middle third of the pier. This indicates that the maximum axial tensile stress is acting at the lower half of the active zone of the soil (the depth of the active zone of this soil is considered as 4 m).

The vertical displacements obtained by the computer program after saturation of soil are presented in Figure 16.6 for a pier length of 6 m. The figure shows the upward movements

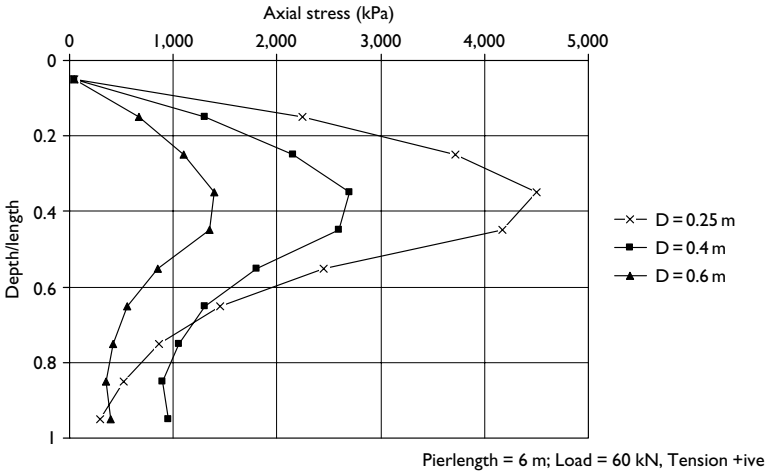

Figure 16.5 Effect of the pier diameter on stress.

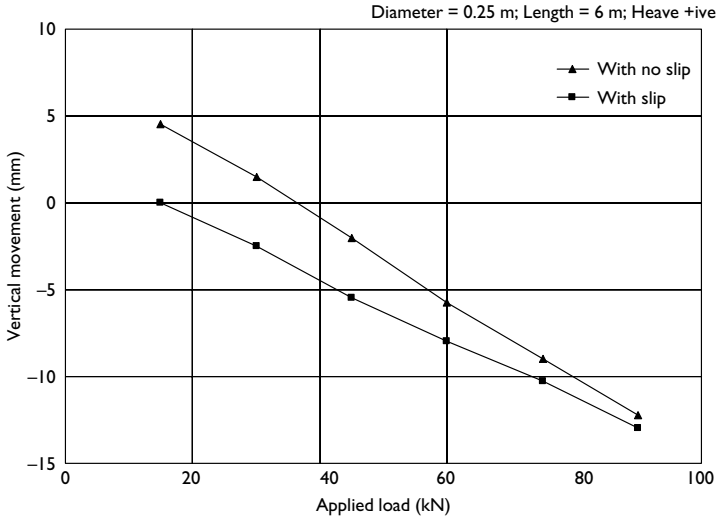

Figure 16.6 Effect of slip at the interface on pier movement.

for the two cases with slip and without slip at the interface. It is clear that the slip is reducing the upward movement of the pier due to swelling. The same trend is shown for different pier diameters in Figure 16.4. Thus the slip at the interface is important and can affect the results specially for light applied loads and large diameter piers. This is of practical

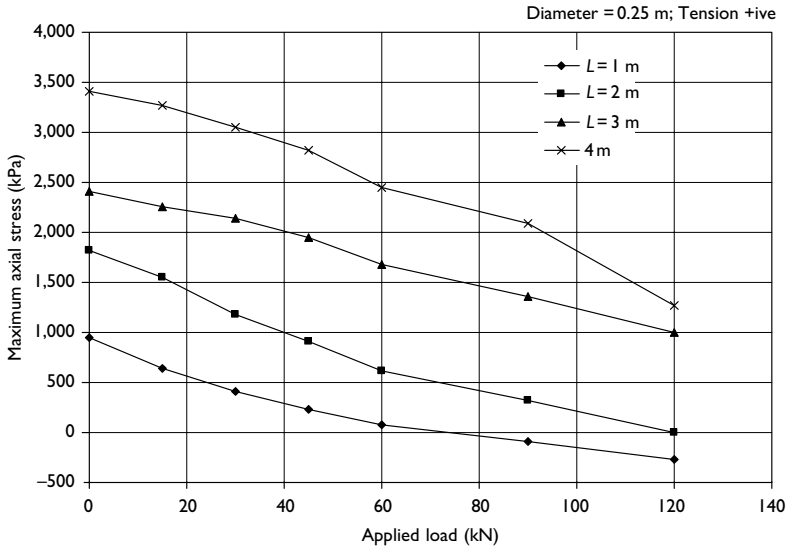

Figure 16.7 Effect of the pier length and the applied load on the maximum stress.

importance since it simulates the current practice of supporting light weight structures on relatively large diameter piers.

One of the benefits of this computer program is that the stresses at any point within the pier-soil system can be determined. The values of these stresses are very useful because they can be used for the determination of the area of steel required to resist tensile stresses in the pier. The maximum tensile stresses due to heave versus load for different pier lengths are plotted in Figure 16.7. As expected the maximum tensile axial stress increases with the pier length since all pier lengths considered are within the zone of soil heave (active zone). The relation between load and maximum tensile stress is approximately linear. The maximum axial tensile stresses decrease when the applied axial load increases.

The maximum axial tensile stresses due to swelling must not exceed the maximum tensile stress of concrete that is usually taken as 1/8 of the cubic strength of concrete (e.g. for f_{cu} = 40,000 kPa, the maximum tensile strength of concrete = 5,000 kPa). The maximum axial tensile stresses predicted by the program was 3,400 kPa for a pier length = 4 m which is less than the maximum tensile strength of concrete. However, as the pier length increases the maximum tensile stress will increase and may exceed the elastic limit, that is, it will exceed the maximum tensile strength of concrete. Thus the assumption of linear elastic behavior for the pier material may not be justified and non-linear stress-strain relationship should be used for the pier material.

The distribution of axial stress in the pier due to heave under different applied axial loads is plotted for a pier length = 3 m and a diameter = 0.25 m in Figure 16.8. From this figure the maximum tensile stress in a pier caused by an expansive soil usually occurs near the

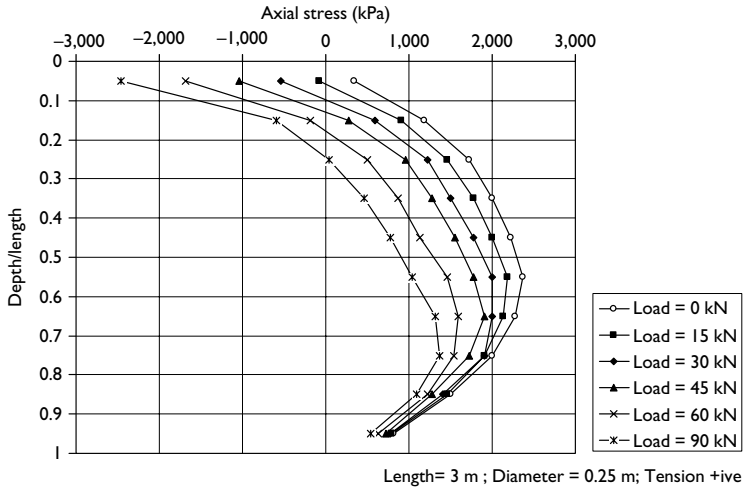

Figure 16.8 Distribution of the stress within the pier.

middle third of the pier. The figure also indicates the presence of tensile stresses throughout the lower third of the pier length. Thus steel reinforcement to resist tensile stresses in the pier must extend to the total depth of the active zone.

Conclusions

The finite element program described in this chapter can be used to find the distribution of tensile stresses in a pier needed for design against tensile failure and the optimum pier length and diameter needed to resist upward movements due to soil heave. The analysis can be used to gain more insight in the behavior of piers in expansive soils. A parametric study such as the one reported in this chapter can be utilized to establish design charts for a given type of expansive soil by taking into consideration all the environmental factors and system variables.

Allowing slip at the soil-pier interface improved the predicting capabilities of the finite element program. The following was observed when slip was allowed: pier settlement due to applied loads decreased, pier heave due to change of soil moisture content decreased, the maximum axial tensile stresses in case of slip were greater than the maximum axial tensile stresses without slip, and the slip at the interface was important for light-weight structures supported on relatively large diameter piers.

An increase in pier length decreased the upward vertical movement of the pier due to soil heave. The upward vertical movement also decreased with an increase in axial compressive load. The decrease in heave due to increase in pier length was more significant than that due to increase in axial compressive load. For long piers increasing the pier diameter decreased both the pier settlement and heave. The maximum axial tensile stress increased when the

pier length increased for piers installed completely in the active zone. The maximum axial tensile stress decreased with increasing pier diameter. For piers entirely within the active zone the tensile stress in the piers was smaller than those for piers extending below the active zone. The tensile stress decreased as the axial load increased and eventually the pier may be subjected only to compressive stresses. The maximum tensile stress in the axially loaded pier usually occurred within the depth of the active zone. For piers completely within the active zone the maximum tensile occurred near the middle third of the pier. For long loaded piers tensile stresses occurred throughout the lower length of the pier below the active zone. The maximum tensile stresses may exceed the tensile strength of concrete and thus this factor must be taken into account.

References

Abdel-Halim, M.H.and Al-Qasem, M.M. (1995). Model studies on bored piles in stiff expansive clay. *International Journal of Structures*, Vol. 15, No. 1, pp. 35–59.

Amir, J.M. and Sokolov, M. (1976). Finite element analysis of piles in expansive soils. *Journal of Soil Mechanics and Foundation Engineering, ASCE*, Vol. 102, No. 7, pp. 701–719.

Army Manual TM5 (1983). Foundations in expansive soils. Technical Manual No. 5-818-7, Headquarters, Department of the Army, Washington, DC, USA.

Bathe K.J. (1996). *Finite Element Procedures in Engineering Analysis*. Englewood Cliffs, NJ.

Blight, G.E. (1984). Uplift forces measured in piles in expansive clay. Proceedings of the Fifth International Conference on Expansive Soils, Adelaide, Australia, pp. 240–244.

BRE and CBRI (1986). Behavior of under-reamed piles in expansive soils. A Collaborative Project between Building Research Establishment (BRE), UK and Central Building Research Institute (CBRI), India.

Chapel, T.A. and Nelson, J.D. (2000). Strain measurements of concrete piers in expansive soils. *Geotechnical Special Publication*, No. 106, pp. 151–163.

Chen, F.H. (1988). *Foundations on Expansive Soils*. American Elsevier Sciences Publisher, New York.

Crilly, M.S. and Driscoll, R.M.C. (2000). Behavior of lightly loaded piles in swelling ground and implications for their design. Proceedings of the Institute of Civil Engineering, *Geotechnical Engineering*, Vol. 143, No. 1, pp. 3–16.

David, D. and Komornik, A. (1980). Stable embedment depth of piles in swelling clays. Proceedings of the fourth International Conference on Expansive Soils, Denver, CO, USA, pp. 798–805.

Desai, C.S., Zaman, M.M., Lightner, J.G., and Siriwardane, H.J. (1984). Thin- layer element for interfaces and joints. *Proceedings of the International Journal for Numerical and Analytical Methods in Geomechanics*, Vol. 8, pp. 19–43.

Dhowian, A.W., Erol, A.O. and Youssef, A. (1988). *Evaluation of Expansive Soils and Foundation Methodology in the Kingdom of Saudi Arabia*. King Abdulaziz City for Science and Technology, Saudi Arabia.

Duncan, J.M., Byrne, P., Wong, K.S.. and Mabry, P. (1978). Strength, stress strain and bulk modulus parameters for finite element analysis of stress and movements in soil masses. Report No. UCB(GT(78–02)), University of California, Berkeley, CA USA.

Ellison, R.D., D' Appolnia, E. and Thiers, G.R. (1971). Load deformation mechanism for bored piles. *Journal of Soil Mechanics and Foundation Engineering, ASCE*, Vol. 97, pp. 661–672.

Holland, J.E. and Richards, J. (1984). The practical design of foundation for light structures on expansive clays. Proceedings of the Fifth International Conference on Expansive Soils, Adelaide, Australia, pp. 154–158.

Johnson, L.D. (1979). Overview for design of foundations on expansive soils. US Army of Engineers, Waterways Experiment Station, Vicksburg, MS, USA, Miscellaneous Paper GL-79-21.

Justo, J.L., Rodrifuez, J.E., Delgado, A., and Jaramillo, A. (1984). A finite element method to design and calculate pier foundations in expansive soils. Proceedings of the Fifth International Conference on Expansive Soils, Adelaide, Australia, pp. 119–123.

Kariuki, P.C. and Van der Meer, F.D. (2003). Determination of cation exchange capacity from spectroscopy. *International Journal of Remote Sensing*, Vol. 24, No. 1, pp. 161–167.

Kariuki P.C., Woldai, T., and Van der Meer, F. (2004). Effectiveness of spectroscopy in identification of swelling indicator clay minerals. *International Journal of Remote Sensing*, Vol. 25, No. 2, pp. 455–469.

Lytton, R.L. (1977). Foundations in expansive soils. In *Numerical Methods in Geotechnical Engineering*. Desai, C.S. and Christian, J.T. (Eds), McGraw Hill Book Company, New York, pp. 427–457.

Mckeen, R.G. (1980). Field study of airport pavements on expansive clay. Proceedings of the Fourth International Conference on Expansive Soils, Denver, CO, pp. 242–261.

Mitchell, P.W. and Avalle, D.L. (1984). A technique to predict expansive soil movement. Proceedings of the Fifth International Conference on Expansive Soils, Adelaide, Australia, pp. 124–130.

Mohamedzein, Y.E.-A. (1989). Non-linear finite element analysis of soil culvert interaction. Ph.D. thesis, School of Civil Engineering, Purdue University, West Lafayette, IN, USA.

Mohamedzein, Y.E.-A., Mohamed, M.G. and Elsharief, A.M. (1999). Finite element analysis of short piles in expansive soils. *Journal of Computer and Geotechnics*, Vol. 24, No. 3, pp. 231–243.

Nelson, J.D. and Miller, D.J. (1992). *Expansive Soils: Problems and Practice in Foundation and Pavement Engineering*. John Wiley and Sons Inc, New York.

Nour Eldayem, F.E. (1999). The effect of interface on soil-pile interaction in expansive soil. A Thesis Submitted in Partial Fulfillment of the Degree of Master of Science in Structural Engineering, Department of Civil Engineering, University of Khartoum, Khartoum, Sudan.

O'Neil, M.W. (1988). Special topics in foundations. Proceedings of the Geotechnical Engineering National Convention, ASCE, Nashville, TN, USA, pp. 1–22.

O'Neil, M.W. and Poormoayed, N. (1980). Methodology for foundations on expansive soils. *Journal of Geotechnical Engineering Division, ASCE*, Vol. 106, No. GT12, pp. 1345–1367.

Osman, M.A. and EIsharief, A.M. (1999). Field experiments on piles in the expansive soils of Central Sudan. *Building and Road Research Journal*, Building and Road Research Institute, University of Khartoum, Khartoum, Sudan, Vol. 2, pp. 17–26.

Poulos, H.G. and Davis, E.H. (1980). *Pile Foundation Analysis and Design*. John Wiley, New York.

Simons, K.B. (1991). Limitations of residential structures on expansive soils. *Journal of Performance of Constructed Facilities, ASCE*, Vol. 5, No. 4, pp. 258–270.

Snethen D.R. and Huang, G. (1992). Evaluation of suction-heave prediction methods. Proceedings of the Seventh International Conference on Expansive Soils, Dallas, TX, pp. 12–17.

Chapter 17

Prediction of swelling pressure of expansive soils using Neural Networks

Yahia E.-A. Mohamedzein,[1] *Rabab Ibrahim,*[2] *and Assim Alsanosi*[3]

Summary

Artificial Neural Networks (ANNs) overcome the limitations of empirical correlations and can be used as an alternative approach. ANN is an efficient tool in identifying complex, non-linear, and causal relations. In this chapter, the ANN model was developed to predict the swelling pressure of the soil. The model produced acceptable results when compared to actual measurements. Charts were developed to estimate the swelling pressure based on typical index parameters such as Atterberg limits, natural water content, and percent of fines.

Introduction

Foundations constructed on expansive soil are subjected to large uplifting forces (i.e. swelling pressures) caused by the swelling. These forces will induce heaving, cracking, and break-up of buildings. Knowledge of these swelling pressures is very important in the design of shallow and deep foundations in expansive soils.

The swelling pressure can be estimated using laboratory tests and empirical correlations. Laboratory tests use the consolidation cell. There are two variations of the tests: consolidation-swelling and constant volume (Nelson and Miller, 1992; ASTM D4546, 1996). In the consolidation-swelling test, an initial prescribed load is applied to an unsaturated sample. The sample is then allowed to swell under that load when water is added. The initial load may represent overburden stress, overburden stress plus structural load, or some other arbitrary surcharge. After swelling, the sample is further loaded and unloaded as in the conventional consolidation test.

The constant volume or swell pressure test involves inundating the sample in the oedometer while preventing the sample from swelling. The swell pressure is reported as the maximum applied stress required to maintain a constant volume. Once the swelling pressure stops increasing after soaking, the sample may be rebounded by complete load removal or incremental load removal. Alternatively, it may be loaded beyond the swell pressure and unloaded following the conventional consolidation test procedure.

Empirical correlations have been proposed in the literature using the results of laboratory swelling tests and actual field measurements. The swelling pressure was related to the

[1] Department of Civil and Architectural Engineering, Sultan Qaboos University, PO Box 33, Al-Khod 123, Sultanate of Oman; Tel: 968 24415 331 (ext. 2577), Fax: 968 24413 416; email: yahiaz@squ.edu.om
[2] Al-Amin Engineering Company, Khartoum, Sudan.
[3] Department of Civil Engineering, University of Khartoum, Khartoum, Sudan.

Table 17.1. Prediction equations for swelling pressure

Equation	*Author*
$\log_{10}SP = 20132 + 0.208\ LL + 0.000665\gamma_d\ 0.0269wc$	Komornik and David (1969)
$\log_{10}SP = (0.4LL - wc - 0.4)/12$	Vijayvergiya and Ghazzaly (1973)
$\log_{10}SP = (\gamma_d + 0.65\ LL - 139.5)/19.5$	
$\log_{10}SP = 5.3 - 147e/PI$; $\log_{10}\ SP = 5.3 - 2.77e$	Brackley (1975a,b)
$\log_{10}SP = 2.5011\gamma_d + 1.055615 + 0.01LL - 1.8218$	Elsharief (1987)

Notes
SP = Swelling pressure; LL = Liquid limit; PI = Plasticity index; WC = Water content; e = void ratio; γ_d = Dry unit weight; and *s* = Degree of saturation.

important soil properties that influence the swelling such as Atterberg limits, dry unit weight, water content, degree of saturation, and void ratio. Typical correlations are shown in Table 17.1.

Performing the swelling pressure laboratory test on every soil sample is time consuming and therefore not practical. Also some soil samples may be disturbed. On the other hand, empirical correlations suffer from two limitations: the correlations are based on a limited database, and the number of variables considered is usually limited to two (Table 17.1). (ANNs) overcome the limitations of empirical correlations and can be used as an alternative approach. ANN is an efficient tool in identifying complex, non-linear, and causal relations. In this chapter, the ANN model was developed to predict the swelling pressure of the soil. To our best knowledge, this is the first attempt in the geotechnical literature to predict the swelling pressure using ANN.

Applications of ANNs in geotechnical engineering

ANNs are forms of artificial intelligence motivated by the studies of the brain and nervous system (Flood and Kartam, 1994; Ural and Saka, 1998). ANNs are connectionist systems that have an ability to learn and generalize from examples. They can provide meaningful solutions to problems even when input data contain errors or are incomplete. ANNs are composed of a collection of layers each consisting of neurons or nodes. Each neuron in a layer is connected to the neurons in adjacent layers. The ANN performs a series of analyses after receiving input signals through the input layer. The last layer in the series produces the outputs.

ANNs are used to solve many problems in civil engineering including geotechnical ones (Toll, 1996; Kartam *et al.*, 1997). Problems in geotechnical engineering are suitable for use of ANNs because of an inadequate understanding of the phenomena involved and the factors affecting them, as well as a limited quantity and inexact quality of information available (Chameau *et al.*, 1983). In these situations, engineers generally rely on empirical design solutions. The information is usually gathered, synthesized, and presented in the form of design charts or tables, or numerically, using empirical formulae. Several examples of applications of ANNs to geotechnical problems will be given in this chapter and will be used as guidelines for development of an ANN model for prediction of swelling pressure.

Basma and Kallas (2003) modeled the collapse potential of soils using a back-propagation ANN model. A special testing program was conducted to measure the collapse for eight types

of collapsible soils. A database consisting of 138 data sets was generated and used in training and testing of the model. The architecture of the model consisted of three layers. The input parameters were coefficient of uniformity, initial water content, compaction unit weight, applied pressure at wetting, percent sand, and percent clay. The model was further validated using information available in the literature. The results proved that the neural network was very efficient in assessing the complex behavior of collapsible soils with minimal processing of data.

Penumadu and Zhao (1999) used the ANN to predict the stress–strain and volume change behavior of sand and gravel under drained triaxial compression test conditions. They employed feed-back ANNs. A large experimental database obtained from published literature was used in training, testing, and prediction phases of three neural network-based soil models. The data-base consisted of a total of 126 and 125 triaxial compression tests for sand and gravel respectively. The input parameters consisted of mineralogy, particle shape, coefficient of uniformity, coefficient of curvature, effective particle size, void ratio, and effective confining pressure. The observed behavior in terms of a non-linear stress–strain relation, compressive volume change at low stress levels, and volume expansion at high stress levels were captured well by the ANN models.

Shahin *et al.* (2002) used a back-propagation ANN model to predict settlement of shallow foundations bearing on cohesionless soils. A database consisting of 189 case records of actual measured settlements was used to develop and verify the ANN model. The network was composed of three layers. The input parameters consisted of footing width, net applied pressure, SPT N-value, footing geometrical ratio of length over width, and footing embedment ratio of depth over width. The results indicated that ANNs were useful techniques for prediction of settlement of shallow foundations on cohesionless soils. They outperformed the traditional methods.

Ural and Saka (1998) developed an ANN model for prediction of liquefaction potential. The parameters used in neural network application were relative density, shear modulus, friction angle, shear wave velocity, porosity, total vertical stress, effective vertical stress, earthquake magnitude, peak ground surface acceleration, and cyclic stress ratio. The data sets consisted of 117 patterns for training the network, 39 patterns for testing and 52 for a validation prediction study. The results from the ANN were compared to the classical method for prediction of liquefaction. Out of the 52 cases considered, the ANN predicted 42 cases correctly (i.e. an 81% agreement with the classical method). They concluded that the prediction of the ANN will be improved further as a large number of input variables become available.

Nawari *et al.* (1999) developed ANN models for analysis and design of piles. The models were based on back-propagation and generalized regression techniques. The data consisted of 90 sets of which 60% were used for training and 40% for testing. The input data consisted of SPT-values and geometrical properties such as pile length, cross sectional area, circumference, and the amount of steel reinforcement. The predicted axial and lateral load capacities by the ANN models were comparable with the predictions of the classical methods.

The application of back-propagation neural network to evaluate the skin friction (f_s) of driven piles was presented by Goh (1995). The data were drawn from load test records presented in the literature for driven piles in clays. The embedded pile length (L) ranged from 4.7 to 96 m, the undrained shear strength (S_u) ranged from 9 to 335 kPa, and the friction coefficient (α) was in the range 0.42–1.73. Most of the f_s values were derived from pile compression load tests after allowance for end-bearing, with unit end-bearing assumed

to be 9 S_u at the pile tip. The undrained shear strength was determined mainly from unconfined compression tests. A total of 45 data sets were used for training the neural network and 20 data sets (randomly selected) for testing the ability of the neural network to interpolate the correct responses for patterns that only broadly resemble the training data. Training was carried out until the average sum square error over all the training patterns was minimized. The number of input and hidden neurons was varied to determine the most reliable model. A single output neuron was used to represent f_s. Experimentation indicated that there was no significant improvement in the error as the number of hidden neurons increased beyond three. The model with the input parameters consisting of pile length, undrained shear strength, the friction coefficient, and the effective overburden stress gave the highest coefficient of correlation and the lowest error rate for the training and testing data. The results indicated that the neural network was successful in modelling the non-linear relationship between f_s and the other parameters.

Modelling of swelling pressure using ANN

In this study, the back- propagation algorithm was used because it was the most popular neural network paradigm that has been applied successively in a broad range of geotechnical engineering problems. The development of the ANN model involved the determination of the model inputs and outputs, division and preprocessing of the available data, design of network architecture, selection of connection weights and internal parameters, selection of stopping criteria, training, testing, and model validation.

Data collection

The data shown in Table 17.2 was collected from the geotechnical investigation studies carried by Building and Road Research Institute (BRRI), University of Khartoum, Sudan. The data was collected from 25 sites in different regions of Sudan such as Khartoum, Algezira, White Nile, and Blue Nile States. The total number of complete data sets was 154. The soil conditions in these regions were similar and consisted of thick alluvial deposits. A typical soil profile consisted of top layer of highly plastic clays which graded with depth into low plastic silty clay or clayey silt. Below this layer, sand deposits extended to the bedrock. The highly plastic clay layer, known as Black Cotton Soil, was active with moderate to very high swelling pressure because of the dominant presence of the montmorillonite clay mineral.

The climate in the study area ranged from poor Savannah to rich Savannah with annual precipitation of up to 1,500 mm (Osman and Charlie, 1984). However, in most areas the rate of transpiration exceeded the rate of precipitation, resulting in a net soil moisture deficit. This resulted in a relatively high depth of the active zone of about 3 to 4 m.

The following laboratory tests were performed on each sample: Atterberg limits, grain size distribution, shear strength, natural moisture content, and swelling pressure tests.

Model inputs and outputs

The first step in development of an ANN model is to identify the target parameters (output) and the factors that affect them (input). In this case the desired parameter is the swelling pressure. The following parameters affect the swelling pressure: natural water content, liquid limit, plastic limit, and percent of fines.

Table 17.2 Data collected

Source	*Depth (m)*	*Liquid limit (%)*	*Plastic limit (%)*	*Natural water content (%)*	*Percent of fines*	*Welling pressure (kN/m²)*
Chinese embassy building1	1	84	30	29.5	83.2	40
	4	85	31	29.1	90.6	105
	5	53	26	23.5	80.5	52.5
	1.5	47	19	18	67.3	52.5
	1	69	28	26.1	77.2	50
	3	54	26	12.4	65.6	50
	5	61	30	26	75.3	105
	6	46	24	20.7	67.8	17.5
Diesel station in Elfao	1	80	39	33.7	94.3	35
	5	71	35	21.3	87.7	100
	5	66	34	22.1	75.9	55
	0.5			30	93.4	50
	1	77	38	30	92	45
	3	67	35	24.1		150
	4	64	34	22.6	94.3	35
	6.5	77	37	23.1	93.6	220
	0.5	74	37	23.9	91	130
	5	65	33	18.6	60.1	50
	8	72	34	21.4	86.6	35
	1	79	35	23.9	85	35
	4	62	33	20.7	87.6	160
	6.5	75	38	26.5	97.8	50
	8	69	22	19.5		120
	1	80	35	26.6	96.2	80
	6.5	80	35	17.8	81.7	65
	0.5	77	35		93.3	100
	2	72	32	32.4	92.1	25
	6.5	76	37	12	91	65
	8	77	34	34.2	89.2	60
	1	84	37		94.4	85
	4	63	31	24.7	88.4	80
	1	77	36	31	97.9	20
	3	77	34	31.4	94.7	55
	4	63	32	21.4	87.1	40
	8	78	34	23.1	87.5	240
	0.5	81	38	27.4	94	210
	2	75	37	30.4	92	70
	8	64	29	21.2	84.9	185
	0.5	76	33		94.8	90
	2	78	36	30.7	94.8	35
	3	65	30	30.7	97	50
	1	80	37	33.8	95.4	30
	3	72	36	28	97.5	75
	6.5	76	33	21	69.5	70
	0.5	74	33	25.7	91.8	70
	2	75	39	29.6	96.2	40
	5	66	31	27.9	88.5	85
	6.5	74	37		90.8	60
	2	67	35	24.9	75.2	70
	4	67	37	30	87.6	40
	6.5			22	92.1	180

(*continued*)

Table 17.2 Continued

Source	*Depth (m)*	*Liquid limit (%)*	*Plastic limit (%)*	*Natural water content (%)*	*Percent of fines*	*Welling pressure (kN/m²)*
White Nile	1.5	81	27	11.1	86.5	250
sugar factory	1.5	93	30	22.7	92.2	200
at Elmasalamab	6	117	35	24	95.3	100
	3	97	30	21.7	91.2	200
	4.5	32	28	21.3	65.5	52.5
Alhalamia	3	72	23	14.6	80.7	110
	3	76	23	19.3	68.3	70
Ariab com.	3	44	17	12.7	58.9	20
headquarters	4.5	82	25	21	81.1	140
building	4.5	83	24	19.6	87.6	157.5
	3	50	28	22	71.3	245
	4.5	81	31	21.7	75.6	122.5
Khartoum univesity	2	53	22	22.7	68.3	52.5
adminstration	2	53	22	18.4	71.3	122.5
building	2	56	21	29.4	71.9	20
	3.5	95	32	33	89.7	70
Dental hospital	4	64	26	18.8	68.6	200
Pital-Khartoum	7.5	53	32	21.5	80.3	85
	4.5	81	37	20.9	83.7	220
	4.5	40	39	14.3	72.9	180
	4.5	72	36	25	89.5	620
Building	4.5	71	32	27.4	97.2	110
Block14	6	54	26	27.1	69	20
	7.5	37	19	21.3	53.8	0
Botana building	1.5	60	28	24.8	59.8	115
	3	55	30	29.1	85.9	44
Plot18	4.5	62	28	20.4	82	250
Elmanshia	6	47	26	20	72	70
Kilo x gas	0.5	66	31	24	82.6	35
turbin	1	82	30	28	82.1	60
	1.5	82	30	23.4	91	120
	2	79	28	17.2	85	150
B.No66B14	0.75	53	24	33.9	73.8	50
	2	84	26	29.2	82.2	115
	3	41	33	21.8	78	85
	5	66	27	27	89	100
	1.5	37	26	38	92	45
	1.5	40	25	33	93	3.5
	4.5	53	25	16	79	66
	4.5	32	26	23	91	180
	4.5	76	26	20	71	104
Animal resources	3	72	29	28.5	66.6	40
	6	73	31	27	58.8	25
School of management	4.5	40	29	26	79	14
	6	34	23	30	77	24
	6	33	27	44	86	6
EPI HQ South Sahafa	4.5	86	31	24	88	315
	3	83	26	24	85	360
	4.5	64	24	23	73.5	140
	4.5	48	26	20	83.5	56
	4.5	59	26	21	74	100
	1.5	92	26	27	83	200

(*continued*)

Table 17.2 Continued

Source	*Depth (m)*	*Liquid limit (%)*	*Plastic limit (%)*	*Natural water content (%)*	*Percent of fines*	*Welling pressure (kN/m^2)*
Multistorey building	4.5	82	35	30.9	82.9	120
No. 2/2	1.5	60	30	19.4	91.7	70
Water station extension project	3	37	31	27	84	53
	4.5	35	24	27	68	7
	3	43	29	25	85.5	50
	6	43	24	26	80	4
	4.5	47	29	29	91	7
	6	43	29	20	98	8
	4.5	46	28	33	88	7
Alhalfaya health center	1.5	77	30	34	94	35
	3	61	31	21	92	37
	1.5	64	27	23	92	28
	1.5	68	28	16	90.5	26
Building at Elhalfaya	1.5	86	33	27	94	112.5
	3	88	27	22	93	227.5
Guneid sugar factory	3	57	23	27	84.8	52.5
	4	57	22	26	74.9	20
	5	49	21	22	63.1	20
	3	54	21	26	79	20
	4	61	24	26	79.6	17.5
	3	50	26	13.1	83.1	50
Millitary factory	3	80	21	28	81.8	200
Singa TV	1.5	81	42	22	89.3	200
	1.5	58	39	22	81.8	210
Nile cement factory	2	39	16	12.3	24	350
	3	53	25	12.3	62	280
	10.5	79	31	19	75	245
	7.5	108	30	21	80	140
Plastic bags factory	1	58	24	12	72.8	140
	2	66	31	20	78	245
	3	61	27	17	68	70
	4	67	26	16	69	245
	3	52	25	14	65.8	175
	2.5	65	28	19.5	72.8	230
	2	59	33	17	77.7	350
	3.5	59	23	14	63	400
	1	61	27	18	64	240
Sinnar sugar project	5	72	32	19.8	85.4	300
	3	76	34	28	87.4	18
	4	75	32	28.5	87.3	60
	1	63	31	24.3	75.4	150
	3	72	29	27	74.2	18
	3	53	25	24.2	55.2	9
	5.5	74	30	30.7	84.3	9
Sinnar yeast factory	3	72	31	20	88	595
	4	72	30	21	80	385
	3	73	30	13	87	160
	5	69	30	19	88	30

The data was divided into three subsets for training, testing, and validation. Each input parameter was normalized to a number between 0 and 1 based on the minimum and maximum values of that parameter using the following equation:

$$\text{Normalized value} = \frac{\text{Actual value} - \text{min value}}{\text{max value} - \text{min value}} \tag{17.1}$$

Network architecture

Network architecture and topology varies from one problem to another. Trial and error is usually used to identify the suitable network topology. In this study, a network consisting of four layers as shown in Figure 17.1 was used. The first layer is the input layer and consists of four neurons (the input parameters). The last layer is the output layer and consists of one neuron (the output parameter). An initial number of hidden layers and the associated neurons can be based on the guidelines published in the literature (e.g. Agrawal *et al.*, 1997). The final numbers can be obtained by performing parametric study during the training and testing processes. In this study, two hidden layers each with seven neurons were obtained after performance of a number of tests.

The computer program

Microsoft Excel's Solver provides a powerful tool for optimizing complex problems that involve multiple variables subject to multiple constraints and it was used in this study. The following provides some features of the solution process.

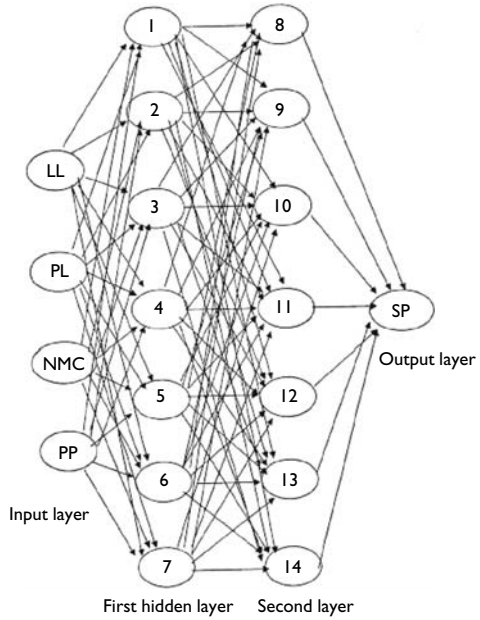

Figure 17.1 Network architecture.

Table 17.3. Final errors resulting from training

Error type	*Error (%)*	*Absolute error*
Minimum	−20.8748	0.001
Maximum	35.35262	35.35262
Average	0.847849	4.602684

The model was programmed as follows: The normalized inputs of the training set were introduced to the input layer. The outputs of the input layer were multiplied by weights and were introduced to the hidden layer. The outputs of the first hidden layer were multiplied by weights and were introduced to the second hidden layer. The outputs of the second hidden layer were multiplied by weights and were introduced to the output layer. Finally the output was received through the output layer. Since the input data was normalized, then the output received will also be normalized. To convert the normalized output to actual values the following equation was used:

$$SP_{model} = O_{model}(SP_{max} - SP_{min}) + SP_{min} \tag{17.2}$$

where: SP_{model} = the model swelling pressure; O_{model} = the model output; SP_{max} = the maximum swell pressure; and SP_{min} = the minimum swell pressure

The error between the swelling pressure predicted by the ANN and the actual swelling pressure was computed as:

$$e = SP_{model} - \text{actual swelling pressure} \tag{17.3}$$

The sum of errors for all training sets was calculated as:

$$E = \sum e^2 \tag{17.4}$$

The analysis process continues until the sum of errors is within the acceptable limits. Table 17.3 shows the errors for the proposed model. The table indicates that the prediction capabilities of the model are acceptable and the model can be used to estimate the swelling of these types of soils.

Charts for estimation of swelling pressure

Here the trained network is used to establish charts for estimation of the swelling pressure if some of the input parameters are known.

Charts based on liquid limit

A swelling pressure chart based on different liquid limit (LL), different plastic limit, constant natural moisture content, and constant percent passing sieve No. 200 is shown in Figure 17.2. The figure indicates that as the LL increases the swelling pressure increases at a moderate rate. However, when the LL reaches about 75%, the swelling pressure starts to increase at a higher rate. The figure also indicates that for LL $<$ 75% the

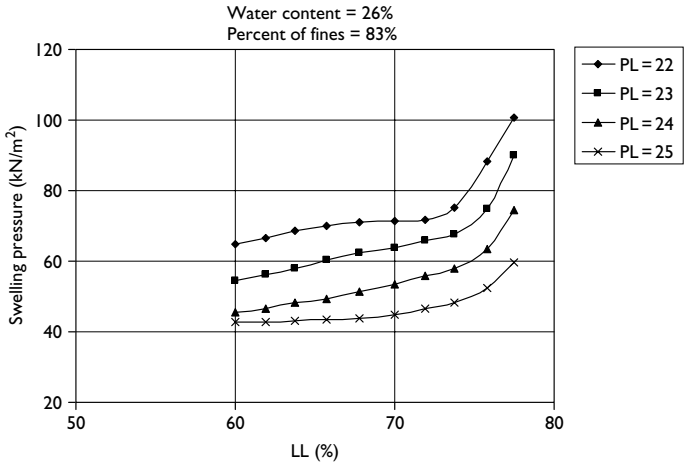

Figure 17.2 Swelling pressure charts for different values of LL and PL.

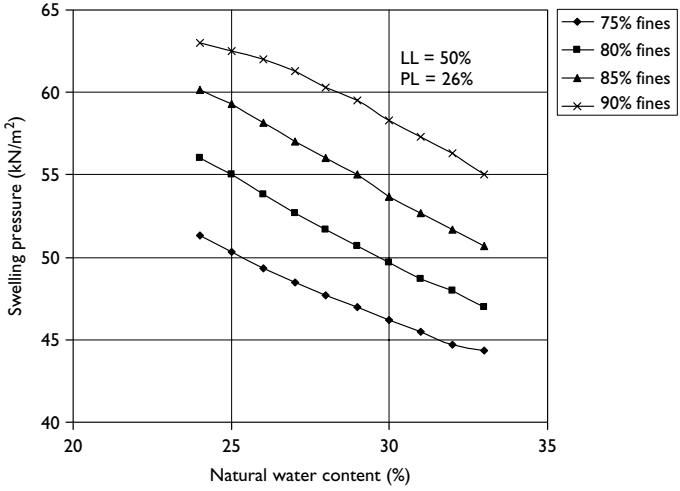

Figure 17.3 Swelling pressure charts for different values of natural water content and percent of fines.

effect of plastic limit (PL) (or the plasticity index) is significant. Above that value the effect of LL is dominant.

Charts based on natural water content

Figure 17.3 shows a swelling pressure chart based on different values of natural moisture content, different values of percent of fines, constant LL, and constant PL. This figure

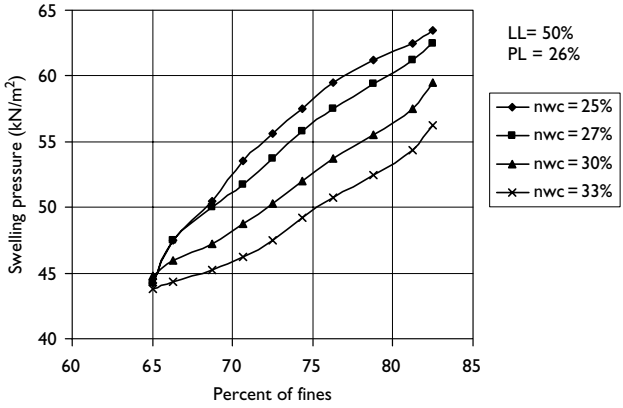

Figure 17.4 Swelling pressure charts for different values of percent of fines and natural water content.

indicates that increasing the natural moisture content tends to decrease the swelling pressure and the swelling pressure increases at a proportional rate with the increase in the percent of fines.

Figure 17.4 shows a swelling pressure chart based on different values of natural moisture content, different values of percent of fines, constant LL, and constant PL. This figure shows that the swelling pressure decreases with the increase in the natural moisture content.

Conclusions

In closing, artificial neural networks overcome the limitations of empirical correlations and can be used as an alternative approach. The ANN is an efficient tool in identifying complex, non-linear, and causal relations. As far as the authors are aware, this is the first time that ANNs have been used to predict the swelling of soils. The results showed that the proposed neural network model can predict the swelling pressure of expansive soils. Charts were developed to estimate the swelling pressure based on typical index parameters such as Atterberg limits, natural water content, and percent of fines.

References

Agrawal, G., Chameau, J.-L.A. and Bourdeau, P.L. (1977). Assessing the Liquefaction Susceptibility at a Site Based on Information from Penetration Testing. In Kartam, N., Flood, I., and Garrett, J.H. (Eds), Artificial Neural Networks for Civil Engineers: Fundamentals and Applications, Monograph, ASCE.

ASTM Designation D 4546 (1996). Standard Test Methods for One-Dimensional Swell or Swell Settlement Potential of Cohesive Soils. Annual Book of ASTM Standards, Vol. 04.08.

Basma, A.A. and Kallas, N. (2003). Modelling Soil Collapse by Artificial Neural Networks. *Geotechnical and Geological Engineering Journal*, Vol. 22, No. 3, pp. 427–438.

Brackley, I.J.A. (1975a). Model of Unsaturated Clay Structure and its Application to Swell Behaviour. Proceedings of the 6th Regional Conference for Africa on Soil Mechanics and Foundation Engineering, Durban, South Africa, pp. 71–79.

Brackley, I.J.A. (1975b). Swell under load. Proceedings of the 6th Regional Conference for Africa on Soil Mechanics and Foundation Engineering, Durban, South Africa, pp. 65–70.

Chameau, J.-L., Altschaeffl, A.G., Michael, H.L., and Yao, J.T.P. (1983). Potential Applications of Fuzzy Sets in Civil Engineering. *International Journal of Man-Machine Studies*, Vol. 19, No. 1, pp. 9–18.

EISharief, A.M. (1987). Field and Laboratory Investigation of Expansive Soil Heave and the Behavior of Short Piles in Expansive Clays. MSc Thesis, Building and Road Research Institute, University of Khartoum, Khartoum, Sudan.

Flood, I. and Kartam, N. (1994). Neural Networks in Civil Engineering I: Principles and Understanding. *Journal of Computing in Civil Engineering*, ASCE, Vol. 8, No. 2, pp. 131–148.

Goh, A.T.C. (1995). Empirical Design in Geotechnics Using Neural Networks. *Geotechnique*, Vol. 54, No. 4, pp. 709–714.

Kartam, N., Flood, I. and Garrett, J. H. (Eds) (1997). Artificial Neural Networks for Civil Engineers: Fundamentals and Applications, Monograph, ASCE.

Komornik, A. and David, D. (1969). Prediction of Swelling Pressure of Clays. *Journal of Soil Mechanics and Foundation Engineering, ASCE*, Vol. 95, No. 1, pp. 209–226.

Nawari, N.O., Liang, R. and Nusairat, J. (1999). Artificial Intelligence Techniques for Design and analysis of Deep Foundations. *Electronic Journal of Geotechnical Engineering (EJGE)*, Vol. 4, http://www.ejge.com

Nelson, J.D. and Miller, D. J. (1992). *Expansive Soils: Problems and Practice in Foundation and Pavement Engineering*. John Wiley and Sons Inc., New York.

Osman, M.A. and Charlie, W.A. (1984). Engineering Properties of Expansive Soils in Sudan. Proceedings of the Fifth International Conference on Expansive Soils, Adelaide, Australia, pp. 311–315.

Penumadu, D. and Zhao, R. (1999). Triaxial Compression Behaviour of Sand and Gravel Using Artificial Neural Networks (ANN). *Computer and Geotechnics*, Vol. 24, No. 3, pp. 207–230.

Shahin, M.A., Maier, H.R. and Jaksa, M.B. (2002). Predicting Settlement of Shallow Foundations Using Neural Networks. *Journal of Geotechnical and Geoenvironmental Engineering*, *ASCE*, Vol. 128, No. 9, pp. 785–793.

Toll, D. (1996). Artificial Intelligence Applications in Geotechnical Engineering. *Electronic Journal of Geotechnical Engineering (EJGE)*, Vol. 1, http://www.ejge.com

Ural, D. N. and Saka, H. (1998). Liquefaction Prediction by Artificial Neural Networks. *Electronic Journal of Geotechnical Engineering (EJGE)*, Vol. 3, http://www.ejge.com

Vijayvergiya, V.N. and Ghazally, O.I. (1973). Prediction of Swelling Potential of Natural Clays. Proceedings of Third International Research and Engineering Conference on Expansive Clays, pp. 227–234.

Chapter 18

Shrinkage strain characterization of expansive soils using digital imaging technology

Anand J. Puppala,[1] *Siva Pathivada,*[1]
Venkat Bhadriraju,[1] *and Laureano R. Hoyos*[1]

Summary

The main objective of this chapter was to describe various shrinkage strain estimation methods followed in geotechnical practice and then introduce a novel method of estimating shrinkage volume changes in soils by testing a cylindrical specimen prepared at various expected moisture contents in the field. The procedure uses digital image analyses, which eliminates operator dependency on test measurements. Two separate experimental studies were presented here which cover linear and three-dimensional volumetric shrinkage test measurements conducted on natural and stabilized expansive clayey soils. Variations in measurements indicated larger shrinkage strains with digital when compared to manual measurements, indicating erroneous characterization of the severity nature of the soil with manual measurements. Major findings from test methods, repeatability, reliability, and future research needs were also addressed.

Introduction

Expansive soils are characterized as problematic as they exhibit swelling with absorption of water and shrinking with desorption. Such volume changes caused by swelling and shrinking movements often distress the infrastructure that is not designed to withstand those movements. In addition to swelling, shrinkage-related volume change is critical in influencing the overall volume change properties of the soil. Field conditions that promote shrinking or shrinkage-induced crack formation include environmental changes, construction process, and surcharge loading (Katha, 2002). Environmental changes include freezing (the growth of ice lenses), differential swelling (coupled with the weakening of interparticle forces during rapid wetting), and drying (shrinkage of clay mass) (Katha, 2002).

Characterization of expansive soils in the current literature is more or less based on various methods or empirical relations with emphasis on potential heave problems (Puppala *et al.*, 2004). Shrinkage characterization has been, to a certain extent, overlooked as a potential distress causing mechanism in the design of foundations and earth structures.

[1] Department of Civil and Environmental Engineering, The University of Texas at Arlington, Arlington, Texas 76019, USA.

Though a few of the foundation design practices in expansive soils include shrinkage-related curling movements in their foundation design methodologies, methods to determine shrinkage strain potentials are based on empirical models or Atterberg limits (Katha, 2002).

Also, shrinkage cracking in expansive soils often lead to increased heaving in soils since surficial shrinkage cracks will allow more moisture ingress into underlying expansive soils and cause further soil heaving. As a result, heave will be quite high at surface levels, which will further distress infrastructures built above them. This signifies the importance of including accurate shrinkage strain characterization in par with the swell behavior estimation in expansive soils. Such inclusion will provide a better understanding of expansive soil behavior and lead to a better foundation design practice.

In this chapter, the authors describe the current state of knowledge on the shrinkage strain characterization of expansive soils, manual shrinkage strain measurement methods, a new approach to measure both linear shrinkage and volumetric shrinkage strain potentials using a digital imaging method, advantages and limitations of these methods, and future research needs.

Background

Any change in the soil water chemistry induces an inter-particle force field resulting in a change in the internal forces, which are subsequently balanced by a change in the particle spacing and orientation in an attempt to attain equilibrium (Mitchell, 1993). This change in particle orientation may be termed as shrinkage or swelling. Shrinkage in expansive soils has always been interrelated to swelling. Due to shrinkage, the surface of the soil layers settle and hence cracking will take place and propagate downward forming cracked soil columns with a desiccated surface crust.

In the case of pavements, transverse cracks develop from the shoulder and propagate on to the pavement as longitudinal cracks leading to major pavement distress (Figure 18.1). Thus, the influence of shrinkage cracks on all aspects of geotechnical engineering is considerable. Thus, a clear understanding of different phases of shrinkage and mechanics of

Figure 18.1 Photograph showing propagation of cracks from sub-grades to the adjacent pavement.

desiccation crack formation are always important for better characterization of severity nature of expansive soils.

Desiccation cracking of soil is a problem encountered in many engineering disciplines, including geotechnical and environmental engineering. Jointing in desiccated clays has significant effects on the hydraulic conductivity, shear strength, compressibility, and slope stability of these soils (Bosscher and Connell, 1988). A variety of research efforts have attempted to address the problems of desiccation cracking. Some have considered the use of surface moisture barriers to encapsulate the expansive soil layer; others have considered decreasing the crack potential of the soil by stabilizing them. Among these latter efforts, a few have considered soil additives to increase the soil strength and resistance to cracking.

Leung and Vipulanandan (1995) studied the effects of soil additives including lime and cement on the volumetric shrinkage and hydraulic conductivity of clay soil. The results indicated that soil shrinkage was reduced but the hydraulic conductivity increased in some cases such as in lime stabilization. Soil plasticity was also reduced thereby decreasing the potential of compacted clay soil to crack due to shear forces.

Mechanism of crack formation

Soil cracking is a natural phenomenon and is frequently observed in natural and man-made earth structures. Desiccation-induced cracking in unsaturated expansive soil fills occurs due to the presence of tensile stresses, which exceed the tensile strength of the soil. Fang (1994) reported that when moisture is lost from the surface soil mass, tensile forces will be generated in the drying surface layer. Because of the loss of water and low tensile strength, soil looses the ability to relieve or withstand these tensile forces. These stresses are finally relieved by the formation of shrinkage cracks, as soil particles move closer together, that break up the surface layer into pieces of more or less distinct geometric shapes. The geometric shape of the cracks depends on the soil particle composition, the heating process, and the pore fluids. An investigation conducted to study the surficial characteristics of cracking showed that crack geometry was a function of duration of desiccation and corresponding soil moisture suction.

Morris *et al.* (1992) reported that macrocracks were produced by the growth of microcracks under tensile loading at the crack tips as a result of increased pore water suction. The pore water suction is inversely proportional to the radius of the capillaries and hence to the particle size. The capillary forces associated with soil moisture loss to the atmosphere cause the soil to shrink. Morris *et al.* (1992) also showed that soil macrocracks due to pore water suction are more readily produced in unsaturated fine-grained soils. This is because fine-grained soils have smaller particle size and hence smaller intergranular voids. The smaller voids support larger pore water suction. They also reported that conditions for crack propagation are most favorable at the ground surface where pore water suctions are generally largest and self-weight stresses are zero. The depth to which the crack extends is ultimately constrained by the increasing stresses due to self-weight of soil, and the planar length of the crack is limited by intersection with other cracks.

Many detailed empirical and theoretical approaches have been developed to explain the mechanics of desiccation crack formation. The first theoretical approach was that of Lachenbruch (1961), who developed an approximate mathematical solution to the Airy stress function, which is used in a classical fracture mechanics framework to describe stress fields around a crack. Later, Bazant and Cedolin (1991) using the energy balance approach

to fracture mechanics, developed a theoretical model to determine minimum spacing of simultaneously formed parallel cracks.

Empirical studies by Corte and Higashi (1964) and Dexter (1988) assumed that the internal soil stress is a function of the soil water suction and is a result of any shrinkage perpendicular to the crack plane being prevented by constrained boundary conditions. A commonly reported observation of desiccation cracking is that the spacing of cracks depends on the rate of drying.

Laboratory measurements of shrinkage strains

Shrinkage tests are in limited use in expansive soil characterization. Currently either linear shrinkage strain tests or Atterberg limit test methods or both are used to measure and interpret shrinkage cracking behavior of soils. Another method, which incorporates the measurement of linear extensibility of the soil, is coefficient of linear extensibility (COLE) method. This method is mostly used by federal agencies to describe the shrinkage strain potential behavior of soil. This is used routinely by the National Soil survey laboratory to characterize shrink-swell potential of soils. In this method, the shrinkage potential is determined by measuring the change of the soil specimen from moist state to dry state.

Linear shrinkage bar test method

As discussed earlier the bar linear shrinkage test is one of the most commonly used test methods for determining the shrinkage strain potential. This test is carried out on the fraction soil sample passing through the 0.425 mm sieve. The soil material should be moistened until it reaches the liquid limit, placed in the mold, and oven dried for at least 12 hours at 105°C. The change in length of the sample is then measured manually by using vernier calipers and the percentage shrinkage is calculated. This test method is restricted by several limitations including small specimen sizes, molds with rigid walls that restrain shrinkage strains in lateral directions, and manual measurement errors. Moreover, these methods are considered poor since they do not simulate to the soil conditions in actual field and this is operator dependent and results often depend on skills of operators performing the tests. To overcome some of the limitations in linear shrinkage strain test measurements, a volumetric shrinkage measurement approach was introduced at the University of Texas at Arlington (UTA) to measure volumetric shrinkage strain potentials of a cylindrical and compacted soil specimen. Details of this test procedure are given in the following section.

Volumetric shrinkage strain test method

The soil, after being crushed, is placed in an oven for 24 hours. This dried soil is passed through a 0.425 mm sieve. This fine fraction of soil is collected and mixed with water at targeted moisture content. The prepared mixture is compacted in a volumetric shrinkage mold of height 5.0 in. and diameter 2.3 in. This mold is left at room temperature for at least 12 hours. The dimensions of the compacted soil sample are then recorded manually using vernier calipers. The specimen is then transferred to the humidity room and then allowed to oven dry at 70°C for 24 hours. This dried shrunk compacted soil sample dimensions are also measured manually and these dimensions are used to measure volumetric shrinkage strains. Thus, this test is termed here as a manual three-dimensional or three-dimensional shrinkage strain test method.

This method is also limited by the manual measurement difficulties in calculating volume changes of soil specimens. The main drawback of this manual measurement method is that it does not account for the crack widths and in some cases hairline cracks form on the surface of the soil specimen after drying. Hence, manual measurements often underestimate true volumetric shrinkage strains. Hence, a new measurement software technology, basically an image processing and analysis of tasks was formulated by Puppala *et al.* (2004) to provide concordant results with reliable measurements. This technology was termed as digital imaging technology.

Digital imaging technology

Digital imaging

Digital imaging is a relatively new tool for analyzing digital images and finding relevant parameters from these images to correlate performance-related engineering parameters. This method is receiving increasing attention, mainly due to the non-destructive nature of the method, which makes its use popular in various civil engineering application areas. A few such areas are pavement distress assessment, site evaluation using satellite imagery studies, crack propagation and microstructure studies in cement-based materials, and fabric study in soils (Frost and Wright, 1993).

In the next section, a few digital imaging applications in geotechnical and highway engineering, followed by definitions of various terms used in digital imaging and instrumentation used for image analysis are presented.

Applications in geotechnical and highway engineering fields

In the geotechnical and highway engineering fields, the use of digital image processing methods has provided numerous opportunities for direct or indirect estimation of various soil and pavement properties (Mitchell, 1993; Hryciw and Raschke, 1996; Kuo and Frost, 1996). The research performed in civil engineering fields ranges from satellite imagery (large-scale images) to clay microfabric images (microscopic-scale images) (Prestridge, 1993).

Digital image processing techniques have also been applied on digital images of soil specimens to obtain information such as soil stratigraphy and grain-size distribution (Hryciw *et al.*, 1997). A three-dimensional analysis of aggregate particles from orthogonal projections in a digital image was used to provide elongation and flatness of each soil grain (Luo *et al.*, 1997). The homogeneity and uniformity of granular materials was addressed in other investigations by studying three fabric parameters in a digital image: particle shape, particle orientation, and local void ratio (Kuo and Frost, 1996).

Macari *et al.* (1993) developed methods to measure volume changes in a soil specimen in a triaxial test by using video cameras to capture top and front views of the soil specimen. These video images were used and analyzed to interpret volume changes in soil specimens which showed a good correlation with conventional triaxial volumetric strain measurements. Digital imaging techniques were also used to understand geotextile fabric distribution. Geotextile image analyses were used to interpret flow-related characteristics that are needed in the design of filters in dams, landfills, edge drains, and retaining walls. Current advances in digital imaging studies focus on the X-ray computed tomography (CT) methods to study localized deformations in granular soils.

Pavement cracks have been subjected to digital imaging techniques. Many algorithms were developed to measure the unified crack index, which was used to address the pavement distress (Jitprasithsiri *et al*., 1996). An Automated Road Analyzer (ARAN) system, a van equipped with instruments to analyze roads, provided pavement distress data from analyzing digital images of cracks on pavements (Klassen and Swindall, 1993). This processing system uses an image analysis algorithm for distinguishing pavement cracks.

Definitions

The main focus is to obtain accurate volumetric shrinkage strain measurements by capturing and analyzing digital images of cracked soil specimens. A digital image is a rectangular array of pixels, or picture elements, and is described in terms of geometry and radiometry (Katha, 2002). The smallest unit in a digital image is called a *pixel*. The magnitudes of the pixels indicate the average light intensity on the pixel known as *pixel intensity* (or gray value). Each pixel represents a color and has an intensity value ranging from 0 to 255. The density of pixels in an image reflects the resolution of the image.

The function that separates the cracked area of a shrunken soil specimen is a *threshold function* with a certain value of pixel intensity. The threshold value sets the background to black for pixels below a threshold value T, and sets values above the threshold value to white in a digital image picture. These image change that are obtained by setting off threshold values will help in the accurate estimation of cracked areas by measuring the number of pixels in either black or white background.

Accessories used for digital imaging

Many devices are used to capture digital images of soil specimens. Scanning electron microscope (SEM) may be considered as the most important device for producing digital images. Fine particulate matter such as soils can be characterized in terms of size, shape, and distribution and a statistical analysis on digital images of soil particles can provide this information. The light polarizing microscope, an optical measuring instrument can be used for the detailed examination of soil samples producing less magnified digital images than SEM images. It is widely used for chemical microscopy and optical microscopy. Digital cameras and Videos provide digital images with various intensities. Scanners convert optical images to a digital format, which can be used for the image analysis.

Digital image-based measurements of shrinkage

Hardware and software features

The present digital measurement procedure was developed after reviewing existing methodologies used in the practice for measuring volume changes in soils. One important variation between present research and previous studies in the measurement of volume changes is the need to consider and evaluate even small hairline, surficial cracks on soil samples, while estimating the cracked area of a shrunk soil specimen. Because of this requirement, digital image studies were considered for accurately incorporating the reduction in surface area into the total volumetric shrinkage. For such digital based analyses, the following software and hardware are acquired.

The software "Scion Image" was used to analyze the digital images. This software has several features in digital image processing to display, edit, enhance, and analyze digital images at different resolutions. It also supports standard digital image-processing functions such as the enhancement of contrast, smoothening, sharpening, threshold, and edge detection. The Scion Image software has capabilities to measure area and perimeter of a user-defined image in pixels, the mean and standard deviation of pixel intensities, and the centroid of a given image area.

The hardware requirements for this test are minimal since any Pentium computer has capabilities to perform digital image studies. A digital camera was used to capture images of shrunk and unshrunk soil specimens for measurement analysis. The camera used was one of the first digital cameras developed with two-mega pixel imaging capabilities.

Digital image analysis for measurement of linear shrinkage strain

The manual measurement of the shrinkage strain of the shrunk sample from linear shrinkage test was discussed in the previous paragraph. In this section the digital measurements of the shrunk sample from linear shrinkage test are discussed. A digital photograph of the shrunk sample was captured along with the linear shrinkage mold. This photograph is trimmed as shown in the Figure 18.2.

This photograph is opened in Scion Image software and the area of the cracks in pixels is measured. The original area of the linear shrinkage bar image in pixels I measured. The ratio of the area of the threshold image in pixels to the area of the original image in pixels gives the total areal shrinkage of the soil sample. Katha (2002) performed many tests both manually and digitally to determine the shrinkage of soil samples. In the research performed by Katha (2002) at The UTA, four clays (two artificial and two natural clays) were considered. Manual measurements using vernier calipers and digital image technique were performed on the samples to determine the shrinkage strain potential. The results obtained from digital analysis were found to provide repeatable and reliable values, mainly representing shrinkage strains experienced by soils in real field conditions. A graph comparing manual and digital measurements of all the soil types is shown in Figure 18.3.

This figure explains the variations in linear and areal shrinkage strains of same soils. It was found that the differences in shrinkage strain potentials between areal and linear measurements varied from 3% to 12%. Such large variation was attributed to several factors including manual errors in measurements and type of measurements (two-dimentional areal digital measurements versus one-dimentional linear measurements). Other problems included lack of incorporation of compaction conditions in linear bar specimens. Overall, this analysis showed the fallacies in a linear shrinkage bar test method, which was overcome by using a cylindrical shrinkage specimen test and digital measurements.

Figure 18.2 Typical trimmed photograph of soil sample (Katha, 2002).

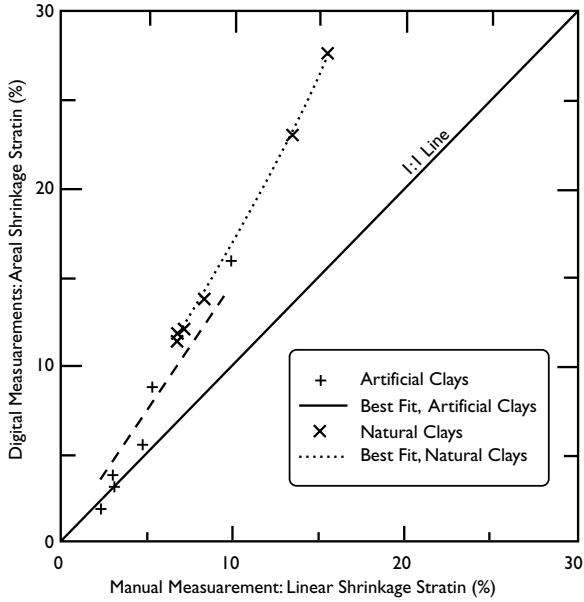

Figure 18.3 Variation of shrinkage strain (%) between manual and digital measurements (Katha, 2002).

As explained earlier, the volumetric shrinkage test can be performed on compacted soil specimens of desired moisture content and dry unit weight, which are then tested in a dry environment similar to linear shrinkage bar test. Reduced dimensions of specimen height and diameters are determined on the dried and shrunk soil specimen and these are used to estimate volumetric shrinkage strains, referred to here as manual volumetric shrinkage measurements. Details of this test can be found in Puppala *et al.* (2004). Details of digital image analysis to measure volumetric shrinkage strains are presented in the next section.

Digital image analysis for measurement of volumetric shrinkage strain

The equation for determining the volumetric shrinkage strain and its parameters are discussed in this section. Assuming that the soil cylindrical specimen has an initial radius (r) and height (h) before subjecting to shrinkage, and assuming the area ratio of the soil specimen as R_s (A_{sf}/A_{si}), the area ratio of circular area of soil specimen as R_c (A_{cf}/A_{ci}), and the perimeter ratio of circular area of soil as R_p (P_{cf}/P_{ci}), the volumetric shrinkage of the soil specimen is given as:

$$VS = 1 - \left(\frac{R_s \times R_c}{R_p}\right)$$

where

A_{sf} = area of the final surface area of soil specimen after shrinkage in pixels.

A_{si} = area of the initial surface area of soil specimen before shrinkage in pixels.
A_{cf} = area of the final circular area of soil specimen after shrinkage in pixels.
A_{ci} = area of the initial circular area of soil specimen before shrinkage in pixels.
P_{cf} = perimeter of the final circular area of soil specimen after shrinkage in pixels.
P_{ci} = perimeter of the initial circular area of soil specimen before shrinkage in pixels.

This equation can be used to determine volumetric shrinkage strain from the digital image technique by taking various images of the soil sample which is discussed in the following paragraphs. The manual volumetric shrinkage strain determination of the soil specimen compacted at the targeted compaction moisture content was described in the earlier section. The digital image analysis technique is performed on the shrunk sample. Four digital photographs of the total surface area of the cylindrical specimen mounted on a marked and rotating pedestal were taken along the circumference of the cylinder at four different equal angles covering the whole circumference of the soil sample with a digital camera. While taking the photographs, the most important factor to be considered is to maintain same resolution and distance between the specimen and the camera. A dummy black cardboard cylinder representing the inner cylinder of the volumetric shrinkage mold was imaged to measure the initial soil cylinder dimensions before shrinkage. The soil specimen was imaged immediately after the shrinkage test as mentioned earlier. These digital images were stitched together as shown in the Figure 18.4

Two more images of the top and base views of the soil sample were taken to determine the average cross-section areas and perimeters. Thus a total of six digital photographs were taken and used in the digital analysis to obtain the volumetric shrinkage strains of the soil. Figure 18.4 presents the cracked surface area of the soil specimen after stitching of the images as discussed earlier along with the threshold image from the digital image technique.

Volumetric shrinkage strains of expansive soils

Katha (2002) performed volumetric shrinkage strain tests on four clays (two artificial and two natural clays). The shrinkage strains obtained from digital imaging were found to be more

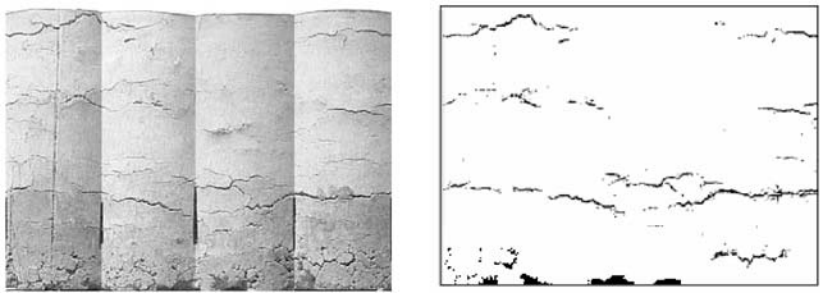

Figure 18.4 Cracked surface area of the soil specimen. (*a*) typical photograph of a soil specimen surface area with cracks, (*b*) threshold image of the surface area showing only cracks (Puppala *et al.*, 2004).

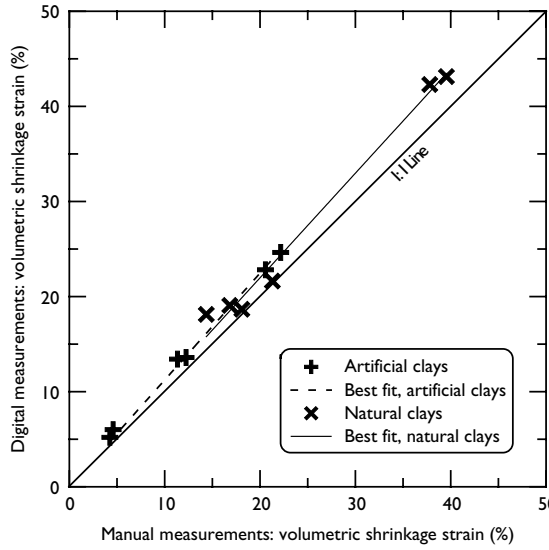

Figure 18.5 Variation of volumetric shrinkage strain (%) between manual and digital measurements. Source: Katha, 2002.

than the ones measured manually. A graph comparing manual and digital measurements of all the soil types as shown in Figure. 18.5 clearly explains that the digital analysis measurements provided consistently higher volumetric shrinkage strains than manual measurements.

It was also found that the differences between digital and manual volumetric shrinkage strains varied between 2% and 5%. This indicated the underestimation of volumetric shrinkage when measured manually. Also, the variations of 2% to 5% represented the differences between two characterization levels, medium to high severity levels.

Volumetric shrinkage strains of stabilized expansive soils

Soil reinforcement using materials relatively stronger in tension has been an attractive option to mitigate shrinkage cracking. Many reinforcing techniques use planar inclusions oriented in preferred directions (geotextiles, geogrids), which sometimes are proven expensive and forming possible planes of failures if not engineered properly. A considerable amount of research on the usage of discrete, randomly distributed, synthetic and natural fibers in soil stabilization has been performed, which always concentrated on the strength and stiffness improvements ensuring isotropy (Musenda, 1999). The current section concentrates on the influence of fiber inclusion on the shrinkage strain potentials of a natural expansive soil measured from the volumetric digital imaging method.

The expansive soil used in the current research was sampled from Arlington, Texas. Carbon fiber dosages of 0.4%, 0.6%, and 1.0% by dry weight of soil were added respectively. Details on the fiber type can be found in Bhadriraju *et al.* (2005). Based on the test results

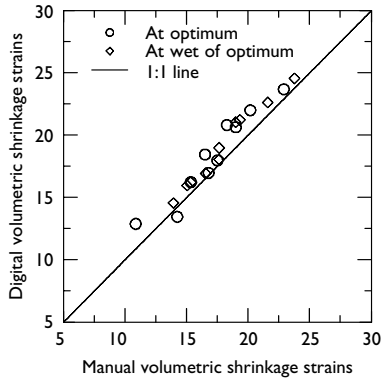

Figure 18.6 Comparisons between manual and digital volumetric shrinkage strain measurements of fiber-treated soils.

from standard Proctor compaction tests on composite soil-fiber matrix, specimens were compacted in steel molds 58 mm in diameter and 125 mm in height with a flat and rigid rectangular base.

The first step in the analysis was to compare both manual (measured average of diameter and length at three different points along the specimen) and digital image-based measurements of shrinkage strain potentials of natural expansive soils. As can be seen from Figure 18.6, comparisons between measurements have shown an absolute shrinkage strain variation of 1% to 5%, with digital measurements consistently providing higher volumetric shrinkage strains. This observation is important since shrinkage strain potentials are often used to characterize the severity nature of expansive soils.

A volumetric shrinkage strain less than 17% is approximated as low severity level whereas volumetric shrinkage strains of above 20% is considered highly problematic and above 24% is considered as very highly problematic (Puppala *et al.*, 2004). For low overburden structures, shrinkage strains less than 17% may also induce distress problems. Considering the small range of shrinkage strain magnitudes that separate low to high shrinkage strains, it is important to use a more accurate method that can account for all cracks in soils that contribute to shrinkage cracking.

When the soil was treated with carbon dosages, added as a percentage of dry weight soil, the weight of the composite soil specimen decreased with increase in fiber dosages. Figure 18.7 presents typical volumetric shrinkage strain results of carbon fiber reinforced expansive soils measured using the digital imaging technique. The following mechanisms describe the potential causes for these improvements. During oven drying, when the soil specimen undergoes shrinkage, fibers start mobilizing tensile resistance and induce this resistance as a part of adhesive forces to the soil particles that come into contact and resist shrinkage cracking. Additionally, fiber modifications result in the decrease of dry unit weights and slight increase in optimum moisture content levels. Low compaction dry unit weights typically result in mitigation of swell and shrinkage behavior of expansive soils

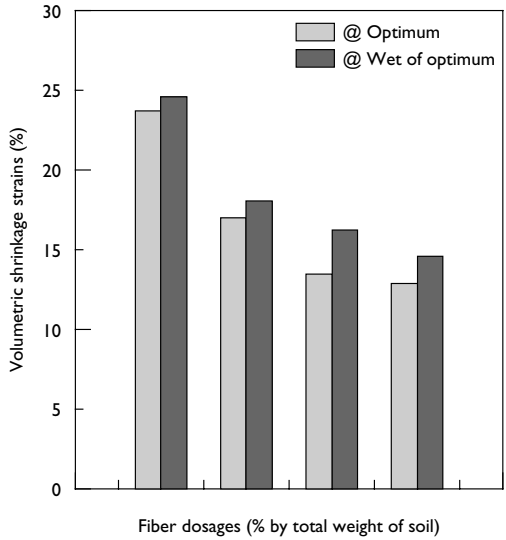

Figure 18.7 Effect of carbon fiber dosages and compaction moisture content on volumetric shrinkage strain.

(Kota *et al.*, 1996). Hence, both tensile strength enhancements and low compaction conditions contribute to the reductions in shrinkage strain potentials.

Based on the expansive soil characterization noted earlier, all fiber-treated soils yielded low severity levels. For carbon fibers, the dosage level corresponding to low severity level was around 0.4%, owing to the high tensile resistance of these fibers. This particular demonstration emphasized that digital imaging technique can successfully be applied on both untreated and stabilized soils for better characterization of shrinkage strains.

Conclusions

Volumetric shrinkage strains measured by digital imaging were higher than those measured by manual methods since the irregular surfaces and hairline cracks were taken into account. Relatively higher volumetric shrinkage strains were measured with digital techniques, which otherwise would underestimate the shrinkage potential of expansive soils. Also, digital measurements were repeatable, and provided reliable and consistent results. This test method can also be used to address compaction state effects on volumetric shrinkage measurements, which was not possible in the current linear shrinkage bar tests.

Better characterization of shrinkage potentials of expansive clays will help in deciding stabilization strategies to mitigate shrinkage cracking, evaluate potential shrink-swell movements to include in the foundation design, estimations of shrink or curling pressures, and interpreting hydraulic conductivity nature of desiccated clays. Hence, the present

volumetric shrinkage tests could be used to assess or evaluate shrinkage strain potentials of expansive soils located in foundation sub-grades, embankments and slopes, retaining walls, and even landfill clay liners.

References

Bazant, Z.P. and Cedolin, L., (1991). *Stability of Structures*. Oxford University Press, Oxford.

Bhadriraju, V., Puppala, A.J., Enayatpour, S., and Pathivada, S., (2005). "Digital imaging technique to evaluate shrinkage strain potentials of fiber reinforced expansive soils," Geo-Frontiers 2005, ASCE, Austin, pp. 2251–2262.

Bosscher, P.J. and Connell, D.E., (1988). "Measurement and analysis of jointing properties in fine-grained soils," *Journal of Geotechnical Engineering, ASCE*, Vol. 114, No. 7, pp. 826–843.

Corte, A. and Higashi, A., (1964). "Experimental Research on Desiccation Cracks in Soil," Research Report 66. U.S. Army Materiel Command. Hanover, New Hampshire: Cold Regions Research and Engineering Laboratory (CRREL).

Dexter, A.R., (1988). "Advances in characterization of soil structure," *Soil and Tillage Research*, Vol. 11, pp. 119–23C.

Fang, Hsai-yang (1994). "Cracking and Fracture Behavior of Soil," Geotechnical Special Publication Fracture Mechanics Proceedings of the ASCE National Convention, No. 43, pp. 102–117.

Frost, J.D. and Wright, J.R. (1993). *Digital Image Processing: Techniques and Applications in Civil Engineering*, American Society of Civil Engineers, New York.

Hryciw, R.D. and Raschke, S.A., (1996). "Development of computer vision technique for in situ soil characterization," Transportation Research Record, No. 1526, National Academy Press, Washington, DC, pp. 86–97.

Hryciw, R.D., Ghalib, A.M., and Raschke, S.A., (1997). "Methods for Soil Characterization from Images of Grain Assemblies," Imaging Technologies: Techniques and Applications in Civil Engineering, American Society of Civil Engineers, Reston, Virginia, pp. 88–99.

Jitprasithsiri, S., Lee, H., Sorcic, R.G., and Johnston, R., (1996). "Development of digital image-processing algorithm to compute unified crack index for salt lake city," Transportation Research Record, No. 1526, National Academy Press, Washington, DC, pp. 142–148.

Katha, B.R., (2002). "Shrinkage Strain Characterization of Expansive Soils Using Digital Imaging Technology," M.S Thesis, The University of Texas at Arlington, Texas, 101 pages

Klassen, G., and Swindall, B. (1993). "Automated Crack Detection System Implementation in ARAN," Digital Image Processing: Techniques and Applications in Civil Engineering, American Society of Civil Engineers, New York, pp. 179–185.

Kota, P.B.V.S., Hazlett, D., and Perrin, L., (1996), "Sulfate-Bearing Soils: Problems With Calcium Based Stabilizers," TRR 1546, Transportation Research Board, Washington, DC, pp. 62–69.

Kuo, C.Y., Frost, J.D., Lai, J.S., and Wang, L.B., (1996). "Three-Dimensional Image Analysis of Aggregate Particles from Orthogonal Projections," Transportation Research record, No. 1526, National Academy Press, Washington, DC, pp. 98–103.

Lachenbruch, A.H., (1961). "Depth and spacing of tension cracks," *Journal of Geophysical Research* Vol. 66, pp. 4273–4292.

Leung, M. and Vipulanandan, C., (1995). "Treating Contaminated, Cracked and Permeable Field Clay with Grouts," Geotechnical Special Publication Proceedings of the Speciality Conference on Geotechnical Practice In Waste Disposal, part 1, No. 46, ASCE New York, pp. 829–843.

Luo, D., Leng, X., Henderson, A.E., Cowan, J., Macleod, J.E.S., and Smart, P., (1997). "Recent Studies in Geotechnical Image Analysis," Imaging Technologies: Techniques and Applications in Civil Engineering, American Society of Civil Engineers, Reston, Virginia, pp. 56–65.

Macari, E.J., Costes, N.C., and Parker, J.K., (1993). "Digital Image Techniques for Volume Change Measurements in Triaxial Tests," Digital Image Processing: Techniques and Applications in Civil Engineering, American Society of Civil Engineers, New York, pp. 211–219.

Mitchell, J.K., (1993). "*Fundamentals of Soil Behavior*," John Wiley and Sons, Inc., New York.

Morris P.H., Graham, J., and Williams, D.J., (1992). "Cracking in drying soils," *Canadian Geotechnical Journal*, Vol. 29, pp. 263–277.

Musenda, C., (1999). "Investigations on the Effects of Using Discrete Randomly Distributed Fiber Reinforcement in Expansive Foundation Soils," M.S Thesis, The University of Texas at Arlington, Texas, p. 118.

Prestridge, E.B. (1993). "Digital Image Processing and Analysis in Materials Science," Digital Image Processing: Techniques and Applications in Civil Engineering, American Society of Civil Engineers, New York, pp. 31–35.

Puppala, A.J., Katha, B., and Hoyos, L.R., (2004). "Volumetric shrinkage strain measurements in expansive soils using digital imaging technology," *Geotech Testing Journal, ASTM*, Vol. 27, No. 6.

Part 5

Site characterization

Chapter 19

Swelling behavior of expansive shale

A case study from Saudi Arabia

Abdullah I. Al-Mhaidib[1]

Summary

Severe and widespread damage in residential buildings, sidewalks, and pavements can be caused by the development of heave and swelling pressure in expansive shale. This chapter presents the problems and the geotechnical and physicochemical properties of expansive shale using the middle region of Saudi Arabia as the case study area. Swell tests were conducted under different loading conditions and following different procedures to quantify the amount of vertical swell and swelling pressure. Conventional one-dimensional oedometer swell tests were performed using three different procedures, namely, free swell, constant volume swell, and swell overburden. In addition, swell tests were performed using a stress path triaxial apparatus. Tests under different vertical stresses and confinements were conducted. Vertical swell and swelling pressure obtained from the various methods were compared. The reliability of the different methods for estimation of swelling potential was discussed.

Introduction

Damages to structures from the swell of foundation soils due to change in moisture conditions are common problems that occur frequently in many parts of the world including vast areas of the Kingdom of Saudi Arabia. Damages inflicted on superstructures by expansive soils each year are enormous. Although there has been no precise estimate, annually in Saudi Arabia, expansive soils are responsible for millions of dollars worth of damage to man-made structures (Ruwaih, 1987; Dhowian *et al.*, 1990). Damages can range from minor cracking of pavement or interior finishes in buildings, which is very common, to irreparable displacement of footings and superstructure elements (Puppala *et al.*, 2004).

It is estimated that expansive soils cover an area of about 800,000 km^2 in the Kingdom (Ruwaih, 1987) (Figure 19.1). Expansive soils are encountered over a large area due to geological history, sedimentation, and climatic conditions (Slater, 1983). Shale formation prevails in different parts of the country including Al-Ghatt, Tabuk, Tayma, and Sharorah. The shale of the town of Al-Ghatt was chosen in this study because Al-Ghatt experiences some of the largest differential ground movements in Saudi Arabia (Dhowian, 1990).

This chapter presents the results of a laboratory investigation of the swelling behavior of expansive shale from the middle region of Saudi Arabia. The investigation included the

[1] Civil Engineering Department, College of Engineering, King Saud University, PO Box 800, Riyadh 11421, Kingdom of Saudi Arabia; e-mail: muhaidib@ksu.edu.sa

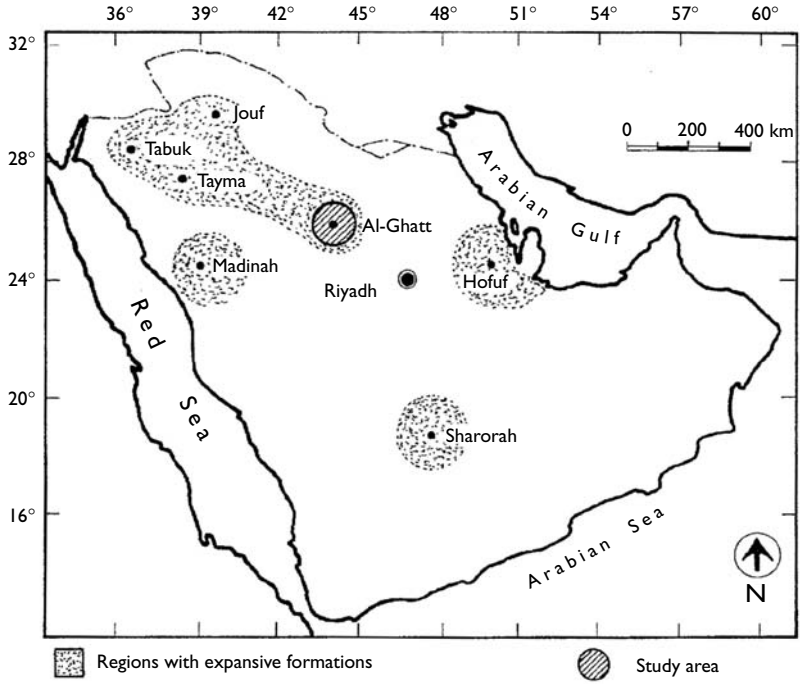

Figure 19.1 Map of case study area in Saudi Arabia showing the distribution of the expansive formations (adapted from Ruwaih, 1987).

determination of geotechnical and physicochemical properties, mineralogical composition, and swelling characteristics of the tested shale. Experiments using various methods to determine the swelling potential of the shale were performed to quantify the amount of vertical swell and swelling pressure. Swell tests were conducted under different loading conditions and following different procedures. The conventional one-dimensional oedometer swell test was performed using three different procedures: free swell, constant volume swell, and swell over-burden. In addition, swell tests were performed in the stress path triaxial apparatus. Tests under different vertical stresses and confinements were conducted. A comparison of the results is presented and discussed in terms of percentage of vertical swell and swelling pressure.

Problem description

Al-Ghatt is a small town in the middle region of Saudi Arabia, 270 km northwest of Riyadh, the capital of Saudi Arabia (Figure 19.1). More than four hundred, one-story residential buildings were constructed as a part of a housing development. The buildings were made of rigid reinforced concrete frames with hollow concrete block partitions and panels. The problems in this town started by the development of cracks after the buildings were occupied. The cracks extended to include slabs, beams, and columns.

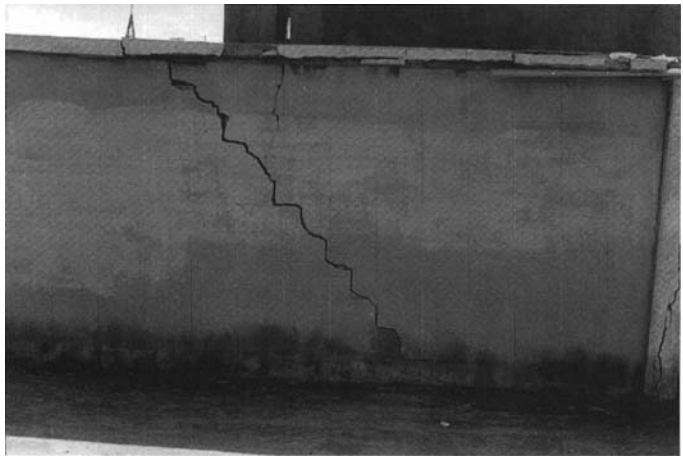

Figure 19.2 Cracking in a masonry wall due to expansive soil.

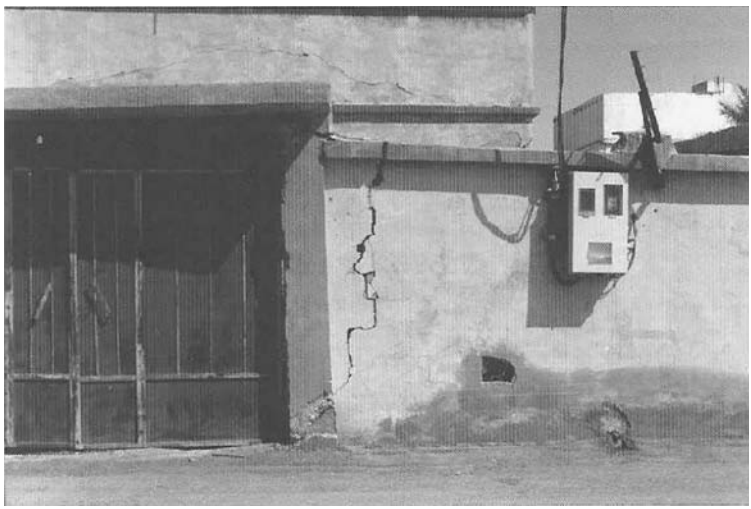

Figure 19.3 Cracks in a reinforced concrete gate and adjacent wall.

Figures 19.2 to 19.5 show examples of the kind of structural damage experienced in the town. Damage to the buildings was caused mainly by differential heave of the foundation subsoil. The damage includes cracking of masonry walls in a diagonal pattern (Figure 19.2). The cracks are typical expansive soil cracks being wide at the top and getting narrower at the bottom of the wall. Also shown are cracking of reinforced concrete gates (Figure 19.3), columns (Figure 19.4), and ground beams.

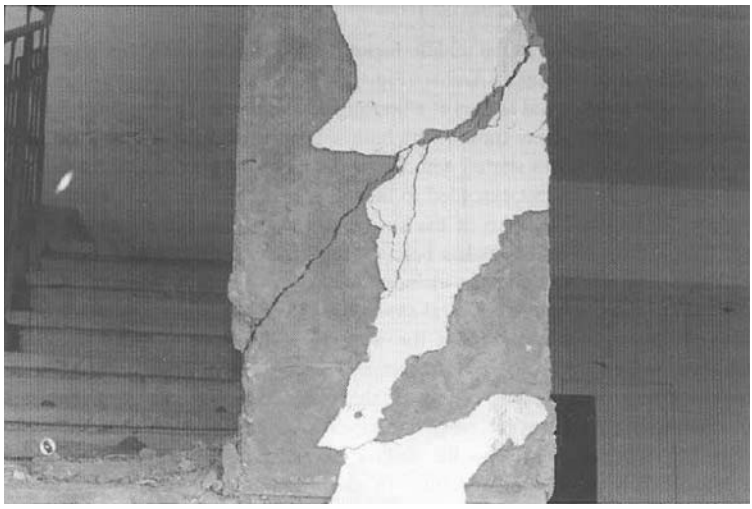

Figure 19.4 Cracks in a reinforced concrete column.

Figure 19.5 Cracks in a road pavement in the town.

Figure 19.5 shows cracking of a road pavement in the town. Damage was attributed to the excessive moisture content. This increased due to water infiltration from domestic sources and garden watering as well as from the surface cover by paving the areas around the buildings. This cover protected the moisture in the ground from outside dry weather.

Domestic waste water soaked into the soil as there was no public sewerage system in the town.

A test pit was excavated in a damaged area and soil samples were obtained at a depth of about 3 m and brought to the soil mechanics laboratory in the Civil Engineering Department, King Saud University. A laboratory testing program was designed to determine the geotechnical and physicochemical properties, mineralogical composition, and the swelling characteristics of the soil.

Soil characteristics

Geotechnical properties

Soil samples were subjected to moisture content, unit weight, grain-size analysis, and Atterberg limits tests using American Society for Testing Materials (ASTM) standard procedures. Table 19.1 shows the geotechnical properties as well as the chemical composition of the investigated soil. The grain-size distribution curve, shown in Figure 19.6, indicated that more than 99% were passing through ASTM sieve No. 200 (75 μm), from which the soil could be described as purely fine grained. The soil was composed of predominantly clay size of about 80% and silt size of about 20%. The soil was classed as inorganic clay of high plasticity (CH) in the unified soil classification system.

Table 19.1 Geotechnical properties and chemical composition of the tested soil

Parameter	*Value*
Specific gravity	2.8
Natural water content (%)	22
Dry unit weight (kN/m^3)	18
Consistency limits	
Liquid limit (%)	60
Plastic limit (%)	31
Plasticity index (%)	29
Shrinkage limit (%)	16
Classification	
Unified soil system	CH
AASHTO classification system	A-7-6
Chemical composition	
Cations (ppm)	
Ca^{2+}	270
Mg^{2+}	50
Na^{+}	8570
K^{+}	6000
Anions (ppm)	
SO_4^{2-}	53800
Cl^{-}	240
CO_3^{-}	Trace
HCO_3^{-}	3
pH	8.0

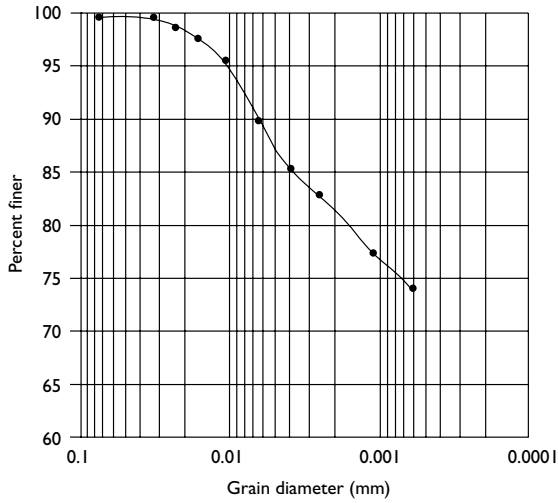

Figure 19.6 Grain-size distribution curve for the tested soil.

The shale was highly weathered, and with the arid and dry desert climate in the town, it had relatively high swell potential. The geotechnical properties of the tested soil showed that the soil had a swelling potential of high (Seed *et al.*, 1962; Dakshanamurthy and Raman, 1973) to very high (Van Der Merwe, 1964).

Soil composition

X-ray diffraction analysis was performed on the clay fraction of the tested soil to identify the clay minerals. A Philips PW 1050 diffractometer was used with a PW 1373 goniometer supply operating at 35 kV and 20 mA, with CuKα radiation, and Ni-filter.The XRD patterns shown in Figure 19.7 indicate that the clay minerals were mostly kaolinite and some illite but no montmorillonite was present. Quartz and calcite were found in relatively small quantities. The results of the chemical tests (Table 19.1) indicated that the soil had high concentrations of K and Na. These monovalent exchangeable cations caused more swelling with water addition when compared with the divalent exchangeable cations such as Ca and Mg which the soil contained in lesser amount. Furthermore, the soluble sulfate concentration was 53,800 ppm, which was believed to have had a significant effect on the swelling potential of the tested soil. The pH value of 8.0 put the soil in the slight alkaline range.

Laboratory swell tests

The amount of vertical swell and swelling pressure of the tested soil were obtained using the three oedometer testing procedures: free swell, constant volume swell, and swell overburden

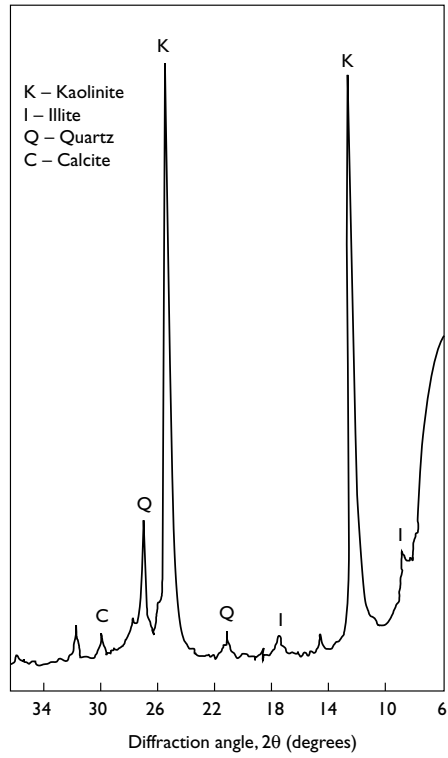

Figure 19.7 X-ray diffraction pattern for the tested soil.

tests described in ASTM standard No. D4546. In addition, swell tests were performed in the stress path triaxial apparatus. Tests under different vertical stresses and confinements were conducted.

Sample preparation

The soil was oven dried for approximately 24 hours, crushed, and sieved through ASTM sieve No. 40 (425 μm). Then it was thoroughly mixed with the amount of water calculated as necessary to obtain the 22% initial moisture content. The mixture was sealed in an air-tight plastic bag and placed in a moist desiccator. It was allowed to cure at room temperature for about 24 hours. Thereafter, the 70 mm diameter, 19 mm thick oedometer samples were prepared in a purpose-made compaction unit containing the oedometer ring at an initial dry unit weight of 18 kN/m^3. Immediately after compaction, samples were transferred to the oedometer and the swell tests were performed.

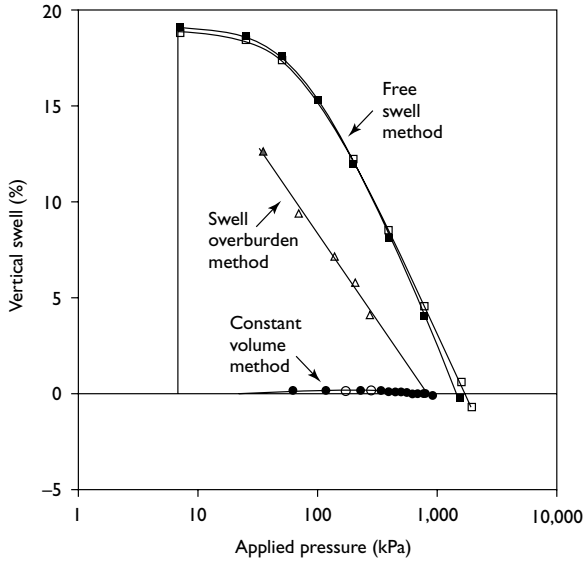

Figure 19.8 Comparison of test results from the three oedometer tests.

Free swell test

In this test, the specimen was inundated and allowed to swell freely under a seating load of 7 kPa until primary swell was complete. Thereafter, it was loaded (after primary swell has occurred) until its initial void ratio (height) was obtained. The swelling pressure was taken as the pressure that brings the sample back to its initial height (i.e. at 0% vertical swell). Two replicate tests were conducted and the results obtained are presented in Figure 19.8. The two tests led to a mean value of 19% vertical swell and 1700 kPa swelling pressure.

Constant volume test

Soil specimen was placed in the oedometer and its vertical expansion when flooded with water was prevented throughout the test. Sufficient load was applied to the specimen in increments until swell pressure was fully developed in soaked conditions. The pressure developed by the specimen when saturation was completed represented a direct measure of swelling pressure. The results of the two replicate tests are shown in Figure 19.8. The swelling pressure was found to be 960 kPa (mean of two tests). The swelling pressure was calculated from the sum of the load increments divided by the cross-sectional area of the sample.

Swell overburden test

In the swell overburden test, the specimen was loaded to vertical in situ overburden pressure and inundated under this pressure until the primary swell was completed. Five vertical

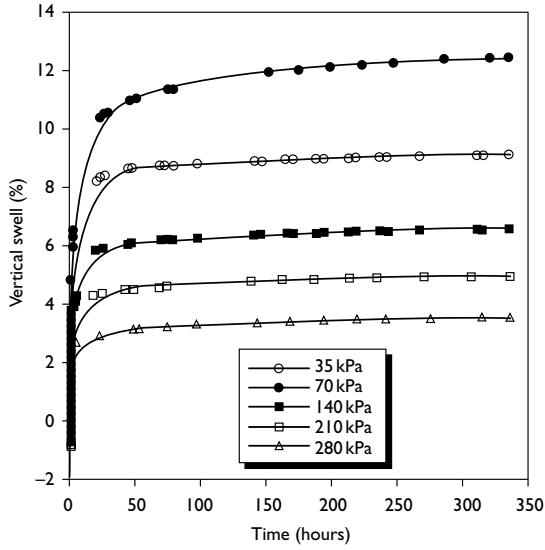

Figure 19.9 Variation of vertical swell with time from the swell overburden oedometer tests under different applied pressures.

pressures (35, 70, 140, 210, and 280 kPa) were applied on the samples in the oedometer. For each vertical pressure, two replicate tests were performed to ensure repeatability of test results. The total number of swell tests in this method was ten. The variation of vertical swell with time is shown in Figure 19.9 for the applied pressures. The vertical swell-time curves could be represented by a rectangular hyperbola which is in agreement with the findings of Dakshanamurthy (1978). The time/vertical swell versus time relationship could be represented by a straight line (Figure 19.10). The reciprocal of the slope of the straight line for each pressure in Figure 19.10 gives the maximum vertical swell. The swelling pressure in this method was determined to be approximately 880 kPa.

Triaxial swell test

The tests were conducted using a hydraulic triaxial stress path cell of the type reported by Bishop and Wesley (1975). In this apparatus, it is possible to measure the vertical swell of the sample directly, whereas in the conventional triaxial apparatus it has generally been possible only to measure the total volume change of the sample. Similar to the oedometer tests, samples were prepared after about 24 hours curing time with an initial moist content of 22% and initial dry unit weight of 18 kN/m^3. Preparation of the 35.5 mm diameter, 71 mm long triaxial samples consisted of statically compacting the soil in a purpose-made vertically split mold. Thereafter, the samples were transferred to the triaxial apparatus and the swell tests were initiated. Details of the procedure of swell testing in stress path triaxial apparatus are given by Al-Shamrani and Al-Mhaidib (1999). The same five vertical pressures used in

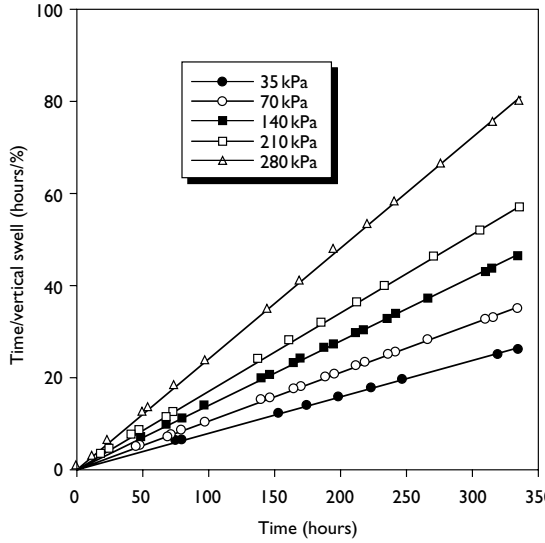

Figure 19.10 Time/vertical swell versus time from the swell overburden oedometer tests under different applied pressures.

the overburden swell oedometer tests were applied on the soil samples. The total number of swell tests was 10; 2 replicate tests for each vertical pressure were performed.

Figure 19.11 shows the swell behavior of the tested soil under the pressures applied. The time/vertical swell versus time relationship is shown in Figure 19.12. A straight line was not observed. Therefore, vertical swell-time curves can not be represented by a rectangular hyperbola. This method gave a swelling pressure of 1000 kPa.

Comparison of results

The magnitudes of vertical swell and swelling pressure obtained from the three methods of the oedometer test are listed in Table 19.2 and compared in Figure 19.8. There appears to be no definite relationship between the values from the three methods. Free swell test gives the highest value of vertical swell and swelling pressure and the swell overburden method gives the lowest value of swelling pressure. The magnitude of swelling pressure obtained from the constant volume method is in between. Free swell method is time-consuming since the specimen passes through two phases of deformation, complete expansion under seating load, and complete compression under different loads, whereas the constant volume method is quick. For both methods, only one specimen is required. The constant volume method provides a direct measure of the swelling pressure. The swell overburden method has the merit that it follows the probable stress path that a soil may undergo in the field. However, it requires at least three specimens, but it is less time consuming.

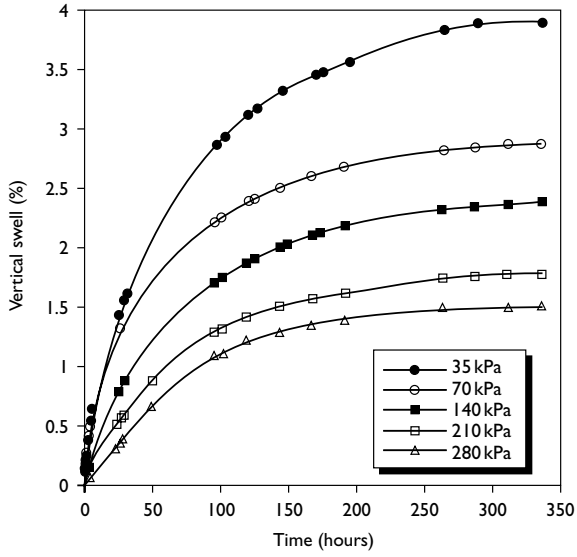

Figure 19.11 Variation of vertical swell with time from triaxial tests under different applied pressures.

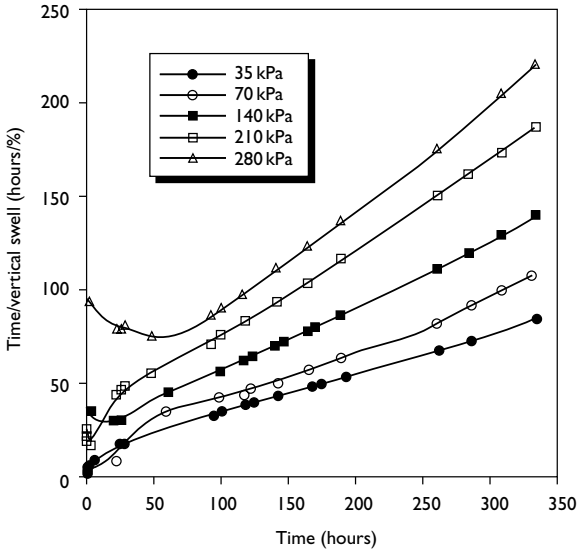

Figure 19.12 Time / vertical swell versus time from triaxial tests under different applied pressures.

Table 19.2 Comparative values of swelling potential by different oedometer methods

Method	*Maximum swelling potential*	
	Vertical swell (%)	*Swelling pressure (kPa)*
Free swell	19	1,700
Constant volume	—	960
Swell overburden	—[a]	880

Note
a see Table 19.3.

Table 19.3 Percentages of vertical swell from swell overburden oedometer test and triaxial test under different applied pressures (average of two tests)

Apparatus type	*Vertical pressure (35 kPa)*	*Vertical pressure (70 kPa)*	*Vertical pressure (140 kPa)*	*Vertical pressure (210 kPa)*	*Vertical pressure (280 kPa)*	*Swelling pressure (kPa)*
Oedometer	12.67	9.43	7.17	5.84	4.14	880.00
Triaxial	3.89	2.88	2.38	1.78	1.51	1000.00
Triaxial/oedometer	0.31	0.31	0.33	0.30	0.36	0.32[a]

Note
a Mean value.

The discrepancies in the swelling potential (vertical swell and swelling pressure) are due to differences in loading and wetting conditions in the oedometer tests. The free swell test does not represent the normal sequence of load wetting in the field. The soil in the field will not absorb water and swell first with the structural load applied later, but rather vise versa. The constant volume method also does not simulate the in situ condition, where the applied load after the structure is in service does not change with time. In addition, it does not present the expected amount of heave under the application of a certain load (structure load). The swell overburden method has the important advantage of being more representative of actual field loading and wetting conditions (El Sayed and Rabbaa, 1986). The data obtained by this method can provide useful information for design, such as swelling pressure corresponding to zero volume change, the expected vertical heave under the loads imposed by the structure, and the loads that could be applied to develop a certain swelling within tolerable imits.

The values of maximum vertical swell obtained from swell overburden oedometer tests and triaxial tests under different applied pressures are shown in Table 19.3. The maximum vertical swell was calculated by dividing the maximum increase in height of the sample by its initial height before it was given free access to water. The relationships between the mean of the maximum vertical swell (two tests) and logarithm of the applied pressure for the samples tested in oedometer (swell overburden method) and triaxial tests are shown in Figure 19.13. The relationships can be approximated by the following equations with a correlation coefficient, r^2, of approximately 0.99:

$$S_p(\%) = 26.5 - 9 \times \log(p) \quad \text{(oedometer test)} \tag{19.1}$$

$$S_p(\%) = 7.8 - 2.6 \times \log(p) \quad \text{(triaxial test)} \tag{19.2}$$

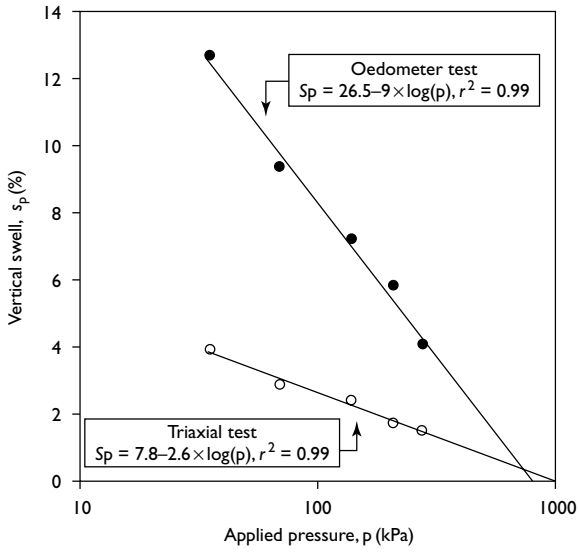

Figure 19.13 Comparison of vertical swell from swell overburden oedometer and triaxial tests.

where S_p is the vertical swell and p is the applied pressure (kPa). From these equations, the swelling pressure was determined to be approximately 880 kPa for oedometer tests and 1000 kPa for triaxial tests at 0% vertical swell. Furthermore, Equation 19.1 predicted the vertical swell under a pressure of 7 kPa to approximately 19%, the same as that found by the free swell test.

The values of vertical swell from the oedometer tests are higher than those from the triaxial tests for all the pressures applied. This may be due to many factors; the most significant are the differences in loading and wetting conditions in both types of equipment. The direction of swelling, lateral restraint in the apparatus, and the wetting of the sample are different in both types of equipment (Al-Shamrani and Al-Mhaidib, 2000). The triaxial test is more representative of the field conditions than the oedometer.

The variation of the ratio of vertical swells obtained from triaxial tests to those obtained from oedometer tests with the applied pressure is shown in Figure 19.14. The mean value of this ratio was approximately one-third (Table 19.3). Previous investigators (Gizienski and Lee, 1965; Dhowian *et al.*, 1990; Erol, 1992) found that laboratory results from oedometer tests overestimated the in situ heave by a factor of three. The reason for this discrepancy may be attributed to the fact that, in the field, swelling takes place in three dimensions rather than one dimension as imposed by laboratory oedometer tests. Other reasons are related to the fact that the in situ stresses on the soil were released after the soil sample was disturbed and brought to the laboratory to be tested. Dhowian *et al.* (1990) and Erol (1992) suggested that approximately one-third of the volume changes are reflected as a surface heave, while the remainder will be lateral. Therefore, when considering a restraint factor of one-third, swell overburden oedometer tests predict vertical swell very well when compared with the

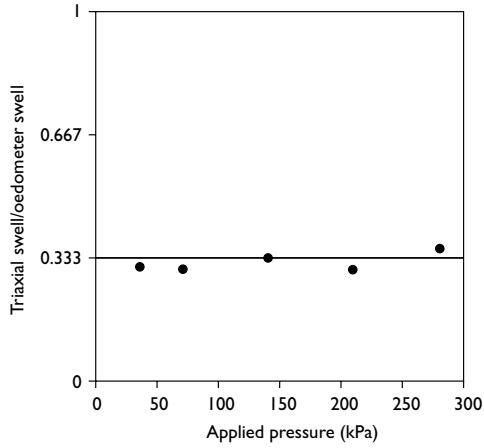

Figure 19.14 Ratio of triaxial vertical swell to oedometer vertical swell versus applied pressure.

measured swell in the field (Dhowian *et al.*, 1990; Erol, 1992). The results of the stress path triaxial tests provided good prediction of the vertical swell without using any restraint factor.

Dhowian (1990) found the percentage of swell in the field in the town of Al-Ghatt to be in the range of 3%–4% throughout the depths investigated (up to 5 m). The vertical overburden stresses in the field were approximately 66 kPa and 110 kPa at depths of 3 m and 5 m, respectively. The vertical swells obtained from the stress path triaxial tests were approximately 2.8% and 2.4% under pressures of 70 and 140 kPa, respectively. Therefore, it may be concluded that the stress path triaxial tests can predict the expected heave better than the swell overburden oedometer tests. Furthermore, the swelling pressure from the triaxial tests was found to be approximately 1000 kPa, close to that obtained by the constant volume oedometer test (960 kPa) which directly measures the swelling pressure.

Conclusions

The results of the different swell tests conducted on expansive shale from the case study area, middle region of Saudi Arabia, indicated significantly different values of swelling potential depending on the test technique used. The free swell test gave an upper bound value for swelling pressure, the swell overburden test provided the smallest value, and the constant volume method gave an intermediate value. This may be attributed to the differences in loading and wetting conditions followed in each method. The free swell method is time consuming but only one specimen is required. The constant volume method is a quick test, requires only one specimen, and provides a direct measure of the swelling pressure. The swell overburden method has the important advantage of being more representative of actual field loading and wetting conditions. However, it requires at least three specimens in identical initial conditions.

A comparison of the results from swell overburden oedometer tests and triaxial tests showed that triaxial tests provide lower values of vertical swell than those from the swell

overburden oedometer tests (i.e. approximately one-third). This ratio was in agreement with those suggested in the literature for the prediction of field heave from oedometer tests. Triaxial tests provided good prediction of vertical swell when compared with field data and also provided a swelling pressure value close to that obtained from the constant volume oedometer method which directly measures the swelling pressure. The stress path triaxial technique could predict the swelling potential of the soil better than the oedometer method.

References

Al-Shamrani, M.A. and Al-Mhaidib, A.I. (1999) Prediction of Potential Vertical Swell of Expansive Soils Using a Triaxial Stress Path Cell, *The Quarterly Journal of Engineering Geology*, 32, 45–54.

Al-Shamrani, M.A. and Al-Mhaidib, A.I. (2000) Swelling Behavior Under Oedometeric and Triaial Loading Conditions. *Geotechnical Special Publication No. 99, Advances in Unsaturated Geotechnics, Proceedings of Sessions of Geo-Denver 2000*, Denver, USA, pp. 344–360.

Bishop, A.W. and Wesley, L.D. (1975) A Hydraulic Triaxial Apparatus for Controlled Stress Path Testing, *Geotechnique*, 25, 657–670.

Dakshanamurthy, V. (1978) A New Method to Predict Swelling Using a Hyperbolic Equation, *Geotechnical Engineering*, 9, 29–38.

Dakshanamurthy, V. and Raman, V. (1973) A Simple Method of Identifying Expansive Soil, *Soils and Foundations*, 13, 97–104.

Dhowian, A.W. (1990) Field Performance of Expansive Shale Formation, *Journal of King Abdulaziz University* (*Engineering Sciences*), 2, 165–182.

Dhowian, A.W., Erol, A.O., and Youssef, A. (1990) *Evaluation of Expansive Soils and Foundation Methodology in the Kingdom of Saudi Arabia*, Final Report, KACST, AT-5-88.

El Sayed, S.T. and Rabbaa, S.A. (1986) Factors Affecting Behavior of Expansive Soils in the Laboratory and Field- A Review, *Geotechnical Engineering*, 17, 89–107.

Erol, A.O. (1992) In-situ and Laboratory Measured Suction Parameters for Prediction of Swell, in *Proceedings of the Seventh International Conference on Expansive Soils*, Dallas, TX, USA, pp. 30–32.

Gizienski, S. F. and Lee, L. J. (1965) Comparison of Laboratory Swell Tests to Small Scale Field Tests, in *Engineering Effects of Moisture Changes in Soils; Concluding Proceedings of the International Research and Engineering Conference on Expansive Clay Soils*, Texas A&M Press, Texas, USA, pp. 108–119.

Puppala, A.J., Katha, B., and Hoyos, L.R. (2004). Volumetric shrinkage strain measurements in expansive soils using digital imaging technology, *Geotech Testing Journal.*, *ASTM*, Vol. 27, No. 6.

Ruwaih, I.A. (1987) Experiences with Expansive Soils in Saudi Arabia, *Proceedings of the Sixth International Conference on Expansive Soils*, New Delhi, India, pp. 317–322.

Seed, H.B., Woodward, R.J. Jr, and Lundgren, R. (1962) Prediction of Swelling Potential for Compacted Clays, *Journal of Soil Mechanics and Foundation Engineering Division, ASCE*, 88, 53–87.

Slater, D.E. (1983) Potential Expansive Soils in Arabian Peninsula, *Journal of Geotechnical Engineering, ASCE*, 109, 744–746.

Van Der Merwe, D.H. (1964) The Prediction of Heave from the Plasticity Index and Percentage Clay Fraction of Soils, *Civil Engineers in South Africa*, 6, 337–342.

Chapter 20

Volume change characteristics of compacted Ankara clay

Erdal Cokca[1] *and Ozlem Cora*[1]

Summary

Volume change characteristics of compacted clays are very important in geotechnical problems. In the case study area in Turkey, heave of earth embankments constructed by Ankara clay have been observed. In this investigation, the effects of swell on volume change characteristics of compacted Ankara clay specimens were investigated. To identify the volume change behavior of samples, compaction water contents were at the dry side of optimum (i.e. $w/c = 17\%$), at optimum (i.e. $w/c = 23\%$), and at the wet side of optimum (i.e. $w/c = 24.5\%$). Oedometer tests were done on both the compacted specimens at compaction moisture content and on soaked specimens (i.e. after swell). According to test results, vertical displacement under the same consolidation pressure for soaked specimen (i.e. after swell) was greater than for specimens compacted at compaction moisture content. The coefficient of volume compressibility decreased with increasing water content and stress level. Under the same consolidation pressure, the value of the coefficient of volume compressibility for soaked specimens (i.e. after swell) was greater than for specimens at compaction moisture content.

Introduction

Most man-made earth structures involve the use of compacted soils. Volume change behavior of compacted soils has been an important subject for soil engineers and has been studied extensively (Ladd, 1959; Seed, *et al.*, 1962a,b; Aitchinson, 1965; Burland, 1965; Fredlund and Morgenstern, 1977; Fredlund and Rahardjo, 1993).

The amount of surface heave/settlement depends on the soil composition (i.e. compacted soils may contain expansive clay minerals), fill depth, compressibility characteristics of the soil, and the extent of wetting. An estimate of heave/settlement can be made based on laboratory test results and assuming full wetting, or partial wetting. It seems prudent to make conservative estimates of future wetting at the design stage. The source of wetting is primarily by rainfall. Occasionally rising groundwater may be a source of wetting. In addition, broken utility lines, utility trenches, street subgrades, permeable layers, gravel packed subdrains, all act as subsurface conduits that lead water to fill. It seems, therefore, that the

[1] Department of Civil Engineering, Middle East Technical University, 06531 Ankara, Turkey; email: ecokca@metu.edu.tr

practical design approach would be to assume that the significant part of the fill mass will eventually get soaked to some degree.

Compacted soil offers a good opportunity for obtaining a desirable soil structure (Mitchell, 1993). In clays, the moisture content controls the ease with which particles and particle groups can be rearranged under the compactive effort (Mitchell 1993, Cokca *et al.*, 2004). Increasing the moisture content tends to increase the interparticle repulsions, thereby permitting a more orderly arrangement of the soil particles to be obtained with a given amount of effort. Clay compacted dry of optimum simulates a flocculated structure, clay compacted wet of optimum simulates a dispersed structure, and clay compacted at optimum moisture content simulates an intermediate soil structure (Lambe and Whitman, 1979).

The term expansive soil applies to soils which have the tendency to swell when its moisture content is increased (Chen, 1975). According to Nelson and Miller (1992) flocculated clays are more expansive than dispersed clays.

In the case study area, Ankara, heave of earth embankments constructed by Ankara clay have been observed (Cokca, 1991, Avsar *et al.*, 2005). The present work studied the influence of initial soil structure and swell on the volume change characteristics of compacted Ankara clay. For identifying the behavior of specimens more clearly, oedometer tests were performed on both compacted specimens at compaction moisture content and on soaked specimens (i.e. after swell). The effect of swell on the volume change of the soil sample was observed and results were evaluated.

Experiment

Soil properties

The soil, Ankara clay, was classified as a CL soil according to Unified Soil Classification System (ASTM D 2487-92) (Table 20.1). The grain-size and dry density versus moisture content curves of the soil sample used are shown in Figures 20.1 and 20.2 respectively. Compaction tests were performed on soil samples in a proctor compaction mold using standard compactive effort. According to the Standard Proctor Compaction test results the maximum dry density of the soil sample was 1.565 Mg/m^3 and the optimum moisture content was 23%.

Oedometer test

To evaluate volume change characteristics of soil samples with varying moisture contents volume change tests (oedometer tests) were performed in the laboratory. In these tests, volume

Table 20.1 Soil properties

Clay content (grain size <2 μm)	(ASTM D 422-1963 and D 1140-92)	20%
Liquid limit, LL	(ASTM D 4318-84)	48%
Plastic limit, PL	(ASTM D 4318-84)	25%
Plasticity index, PI	(ASTM D 4318-84)	23%
Specific gravity, G_s	(ASTM D 854-92)	2.66
Activity = PI/(C-10)		2.3

Note
C: % finer than 2 μm.

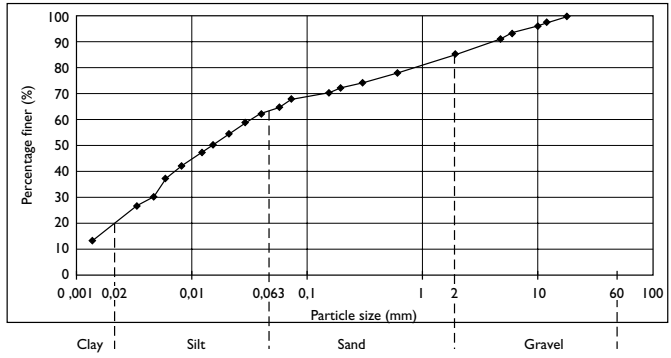

Figure 20.1 Grain-size curve.

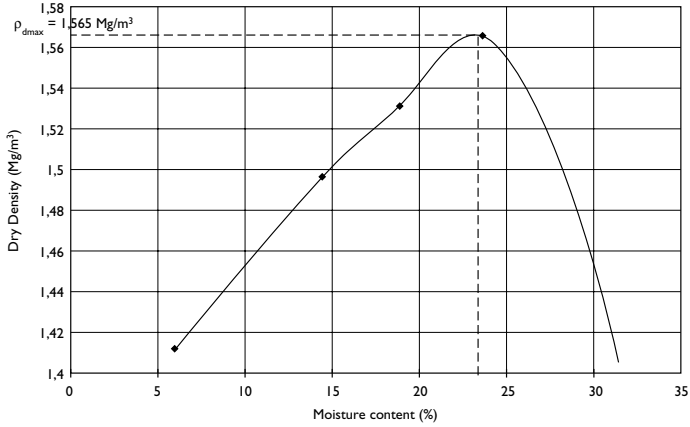

Figure 20.2 Dry density versus moisture content.

change of soil specimens under various surcharge pressures and with various moisture contents were obtained. The oedometer tests (ASTM D 4546-96) were conducted on compacted soil at different compaction states; dry side of optimum (i.e. $w/c = 17\%$), at optimum (i.e. $w/c = 23\%$), and at the wet side of optimum (i.e. $w/c = 24.5\%$) moisture contents (ASTM D 4959–89). In the experiments four different surcharge loads were applied to specimens, these are 25, 75, 150, and 225 kPa. All tests were performed on the specimens compacted at the compaction moisture content and on soaked (after swelling) specimens to see the effect of compaction moisture content and soaking on the volume change properties of the specimens. Consolidation machines that are used for consolidation tests of this study were "Soil Test Inc." type.

In order to prepare and test remolded soil sample at compaction moisture content, a predetermined weight of oven-dried soil sample pulverized and passing sieve number 40

was used to get the required initial dry density. Appropriate amount of water was added to the dried soil and mixed carefully to get the required initial water content. Then the mixed soil was kept in an airtight container for 24 hours to allow for uniform distribution of moisture. Soil was placed into the mold and the standard 2.5 kg hammer was dropped 25 times on each layer and soil was compacted in three layers. Specimen was taken from the mold, placed in the oedometer and exposed to loadings of 25, 75, 150, and 225 kPa. For each loading different specimens were prepared at desired water content. After 24 hours, settlement readings were completed.

In order to prepare and test the soaked soil sample, specimens were prepared at Proctor compaction mold at desired water content. Specimens were taken from the mold and placed in the oedometer. After that specimen was soaked (i.e. allowed to swell), there was a 24-hour waiting period without any loading. After this period, specimens were loaded at consolidation loading (i.e., 25, 75, 150, and 225 kPa). After 24 hours of loading, the settlement readings were completed. After the consolidation tests were completed strain versus applied pressure graphs were obtained for each specimen (Figure 20.3).

Swell potential

The specimens in this test were prepared at the given dry density and water content and then placed in the oedometer. After the specimen was placed in the oedometer device, water was added and the sample was allowed to swell under an applied pressure of 7 kPa (ASTM D 4546-96). Readings of swell deformation due to addition of water were taken. It was seen that 24 hours was enough to reach the ultimate swell. The swell potential was calculated as the ratio of the maximum swell height of the specimen due to wetting to the initial height of the specimen. Swell potentials were found as 7.5%, 6.9%, and 6.9% for specimens compacted at dry of optimum, at optimum and at wet of optimum moisture contents respectively. According to Seed *et al.* (1962b) specimens have high swell potentials.

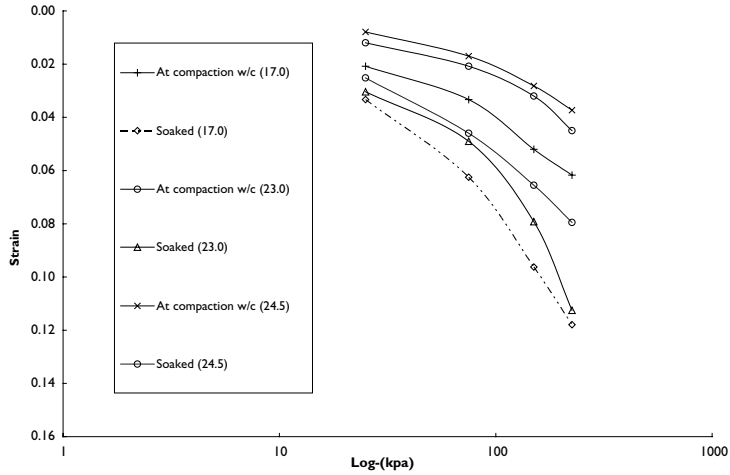

Figure 20.3 Strain versus log pressure relationships.

Table 20.2 Coefficient of volume compressibility (m_v) values (m^2/MN)

Initial water content (%)	*Normal stress range* σ					
	Sample compacted at compaction water content			*Soaked sample*		
	25–75 (kPa)	*75–150 (kPa)*	*150–225 (kPa)*	*25–75 (kPa)*	*75–150 (kPa)*	*150–225 (kPa)*
17.0	0.265	0.200	0.130	0.610	0.480	0.320
23.0	0.175	0.150	0.095	0.317	0.350	0.300
24.5	0.187	0.148	0.125	0.423	0.267	0.196

Table 20.3 Ratio of coefficient of volume compressibility (m_v) values of soaked and compaction water content samples

Initial water content (%)	$m_{v\,(\text{soaked})}$ / $m_{v\,(\text{compaction water content})}$		
	Normal stress range, σ *= 25–75 (kPa)*	*Normal stress range,* σ *= 75–150 (kPa)*	*Normal stress range,* σ *= 150–225 (kPa)*
17.0	2.3	2.4	2.5
23.0	1.8	2.3	3.2
24.5	2.3	1.8	1.6

Results and discussion

In this study volume change characteristics of compacted Ankara clay were investigated. To identify the volume change behavior of samples more clearly, experiments were done on both compacted samples at compaction moisture content and on soaked samples (after swell). Compaction water contents were at dry side of optimum (i.e. $w/c = 17\%$), at optimum (i.e. $w/c = 23\%$), and at wet side of optimum (i.e. $w/c = 24.5\%$).

Figure 20.3 shows that vertical strain at the same consolidation pressure for soaked samples (after swell) was greater than for samples compacted at compaction moisture content. It can be seen from Tables 20.2 and 20.3 that the coefficient of volume compressibility for soaked samples (after swell) were, on average, more than two times greater than for samples compacted at compaction moisture content (i.e. at dry of optimum, at optimum, and at wet of optimum moisture contents). Table 20.2 shows that the coefficient of volume compressibility decreased with increasing pressure for the samples compacted at compaction moisture content and for the soaked samples.

In closing, if Ankara clay is to be used as a fill material, damage to structures may not only be due to swelling and shrinking, but also due to a change in the compressibility of the soil due to the swelling.

References

Aitchinson, G.D. 1965. Shear strength and consolidation, *Proceedings of the 6th International Conference on Soil Mechanics and Foundation Engineering*, Session 2 – Division 2, Vol. 3, 318–321.

ASTM 1963. *Standard test method for particle-size analysis of soils*. Annual Book of ASTM Standards, D 422-63, 04.08, 93–99.

ASTM 1984. *Standard test method for liquid limit, plastic limit, and plasticity index of soils*. Annual Book of ASTM Standards, D 4318-84, 04.08, 682–691.

ASTM 1989. *Standard test method for determining of water (moisture) content of soil by direct heating method*. Annual Book of ASTM Standards, D 4959-89, 04.08, 1153–1156.

ASTM 1992. *Standard test method for specific gravity of soils*. Annual Book of ASTM Standards, D 854-92, 04.08, 176–179.

ASTM 1992. *Standard test method for amount of material in soils finer than the no.200 sieve.* Annual Book of ASTM Standards, D 1140-92, 04.08, 191–193.

ASTM 1992. *Standard classification of soils for engineering purposes (unified soil classification system)*. Annual Book of ASTM Standards, D 2487-92, 04.08, 325–334.

ASTM 1996. *Standard test method for one – dimensional consolidation properties of soils*, Annual Book of ASTM Standards, D 4546-96, Vol. 04.08, Philadelphia, USA, 210–219.

ASTM 1996. *Standard test method for one-dimensional swell or settlement potential of cohesive soils*, Annual Book of ASTM Standards, D 4546-96, Vol. 04.08, Philadelphia, USA, 672–678.

Avsar E., Ulusay, R. and Erguler, Z.A. 2005. Swelling properties of Ankara (Turkey) clay with carbonate concretions, *Environmental and engineering geoscience*, XI(1), 75–95.

Burland, J.B. 1965. Some Aspects of the Mechanical Behaviour of Partly Saturated Soils, Moisture Equilibrium and Moisture Changes in Soil Beneath Covered Areas, Australia, Butterworth.

Chen, F. H. 1975. Foundations on expansive soils, *Developments on geotechnical engineering* 12, Elsevier Scientific Co., Amsterdam.

Cokca, E. 1991. Swelling Potential of Expansive Soils with a Critical Appraisal of the Identification of Swelling of Ankara Soils by Methylene Blue Test, PhD Thesis, Department of Civil Engineering, Middle East Technical University, Ankara, Turkey, p. 325.

Cokca E., Erol, O., and Armangil, F. 2004. Effects of compaction moisture content on the shear strength of an unsaturated clay, Technical Note, *Geotechnical and geological engineering*, 22, 285–297.

Fredlund D.G. and Morgenstern N.R. 1977. Stress-state variables for unsaturated soils, *ASCE, Journal of Geotechnical Engineering Division*, GT5, Vol. 103, 1415–1416.

Fredlund D.G. and Rahardjo, H. 1993. *Soil mechanics for unsaturated soils*, John Wiley and Sons Inc., pp. 38–105, 247–258.

Ladd C.C. 1959. Mechanism of swelling by compacted clay, *Highway Research Board*, Bulletin, Annual Meeting.

Lambe, T.W. and Whitman, R.W. 1979. *Soil mechanics*, John Wiley and Sons, New York.

Mitchell, J.K. 1993. *Fundamentals of soil behaviour*, John Wiley and Sons, New York.

Nelson, J.D. and Miller, D.J. 1992. *Expansive soils, problems and practice in foundation and pavement engineering*, John Wiley and Sons Inc., New York.

Seed, H.B., Mitchell, J.K. and Chan, C.K. 1962a. Studies of swell and swell pressure characteristics of compacted clays, *Highway Research Board Bulletin*, Vol. 313, 12–39.

Seed, H.B., Woodward, R.J. and Lundgren, R. 1962b. Prediction of swelling potential of compacted clays, *Journal of ASCE, Soil Mechanics and Foundations Division*, Vol. 88, SM3, 53–87.

Chapter 21

Influence of trees on expansive soils in southern Australia

Donald A. Cameron,[1] *Mark B. Jaksa,*[2] *Wayne Potter,*[1] *and Aaron O'Malley*[1]

Summary

Tree-related desiccation is likely to cause greater ground movements than normal in the dry season. This extra soil movement may result in unsightly and perhaps structural damage. This chapter will present a review of the influence of trees on expansive clay soils and how designs might be attempted to minimize the risk of damage to buildings, due to the deep drying that can result from trees. Results will be presented on two major projects dealing with trees and foundations. The first study will demonstrate that trees in the right situation (rail corridor) can actually help to stabilize foundations. The findings of the second study will demonstrate that demand for water is dependent on species.

Introduction

The combination of reactive soils and semi-arid climates means that houses and pavements must withstand significant soil movements. Trees in an urban environment can add to these movements and can cause unacceptable distortions and cracking. However, trees are an environmentally desirable part of urban streetscapes. In Australia, street trees are provided by Local Government Authorities to improve the landscape, enhance the environment, and usually to maintain or increase land values. Apart from their aesthetic value, trees provide a valuable habitat for fauna and extend the urban wildlife corridor, thereby protecting and enhancing biodiversity (Moore, 1997). Trees however, may present a nuisance if they become too large for the streetscape, lose branches in storms or uplift pavements.

The research reported in this chapter is concerned with the indirect damage to pavements and buildings caused by trees, through the extraction of moisture from clay soils, causing deep drying and shrinkage settlement. Past research has shown that tree root systems can generate shrinkage settlements in reactive clay soils at appreciable depths of over four metres or more (Richards *et al.*, 1983; McInnes, 1986). Tree-related desiccation is likely to cause greater ground movements than normal in the dry season. This extra soil movement may result in unsightly and perhaps structural damage.

Generally, free-standing masonry or masonry veneer houses in Australia over 10 years old have not been designed to cater for tree-drying effects and are at a greater risk of damage

[1] University of South Australia, School of Natural and Built Environments; email: donald.cameron@unisa.edu.au
[2] University of Adelaide, School of Civil & Environmental Engineering.

than recently built houses. Indeed, even the current Australian Standard AS2870-1996 (Standards Australia, 1996) for the design of footings does not provide directly for the influence of trees on foundations. Rather, the Standard encourages the avoidance of manageable extreme moisture changes and in particular, distancing trees from dwellings. The site classification scheme, which affects footing design, assumes reasonable site maintenance practices are adhered to throughout the life of the dwelling and trees are kept sufficiently far away, so that they have no influence on the design site movement. Design suction changes are assigned to regional areas throughout Australia for a range of climatic conditions.

AS2870 recommends proximity rules, which are designed to keep vegetation sufficiently far from houses so as to minimize their influence. Proximity rules are expressed in terms of the ratio D : H, where D is the minimum horizontal distance between the tree trunk and the walls of the building, and H is the mature height of the tree. The proximity ratios recommended by AS2870-1996 can be more stringent than Ward's (1953) rule (D : H = 1). The D : H ratio increases with the level of site classification for expansive clay movement as described by AS2870-1996, and also if more than one tree is present. AS2870's planting guidelines do not distinguish movement risk on the basis of species.

With the current trend in Australia toward smaller housing allotments, the prescribed safe distances for rows of street trees may lead to a relatively treeless urban environment in areas of clay-rich soil profiles, a situation which would be aesthetically unacceptable (Flora, 1978). Building over once-treed sites also poses a problem, as soil moisture is regained and the soil swells within the previous area of influence of the trees and below the new construction (Samuels and Cheney, 1975). Although AS2870 recognizes the problem, it does not provide any specific guidelines for designers. Attempts have been made in the past to pre-water sites. Such attempts require an understanding of the drying zone, which is commonly deep, so watering of deep boreholes is required usually to effectively recover water loss. Ground movements and soil moisture changes should be monitored while watering to evaluate the extent of recovery.

Footing design engineers try to minimise the risk of soil shrinkage settlements by excluding trees or, more recently, by designing footings according to local rules to cater for anticipated soil movement (without trees). Current design criteria for "tree-designs" are based on simplistic empiricism, as very little information is available on the relative water usage of different tree species in the urban environment. Without this information, footings are either being overdesigned, adding substantially to building costs, or underdesigned, resulting in footing failures as the trees reach maturity.

This chapter will present a review of the influence of trees on expansive clay soils and how designs might be attempted to minimize the risk of damage to buildings, due to the deep drying that can result from trees.

National guidelines

The South Australian capital, Adelaide, and its suburbs, suffers the most powerful combination of expansive soils and climate of any capital city within Australia. Footing design has developed substantially there and has provided guidance to the rest of Australia. International research influenced Australian developments, especially that of Lytton from Texas A&M (e.g. Lytton, 1972). The first release of national design guidelines for identification of reactive soil sites and design of shallow footings (raft slabs, strip footings) was in 1986, with two subsequent major revisions culminating in AS2870-1996. Examples of the

research effort that resulted in the Standard can be found in papers by Aitchison *et al.* (1973), Holland (1981), Mitchell (1984), Walsh (1985), and Cameron (1989).

Currently, expansive (or reactive) clay sites are classified in accordance with the Australian Standard 2870-1996 as "Slightly," "Moderately," "Highly," or "Extremely" reactive, depending on the amount of the design ground surface movement, y_s, expected over the 50 year design life of a house in an urban environment. The site classification assumes reasonable site maintenance practices are adhered to throughout the life of the dwelling. New homeowners are supplied with CSIRO Building Technology File pamphlet, BTF18 (CSIRO, 2003), which advises homeowners on site maintenance and expected footing performance, and which discusses the threat of shrinkage settlement represented by close trees on reactive clay sites.

Regional environmental conditions play an important role in the behavior of soils. Climate dictates the design level of soil moisture changes at a site and therefore the site classification. Annual variations in intensity of rainfall and evaporation, depth of ground water table and site drainage patterns influence both the extent and the pattern of ground movements on a reactive site. Soil profiles at a site can vary markedly, leading to differences in movement across a site, even if the site experiences a uniform change in soil moisture condition.

Australian Standard AS2870 recognizes that urbanization causes environmental changes, which can lead to greater depths of movement and a moderation of seasonal climatic effects. On a well-drained and uniformly reactive site, these environmental changes lead to initial dishing of the ground under a house and, in subsequent years, a doming distortion is likely to develop. As the soils beneath the edges of a house undergo almost seasonal variation in moisture condition, dishing is most noticeable over the winter–spring period in a semi-arid environment, while doming is most distinct during summer–autumn. Civil engineers design footings to moderate these movements in order to avoid large deflections of the structure, and hence significant distortion and cracking of susceptible walls.

Soil suction

Australian Standard AS2870 relies on total suction changes (the sum of matric and solute suction changes) to define desiccation in soil profiles and to predict the volume changes within the soil profile. Soil suction is the negative pressure of the pore water in the soil, usually expressed on a logarithmic scale. High suctions infer low moisture contents or dry soil. The usual range of soil suctions in the field in a semi-arid climate is approximately 100 kPa to 10 MPa. Soil suction is related to the moisture content of a soil, but the relationship changes with each and every soil type. A linear relationship is usually assumed between suction and gravimetric moisture content, although it seldom is linear over the full range of moisture conditions.

In Australia, laboratory hygrometers are used to measure total suction on soil cores in a controlled environment. The determination relies on the measurement of dew point temperature of a small air space above the soil, which has come into equilibrium with the soil sample at the ambient temperature.

Influence of trees on clay

Much of what we know about trees is based on indirect evidence. For example, the aggressiveness of different root systems of trees near water pipes was revealed in studies of

root chokes by the Engineering and Water Supply Department (South Australia) in Adelaide (Baker, 1978). Cameron and Earl (1982) published information on potential damage to houses by trees, based on this information. It was assumed in the adoption of these species that climate differences around Australia would make little difference, although it is well known that the extent of a tree root system is greatly affected by water availability (Yeagher, 1935).

Ward (1953) in the UK recommended safe planting distance of trees to avoid soil shrinkage settlement and damage to buildings. He prescribed the first "proximity rule" of D : H equal to one. In Canada, Bozozuk (1962) demonstrated the decrease of drying settlements with distance from a row of 17 m high elm trees. In the UK in the mid 70s, a severe drought caused much shrinkage settlement and it was realised that a large proportion of the ground movement under footings was related to the drying effects of trees. Further research effort was initiated in response to the widespread damage observed during the drought (e.g. Cutler and Richardson, 1981; Biddle, 1983; Driscoll, 1983).

Biddle (1983, 2001) conducted studies of soil moisture deficits around specimens of certain tree species in open grassland. Five different clay soil profiles were investigated at three locations underlain by clay soils. Soil moisture was monitored with a down-hole neutron moisture meter to a maximum depth of 4 m. Generally, it was seen that the lateral extent of drying was contained within a radius equal to the height of the tree. However, the depth and radius of drying, both horizontally and vertically, appeared to be species-dependent. Poplars caused drying to a radius of over 1.5 times the tree height and caused the deepest drying close to the trees, probably to a depth in excess of 4 m.

Cutler and Richardson (1981) reported on 2,600 cases of building damage in the UK. Trees implicated as a cause of the damage were recorded and their proximity to the building noted. A database of species was established and was reviewed to find the maximum distance for a tree to "cause" damage in 75% of the cases recorded for that species. The greater the distance relative to the height of the tree ($D : H_{75\%}$), the more dangerous the tree. Unfortunately, the information has had little impact on Australian practice owing to differences in climate, differences in tree species, and different sensitivities to damage between homeowners in the UK and Australia (Radevsky, 2000). In fact, the degree of damage was not considered and may have often been insignificant in the Australian context. Furthermore, the usual construction in England is cavity brick walls on strip footings, which is far less tolerant to movement than masonry veneer walls on a stiffened raft, the dominant construction style in Australia.

In the USA in Texas, Tucker and Poor (1978) studied a housing estate, which was in the process of being demolished because of the extent of damage to the houses (masonry veneer walls on slabs). Tree species were mulberry, elm, cottonwood, and willows. Differential movements were measured and compared with D : H ratios. The results of the study revealed an average background movement of approximately 50 mm due to site reactivity, which was apparent at D : H ratios above two. The data strongly indicated that tree effects were significant at D : H values greater than one. Differential movements in excess of 120 mm were observed, where trees were close to the building.

In New Zealand, Wesseldine (1982) demonstrated the influence of the silver dollar gum (E. cinerea) on houses. The research indicated a threshold value of D : H of 0.75 for single trees to cause damage and 1.0 to 1.5 for groups of these trees. The extent of damage was not included in the correlation.

Early research in Australia on the effects of trees was not reported widely until the mid-1980s (e.g. Richards *et al.*, 1983; Cameron and Walsh, 1984; Pile, 1984). This research

was related largely to appraisals of damaged buildings. In Melbourne, studies of damaged masonry veneer houses on strip footings (Holland, 1982; Cameron and Walsh 1984) concluded that significant damage was only likely if the proximity of a single tree was less than or equal to 0.5 times the tree height, H. Pile (1984) reported building distortions and suction profiles to a maximum depth of 4 m in Adelaide, which were affected partly by trees.

Richards *et al.* (1983) studied total soil suction regimes near groups of three different species of trees in parkland in Adelaide, South Australia. The tree groups were described as eucalypts, casuarinas, and pines. Soil samples were taken from boreholes made progressively away from the tree groups. The eucalypts had the greatest drying effect, while the pines had little effect on the surrounding clay soil. For the eucalypt site, the total soil suction reached 3.5 MPa at depth below the group of trees, and was not lower than 2 MPa throughout the exploration depth of 8 m. The radial extent of near-surface drying appeared to be 1.3 times the average height of the trees, H_{av}. The depth of drying decreased with distance away from the group.

Silvestri *et al.* (1992) studied movements over three years of two damaged buildings in Montreal, Canada, and the associated patterns of soil movements, particularly around rows of maple trees adjacent to the buildings. Two catalpa trees also influenced the more severely damaged building. This work was unique in that investigations of building distress were allowed to continue over a significant period of time, allowing the installation of 3 or 4 neutron moisture meter access holes at each site to a depth of about 3 m, and the monitoring of soil moisture.

Wilting point concept

Vegetation is unable to draw moisture from the soil at high levels of soil desiccation, or soil suction. The "limit" at which this occurs is termed the wilting point and its value differs with species. Values of total suction of 1.55 to 3.1 MPa corresponding to the wilting point have been reported by McKeen (1992). If roots encounter soil at the wilting point, then the roots may extend into new areas of the profile, where there is greater water availability, otherwise the vegetation may die, or the plant may become dormant until water becomes available; all these possibilities being dependent on species.

Cameron (2001) inferred the wilting points of trees from total soil suction data gathered around damaged house sites. Trees were found to cause deep drying in Adelaide soils to approximately 4 m depth for an isolated tree and 6 m for a group or cluster of trees. Tree roots could not compete with the high levels of near surface desiccation in seasonally dry periods.

Cameron recognized that the differences in total suction across a site were more important than the absolute values of suction, particularly as soil salinity can affect the suction values from one site to another (Richards *et al.*, 1983). So the divergence from the equilibrium soil suction was used to express the level of soil desiccation caused by a given species. It is generally accepted that total soil suctions become relatively constant at depth, in soil profiles with deep water tables, which are unaffected by vegetation. This suction value is termed the deep equilibrium suction, u_{eq}, which is also the suction expected under the center of a large paved area in the same environment (Richards and Chan, 1971).

Jaksa *et al.* (2002) adopted a similar strategy to that of Cameron (2001) for analysis of a further two treed sites in Adelaide, with one site having a group of trees and the other site accommodating a single large eucalypt.

Current footing design practice in Australia

In 1986, Standards Australia, AS2870, adopted a philosophy of designing for footings, assuming that trees were sufficiently distant from the structure not to cause any untoward effects. The proximity rules were modified to include potential effects of site reactivity and the density of tree planting, but not tree species. This philosophy has remained intact. Despite there not being a prescriptive Standard for designing for the tree drying, engineers have been pressed by the community to accommodate the extra soil settlement that may arise. Knowledge of the in situ soil suction changes around trees is essential to reliably estimate the ground movement in expansive clay soils. Once the magnitude and pattern of the ground movement is known, footings can be structurally designed to mitigate adverse effects and to facilitate an acceptable performance of the structures they support.

Currently, additional design soil suction changes are provided in the guidelines of the Footings Group (1996), where trees are present on a site. These suction changes do not recognize either any influence from tree species or the concept of "wilting point." Design suctions generated by trees using the Footings Group approach tend to be much higher than observed suctions at the wilting point, especially for groups of trees. However, no account is taken of the potential extra drying depth associated with tree groups.

Water potential of plants

As water is lost from the leaves of a tree through transpiration, an essential part of photosynthesis, a negative potential or suction is set up within the leaf (Kozlowski, 1982). The suction caused by leaf water loss provides the pulling power to drive water from the soil through the plant's continuous system to the foliage (Biddle, 2001). This "continuous system" is composed of the interactions between the soil, root, xylem, and foliage (O'Malley, 2001).

A measure of the components of water potential in a plant is necessary to fully understand and explain the nature of plant water stress and soil water deficits (Campbell, 1985). The components of water potential, namely osmotic, turgor, and matric potential, represent the principal forces affecting the energy status of water in plant tissues (Wiebe, 1972).

Leaf water potential (LWP) is one measure of the potential of the tree to extract water from the soil, similar in concept to soil suction. Hygrometers may be used to measure total suction indirectly through measurement of dew point temperature in situ on intact leaves; the LWP is reported in MPa. A negative potential or suction is needed to drive the water through the plant and the atmosphere, through humidity, providing the potential to move water from the soil through the plant's xylem to the foliage (Knox *et al.*, 1994). Leaf water potential does not, however, measure the water use of trees. It does indicate the potential of the species to extract water from the soil under differing conditions.

Xylem pressure or stem suction is another measure of the potential of trees to extract water from the soil. A freshly cut stem is placed in a chamber with one end outside the chamber. The chamber is pressurized until sap is seen to exude from the stem. The pressure at which this occurs is equivalent to the stem suction (Dixon and Tyree, 1984). Only a few attempts have been made to directly correlate LWP and xylem pressure and only on a limited number of species (Dixon and Tyree, 1984; Savage and Cass, 1984; Schaefer, 1989; Melcher *et al.*, 1998; Bernardi, 2000).

Research on soil water extraction, evapotranspiration, tree water use, and stomatal behavior is mainly associated with forestry plants and agricultural crops (Ravina, 1983; Balling and Zimmermann, 1990; Raper, 1998; Stewart and Sand, 1998; Hatton *et al.*, 1999; Bernardi, 2000), but similar information for ornamental plant species used in urban areas is very limited. The research of Misra and Sands (1989) was unique in that it investigated the physiology (by measuring sap flux) of two ornamental species, as well as ground movements, in a park in Melbourne, the capital city of the State of Victoria in Australia.

Research data on the role of trees in extracting water from the soil and tree desiccation (i.e. suction profiles) is also very limited, particularly for trees in an urban environment. Consequently, there are no rational planting guidelines for tree species or footing designs for reactive sites planted with trees.

Research with trees on reactive clay sites

Researchers at the University of South Australia are involved in two major research projects concerned with trees on expansive clay soils. One project is investigating the feasibility of stabilizing poorly-drained, clay subgrades under rail formations by re-vegetating the rail corridor. Although the drying effect of the trees on the soil will cause shrinkage settlement, these movements can be managed; in the long term the rail formation will be more stable to loads from train traffic, as the strength and stiffness of the subgrade will be improved. The improvement in soil properties has been demonstrated at four sites by comparing treed and non-treed sections of the sites at the peak seasonally dry and wet periods (Potter *et al.*, 2004; Potter and Cameron, 2005).

The second project is a long-term investigation of the influence of a range of street trees on soil moisture patterns within a modern housing subdivision (generally consisting of single storey, masonry veneer construction on concrete raft slabs). A number of sites within the subdivision have been monitored for three years. Most of the sites are on extremely reactive clay sites. It is a long-term research project as the trees are immature and the garden watering regime has been excessive – to date, the influence of the trees has been negligible. However, observations of tree physiology have been made, which suggest that movements due to street trees may become significant.

Trees in rail corridor

Details of the sites and the methodology of the research are reported by Potter *et al.* (2004) and Potter and Cameron (2005). In the present paper, only the suction data will be discussed for the three Victorian sites, which were generally within the same regional climate.

Average climate data for Western Victoria are provided in Figure 21.1. The three sites were within 100 km of each other across an area which is classified as semi-arid. The average climate data shows that Western Victoria usually experiences highest rainfalls during the winter months (June to August) when temperatures and evaporation rates are at their lowest levels. Monthly rainfall exceeds pan evaporation in both June and July.

Existing trees in the rail corridor are planted in rows, sometimes along each side of the corridor, as at the Wal Wal site, but often along just one side, as at Miram and Horsham. Table 21.1 provides details of trees at the vegetated sites and their proximity to the rail line. Sketches of the sites are provided in Figures 21.2 to 21.4 to provide perspective of scale.

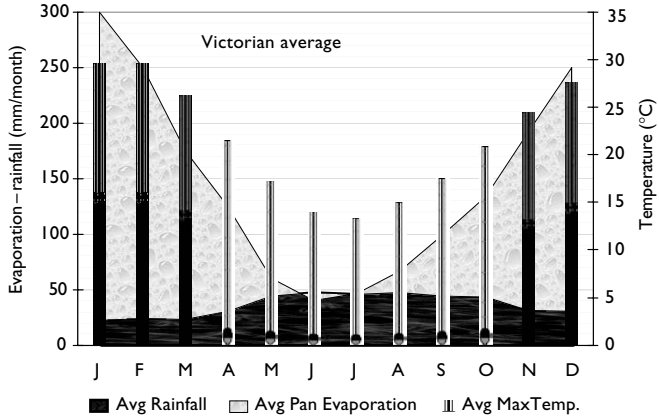

Figure 21.1 Climate data for Western Victorian sites.
Source: Data source Bureau of Meteorology, 2004.

Table 21.1 Details of trees at the vegetated sites

Site	*Species (common name)*	*Approx height of trees (m)*	*Sides*	*Average distance from ballast toe (m)*
Miram	Blackbox	7	1	3
Horsham	Red gum and sugar gum	15	1	4
Wal Wal	Various types of gums and wattles	10	2	12

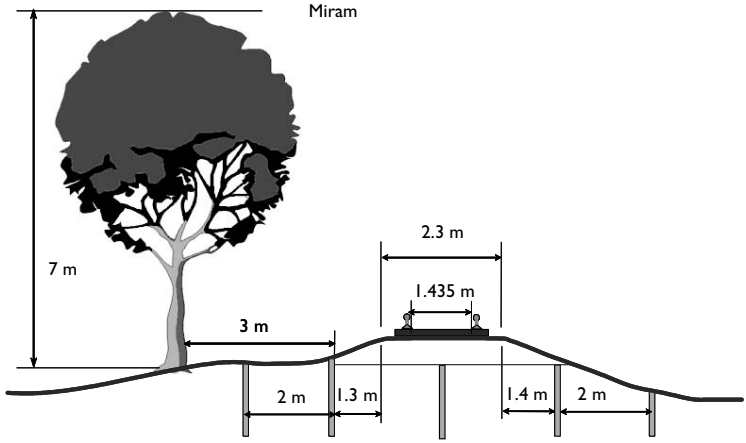

Figure 21.2 The Miram site.

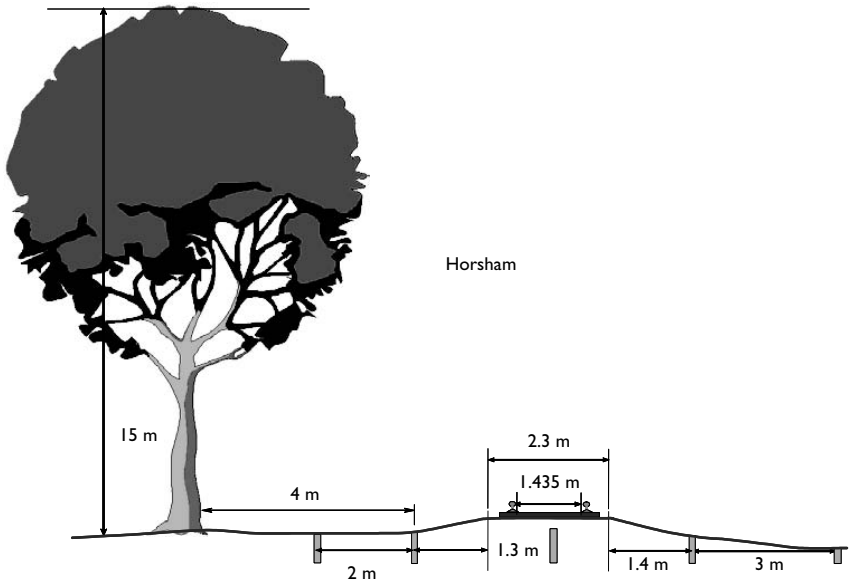

Figure 21.3 The Horsham site.

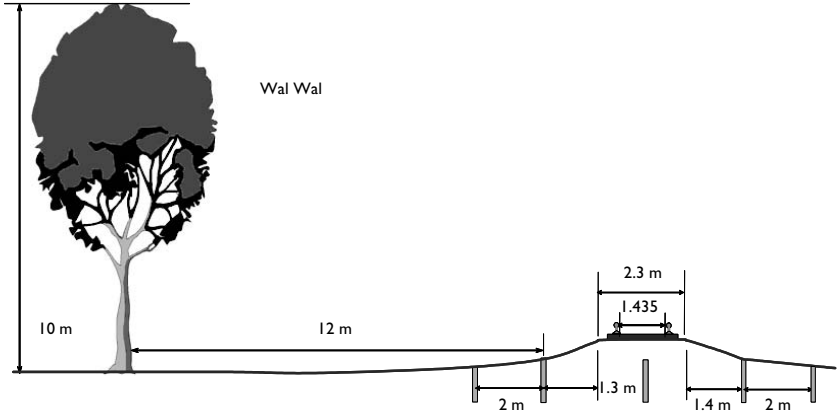

Figure 21.4 The Wal Wal site (trees are shown on only one side for convenience).

Table 21.2 Soil descriptions for the vegetated sites

Site	*Soil type (after Northcote et al., 1975)*	*Dominant soil classification*	*Comments*
Miram	Red duplex clay	CH	
Horsham	Grey cracking clay	CH–CV	
Wal Wal	Yellow duplex clay	CI	CI to 3.5 m depth, underlain by CH clays: sandy lenses in the first 4 m depth

Influence on soil suction

The soils at each site differed as indicated in Table 21.2. While the Miram and Horsham soil profiles both consisted of high plasticity clays generally, the clay at Wal Wal was less plastic and was interspersed with sandy lenses.

It should also be noted that at Wal Wal, the corresponding non-vegetated site's soil profile differed significantly from the vegetated site's profile, being less plastic and more permeable.

The normal proximity rules are influenced by the rail formation, as railway ballast is designed to be permeable. Rainfall infiltration below the level of the rail can affect the patterns of soil moisture and suction distribution – capillary action can reduce evaporation from the surface, so moisture levels can be expected to be greater below and beside the ballast.

Total soil suction profiles are provided in Figures 21.5 and 21.6 for the three sites relevant to the second round of soil sampling after a relatively dry period. Proximity ratios are provided in the legend to each figure, which can be related to the sketches of the sites in Figures 21.2 to 21.4. At Miram, the trees were quite close relative to their average height, and it can be seen that the soil suction profiles from boreholes 2 m either side of the ballast were as expected; close to the tree, significant drying was recorded to 2 m depth when compared with the profile from the borehole at D : H of 1.4. It was also relatively dry below the center of the track.

A similar pattern was observed at Horsham; although the closest borehole (D : H = 0.13) was drier between 1 and 3 m depth, it appeared that in the top 0.8 m of the profile at D : H of 0.8, the soil was drier. It could be conjectured that this difference was due to shading of the ground close to the tree, reducing evaporation rates locally, although a similar effect was not apparent at Miram, possibly because of the relatively small leaf area of the black box tree.

At Wal Wal, trends were less evident immediately as trees were located on either side of the track and relatively far away ($D : H_{min} = 1$). However, the greatest drying was evident at this proximity ratio and beneath the center of the track the soil was noticeably wetter below a depth of 1.5 m. Suction profiles from either side of the track center were similar for each proximity ratio.

In order to gauge the influence of the trees on the rail corridor, estimates of the deep equilibrium suction, u_{eq}, were made for each site. The estimate of u_{eq} was based on the average suction of all samples, except those from below the center of the track, at 4.5 m depth from the non-vegetated (NV) site over two rounds of soil sampling. These estimates were 750, 1,050, and 300 kPa for Miram, Horsham, and Wal Wal, respectively. The last estimate of u_{eq} may not be as reliable for the other two sites because of the differences in soil profile between the vegetated and NV sites, as previously noted.

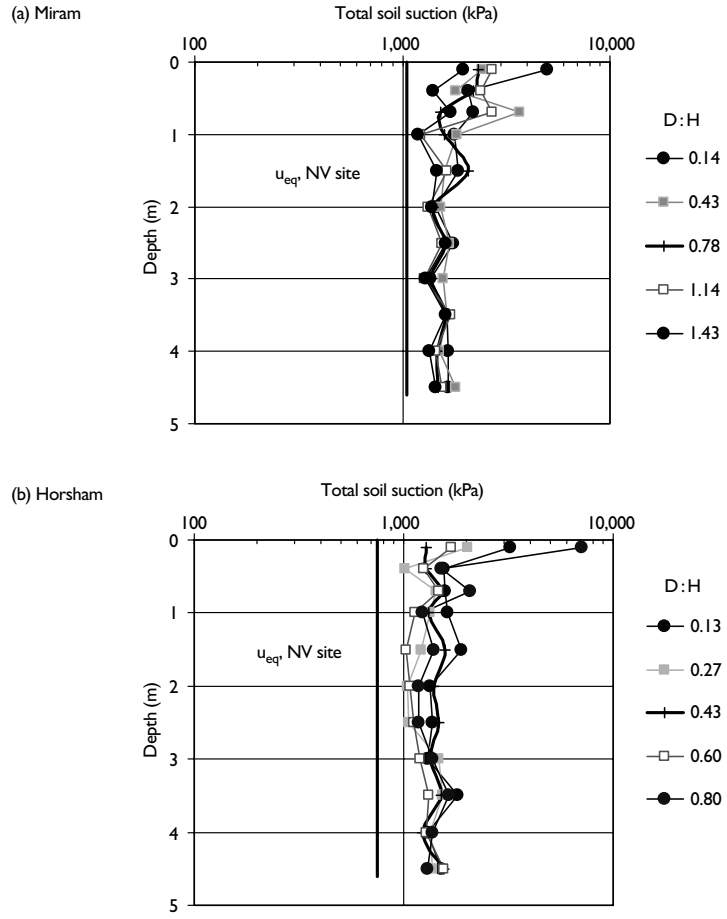

Figure 21.5 Total soil suction profiles at the vegetated sites, Miram and Horsham.

The drying influence of the trees at each of the sites is quite apparent. Further evidence of the drying below the center of the track at each site is provided in Figure 21.7. The logarithm of the difference in total suction in kPa is given between the vegetated and corresponding NV sites. In these terms, the greatest drying effect that has been observed is at Horsham, where consistent relative drying is evident for the full depth of exploration. At both Miram and Wal Wal, the drying influence below the center of the track was most pronounced in the top 2 m of the soil profile, and although still significant, was reduced at greater depth. It should be noted that the trees were closest at the Horsham site and most distant at Wal Wal.

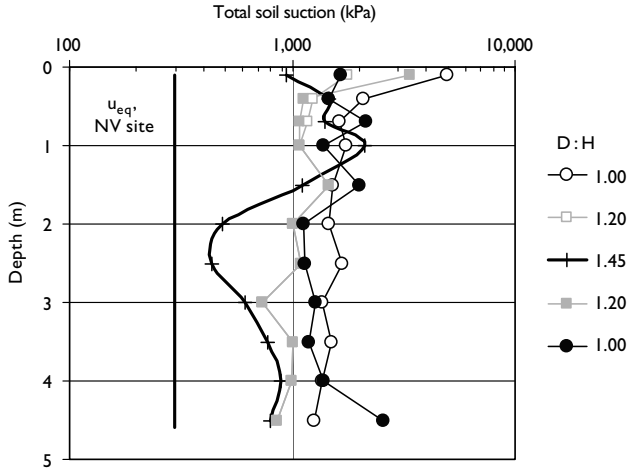

Figure 21.6 Total soil suction profiles at the vegetated site, Wal Wal.

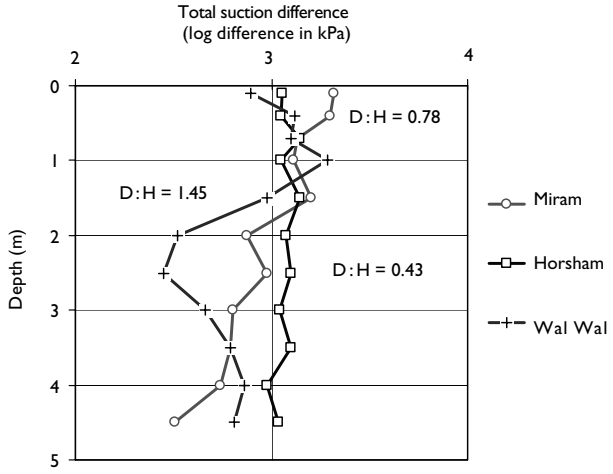

Figure 21.7 Difference in total soil suction profiles below track center between vegetated and non-vegetated sites.

Influence of soil suction on engineering soil properties

It has long been recognized that high soil suctions will lead to greater soil strength, stiffness, and resistance to repeated load (Brown *et al.*, 1987). Laboratory testing of the soil to a depth of one metre below the rail formation was undertaken to appraise strength and stiffness variations due to soil moisture differences. Shear strengths were determined by three-stage,

Table 21.3 Shear strength variations between vegetated and non-vegetated sites

Site	τ_{50} *(kPa)*	
	Non-vegetated	*Vegetated*
Miram	30–80	90–350
Horsham	25–40	60–140
Wal Wal	25–60	80–265

Table 21.4 Resilient moduli variations between vegetated and non-vegetated sites

Site	$M_{r,bp}$ *(MPa)*	
	Non-vegetated	*Vegetated*
Miram	20–55	75–660
Horsham	10–40	30–155
Wal Wal	20–65	85–760

unconsolidated, undrained triaxial tests on 50 mm diameter samples from thin-walled sampling tubes. To enable comparison of shear strengths, a nominal normal stress of 50 kPa was adopted, thereby providing the estimate of shear strength, τ_{50}. A summary of the ranges of measured values of τ_{50} is provided in Table 21.3.

Resilient modulus, M_R, is a measure of the cyclic stiffness of a soil, or, more simply, the soil's ability to recover elastically under dynamic loading. M_R values are dependent on both confining pressure and deviator stress. The resilient moduli of clay subgrades are affected also by soil suction (Selig and Waters, 1994; Phillip and Cameron, 1995; Lee *et al.*, 1997), with the stiffness of the soil increasing with the level of suction.

Resilient moduli were determined by constant confining pressure tests in a triaxial cell on 72 mm diameter samples of the rail subgrade (to a depth of 1 m below the formation), which were taken by thin-walled sampling tubes. Axial strains were measured over the middle third of each specimen. For the purpose of comparison of resilient moduli, the concept of a breakpoint resilient modulus ($M_{R,bp}$) was adopted (Thompson and Robnett, 1979). Essentially, the breakpoint modulus pertains to a specific confining pressure and deviator stress. Ranges of values of the breakpoint modulus are presented in Table 21.4.

It is evident from Tables 21.3 and 21.4 that the strength and cyclic stiffness of the subgrade soils at the vegetated sites were significantly greater than those from the NV sites. Correlations were attempted between total soil suction and the engineering soil properties. General trends of increasing strength and stiffness with suction are evident in the two plots provided in Figure 21.8, which contain the data for all three sites across two rounds of sampling. No attempt was made to account for differences in soils in these plots.

Trees in streetscape

Details of the sites, the methodology of the research, and early findings are reported by Cameron and O'Malley (2003). In the following sections, the discussion will concentrate

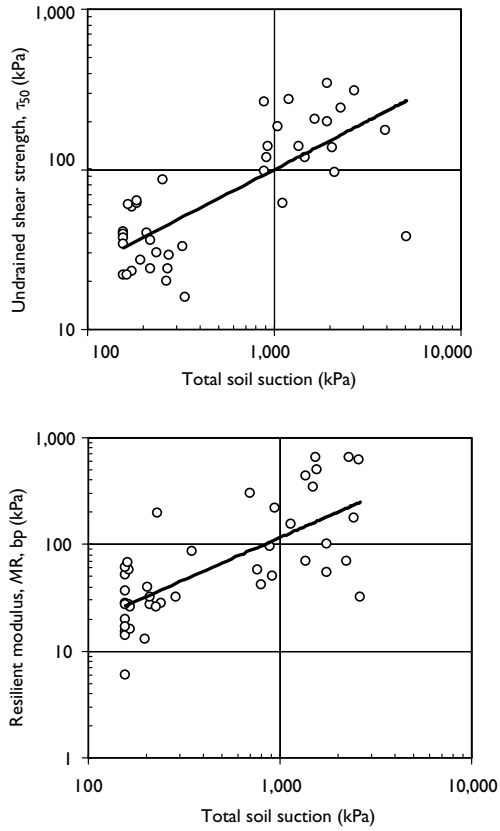

Figure 21.8 Variation of engineering properties with soil suction.

on aspects of tree physiology revealed by monitoring leaf water potential and xylem pressures.

Four tree species were monitored across the six sites in the subdivision, namely, Chinese Elm, Golden Raintree, Ornamental Pear, and Coral gum. Three of these species were exotics, however the Coral Gum is an Australian native eucalypt. The oldest trees at the beginning of the research project were the elm trees, which were stock planted in 1999; whereas the Coral gums were stock planted in 2002. Tree heights are provided in Table 21.5, where it can be seen that the trees were quite immature street plantings. Nonetheless, monitoring of plant–water relations of even young trees can indicate the potential for soil drying as the trees reach maturity.

Sampling of LWP and xylem sap pressures

Monitoring of the species water relations was conducted on a monthly basis, since February 2002. On each tree the middle canopy section was sampled with both instruments, as past

Table 21.5 Details of tree species and locations

Site name	*Tree species, common name*	*Tree height (m)*
Homestead Av.	*Ulmus parvifolia* Chinese elm	4.5
Legend Av.	*Pyrus ussuriensis x calleryana* Pear tree	1.7
Dene St.	*Pyrus ussuriensis x calleryana* Pear tree	2.4
Drover Ct.	*Koelreuteria paniculate* Golden raintree	3.4
Saddle Cr.	*Koelreuteria paniculate* Golden raintree	3.1
Station Ct.	*Eucalyptus torquata* Coral gum	1.7

research by O'Malley (2001) showed that this section provided the best overall water relations for the tree species at the time of sampling. Usually just one tree from each of the six sites was sampled.

Three sub-samples of the tree leaf area or stem were measured on each tree and the readings were then averaged. All measurements of LWP and stem pressures were collected in the afternoon (12 to 5 pm) when the plants' suctions were high. A previous study had revealed that this period of the day provided the greatest magnitude of plant stress (O'Malley, 2001). It was found that the highest suction is measured during the early afternoon period, as the trees become more stressed, whereas the lowest suction was observed in the pre-dawn period, when LWP is likely to be in equilibrium with the soil.

The tree species' water relations (water potential and sap pressure) were measured using a Wescor in situ hygrometer and a custom-built xylem pressure chamber. The hygrometer measures only leaf potential, while the pressure chamber can be used for leaves, petiole, or stem potential measurements. Unfortunately, the hygrometer cannot be used on deciduous trees after leaf fall. Since 3 of the 4 trees were exotic deciduous species (refer Table V for species), the xylem pressure observations were of considerable benefit and so the following section discusses the xylem pressure observations and provides only a comparison between the two devices on one tree.

Xylem pressures and leaf water potentials

The data of average xylem pressure against time over approximately 2.5 years are presented in Figures 21.9 and 21.10 for the four species of trees. Generally, the trees were under greater stress during the warmer months. Higher negative potentials or lower suctions occurred during the colder, wetter months when there was more water in the soil available to plant life.

From Figure 21.9 and from the data not shown in this chapter, leaf suctions tended to reflect the xylem suctions, but were, generally speaking, a little lower. Variations did occur between the two species, which were duplicated at other sites in this project, but were similar within each species, and the maximum and minimum potentials that were measured were applicable for both specimens.

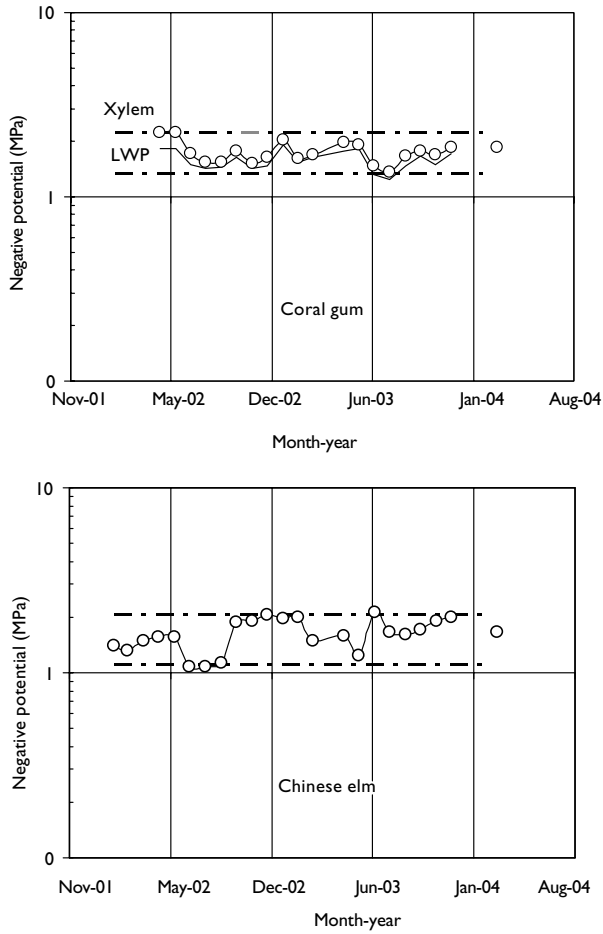

Figure 21.9 Tree water relations for the Coral gum and Chinese elm.

The patterns of moisture demand varied between species. Most noticeably, the range of xylem suctions was greatest for the pyrus species and smallest for the eucalypt or Coral gum. The seasonal demand for water of both the Pear and Golden Raintree exotics fluctuated strongly. The range of suctions developed in the elm tree was similar, but slightly greater than that of the native eucalypt.

The greatest suction within the monitoring period was developed in both the Coral gum and the Chinese elm (2.25 MPa). The elm trees were located on a site that was heavily affected by over-irrigation, causing saline levels within the soil to increase and consequently

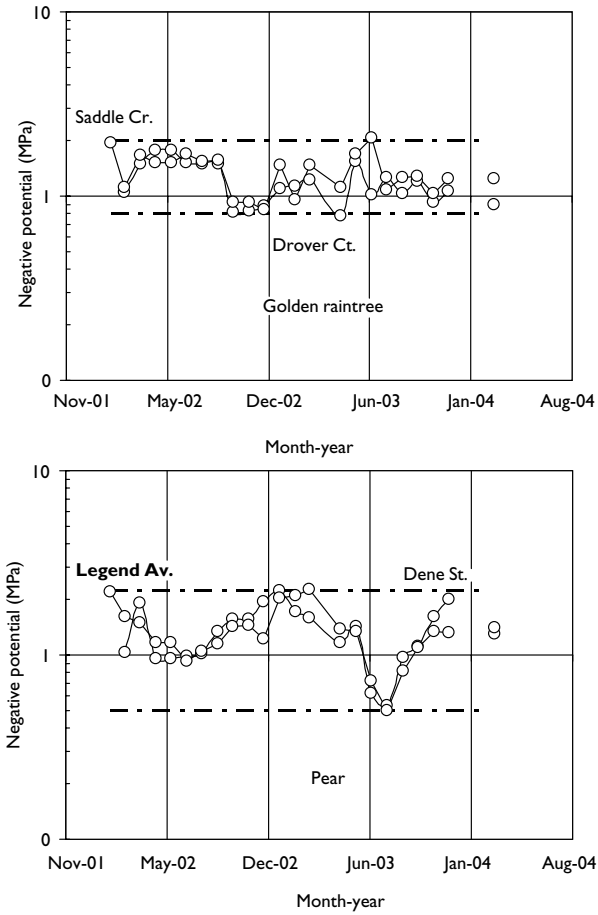

Figure 21.10 Xylem pressure variation with time for two exotic tree species.

noticeable stress to the trees. Even the Golden raintree and Pear trees produced xylem suctions as high as 2 MPa.

Unfortunately, such data serve only to indicate the level of drying that might be passed onto the soil in the root zone. For the four species in this study, it would appear that the evergreen Coral gum consistently places demand on the water held within the root zone. The Chinese elm, despite being deciduous, can also demand a similar level of water uptake, although, in cooler wetter periods, the soil may, to some extent, be more able to be replenished. The deciduous nature of both the Golden raintree and Pear trees impacts more significantly on soil–water demand, with modest levels of suctions ($\leq$ 1 MPa) being developed within these plants in the winter periods.

Concluding remarks

Trees require water and so can deplete soil water reserves, if they can develop suctions greater than those in the root zone. This chapter has presented a review of the influence of trees on expansive clay soils and how designs might be attempted to minimize the risk of damage to buildings, due to the deep drying that can result from trees. Results have been presented on two major projects with trees and foundations. The first study demonstrated that trees in the right situation (rail corridor) can actually help to stabilize foundations. The findings of the second study, with its long-term goal concentrating on tree–water relations, demonstrated that demand for water is dependent on species. However, the great divide that has been hypothesized between deciduous and evergreen plants may not always be that distinct, as in the case of the Coral gum and Chinese elm trees monitored in this study.

The research that has been discussed in this chapter is ongoing, thanks to the support of local government and the Cooperative Research Centre for Rail Technology. Numerical modeling of potential drying due to trees is being developed at the University of Wollongong in conjunction with the rail research. In the future, the monitoring of the rail sites will be restricted to a single site (Miram). Studies of root distributions have been undertaken and will be supported by monitoring of sap flux for the trees over approximately a year. Soil moisture distributions will be compared with vapour pressure deficits derived from a local weather station and the transpiration rates of the trees.

References

Aitchison, G.D., Peter, P., and Martin, R. (1973). The quantitative description of the stress deformation behaviour of expansive soils. *Proceedings of 3rd International Conference on Expansive Soils*, Haifa, Israel, V2, 79–82.

Baker, P.D. (1978). Tree root intrusion into sewers. *Progress Report No. 2: Analysis of Root Chokes by Species*. Engineering and Water Supply Department, Sewerage Branch, SA, Australia, August.

Balling, A. and Zimmermann, U. (1990). Comparative measurements of the xylem pressure of Nicotiana plants by means of pressure bomb and pressure probe. *Planta*, 182, 325–338.

Bernardi, A.L. (2000). Branch water potential; a useful indicator of plant water potential in comparison to leaf water potential in canola. *Australian Journal of Experiment Agriculture*, 40, 687–692.

Biddle, P.G. (1983). Patterns of soil drying and moisture deficit in the vicinity of trees on clay soils. *Geotechnique*, 33, 2, 107–126.

Biddle, P.G. (2001). Tree root damage to buildings. *ASCE Geotechnical Special Publication*, 115, 1–23.

Bozozuk, M. (1962). Soil shrinking damages shallow foundations at Ottawa, Canada. *Research Paper 163*, Division Building Research, NRCC, Canada.

Brown, S.F., Tam W.S. and Brunton, J.M. (1987). Structural evaluation and overlay design: analysis and implementation. *Proceeding of 6th International Conference Structural Design of Asphalt Pavements*, Ann Arbor, MI, 1013–1028.

Bureau of Meteorology (2004). *Climate data accessed online*, 13th May 2004, URL: http://www.bom.gov.au/climate/

Cameron, D.A. (1989). Tests for reactivity and prediction of ground movement. *Civil Engineering Transactions*, I.E. Aust., CE 31, No. 3, December, 121–132.

Cameron, D.A. (2001). The extent of soil desiccation near trees in a semi-arid environment, *Footings Group*, IE Aust SA, 17.

Cameron, D.A. and Earl, I. (1982). *Trees and Houses: A Question of Function*. Cement and Concrete Association of Australia, p. 20.

Cameron, D.A. and O'Malley, A.P.K. (2003). Movements in an urban development on extremely reactive soil: the first year. *Proceedings of 2nd Asian Conference on Unsaturated Soils*, Osaka, Japan, November, 265–270.

Cameron, D.A. and Walsh, P.F. (1984). *Damage to Buildings on Clay Soils*. National Trust of Australia (Victoria), Technical Bulletin 5.1.

Campbell, G.S. (1985). Instruments for measuring plant water potential and its components. In *Instrumentation for Environmental Physiology* (eds Marshall, B. and Woodward, F.), Cambridge University Press, Cambridge, 193–209.

Commonwealth Scientific and Industrial Research Organisation (CSIRO) (2003). Foundation maintenance and footing performance: a homeowner's guide. *Building Technology File 18*, CSIRO Publishing, Australia.

Cutler, D.F. and Richardson, I.B.K. (1981). *Trees and buildings*. Construction Press: London.

Dixon, M.A. and Tyree, M.T. (1984). A new stem hygrometer corrected for temperature gradients and calibrated against the pressure bomb. *Plant Cell Environment*, 7, 693–697.

Driscoll, R. (1983). The influence of vegetation on the swelling and shrinkage of clays in Britain. *Geotechnique*, 33 (2), 93–105.

Flora, T. (1978). Treeless towns? *Journal of Institute Landscape Architecture*. 121, 10–12.

Footings Group (1996). *Special provisions for the design of residential slabs and footings*. IEAust SA, August.

Hatton, T., Landsberg, J., Reece, P., and Knight, J. (1999). The ways tree use water. *Water and Salinity Issues in Agroforestry*, No. 5. Rural Industries Research and Development Corporation Publication No. CSM-4A, Wembley, WA, 107.

Holland, J.E. (1981). The Design, Performance and Repair of Housing Foundations. *Seminar Proceedings*, Swinburne College Press, Swinburne, Melbourne, Victoria.

Holland, J.E. (1983). The relationship of trees and housing. *Landscape Australia*, 3/82, 251–260.

Jaksa, M.B., Kaggwa, W. S., Woodburn, J. A., and Sinclair, R. (2002). Influence of large gums trees on the soil suction profile in expansive clays. *Australian Geomechanics*, 71(1), 23–33.

Knox, B., Ladiges, P., and Evans, B. (1994). *Biology*. McGraw-Hill, Australia.

Kozlowski, T.T. (1982). Water supply and tree growth. *Forestry Abstracts*, 43(2), 57–95.

Lee, W., Bohra, N., Altschaeffl, A., and White, T. (1997). Resilient modulus of cohesive soils. *Journal of Geotechnical and Geo-environmental Engineering*, ASCE, 123(2) 131–136.

Lytton, R.L. (1972). Design methods for concrete mats on unstable soils. *Proceedings of Inter-American Conference on Materials Technology*, Rio de Janeiro, Brazil, 171–177.

McInnes, D.B. (1986). Drying effect of different verge planted tree species on urban roads. *Proceedings of 13 ARRB, 5th REAAA Comb Conference*, 13(4), 54–66.

McKeen, R.G. (1992). A model for predicting expansive soil behaviour. *Proceedings of 7th International Conference on Expansive Soils*, Dallas, 1, 1–6.

Melcher, P.J., Meinzer, F.C., Yount, D.E., Goldstein G. and Zimmermann U. (1998). Comparative measurements of xylem pressure in transpiring and non-transpiring leaves by means of the pressure chamber and the xylem pressure probe. *Journal of Experiment Botany*, 49, 1757–1760.

Misra, R.K. and Sands, R. (1989). Physical and physiological basis of soil water extraction by various tree species and their possible impact on building foundations in clay soils. Report to the Melbourne City Council.

Mitchell, P.W. (1984). A simple method of design of shallow footings on expansive soil. *Proceedings of 5th International Conference on Expansive Soils*, Adelaide, 159–162 and 232–233.

Moore, G.M. (1997). The benefit of street trees. *The Australian Arbor Age*, 2, 8–15.

O'Malley, A.P.K. (2001). Water relations of four urban street tree species using a Wescor in-situ hygrometer in the City of Salisbury, South Australia. *Honours Thesis*, University of South Australia, 123.

Phillip, A.W. and Cameron, D.A. (1995). The influence of soil suction on the resilient modulus of expansive soil subgrades. *Proceedings of 1st International Conference on Unsaturated Soils* (eds, Alonso, E.E. and Delage, P.), Balkema, Rotterdam, Paris, France, September, V1, 171–176.

Pile, K.C. (1984). The deformation of structures on reactive clay soils. *Proceedings of 5th International Conference on Expansive Soils*, Institution of Engineers, Australia, Pub. N. 84/3, Adelaide, 292–299.

Potter, W. and Cameron, D. A. (2005). Potential remediation of rail track foundations in poorly drained clay sites with native vegetation. *Proceedings of 7th International Conference on the Bearing Capacity of Roads, Railways and Airfields*, June, Trondheim, Norway, (published on CD).

Potter, W., Londema, W. and Cameron, D.A. (2004). The influence of vegetation on rail track stability. *Proceedings of 9th Australia New Zealand Conference on Geomechanics*, Auckland NZ, 2, 895–901.

Radevsky, R. (2000). Subsidence – a global perspective. *Association of British Insurers, Research Report No. 1*, London, UK.

Raper, P. (1998). Agroforestry water use in Mediterranean regions of Australia. Water and Salinity Issues in Agroforestry, No. 2. *Rural Industries Research and Development Corporation, Publication No. DAW-35A*, Bunbury, Western Australia.

Ravina, I. (1983). The influence of vegetation on moisture and volume changes. *Geotechnique*, 33 (2), 151–157.

Richards, B.G. and Chan, C.Y. (1971). Theoretical analyses of subgrade moisture under environmental conditions and their practical implications. *Australian Road Research*, 4, (6), 32–49.

Richards, B.G., Peter, P., and Emerson, W.W. (1983). The effects of vegetation on the swelling and shrinking of soils in Australia. *Geotechnique*, 33, (2), 127–139.

Samuels, S.G. and Cheney, J.E. (1975). Long term heave of a building on clay due to tree removal. *Proceedings of Conference on Settlement of Structures*, British Geotechnical Socities, Pentech Press, Cambridge, 212–220.

Savage, M.J. and Cass, A. (1984). Psychrometric field measurement of water potential changes following leaf excision. *Plant Physiology*, 74, 96–98.

Schaefer, N.L. (1989). In-situ measurement of plant water potential. *Moderne Plant Analytical*, 9, 135–160.

Selig, E. and Waters, J. (1994). *Track structure and substructure management*. Thomas Telford Publications, London.

Silvestri, V., Soulié, M., Lafleur, J., Sarkis, G., and Bekkouche, N. (1992). Foundation problems in Champlain clays during droughts. II. Case histories. *Canadian Geotechnical Journal*, 29,169–187.

Standards Australia (1996). Residential slabs and footings – construction. *AS2870–1996*, Homebush, Sydney.

Stewart, M. and Sand, R. (1998). Soil movement and water potentials in trees growing in expansive clay soils. *Arboricultural Journal*, 22, 343–357, Great Britain.

Thompson, M.R. and Robnett, Q.L. (1979). Resilient properties of subgrade soils. *Transportation Engineering Journal,* ASCE, 105, No. TE1.

Tucker, R.L. and Poor, A.R. (1978). Field study of moisture effects on slab movements. *Journal of Geotechnical Engineering*, ASCE, 104(4), 403–415.

Walsh, P.F (1985). Load factors and design criteria for stiffened rafts on expansive clays. *Civil Engineering Transactions, I. E. Aust*., CE27, February, 1, 119–123.

Ward, W.H. (1953). Soil movements and weather. *Proceedings of 3rd International Conference Soil Mechanics*, Zurich, 2, 477–481.

Wesseldine, M.A. (1982). House foundation failures due to clay shrinkage caused by gum trees. *Transactions, Institution of Professional Engineers*, NZ, March, CE9(1).

Wiebe, H.H. (1972). The role of water potential and its components in physiological processes of plants. In: *Psychometry in water Relations Research* (eds Brown, R.W. and van Haveren, B.P.), Utah Agricultural Experiment Station, Utah State University, 194–197.

Yeagher, A.F. (1935). Root systems of certain trees and shrubs grown on prairie soils. *Journal of Agricultural Research*, 51(12), 1085–1092.

Part 6

Lime stabilization

Chapter 22

Stabilization of expansive Ankara Clay with lime

Mehmet Celal Tonoz,[1] *Candan Gokceoglu,*[1] *and Resat Ulusay*[1]

Summary

The specific objectives of the study reported in this chapter were to investigate the performance of the lime column technique and the effects of quick lime in powder form as the stabilizing agent on index, strength, compaction, compression, and swelling characteristics of Ankara Clay using laboratory-scale models. A site was selected at the southwestern part of the Ankara metropolitan area, where structural damages and high swelling pressures were reported. Engineering properties of the untreated (natural) and treated samples were determined. In the evaluations, prime consideration was paid to the effect of the lime–clay mixture and the spacing between lime columns, on engineering properties of the soil by comparing the results of the tests from the untreated and treated specimens. Finally, improvement in engineering properties of the clay was discussed.

Introduction

Excessive heave, settlement, low shear strength, and internal erosion of soils can cause damage to engineering structures. In order to overcome these difficulties and to prevent structural damages during the site selection and/or construction stages, engineers have developed several techniques. They avoid potential soil problems by selecting an alternative site or by removing the undesirable soil and replacing it with desirable soil. Engineering designs have been adopted for the conditions at hand, lastly the soil can be improved. The last approach, improvement or stabilization of a soil, is becoming the more attractive method for the soil engineers. Stabilization of clay soils using lime, cement, or fly ash has long been used to improve the workability and mechanical characteristics of the soils in geotechnical engineering. Fundamentally, lime stabilization refers to stabilization of the soils by the addition of burned limestone products, either calcium oxide or calcium hydroxide (Bell, 1988a). Lime is the most effective and widely used chemical additive for expansive soils (Nelson and Miller, 1992), because after adding the lime to a clay soil, many chemical reactions such as cation exchange, flocculation – agglomeration, lime carbonation, and pozzolanic reaction occur. For this reason, the chemical theory involved in the lime reaction is considerably complex (Thompson, 1966). In spite of this complexity, it is still possible to find many

[1] Department of Geological Engineering, Applied Geology Division, Hacettepe University, 06532 Beytepe, Ankara, Turkey.

successful applications of lime stabilization in the literature. Lime stabilization techniques can be divided into two groups, namely lime columns and lime mixture technique for deep and shallow improvements, respectively.

The lime column technique consists of holes in the ground filled with lime. Lime columns are constructed in situ by mixing quicklime with the natural soils using a giant egg-beater auger. To construct a column the auger is drilled into the soil to the required depth, the direction of rotation is reversed, and the auger is slowly withdrawn. As the auger is withdrawn, powdered quicklime is pneumatically pumped into the soil (Rogers and Bruce, 1991). The stabilization process provided by the lime columns is controlled mainly by the lime migration. It is thus widely reported that lime migrates from the piles or columns and reacts with, and hence stabilizes, the surrounding ground (Rogers and Glendinning 1997). However, the migration distances are small in clay soils, because they have low to very low permeability. For an efficient stabilization, calcium and hydroxyl ions should migrate through the clay, because hydroxyl ions cause highly alkalinic conditions in clay soil. Highly alkalinic conditions give rise to the slow solution of alumino-silicates which are then precipitated as hydrated cementitious reaction products (Diamond and Kinter, 1966). These reaction products contribute to flocculation by bonding adjacent soil particles together and as curing occurs they strengthen the clay soil. Such pozzolanic reactions are time dependent and strength develops gradually over a long period (Bell, 1996; Sivapullaiah *et al*., 2000).

The other lime stabilization technique is the lime mixture. This technique is widely used in the construction of roads, airports, embankments, or canal linings by intimate mixing with clay subgrades to improve workability, strength, swelling characteristics, and bearing capacity. Generally, from 3% to 8% by weight hydrated lime is added to the top layer of the soil (Nelson and Miller, 1992). The effects of lime stabilization on clay soils have been investigated by numerous groups (e.g. Bell, 1988b; Indrartna *et al*., 1995; Popescu *et al*., 1997; Afes and Didier, 2000). Since the properties of soil–lime mixtures depend upon the character of the clay soil, and the type and period of curing, the method and quality of construction and the proper amount of lime to be used should be investigated before the application of the lime–soil mixture technique.

Approximately two-thirds of the settlement of Ankara, the capital of Turkey, is founded on a clayey soil called Ankara Clay and classified as medium to highly plastic expansive soil. Damage has been reported to light one-storey buildings, garden walls, roads, and buried utilities such as water pipes due to excessive heave of Ankara Clay particularly at the southwestern part of the city, where there is a rapid dense urbanization (Ordemir *et al*., 1977; Erguler and Ulusay, 2003) (Figure 22.1). Sufficient attention has not been given to the treatment of this clay to control the swelling pressure. Although there exists experimental investigations on the swelling properties of Ankara Clay (Birand, 1963; Uner, 1977; Furtun, 1989; Cokca, 1991; Erguler and Ulusay, 2003). Very little work has been reported on the stabilization of this clay with the lime mixture technique (Oral, 1964) . Due to the expensive nature of the clay and the lack of information about its stabilization, there was a need for further studies on soil treatment with lime.

The specific objectives of the study reported in this chapter were to investigate the performance of the lime column technique and the effects of quick lime in powder form as the stabilizing agent on index, strength, compaction, compression, and swelling characteristics of Ankara Clay using laboratory-scale models. A site was selected at the southwestern part of the Ankara metropolitan area, where structural damages and high swelling pressures were reported (Erguler and Ulusay, 2003), and five undisturbed block samples (approximately

Figure 22.1 (a) A typical damaged one-storey building, and (b) cracks and heave on the asphalt pavement due to expansion of the investigated soil.

$35 \times 35 \times 30$ cm in dimension) from different locations at the site were collected (Figure 22.2). Engineering properties of the untreated (natural) and treated samples were determined. In the evaluations, prime consideration was paid to the effect of the lime–clay mixture and the spacing between lime columns, on engineering properties of the soil by comparing the results of the tests from the untreated and treated specimens. Finally, improvement in engineering properties of the clay was discussed.

Lithological, mineralogical, and engineering characteristics of Ankara Clay

The city of Ankara is located in the Ankara Basin which is 18 to 20 km long and 6 to 8 km wide depression bounded by a series of highlands. Both rock and soil units are observed in the city. The rock units are represented by andesite, spilite, and schist in different ages. The soil units, which fill the Ankara Basin, are composed of river and lake sediments of Late Pliocene and Quaternary aged alluviums (Kocyigit and Turkmenoglu, 1991). The Late Pliocene sequence (Calgin *et al*., 1973) is mainly composed of clay and occasional sandy and gravely layers, and generally called as Ankara Clay (Birand, 1963). This clay soil with typically reddish–brown color is the weathering product of the volcanic rocks, particularly the andesites surrounding the basin from the north and east (Calgin *et al*., 1973; Aras, 1991). Lime nodules and lime concentrations occasionally appearing at very shallow depths within the clay have no lateral continuity. It is preconsolidated, stiff, and fissured clay, and according to Erol (1976) its thickness reaches up to 200 m in the central part of the basin.

X-ray diffraction (XRD) analyses were performed on the samples in order to assess the relative quantity of clay minerals and whole sample mineralogy. The XRD diffractograms were obtained at Hacettepe University X-ray Micro-analysis Laboratory using a Philips PW-1140 model diffractometer with a goniometer speed of 2°/min. Semi-quantitative estimates of the minerals were determined from the powder diffractograms following an external standard method developed by Gundogdu (1982). In this method, samples were mounted in the same way and the characteristic peak intensities (I) of the minerals were normalized to that of the reflection of dolomite. In other words, a K factor for each mineral, including clays with peaks between 19 and 20° 2q, was determined as $K_{dolomite}/I_{mineral}$ in a

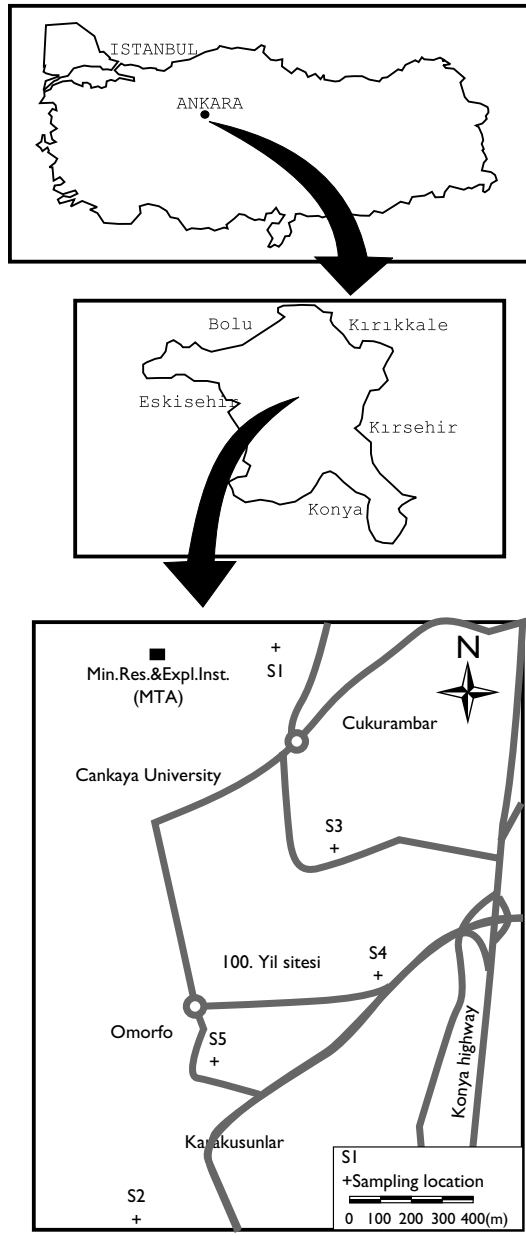

Figure 22.2 Sampling locations.

Table 22.1. The results of the XRD analysis from untreated clay samples

Sample No.	*Clay and non-clay minerals (%)*				*Clay minerals (%)*		
	Clay	*Calcite*	*Quartz*	*Feldspar*	*Smectite*	*İllite*	*Kaolinite*
S1	64.8	12.7	14.5	8.0	43.2	9.3	12.3
S2	64.0	13.0	19.4	3.5	34.0	16.0	14.0
S3	73.0	8.3	14.1	4.4	36.5	20.5	16.0
S4	77.0	8.5	11.3	3.2	28.9	28.9	19.2
S5	73.0	9.2	15.0	2.7	38.5	16.0	18.5

1/1 dolomite–mineral mixture by weight. Percentages of the minerals, a, was calculated from the following equation:

$$a = 100\,K_aI_a/K_aI_a + K_bI_b + \cdots\cdots\cdots\cdots + K_nI_n \tag{22.1}$$

where $K_{a,b,\ldots,n}$ and $I_{a,b,\ldots,n}$ are the K factor and intensity of each mineral identified, respectively.

The diffractograms from normal, oven-dried, and ethylene-glycol-treated preparations were evaluated and the results were semi-quantitatively calculated (Table 22.1). Typical X-ray diffractograms of a sample from the Ankara Clay are shown in Figure 22.3. Table 22.1 suggests that the minerals present in the samples were clay, calcite, quartz, and feldspar. Clay dominated the samples, accounting for some 64%–77%. The chief clay mineral was smectite which exhibited a high swelling potential.

Engineering properties of untreated samples

Laboratory tests that were carried out on untreated samples of Ankara clay included the determination of physical and index properties, unconfined compressive strength, and consolidation and swelling characteristics. The tests were conducted by following the procedures suggested by ASTM (1994).

Physical and index properties

Since lime stabilization affects the physical and index properties of the clay soil, unit weight, specific gravity, natural moisture content, Atterberg limits, grain size distribution, and activity of the untreated (natural) samples were determined and compared with those from treated samples. The grain size distribution analysis results (Table 22.2) revealed that clay-sized grains were dominant particle size, comprising between 43% and 55%. The clay samples displayed a narrow range of liquid and plastic limit values. The liquid limits greater than 50% indicated the presence of smectite and confirmed the results from the X-ray diffraction analysis. The samples from Ankara clay were classified as CH and MH soils.

Skempton (1953) stated that the activity of a soil is related to its mineralogy and geological history. Figure 22.4 and Table 22.2 suggest that the activity of the samples did not vary significantly and that the clay samples were potentially highly expansive. This was supported by the shrinkage limits of these samples indicating that they both shrank and

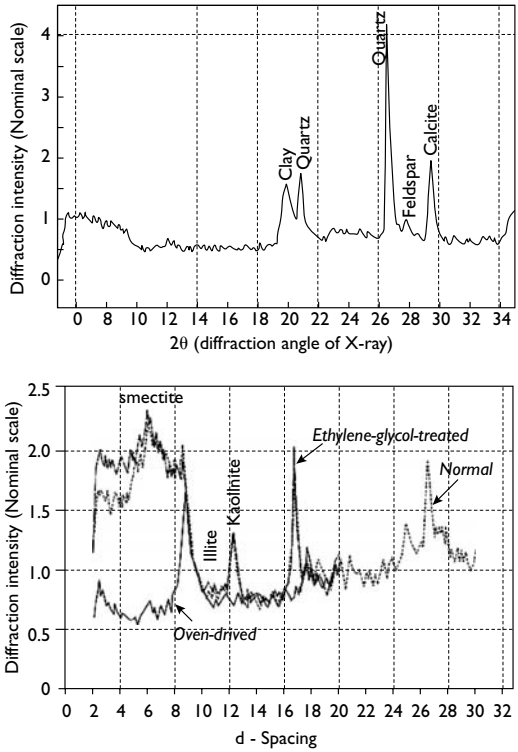

Figure 22.3 Example X-ray diffractograms from Ankara Clay (sample S5): (a) bulk sample and (b) clay fraction.

expanded considerably. The standard Proctor compaction tests were carried out on the untreated samples to prepare soil specimens for unconfined compressive strength and swelling tests after treatment and to understand the changes sourced from the application of the lime mixture technique. Figure 22.5 illustrates the relationships between dry density and moisture content for the samples tested. The soil samples had maximum dry density values varying between 1.41 and 1.53 g/cm^3 and an optimum moisture content of about 30%.

Unconfined compressive strength

The unconfined compressive strength of the untreated soil samples was determined using remolded specimens due to difficulties experienced during the preparation of standard undisturbed specimens with a height to diameter ratio of 2.5 from the block samples. Considering the optimum moisture content and dry density of each sample, the specimens extracted from the block samples were compacted in a standard Proctor mold and tested in accordance with the procedure suggested by ASTM (1994). During the tests, strains were

Table 22.2 Physical and index properties, and unconfined compressive strength of the untreated samples from Ankara Clay

Sample No.	*Natural moisture content (%)*	*Grain size (%)*				*Specific gravity*	*Atterberg limits (%)*				*Unified Soil Classification*	*Natural bulk density (g/cm^3)*	*Dry density (g/cm^3)*	*Activity*	*UCS (kPa)*
		Gravel	*Sand*	*Silt*	*Clay*		*LL*	*PL*	*PI*	*SL*					
S1	27.0	6.0	28.0	21.0	45.0	2.57	64.0	31.0	33.0	23.0	CH	2.00	1.87	0.73	52.8
S2	25.0	10.0	22.0	17.0	51.0	2.52	65.0	33.0	32.0	15.0	MH	1.81	1.64	0.63	64.9
S3	30.0	9.0	15.0	24.0	52.0	2.59	66.0	37.0	29.0	18.0	MH	1.68	1.52	0.56	62.0
S4	29.0	8.5	16.5	20.0	55.0	2.64	75.0	43.0	32.0	18.0	MH	1.68	1.46	0.58	82.0
S5	33.0	10.5	13.1	33.4	43.0	2.61	68.0	34.0	34.0	14.0	CH	1.52	1.39	0.79	59.0

Notes
LL: Liquid limit; PL: Plastic limit; PI: Plasticity index; SL: Shrinkage limit; UCS: Unconfined compressive strength.

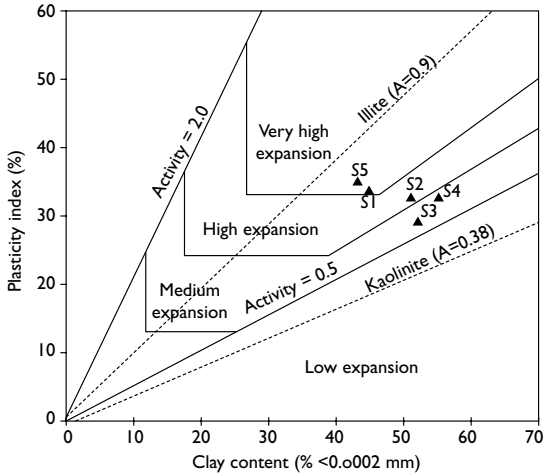

Figure 22.4 Swelling potential classification for the samples of Ankara Clay.

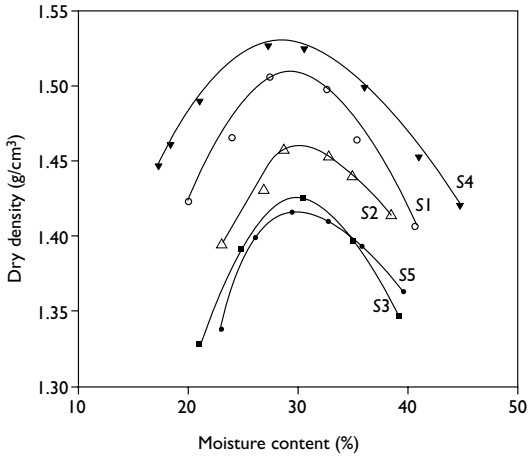

Figure 22.5 Moisture content–dry density curves for the untreated samples.

also calculated to obtain the stress–strain curves of each specimen. Generally, failure occurred at a strain of about 0.8%. However, for some specimens strains were between 0.4% and 0.5% (Figure 22.6). All the specimens failed in shear and there was evidence of barreling. The unconfined compressive strength of the soil samples ranged between 53 and 82 kPa (Table 22.2).

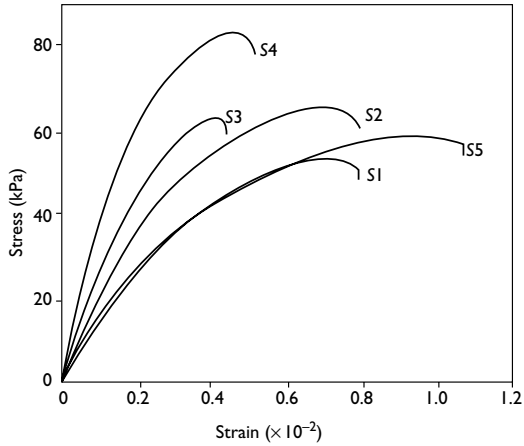

Figure 22.6 Stres–strain curves of the untreated samples obtained from uniaxial compression tests.

Swelling characteristics

Erguler and Ulusay (2003), who studied the swelling behavior of Ankara Clay at the same site, indicated that the moisture content of the clay was less than its shrinkage between depths of 0 and 1.8 m in the arid season, while the footings of the light buildings are placed directly on the surface and/or at such shallow depths as 1 m. Based on this information, the specimens were tested at water contents less than their shrinkage limits and the swelling tests were conducted after the specimens were dried in the oven for about 24 h. For each condition of moisture content and dry density, specimens were subjected to free swell test. The tests using an oedometer were carried out on compacted specimens. For further details see the paper by Erguler and Ulusay (2003). The swelling pressures of five samples from the blocks tested varied from 25 to 96 N/cm^2.

Compressibility characteristics

Conventional oedometer tests on untreated specimens taken from the blocks of Ankara Clay were carried out to determine their consolidation characteristics such as preconsolidation pressure, compression index (C_c), and coefficient of volume change (m_v). The tests were carried out at pressure intervals between 25 and 200 kPa, similar to the estimated loads imposed by the light buildings at the sampling site. Consolidation was determined from the observed consolidation curve of each specimen using the procedure recommended by ASTM (1994). Preconsolidation pressures from the compression curves, and the compression index, and the coefficient of volume change for each specimen at the different pressure intervals are shown in Figure 22.7 and given in Table 22.3, respectively. Although the block samples were taken at shallow depths under about 40 kPa overburden pressure, the preconsolidation pressures were much higher than the overburden pressure. This situation suggests

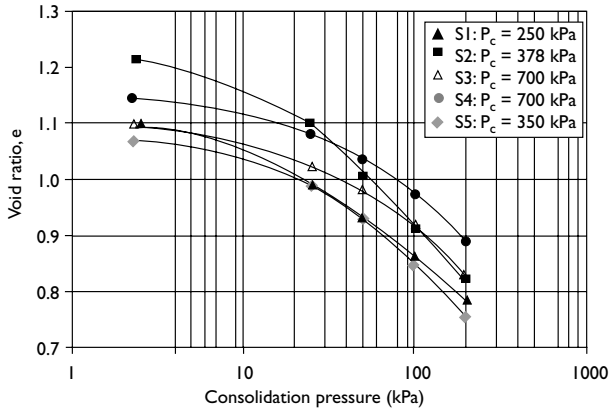

Figure 22.7 Compression curves for the tested specimens.

Table 22.3 Consolidation characteristics of the untreated samples for different pressure intervals

Sample No.	*Pressure interval*					
	25–50 kPa		*50–100 kPa*		*100–200 kPa*	
	C_c	m_v	C_c	m_v	C_c	m_v
S1	0.093	0.777	0.289	0.658	0.308	0.432
S2	0.122	0.758	0.229	0.720	0.269	0.438
S3	0.165	0.865	0.242	0.711	0.36	0.502
S4	0.132	0.646	0.192	0.518	0.272	0.345
S5	0.192	1.166	0.275	0.859	0.75	0.546

Notes
C_c: compression index; m_v: coefficient of volume change (m^2/MN).

that Ankara Clay is an overconsolidated clay, as indicated by previous investigators (e.g. Arda 1966; Ordemir *et al.*, 1977; Kiper 1983).

Effects of lime stabilization on engineering behavior of Ankara Clay

In order to assess the performance of lime stabilization in laboratory scale, two techniques namely lime column and lime mixture were employed. The soil specimens taken from the site (Figure 22.2) were stabilized by adding varying percentages of lime and constructing lime columns arranged at different distances. Then the results obtained both from the treated and natural soil samples were compared to assess the influence of lime stabilization by two methods.

Performance of lime column technique

Preparation of laboratory-scale model

The lime column techniques can be classified into two main groups such as drill hole lime or lime column and pressure injected lime. The lime columns can be constructed using the quick lime in a slurry form (Nelson and Miller, 1992) or powder form. In this study, using five undisturbed soil blocks from the site, the specimens were extracted at different distances from the laboratory-scale lime columns. Then the effective radius of the lime-treated zone by lime migration on hole diameter was investigated. Since a very limited amount of information was available on the distance between the columns and column diameter based on laboratory-scale models (Nobel and Anday, 1967; Brandl, 1981; Chummer, 1987), the data from in-situ investigations on lime columns (Tystovich *et al*., 1971; Brandl, 1981; Kitsugi and Azakami, 1982) were also considered. By employing the data from these investigations, and the pairs of holes (column), diameter (D), and the radius of effective distance of lime migration (R), a linear relationship (Figure 22.8) was obtained. This figure, implies that D–R data pairs of lime columns from the laboratory investigations range between 0 and 10 cm (D) and 0 and 20 cm (R), and the appropriate distance between the columns would be 14 cm for a column diameter of 2 cm (i.e. 7 times the diameter of the column). Using 2 hand augers with different diameters, 4 holes at 14 cm centers were opened in the blocks labeled S1, S3, and S4 (Figure 22.9a), while only 1 hole with a diameter of 4.8 cm was opened in blocks S2 and S5. The depths of the holes ranged between 25 and 28 cm depending on the thickness of the block samples, and they were cleaned by a spiral brush before they were filled with lime. In the field application, a hollow tube is pushed into the soil to the required depth and quicklime is then forced into the pile or column by air pressure as the tube was withdrawn. To simulate this process in laboratory conditions, each hole was filled with the quicklime in powder form in four successive layers and each layer was separately

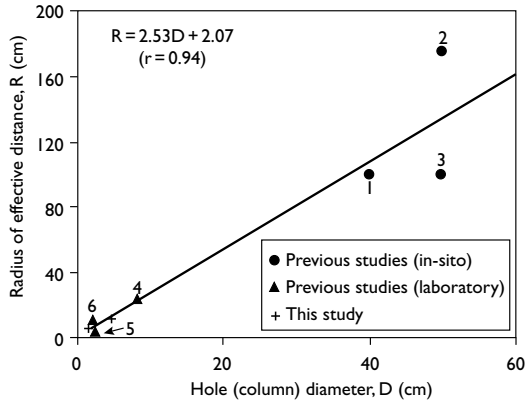

Figure 22.8 Column diameter vs. radius of effective distance of lime migration.

Notes
1: Kitsugi and Azakami (1982); 2 and 4: Brandl (1981); 3: Tystovich *et al.* (1971); 5: Noble and Anday (1967); 6: Chummer (1987).

compacted. Ruenkrairergsa and Pimsarn (1982) suggested that the lime columns should be constructed before the rainy season in order to allow ion migration from the column. In the study reported in this chapter, therefore, water was introduced into both the lime columns and the soil to allow for the migration of ions and to keep the moisture content of the samples at least 50%. Previous investigations (Ruenkrairergsa and Pimsarn, 1982; Rogers and Bruce, 1991; Rogers and Glendinning, 1997) on lime columns showed that the curing period ranges between 28 days and 2 years. Therefore, in this study, curing times of 28 and 56 days were considered. At the end of each curing time, the samples were extruded by an auger from the soil block at various distances from the lime columns as illustrated in Figure 22.9b. These samples were then subjected to laboratory tests for assessing the performance of the stabilization by lime column.

Gradation and consistency

The upper and lower bounds of the grain size distribution of the untreated and treated samples in terms of curing time were compared in Figure 22.10. Results indicated that the clay particles underwent flocculation to form aggregates after treatment and the aggregates behaved like particles of silt. In addition, the decrease in the amount of clay particles after treatment was greater at 56 days of curing time when compared to that at 28 days of curing. The histograms in Figure 22.11 suggested that the maximum decrease in percentage of clay occurred at a distance approximately the diameter of the columns. However, beyond this distance, the percentage of clay particles tended to increase and approached those of the natural samples. In the zone of influence of the lime columns, depending on curing time, a decrease in clay particles of about 40% occurred.

Figure 22.12 indicated that the liquid limit and plasticity index fell rapidly within 28 days and thereafter they inclined slightly, with the greatest changes close to the columns (i.e. at a distance approximately equal to two times the diameter of the column). The overall effect was an increase in the plastic limit as the distance to the column increased. Figure 22.12 also implied that a curing time of 28 days seemed to be suitable to achieve the maximum improvement in terms of plasticity.

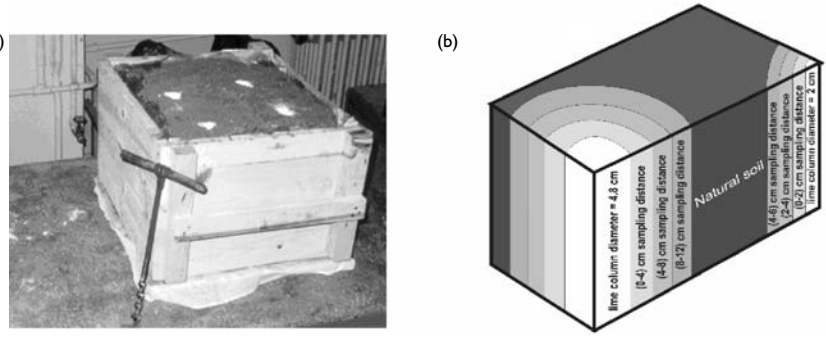

Figure 22.9 (a) A view from the laboratory-scale lime columns constructed in the soil block, and (b) methodology for extracting threated samples at diffrerent distances to lime columns.

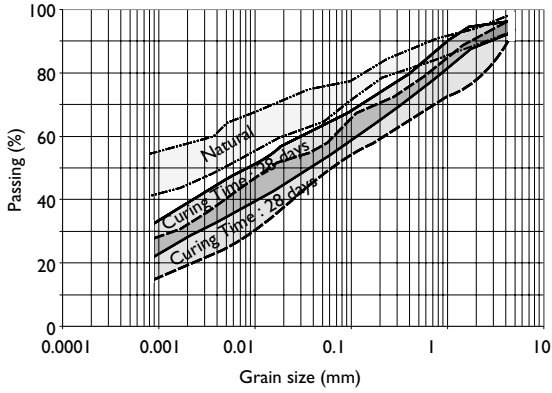

Figure 22.10 Grain size distributions of the natural and lime-column treated samples.

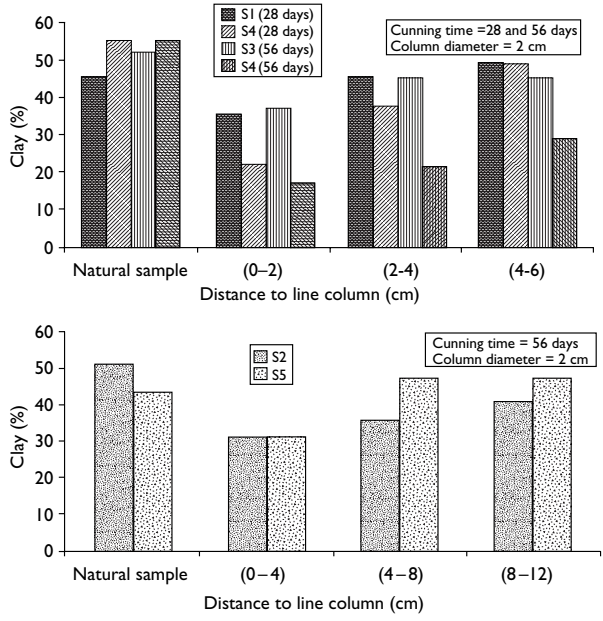

Figure 22.11 Influence of lime columns in different diameters on clay percentage in terms of different distances to columns and curing times.

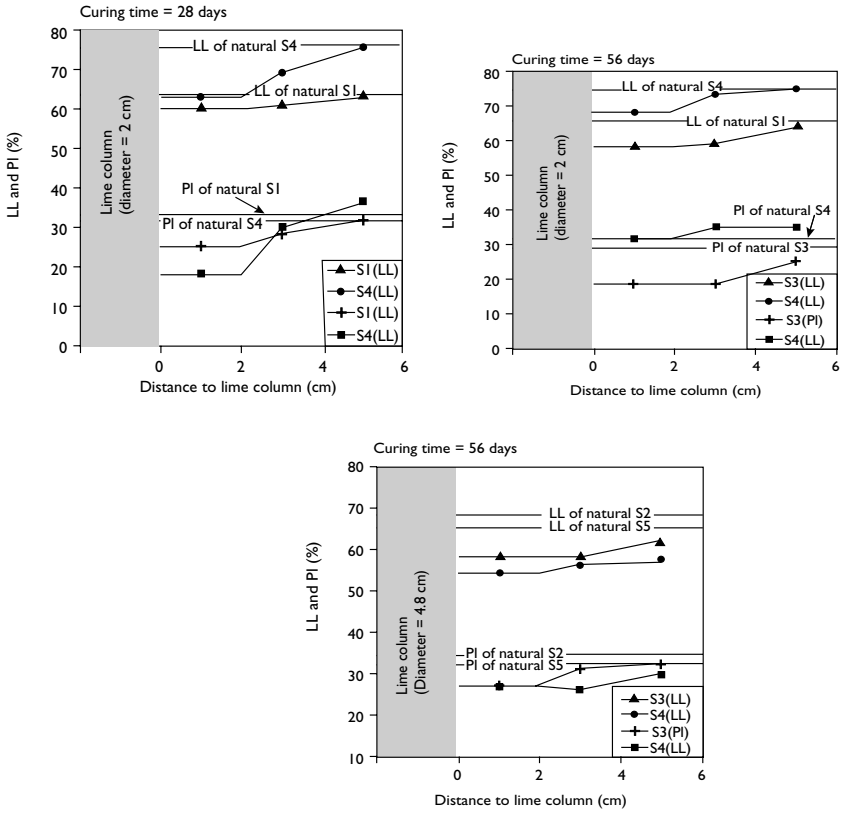

Figure 22.12 Effects of distance to column and curing time on consistency of the soil samples.

Strength

In this study, the unconfined compressive strength of the cylindrical specimens extracted from the close vicinity to the columns was determined in order to compare the variation in the unconfined compressive strength with the distance from the lime column. Specimens from blocks S1, S3, and S4 crumbled during the sampling and hence neither the undisturbed specimens nor the compacted specimens could be prepared due to the limited amount of soil samples. Strength tests of the treated specimens were, therefore, conducted only on the compacted specimens prepared from blocks S2 and S5 at a curing period of 56 days. It was evident from Figure 22.13a that the strength of the soil increased when treated. The most clear effect of the lime migration occurred at a distance approximately twice the column diameter (i.e. 0–8 cm). It was also noted that although the strength of the natural sample S2 was greater than that of sample S5 (Table 22.2), lime stabilization had a greater effect on the

strength of sample S5 (about 80% increase in strength) due to its higher clay particle and smectite contents compared to those of sample S2.

Although the stress–strain curves for the natural samples did not exhibit pronounced peaks, (Figure 22.6), the stress–strain curves of the treated samples had slight peaks due to cementation of soil particles by pozzolanic compounds formed by reactions between the soil and lime (Figure 13b).

Swelling

The change in swelling pressure of the soil after the treatment by lime columns was investigated by a series of free swell tests carried out on samples taken at different distances from the lime columns. The changes in swelling pressures after the treatment in terms of two different column diameters are depicted in Figure 22.14. The percentage

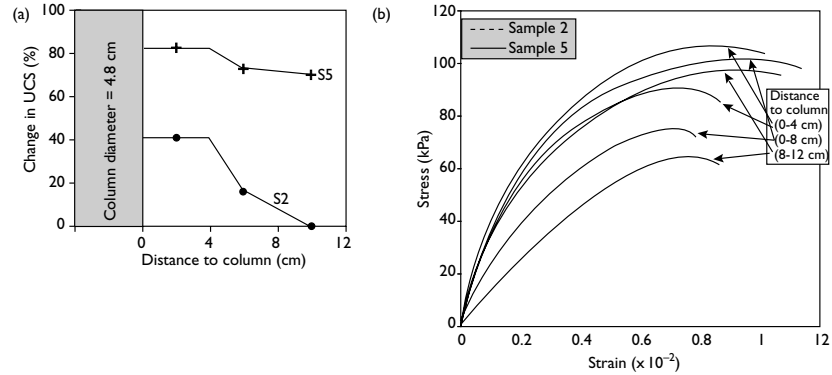

Figure 22.13 (a) Variation of unconfined compressive strength (UCS) of the soil in terms of distance to column, and (b) effect of lime on stress–strain behavior of the treated samples for different distances to column.

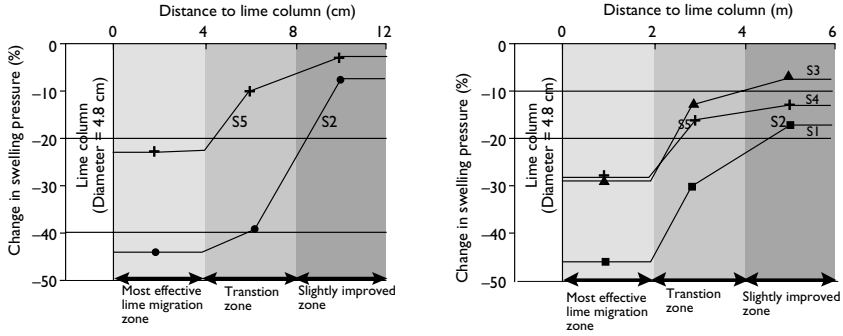

Figure 22.14 Change in swelling pressure of the treated samples with distance to lime column.

variation in swelling pressure (VSP) of the soil samples was calculated from the following expression:

$$\mathrm{VSP}(\%) = ((\mathrm{SP_T} - \mathrm{SP_N})/\mathrm{SP_N}) \times 100 \tag{22.2}$$

where $\mathrm{SP_T}$ and $\mathrm{SP_N}$ are the swelling pressures determined from the treated and natural samples respectively.

Figure 22.14 suggests that a decrease in swelling pressure occurred between 40% and 75% up to a distance of two diameters from the column. It was apparent that the change was about 15% at 60 mm to about 70% adjacent to the column, a decrease in swelling pressure of about 55%. The maximum decrease in swelling pressure of 75% was obtained with sample S1, probably due to its higher smectite content when compared to those of other samples, although the liquid limits of the samples were approximately identical.

Compressibility

In the literature, prime consideration has been paid to the effect of lime stabilization on the strength and swelling characteristics of expansive soils (Tuncer and Basma, 1991; Nicholson *et al*., 1994). The exception is a study conducted by Nalbantoglu and Tuncer (2001) who assessed the compressibility of a clay–lime mixture. In the study reported in this chapter, therefore, a series of one-dimensional consolidation tests were also conducted on undisturbed treated soil specimens to investigate the effects of lime columns on their consolidation characteristics. Undisturbed samples were taken from the blocks from different distances to the column after 28- and 56-day curing periods. The void ratio versus logarithmic pressure diagrams of the treated specimens are shown in Figure 22.15a. When compared to those in Figure 22.7, Figure 22.15a indicated a reduction in the slope of the virgin curve for all specimens. Due to cation exchange reaction, an increase in the flocculation and aggregation caused a chemically induced preconsolidation effect, resulting in an increase in the vertical effective stress and reduction in the compressibility characteristics. It was apparent from a comparison of the compression curves in Figures 22.7 and 22.15a that there was an increase in preconsolidation pressure. Figures 22.15b and 22.15c suggested that the preconsolidation pressure increased rapidly at a distance equal to the diameter of the column. These figures also suggested that the curing time did not have any considerable effect on the preconsolidation pressures. A curing time of 28 days seemed to provide an efficient treatment.

The test results on the treated samples showed a dramatic decrease in C_c and m_v in close vicinity to the column (Figure 22.16). The highest reduction in the values of C_c and m_v was obtained for the samples at a distance equal to the diameter of the column. Beyond this distance, the effect of the lime column on these parameters tended to slowly decrease as seen in Figure 22.16. This indicated the increased tendency of the soil treated with lime columns to resist compression and expansion. However, as with preconsolidation pressure, the effect of the curing period on these compressibility characteristics of the soil was not evident, indicating a curing period of 28 days is likely to be satisfactory.

Performance of lime mixture technique

Mixture and specimen preparation

An experimental program was performed on the samples from Ankara Clay that were from the locations of those used in lime column experiments. In laboratory experiments, the

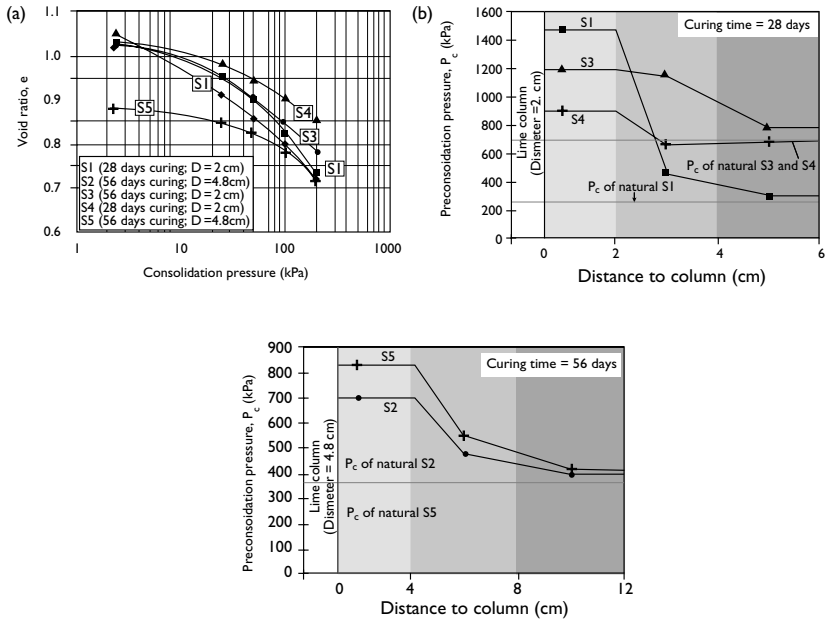

Figure 22.15 (a) Compression curves for the samples treated by lime column, and (b) and (c) effect of lime on preconsolidation pressure in terms of distances to lime and curing periods.

mixture design procedure developed by Thompson (1966) was utilized on disturbed soil samples. By employing approximately 100 kg disturbed sample, five different types of lime–soil mixtures (2%, 4%, 6%, 8%, and 10% lime by weight) were prepared and engineering properties of each were determined after 3, 7, 14, and 28 days. Prior to the preparation of lime-treated samples, pH tests were also carried out to obtain general information on the amount of lime to be mixed into the soil. Eads and Grim (1966) developed a quick test to determine if a soil is lime-reactive and how much lime, in percent by weight, is necessary to achieve a desired volume change reduction. The lowest percent lime to produce a pH of 12.4 is termed "lime modification optimum" (Nelson and Miller, 1992). In the current study, a pH value (12.2) close to 12.4 was achieved in the case of a 6% lime mixture.

Gradation and consistency

Flocculation of clay particles is one of the fundamental effects of lime stabilization on clay soils. A change in soil texture through flocculation of the clay particles takes place when lime is mixed with clay. As the concentration of lime is increased, there is an artificial reduction in clay content. Variations in grain size distribution, depending on lime content and curing time, are evaluated by the grain size distribution analyses. Variation in grain size distribution of the samples in 28 days curing period is shown in Figure 22.17a as an example. It was evident from Figure 22.17a that the amount of clay fell below 10% when lime content achieved was 4% or more. The lowest clay content (2%) was obtained at

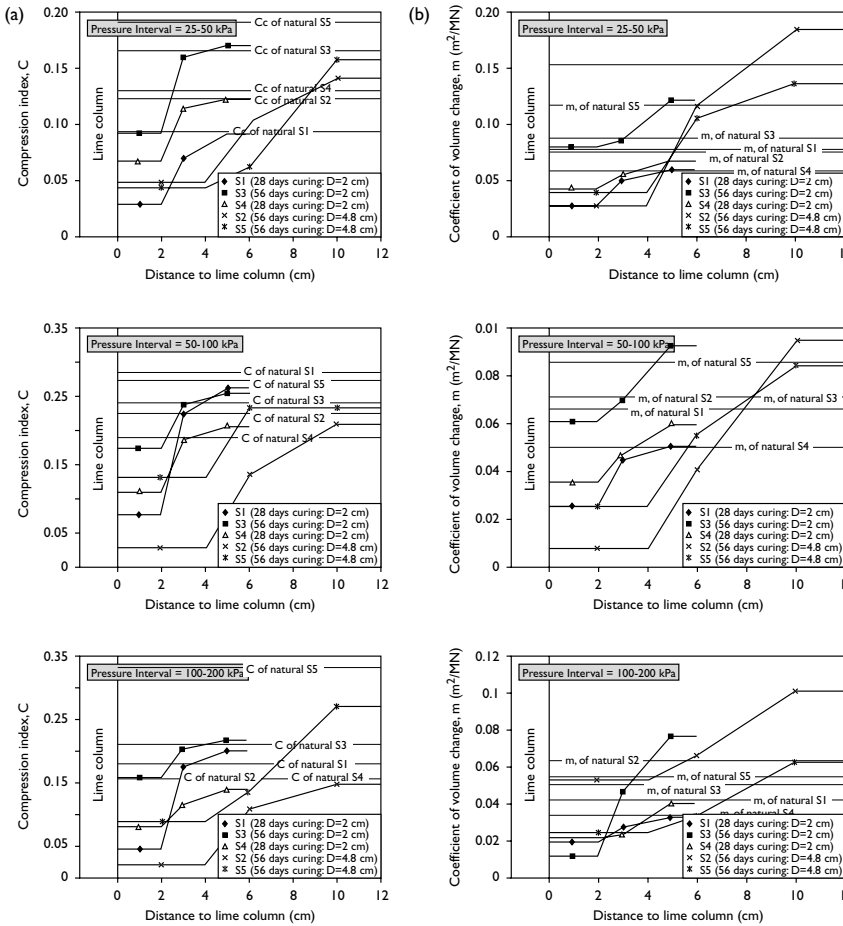

Figure 22.16 (a) Influence of lime stabilization on the compression index and (b) coefficient of volume change depending on distance to column and curing period.

4% lime content for each curing period employed. Due to this, the percent of "sand and gravel" increased as the lime content increased (Figure 22.17b).

In most cases, the effect of lime on plasticity of a clay soil is instantaneous and the calcium ions from the lime cause a reduction in plasticity. Due to this effect, the soil becomes more friable and more easily worked. The clay particles undergo flocculation to form aggregates, which behave like silt particles. Bell (1996) stated that very small quantities (from 1% to 3%) of lime are sufficient to bring about these changes in plasticity. Since the amount of clay-sized particles considerably decreases in the case of lime contents equal

to 4% and more, the effect of lime mixture stabilization on Atterberg limits was only examined on a sample with a lime content of 2% for four different curing periods. Figure 22.18a suggested that the effect of application of the lime mixture technique on Atterberg limits was very quick and evident in the first 7 days, while it gradually decreased between 7 and 14 days. For curing periods longer than 14 days it tended to be stationary. Although an increase was expected in plastic limit, it tended to decrease. This behavior was considered probably due to the presence of quartz and kaolinite minerals in the sample.

Compaction characteristics

An increase in optimum moisture content and reduction of maximum dry density for the same compaction effort can be achieved when lime is added to all clay soils (Bell, 1988a). The results obtained by Afes and Didier (2000) indicated that the optimum moisture content increased from 20.5% to 24.5% while the maximum dry density decreased from 1.65 g/cm^3 to 1.52 g/cm^3. These results reveal the soils in wetter than original condition to be compacted satisfactorily. The results obtained from the lime-treated samples prepared in our study are shown in Figure 22.18b as moisture content-dry density curves. Figure 22.18b suggested

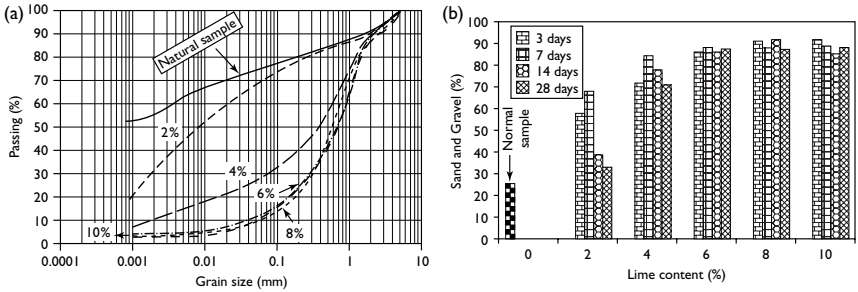

Figure 22.17 (a) Influence of lime content on the gradation curve of the soil (28 days curing) and (b) "sand and gravel" percent.

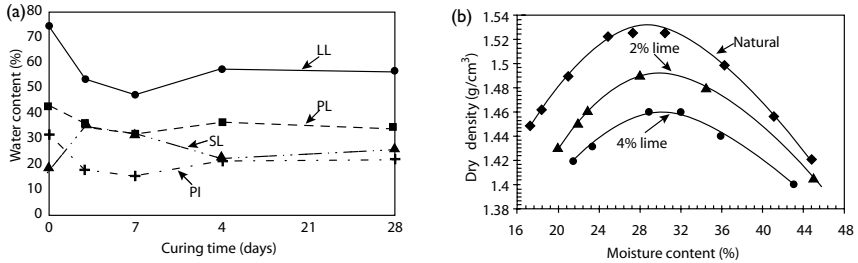

Figure 22.18 (a) Effect of curing time on consistency of the soil with 2% lime content, and (b) compaction curves of the natural and treated samples.

a decrease in the maximum dry density and increase in optimum water content after lime stabilization when compared to those of the untreated samples shown in Figure 22.5.

Strength

The unconfined compressive strength tests were performed on the remolded specimens to evaluate the effects of lime on the unconfined compressive strength of Ankara Clay. However, when 6% or more of lime was mixed with Ankara Clay, remolded specimens could not be prepared. Due to this difficulty, only 2% and 4% of lime contents were used. As seen in Figure 22.19a, for the curing periods shorter than 28 days, the unconfined compressive strength of the untreated sample was higher than those of the treated samples. This suggested that the pozzolanic reactions were slower than the flocculation of the Ankara clay. The maximum improvement on the strength was obtained at 4% lime content for 28 days curing period. The stress–strain curve of the sample having 4% lime and 28 days curing period is shown in Figure 22.19b. This figure illustrated that the treated sample suffered lesser deformation when compared to the untreated sample, and therefore, Young's modulus increased about 60% with the application of lime-mixture technique.

Swelling

A series of swelling tests were performed on the treated clay samples to assess the effect of lime-mixture stabilization technique on swelling characteristics of the soil by considering different lime mixtures and curing periods. Figure 22.20 indicated that swelling pressure sharply decreased at the end of the third day curing period, and 100% reduction in swelling period was recorded for the sample with 4% lime content which seemed to be the most suitable mixture design. Basma and Al-Sharif (1994) pointed out that lime contents between 3%–9% are required to reduce the swelling pressure to zero depending on the properties of clay soils. The optimum lime content obtained in the present study fell into the range mentioned here.

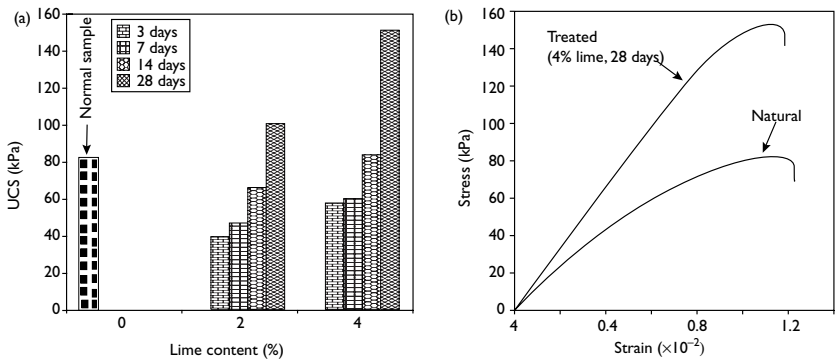

Figure 22.19 (a) Variation of unconfined compressive strength (UCS) with lime content, and (b) stress–strain behaviour of the soil after stabilization by lime-mixture technique.

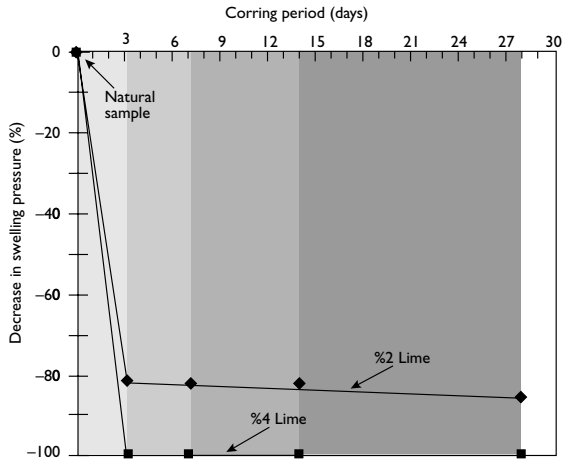

Figure 22.20 Effects of lime content and curing period on swelling pressure.

Conclusions

The particle size distribution analysis results showed that the soils used were mostly composed of fine particles. The amount of clay size fraction in the samples tested was between 64% and 77%, and the smectite mineral content between 29% and 43%. The ranges of liquid limit, plastic limit, and plasticity index of the untreated soil samples varied between 64% and 75%, 31% and 43%, and 29% and 34%, respectively. The samples fell into the MH and CH soil groups of the Unified Soil Classification System, and had a high expansion capacity. It was noted that there was little change in the geomechanical parameters of the Ankara Clay tested. Based on the lime mixture experiments, a lime content of 4% in 28 days curing period provided maximum improvement in engineering properties. A reduction in the clay content of the soil by addition of lime resulted in a reduction of the amount of swelling, particularly at 4% lime content.

The decrease in clay particles in the soil in the close vicinity of the columns (approximately at a distance twice the column diameter) was between 20% and 40% after treatment depending on curing time. This indicated that considerable flocculation due to lime migration had occurred. A similar trend was also observed in consistency limits, and the decrease in plasticity was rapid in the 28-day curing period and pronounced at a distance of approximately twice the column diameter.

As a result of pozzolanic reactions, the unconfined compressive strength of the soil was increased with the introduction of lime columns. The highest gain in strength was about 80%. The sample with the highest smectite content exhibited a more pronounced response to treatment. The stress–strain curves of the treated soils showed slight peaks and the soil tended to behave in a slightly brittle manner.

Lime column installation resulted in a drastic reduction in swelling pressure, reaching up to 40%–75%. The maximum decrease in swelling pressure was achieved at a distance equal to the column diameter, and the swelling pressure tended to slightly increase beyond this zone, as the distance from the column increased. The construction of lime columns caused a chemically induced preconsolidation effect resulting in an increase in the vertical effective stress and a reduction in the compressibility characteristics of the soil.

The study showed that treatment by the lime column technique and lime-mixture techniques can be used effectively in the stabilization of the expansive Ankara Clay. The laboratory-scaled lime column models indicated that the most effective treatment may be achieved at a distance of approximately twice the column diameter. The optimum curing time for lime-mixture technique obtained for the Ankara Clay was 28 days. Although this study was a preliminary work based on laboratory-scale models, it was a first trial on the performance of lime column techniques to stabilize the expansive Ankara Clay. The results from this study may provide useful information for future in-situ lime column and lime-mixture works using this clay.

References

Afes, M. and Didier, G., 2000. Stabilization de sols gonflants: cas d'une argile en provenance de Mila (Algerie). *Bulletin of Engineering Geology and the Environment*, 59, 75–83.

Aras, I.A., 1991. Clay mineralogy and sedimentological features of the Late Pliocene sediments in Ankara area. MSc Thesis, Department of Geological Engineering, Middle East Technical University, Ankara, Turkey.

Arda, S., 1966. Preconsolidation of Ankara clay. MSc Thesis, Department of Civil Engineering, Middle East Technical University, Ankara, Turkey.

ASTM, 1994. Annual Book of ASTM Standards Soil and Rock, Building Stones, Section 4, Construction, V. 04.08. American Society for Testing and Materials, Philadelphia.

Basma, A.A. and Al-Sharif, M.A., 1994. Treatment of expansive soils to control swelling. *Geotechnical Engineering Journal*, 25(2), 3–19.

Bell, F.G., 1988a. Stabilization and treatment of clay soils with lime, Part – 1: basic principles. *Ground Engineering*, 21(2), 10–15.

Bell, F.G., 1988b. Stabilization and treatment of clay soils with lime, Part – 2: some applications. *Ground Engineering*, 21(2), 22–30.

Bell, F.G., 1996. Lime stabilization of clay minerals and soils. *Engineering Geology*, 42, 223–237.

Birand, A., 1963. Study of the characteristics of Ankara Clay showing swelling properties. MSc Thesis, Department of Civil Engineering, Middle East Technical University, Ankara, Turkey.

Brandl, H., 1981. Stabilization of slippage-prone slopes by lime piles. *Proceedings of the 8th International Conference on Soil Mechanics and Foundation Engineering*, 3, 738–740.

Calgin, R., Pehlivanoglu, H., Ercan, T., and Sengün, M., 1973. Ankara civari jeolojisi. Mineral Research and Exploration Institute of Turkey (MTA), Report No. 18, Ankara (in Turkish).

Chummer, A.V., 1987. Ground improvement by sand lime piles. *Proceedings of the 9th SE Asian Geotechnical Conference, Bangkok, Thailand*, 611–619.

Cokca, E., 1991. Swelling potential of expansive soil with a critical appraisal of the identification of swelling of Ankara soils by methylene blue tests. PhD Thesis, Department of Civil Engineering, Middle East Technical University, Ankara, Turkey.

Diamond, S. and Kinter, E.B., 1966. Adsorption of calcium hydroxide by montmorillonite and kaolinite. *Journal of the Colloid Interface Science*, 22, 240–249.

Eads, J.L. and Grim, R.E., 1966. A quick test to determine lime requirements for lime stabilization. *Highway Research Bulletin*, 139, 61–72.

Erguler, Z.A. and Ulusay, R., 2003. A simple test and predictive models for assessing swelling potential of Ankara (Turkey) Clay. *Engineering Geology*, 76, 331–352.

Erol, O., 1976. Ankara sehrinin gelismesinde dogal kosullarin etkisi. Ankara Universitesi, Dil ve Tarih Cografya Fakültesi 50. Yil Konferanslari, 45–55 (in Turkish).

Furtun, U., 1989. An investigation on Ankara soils with regard to swelling. MSc Thesis, Department of Civil Engineering, Middle East Technical University, Ankara.

Gundogdu, M.N., 1982. Neojen yasli Bigadic sedimanter baseninin jeolojik, mineralojik ve jeokimyasal incelenmesi. PhD Thesis, Department of Geological Engineering, Hacettepe University, Ankara, Turkey (in Turkish).

Indraratna, B., Balasubrayaniam, A.S., and Khan, M.J., 1995. Effect of fly ash with lime and cement on the behaviour on a soft clay. *Quarterly Journal of Engineering Geology*, 28, 131–142.

Kiper, O.B., 1983. Etimesgut-Batikent yöresindeki Ust Pliyosen cökellerinin jeo-mühendislik özellikleri ve konsolidasyonu. PhD Thesis, Department of Geological Engineering, Hacettepe University, Ankara (in Turkish).

Kitsugi, K. and Azakami, H., 1982. Lime-column techniques for the improvement of clay ground. *Proceedings of the Symposium on Recent Developments in Ground Improvement Techniques*, Bangkok,105–115.

Kocyigit, A., and Türkmenoglu, A., 1991. Geology and mineralogy of the so-called Ankara Clay formation: a geologic approach to the "Ankara Clay" problem. 5. Ulusal Kil Sempozyumu Bildiriler Kitabi, Eskisehir, Turkey, 112–125 (in Turkish).

Nalbantoglu, Z. and Tuncer, E.R., 2001. Compressibility and hydraulic conductivity of a chemically treated expansive clay. *Canadian Geotechnical Journal*, 38, 154–160.

Nelson, J.D., and Miller, D.J., 1992. *Expansive Soils – Problems and Practice in Foundation and Pavement Engineering*. John Wiley and Sons, p. 259.

Nicholson, P.G., Kashyap, V., and Fujii, C.F., 1994. Lime and fly ash admixture improvement of tropical Hawaiian soil. *Transportation Research Record*, 1440, 71–78.

Noble, D.F. and Anday, M.C., 1967. Migration of lime deposited in drill holes. Virginia Highway Research Council Publication, Portsmouth, p. 321.

Oral, C., 1964. Stabilization of Ankara Clay. MSc Thesis, Department of Civil Engineering, Middle East Technical University, Ankara, Turkey.

Ordemir, I., Soydemir, C., and Birand, A., 1977. Swelling problems of Ankara Clay. *Proceedings of the 9th International Conference on Soil Mechanics and Foundation Engineering*, Tokyo, Japan, 243–346.

Popescu, M.E., Constantinescu, T., Ferrando, C., and Quintavalle, F., 1997. Treatment of subgrade expansion soil at the extension of Bucharest–Otopeni International Airport. *Proceedings of the Intertaional Symposium on Engineering Geology and the Environment*, Athens, Greece, 331–338.

Rogers, C.D.F., and Bruce, C.J., 1991. *Slope Stability Engineering*. Thomas Telford, London, p. 443.

Rogers, C.D.F., and Glendinning, S., 1997. Improvement of clay soils in-situ using lime piles in the UK. *Engineering Geology*, 47, 243–257.

Ruenkrairergsa, T., and Pimsarn, T., 1982. Deep hole lime stabilization for unstable clay shale embankment. *Proceedings of the 7th SE Asia Geotechnical Conference*, Hong Kong, 631–645.

Sivapullaiah, P.V., Sridharan, A., and Ramesh, H.N., 2000. Strength behaviour of lime-treated soils in the presence of sulphate. *Canadian Geotechnical Journal*, 37, 1358–1367.

Skempton, A.W., 1953. The colloidal activity of clays. *Proceedings of the 3rd International Conference on Soil Mechanics*, Zurich, 57–61.

Thompson, M.R., 1966. Lime reactivity of Illinois soils. *Journal of Soil Mechanics and Foundation Engineering Division ASCE*, 92, 67–92.

Tuncer, E.R. and Basma, A.A., 1991. Strength and stress–strain characteristic of a lime treated cohesive soil. *Transportation Research Record*, 1295, 70–79.

Tystovich, N.A., Abelev, M. Yu., and Takhirov, I.G., 1971. Compacting saturated loess soils by means of lime piles. *Proceedings of the 4th Conference on Soil Mechanics*, Budapest, 837–842.

Uner, A.K., 1977. A Comparison of Engineering Properties of Two Soil Types in the Ankara Region. MSc Thesis, Department of Civil Engineering, Middle East Technical University, Ankara, Turkey.

Chapter 23

Lime stabilization of expansive clay

Zalihe Nalbantoglu[1]

Summary

The effect of lime treatment on the engineering properties of soil was investigated by comparing the physical properties, strength, compressibility, and swelling potential of natural and lime treated expansive soils. Test results indicated that addition of lime increased the valency of absorbed cations associated with cation exchange phenomenon and decreased plasticity. Significant reduction in the swell potential and compressibility of the lime treated soils was obtained. Scanning electron microscope (SEM) was used to bring out the qualitative changes occurring in the microstructure of the lime treated soils. Lime treatment produced a soil with a more open fabric and less water absorption potential. Lime treatment has tremendous potential as an economical method for soil stabilization.

Introduction

In geotechnical engineering practice, the soils at a given site are often less than ideal and may cause damage to structures. In the United States, damage from swelling soils annually causes a greater economic loss than floods, hurricanes, tornadoes, and earthquakes (Jones and Holtz, 1973). Recently, there has been a worldwide interest in expansive clays and shale. Usually, expansive soils are found in abundance in semi-arid regions of tropical and temperate climatic zones, where annual evapotranspiration exceeds precipitation. The alkaline environment and lack of leaching favor the formation of montmorillonite minerals which have a very high swell potential (Abduljauwad, 1993).

The modification of engineering properties of expansive soils has become very important to geotechnical engineers, as soils that are ideal become less available. There are a number of additives which may be utilized for ground modification. The most commonly used additives are Portland cement, lime, fly ash, and lime–fly ash. Lime treatment in cohesive soils generally causes a decrease in plasticity, dispersion, and volume change potential, and an increase in particle size, permeability, and strength (Broms and Boman, 1977; El-Rawi and Awad, 1981; Locat *et al*., 1990; Tuncer and Basma, 1991; Nalbantoglu and Gucbilmez, 2001). Various researchers have suggested different methods of stabilization to modify and improve soil properties (Highway Research HPR Report, 1967; Mowafy *et al*., 1985;

[1] Department of Civil Engineering, Eastern Mediterranean University, Gazimagusa, Mersin 10, Turkey; email: zalihe.nalbantoglu@emu.edu.tr

Kennedy *et al*., 1987; Basma and Tuncer, 1991, Al-Rawas *et al*., 2002; Nalbantoglu and Gucbilmez, 2002; Al-Rawas *et al*., 2005).

Scanning electron microscope (SEM) has been used to identify the nature of clay particle aggregates and their arrangement in soils. It gives information about the visible changes at the microstructure level. The main purpose of the microscopic examination is to determine mineralogical composition, texture, and internal structure. SEM has also been used to investigate the secondary products formed from pozzolanic reactions. In previous studies, SEM was used to investigate the changes in soil fabric. Croft (1967) made use of SEM to identify the structure of soils stabilized with cementation compounds. Narasimha and Rajasekaran (1996) observed aggregated particles of lime-treated soils with an open type of fabric arrangement. The gel coatings of the aggregates cemented the particles together and formed aggregated crumbs. Locat *et al*. (1996) used SEM to explain the changes in the behavior of lime-treated soils relative to compressibility, shear strength, and hydraulic conductivity. They found that pozzolanic reactions filled parts of the interaggregate pore network and coated most aggregate external surfaces with secondary minerals resulting in a decrease in the average pore radius.

In the study reported in this chapter, hydrated lime was used as a chemical stabilizer to improve the engineering properties of an expansive soil. Scanning electron microscope was used to bring out the qualitative changes occurring in the microstructure of the lime treated soils.

Materials and methods

The site selected was based on the reported structural damage in an area in which serious cracks were observed on buildings and pavement. The soil had a high expansive character. The physical and mineralogical properties of the soil are given in Table 23.1.

Soil specimens were collected from a depth of 1.5 m below the ground surface. A series of tests were first performed on compacted soil specimens without admixture followed by additional tests in which lime was added in different percentages. Soil-lime mixtures were prepared with lime of 3%, 5%, and 7% by dry weight of soil. All specimens were compacted

Table 23.1 Physical and mineralogical properties of soil at case study site

Properties	*Test values*
Calcite (%)	23.0
Quartz (%)	20.0
Chlorite (%)	5.0
Illite (%)	3.0
Plagioclase (%)	4.0
Dolomite (%)	7.0
Kaolinite (%)	21.0
Smectite (%)	17.0
Liquid limit (%)	67.8
Plastic limit (%)	22.2
Plasticity index (%)	45.6
% Clay fraction (<2 μm)	33.0
Activity	1.38

before testing by using a standard Proctor compaction effort at optimum water content. Naturally available commercial high calcium hydrated lime ($Ca(OH)_2$) was used as a chemical additive.

Results and discussion

The effect of lime treatment on Atterberg limits is given in Figure 23.1. As percent lime increased, the liquid limit decreased and an increase in the plastic limit values was obtained. When lime was added to clay, a cation exchange reaction took place. This reaction decreased the double-layer thickness, resulting in an increase in the attraction forces which led to a better flocculation of the particles. There was also a gradual reduction in the linear shrinkage values of the treated soils.

Many of the engineering properties of soils such as compressibility, volume change potential, hydraulic conductivity, and compressive strength are dependent on the moisture and density values at which the soil is compacted. Therefore, it is important to achieve the desired degree of relative compaction necessary to meet the desired soil properties. Test results in Figure 23.2 indicated that when materials with low specific gravity, like lime, are added to the soil, the maximum dry unit weight of the soil decreases and optimum water content increases with an increase in percent lime. Flocculation and aggregation of the soil particles make the soil more difficult to compact. As percent lime increased, the compaction curve obtained for the soils got flatter. This made the moisture control less critical and reduced the variability of the density produced.

The stress–strain behavior of natural and lime-treated soils at different curing times is shown in Figure 23.3. The shape of the stress–strain diagram of the natural and lime-treated soils at zero curing time were similar to that of normally consolidated soils rather than cemented soils. As curing time increased, the unconfined compressive stress values increased and the shape of the stress–strain diagram changed and became steeper,

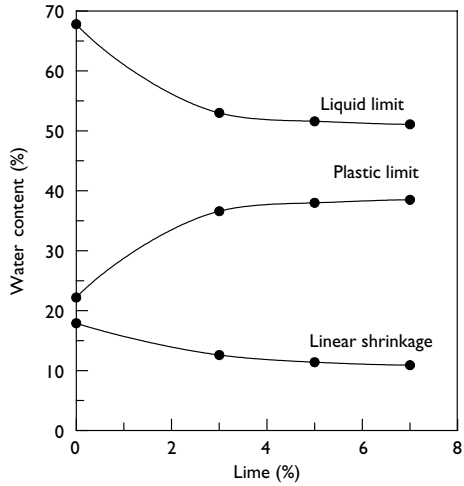

Figure 23.1 Effect of lime on consistency of lime-treated soils.

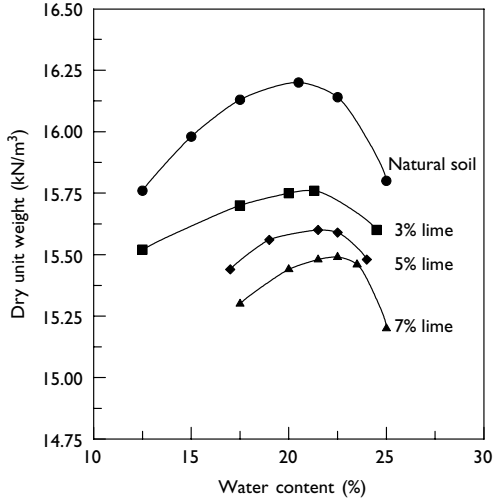

Figure 23.2 Effect of lime treatment on compaction characteristics.

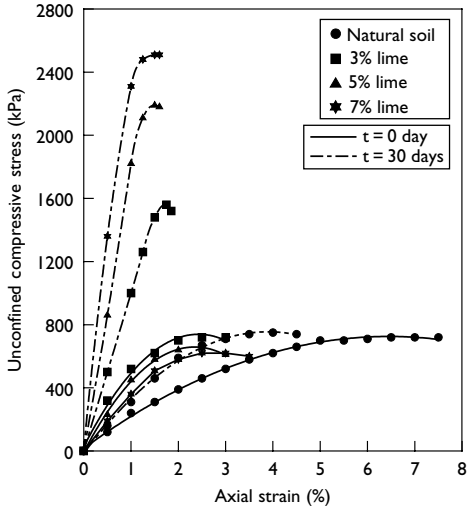

Figure 23.3 Stress–strain diagrams of the natural and lime-treated soils.

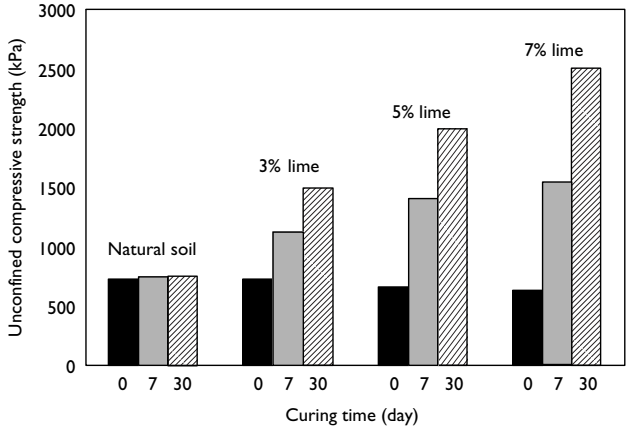

Figure 23.4 The unconfined compressive strength values of natural and lime-treated soils at different curing times.

representing a stress–strain diagram similar to that of over-consolidated clays. This change indicated that a reduction in the compressibility of the lime treated soils was expected.

The effect of lime treatment on unconfined compressive strength (q_u) of soil is given in Figure 23.4. The natural soil, compacted at optimum water content gave an unconfined compressive strength of 720 kPa. Lime treatment and curing time increased the unconfined compressive strength of the soils. At a curing time of 30 days, the unconfined compressive strength value of 7% lime-treated soil increased to 2510 kPa.

The compression and rebound indices (c_c and c_r) obtained from the one dimensional consolidation test data are plotted against percent lime in Figure 23.5. The results indicated the increased tendency of lime-treated soils to resist compression and expansion. A dramatic decrease in c_c and c_r values of the treated soils was seen. This reduction in c_c and c_r was in good agreement with previous findings.

A significant decrease in the swell pressure values of the lime treated soils was observed (Figure 23.6). The swell pressure was obtained by consolidating the pre-swollen specimens to their initial height. The swell pressure of the natural soil was 480 kPa. With only 3% lime treatment, the swell pressure decreased to 98 kPa. The results indicated that the swell pressure values of the treated soils decreased further with an increase in curing time. This was ascribed to the cementing ability of lime-treated soils which reduced the water absorption tendency of the calcium-saturated clays.

Mixing a reactive clay soil with chemical additives resulted in changes in the microstructure of stabilized soils. Reactions between soil–lime–water resulted in attack at sites of structural weakness of clay mineral and caused the crowding of calcium ions on the clay mineral surface. This resulted in changes in soil engineering properties and visible changes at the microstructure level of the stabilized soils.

Changes in the microstructure of lime treated soils occurred. Untreated soil samples showed a uniform clay-like structure with some individual aggregates Figure 23.7

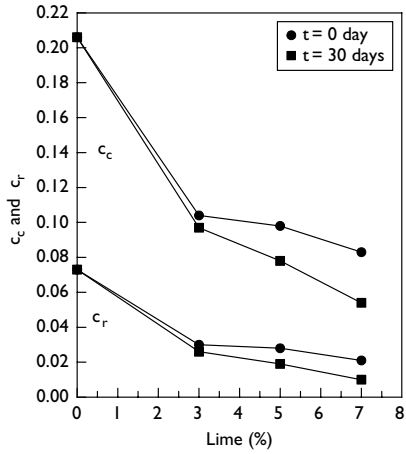

Figure 23.5 Effect of lime and curing time on the compression and rebound indices.

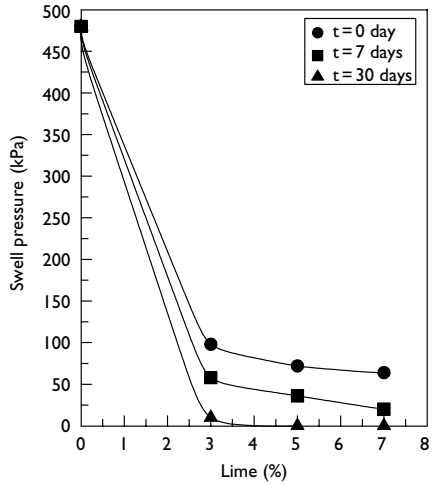

Figure 23.6 Effect of lime and curing time on the swell pressures.

(a). In Figure 23.7 (b) the SEM micrograph of 3% lime-treated soil is given. The results indicated that a small amount of aggregation started with 3% lime treatment. In Figure 23.7 (c), the sample was treated with 5% lime and indicated new soil formation with more flocculated fabric. At a higher magnification (Figure 23.7 (d)) the clay particles appeared to be in a highly porous arrangement, and further, a sponge-like structure could be seen.

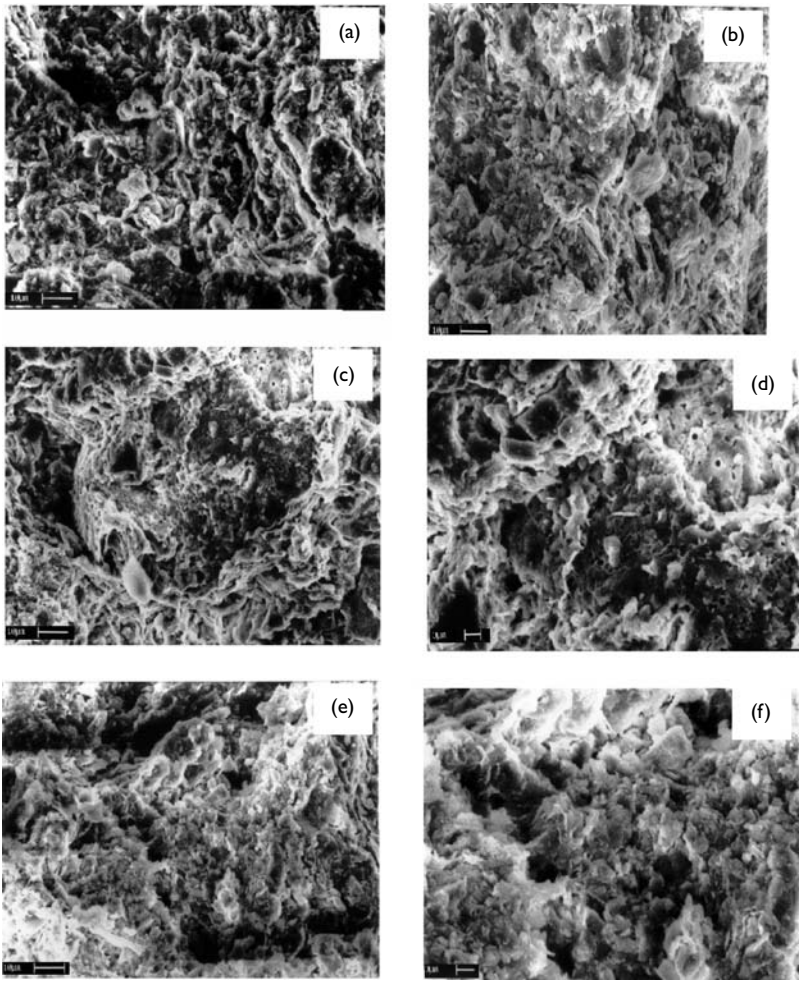

Figure 23.7 Scanning electron micrographs of the natural and lime-treated expansive soils after 30 days of curing: (a) natural soil, (b) soil treated with 3% lime (c and d) soil treated with 5% lime, (e and f) soil treated with 7% lime.

The SEM micrograph for 7% lime-treated soil is given in Figure 23.7 (e). The results showed the flocculation and the formation of new phases due to lime treatment. The soil particles were fused together into a larger aggregate mass and resulted in a more open fabric arrangement. At a higher magnification (Figure 23.7 (f)), the highly open fabric arrangement could clearly be seen. The cementing phases, due to gradual crystallization of the new secondary minerals, caused an increase in the strength of the stabilized soils (Locat *et al*., 1996).

Conclusions

Lime was very effective in increasing the unconfined compressive strength of treated soils. The unconfined compressive strength values of the soils increased with an increase in percent lime and curing time. Swell pressure values of the treated soils decreased and with the increase in curing time further reduction in these values were obtained. This was ascribed to the cementing ability of lime-treated soils which reduced the water absorption tendency of the calcium-saturated clays. The analyses of the SEM micrographs of the natural and treated soils indicated that soil treatment produced new phases with a highly open fabric arrangement. This caused a decrease in water absorption potential. The formation of new cementation compounds also provided for a long-term strength development of stabilized soils.

References

Abduljauwad, S.N., 1993. "Treatment of calcareous expansive clays," *Fly Ash for Soil Improvement, Geotechnical Special Publication*, ASCE, 36, pp. 100–115.

Al-Rawas, A.A., Taha, R., Nelson, J.B., Beit Al-Shab, T., and AL-Siyabi, H., 2002. "A comparative evaluation of various additives used in the stabilization of expansive soils," *Geotechnical Testing Journal, GTJODJ*, ASTM, 25(2), pp. 199–209.

Al-Rawas, A.A., Hago, A.W., and Al-Sarmi, H., 2005. "Effect of lime, cement and sarooj (Artificial Pozzolan) on the swelling potential of an expansive soil from Oman," *Building and Environment*, 40(5), pp. 681–687.

Basma, A.A. and Tuncer, E.R., 1991. "Effect of line on volume change and compressibility of expansive clays," *Transportation Research Record*, 1295, pp. 52–61.

Broms, B. and Boman, P., 1977. *Stabilization of Soil with Lime Columns*, Royal Institute of Technology, Department of Soils and Rock Mechanics, Sweden, Design Handbook.

Croft, J.B., 1967. "The structures of soils stabilized with cementitious agents," *Engineering Geology*, 2, pp. 63–80.

El-Rawi, M.N. and Awad, A.A.A., 1981. "Permeability of lime stabilized soils," *Journal of Transportation Engineering Division*, ASCE, 107, TE1, pp. 25–35.

Highway Research HPR, 1967. *Lime and Lime-Fly Ash Soil Stabilization*, Report 26, Alabama Department of Highways.

Jones, D.E. and Holtz, W.G., 1973. "Expansive soils-the hidden disaster," *Civil Engineering*, ASCE, 43, pp. 49–51.

Kennedy, T.W., Smith, R., Holgreen, R.J., and Tahmoressi, M., 1987. "An evaluation of lime and cement stabilization," *Transportation Research Record 1119,* pp. 11–25.

Locat, J., Berube, M.-A., and Choquette, M., 1990. "Laboratory investigations on the lime stabilization of sensitive clays: shear strength development," *Canadian Geotechnical Journal*, 27, pp. 294–304.

Locat, J., Tremblay, H., and Leroueil, S., 1996. "Mechanical and hydraulic behaviour of a soft inorganic clay treated with lime", *Canadian Geotechnical Journal*, 33, pp. 654–669.

Mowafy, Y.M., Bauer, G.E., and Sakeb, F.K., 1985. "Treatment of expansive soils: a laboratory study," *Transportation Research Record 1032,* pp. 34–30.

Nalbantoglu, Z. and Gucbilmez, E., 2001. "Improvement of calcareous expansive soils in semi-arid environments," *Journal of Arid Environments*, 47(4), pp. 453–463.

Nalbantoglu, Z. and Gucbilmez, E., 2002. "Utilization of an industrial waste in calcareous expansive clay stabilization" *Geotechnical Testing Journal*, ASTM, 25(1), pp. 78–84.

Narasimha, R.S. and Rajasekaran, G., 1996. "Reaction products formed in lime-stabilized marine clays," *Journal of Geotechnical Engineering*, ASCE 122(5), pp. 329–336.

Tuncer, E.R. and Basma, A.A., 1991. "Strength and stress-strain characteristics of a lime treated cohesive soil," *Transportation Research Record*, 1295, pp. 70–79.

Chapter 24

Combined lime and polypropylene fiber stabilization for modification of expansive soils

Anand J. Puppala,[1] *Ekarin Wattanasanticharoen*,[2] *and Ali Porbaha*[3]

Summary

Swell and shrinkage-related volume changes of unsaturated expansive soils cause severe distress to infrastructures. Recent research showed that polypropylene (PP) fibers could reduce volumetric shrinkage strains of expansive soils by 15% to 30%. It is assumed that the combined lime and fiber stabilization could reduce total volumetric movements of expansive soils and mitigate distress problems. The present research was conducted to address the effectiveness of combined quick lime and PP fiber stabilization to enhance swell, shrinkage, and strength properties of four expansive clayey soils. Fiber distributions in soil specimens and repeatability of test results were first addressed. Engineering test results showed considerable reductions in swell and shrinkage strains, and these reductions will lead to better treatments of expansive soils by controlling moisture movements through cracks. Test results indicated statistically significant improvements in the expansive soil properties, indicating the effectiveness of this treatment method. Contributions of lime and fibers to enhance soil properties were also addressed.

Introduction

Expansive soils, when subjected to moisture content fluctuations caused by rainfall events, severe droughts, and plumbing leaks, generally undergo large soil movements. Such soil movements cause extensive structural damages to pavements, runways, residential and industrial structures, and foundations (US Army Corps of Engineers Report, 1983; Chen, 1988; Nelson and Miller, 1992). Jones and Holtz (1973) mentioned that the infrastructure damages caused by expansive soils alone are comparable to the combined damages caused by tornados, hurricanes, and floods. Annual maintenance costs to repair afflicted infrastructures from expansive soil movements are estimated to be several billion dollars (Chen, 1988; Nelson and Miller, 1992). This explains the importance of stabilization of these soils prior to infrastructure construction.

[1] Email: anand@uta.edu, Tel # (817) 272-5821 and Fax # (817) 272-5630; corresponding author.
[2] Department of Civil and Environmental Engineering, Box: 19308, The University of Texas at Arlington, Arlington, TX 76019; email: ekarin5@ce.uta.edu, Tel # (817) 272-5737.
[3] Division of Research & Innovation, California Department of Transportation, 5900 Folsom Blvd, Sacramento, California 95819; e-mail: ali_porbaha@dot.ca.gov, Tel # 916-227-7161.

Chemical and mechanical stabilization methods have been used to modify expansive soils (Bugge and Bartelsmeyer, 1961; Diamond and Kinter, 1965; Little, 1987; Hausmann, 1990; Mitchell, 1993; Sherwood, 1995). Among the chemical treatments, lime stabilization is frequently used to treat expansive soils since it chemically alters the plasticity soil properties (Diamond and Kinter, 1965; Little, 1987; Hausmann, 1990). Though lime stabilization is quite effective, it is often limited by leaching problems, moderate strength enhancements, and unsuitable for stabilizing sulfate rich soils. Mechanical stabilization methods including preloading and prewetting techniques are successfully used to modify expansive soils (Hausmann, 1990). However, they do not enhance strength properties and are time consuming.

A mechanical fiber reinforcement method using polypropylene fibers showed promising improvements in expansive soil properties by reducing volumetric shrinkage strain potentials (Puppala and Musenda, 2000). However, this method had no influence on swell strain potentials. Any reductions in shrinkage or desiccation cracks of expansive soils caused in dry environments could lead to lessening of potential heave distress of same soils since moisture access to underlying subgrades through desiccation cracks at surfaces would be limited (Poor, 1974). Hence, the potential utilization of fibers along with chemical additives that reduce swell strains could lead to a complete and effective treatment of natural expansive soils.

The present research was conducted at The University of Texas at Arlington (UTA) to investigate the effectiveness of combined stabilization method utilizing polypropylene fibrillated fibers and quicklime stabilizer (Wattanasanticharoen, 2001). Lime stabilizer was selected since it is well known for mitigating expansive soil behavior. Four expansive soils were considered as control soils. This chapter provides a summary and analysis of laboratory test results, evaluation studies conducted on combined stabilization, material cost details, and construction specifications for field mixing.

Background

In this section, the main focus is on fiber reinforcement studies covered in the literature. Fibers come in two forms, natural and synthetic fibers. Natural fibers investigated in earlier studies include reeds, palmyra (a fiber acquired from the African palmyra palm), wood pulp, coir (coconut fibers), and bhabar, a natural fiber used to make cleaning brushes (Gray and Ohashi, 1983; Ranjan *et al.*, 1996). Synthetic and other fibers include polypropylene (fibrillated, discrete, in bundles, and in meshes) (Gray and Ohashi, 1983; Khire and Benson, 1994; Maher and Ho, 1994; Ranjan *et al.*, 1996; Murray *et al.*, 2000; Wattanasanticharoen, 2001), polyamide (Michalowski and Zhao, 1996; Michalowski and Čermák, 2003), and polyvinyl chloride (PVC) fibers (Gray and Ohashi, 1983). Other fibers include glass (Ranjan *et al.*, 1996), chopped fiberglass (Consoli *et al.*, 1998), and steel fibers (Michalowski and Zhao, 1996; Michalowski and Čermák, 2003). The following discussions cover various geotechnical application areas of fibers.

Gray and Ohashi (1983) studied mechanics of fiber reinforcements in sands and showed that the inclusion of fibers in sands increased peak shear strength and limited post peak reduction in shear resistance. Maher and Ho (1994) noted that the fibers reinforce sandy soils through a combination of particle-fiber frictional contacts and tension mobilized within the fibers due to applied stresses resulting in a particle-interlocking effect within the sand matrix.

Studies on fiber-reinforced sands by Michalowski and Zhao (1996) and Michalowski and Čermák (2003) showed an increase in the failure stress of composite materials, a decrease

in initial stiffness, and an increase in the axial strain to failure. Michalowski and Čermák (2003) introduced a concept of macroscopic friction angle for fiber-reinforced sands and provided description on fiber geometry and their role in the enhancements of strength properties of soils. Tingle *et al.* (1999) concluded that fiber reinforcement in sands is most effective between dry of optimum and optimum moisture contents of the sand. They attributed this effectiveness to an increase in the adhesive capacities of the fibers to sands at these moisture content conditions.

Researchers also focused on stabilization effects of fibers in clays, including expansive clays (Andersland and Khattack, 1979; Gray and Al-Refeai, 1986; Maher and Ho, 1994; Shulley *et al.*, 1997; Ziegler *et al.*, 1998; Puppala and Musenda, 2000). Andersland and Khattack (1979) studied the effect of adding pure cellulose pulp fibers on the shear strength and stress-strain behavior of Kaolinite clay. Triaxial test results showed that the fiber inclusion increased the peak shear strength of Kaolinite under all testing conditions (Andersland and Khattack, 1979).

Inclusion of fibers has shown to increase shear strength of cohesive soil under static loads (Gray and Al-Refeai, 1986). A variety of tensile inclusions ranging from low-modulus polymeric materials to relatively stiff, high-strength metallic inclusions were used to reinforce soils. These tensile inclusions come in many forms ranging from strips and grids to discrete fibers and woven and non-woven fabrics (Gray and Al-Refeai, 1986). Fiber reinforcement of clays, particularly at shallow depths (lower confining pressures), was reported to occur through the adhesion between clay and fibers rather than the friction between clay particles and fibers, as in the case of cohesionless soils (Shulley *et al.*, 1997; Gregory and Chill, 1998; Ziegler *et al.*, 1998). The adhesion can be increased with the fiber surface area by increasing length or width of fibers (Shulley *et al.*, 1997; Ziegler *et al.*, 1998). All these studies concluded that the fiber incorporation in sands and clays contribute to soil reinforcement and stabilization.

Very few studies involving fiber treatments addressed expansive soil modifications (Ziegler *et al.*, 1998; Puppala and Musenda, 2000; Punthutaecha *et al.*, 2003). Two recent studies showed moderate to considerable reductions in shrinkage strains of expansive soils in dry environments (Ziegler *et al.*, 1998; Puppala and Musenda, 2000). The same fiber treatments, however, resulted in an increase in swell strain potentials of expansive soils (Puppala and Musenda, 2000). Punthutaecha *et al.* (2003) studied matric suction potentials and soil water characteristic curves of unsaturated expansive soils modified by fibers. This study indicated that fibers had minor or no improvements in swell properties and significant improvements of shrinkage-related volume changes of expansive soils (Punthutaecha *et al.*, 2003). Nevertheless, the fibers' treatments can be quite effective in stabilizing expansive soils since they can mitigate shrinkage cracks in soils. These cracks in soils are known to cause or worsen heaving problems by saturating large amounts of underlying expansive soils so that water can reach through shrinkage or desiccation cracks.

It is assumed here that combining fibers with chemical additives such as lime stabilizer could lead to an effective and complete treatment of expansive soils since lime and polypropylene fibers could reduce swell and shrinkage-related volume changes in soils. Additionally, the combined stabilization, if effective, could lead to better treatments of sulfate-rich expansive soils by reducing the amounts of calcium stabilizer and replacing it with fibers. Better treatments to sulfate soils are expected since reduced amounts of calcium stabilizer treatments may result in low amounts of swell-prone crystalline mineral (ettringite) formation in soils. All these assumptions require experimental verifications. The present

research was hence conducted to evaluate the effectiveness of combined lime and fiber treatment to stabilize sulfate-rich expansive soils.

Lime stabilizer was considered as the sole calcium stabilizer since a majority of the case studies involving sulfate heave problems were predominantly associated with lime stabilization (Puppala *et al.*, 2001). Results presented in this chapter address the effectiveness of lime-fiber stabilization in laboratory conditions. Verification studies are needed for further evaluation of this method in true field conditions.

Experimental program

The research was conducted to test four expansive soils sampled from four different locations in Arlington, Texas. These soils were termed with their sampling location names, Walnut Creek (WC), Quail Creek (QC), South Cooper Estate East (SE), and South Cooper Estate West (SW). Table 24.1 presents basic physical properties of these soils. This table indicates that all soils contain large amounts of soluble sulfates, which make them appropriate as base soils for the present research.

Table 24.2 presents physical and engineering properties of polypropylene fibers. The fibers provide excellent resistance to chemical and alkali reactions and are not affected by the presence of sulfates and other inorganic chemicals. Quick lime used in the combined treatment was reduced from usual amounts of 10% to 12% to 8% since reduced calcium content was expected to reduce sulfate heaving distress in present sulfate-rich expansive soils. This heave was later addressed by assessing the ettringite formation in lime-fiber treated soils via mineralogical studies.

Stabilizer-related variables studied here were percent amounts of polypropylene fibers and curing periods adapted. Two fiber amounts (0.15% and 0.30% by dry weight of soil) and three curing periods including short (3 days), medium (7 days), and long (14 days) time periods were studied. These variables along with four control expansive soils increased the total number of variables in this research. Additionally, lime stabilization studies were

Table 24.1 Physical properties of control soils

Soil properties	*Soil sampling location*			
	Walnut Creek (WC)	*Quail Creek (QC)*	*South Cooper Estate West (SE)*	*South Cooper Estate West (SE)*
Passing #200 (%)	90	93	89	91
Specific gravity	2.87	2.80	2.76	2.85
Liquid limit (%)	69.4	69.0	70.6	73.9
Plasticity index, PI (%)	42.7	41.1	42.2	45.0
Natural moisture content (%)	6.0	5.7	7.2	6.6
pH	7.96	8.20	8.13	8.08
Soluble sulfate content (ppm)[a]	32,122	5,688	4,737	33,048
USCS classification	CH	CH	CH	CH

Source: Puppala *et al.*, 2002.

Note
a Based on Modified UTA method.

Table 24.2 Physical and engineering properties of polypropylene fibers

Descriptions	*Magnitudes*
Material	Polypropylene
Tensile strength	0.67 kN/mm^2 (97 ksi)
Modulus (Young's)	4.0 kN/mm^2 (580 ksi)
Melt point	165°C (330°F)
Chemical resistance	Excellent
Alkali resistance	Excellent
Acid and salt resistance	High
Ignition point	600°C (1,100°F)
Absorption	NIL
Specific gravity	0.91
Density, bulk	8.79 kN/m^3 (56 lb/ft^3)
Density, loose	2.35–3.92 kN/m^3 (15–25 lb/ft^3)
Dosage (Normal)	0.009 kN/m^3 (1.5 lb/yd^3)
Fiber length (Normal)	18 mm (3/4″)
Form	Fibrillated polypropylene
Color	White
Fiber count	1.8–2.7 million/N (8–12 million/lb)

investigated on the same soils to understand the relative contributions of lime and fibers' treatments to the enhancements in soil properties.

The following notation system is used in this chapter for simple identification of each soil, curing period, and percent amounts of each stabilizer. Each sample was given a notation in the form of WC-LF-3-0.15%. The first index of the notation, WC, indicates Walnut Creek location from which the soil was sampled. The second index represents stabilizer type, with LF indicating combined lime-fiber stabilization and L indicating lime stabilization alone. The third index describes the curing period in days. The fourth index is the amount of fibers in the soil sample expressed in percent. For example, "WC-LF-3-0.15%" indicates a three-day cured soil specimen prepared with Walnut Creek soil and stabilized with lime and fibers at 0.15%. The next section describes the soil specimen preparation procedure adapted in this study.

Soil specimen preparation

Compaction moisture contents of stabilized soils differ from those of control soils. Hence, standard Proctor tests were conducted on combined lime-fiber treated soils to determine compaction characteristics. Figures 24.1 and 24.2 present compaction relationships of control and treated soils, respectively. Compaction moisture contents and dry unit weights were established and these results were used to prepare soil specimens for engineering tests. The following section describes the steps followed in the specimen preparation.

The soil in dry state was thoroughly mixed with the lime at the targeted moisture content for approximately 20 minutes until the mixture appeared uniform in color and texture. At this stage, polypropylene fibers were added to the soil-lime mixture as per the targeted fiber amount. As noted, two fiber amounts, 0.15% and 0.30% by dry weight of the soil, were used here and these levels represent practical amounts used in the field. Fiber mixing was performed as per the procedure described by Gregory and Chill (1998). Care was taken to

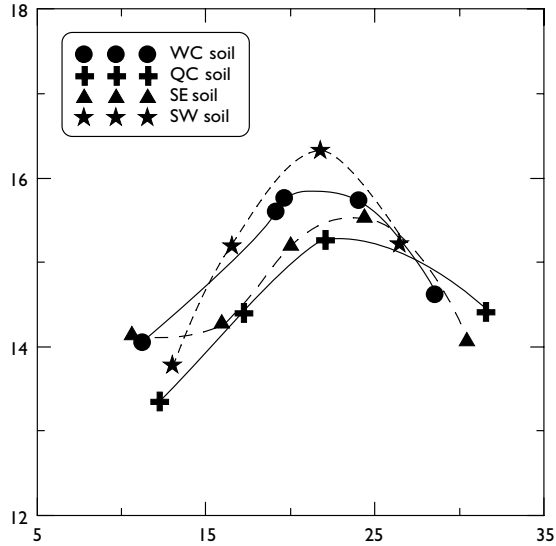

Figure 24.1 Compaction relationships of control soils from standard Proctor tests.

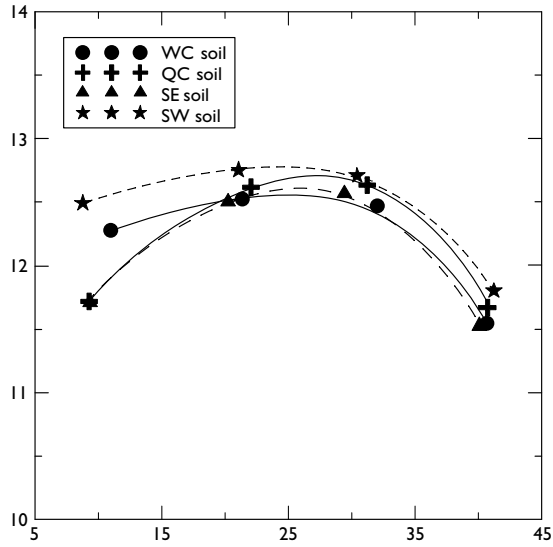

Figure 24.2 Compaction relationships of lime-fiber treated soils from standard Proctor tests.

mix fibers with low amounts of treated soils by selecting three equal portions for each soil specimen. This treatment sequence was followed since initial lime treatment makes soils friable, a state at which fibers can be easily mixed.

Once mixing was completed, soil samples were prepared, mellowed for 24 hours and then compacted into 70-mm (2.8-in.) molds. The specimen was compacted in three layers using a rammer, applying the same number of blows per layer. Compacted soil samples were then wrapped with a geotextile layer and sealed in a moisture-tight plastic bag. These samples were transferred to a 100% humidity controlled room for curing. After curing of 3, 7, and 14 days, soil samples were subjected to a multitude of geotechnical tests. These tests were conducted on both control and treated soils to assess improvements in physical and engineering characteristics from stabilization.

Engineering tests performed include unconfined compressive strength or UCS tests based on ASTM D-2166, (ASTM, 1995) and volume change behavioral tests such as one-dimensional free swell and linear shrinkage strain bar tests (based on Tex-107-E method of Texas Department of Transportation material testing procedures). The UCS tests provide maximum shear strength of soils under unconfined conditions. Both free vertical swell and linear shrinkage tests provide maximum swell and shrinkage strain potentials of soils. Prior to these tests, combined lime-fiber treatment method was addressed for producing uniform soil specimens and yielding repeatable test results.

Uniformity of soil specimens

Lime treatment of soils is well established and usually provides reproducible specimens. On the other hand, randomly oriented fiber mixing and their distributions are not well understood and hence soil specimens were evaluated in this research to address the distribution of fibers in compacted soil specimens. This evaluation was attempted by slicing soil samples into three equal parts and then drying and sieving each one of them. Fibers in each slice were measured and used to calculate percent fibers in each slice. Table 24.3 shows test results of fiber amounts in four randomly selected soil specimens. These results indicate that fiber content in each slice was close to targeted fiber contents, which confirm that soil specimen preparation steps followed here resulted in uniform distribution of fibers along the depth of the soil samples.

Repeatability of test results

The number of tests was selected based on repeatability assessments. These assessments were conducted very early in the experimental program. Six control and six stabilized soil

Table 24.3 Percent fiber content in sliced soil specimens

Specimen slices	*Fiber content (% by dry weight of soil)*			
	Specimen 1 0.15%	*Specimen 2 0.15%*	*Specimen 3 0.30%*	*Specimen 4 0.30%*
Top slice	0.14	0.16	0.32	0.27
Middle slice	0.17	0.15	0.30	0.32
Bottom slice	0.14	0.13	0.28	0.30
Average	0.15	0.15	0.30	0.29
Standard deviation	0.014	0.015	0.020	0.015

Table 24.4 UCS and free swell test results of control and treated soil samples

Test	*Test results on three identical samples*			*Average*	*Standard deviation and COV (%)*
UCS of control SE soil in Mpa	0.13	0.14	0.15	0.14	0.01 and 0.010
UCS of treated (3 days) QC soil in MPa	0.86	0.88	0.86	0.87	0.01 and 0.013
Free swell of control QC Soil in %	12.1	12.3	12.1	12.1	0.12 and 1.333
Free swell of treated SE soil (3 days) in %	2.28	2.47	2.63	2.46	0.18 and 3.070

Notes
Treated soils – 8% lime and 0.15% fibers; 1 psi = 6.9 kPa; COV = Coefficient of variation in %.

specimens were prepared and subjected to both unconfined compressive strength and free swell strain tests. Treated soils were cured for three days.

Table 24.4 presents UCS and free swell strain test results along with standard deviation and coefficient of variations. Both tests provided similar results with low standard deviations. The COV values varied between 0.9% and 7.4%, indicating that both strength and free swell test results of control and lime-fiber treated soils were repeatable. This reconfirms that the combined treatment resulted in well-mixed uniform soil samples, which yielded similar results under strength and swell testing.

Results and discussion

Table 24.5 presents a summary of plasticity index, unconfined compression strength, swell strain, and linear shrinkage strain test results of control and treated soils. Both lime (L) and lime-fiber (L-F) treatment results are included in this table. These results are analyzed and used in the following assessments.

Plasticity properties

The PI (Plasticity index) values of all four soils (shown in Table 24.5) indicate that the lime treatment resulted in lower plasticity properties when compared to control soils. All four soils showed similar reductions in PI properties. These low PI properties of treated soils are close to non-plastic conditions which are well known and are attributed to chemical reactions between lime and soils including ion exchange and associated flocculation reactions. Atterberg limits tests were difficult to perform on lime-fiber treated soil samples since fibers impede the mechanisms of plastic limit and liquid limit tests. Lime treatments were applied prior to fiber treatments, hence the PI properties of lime treated soils were taken as those of lime treated soils.

Shear strength properties

Unconfined compressive strength test results shown in Table 24.5 indicate substantial increase in strength due to combined lime-fiber treatment. The brittle soil failure was not

Table 24.5 Atterberg limits, unconfined compressive strength, free swell strain, and linear shrinkage strain test results of control and treated soils

Stabilizers (%)	*Walnut Creek clay curing periods (days)*				*Quail Creek clay curing periods (days)*				*South Cooper Estate East clay curing periods (days)*				*South Cooper Estate west clay curing periods (days)*			
	0	*3*	*7*	*14*	*0*	*3*	*7*	*14*	*0*	*3*	*7*	*14*	*0*	*3*	*7*	*14*
Atterberg limits (%)																
Control	43	43	43	43	41	41	41	41	42	42	42	42	45	45	45	45
L 8	—	NP	NP	NP	—	NP	NP	NP	—	NP	NP	NP	—	NP	NP	NP
L 8, F 0.15	—	NP	NP	NP	—	NP	NP	NP	—	NP	NP	NP	—	NP	NP	NP
L 8, F 0.30	—	NP	NP	NP	—	NP	NP	NP	—	NP	NP	NP	—	NP	NP	NP
Unconfined compressive strength (Mpa)																
Control	0.19	0.19	0.19	0.19	0.23	0.23	0.23	0.23	0.14	0.14	0.14	0.14	0.20	0.20	0.20	0.20
L 8	—	0.56	0.58	0.96	—	0.61	0.82	1.02	—	0.71	0.86	1.05	—	0.85	1.04	1.22
L 8, F 0.15	—	0.77	0.89	1.26	—	0.64	0.86	1.07	—	0.73	0.89	1.07	—	0.86	1.06	1.28
L 8, F 0.30	—	0.79	0.92	1.30	—	0.87	0.92	1.15	—	0.74	0.98	1.19	—	0.94	1.14	1.56
One-dimensional free swell strain (%)																
Control	20	20	20	20	12.1	12.1	12.1	12.1	15	15	15	15	18	18	18	18
L 8	—	1	0.2	0.1	—	0.52	0.21	0.01	—	0.8	0.6	0.2	—	9.9	3.5	1.9
L 8, F 0.15	—	3.74	1.21	0.81	—	3.44	1.00	0.63	—	2.46	0.11	0.08	—	2.74	1.38	0.97
L 8, F 0.30	—	1.74	0.78	0.41	—	1.33	0.54	0.47	—	0.11	0.00	0.00	—	2.23	0.89	0.48
Linear shrinkage strain (%)																
Control	18	18	18	18	17	17	17	17	17	17	17	17	17	17	17	17
L 8	—	1.2	0.4	0	—	0.9	0.5	0	—	1.8	1.5	0.3	—	0.5	0.3	0
L 8, F 0.15	—	0.4	0.2	0.2	—	0.4	0.2	0.1	—	0.35	0.2	0.1	—	0.45	0.25	0.1
L 8, F 0.30	—	0.2	0.1	0.0	—	0.2	0.1	0.0	—	0.3	0.15	0.0	—	0.2	0.1	0.0

Notes
NP – non-plastic; L – % lime; F – % fibers; 1 psi – 6.9 kPa.

Figure 24.3 Soil specimens treated with lime and fibers and subjected to UCS tests.

Table 24.6 Percent increase in UCS of control, lime, and lime-fiber treated soils

Soil locations		*Percent increase in UCS*								
		Control and lime treated soils			*Control and lime mixed with fibers at 0.15%*			*Control and lime mixed with fibers at 0.30%*		
	Curing period	*3*	*7*	*14*	*3*	*7*	*14*	*3*	*7*	*14*
WC		195	205	405	305	368	563	316	384	584
QC		165	257	344	178	274	365	278	300	401
SE		407	514	650	421	536	664	429	600	750
SW		325	420	510	330	430	540	370	470	680

noticed in the lime-fiber treated soils, which was attributed to the presence of flexible fibers (Figure 24.3). The failure planes of these soil specimens were not unique, possibly due to random orientation and distribution of fibers in the soil specimens.

Isolated lime stabilization study results were compared here with combined treated soils to understand approximate percent contributions of lime and fibers to the overall strength of treated soils. Table 24.6 presents comparisons of strength increase between control and lime treated soils as well as control and lime-fiber treated soils. These results indicate that the majority of strength increase (an average strength increase close to 480%) in treated soil properties was attributed to lime reactions with clayey soils. The fibers' contribution to overall strength appears to be moderate at 0.15% fiber content and substantial at 0.30% fiber content.

The major source of the strength increase in combined treated soils was attributed to lime stabilization reactions, which include cationic exchange, flocculation, pozzalonic, and agglomeration reactions, which are also well established in the literature. Fiber treatments also enhanced shear strength by increasing tensile resistance of treated soils, which can be expressed in the form of an apparent cohesion intercept. A few direct shear tests conducted separately on selected control and QC-treated soils showed 2 to 3° improvements to friction angle properties from combined treatment. These low friction angle improvements are attributed to agglomeration reactions of lime treatment. Fibers' contribution to friction properties is small possibly due to smooth surface characteristics of fibers.

Figure 24.4 presents graphical representation of same overall percent increases in UCS properties of all four soils due to lime and fiber modifications. This figure indicates that the

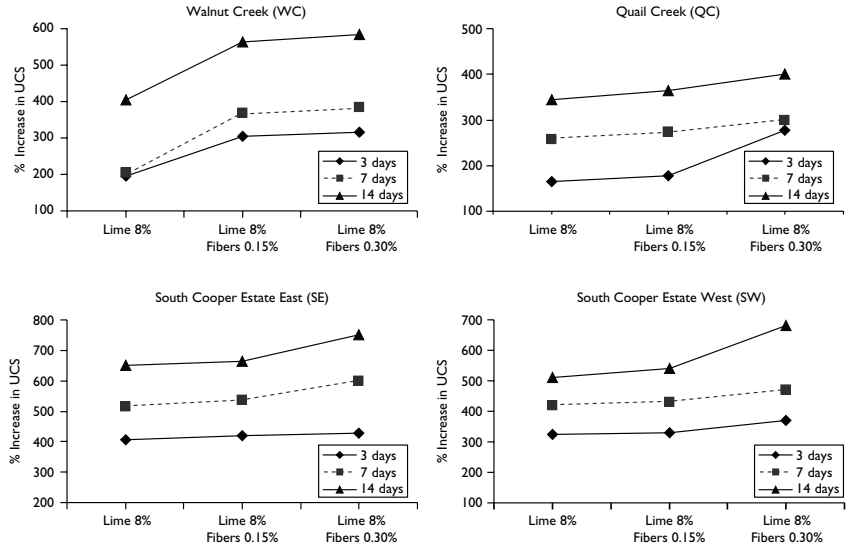

Figure 24.4 Influence of lime-fiber and lime treatments on percent increase in UCS properties of control soils.

percent increase in UCS from combined treatments ranged between 170% and 750%. Among all soils, strength enhancements are higher for SE soils, possibly due to large amounts of clay minerals present in them. All four soils showed similar trends. As noted earlier, an increase in fibers from 0.15% to 0.30% amounts resulted in moderate to substantial increase in shear strength of control soils. Moderate enhancements were noted in the case of WC and QC soils and substantial enhancements were noted for SE and SW soils. These enhancements appear to be dependent on adhesion attractive forces between SE, SW soils and fibers, which are higher than those in WC and QC soils. Overall, the optimum fiber percent for best strength enhancements of combined lime-fiber treatments in present soils is close to 0.30%.

Free swell strain properties

Figure 24.5 presents the percent decrease in free swell strains of all four lime-fiber treated soils. The decrease in free swell strains varied between 70% and 98%, which indicates a strong improvement in swell strain properties from lime-fiber treatment. Free swell test results shown in this figure and Table 24.5 indicate that the lime-fiber treatment reduced free swell strains of all four control soils with SE soil again showing maximum reductions in swell strain potentials. The maximum enhancements in swell strains were attributed to lime reaction that result in reductions of plasticity properties and enhancements in strength properties of soils.

Fibers initially increased swell strains of lime treated soils at low fiber content of 0.15%. The fiber content then decreased swell strains at high fiber amounts of 0.30%. Curing period had a direct and significant influence on these reductions in free swell strains. The results in

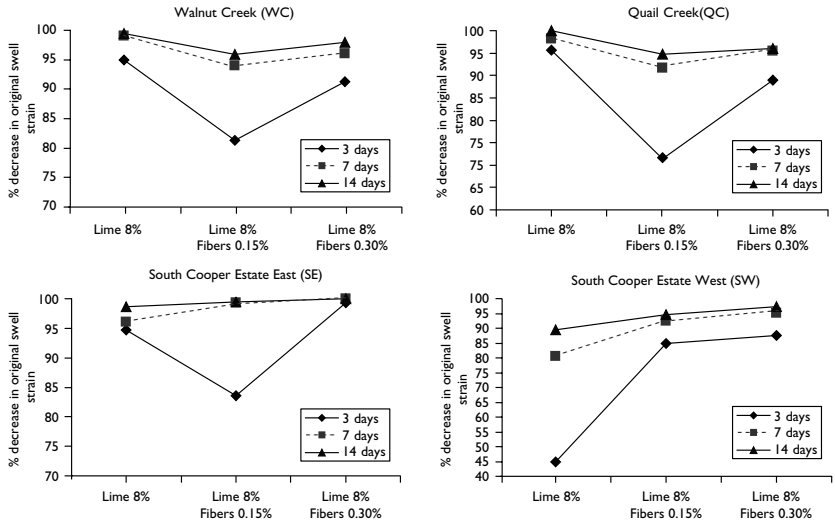

Figure 24.5 Influence of lime-fiber and lime treatments on percent decrease in free swell of control soils.

Figure 24.5 indicate that the swell strain variations at 7- and 14-days curing appeared to be more definitive than the variations noted at 3-days curing.

A comparison between swell test results of both lime and lime-fiber treated soils of Table 24.5 indicate two distinct trends. These trends make it difficult to generalize the present observations noted in free swell strain enhancements. The free swell strains of combined lime-fiber treatments of SE and SW soils were slightly lower than the lime treated same soils, whereas opposite trends were noticed in the case of QC and WC soils with higher enhancements noted in lime-fiber treatments. The following explains possible causes for these variations in the trends.

The high amounts of decrease of free swell strains in lime-fiber treated SE and SW soils are attributed to the following two mechanisms. First, fibers may have facilitated better distribution of moisture content within these treated soils, which may have accelerated reactions between lime and soil. Second, the increase in strength has provided resistance to free swell-related dispersive forces during testing. High increase in soil strength implies substantial improvements in swell strains.

The low amounts of increase in swell strains of lime-fiber treated WC and QC soils attributed to open void structures (low unit weights) formed in fiber-treated soils, which may have raised swell strains of soils. Overall, authors opine that swell mechanisms of lime-fiber treated soils depend on both void distributions and strength enhancements, with strength improvements showing considerable influence on final swell strains. Strength or UCS increase in SE and SW soils is substantially higher than those in WC and QC soils, indicating that the increased shear strengths of SE and SW soils provide ample resistance to disruptive dispersive forces generated during swell test conditions. Hence, low swell strains

were measured for lime-fiber treated SE and SW soils. Further research on additional soil types would corroborate these swell property interpretations in lime-fiber treated soils.

Linear shrinkage strain properties

The linear shrinkage test measures percent shrinkage strain of an elongated soil specimen placed in an aluminum box that was subjected to drying in an oven for 24 hours. Figure 24.6 presents photographs of present soil specimens subjected to linear shrinkage strain bar tests. The first photograph (a) indicates large shrinkage cracks developed in a control soil and the second photograph (b) indicates minute shrinkage strains of the same control soil after lime and fiber treatment. This figure explains the substantial reductions in shrinkage strains due to combined treatment.

Linear shrinkage strain results presented in Table 24.5 indicate that all four soils showed similar and substantial reductions in shrinkage strains after lime-fiber treatment. Similar decrease was also noted in the case of lime treatment indicating that the majority of the decrease in shrinkage strains was due to chemical reactions between lime and control soils, which result in reductions in plasticity properties and related shrinkage strains.

Overall, it can be summarized that both lime-fiber and lime treatments were equally effective in reducing linear shrinkage strains with combined treatment at 0.3% fiber amount level providing the lowest shrinkage strains (0.3% or less). These reductions are quite significant since expansive soils with such low shrinkage strains are considered non-problematic since they do not undergo any desiccation cracks. This confirms the importance of including fibers in the combined treatment for an effective mitigation of shrinkage strain-induced cracking in soils.

Mechanism of fibers in restraining linear shrinkage movements is explained here. The shrinkage cracking resistance in soils is contributed by fibers which induce additional tensile strength or apparent cohesive intercept to composite soil mass. This additional strength counters tensile forces generated in soils during shrinkage environments. As a result, the original linear shrinkage strains were decreased. Also, curing period had similar effect on shrinkage strains as those noticed on swell strains.

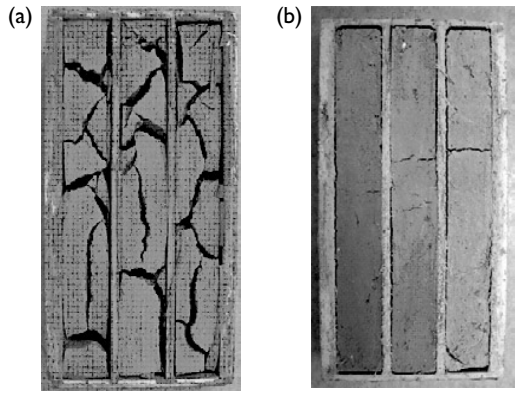

Figure 24.6 (a) Linear shrinkage bar test results of (a) untreated QC soil and (b) lime mixed with fiber treated QC soil.

X-Ray diffraction studies

Powder diffraction studies were conducted on the lime treated soils to verify the ettringite mineral formation in them. Figure 24.7 presents X-Ray Diffraction (XRD) results of lime treated SE and SW soils after a curing period of 14 days. The XRD results in the figure indicate no evidence of ettringite mineral formation in the treated soil. Further analyses on

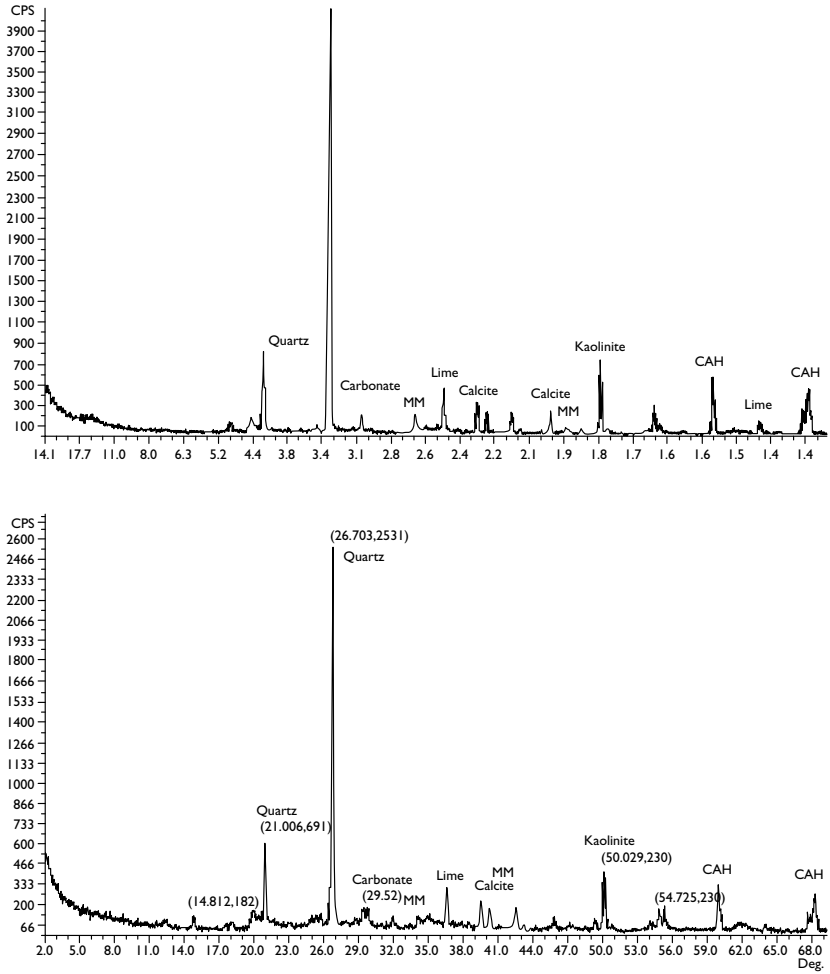

Figure 24.7 XRD analysis results of lime treated clays after 14-days curing; (a) SE soil and (b) SW soil.

Notes
CAH: calcium aluminum silicate hydroxide.
MM: Montmorillonite.

the XRD data showed the presence of a few stabilization compounds including carbonates and calcium aluminum silicate hydroxide (CAH) gels. These gels are known to bond soil particles, which result in the enhancements of soil strength.

In few case studies, ettringite was reported to form a few months after lime stabilization (Puppala *et al.*, 2001). Hence, further mineralogical assessments are needed on treated soils that are subjected to longer curing periods than 14 days to address ettringite formation.

Statistical analyses

The combined stabilization method provided effective stabilization of all four soils by enhancing control soil properties. However, the effectiveness of this stabilization needs to be measured in statistically significant terms. Therefore, statistical analyses were conducted on the present laboratory test data by pooling results from all four soils. One-way analysis of variance method (ANOVA) was used in this analysis.

This statistical evaluation was performed by comparing test results of both control and stabilized soils. The significance level of a test is the probability of exceeding the value of the test statistic under the null hypothesis condition. The probability factor called the F statistic is referred to as the "P-value." The magnitude of the P-value is used to decide the statistical significance of the F factor in the analysis of variance. If the probability is less than the traditional significant level of 0.05 (represents 5% probability error), also known as the alpha or cut-off value for statistical significance, then it can be concluded that the treated soil data is statistically significantly different from the control soil data. The effectiveness can then be measured by assessing whether there is an increase in strength, or decrease in swell or shrinkage strain potentials.

Tables 24.7 and 24.8 present the ANOVA analyses results of test results of both lime and lime-fiber treated soils at various curing conditions. Results in these tables indicate that both lime-fiber and lime stabilizations provided statistically and significant improvements in all soil properties considered in this research. These improvements are also effective since plasticity and volume change properties were reduced and strength properties were enhanced.

Table 24.7 ANOVA analyses on test results of lime treated soils

Comparison groups	*Type of test*	*Control soil and L-3*	*Control soil and L-7*	*Control soil and L-14*
Probability *(P)*	UCS	0.029	0.0003	0.029
	FS	0.029	0.029	0.029
	LS	$<$0.0001	$<$0.0001	$<$0.0001
Statistically significant? ($P < 0.05$)	UCS	Yes	Yes	Yes
	FS	Yes	Yes	Yes
	LS	Yes	Yes	Yes
Treatment: effective or not effective	UCS	Effective	Effective	Effective
	FS	Effective	Effective	Effective
	LS	Effective	Effective	Effective

Notes
UCS – Unconfined compressive strength; FS – Free swell strain; LS – Linear shrinkage strain.

Table 24.8 ANOVA analyses on test results of control and lime-fiber treated soils

Comparison groups	*Type of test*	*Control soil and LF-3-0.15*	*Control soil and LF-3-0.30*	*Control soil and LF-7-0.15*	*Control soil and LF-7-0.30*	*Control soil and LF-14-0.15*	*Control soil and LF-14-0.30*
Probability *(P)*	UCS	0.04	<0.0001	0.0003	0.0004	0.03	0.03
	FS	0.03	0.03	0.03	0.03	0.03	0.03
	LS	<0.0001	<0.0001	<0.0001	<0.0001	<0.0001	<0.0001
Statistically significant? ($P < 0.05$)	UCS	Yes	Yes	Yes	Yes	Yes	Yes
	FS	Yes	Yes	Yes	Yes	Yes	Yes
	LS	Yes	Yes	Yes	Yes	Yes	Yes
Treatment: effective or not effective	UCS	Effective	Effective	Effective	Effective	Effective	Effective
	FS	Effective	Effective	Effective	Effective	Effective	Effective
	LS	Effective	Effective	Effective	Effective	Effective	Effective

Notes
UCS – Unconfined compressive strength; FS – Free swell strain; LS – Linear shrinkage strain; LF – Combined stabilization.

Table 24.9 Approximate cost estimates of lime and fibers

Stabilization method and amount levels	*Weight of stabilizer (N) needed to treat 1,080 m^2*	*Unit cost of the stabilizer per 8,800 N[a] ($)*	*Costs of the stabilizer ($)*	*Total cost ($) (increase over lime in %)*
Lime 8%	Lime 306,856	83	2,894	2,894 (0)
Lime 8% and fibers 0.15%	Lime 306,856 Fibers 5,753	83 2,333	2,894 1,525.5	4,409.5 (52)
Lime 8% and fibers 0.30%	Lime 306,856 Fibers 11,506	83 2,333	2,894 3,051	5,945 (105)

Notes
1 lb = 4.4 N; 1 yard = 0.9 m.
a Freight costs are not included and material cost details are provided by City of Arlington, Texas; thickness of stabilized subgrade is 8″.

Cost analysis

Another important factor in the selection of stabilization methods for field practices is cost details of the stabilizers. It should be noted that the cost analysis presented here would be replaced in the future with AASHTO recommended cost benefit studies. Cost benefit studies address capital and maintenance costs over a period of several years and hence require field performance data of several years. Currently, due to lack of field performance data, cost details of stabilizers are only reported in this section.

Table 24.9 provides approximate cost estimation details of lime and fibers used in this research. These costs are based on stabilizing subgrade up to a depth of 200 mm (8 in.). The 200-mm thickness of subgrade represents the current chemical stabilization practice of a

local city, Arlington, Texas. Costs of materials are estimated to stabilize a test pavement section of a planar area of 1080 m^2 (40′ × 300′). A dry unit weight of 17.5 kN/m^3 of compacted subsoil is used in the cost analysis. Costs of the materials were provided by the City of Arlington, Texas.

The cost calculations indicate that the percent fibers inclusion can significantly increase the overall material costs by 50% at 0.15% of fiber dosage to as high as 100% at 0.30% of fiber dosage. Such high initial costs will be justified if the field performance shows substantial reductions in the annual pavement maintenance costs in life cycle cost analysis.

Specifications for field mixing

In this section, a few details regarding field mixing and compaction of lime and fiber treatments are presented. Since fibers are recommended in combination with chemical stabilizers for field treatments, construction specifications need to be established. This section provides a summarized version of these specifications. Prior to stabilization, the subgrade soil shall be scarified. The polypropylene fibers shall be applied to the subgrade by uniformly distributing them over the scarified subgrade. The fibers should be spread on the subgrade material by using leaf rakes. A rotomixer should be used to mix and distribute fibers along the depth of the subgrade. The maximum lift thickness for fiber mixing should be 200 mm (8 in.). The soil shall then be kept close to optimum moisture content for 72 hours prior to adding lime.

Lime and water required to achieve compaction moisture content shall be mixed to form a mixture for the lime application. Mixing with a pulvamixer will immediately follow lime application until the entire soil mixture passes through a 50 mm (2 in.) sieve. The lime treated subgrade shall then be sealed with a pneumatic roller and left for an initial curing (mellowing) period of no less than 24 hours measured from initial application. The final remix and compaction shall be completed within seven days as measured from the date of the initial application. This procedure is currently under research evaluation in field settings.

Conclusions

The combined lime-fiber treatment method provided reproducible samples which yielded repeatable strength and swell strain results with low standard deviations. The combined lime-fiber stabilization enhanced UCS properties of control soils by a range of 170% to 750%. Possible mechanisms for strength improvements in soils were ion exchange, flocculation, and pozzalonic reactions of lime stabilizer and mechanical interlocking of fibers with soils. The majority of strength increase was, however, attributed to lime stabilizing reactions. Combined stabilization reduced free swell strain potentials of all four control soils. Though lime reactions resulted in substantial reductions in swell strains, fiber modification also provided small reductions in overall swell potentials. Fibers might have facilitated moisture access for enhanced chemical reactions and resulted in an increase in the total shear strength of soils. The increased strength in soils has provided ample resistance to disruptive dispersive forces generated during swelling. Hence, low swell strains were measured in combined treatments. The combined stabilization reduced shrinkage strain potentials of all four soils since lime and fibers contributed additional tensile resistance of soils. The increased tensile resistance of lime-fiber treated soils countered shrinkage strain-induced tensile stresses in soils during dry environments. As a result, low shrinkage strains were recorded.

Curing period had considerable influence on strength enhancements and swell reductions and moderate influence on shrinkage strain reductions in control soils. Based on all test results, lime at 8% amount, polypropylene fibers at 0.3%, and a curing period of seven days are recommended for field stabilization. As expected, soils cured for 14 days yielded better properties than soils cured for 7 days. However, seven-day curing is recommended for field treatments based on the fact that improvements gained during additional seven days of curing are not significant enough to delay the construction. Statistical analyses on both control and lime-fiber treated soil properties indicated that the combined stabilization method provided not only effective, but also statistically significant improvements to all soil properties. It is recommended that this stabilization technique be assessed under field conditions, and that other hybrid stabilization methods be tried using inexpensive and recycled stabilizers.

Acknowledgments

Authors would like to acknowledge the City of Arlington, Texas, USA for funding this research. Authors would like to acknowledge Mr William Verkest, Mr Keith Melton, and Mr Martin Phillips of the City of Arlington for their involvement in the research. Partial funding from Texas Higher Education Coordinating Board (THECB) under the "Advanced Technology Program (ATP) Grant No. 1407610-50" is also acknowledged. Authors would like to acknowledge Mr Ken McCleskey of US Army Corps of Engineers, Fort Worth District for the extensive literature review provided on fiber materials.

References

AASHTO. (1993). *Guide for Design of Pavement Structures*. Washington, DC.

Andersland, O.B. and Khattak, A.S. (1979). "Shear strength of kaolinite/fiber soil mixtures." *Proceeding of International Conference on Soil Reinforcement: Reinforced Soil and Other Techniques*, Vol. 1, pp. 11–16.

ASTM. (1995). "Annual book of ASTM standards." Section 4, Construction, *American Society of Testing and Materials*, Philadelphia, PA.

Bugge, W.A. and Bartelsmeyer, R.R. (1961). *Soil stabilization with portland cement.* Highway Research Board, No. 292, National Research Council, Washington, DC, pp. 1–15.

Chen, F.H. (1988). "Foundations on expansive soils." *Developments in Geotechnical Engineering*, Vol. 12, Elsevier Publications, The Netherlands.

Consoli, N.C., Prietto, P.D.M., and Ulbrich, L.A. (1998). "Influence of fiber and cement addition on behavior of sandy soil." *Journal of Geotechnical and Geoenvironmental Engineering*, Vol. 124, No. 12, pp. 1211–1214.

Department of the United States Army. (1983). *Foundations in expansive soils*. US Army Corps of Engineers Report.

Diamond, S. and Kinter, E.B. (1965). *Mechanisms of soil-lime stabilization: and interpretive review*. Highway Research Record 92, Transportation Research Board, Washington, DC, pp. 83–96.

Gray, D.H. and Al-Refeai, T. (1986). "Behavior of fabric-vs. fiber-reinforced sand." *Journal of Geotechnical Engineering*, Vol. 112, No. 8, pp. 804–820.

Gray, D.H. and Ohashi, H. (1983). "Mechanics of fiber reinforcement in sand." *Journal of Geotechnical Engineering*, Vol. 109, No. 3, pp. 335–353.

Gregory, G.H. and Chill, D.S. (1998). "Stabilization of earth slopes with fiber reinforcement." *Proceedings of 6th International Conference on Geosynthetics*. Atlanta, GA.

Hausmann, M.R. (1990). *Engineering Principles of Ground Modification*. McGraw Hill, New York.

Jones, D.E., Jr and Holtz, W.G. (1973). "Expansive soils – the hidden disaster." *Civil Engineering*, August, Vol. 43, No. 8.

Khire, M. and Benson, C.H. (1994). "Reinforcing sand with strips of reclaimed high-density polyethylene." *Journal of Geotechnical Engineering*, Vol. 120, No. 5, pp. 838–855.

Little, N.D. (1987). "Fundamentals of the stabilization of soil with lime." *National Lime Association Bulletin*, No. 332.

Maher, M.H. and Ho, Y.C. (1994). "Mechanical properties of kaolinite/fiber soil composite." *Journal of Geotechnical Engineering*, Vol. 120, No. 8, pp. 1381–1393.

Michalowski, R.L. and Čermák, J. (2003). "Triaxial compression of sand reinforced with fibers." *Journal of Geotechnical and Geoenvironmental Engineering*, Vol. 129, No. 2, pp. 125–136.

Michalowski, R.L. and Zhao, A. (1996). "Failure of fiber-reinforced granular soils." *Journal of Geotechnical Engineering*, Vol. 122, No. 3, pp. 226–234.

Mitchell, J.K. (1993). *Fundamentals of Soil Behavior*. John Wiley and Sons, New York.

Murray, J.J., Frost, J.D., and Wang, Y. (2000). *Behavior of sandy silt reinforced with discontinuous recycled fiber inclusions*. Transportation Research Record 1714, TRB, National Research Council, Washington, DC, pp. 9–17.

Nelson, D.J. and Miller, J.D. (1992). *Expansive Soils: Problems and Practice in Foundation and Pavement Engineering*. John Wiley & Sons, New York.

Poor, A. (1974). "Behavior of residential slabs on expansive clays." Construction Research Center Report, The University of Texas at Arlington, Arlington, Texas, 53 pages.

Punthutaecha, K., Puppala, A.J., and Hoyos, L.R. (2003). "Relationships between matric suction potentials and swell strains of fly ash stabilized soils." *Proceedings of 2nd Asian Conference on Unsaturated Soils*, UNSAT ASIA-2003, Osaka, Japan, April.

Puppala, A.J. and Musenda, C. (2000). *Effects of fiber reinforcement on strength and volume change behavior of expansive soils*. Transportation Research Board, TRR No. 1736, pp. 134–140, Washington, DC.

Puppala, A.J., Suppakit, C., Viyanant, C., and Perrin, L. (2001). "Sulfate heaving problems in stabilized soils: observations from a few case studies." *Proceedings of 2nd International Conference on Engineering Materials*, San Jose, California, August.

Ranjan, G., Vasan, R.M., and Charan, H.D. (1996). "Probabilistic analysis of randomly distributed fiber-reinforced soil." *Journal of Geotechnical Engineering*, Vol. 122, No. 6, pp. 419–426.

Sherwood, P.T. (1995). "*Soil Stabilization with Cement and Lime*." HMSO Publications Center, pp. 14–55.

Shulley, S., Leshchinsky, D., and Ling, H.I. (1997). *Effects of short polymeric fibers on crack development in clays*. US Army Corps of Engineers Technical Report REMR-GT-25, p. 102.

Tingle, J.S., Webster, S.L., and Santoni, R.L. (1999). *Discrete fiber reinforcement of sands for expedient road construction*. US Army Corps of Engineers Technical Report GL-99-3, 110 pp.

Wattanasanticharoen, E. (2001). "Laboratory investigations on four novel treatment methods to stabilize soft subgrade soils of southeast Arlington." MS Thesis, The University of Texas at Arlington, Arlington, Texas.

Ziegler, S., Leshchinsky, D., and Ling, H.I. (1998). "Effect of short polymeric fibers on crack development in clays." *Soils and Foundations*, Vol. 38, No. 1, pp. 247–253.

Part 7

Cement-stabilization

Chapter 25

Assessment of anisotropic behavior of swelling soils on ground and construction work

Evangelos I. Stavridakis[1]

Summary

The main aim of the study reported in this chapter was to assess the anisotropic behavior of swelling soils on ground and construction work. In particular, the mechanism and factors affecting expansion were presented. Confronted with major geotechnical problems in construction involving swelling soils, several protection measures were described so that difficulties due to soil expansion may be overcome.

Introduction

Problematic swelling soils have generally been ignored in favor of higher quality soils with reduced technical difficulties and lower construction costs. Alternative areas for construction, however, have become more and more important during the last decade due to a growing shortage of quality soils for building (Pinto *et al*., 2003). The geotechnical engineering community has recognized that swelling soils may result in considerable distress and consequently in severe damage to overlying structures.

Swelling soils exhibit high plasticity, high compressibility, high swelling potential (due to swelling minerals and environmental conditions), reduced strength, low coefficient of internal friction, and durability. Consequently, they are low quality material for construction and present difficulties. It is worth mentioning that in the USA, damage caused by this phenomenon is more than twice that from earthquakes, tornadoes, hurricanes, and floods combined. This is explained by the fact that over 20% of US land is affected by soil expansion while only 14% is affected by the other mentioned physical phenomena (Gromko, 1974).

China is one of the countries with a large distribution of expansive soils. This has been found in more than 20 provinces and regions, occupying nearly 6,00,000 km^2. Expansive soils constitute the most vulnerable natural hazard to buildings on shallow foundations in China. According to incomplete estimates, the houses destroyed by expansive soils amount to a floor space of 10 million m^2. The immediate economic loss in China exceeds 1 billion US dollars annually (Bin *et al*., 2002).

When dry conditions are dominant, swelling soils are hard and strong, like a rock, but when water is added due to, for example, environmental flooding these soils expand and

[1] Geotechnical Engineering Division, Department of Civil Engineering, Aristotle University of Thessaloniki, 541 24 Thesssaloniki, Greece, Tel: 00302310 995814 – FAX: 00302310995619; stavrid@civil.auth.gr

soften. In pure form of montmorillonite clays they may expand to over 15 times of their dry volume. On the other hand, most soils contain only a small amount of montmorillonite. They may expand not more than $1\frac{1}{2}$ times their dry volume. When the swollen soils are expanded and saturated with water, they lose much of their strength (Sridhara, 1998).

Water intrusion during wetting in active clay minerals such as bentonite, creates swelling and disrupts the interpartical contacts and bonds. The bonds between particles are weakened as the particles are moved further apart and simultaneously disruptive internal pressures appear through the clay system making this more susceptible to erosive forces (loss of internal strength) (Stavridakis, 2003). From this point of view the expansion of the remolded specimens will be considerably greater compared with the volume increase of undisturbed specimens of the same soil. This is due to a remolded or undisturbed stage. Bonding determines the ease with which microfractures (swelling effect) can propagate through the specimen by disrupting the structure and breaking the bonds within the soil mass. The bonding effect is less than in the undisturbed stage.

Akpokodje, 1986, suggested that the presence of appreciable proportions of carbonate (up to 20%) tends to increase the resistance to water intrusion within the mass of a swelling soil, such as in bentonite. In contrast, kaolinite, illitic, and well-organized (well-crystallized) soil minerals are largely inert and resistant to water penetration. On the other hand, under drying conditions the clay – cement system shrinks as the water moves further apart with a resulting breaking of the soil – cement bonds. The type of bonding agent (mineralogy bonding or additives for soil improvement), degree of bonding, and percentage of a dominant active mineral such as bentonite are the more important factors that control strength (bearing capacity), internal friction, cohesion, and durability (strength of mineral or additive - soil bonds, internal strength).

Finally, other adverse effects of swelling soils include: settlement of building foundations, increase in loosening of the surrounding soil in excavation work, increase of volume change and erosion deterioration, increase in loss of strength and durability, increase of erosion, and increase of erosion damage (land subsidence). The main aim of the study reported in this chapter is to assess the anisotropic behavior of swelling soils on ground and construction work.

Global distribution of expansive soils

The distribution of expansive soils has a close relationship with the regional geological background, climate, hydrology, and geomorphology (Figure 25.1). The countries suffering from construction damage due to expansive soils include: Argentina, Cuba, Greece, Mexico, Rumania, Turkey, Australia, Cyprus, India, Moroco, South Africa, USA, Burma, Ethiopia, Israel, Norway, Spain, Venezuela, Canada, Germany, Iran, Oman, Sweden, China, Ghana, Maroco, Rhodesia, and Japan. Expansive soils can be found almost anywhere in the world. It can be expected that more of this type of soil will be discovered in future as the amount of construction increases (Donaldson, 1969).

There is no single soil type that can be named as “the expansive soil” as there are soils that do not contain appreciable amounts of the active clay minerals. These behave in a different way from the classical ones. As examples, there are the pyretic shales of Cleveland, Oslo, and Pittsburgh which contain iron pyrites which oxidize and, in so doing, they swell and damage structures as well as other soil minerals such as anhydrite (which forms chemical sediments, $CaSO_4$), certain micas that react with phosphates, and the clay mineral attapulgite. However, the range of expansive soils contains all clayey materials including clayey silts and clayey sands which may have a relatively high potential of expansiveness.

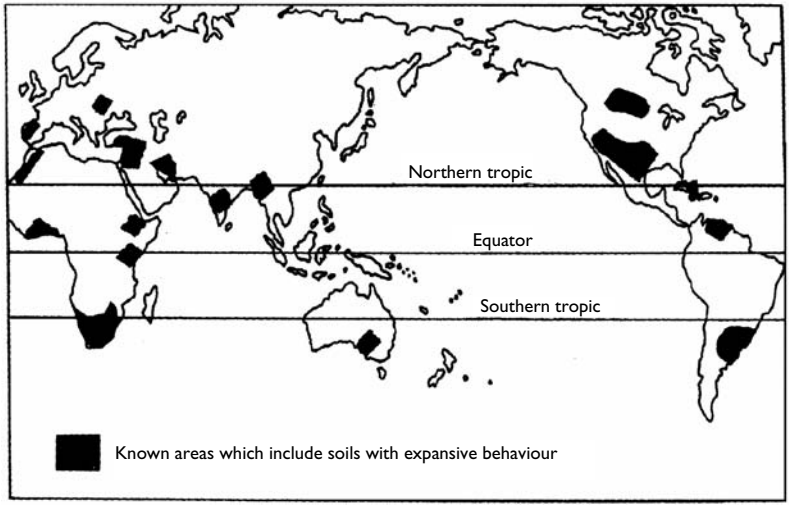

Figure 25.1 Global distribution of reported expansive behavior of swelling soils.
Source: After Donaldson, 1969.

Generally, the material sources of expansive soils are from the weathering (epigenic or hypogenic processes) of various types of rocks such as basic and ultrabasic igneous rocks, metamorphic rocks, and sedimentary rocks such as limestone, sandstone, and mudshale, which contain plenty of silicate minerals and easily convert into clay minerals such as montmorillonite, illite, and kaolinite through oxidation and reduction, hydration and dehydration, ion exchange, and leaching.

There are, basically, two major groups of parent materials that can be associated with expansive soils. The first group is comprised of basic igneous rocks, such as the basalts of Deccan Plateau in India, the dolerite sills and dykes in the central region of South Africa, and the gabbros and norites north of Pretoria. In these soils, the feldspar and pyroxene minerals of the parent rock have decomposed to form montmorillonite and other secondary minerals. The second group comprises the sedimentary rocks that contain montmorillonite as a constituent. These break down physically to form expansive soils. In North America, bedrock shale found in Denver Formations are examples of this type of rock, as are the clay-shales of Canada. In Israel there are the marls and limestones (Blyth and Freitas, 1976).

Expansive soils contain a relatively large amount of the clay mineral montmorillonite. They are generally found as residual soils from basic igneous rocks and montmorillonitic sedimentary rocks or as transported materials derived from the same parent materials. On the other hand, bentonite (swelling type of montmorillonite) is a clay formed by the devitrification and other chemical alteration of volcanic tuff or ash.

The climate of arid and semi-arid regions consists of an annual evaporation that exceeds the annual precipitation. The dryness ratio (annual evaporation/ annual precipitation) is over

1.5. The maximum reaches 4.3, which creates a favorable water cyclic environment for the formation of expansive soil. On the other hand, the process is restrained to a certain extent, so that the alkaline-earth elements such as calcium and magnesium and silica in soil are leached very slowly, which creates an ideal material condition for the formation of hydrophilic clay minerals. Finally, expansive soils mainly occur on upland hills, terraces, intermountain basins, and pro-mountain plains. Expansive soils have diverse origins, including lacustrine, residual, alluvial, and pluvial.

Mechanism of soil expansion

Clay particles are mainly flat and electrically charged (usually negative). This high potential is concentrated on the surface of the clay particles causing attraction of bipolar H_2O molecules. Thus an orientation of H_2O molecules on the clay surface is achieved. Due to these electronic forces the water molecules are distinguished in layers related to the attraction forces as distance from the clay surface increases, (Figure 25.2).

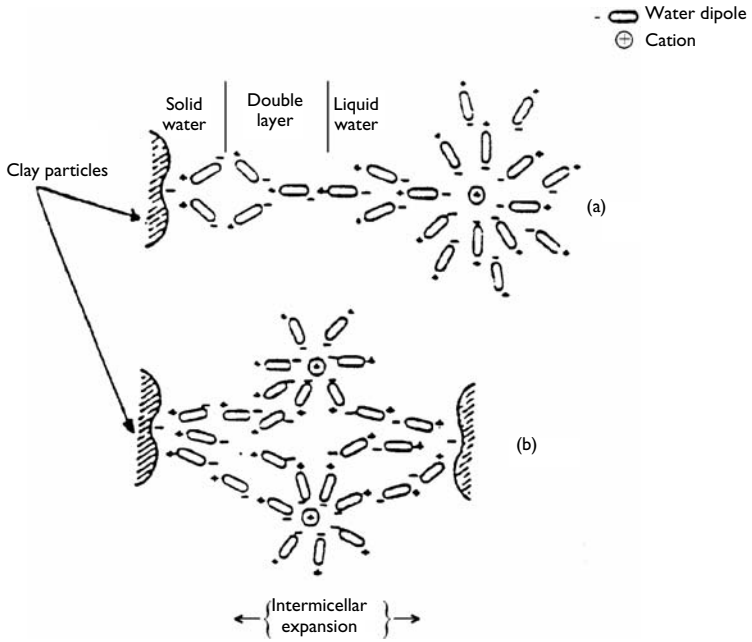

Figure 25.2 Representation of water molecules layers absorbed and held by high potential of clay particles.

Notes
Solid water (adsorbed) held very firmly in a thin layer of clay surface. Double layer (like water) held with less attractive forces in a thick layer and liquid water, a viscous thick, middle layer between the grains which is responsible for the plasticity of clay. Within this layer the grains of clay can slip on each other without elastic rebound, without rupture and volume change.

If a soft, loose, low shear strength clay is formed, the pressures of the overburden load (including man-made construction), causes a denser soil to form as the particles come closer to each other. This happens only if appreciable water of low viscosity is squeezed out from the grain spaces under the high pressure at the points of contact. The double layer water requires higher pressures and long periods (long-term stability-drained conditions) of time to be squeezed out. Finally, a state is reached in which particles are held by the solid (adsorbed) water. In the previous undisturbed stage the clay is loose. It possesses a relatively high shear strength and has a brittle quality. If this hard clay is submerged in water, soil expansion will occur, because the clay is partially an elastic material and so when this is submerged in water, there is no surface tension at the clay surface and hence no capillary compression. An elastic rebound occurs due to removal of the compressive forces. Furthemore, restoration of the sorbing capacity of the clay will also occur. This was overcome by evaporative forces during desiccation. When the latter vanishes, the clay pores again are filled with adsorbed water.

Factors affecting volume change

The amount of volume change depends on percentage and type of dominant active mineral such as montmorillonite. The density of an expansive clay soil or bedrock greatly affects expansion. A greater volume increase will take place in a wetted dense soil than in a loose one because the former has more clay particles packed into a unit volume. In dry expansive clay the thickness of the clay mineral is relatively small. When water is added it causes an increase in the thickness. Also the capillary and other tension forces of moisture films are very active in clays and become great upon drying, causing higher shrinkage.

It has been noted that highly expansive clays expand very little at low densities and high moistures, but expand greatly when compacted at high densities and low moistures. If sufficient external load is applied to balance the internal forces developed in a clay mineral upon wetting, expansion could be held to zero, taking into account the moisture and density. Lesser loads, however, than the previous one will cause expansion until a stage of balance between the internal and external forces are reached.

The structure (bonding effect) of an expansive soil has an influence on the volume change. In undisturbed and remolded specimens of the same soil tested at the same moisture and density conditions, the degree of expansion of the remolded specimen will be considerably greater. Finally, time influences expansion. It is related to the fineness of clay material, transmission of moisture (distance from the surface of water application), and the balance of internal and external forces. Years may be required to saturate a foundation soil or water-retaining embankment of this material.

Generally there are two fundamental types of swelling. Interparticle – intramicellar or interlayer swelling which is the expansion of the crystal lattice of the clay mineral. Clay minerals such as montmorillonite expand when water is adsorbed into the layered structure. Such swelling is a function of the amount and the type of swelling mineral (nature of the interlayer cation, for example, Na^+ in Na-montmorillonite) and properties of the water. Intermicellar expansion is related strongly with the adsorption of water molecules between individual clay minerals.The first expansion occurs mainly in smectite family of clay minerals and of montmorillonite in particular and can be identified by using x-ray diffraction (e.g. glycerol method) (Attewell and Farmer, 1976). The second expansion (intermicellar) can be identified and measured physically (e.g. method of free swelling).

Geotechnical problems associated with construction work

While expansion is a problem in arid and semi-arid regions, shrinkage caused by desiccation can affect structures in areas with sizable precipitation. In many cases trees are planted near houses and along streets underlain by montmorillonite clays. By the time these trees mature, they will have withdrawn considerable more soil moisture than that which has been replenished by nature, causing shrinkage of soil due to drying. The resulting soil movements disrupt houses, sidewalks, streets, and other structures. Structural damage to homes can often originate from expansive soil heaving due to water from a leaking sewer (Sultan, 1969).

Buildings

Many buildings on lightly loaded slabs or footings, such as residential houses, motels, and garages have suffered erratic cracking consisting of corner-down type of construction, upward heaving near the middle of walls, slight rotation of stemwalls, horizontal translation outward, and slight rotation of corner about a vertical axis, (Popa, 1997). The predominant movement observed in buildings on expansive soils is one of upward heave or a dome-shaped heave with the greatest upward movement occurring at the center of the building.The resulting cracking pattern have the appearance of a corner-down distortion (Figure 25.3). Stresses at the corners are relatively higher than along the rest of the longitudinal footings due to the presence of windows and doors opening over the latter. Therefore it may be expected that the corners of the footings would settle more than the middle.

During the summer the soil shrinks by desiccation. Since the soil around corners is exposed to more drying than at the sides of the house, more shrinkage would be expected at the corners than at the middle of the footings. When the soil is subsequently wetted either by rainfall or domestic watering, the middle of the footing would be experience more expansion than the corners due to the smaller surcharge over the former. This would result in larger differential movement (e.g. differential settlement) between the corner and the middle of the footing causing the corners to assume a lower elevation (Figure 25.4).

Differential heave is a function of a number of variables, such as thickness of the clay strata, variations in water content beneath the structure (due to domestic sewer system, environmental conditions, or water table fluctuations), nonuniformity of the soils,

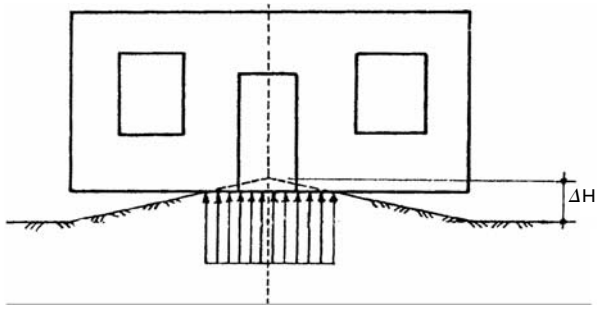

Figure 25.3 Dome-shaped heave disturbance.

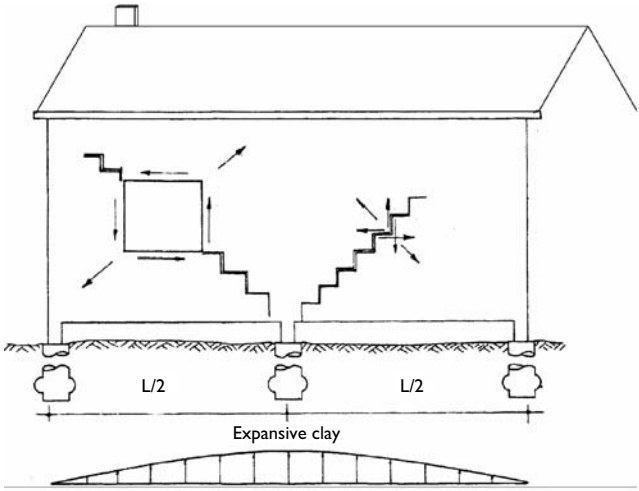

Figure 25.4 Differential heave disturbance (structure subjected to center column heave).

and other reasons related to the use and occupation of a particular building. The differential movements may be too severe and cracking may occur in the footing stemwalls and concrete walls which may be attributed to a lack of structural continuity in the houses where no reinforcement was incorporated either in the footing or in the stemwall (Means, 1959). Even multistorey buildings have suffered severe damage since in these cases of foundations different intensities of loading at different levels were reflected in the subsoil. Differential movement of these buildings may cause undesirable floor tilting (moments), cracks, and other hazards.

Roads

Building highways on water-sensitive expansive soils often is a major problem. The degree of movement of a road surface closely agrees with that observed for light buildings. The distortions are also very similar. Differential movement occurs because of variations in profile thickness of any expansive strata as well as trees or water concentrations. In severe cases the whole road surface fails.

Earth dams

The damage could be either in the concrete parts or the slope of the dam area. A failure could have the shape of Figure 25.5 if the slope is made of expansive material (even though it is well-compacted) that swells in contact with water and loses all (Na-montmorillonite-dispersion) or part (Ca-montmorillonite) of its shearing strength. This loss of strength is not necessarily instantaneous and depends on the fluctuation of water level in reservoir area.

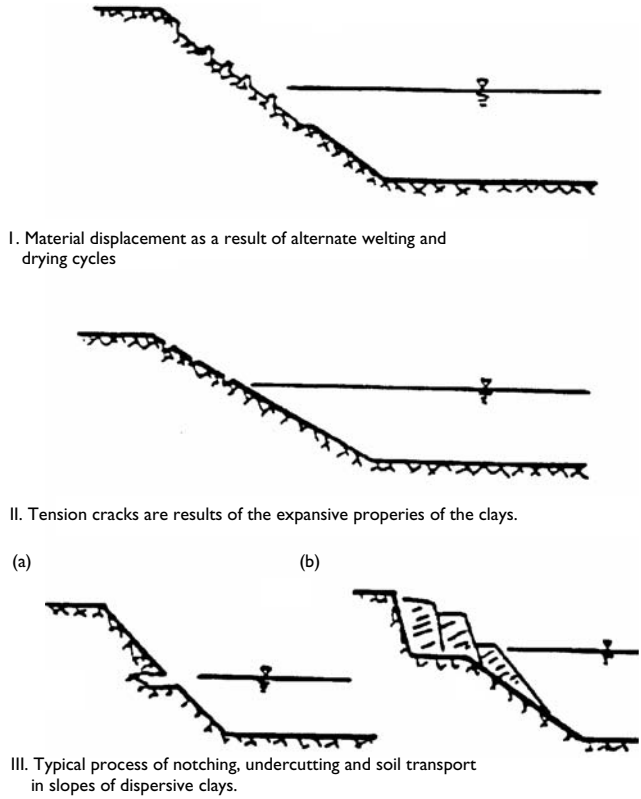

Figure 25.5 Patterns of slope erosion in expansive clays.
Source: After Ghuman *et al.,* 1977.

Slopes

The construction of foundations on hillsides where expansive clays are encountered causes problems because of the tendency of the clay to creep down hill. Although proper drainage and terraced excavations may help, there is always a possibility that deep creep will damage the structure. So the best solution is that these areas should not be used for building purposes but instead should be used as parks.

Another point to take into consideration is that highway builder can make cut or fill slopes steep as most highway landslides can be repaired quickly and easily. In cities, however, landslides may damage structures, so slopes near buildings should be much less steep than the usual highway side slopes.

A chemical change which can occur rapidly in geological materials is the expansion of anhydrite on hydration which can affect the short-term stability of slopes as it drastically reduces their stabilities.

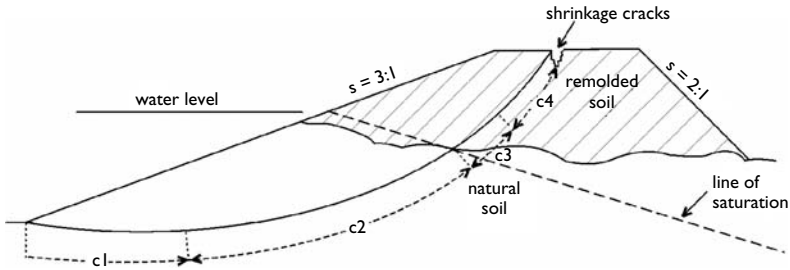

Figure 25.6 Disturbance of cohesion (internal strength) and stability conditions of a slope in canal due to presence of expansive soils.

Canals

A typical slope condition for a canal in expansive clay is divided into stability zones related to the surface of the water table saturation line (Figure 25.6). There are several factors to be considered in any stability study. In the first zone, the cohesion (C_1) and so the stability of the base (toe) of the sliding arc, below the saturation line, will be influenced by saturation, low loadings, and possible drying and resaturation. In the second zone, the soil above the aforementioned segment and below the saturation line will be saturated, will be moderately loaded and will be less likely to be subject to severe cycles of wetting and drying. Therefore, the cohesion of this segment (C_2) may be greater than C_1. Above the line of saturation, in the third zone, free water conditions do not exist and the cohesion of the soil (C_3) is influenced by capillary and other tension forces and may be quite high (more stable conditions). As shrinkage cracks often open to depths of several meters, above the zone with C_3 cohesion, when expansive type clay becomes very dry, at the upper most part of the sliding, the cohesive (C_4) and frictional strength systems cause unsafe stability conditions. On the other hand, deep, longitudinal shrinkage cracks may occur, in a concrete-lined canal, along the banks and the clays at the base of slopes will become soft. Since concrete is very sensitive to expansion pressure, as its weight is insufficient to withstand even moderate pressure, it will suffer from erratic cracking and uplifts pressures related to swelling of clay strata.

Retaining walls and buried structures

While other types of structures are usually subject to vertical expansive forces only, both retaining walls and buried type of structures, such as culverts and shelters, are liable both to horizontal and vertical expansive forces. These horizontal forces reach high values and cause large movements of the retaining walls and cracking of rigid structures.

Underground construction

Local expansion can occur when limited and relatively small amounts of expansive material are encountered. During excavations in Norway (Brekke and Selmer-Olsen, 1965), problems arose from seams of expansive montmorillonite clay. These promoted large falls and resulted in considerable amounts of clay flowing into a heading. Such zones require careful investigation, because when dry they may be sufficiently strong to give no difficulty during construction;

hence their effect on long-term stability of an excavation can easily be underestimated. Another example of a swelling soils disturbance has been recorded by Proctor and White (1946). During the driving of a tunnel through the Alps, layers of shale below the floor of the tunnel were disturbed. This allowed water to enter into thin interbedded seams of anhydrite. This hydrated to gypsum and expanded, raising the tunnel floor for several years at about 25 cm, a year.

Solutions to geotechnical problems related to swelling soils

Stabilization of swelling clayey soils

Several methods can be used to minimize heave of an expansive soil so that difficulties of construction could be overcome. The application of these methods will keep intact over a long period of time the engineering structures such as buildings, highways, dam embankments, and shallow foundations (Van Impe, 1989).

Compaction

The best solution (but often prohibited because of high cost) is to remove the expansive soil before construction and replace it with compacted, nonexpansive material. In general, a compacted clay will expand less under a given load than the same clay in an undisturbed state. A sample of desiccated clay from central Oklahoma which in its natural state expanded under load up to 468 kN/m^2 required only about 104 kN/m^2 to prevent expansion when compacted on the dry side with a standard hammer. In some cases where it has been positively established that the expansive layer is only of limited thickness, only the upper strata of the expansive soil should be removed and replaced by inert material compacted in 23 cm layers. Excavation and removal deeper than 1.5 m, however, have proved uneconomical. Finally, a good precaution is, of course, to avoid building on an expansive soil when it is in a desiccated state.

Prewetting

The purpose of prewetting is to allow desiccated foundation soils to swell prior to placement of a structure. One of the most common wetting methods is ponding or submerging of an area in water. However, wetting the foundation subsoil by ponding may require many months or even years to increase the water content to the required depths unless the clay contains a fissure system to pass water percolation through the soil. Furthermore, the completed structure may continue to rise for some time after prewetting.

Prewetting can be facilitated by the installation of a grid of vertical wells (drainage system) prior to flooding. This can reduce the time necessary to adjust the soil water content up to the point where maximum heave will occur within a few months of flooding.

Constant water content

Most moisture control methods are applied around the perimeter of structures in an attempt to minimize edge wetting or drying of foundations. One of the more common methods of maintaining constant moisture is through the installation of impermeable barriers, adequate drainage systems, and control of vegetation coverage.

Chemical stabilization

Lime stabilization develops because of base exchange and cementation processes between clay particle and lime. The primary effect of small lime additions (2%–8%) is to decrease significantly the liquid limit, plasticity index, maximum dry density, and swelling pressure, and to increase the optimum water content, strength, and durability of expansive type clays (Glendinning, 1996).

Cement stabilization develops from the cementitious bonds between the calcium silicate (three-calcium silicate) and aluminate hydration products of cement and the soil particles. The action of cement reduces both the swelling types: either the interlayer or the intermicellar swelling (Van der Kerkhof, 2001). The basic strategy of cement stabilization is to reduce the liquid limit, plasticity index, permeability, deformation, and potential volume change and to increase the shrinkage limit, strength, and durability.

Organic compounds (chemical substances) stabilize expansive soils by water proofing, by retarding water adsorption, or by hardening (increase of strength and durability) the soil with resins. Particularly, the acrylic resin prevents, by making the clay-cement system more impermeable, from the adsorption of deleterious substances such as sulphates or probably organic compounds from ground, with small chains. However, the estimated costs of this method can be as much as twice that of cement or lime in similar applications' problems.

Electrosmosis stabilizes clay soils primarily by dewatering and ion exchange processes. Also, some cementations (increase of strength and durability) have been observed. Unfortunately, the cost of electricity used for this method has so far damped enthusiasm.

Protecting structures from disturbances caused by soil swelling

Footing size

When footings are employed for foundations, their sizes can be adjusted for any design contact pressure, thereby preventing expansion of the clay immediately below the footing. But at depths below the footing the load is distributed over an area larger than the footing which reduces the unit pressure on the clay. For this reason small footing carrying light loads can be lifted by expanding clays more easily than large footings carrying heavy loads, even though both are subjected to the same contact pressure. So adjustment in the spacing (distance between footings) and loads should be made as far as possible so that footings both near the surface and near enough to the water table (water stable conditions) under the structure carry the same load and are of the same size in order to prevent unequal (differential settlement results) uplift (upheaval).

Using deep footings

The building may be supported on footings at a depth below the surface near enough to the water table, so that the moisture content will not be affected by environmental changes. Precautions must be taken to prevent damage to the buildings by uplift on parts of the building by expansion of the clay between the footings and the ground beams, floors and other parts of the building at ground (Chey, 1975). Thus the extension of footings to an inactive soil zone below the expansive clay level may offer sometimes the best solution depending

on how thick is the expansive layer. The extension of independent footings to depths of up to 7.5 m in hard desiccated clay could be done quite economically by casting piers with belled footing.

Preventing uplift swelling pressures

Uplift pressures on piles can be used where the thickness of the expansive layer is greater than can be economically excavated. They are expensive and must satisfy several requirements. They must be founded and anchored in stable material, and must be able to carry the design load. Pile must be capable of resisting forces set up by the surrounding material, be corrosion-resistant, and economical.

In cases of light structures, the frictional resistance along the surface should be reduced to a negligible amount so that the clay, as it swells upwards past the pier, cannot exert uplift. Consequently, the uplift pressure can be reduced by drilling an oversize hole for the pier and casting the pier in smaller form in diameter than the hole and filling the remaining space around the pier with a material of low shear strength, but not sand. Sand is not suggested as a filling material in this case because it has high shear strength when subjected to pressure in confined mode (Figure 25.7).

Ground beams cast in contact with desiccated clay are sometimes broken by uplift pressure of expansive clay. Even if they are reinforced at the top of the beam, for taking the induced moments, provision should be made for a void under the ground beams, into which the clay can expand without exerting uplift pressure.

The only methods of preventing damage to floor slab due to expansion of clay is to use coarse broken stone or gravel fill, not compacted, under slabs which will reduce the uplift pressure of expanding clay by providing void spaces into which clay can flow as it expands, (Figure 25.8).

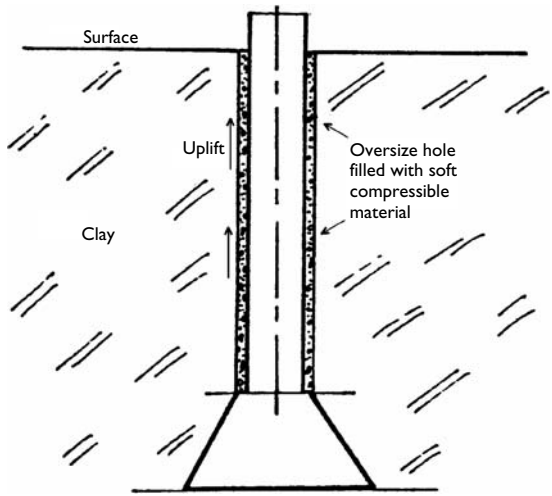

Figure 25.7 Belled footing casted in desiccated clay. Pier casted in oversize hole filled with material of low shear strength to takeover the swelling disturbance.

Figure 25.8 Example of structure damage caused by expansive soil (slab failure).
Source: Prefecture of Rethymnon in Crete island – Greece.

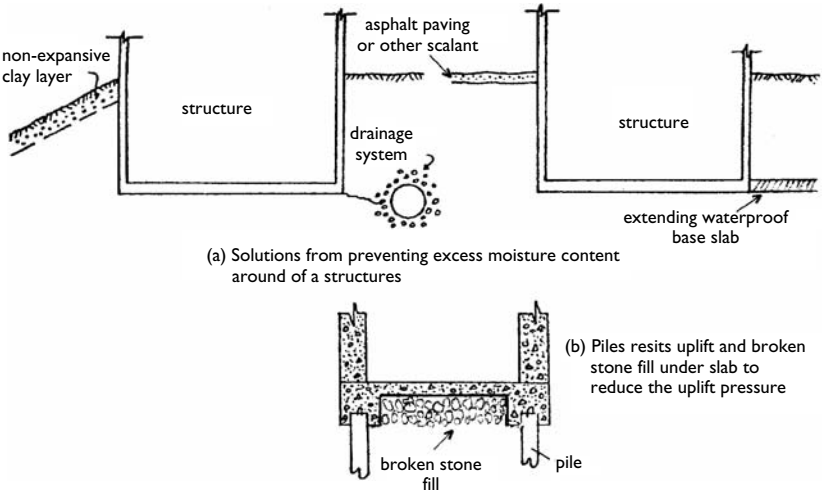

Figure 25.9 Methods of preventing damage from expanding clays.

Using rigid frames or slabs

In some areas where the soil and environmental conditions are exceptionally bad, the method of preventing damage of buildings by placing them on slabs or frames strong and rigid enough to transmit the buildings' loads to the soil without excessive deflection is used extensively (Figure 25.9).

In closing, the study reported in this chapter has helped to increase our understanding of the anisotropic behavior of swelling soils on ground and construction work.

References

Alpokodje, E.G. (1986) "A method of reducing the cement content of two stabilized Niger delta soils," *Quarterly Journal of Engineering Geology*, London, Vol. 19, pp. 359–363.

Attewell, B.P. and Farmer, W.I. (1976). *Principles of Engineering Geology*, Chapman and Hall, Wiley J. and Sons, N.Y.

Bin, S., Hongtao, J., Zhibin, L., and Fang, Y.H. (2002). "Engineering geological characteristics of expansive soils in China," *Engineering Geology* Vol. 67, 1–2, 2002, pp. 63–71.

Blyth, H.G.F. and M.H.de Freitas, (1976). *A Geology for Engineers*, Edward Arnold Limited, London.

Brekke, I. and Selmer-Olsen, R. (1965). "Stability problems in underground construction caused by montmorillonite carrying joints and faults," *Engineering Geology*, 1, pp. 3–19.

Chey, F.H. (1975). *Foundation on Expansive Soils*, Elsevier, New York.

Donaldson, G.W. (1969). "The occurrence of problems of heave and the factors affecting its Nature," *Proceeding of 2nd International Research and Engineering Conference on Expansive Soils*, A.E.M. Press, Texas, pp. 25–36.

Ghuman, O.S., Allen, R.L., and Mc Neil, R.L. (1977). "Erosion corrective maintenance and dispersive clays." Dispersive clays, related piping, and erosion in Geotechnical projects, ASTM STP 632, Eds, J.L. Sherard and R.S. Decker, *American Society for Testing and Materials*, pp. 260–273.

Glendinning, S. (1996). "Lime stabilization of clay soils," *Ground Engineering*, June pp. 33.

Gromko, G.J. (1974). "Review of expansive soils," *Proceedings ASCE* Vol. 44, 6T6, June, pp. 667–687.

Means, R.E. (1959). "Building on expansive clay," *Quarterly of the Colorado School of Mines*, Vol. 54, 4, April, pp 1–31 (Theoretical and Practical Treatment of Expansive Soils).

Pinto, M., Isabel, M. and Oliveira, J. da V. P. (2003). "Use of geosynthetics in embankments on soft soils," Eds, Dr Ian Jefferson and Dr Matthew frost, *Proceedings of an International Conference on Problematic soils*, 29–30 July, Nottingham, UK, Vol. 1, pp. 83–98.

Popa, A. (1997). "Shrinkage–Swelling phenomena effects on buildings," *Engineering of Geology and the Environment*, Vol. 1, Balkema, Rotterdam, pp. 327.

Proctor, R and White, T. (1946). *Rock Tunnelling With Steel Supports*, Commercial Shearing and Stamping Co, Youngstwon, Ohio.

Sridhara, A. (1998). "Volume change behaviour of expansive soils," Eds, Eiji Yanagisawa, Nobuchika Moroto, Toshiyuki Mitachi, *Problematic soils*, Balkema, Rotterdam, pp. 833–840.

Stavridakis, I.E. (2003). "Influence of grain – size on strength and slaking of cement stabilized clayey admixtures," *Proceedings of 56th Canadian Geotechnical Conference and 4th joint IAH – CNC/CGS Conference*, Winnipeg, Manitoba, Canada, September 29–October 1, 2003.

Sultan, H.A. (1969). "Foundation failures on collapsing soils in the Tuscon, Arizona area," *Proceedings of the 2nd International Research and Engineering Conference on Expansive soils* A.E.M. Press, Texas, pp. 394–403.

Van der Kerkhof, E. (2001). "Small scale recycling of plastic soils for trench fills using lime or cement treatment," *1st International Symposium on Subgrade Stabilization and In situ Pavement Recycling Using Cement*. Vol. 1, pp. 531–540, IECA, Salamanca, Spain.

Van Impe, F.W. (1989). *Soil Improvement Techniques and their Evolution.* AA. Bulkema, Rotterdam, Brookfield.

Chapter 26

Stabilization of problematic soils using cement and lime

Evangelos I. Stavridakis[1]

Summary

The primary aim of this chapter was to review studies on the stabilization of problematic soils using cement and lime. The suitability of a soil for effective stabilization and the most appropriate stabilizing agent are dependent on the mineralogical composition of the soil. The proposed classifications of anisotropic engineering behavior of cement-treated clay mixtures will aid in providing solutions to the problem of predicting the suitability of silty-clayey material for cement stabilization.

Introduction

The modification of soils to improve their geotechnical properties is well recognized. Among various stabilizing agents the most prominent are lime and Portland cement. The effect of cation exchange capacity and flocculation are processes that take place in the presence of a stabilizer. Portland cement and lime are capable of providing calcium, but they differ in their chemical nature, their mode of reaction in the presence of water, and their resulting reaction products.

Based upon the results of analytical and mechanical characterizations, the following hypothesis was reported by Herzog and Mitchell, (1963): During the hardening of a clay-cement mixture two processes take place – a primary and a secondary. Hydrolysis and hydration of cement could be regarded as primary reactions. Clay may participate in the secondary processes. The calcium ions produced by cement hydration first convert the clay to the calcium form and tend to intensify the flocculation. Calcium hydroxide used up in the secondary processes could be replenished to some extent by the release of lime from the hydrating cement. Since the secondary cementitious matter (i.e. calcium silicates and calcium aluminates) would be mainly formed on or near the surface of clay particles, the flocculated particles would be glued together at points of contact.

The primary products harden into a high-strength aggregate and differ from normally hydrated cement in that their calcium content is lower. The secondary processes enhance the strength and stability of soil-cement by producing additional cementitious matter which increases interparticle bond strength (i.e. internal strength). According to Stocker (1975),

[1] Geotechnical Engineering Division, Department of Civil Engineering, Aristotle University of Thessaloniki, 541 24 Thesssaloniki, Greece; Tel: 00302310 995814 – FAX: 00302310995619; stavrid@civil.auth.gr

diffuse cementation or lime migration is the form of cementation that takes place when soil is stabilized with both Portland cement and lime. However, additional skeletal cementation can be produced with Portland cement but not with lime.

When lime is added to soil for modification of soil properties, the result is called lime-modified soil. Simple modification of soil properties with Portland cement, as with lime, is termed a cement-modified soil. This modified soil is an improved soil in the unhardened or semi-hardened state. This is achieved by using a lower amount of cement. When the cement content is increased, the resulting material is referred to as hardened soil-cement. The test criteria should be first durability and second strength, but unfortunately while strength is used as a second criterion the durability is absent.

Bonding (clayey soil grains-cement) determines the ease with which microfractures can propagate during slaking process, through the stabilized clay by disrupting the structure and breaking the bonds within the cemented clayey mass.

Durability (slaking), under conditions of wetting-drying and potential stresses (e.g. during seismic events or movements due to landslides), (Tatsuoka *et al.*, 1997) is an aspect of cement stabilized soils behavior that has been neglected in favor of other properties such as strength. However it is an important feature of many commonly encountered engineering problems in transportation (Owttrim, 1988), and in dam construction when the dispersive properties of clays (Na – montmorillonite) are not suitably accounted for in the design of an earth dam or even in grouts where problems of durability in cement-chemical grouted soil arise due to fluctuation of the water table (Stavridakis, 2004a).

The achievement of higher strength with Portland cement than with lime may be attributed to two factors: First, the $Ca(OH)_2$ crystals generated as a by-product of the hydration of calcium silicates are pure and fine and thus more reactive. Therefore these crystals provide the calcium necessary for ion exchange with swelling minerals such as bentonite. Second, there is the formation of a rigid network by the hydration of Portland cement, as occurs in mortar or concrete. This rigid network depends on the amount of Portland cement used. At smaller dosages the networks (skeletal cementation) may be small. With increasing amounts of Portland cement, a three-dimensional network may form where the soil particles are either isolated or may form their own three-dimensional network. This versatility may be of significance when different properties are required from the same soil such as reduced permeability, slaking, and deformability or increase of strength (bearing capacity). In stabilization with Portland cement, the strength development begins early and the contribution of strength to a stabilized soil is superior compared to that achieved with lime stabilization.

The primary aim of this chapter is to review studies on the stabilization of problematic soils using cement and lime.

Influence of clay minerals of soils on their cement-stabilization

Expansive soils contain clay minerals that exhibit high volume change upon wetting. The large volume change causes extensive damage to structures, in particular, light buildings and pavements (Fredlund and Rahardjo, 1993). Confronted with these problems, a suitable ground improvement technique is needed for surface or deep excavations in problematic soils (swelling soils) to increase strength, reduce deformability, provide volume stability, reduce permeability, and increase durability. Techniques such as Soil Mixing, Cement Deep Mixing (CDM), Soil Mixed Wall (SMW), Deep Soil Mixing (DSM) are well known (Kaushinger *et al.*, 1992).

Cement-stabilization (surface or deep) has been used for many diverse applications including foundations (to halt the settlement of existing structures), retaining structures (for temporary support of excavations), liquefaction mitigation (to cut off water infiltration into excavations and sewer lines), water control (foundation curtains that reduce water loss under structures), and pollution control by using stabilization/solidification (S/S) techniques that aim to immobilize the source of contaminants (remediation of contaminated land prior to redevelopment).

Various clay minerals in a clayey soil influence the ease with which it can be stabilized with cement. Kaolinite and well-organized (well-crystallized) soil minerals appear to have little effect on the hydration of cement and hardening proceeds normally by using small amounts of cement. In contrast, clay minerals with an expansive lattice have a profound influence on the hardening of cement and require large amounts of cement, to develop satisfactory strength and durability (Croft, 1967; Bell, 1976). The reason for this is that in a clay-cement mixture, the number of calcium ions liberated from the cement during hydration and hydrolysis depend on the amount of cement used for stabilization. These occupy the positions of exchangeable ions on the clay minerals. The number of these positions depends upon the portion of clay in the soil-cement mixture and on the type of clay minerals. Therefore, the greater the swelling effect of a swelling mineral, the greater is the number of calcium ions (% of cement) to be used for effective stabilization. The order in which swelling potential decreases is as follows: montmorillonite > illite > halloysite > kaolinite (Koncagül *et al.*, 1999).

The types of ions existing as dissolved solids in the wetting fluid also strongly affect the degree of swelling. For example, swelling of montmorillonite decreases as other univalent or divalent ions substitute for Na^+ in the following order: Li > K > Ca > Mg > H. Finally, the number of exchangeable ion positions is connected with the liquid limit which reflects the composition of a clay-soil and are related with the slaking and unconfined compressive strength (Stavridakis and Hatzigogos, 1999).

The effectiveness of cement stabilization increases in the following order: swelling soils < cohesive soils with liquid limit about 60% < clayey soils with liquid limit lower than 60% < clayey soils with liquid limit lower than 40% (Stavridakis, 2003a), (Figure 26.1).

The suitability of a soil for stabilization, the most appropriate stabilizing agent, and the quantity of this agent required, are depended on the mineralogical compositions (qualitative and quantitative); texture (particle size distribution) of a soil as well as its properties needed to be upgraded. The properties of clays which require investigation include their strength, durability, and capacity to swell or shrink which are reflected to strength and durability under soaked and desiccated conditions. These properties can be improved by either converting the soil to a rigid or granular mass or by retarding moisture movement within it.

When enhanced strength or resistance to water penetration is required, stabilization by the addition of cement, or lime, or cement with small proportions of lime, or cement with small proportions of acrylic resin may provide the answer. Acrylic resin is an emulsion of a synthetic elastic chemical substance which as additive in cement paste increases significantly the bonds within the substrate particles as well as the cohesion and the engineering strength. It improves also the durability in chemical intrusion, the impermeability, and finally the durability in cycles of freezing and thawing. The acrylic resin prevents the adsorption of deleterious substances such as sulphates or organic compounds with small chains by making the clay-cement system more impermeable.

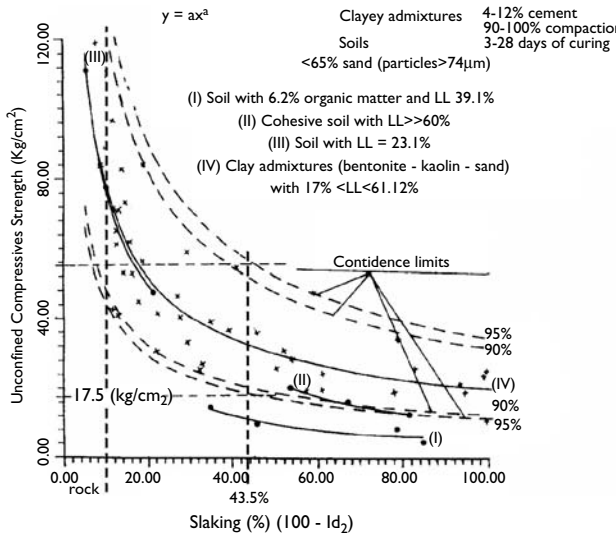

Figure 26.1 Influence of composition of clayey soils on their stabilization by cement.
Source: Stavridakis, 2003a.

The internal force system of a cement-stabilized clayey soil is defined as the resultant stresses established by the bonding potential (A) (attractive forces) of cement and the swelling potential (R) (repulsive forces). The internal force can be illustrated as a combination of R-A: (R-A) < 0 *net attraction*: strength and durability of clay-cement system are increased, (R-A) > 0 *net repulsion*: strength and durability of clay-cement system are decreased. The A-forces and R-forces are highly influenced by the amount of cement, compaction, curing, soaking, and desiccating time, whereas the R-forces change in relation to water intrusion. The internal force system is strongly related to the type and amount of swelling clay in cement stabilized soils. The internal force system influences the resistance against deformation (applied external force-unconfined compressive strength) and durability (bonding effect) (Stavridakis, 2004b).

A classification system is needed for cement-stabilized clayey soils for the evaluation of their engineering and cement stabilization parameters. The additive of an engineering classification scheme is to categorize clayey materials stabilized by cement according to their potential engineering behavior. In this regard, an engineering classification is often oriented toward a specific application. For these reasons empirical relationships were considered between slaking and liquid limit; unconfined compressive strength and slaking (durability) of clayey admixtures stabilized with 4% and 12% cement, at 95% compaction and cured for 28 days (Stavridakis, 2003b).

A composite diagram was drawn containing all the aforementioned parameters, a range of power curves of liquid limits from 15% to 60% and a range of power curves of cement percentages from 4% to 12%, (Figure 26.2). This diagram shows the influence of liquid limit (composition of soil) and amount of cement on the development of strength and durability

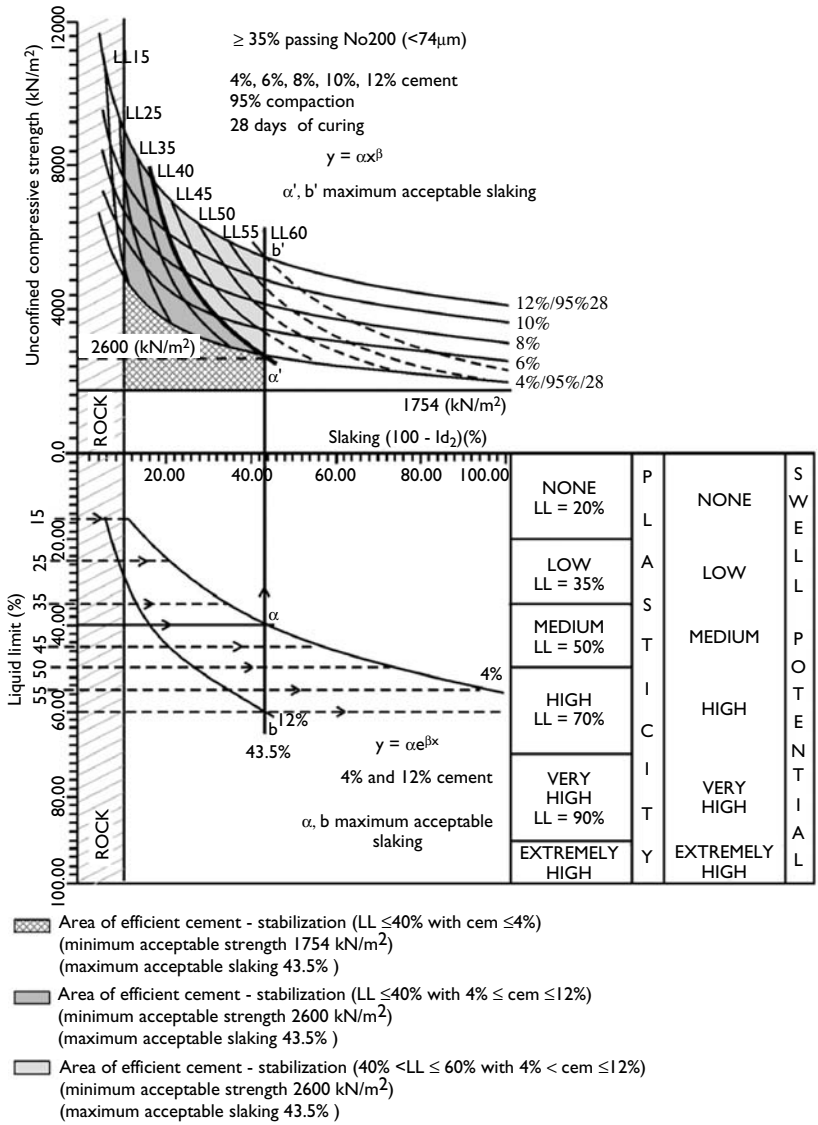

Figure 26.2 Diagrams of influence of plasticity and cement percentage on strength and slaking of cement-stabilized clayey mixtures combined with the swelling potential.

Source: Plasticity and swell potential classification by Dakshanamurty and Raman (1973).

of bentonite–kaolin–sand (active clay mineral-inactive clay mineral-quartz) mixtures stabilized by cement at a constant degree of compaction (95%) and curing time (28 days). The combination of this diagram with the swelling potential classification (Dakshanamurthy and Raman, 1973) classifies, characterizes, and defines areas of strength, durability, liquid limit, cement percentage, and swelling potential for best stabilization effect.

According to the literature, clayey soils with a liquid limit less than 40% are stabilized successfully by using economical amounts of cement (Godin, 1962), while clayey soils with large liquid limits (>60%) usually contain expansive clays and react with large amounts of cement (Croft, 1968). These liquid limit values define an ultimate slaking value (maximum acceptable slaking or minimum acceptable durability) from the slake durability index test (Franklin and Chandra, 1972) accepted for efficient cement stabilization. So in this diagram (Figure 26.2), pairs of values of strength and slaking beyond the limit of 43.5% slaking are unacceptable because clay mixtures having these values need large amounts of cement to develop satisfactory strength and durability for best stabilization effect.

Conventional specifications stipulate a lower limit of 1,754 kN/m^2 unconfined compressive, strength after 7 days of curing for soils stabilized by cement to pass the erosion tests successfully (material loss 7–14% in 12 cycles of freezing and thawing or wetting and drying test as described in ASTM D.560-03 and ASTM D.559-03 respectively) (Croft, 1967; Akpokodje, 1986). From this point of view this classification diagram (Figure 26.2) defines a minimum strength value of 2,600 kN/m^2 revealing that an area of clay mixtures stabilized with less than 4% cement attain the lower limit of 1,754 kN/m^2 unconfined compressive strength and maximum acceptable slaking of 43.5%. Finally it is suggested that slaking value of 43.5% might provide a useful criterion for successful stabilization. Such a value is achieved if a soil having a liquid limit of 40% is treated using 4% cement. To achieve the same slaking value of 43.5% in a soil having a liquid limit of 60% would require the addition of 12% cement. Such a large amount of cement is likely to be uneconomic.

Controlling water flow through soil is important for various reasons. Water leakage into underground openings with the lowering of the ground water table and consolidation settlements of clay layers as a result, can cause surface damage to buildings. Water flow through storage of waste material causes an undesirable contamination of the ground water (Hassler *et al.*, 1987). In order to reduce the water flow, soil-cement mixing is commonly used. In particular, in dam construction, soil-cement stabilization (soil-cement mixing, surface or deep) is a very important method to ensure water tightness because water seepage under dams causes energy loss and erosion of the dam core.

Pollution of the environment due to leakage from waste repositories is a well-known and widespread problem. Therefore, the design of liners for such repositories is based upon hydraulic conductivity, liner composition, environmental conditions (wet–drying), and compaction (De Marco *et al.*, 1998). Many different barrier materials exist, for example, plastic membranes, geotextiles, bentonite, compacted clay, and cement stabilization. As bentonite (swelling soil) is a material with a very low hydraulic conductivity, it is obvious that the higher the percentage of bentonite, the lower the permeability. However, the permeability is not the only criterion to fulfill the requirements to create waste repositories with cement-stabilized clay; strength and durability of this barrier material are also very important so that this construction will remain intact over a long period of time.

Normally the amount of bentonite, in a sand-bentonite mixture used as a barrier constitutes 4%–13% of the dry weight of a bentonite clay-sand mixture (Sällfors and Öberg, 2002). Greater amounts of bentonite tend to form around the sand or inert material grains and the

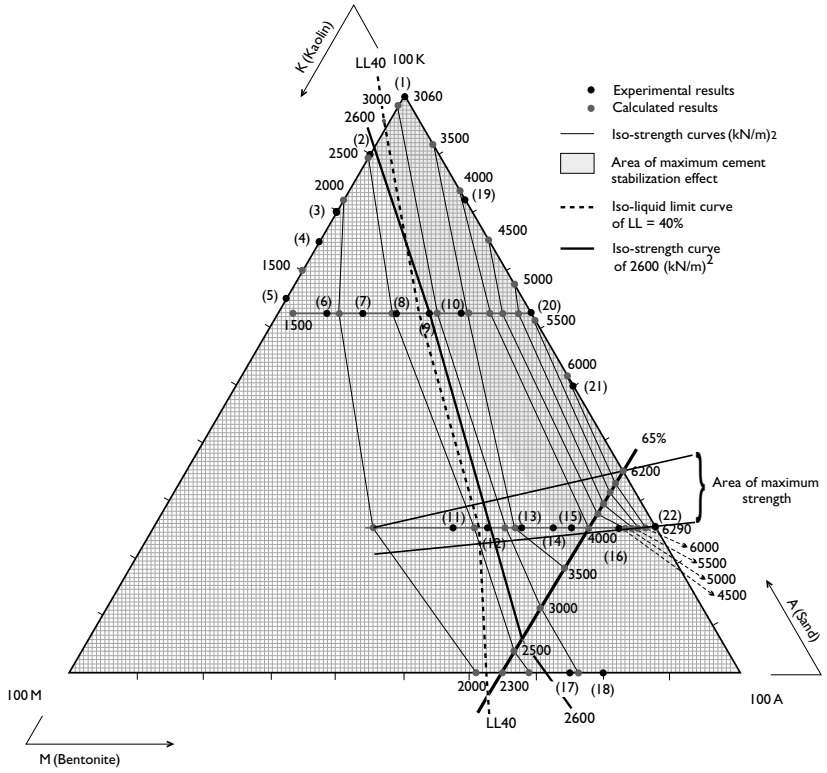

Figure 26.3 Development of unconfined compressive strength of clay-sand mixtures treated with 4% cement, compacted at 95% and cured for 28 days.

mixture becomes plastic and consequently difficult to compact, developing, simultaneously, low strength and durability. Consequently, these limits of bentonite define areas of mixtures for efficient cement stabilization of a swelling clay-sand mixture by using economical amounts of cement. From this point of view, triangular diagrams (Figures 26.3 and 26.4) were prepared on the basis of unconfined compressive strength and slaking experimental results of previous bentonite–kaolin–sand mixtures stabilized with 4% cement, compacted at 95%, and cured for 28 days. The particles of most of these clayey admixtures retained on sieve No 200 (74 μm) are less than 65% and they can be described as silt-clay materials in accordance with the Highway Research Board Classification System. This manner of presentation is very convenient because the iso-strength and iso-slaking curves reveal the development of strength and slaking (durability) through all these clay mixtures.

A basic curve of LL_{40} (LL = 40%), was drawn, divided the triangles in two areas, the first, of clay mixtures with LL ≤ 40% (maximum stabilization effect) and the second with LL > 40% (minimum stabilization effect). Finally from the previous composite diagram

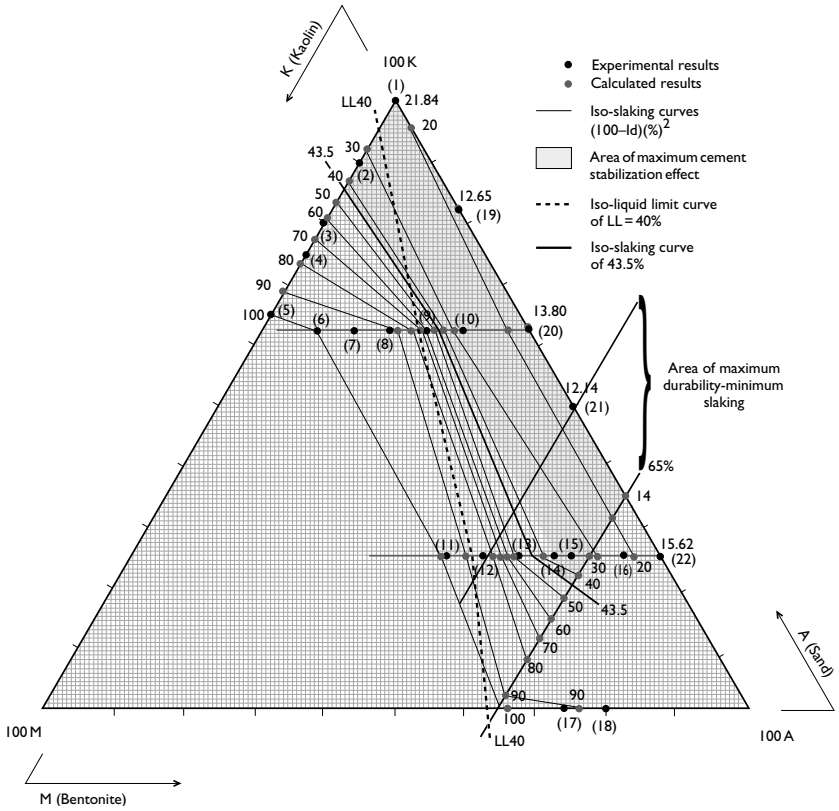

Figure 26.4 Development of slaking of clay-sand mixtures treated with 4% cement, compacted at 95% and cured for 28 days.

(Figure 26.2) the minimum strength of 2,600 kN/m^2 curve and ultimate slaking curve of 43.5% (maximum acceptable slaking or minimum acceptable durability) were drawn. Additionally in the diagrams (Figures 26.3 and 26.4), areas grey in color define the development, through clay mixtures, of triangles with <15% bentonite content, of clay-mixtures used as barrier material. These mixtures exhibit low permeability, strength higher than 2,600 kN/m^2, slaking lower than 43.5%, and form areas of maximum cement-stabilization effect. Also iso-slaking curve of 100% define clay-sand mixtures, which contain 30% of bentonite resulting in complete disintegration. Consequently, this value of bentonite constitutes a limit in cement stabilization.

At the same time these mixtures (with slaking 100%) exhibit strength values between 1,500 and 2,500 kN/m^2. This means that for safety reasons in construction works the slaking (durability) should be considered as a serious safety factor together with strength. Finally these diagrams reveal areas of maximum strength and durability (minimum slaking) of clay mixtures. A combination of maximum strength and durability areas with the areas of

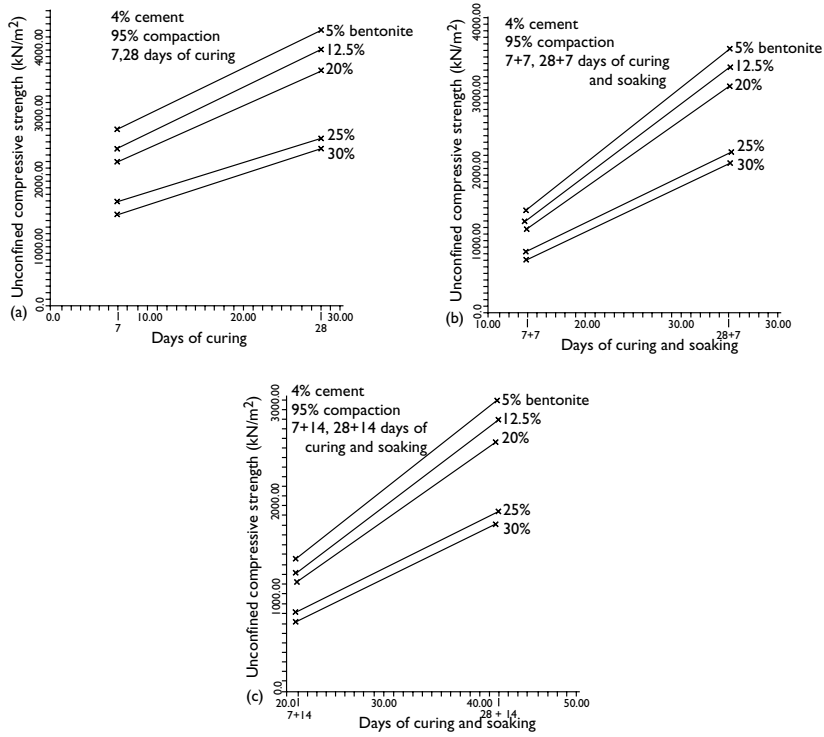

Figure 26.5 Influence of bentonite (swelling material) of clayey mixtures on their strength under cured and soaked conditions.

<15%, or from 15% to 30% bentonite could reveal useful information on the percentages of active, inactive, and sand portion of clay-sand mixtures used in specific applications such as soil-mixing (deep or surface) or control of water flow through soil or even improvement of engineering-geotechnical properties of swelling soils.

Bentonite–kaolin–sand mixtures prepared with constant percentage (25%) of kaolin stabilized with 4% cement, at 95% compaction, cured for 7 and 28 days, and soaked for 7 and 14 days, reveal the influence of bentonite variability from 5% to 30% on the strength and slaking (Figures 26.5 and 26.6). Clay-sand mixtures with 30% bentonite exhibit the lower strength and higher slaking 100% (complete disintegration).

The strong influence of soaking conditions are shown clearly in Figure 26.7: as the soaking time increases, the bentonite–kaolin–sand mixtures exhibit lower strength and durability. Soaked conditions negatively influence the improvement by cement of clayey-sand mixtures when swelling minerals are present, (Figure 26.7). The higher the values of the liquid limit in clay minerals (i.e. higher content of swelling mineral) the more negative the development of strength and durability during soaking conditions of cement-stabilized clayey-sand mixtures.

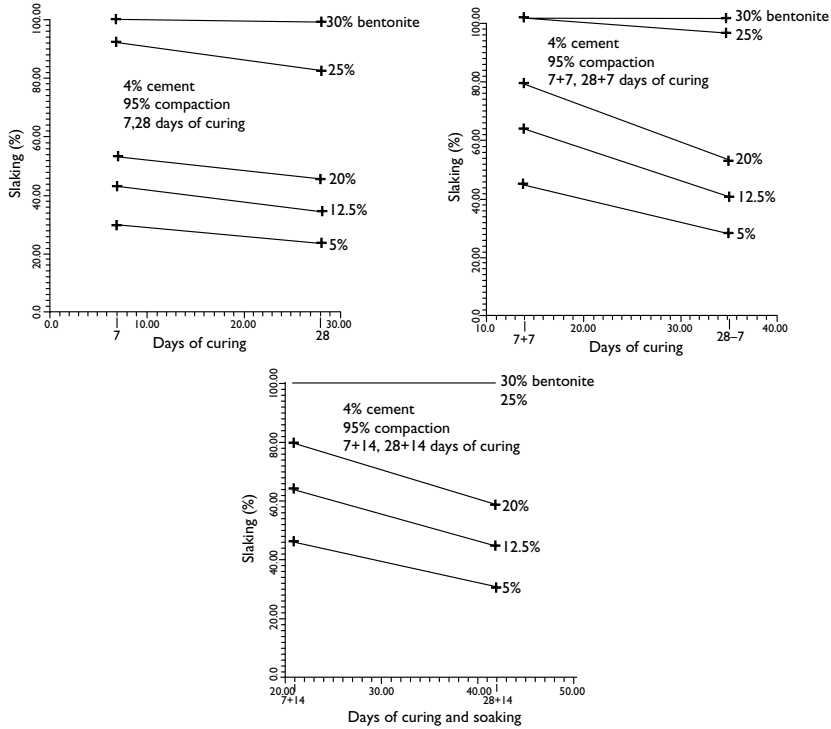

Figure 26.6 Influence of bentonite (swelling material) of clayey mixtures on their slaking under cured and soaked conditions.

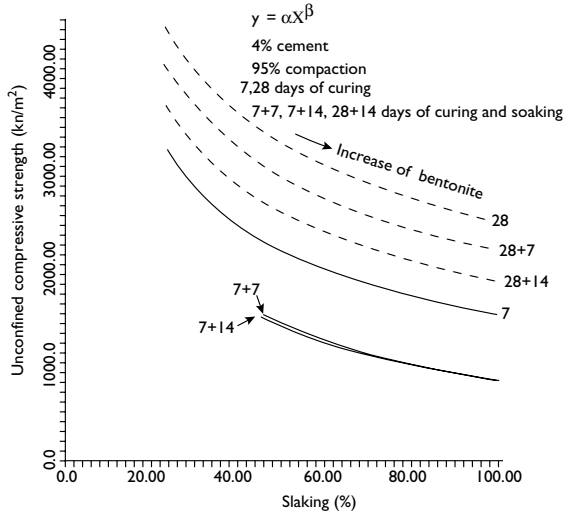

Figure 26.7 Influence of soaked conditions of bentonite-clay admixtures on their stabilization by cement.

Fly ash used for improvement of swelling soils

Fly ash is produced during the combustion of ground or subbituminous coals, exhibiting self-cementing characteristics that can be adapted to a wide range of stabilization applications. Generally, applications for fly ash treatment can be divided into several categories: drying soils to facilitate compaction, treatment of soils to reduce shrink-swell potential, and stabilization to improve engineering properties of a material such as increased strength, durability, or stability.

Fly ash treatment can effectively reduce the swell potential of fat (swelling) clay soils and increase support capacity of pavement subgrades (Kate, 1998). Fly ash also contributes to embankment construction of different configurations. This waste material could be used in the core and layers of embankments or as a soil-fly ash mixture in the construction of an embankment.

Combustion of subbituminous coal produces fly ash rich in calcium (class C) that exhibits self-cementing characteristics, eliminating the need to add activators such as lime or Portland cement. Class F fly ash has low calcium content and does not exhibit self-cementing characteristics. For this reason it is used with addition of lime or cement to cause pozzolanic reactions for the production of cementitious products.

The fly ash consists mainly of CaO and SiO_2 which influence the two fundamental types of swelling, intramicellar (interlayer) and intermicellar expansion, depending on the amount of these oxides. The reduction of swell potential of the material, by using fly ash is generally comparable to lime and cement stabilization. This reduction based on the amount of CaO and SiO_2, appears to be a result of bonding of the soil particles by the cementitious products formed during hydration of the fly ash in addition to flocculation of the clay minerals. Finally, a skeletal cementation can be produced with the aid of Portland cement, thereby increasing the strength and durability of the swelling material.

Conclusions

Lime stabilization (lime modification) influences the intramicellar (i.e. interlayer) expansion. For this reason the lime is more effective for swelling soils stabilization. Cement stabilization (i.e. cement modification) also influences the intermicellar expansion. With Portland cement, the strength and durability contribution to a stabilized soil is superior to that achieved through lime stabilization. A combination of cement with small proportions of lime is more effective for the stabilization of swelling soils. Acrylic resin prevents the clay-cement-lime system from the adsorption of sulphates or organic compounds. A combination of cement with fly ash could contribute strongly to the development of strength and durability of stabilized swelling material.

For construction of embankments, the expansive layer of limited thickness could be removed and replaced in the core or in layers by fly ash material, or the embankments could be constructed only with fly ash-soil material.

The classification system presented characterizes the swelling soils in terms of strength, durability, plasticity, and swelling potential. The triangular diagram defines a maximum limit of bentonite percentage necessary for the stabilization of swelling soils. The value of this limit depends on the portion and type of swelling minerals of the clay-cement system. The triangular diagram defines the development of strength and durability through bentonite–kaolin–sand mixtures as well as areas of best cement-stabilization effect. The composite and triangular diagrams reveal areas of bentonite–kaolin–sand mixtures with maximum and

minimum stabilization effect. The swelling soils could be stabilized with cement, lime, or fly ash if they mix with sand for reducing the swelling portion and consequently the swelling effect. Additionally these mixtures could be used in specific applications such as soil-mixing (i.e. deep or surface) or control of water flow through soil or even improvement of engineering-geotechnical properties of swelling soils. Low permeability of swelling soils is a property that can be used for construction works to control water flow through soil lattice by using bentonite–kaolin–sand mixtures.

References

Akpokodje, E.G. (1986). "A method of reducing the cement content of two stabilized Niger delta soils," *Quarterly Journal of Engineering Geology*, London, Vol. 19, pp. 359–363.

ASTM D.559-03. *Standard Test Methods for Wetting and Drying Compacted Soil – Cement Mixtures*, American Society for Testing and Materials, West Conshohocken, Pennsylvania, USA.

ASTM D.560-03. *Standard Test Methods for Freezing and Thawing Compacted Soil – Cement Mixtures*, American Society for Testing and Materials, West Conshohocken, Pennsylvania, USA.

Bell, F.G. (1976). "The influence of the Mineral Contents of clays on their stabilization by cement," *Bulletin of the Association of Engineering Geologists*, Vol. XIII, 4, pp. 267–278.

Croft, B.J. (1967). "The influence of soil mineralogical composition on cement stabilization," *Geotechnique*, 17, 119–135.

Croft, B.J. (1968). "The problem in predicting the suitability of soils for cementitious stabilization," *Engineering Geology an International Journal*, Vol. 2, 6, pp. 397–424.

Dakshanamurthy, V. and Roman, V. (1973). "A simple method of identifying an expansive soil," *Soils and Foundations, Japanese Society on Soil Mechanics and Foundation Engineering*, 13, 1, 79–104.

De Marco, S., Holden, J., Mc Manus, K., and Pardo, L. (1998). "Application of moisture barriers for expansive soils," *Problematic soils*, eds, Eiji Yanagisawa, Nobuchika Moroto, Toshiyuki Mitachi, Balkema, Rotterdam, pp. 381–386.

Franklin, J.A. and Chandra, R. (1972). "The slake durability test," *International Journal of Rock Mechanics and Mining Sciences*, Vol. 9, pp. 325–341.

Fredlund, D.G. and Rahardjo, H. (1993). "Soil Mechanics for Unsaturated Soils," John Wiley and Sons, Inc.: New York

Godin, P.M. (1962). "Emploi et perspectives de la stabilization au ciment en technique routière," *Annales de l'institut technique du bâtiment et des travaux publics*. 169, pp. 38–64 (in French).

Hassler, L., Stille, H. and Hakansson, U. (1987). "Simulation of grouting in jointed rock," *Proceedings of 6th International Congress on Rock Mechanics*, Montreal, Vol. 2, pp. 943–946.

Herzog, A. and Mitchell, J.K. (1963). "Reactions accompanying stabilization of clay with cement," *Highway Research Record*, National Research Council, Washington, DC, 36, pp. 166–171.

Kate, J. (1998). "Behaviour of expansive soils treated with fly ash," *Problematic Soils*, eds, Eiji Yanagisawa, Nobuchika Moroto, Toshiyuki Mitachi, Balkema, Rotterdam, pp. 293–296.

Kaushinger, J.L., Perry, E.B., and Hankour, R. (1992). "Jet grouting: State of the practice," *Proceedings of the Conference Sponsored by Geotechnical Eng. Division, ASCE, Grouting, Soil Improvement and Geosynthetics*, Vol. 1, pp. 169–181.

Koncagül, C.E. and Santi, M.P. (1999). "Predicting the unconfined compressive strength of the Breathitt shale using slake durability, shore hardness and rock structural properties," *International Journal of Rock Mechanics and Mining Sciences* 36, pp.139–153.

Owttrim, M. W. (1988). "*Erodibility Test*," Mainroads Department, Queensland, Australia.

Sällfors, G. and Öberg-Högsta, A.L. (2002). "Determination of hydraulic conductivity of sand – bentonite mixtures for engineering purposes," *Geotechnical and Geological Engineering* 20, 65–80.

Stavridakis, I.E. (2003a). "Influence of composition of soils on their stabilization by cement," *12th Asian Regional Conference on Soil Mechanics and Geotechnical Engineering* 4–8 August 2003, Singapore, pp. 545–548.

Stavridakis I.E. (2003b). "Effect of cement, compaction and strength on slaking for cement stabilized clayey admixtures," *XIIIth European Conference on Soil Mechanics and Geotechnical Engineering*, 25–28 August, Prague, pp. 913–918.

Stavridakis I.E. (2004a). "The effect of Bentonite on strength and durability of cement stabilized clayey admixtures," *Proceedings of the 5th International Conference on Ground Improvement Techniques*, 22–23 March, K. Lumpur, Malaysia, pp. 297–304.

Stavridakis, I.E. (2004b). "The effect of soaking conditions on durability, of cement treated clayey – sand admixtures," *Proceeding of 15th Southeast Asian Geotechnical Conference*, 22–26 November, Bangkok, pp. 569–574.

Stavridakis, I.E. and Hatzigogos, N.T. (1999). "Influence of liquid limit and slaking on cement stabilized clayey admixtures," *Geotechnical and Geological Engineering*, eds, D.G. Toll and K. Kim, 17, 145–154, Kluwer Academic Publishers, Netherlands.

Stocker, P.T. (1975). "Diffusion and diffuse cementation in lime – and cement – stabilized clayey soils – chemical aspects," *Australian Road Research*, Vermont South, Victoria, Australia, Vol. 5, 9, pp. 6–47.

Tatsuoka, F. Uchida, K., Imai, K., Ouchi, T., and Kohata, Y. (1997). "Properties of cement – treated soils in Trans –Tokyo Bay Highway Project," *Ground Improvement Geosystems*, Tokyo, 1, pp. 37–57.

Chapter 27

Influence of sand content on strength and durability of cement-acrylic resin treated soil

Costas A. Anagnostopoulos[1]

Summary

Cement-acrylic resin was used with different proportions of soft clay to medium-fine sand mixtures to improve their engineering characteristics. A comprehensive laboratory testing program was carried out for studying the effect of cement-acrylic resin on physical and engineering behavior of this soft clay. The properties studied were compressive strength, slake durability, porosity, dry unit weight, and compression index C_c. The improvement of engineering properties of these soft clay-sand mixtures, treated with cement-acrylic resin, was influenced strongly by the medium-fine sand content.

Introduction

Various methods of soil mixing such as mechanical and hydraulic, with and without air, have been used widely in Japan for about 20 years. More recently they have gained wide acceptance in the United States. Soil mixing, a ground modification technique, has been used for many diverse applications including building and bridge foundations (Puppala *et al*., 2003), retaining structures, liquefaction mitigation, temporary support of excavations, water control, and structures to protect the natural environment.

Classifications such as Soil Mixing, Cement Deep Mixing (CDM), Soil Mixed Wall (SMW), Deep Soil Mixing (DSM), are well known. All these methods have the same basic aim – to find the most efficient and economical method of mixing cement with soil so that the properties of a soft soil can be more like the properties of a soft rock such as clayey shale or lightly cemented sandstone (Ahnberg *et al*., 2003).

Mixing of soft clay soils must be carefully controlled in order to avoid significant pockets of untreated soils (homogeneous mixing). Soil mixing is also commonly used as a stabilization or in situ fixation method for isolating hazardous wastes and sludge.

Certain minimum requirements must be satisfied in order to improve the physical and engineering properties of soft soils adequately. If a soft soil is stabilized by cement, factors such as compressive strength (e.g. bearing capacity), durability under environmental conditions of wetting-drying (e.g. strength of cement-soil bonds), porosity (e.g. water or waste leakage through the pore grains), permeability (e.g. containment walls can be constructed with permeability of approximately 5×10^{-7} cm/sec), compression index

[1] Aristotle University of Thessaloniki, Greece; e-mail: kanagnos@civil.auth.gr

(e.g. consolidation-settlement of foundations), and the percentage of sand grains (e.g. grain to grain contact, effective vertical strength) should be taken into consideration (Bell, 1975; Kawasaki *et al*., 1981; Kamruzzaman *et al*., 2000).

In this chapter the following studies are reported: tests of compressive strength and slake durability index were carried out, and parameters such as porosity, dry unit weight, and compression index C_c were estimated in four different mixtures of soft clay (particle size <74 μm) with medium-fine sand (particle size >74 μm) stabilized by 4% and 12% cement and 5% acrylic resin, cured for 7 and 28 days. The main concept assessed in this research work is that the percentage of sand primarily controls parameters such as strength and durability. Specifically, the influence of percentage of sand grains on strength, slaking (i.e. potential weakening of bonds between the grains of cement-acrylic resin stabilized soft soil due to wetting-drying or due to stresses), porosity, dry unit weight, and compression index C_c were assessed. The characterization, classification, and study of higher values of these parameters were investigated for soft-sand mixtures in order to use them as reinforced material in soil-improvement techniques such as soil mixing. Additionally, the acrylic resin used as additive with cement paste was assessed for its ability to increase the bonds within the grains as well as the durability, cohesion, and engineering strength, and its ability to decrease the porosity. Finally, the clay-cement system can be made almost impermeable to the adsorption of deleterious substances such as sulphates and organic compounds with small chains.

Methodology

Materials

Soft soil samples were collected from a depth of 5 to 10 m. The basic physical and engineering characteristics of this soft clay are listed in Table 27.1. The quartz-sand used was uniform with Hazen coefficient $2.19 < 5$ and its range of particle size was 74 μm to 840 μm. Microfine Portland cement was used with Blaine over 4,500 cm^2/g, produced by Titan Co., Greece and its chemical composition is shown in Table 27.2. The acrylic resin (AR) used was an emulsion of a synthetic elastic chemical substance, which strongly increases the bonds between the soft soil-sand-cement particles as well as cohesion and engineering strength. It also improves the durability with regards to chemical intrusion

Table 27.1 Properties of the in situ soft clay

Properties	*Characteristics*	*Properties*	*Characteristics*
Liquid limit LL (%)	51	Grain size distribution	
Plastic limit PL (%)	30	• Clat (%)	55
Plasticity index PI (%)	21	• Silt (%)	40
Water content (%)	49.8	• Sand (%)	5
Activity	0.7	Initial void ratio (e_o)	1.35
Bulk unit weight (KN/M^3)	17.2	pH (Soil : water = 1 : 5)	8
Dry unit weight (KN/M^3)	11.5		Montmorillonite,
Specific gravity	2.7	X-Ray diffraction	Kaolinite, illite
Compression index (C_c)	0.33	Analysis	Chlorite, Quartz,
Porosity (%)	57.4		Calcite
Compressive strength (KPa)	70		

Table 27.2 Chemical composition of the used cement

Chemical component	SiO_2	Al_2O_3	Fe_2O_3	*CaO*	*MgO*	SO_3	K_2O	Na_2O	*Ignition loss*
Amount (%)	30	7.5	2	52	2	3	1.5	0.5	1.5

Table 27.3 Mixing proportions of specimens (by weight)

No.	*Soft soil*	*Fine sand*	*Cement*	*Acrylic resin*
SC1	0.825	0.175	0.04	0.05
SC2	0.7	0.3	0.04	0.05
SC3	0.45	0.55	0.04	0.05
SC4	0.35	0.65	0.04	0.05
SC5	0.825	0.175	0.12	0.05
SC6	0.7	0.3	0.12	0.05
SC7	0.45	0.55	0.12	0.05
SC8	0.35	0.65	0.12	0.05

and the strengthening of bonds between the grains (Grammatikopoulos *et al*., 2000). The amount of AR added in cement-treated soft soil-sand mixtures was 5% by weight of soil-sand mixture for all cement to soil-sand proportions.

Sample preparation

The proportions of cement-acrylic resin treated soft soil-sand mixtures are shown in Table 27.3 and were prepared as follows: In the first stage the soft soil-sand mixtures were prepared and afterwards a required amount of water was added to these soil samples and mixed thoroughly by a high speed rotating stirrer to obtain a water content of 50% (saturated conditions). Continuously, the required quantity of cement in powder form was added to the soil-sand slurry and the whole mixture was stirred for 10 min. Then, the quantity of AR was added and another mixing followed for 5 min. Quantities of the added cement were 4 and 12% by weight of soil-sand mixtures. The samples for compressive strength and slake durability test were kept in plastic bags during the 7 and 28 days of curing. Oedometer specimens were prepared by placing the treated soil directly into the oedometer ring and were kept in airtight plastic bags to prevent moisture loss until the day of their test. The slaking ($100 - I_{d_2}$) was measured using the device and testing procedure developed by Franklin and Chandra (1972). Finally the slake durability index (I_{d_2} – second cycle) was calculated as the percentage ratio of the final to initial dry sample weight.

Results and discussion

The compressive strength, slaking, and compression index C_c, in 7 and 28 days of curing, and porosity of cement-acrylic resin treated soft soil-sand mixtures vs. the fine sand content are shown in Figures 27.1 to 27.4 respectively. It was observed that the compressive strength increased while the percentage of sand was also increasing up to a higher value for soil mixture with 55% sand content for 4% and 12% cement at 7 and 28 days of curing. The reason

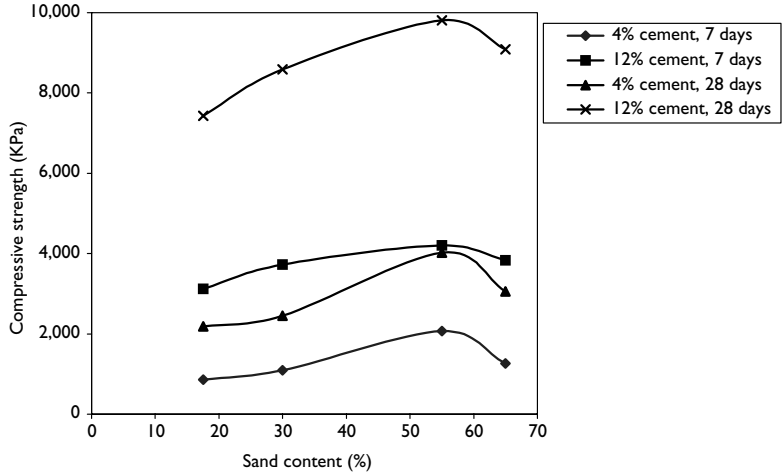

Figure 27.1 Compressive strength versus sand content of soft clay-sand specimens treated with 4% and 12% cement and 5% AR, at 7 and 28 days of curing.

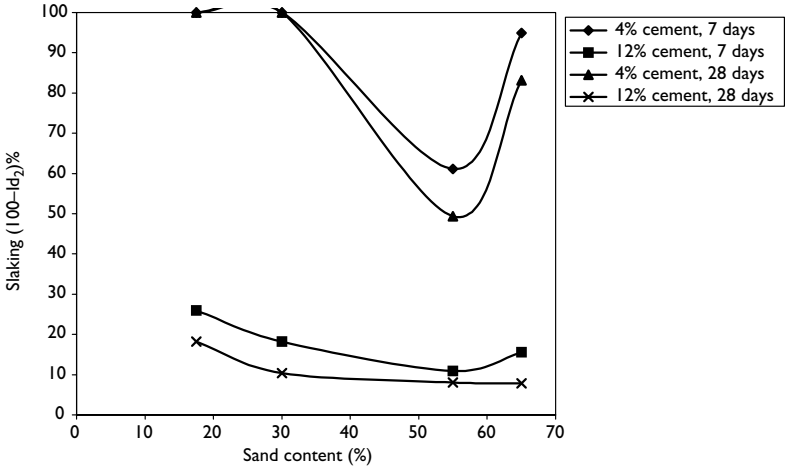

Figure 27.2 Slaking versus sand content of soft clay-sand specimens treated with 4% and 12% cement and 5% AR at 7 and 28 days of curing.

for that is that the fine grains filled all the voids between the soil grains resulting in a gain of strength and durability (lower slaking). This is related with the increased values of dry unit weight shown in Table 27.4 and the decreased values of porosity, which were observed for the soil-sand mixtures, containing 17.5% to 55% sand. In connection to this, as the

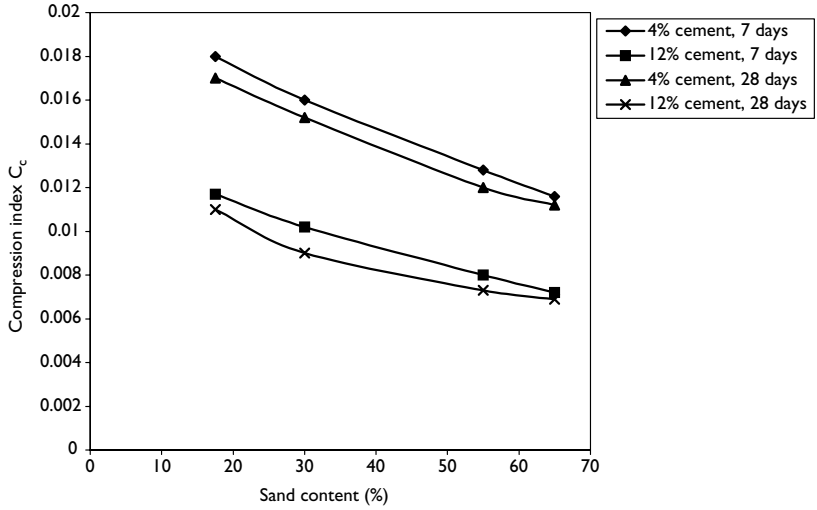

Figure 27.3 Compression index versus sand content of soft clay-sand specimens treated with 4% and 12% cement and 5% AR at 7 and 28 days of curing.

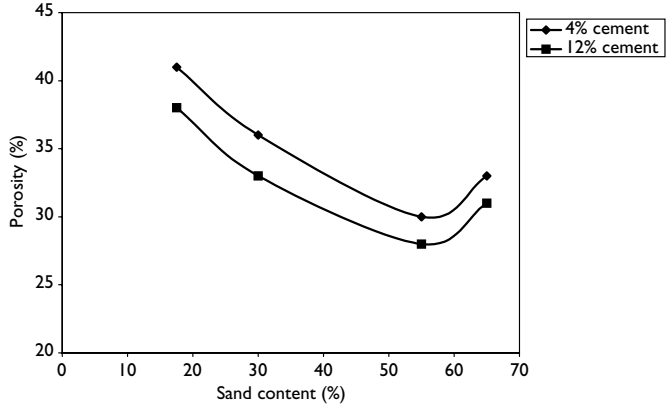

Figure 27.4 Porosity versus sand content of soft clay-sand specimens treated with 4% and 12% cement and 5% AR.

amount of sand grains increases beyond 55%, the number of grain to grain contacts also increased and a greater amount of cement was needed to develop strong bonds in the cement-soil-sand system. This is in the lower values of dry unit weight shown in Table 27.4 and the higher values of porosity for 65% sand (Yoder, 1967 and Stavridakis, 1997).

Table 27.4 Dry unit weight of specimens

No	*Dry unit weight (KN/M^3)*
SC1	15.93
SC2	17.28
SC3	18.9
SC4	18.09
SC5	16.74
SC6	18.09
SC7	19.44
SC8	18.63

The compression index C_c tended to decrease as the cement content was increased. Furthermore the addition of fine sand had a resultant reduction in C_c values. Curing time had only a marginal effect on this improvement.

A soft soil treated with a strong grout may achieve a strength exceeding 7,000 KPa. In the present work the values of strength of soft soil-sand mixtures treated with 12% cement and AR in 28 days of curing, satisfied these specifications outlined by Bell (1975).

Conclusions

The sand content strongly influenced the strength, slaking (i.e. potential weakening of bonds between the grains of cement-acrylic resin stabilized soft soil), porosity, dry unit weight and compression index C_c. Higher values of these stated parameters were observed in soil mixtures with 55% sand. The values of the strength were $>$7000 KPa in soil-sand mixtures stabilized by 12% cement and acrylic resin cured for 28 days.

References

Ahnberg, H., Johansson, S. E., Pihl, H. and Carlsson, T. (2003), "Stabilising effects of different binders in some Swedish soils." *Ground Improvement*, Vol. 7, pp. 9–23.

Bell, F.G. (1975). "Methods of treatment of unstable ground" by Lilley AA, Newnes-Butterworth.

Franklin, J., A. and Chandra, R. (1972). "The slake durability test." *International Journal of Rock Mechanics and Mining Sciences*, Vol. 9, pp. 325–341.

Grammatikopoulos, I. and Anagnostopoulos, C. (2000). 'Properties of acrylic resin-acrylic polymer grouts for soil and rock reinforcement." *Proceeding of 5th International Conference on Environmental Pollution*, ed., A. Anagnostopoulos, Thessaloniki, Greece, pp. 802–810.

Kamruzzaman, M.H.A., Chew, H.S., and Lee, H.F. (2000). "Engineering behaviour of cement treated singapore marine clay." *Proceeding of an International Conference on Geotechnical and Geological Engineering*, 19–24 November, Technomic Publishing Co., Melbourne, Australia.

Kawasaki, T., Niina, A., Satoh, S., Suzuki, Y. and Honjyo, Y. (1981). "Deep mixing method using cement hardening agent." *Proceedings of the Tenth International Conference on Soil Mechanics and Foundation Engineering*, Vol. 1, pp. 721–724.

Puppala, A. J., Wattanasanticharoen, E. and Punthutaecha, K. (2003), "Experimental evaluations of stabilisation methods for sulphate-rich expansive soils." *Ground Improvement*, Vol. 7, pp. 25–35.

Stavridakis, I.E. (1997). "A study of slaking related to the unconfined compressive strength of cement stabilized clayey soils." PhD thesis, Dept of Civil Engineering Aristotle University of Thessaloniki, Greece, (in Greek).

Yoder, E.J. (1967). *Principles of Pavement Design*, John Wiley and Sons, Inc., New York.

Chapter 28

Physical and engineering properties of cement stabilized soft soil treated with acrylic resin additive

Costas A. Anagnostopoulos[1]

Summary

Soil mixing, a ground modification technique, has been used for many diverse applications including building and bridge foundations, retaining structures, liquefaction mitigation, temporary support of excavations, water control, and structures that protect the natural environment. This method has a basic objective – to find the most efficient and economical method of mixing cement with soil so that soft soil obtains properties more like to those of a soft rock, such as a clayey shale or lightly cemented sandstone. Soft soils are well known for their low strength and high compressibility. Usually, due to sedimentary processes, both physical and engineering properties such as void ratio, water content, grain size distribution, compressibility, permeability, and strength show significant variation. Furthermore, they exhibit high compressibility including secondary consolidation, reduced strength, low permeability, and compactness. Consequently they display low quality for construction. Thus, deep mixing has recently been used to improve the strength and deformation characteristics of these soft clays. A comprehensive laboratory testing program was carried out in order to study the effect of inclusion of cement and acrylic resin on the physical and engineering behavior of soft clay. A series of unconfined compression, oedometer consolidation, durability, porosity, and permeability tests were conducted with cement contents varying from 5% to 30% *w/sw* (weight by soil weight) and acrylic resin of 5% *w/cw* (weight by cement weight) and having curing periods of 7 and 28 days.

Introduction

A technique for stabilization and reinforcement of a soft soil is by mixing the ground with cement. This ground modification technique has been used in Japan (mid-1970s), and in Scandinavia (Sweden, Finland), for many diverse applications. Names such as Jet Grouting, Soil Mixed Wall (SMW), Geojet, Deep Soil Mixing (DSM) and Cement Deep Mixing (CDM) have recently gained wide acceptance in the United States (Kaushinger, 1992). The CDM technique, for example, has been used in the following cases:

- Building foundation to reduce settlement by ensuring volume stability or controlling permeability or increasing strength;

[1] Laboratory of Soil Mechanics, Geotechnical Engineering Division, Department of Civil Engineering, Aristotle University of Thessaloniki, 541 24 Thessaloniki Greece, Tel: 00302310 995706; email: kanagnos@civil.auth.gr

- Excavation work to provide better support by strengthening the surrounding soil or varying its permeability;
- Pavement construction to provide more durable and stronger pavements by eliminating volume changes and preventing weathering deterioration;
- Slope stability to prevent slips by strengthening the soil;
- Water retention to ensure safe structures against water erosion;
- Environmental conservation to prevent or repair erosion damage by increasing the resistance of the soil to natural weathering from water (Ingles *et al.*, 1972; Lee, 1974).

Each of these methods has the same basic goal – to allow the engineering structures to remain intact over a long period of time without any required repairs or reconstruction.

During the last decades some limitations have been imposed to constructions – limits on the space occupied and on time for construction, safety, growing environmental concerns, and shortages of traditional natural material. Soft soil deposits are problematic soils for construction and that is why they have been ignored for a long time in contrast with soils of higher quality with their reduced technical difficulties and lower construction costs. Alternative areas for construction, however, have become more and more important during the last decades due to a growing shortage of better quality soils. These limitations may be overcome with the introduction of new mixing materials, such as cement-acrylic resin, and new construction techniques, such as CDM (Pinto *et al.*, 2003).

Several minimum requirements must be satisfied in order to adequately improve the physical and engineering properties of soft soils. If this type of soil is stabilized by cement, factors such as compressive strength (i.e. bearing capacity), durability under environmental conditions of wetting-drying (i.e. strength of cement-soil bonds), porosity (i.e. water or waste leakage through the pore grains), permeability (i.e. containment walls can be constructed with permeability of approximately 5×10^{-7} cm/sec), and compression index (i.e. consolidation-settlement of foundations) should be taken into consideration (Bell, 1975; Kawasaki *et al.*, 1981; Kamruzzaman *et al.*, 2000). For these reasons, tests of compressive strength and slake durability index were carried out, and parameters such as porosity, compression index C_c, apparent swelling index C_{as}, and permeability coefficient, were estimated for soft clay stabilized with 5%, 10%, 20%, and 30% cement addition with/without 5% acrylic resin, cured for 7 and 28 days. The main concept in this research work was the study of the influence of cementing agent on the stabilization-engineering parameters (Anagnostopoulos *et al.*, 2003).

The goals of the study reported in this chapter were to asses the influence of variability percentage of cement on strength, slaking (i.e. potential weakening of bonds between the grains of cement-acrylic resin stabilized soft soil due to wetting-drying or due to stresses), porosity, and compressibility parameters. The characterization, classification and study of higher values of the parameters for this improved soft clay will also be reported in order to use it as reinforced material in soil-improvement techniques such as soil mixing. Additionally, it will be demonstrated that the acrylic resin used as additive with cement paste significantly increased the bonds within the grains as well as the durability, cohesion, and engineering strength, while decreasing porosity.

Methodology

Soil Soft soil samples were collected from excavations at a depth of 10 to 15 m in the wider area of Thessaloniki, Greece. The basic characteristics of the in situ soft soil are listed in Table 28.1.

Table 28.1 Properties of the in situ soft soil

Properties	*Characterists*	*Properties*	*Characteristics*
Liquid limit LL (%)	43.54	Grain size distribution	
Plastic limit PL (%)	25.32	Clay (%)	27
Plasticity index PI (%)	18.22	Silt (%)	40
Water content (%)	61.2	Sand (%)	33
Activity	0.67	Initial void ratio (e_o)	1.653
Bulk unit weight (KN/M^3)	16.68	pH (soil : water = 1:5)	8
Dry unit weight (KN/M^3)	10.17	X-ray diffraction analysis	Montmorillonite, kaolinite, illite, chlorite, quartz, calcite
Specific gravity	2.7		
Compression index (C_c)	0.311		
Swelling index (Ca_s)	0.093		
Shear strength (Kpa)	18.6		

Table 28.2 Chemical composition of the used cement

Chemical component	SiO_2	Al_2O_3	Fe_2O_3	CaO	MgO	SO_3	K_2O	Na_2O	*Ignition loss*
Amount (%)	30	7.5	2	52	2	3	1.5	0.5	1.5

Cement Microfine Portland cement was used with Blaine fineness of approximately 4200 cm^2/g and 28-day compressive strength of 45 MPa, produced by Titan Co., Greece. Its chemical composition is shown in Table 28.2.

Acrylic resin (AR) The acrylic resin which was used is an emulsion of a synthetic elastic chemical substance which as additive in cement paste increases significantly the bonds within the substrate particles as well as the cohesion and the engineering strength. It improves also the durability in chemicals intrusion, the impermeability, and finally the durability in cycles of freezing and thawing. The amount of AR added in cement-treated soil samples was 5% *w*/*cw* (per weight of cement) for all cement/soil ratios.

Sample preparation Cement and cement-acrylic resin treated soil samples were prepared as follows: a required amount of water was added to the soil sample and mixed thoroughly by a high speed-rotating stirrer to obtain saturated conditions. Afterwards a quantity of cement in powder form was added to the saturated soil and the whole mixture was stirred in short time (5 minutes) to avoid hardening of the soil-cement mixture. Then, the quantity of AR (acrylic resin) (5% *w*/*sw*) was added and another mixing followed for 5 minutes. Quantities of cement added to the soil slurry were 5%, 10%, 20%, and 30% *w*/*sw*. The samples for unconfined compression tests were kept in plastic bags during the curing time. Oedometer specimens were prepared by placing the treated soil directly into the oedometer ring. They were then kept in airtight plastic bags to prevent moisture loss until the day of their test.

The samples for compressive strength (ASTM D 1632–96) and slake durability tests were kept in plastic bags during the 7 and 28 days of curing. The strength was measured using a commercially available device named Versa Tester/Soil test Inc. The dimensions of the cylindrical specimens tested were 35.5 mm in diameter and 71 mm in length. The rate of strain was 0.6604 mm/min. The slaking (100 – Id_2) was measured using the device and testing

procedure developed by Franklin (Franklin and Chandra, 1972). Finally, the slake durability index (Id_2 – second cycle) was calculated as the percentage ratio of the final to initial dry sample weight. The dimensions of the cylindrical specimens tested in the slake durability test were 35.5 mm in diameter and 23.7 mm in length.

Permeability coefficient was measured according to ASTM D 5084–00e1 regulation and porosity was measured according to the referenced method of Grimshaw (1971).

Results and discussion

Unconfined compression tests were performed to determine the stress–strain and stiffness characteristics of cement-treated soft soil. The experiments were conducted with cement contents varying from 5% to 30% with/without 5% AR having curing periods of 7 and 28 days. Figures 28.1 and 28.2 illustrate the stress-strain behavior of treated soil for different cement contents with/without AR after 7 and 28 days curing period, respectively. It was found that all soil-cement stabilized samples cured for seven days and treated with acrylic resin revealed lower compressive strength and stiffness compared with soil-cement stabilized samples without AR treatment. The difference in strength was 18%, 28%, 33%, and 48% for 5%, 10%, 20%, and 30% *w*/*sw* cement respectively. The difference was related to the retarding action of the AR on the pozzolanic reactions and consequently on the cement hardness. This adverse action will be diminished by time.

Strength values of soil-cement stabilized samples cured for 28 days and treated with AR were higher than values of soil samples treated only with cement. In case of 5% *w*/*sw* cement addition the increment of strength was 26.5% while in larger amount of cement addition this increment was almost permanent between 18.5% and 19% (Figure 28.3). Figures 28.1 and 28.2 also reveal that higher cement content treated soil exhibits more ductile behavior. More brittle type of failure with low values of failure strain was observed for lower cement content treated soil in both curing periods (Tatsuoka *et al.*, 1996).

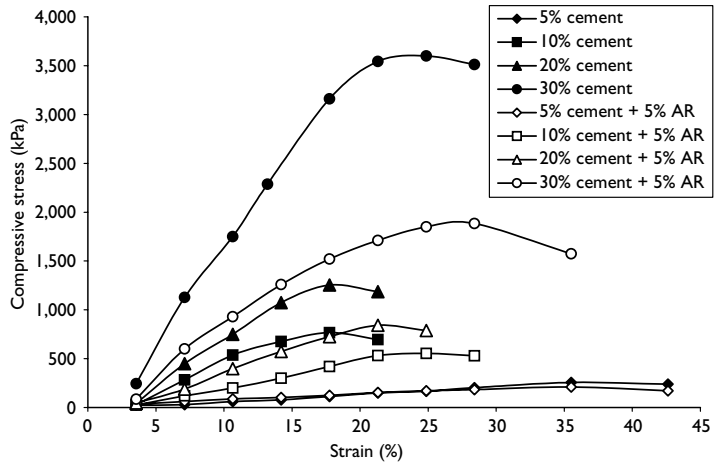

Figure 28.1 Stress-strain behavior of cement and cement-acrylic resin treated soil cured for 7 days.

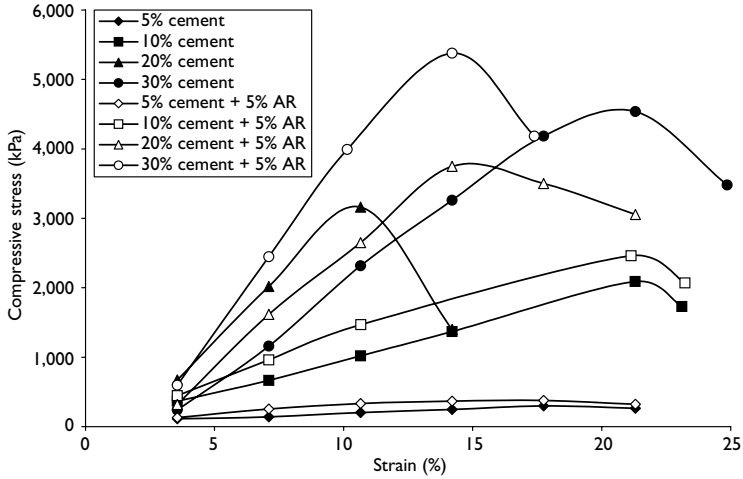

Figure 28.2 Stress-strain behavior of cement and cement-acrylic resin treated soil cured for 28 days.

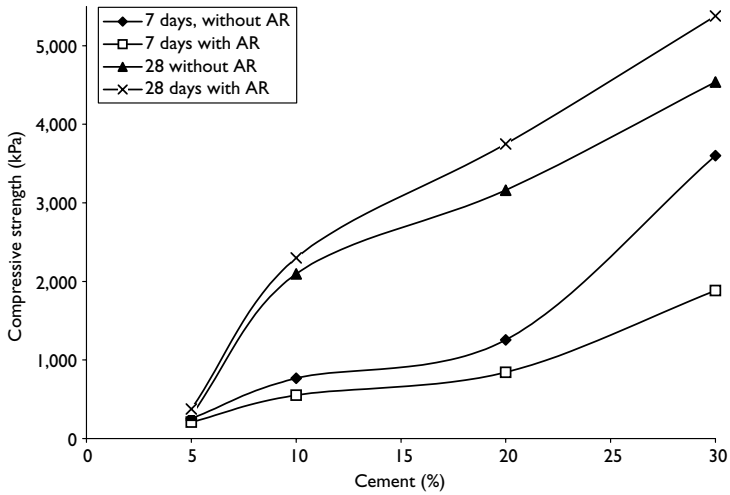

Figure 28.3 Compressive strength versus cement percentage for treated soil cured for 7 and 28 days.

Figures 28.4 and 28.5 show the e-log σ_v' relationship of untreated and treated soil samples aged 7 and 28 days. Figure 28.6 shows the Compression index C_c in relation to cement content of treated soil aged for 7 and 28 days. Consolidation characteristics were improved strongly as the cement content was increased. Curing time had only marginal effect on this

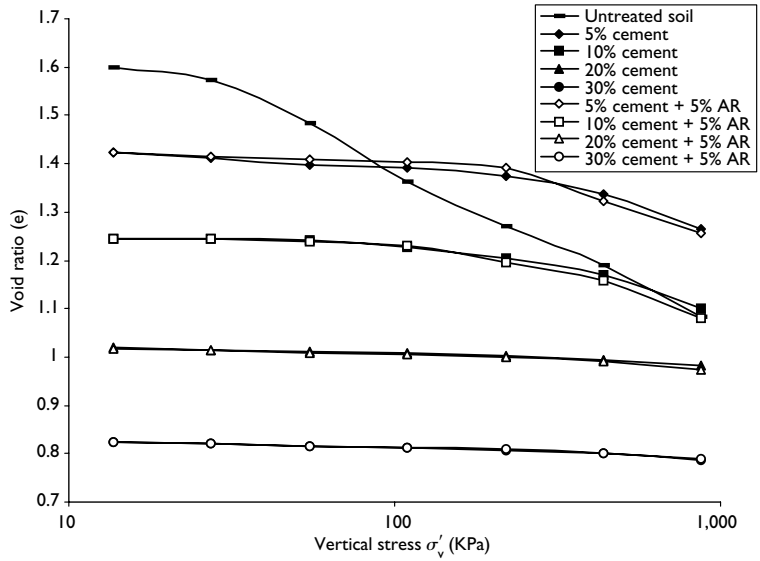

Figure 28.4 e-logσ'_v relationship of treated and untreated soil cured for 7 days.

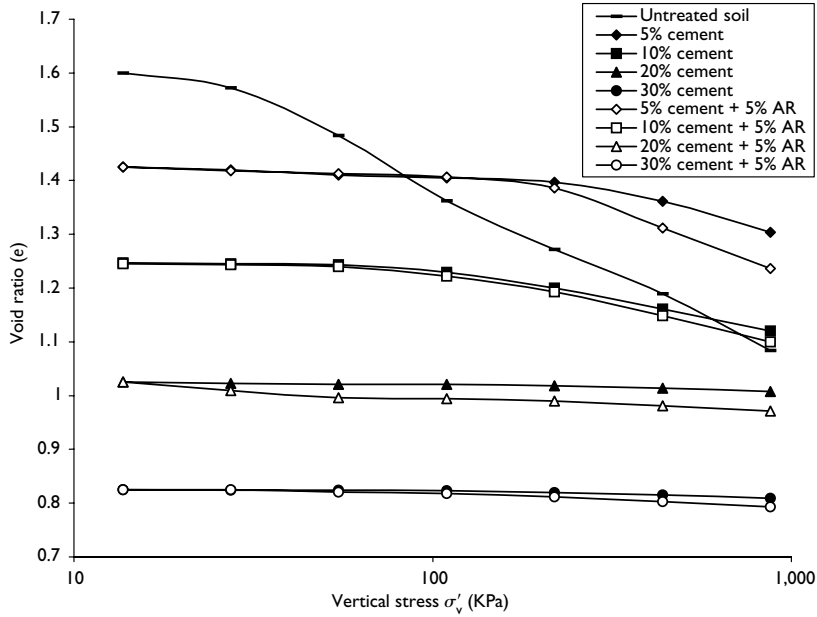

Figure 28.5 e-logσ'_v relationship of treated and untreated soil cured for 28 days.

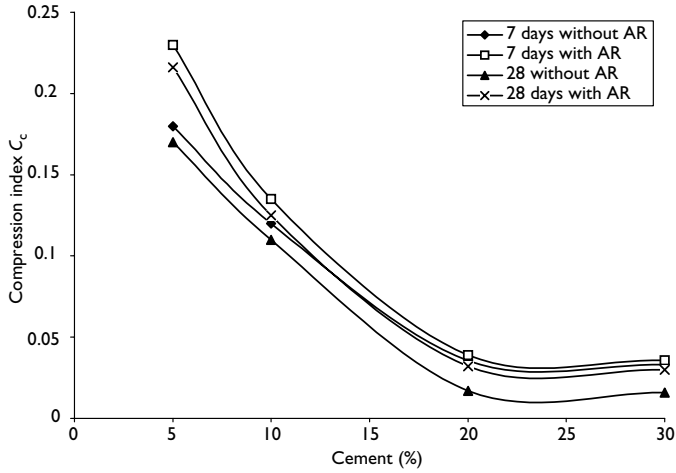

Figure 28.6 Compression index C_c verses cement percentage for treated soil cured for 7 and 28 days.

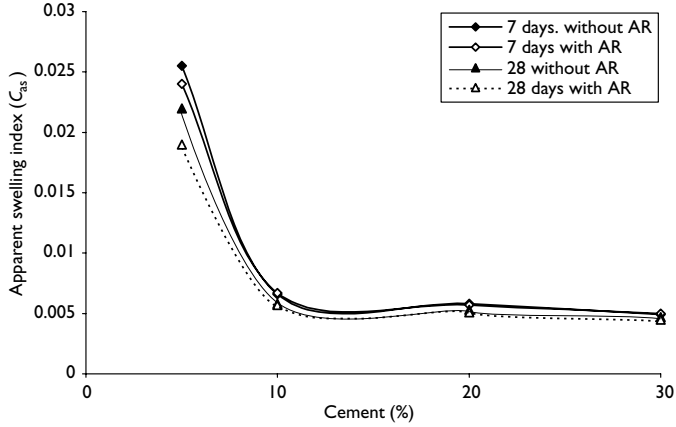

Figure 28.7 Apparent swelling index C_{as} versus cement percentage for treated soil cured for 7 and 28 days.

improvement. The addition of 5%, 10%, 20%, 30% *w/sw* cement decreased the compression index C_c to about 0.17, 0.11, 0.017, and 0.016 correspondingly, in 28 days, from 0.311 of the untreated soil. Acrylic resin caused a small increment of C_c at all percentages of cement due to initial water absorption from the hydrophilic groups of acrylic resin polymeric chains and to its final water loss during loading.

The portion of (e-logσ'_v) relationship before apparent preconsolidation pressure is defined as apparent swelling index (C_{as}). Figure 28.7 illustrates the relation between

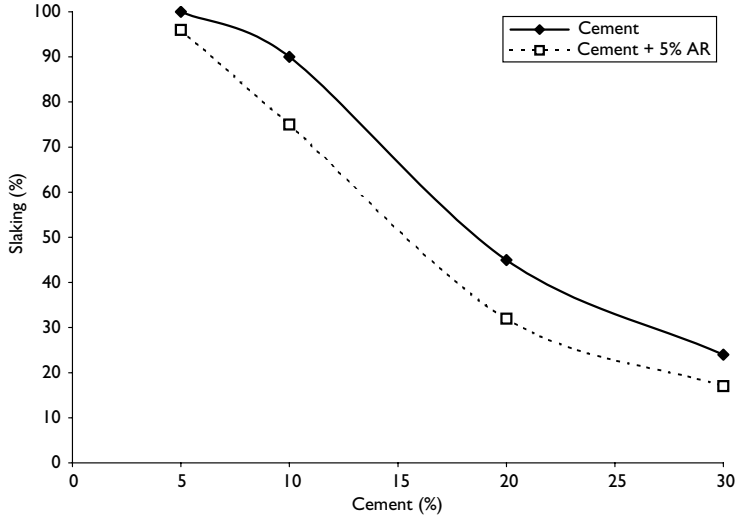

Figure 28.8 Slaking versus cement percentage for treated soil cured for 28 days.

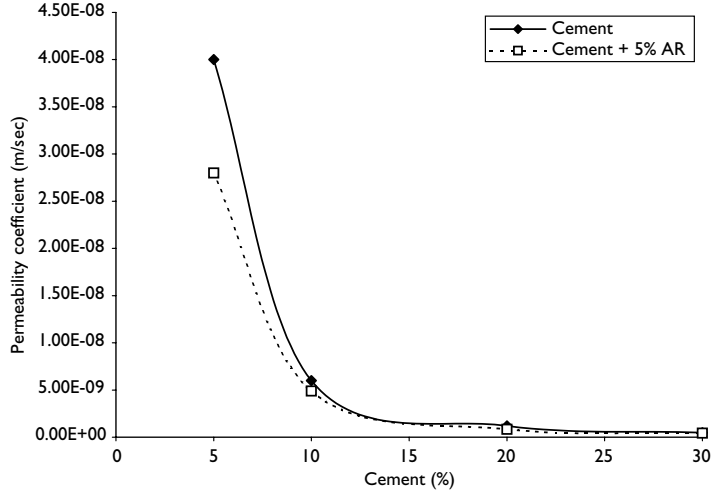

Figure 28.9 Influence of cement content permeability coefficient of treated soil cured for 28 days.

C_{as} and cement content. In case of 5% *w/sw* cement addition, the curing time and AR influenced the C_{as} values. This influence is limited for higher amounts of cement added. Generally AR slightly reduced the C_{as} values due to prevention of water intrusion in the soil mass.

Figures 28.8 to 28.10 show the relation of cement content with slaking, permeability coefficient, and porosity of treated soil cured for 28 days. These results indicate that the

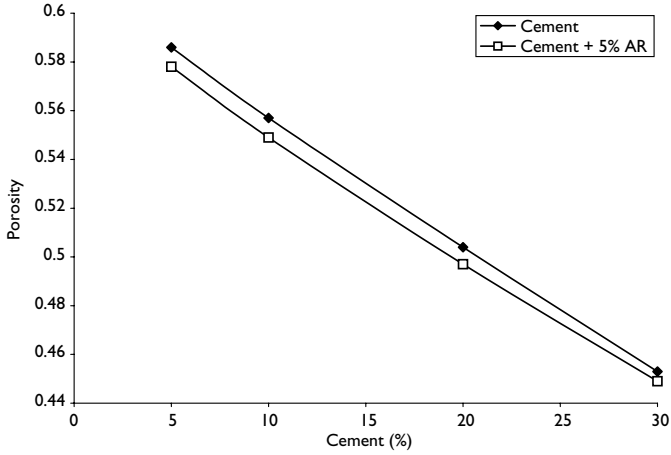

Figure 28.10 Influence of cement content on porosity of treated soil cured for 28 days.

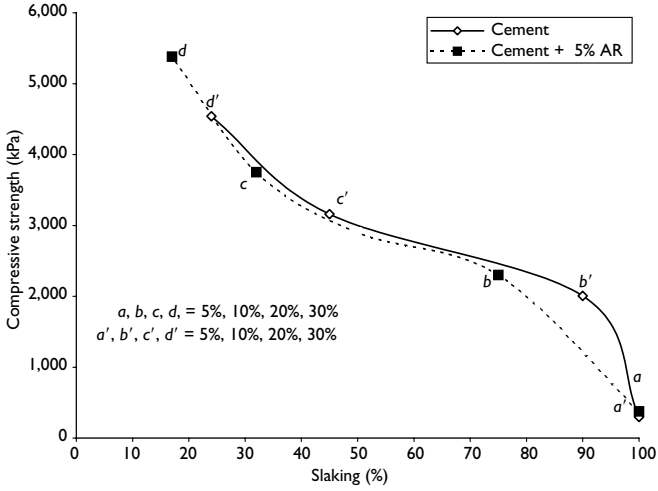

Figure 28.11 Compressive strength versus slaking of treated soil cured for 28 days.

additon of AR decreases the values of slaking, permeability coefficient, and porosity. Also, the increase of cement content decreases strongly the values of slaking, permeability coefficient, and porosity. In relation to this, the slaking decreases because of the potential strengthening of bonds between the grains of cement-acrylic resin stabilized soil. Additionally, AR forms polymer films, which partially fill the voids and micro cracks between the cement-soil grains resulting in the decrease of permeability coefficient and porosity.

Figures 28.11 and 28.12 show the influence of AR on slaking-compressive strength and slaking-porosity, respectively. Slaking (durability) is governed by both cement and AR film

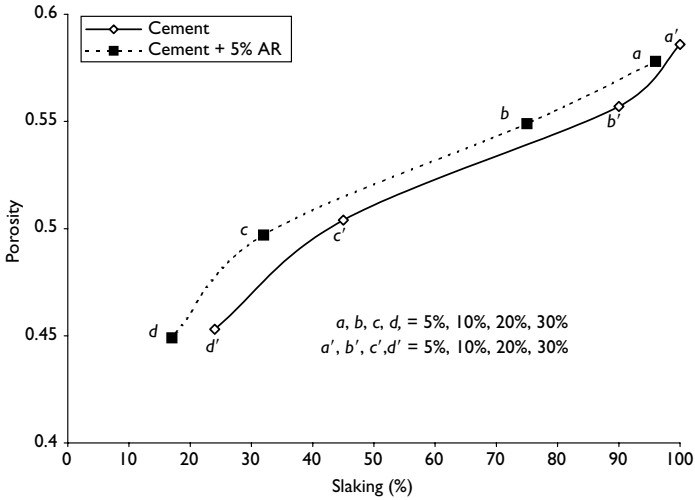

Figure 28.12 Porosity versus slaking of treated soil cured for 28 days.

formation process in their binder phase with soil particles. This significantly improves durability and strength and slightly decreases the porosity of treated soil cured for 28 days (Stavridakis, 1997).

Conclusions

Increasing the amount of cement improved the strength and stiffness of treated soil. Development of strength and stiffness for a short curing time (i.e. 7 days) was delayed significantly as a result of the addition of acrylic resin while for long curing times (i.e. 28 days) the engineering parameters were increased considerably. Compressibility parameters (i.e. compression index and apparent swelling index) were improved significantly as the cement content was increased while there was no effect of curing time. Addition of acrylic resin revealed a small increase in C_c for all percentages of cement because of the tendency of the resin to keep water in its molecule. Addition of acrylic resin and variation in curing time did not influence the C_{as} values for cement more than 5% *w/sw*. The increase in cement content reduced the values of slaking, permeability coefficient and porosity. There was also a significant reduction of these parameters with the addition of 5% acrylic resin.

References

Anagnostopoulos, C., Stavridakis, E., and Grammatikopoulos, I. (2003). "Influence of sand content on strength and durability of cement-acrylic resin treated soil," Proceedings of the 56th Canadian Geotechnical Conference, September, Manitoba, Canada.

ASTM D 1632–96 (1996). "Standard practice for making and curing soil-cement compression and flexure tests specimens in the laboratory," *Annual Book of ASTM Standards*, ASTM International West Conshohocken, PA.

ASTM D 5084–00e1 (2000). "Standard test methods for measurement of hydraulic conductivity of saturated porous materials using a flexible wall permeameter," *Annual Book of ASTM Standards*, ASTM International West Conshohocken, PA.

Bell, F.G. (1975). "Methods of treatment of unstable ground," by Lilley AA, Newnes-Butterworth.

Franklin, J. A. and Chandra, R. (1972). "The slake durability test," *Internationa Journal of Rock Mechanisms and Mining Sciences* Vol. 9, pp. 325–341.

Grimshaw, W. Rex (1971), *The Chemistry and Physics of Clays and Allied Ceramic Materials*, Ernest Benn Ltd., New York.

Ingles, O.G. and Metcalf, J.B. (1972). *Soil Stabilization Principle and Practice*, Butterworths, Melbourne, Australia.

Kamruzzaman, M.H.A., Chew, H.S., and Lee, H.F. (2000). "Engineering behaviour of cement treated singapore marine clay," Proceedings of an International Conference On Geotechnical and Geological Engineering, 19–24 November, Melbourne, Australia.

Kaushinger, J.L., Perry, E.B., and Hankour, R. (1992). "Jet grouting: state of the practice," Proceedings of the Conference Sponsored by Geotechnical Engineering Division, ASCE, Grouting, Soil Improvement and Geosynthetics, Vol. 1, pp. 169–181.

Kawasaki, T., Niina, A., Saitoh, S., Suzuki, Y., and Honjyo, Y. (1981). "Deep mixing method using cement hardening agent," Proceedings of the 10th International Conference On Soil Mechanics and Foundation Engineering, Vol. 1, pp. 721–724.

Lee, I.K., (1974). *Soil Mechanics-New Horizons*, University of New South Wales, Australia, London.

Pinto, M., Isabel, M. and Oliveira, J. da V. P., (2003) "Use of geosynthetics in embankments on soft soils," Proceedings of International Conference on Problematic Soils, 29–30 July, Nottingham, UK, Vol. 1, pp. 83–98.

Stavridakis, I.E. (1997). "A study of slaking related to the unconfined compressive strength of cement stabilized clayey soils," PhD thesis, *Dept of Civil Engineering, Aristotle University of Thessaloniki*, Greece, (in Greek).

Tatsuoka, F., Kohata, Y., Uchida, K., and Imai, K. (1996). Deformation and strength characteristics of cement treated soils in Trans-Tokyo bay highway project, Proceedings of the 2nd International Conference On Ground Improvement Geosystems, Tokyo, 14–17 May, Grouting and Deep Mixing, pp. 453–459.

Part 8

Other treatment methods

Chapter 29

Pozzolanic stabilization of expansive soils

P.V. Sivapullaiah[1]

Summary

The aim of this chapter was to review pozzolanic agents, such as lime and fly ash, in order to assess their effectiveness in controlling swelling in expansive soils induced by moisture content variation. Pozzolanic agents such as lime and fly ash were found to be effective in controlling swelling in expansive soils induced by moisture content variation. The pozzolanic reaction compounds formed bind the soil particles strongly resisting the internal swelling pressure of the clay. Calcium based stabilization is very effective in the presence of alkali solution and has been successfully applied to control the alkali-induced heave in expansive soil.

Introduction

Swelling and shrinkage of expansive soils occur mainly due to a change in the moisture regime and pose serious problems to foundations causing damage to structures founded on them. The hydration of particles is mainly due to a charge on clay particle surface. Most soils have a net negative charge. The total charge on clay mineral surfaces is of two types. The permanent or intrinsic charge is due to structural properties including isomorphic substitution and other alterations, which is independent of soil reaction or pH. There is another charge, which is pH or proton dependent, and is due to the imbalance of complex proton and hydroxyl charges on the surface.

Soils containing montmorillonite, vermiculite, and some mixed layer minerals behave as expansive soils (Figure 29.1). Many of these clay minerals occur as the dominant mineral in some areas and almost all of them occur as minor constituents with other clay minerals. Discrete clay crystals may consist of alternating layers of two or more different clay minerals, which are referred to as mixed-layer clays. Common combinations contain the expandable clay mineral montmorillonite or beidellite, interlayer with chlorite or with mica.

The aim of this chapter is to review pozzolanic agents, such as lime and fly ash, in order to assess their effectiveness in controlling swelling in expansive soils induced by moisture content variation.

[1] Department of Civil Engineering, Indian Institute of Science, Bangalore, India – 560 012; email: siva@civil.iisc.ernet.in

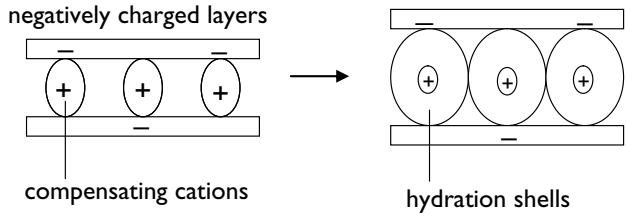

Figure 29.1 Swelling of smectites by hydration.
Source: Stockmeyer, 1991.

Mechanism of swelling

Electrical double layer theory has been successfully used to explain the swelling phenomena in expansive soils (Lal and Shukla, 2004). When clay particles are fully hydrated, the negative charge is balanced by the cations in the soil solution attracted by the Coulomb force. The negative charge on the clay surface and positive charge of the balancing cations create an electrical double layer around the clay particles. According to Guoy (1910) and Chapman (1913), the distribution of ions form a diffuse double layer because cations possess thermal energy that causes a dynamic concentration gradient creating a double layer, which is a condition for maximum entropy. The cations present in the solution neutralize the negative charge on the clay particle and the anions present in the solution. Addition of electrolytes to the system decreases the thickness of the double layer. At relatively short distances from the surfaces of clay particles the orienting and adsorbing forces acting on the water molecules are very strong and the water is believed to be in the solid state rather than in the liquid state. As these adsorbed layers grow during the wetting of a clay, the effective solid volume associated with each particle increases, and if the layers are in contact with each other, the growth of the individual layers will be reflected in an increase in the total volume of the soil structure.

A two parallel plate model can describe the swelling behavior of montmorillonite sheets of clay. These two plates are subjected to repulsive and attractive forces. The energy for attraction is caused by adhesive and van der Waals forces, which depend on the orientation of the plates and pH of soil solution. When pH decreases the charges at the edge of the plate become positive and edge bonding develops, which is more like a plate-like arrangement than parallel arrangement of clay particles. The repulsive forces between two parallel plates with negatively charged surfaces consist of forces owing to double layer and forces owing to the differences in electrolyte concentration between the plates and outer solution. Since the chemical potential of interlayer is greater than outer solution, addition of water causes the plates to drift apart till potential difference reaches equilibrium. The total potential energy is the sum of attractive and repulsive potential energies, which is not necessarily a monotonic function with distance. At low soil moisture content, clay particles are only partially hydrated. Consequently, the double layer is not fully extended and is truncated. Such a truncated double layer has a relatively higher concentration than when the double layer is extended fully. Such a system, therefore, has the capacity to adsorb water or any other polar liquid. Increase in soil moisture content extends the double layer. Swelling is the increase in soil volume due

to the adsorption of water and other polar liquids. Swelling due to diffused double layer repulsion can be curtailed by strong adsorption forces of polyvalent cations. The Coulomb's attraction forces hold the two clay particles together against the double layer repulsion.

The inherent swelling potential of aggregates of clay minerals is closely related to the total external and internal surface areas of clay-mineral particles. Clay minerals are capable of adsorbing water on their outer surfaces, and water so adsorbed will cause a small amount of swelling related to enlargement of the capillary films. When water is introduced to expansive soils, the water molecules are pulled into gaps between the soil plates. As more water is absorbed, the plates are forced further apart, leading to an increase in soil pore pressure. If this increased pressure exceeds surcharge pressure (including the weight of the overlying pavement), the soil will expand in volume to a point where these pressures are once again in balance.

Some clay minerals, however, such as montmorillonite and beidellite of the smectite group, are capable of absorbing appreciable amounts of water between the individual silicate layers of the structural lattice, which results in a high swelling potential. Vermiculite, attapulgite, nontronite, and degraded mica (illite) and chlorite, though less common, are also capable of absorbing appreciable amounts of water. These expandable clay minerals consist of atoms arranged in lattice structures in which sheets or layers of the lattices are bound together by atomic physicochemical forces. The strengths of these forces vary with the types of clay minerals and with the water-retention properties of the cations that occur between the lattice layers. Several methods are available for identification of expansive soils.

In practice, the adsorbed water films in clay grow in thickness until the suction pressure in the water becomes equal to the overburden pressure on the soil due either to self-loading or to externally applied loads. If, when this equilibrium is reached, the loading is increased, the adsorbed water films are reduced in thickness and settlement occurs.

Stages of swelling

The swelling of plate like clay particles can be described by three stages of swelling (Lal and Shukla, 2004). The first stage occurs when the initial distance between the particles is less than two nanometers. During this stage, the swelling is opposed by the electrostatic attraction between cations and negatively charged layers. Swelling beyond 2 nm is possible provided the hydration energy of cation is more than the energy of attraction. With the addition of water the distance between plates increases in discrete steps associated with each molecular water layer formed between the sheets. The swelling continues to the second stage if monovalent cations are present. However, if divalent and trivalent cations are present, swelling ends at the first stage. At the beginning of the second stage, the bonding of molecules to solid surfaces continues as the swelling process continues. The distance between the neighboring sheets rises smoothly up to tens of nm and edges to face forces are important for holding sheets together. In the third stage, the sheets are totally separated and form an arrangement caused by edge to face and edge to edge forces. During drying at first, the decrease in volume is equal to volume of water drained and the degree of saturation remains fairly constant. However, in the second stage, volume decreases less rapidly than water content as air starts entering the soil.

Extent of swelling

The swelling potential of clay is dependent upon the amount and kind of clay minerals present, their exchangeable ions, the electrolyte content of the aqueous solution, particle-size

Table 29.1 Probable expansion as estimated from classification test data

Degree of expansion	*Probable expansion (as a percent of the total volume change)*	*Colloidal content (percent less than 1 μm)*	*Plasticity index*	*Shrinkage limit*
Very high	>30	>28	>35	<11
High	20–30	20–31	25–41	7–12
Medium	10–20	13–23	15–28	10–16
Low	<15	<15	<18	>15

distribution, void size and distribution, water content, superimposed load, and probably other factors (Lal and Shukla, 2004). Volume changes of 1,400–2,000% are reported from laboratory tests in which samples of dry Na-montmorillonite were immersed in water, and changes of 45–145% are reported for Ca-montmorillonite. The inherent swelling capacities of vermiculite, attapulgite, illite, and degraded chlorite have not been fully investigated. Available evidence suggests that they have low to moderate swelling capacities.

The amount of volume change and pressure generated by a swelling clay under laboratory conditions is usually considerably greater than that generated by the same clay in the field under natural conditions. This is possibly due to changes in diagenetic and environmental factors as a consequence of collecting and preparing specimens for testing. Dry swelling clays absorb much larger quantities of water before becoming plastic than do dry, non-swelling clays. They also remain plastic over a wider range of moisture content refered to as the plasticity index (PI). The PI bears a direct relation to the amounts and types of clay minerals present and to the orientation and size of clay particles. Other factors remaining constant, the PI increases with (1) increase in amount of expandable clay minerals, (2) decrease in degree of parallel orientation of the platy clay minerals, and (3) decrease in clay-particle size. Table 29.1 gives a general idea of the types of expansion that can be expected.

Many plastic clays swell considerably when water is added to them and then shrink with the loss of water. Foundations constructed on these clays are subjected to large uplifting forces caused by the swelling. These forces will induce heaving, cracking, and break up of both building foundations and slab on grade members.

Stabilization of expansive soils by chemical additives

Treatment of expansive soils is either to convert the soil to a rigid granular mass, the particles of which are sufficiently strongly bound to resist the internal swelling pressure of the clay, or to retard moisture movement within the soil, provided the retardation is sufficient to overcome normal seasonal changes that is adequate for practical purposes. Impervious membranes are available and useful, but unless they wholly isolate the area to be stabilized their function will be merely to lengthen the path and hence time of the moisture movement. Other than loading to restrict swell, there is no good alternative to stabilization to overcome the disruptive effects of moisture changes in an expansive soil. Densification is almost always a useful means for upgrading the mechanical properties of a soil, whatever additional stabilization systems are employed. Chemical admixture stabilization has been extensively used in both shallow and deep stabilization to improve inherent properties of soil. The role of various chlorides and hydroxides has been investigated in the stabilization of soils.

Pozzolanic stabilization

A pozzolan is a siliceous material, which will react with lime to form cementitious compounds. For production of cementitious compounds, silica in amorphous or noncrystalline form is more effective. Lime, cement, and fly ash have been extensively used to improve the properties of expansive soils. While lime reacts with soil silica to produce cementitious compounds, these compounds are readily available in Portland cement. However, cement is mainly used as pre-treatment before lime stabilization of expansive soils. Fly ashes often contain both lime and reactive silica and produce cementitious compounds in the presence of water. There are three different types of fly ashes from the consideration of pozzolanic nature – self pozzolanic, pozzolanic, and non-pozzolanic. The reactive silica content of fly ash plays an important role in the pozzolanic properties of fly ash. Fly ashes with good reactive silica content and sufficient lime content are called self-pozzolanic (Sivapullaiah *et al.*, 1998b). Fly ashes containing reactive silica but in adequate lime content are pozzolanic and develop good strength with addition of lime. Methods are available for optimising lime content (Sivapullaiah *et al.*, 1995). Fly ashes without reactive silica can not develop strength even with addition of lime and are called non-pozzolanic. Rice husk ash has also been used along with lime or cement.

While most of the stabilizing agents are mixed into the soil, there are also occasions when pozzolanic stabilized materials such lime stabilised rice husk ash can be used as a cushion between expansive soil and foundation to control the swelling of soils. These materials can be better than conventional cohesive non-selling materials as a cushion (Sivapullaiah *et al.*, 2004).

Lime stabilization

The chemical theory involved in the lime reaction is complex. Ignoring carbonation which is a minor cause for strength increase, the major strength gain of lime treated clay is mainly derived from the following reactions:

Dehydration of soil
Ion exchange and flocculation
Pozzolanic reaction

Hydration and flocculation are short-term reactions and pozzolanic reactions are long term. Hydration reaction:

$$CaO + H_2O \rightarrow Ca(OH)_2 + \text{Heat}$$

$$Ca(OH)_2 \rightarrow Ca^{2+} + 2(OH)^- \text{ (280 calories/gm of CaO)}$$

Ion exchange reaction:

$$Ca^{++} + \text{Clay} \rightarrow Ca^{++}\,\text{Clay} + (Na^+, K^+)$$

Pozzolanic reaction:

$$Ca^{++} + 2(OH)^- + SiO_2 \rightarrow CSH$$

$$Ca^{++} + 2(OH)^- + Al_2O_3 \rightarrow CAH$$

The formation of cementitious compounds, calcium silicate hydrate, and calcium aluminate hydrate have been identified by Narasimha Rao and Rajasekaran (1996) by X-ray diffraction and micro-structural analysis of soil lime reaction products. The calcium silicate gel formed initially coats and binds lumps of clay together. The gel then crystallizes to form an interlocking structure.

Effects of lime on expansive soil properties

Most expansive soils respond to lime stabilization very well. Immediately on addition of lime the plastic limit of soil increases up to lime fixation point, the point up to which the monovalent cations of clay particles are replaced with lime. While the liquid limit can increase or decrease on addition of lime depending on the cation exchange and type of exchangeable cations of the clay and associated fabric changes, the plasticity index usually decreases immediately on addition of lime. With curing period the plasticity index is influenced by pozzolanic reactions. The shrinkage of expansive soils is improved by addition of lime. Lime in excess of lime fixation point is used for pozzolanic reactions. The strength of soil with a lime content less than the lime fixation point is affected by water content whereas the strength beyond lime fixation point does not depend on water (Sivapullaiah *et al.*, 1998a). The increase in strength is more due to an increase in cohesive intercept than an increase in the frictional component. Proctor's maximum dry density decreases and optimum water content of expansive soil increases due to flocculation of soil particles. Pozzolanic reactions produce cementitious compounds with curing period up to the optimum lime content. With an increase in lime, the strength of lime treated soil increases only up to the optimum lime content which basically depends on the reactive silica of soil. An increase in the alkalinity increases the reactive silica content of soil. Volume stability of lime treated soil increases considerably. Generally, the permeability of soil increases on treatment with lime due to flocculation of soil clay particles. Factors controlling the characteristics of lime treated clay are – soil factors, type of soil, grain size distribution, clay mineral, soil pH, type of lime, lime content, curing conditions, curing time, curing temperature, etc. Many sodium salts improve the strength of lime treated soils due to increased pozzolanic reactivity and production of more voluminous cementitious compounds of sodium calcium silicate type rather than usual calcium silicate hydrates.

Methods of incorporating lime into soil

The following are some of the more commonly applied methods (Nelson and Miller, 1992) for incorporating lime into the soil.

Mixed in place and recompacted One method of lime application is to mix it mechanically with either a disc harrow or a small ripper. With this method it is difficult to mix deeper than about 30 cm. A second method has also been used to mix to a depth of 45 cm. A root plough can be used on the back of a bulldozer to cut the entire thickness once.

Drill-hole lime The drill-hole technique consists of introducing quicklime or hydrated lime in a slurry form into holes drilled for the purpose. Holes of 15–30 cm in diameter are drilled through the pavements to depths of about 75–125 cm depending on the nature or the problem. This method is also useful as a remedial measure in highway stabilization. As a variation of the method trenches of approximately 15 cm wide and 1 m deep can be used.

Pressure-injected lime The pressure-injected lime (PIL) or lime slurry pressure injection (LSPI) technique was developed in an attempt to produce greater lime slurry

penetration in the drill-hole method. In this method lime slurry is pumped through hollow injection rods at pressures at an interval of about 30 cm. Slurry is injected until either the soil will not take additional slurry, or until injection begins to fracture or distort the surface.

Deep mixing Deep mixing method may be classified into two categories, namely: mechanical mixing and slurry mixing.

Dry jet mixing In this method the cement powder or quicklime is injected into the deep ground through a nozzle pipe with the aid of compressed air and then the powder is mixed mechanically by rotating wings (Figure 29.2). In this method no water is added to the ground and hence much higher improvement is expected than using slurry.

Jet grouting mixing Another improvement is the wet jet mixing method or slurry jet grouting method in which lime/cement is jetted into the clay by a pressure of 20 MPa from a rotating nozzle (Figure 29.3).

Lime piles and columns In certain cases lime piles offer an effective and inexpensive method of compacting saturated soils. One of the reasons for this is the large density difference between oxide (CaO) and hydrate ($Ca(OH)_2$) (i.e. 3.3 as opposed to 2.2) which gives rise to a considerable expansion on hydration. This, in turn leads to lateral consolidation of the soil around the lime piles.

Lime piles can be installed in saturated soils by means of a special metal tube with a closed tip (from 250 to 500 mm in diameter), holes being driven to depths of 5–8 m and spread at 1.5–2.5 m centers. Then the tube is withdrawn from the soil and the hole is filled

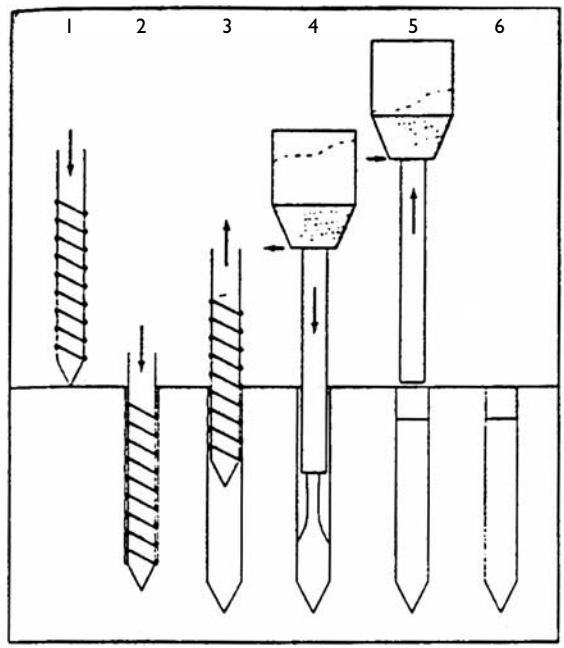

Figure 29.2 Installation of lime/cement column by DJM method.
Source: Kitsugi and Azakami, 1982.

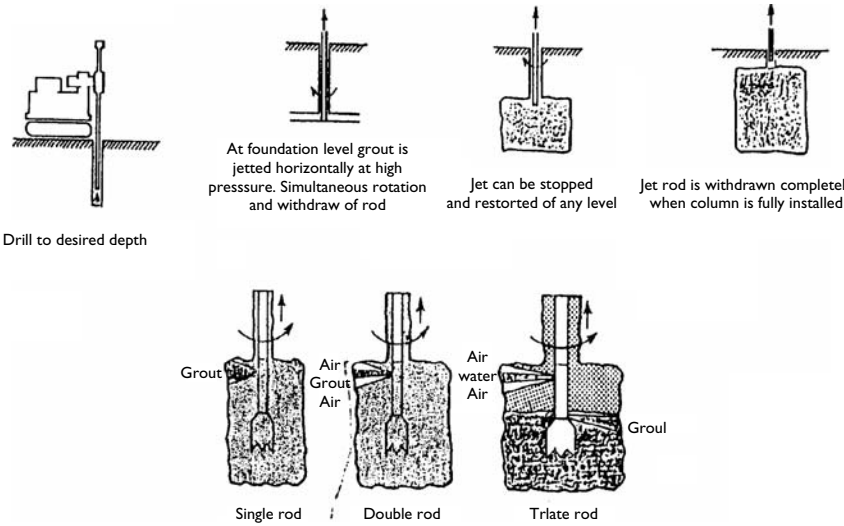

Figure 29.3 Jet grouting system.
Source: After Bergado *et al.* (1996).

with lumps of quicklime. Casing is used if the walls of the hole are unstable. It is extracted as the quicklime is placed. Finally the quicklime is packed by tamping. The process of forming quicklime piles is shown in Figure 29.4.

On contact with groundwater, the quicklime gradually slakes which means, as noted earlier, that the diameter of the pile may expand from 30% to 70% of its original size. Furthermore, a large amount of heat is released as quicklime slakes and this results in evaporation of some of the pore water in the surrounding soil. It also assists flow of water to the pile. In addition, lime penetrates the soil, thereby effecting its stabilization. Lime piles also have been used prior to excavation to increase the strength of cohesive soils, which have permeability above 10^{-7} m/sec and moisture contents of 50% or over.

Yet another application is around structures supported by piles where the lime columns can reduce the negative skin friction and the lateral displacement of the piles due to creep of the surrounding soil. More specifically, where highway cutting are to be constructed through thick soil horizons, the soil is initially piled below the design depth of the cutting. In this way the cutting is produced with a stable floor and sides. Similarly, lime piles can be used to control landslips in thick clay soils.

Lime drains can be installed in situ by means of a tool reminiscent of a giant "eggbeater." The mast and the rotary table are usually mounted on a front wheel-loader. A container is attached to the loader to store the unslaked lime. It takes about 10 minutes to install a drain to a depth of 10 m. The tool is screwed into the soil to the required depth of the drain. The rotation then is reversed and unslaked lime is forced into the soil, by compressed air, through openings placed just above the blades of the mixing tool. The amount of lime used approximates to 5%–8% of the dry weight of the soil. When the tool is extracted, the retrieval rate

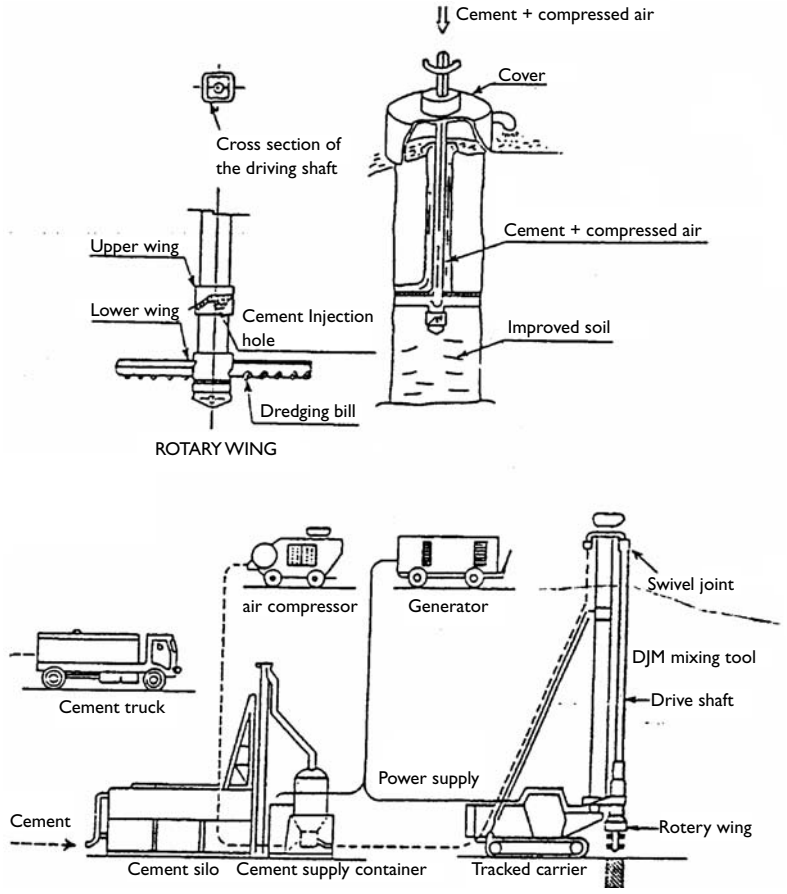

Figure 29.4 Procedure for construction of lime piles.
Source: After Bergado *et al.* (1996).

is about one-tenth of the rate at which it is screwed into the soil, so that the lime can be thoroughly mixed with the soil. This is important since the rate of diffusion of calcium ions in most cohesive soils is low. These lime columns bring about drainage of the soil and compare favorably with sand drains due to their large surface area; they have a diameter of about 0.5 m. The drainage effect of one lime column was equivalent to that of two or three 100 mm wide band drains or three 150 mm diameter sand drains.

Furthermore, lime columns have been used instead of piles as foundations for light structures. The bearing capacity of a 0.5 m diameter lime column varies normally between 50 and 500 kN depending on the soil type and the amount of lime added. The columns reduce total and differential settlements and may be placed in a square pattern with a

concentration beneath the loaded walls. The load of the structure can be distributed to the lime columns by way of a thin concrete slab (e.g. if the number of columns is large the slab need only be about 80 mm thick). In the case of light structures the amount of settlement which occurs usually is a more significant factor than the shear strength of the soil.

The final amount of settlement undergone by soil treated with lime columns generally is calculated by assuming that the stiffness of the foundation corresponds to the sum of the stiffness of the lime columns and of the unstabilized soil between the columns. It therefore is further assumed that the deformation of the lime columns will be the same as that of the unstabilized soil between the columns. The calculation of the time-settlement relationships is usually based on the assumption that the lime columns function as vertical drains in the soil and that drainage takes place horizontally.

Lime columns also have been used to increase the bearing capacity and to reduce the settlement of soft or very soft soils beneath fills or embankments.

Applications of lime stabilized expansive soils

Lime treatment of expansive spoils is used for a variety of engineering applications (Bell, 1988) such as sub-grade and sub-base stabilization, drying of soil, stabilization of embankments and canal linings, foundation soil improvement, and compaction of saturated soil. However, one has to be cautious when using lime to stabilize soils containing sulphate or organic matter. It is known to adversely affect the strength of soil in the presence of sulphate and cause heaving (Sivapullaiah *et al.*, 2000; Puppala *et al.*, 2004). Figure 29.5 shows the effect of presence of 1% sodium sulphate on the stress strain curves of Indian black cotton soil treated with 6% lime after different periods. It can be seen that the strength of lime treated soil decreases with curing period and the strength after curing for one year is less than that of soil without curing period. This has been attributed to formation of swelling type ettringite compounds. Expansive soil stabilized with 7% by weight of expansive soil has been recommended for as liner to resist the effects of chemical attack by Broderick and Daniel (1990).

Fly ash

Fly ash has also been added as an admixture for stabilization of soils. Many studies are conducted on the effect of fly ash with and without lime on the compaction and strength of soils. It is generally known that addition of fly ash or fly ash lime mixture decreases maximum dry density and increases optimum water content. Self-pozzolanic fly ashes without lime and pozzolanic fly ashes with lime can be used to increase pozzolanic reaction in soils. It was suggested that the maximum compressive strength can be obtained when lime–fly ash mixture is used in the ratio of 1 : 2. More rational approaches are now developed to use the lime content of the lime–fly ash mixtures. Attempts are made to find an optimum amount of the fly ash–lime mixture for stabilizing various types of soils for maximum strength. Fly ash is used to control the volume change in expansive soil and reduce the water softening effect on the strength of expansive soils. Many factors such as type of fly ash, particle sizes, influence the strength of expansive soil stabilized with fly ash. It was shown that for reactive fly ashes at a given lime content there will be an optimum fly ash content for maximum strength at lower fly ash contents. However, at higher fly ash contents, as the percentage of fly ash increases, the strength increases. Addition of nonreactive fly ash decreases the strength of expansive soils (Sridharan *et al.*, 1997).

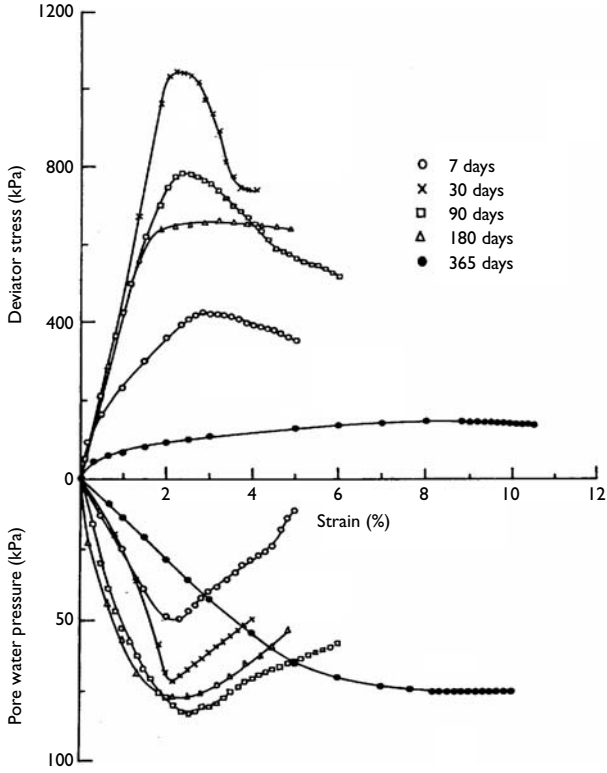

Figure 29.5 Effect of 1% sodium sulphate on the strength of lime stabilised Indian black cotton soil at different curing periods at a confining pressure of 100 kPa.

Rice husk ash

Rice husk ash (RHA) generated by burning rice husks at a temperature of about 450°C, contains amorphous silica which is not a good primary stabilizer but is a good secondary stabilizer in combination with lime or cement. Lazarov and Moh (1970) reported a reduction in the plasticity and maximum dry density of clayey soil with the addition of RHA along with lime. The effectiveness varies with the ratio of lime and RHA. It is generally found that 6% of lime or 10% of cement is adequate for stabilization of RHA with lime.

Use of lime to reduce heave induced by alkali contamination

The solutions used for remedial treatment to control alkali-induced heave include neutralizing with 5% ferric chloride, aluminium sulphate, calcium chloride, and magnesium chloride. The neutralization is reported to be partially successful. A better understanding of soil alkali

reactions has helped in the application of new types of treatments. The soil alkali reactions are specific to the type of hydroxide solution. Thus the hydroxide of calcium (lime) produces different types of compounds, which bind the soil particles, increasing the strength of soil and reducing the volume changes. It is also established that the effect of lime in binding soil particles increases in the presence of alkali due to enhanced chemical reactions such as formation of more cementing agents and different types of compounds (Davidson *et al.,* 1960). Improved methods of application of lime solution as grout mixture at any depth are available (James Warner, 2004). Hence to control the heaving in soils in the presence of alkali solution, calcium chloride, which will form calcium hydroxide, treatment can be an effective measure. Studies conducted on the effectiveness of treating alkali-contaminated soil with calcium chloride to control heave have been elaborated.

Recent studies have shown that swelling can occur even in non-swelling soils due to intense chemical reactions between the soil and alkali, producing mineralogical changes and formation of new compounds (Sivapullaiah and Manju, 2005). Also in some cases it is known to cause a reduction in the shear strength of soil (Sinha *et al.*, 2003). The compounds formed and the volume change behavior depend on the type and amount of clay mineral, alkali concentration, and duration of interaction between the soil and the alkali. Caustic solutions of various concentrations are being used by several industries such as paint and dyes, pulp and paper industries, cotton mills, and aluminium industries. Contamination of soils can occur due to leakage of these solutions from the plant units, infiltration from liquid waste storage facilities, and surface/subsurface disposal of untreated liquid waste from these industries.

Alkalies can trigger changes in charges on clay particles and consequent micro structural changes of soils at lower concentrations (Jozefaciuk, 2002; Jozefaciuk and Bowanko, 2002) and lead to reactions causing mineralogical changes in montmorillonitic soils. One-dimensional consolidation tests were conducted to understand the volume change behavior of expansive soil containing an interstratified clay mineral of montmorillonite and illite (Figure 29.6), with a high concentration caustic solution (4 N NaOH), exhibited an interesting phenomena as shown in Figure 29.7. The specimens compacted to Proctor's density at optimum moisture content in consolidation rings were mounted on to consolidation cells by initially mixing with either water or caustic solution and inundating the consolidation cells with water and caustic solution. From the figure, it can be noticed that specimen mixed with water and inundated with caustic solution as well as specimen mixed with caustic solution and inundated with caustic solution exhibited a steep rebound (swelling) at surcharge lower than 200 kPa and reaching the same initial void ratio as that of soil alone compacted with water at nominal surcharge of 6.25 kPa. The mineralogical changes indicated the formation of new mineral/compounds due to interaction of soil with high concentration caustic solution (Figure 29.8) . These compounds are known to cause swelling in soils. Also the cementation bonds in the soil might have been broken due to leaching.

The efficiency of lime to control the heaving in alkali contaminated soil has been studied. Calcium chloride has been used since calcium chloride can react with hydroxide to form calcium hydroxide by the reaction:

$$CaCl_2 + NaOH \rightarrow Ca(OH)_2 + 2NaCl$$

Calcium hydroxide is known to react with soil better in the presence of sodium chloride. To study this effect consolidation tests were conducted on three specimens compacted by

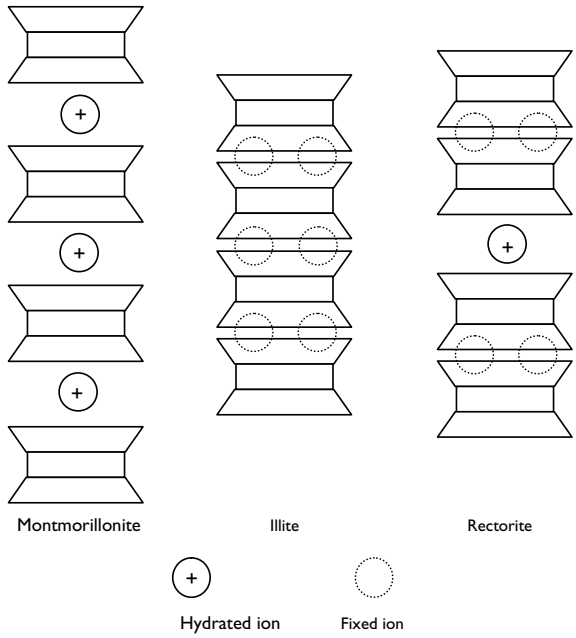

Figure 29.6 Structure of rectorite.

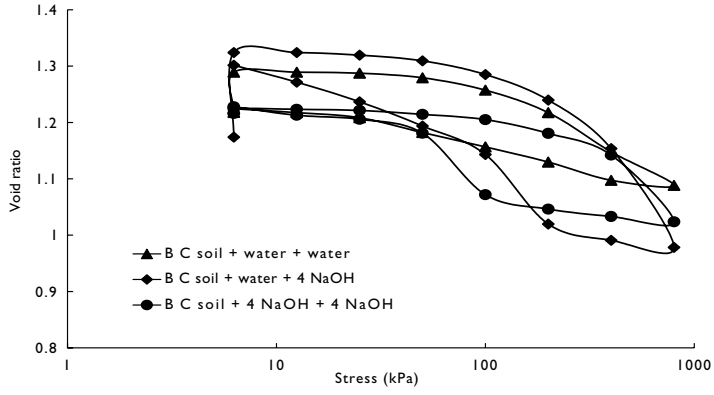

Figure 29.7 Volume change behavior of Indian black cotton soil as affected by alkali contamination.

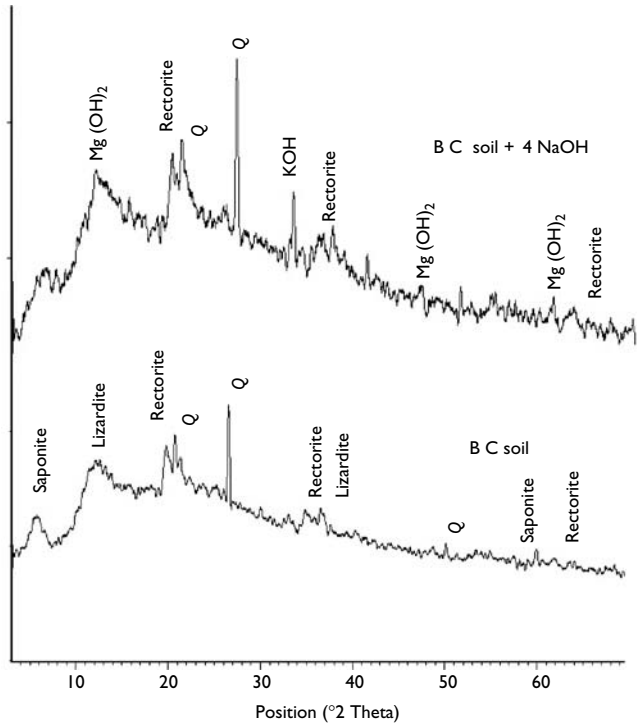

Figure 29.8 X-ray diffraction patterns indicating mineralogical changes due to interaction with alkali in an expansive soil.

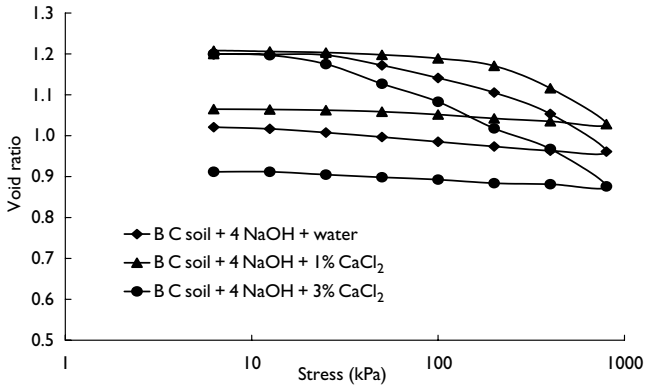

Figure 29.9 Volume change behavior of alkali contaminated black cotton soil as stabilized with calcium chloride.

mixing with 4 N caustic solution and inundated with water, 1% and 3% $CaCl_2$ solutions (10 g and 30 g of calcium chloride in 1 l of water) respectively. From the Figure 29.9 it can be noticed that the specimens did not exhibit abnormal heaving during unloading. The 1% calcium chloride solution is adequate to control the heave induced by caustic solutions.

Conclusions

Pozzolanic agents such as lime and fly ash are effective in controlling swelling in expansive soils induced by moisture content variation. The pozzolanic reaction compounds formed bind the soil particles strongly therefore resisting the internal swelling pressure of the clay. Calcium based stabilization is very effective in the presence of alkali solution and has been successfully applied to control alkali-induced heave in expansive soil.

References

Bell, F.G. (1988) "Stabilization and treatment of clay soils with lime," *Ground Engineering*, 21, 10–15, 25–29.

Broderick, G. and Daniel, D.E. (1990) "Stabilizing compacted clay against chemical attack," *Journal of Geotechnical Engineering*, *ASCE*, 116, 1549–1567.

Chapman, I. (1913) "A contribution to the theory of electrocapillarity," *Philosophical Magazine, Series* 6, 25 (148), 475–481.

Davidson, D.T. and Barnes, H.F. (1960) "Improvement of lime stabilization of montmorillonite clay soils with chemical additives," *Highway Research Board Bulletin*, 262: 33–50.

Gouy, G. (1910) "Sur la constitution de la charge électrique a la surface d'un électrolyte," *Journal de Physique Théorique et Appliquée, Series* 4, 9, 457–468 (in French).

James Warner, P.E. (2004) *Practical Handbook of Grouting, Soil, Rock and Structures*, John Wiley & Sons, Inc., New York.

Jozefaciuk, G. (2002) "Effect of acid and alkali treatments on surface – charge properties of selected minerals," *Clays and Clay Minerals*, 50, 647–656.

Jozefaciuk, G. and Bowanki, G. (2002) "Effect of acid and alkali treatments on surface areas and adsorption energies of selected minerals," *Clays and Clay minerals*, 50, 771–783.

Lal, R. and Shukla, M.K. (2004) *Principles of Soil Physics*, Maracel Decker Inc., New York.

Lazarov, R.C. and Moh, C. (1970) "Stabilisation of deltaic clays with lime and rice husk ash as admixtures," *Proceedings II South East Asian Conference on Soil Engineering*, Singapore, 215–225.

Narasimha Rao, S. and Rajasekaran, G. (1996) "Reaction products formed in lime-stabilized marine clays," *ASCE Journal of Geotechnical Engineering*, 122 (5), 329–336.

Nelson, J.D., and Miller, D.J. (1992) *Treatment of Expansive Soils Problem and Practice in Foundation and Pavement*, John Wiley & Sons, Inc., New York.

Puppala A.J., Griffin J. A., Hoyos L.R., and Chomtid. S. (2004). "Studies on sulfate-resistant cement stabilization methods to address sulfate-induced Soil Heave," *Journal of Geotechnical and Geoenvironmental Engineering*, *ASCE,* 130 (4), 391–402.

Sinha, U.N., Sharma, A.K., Bhargava, S.N., Minocha, A.K., and Pradeep Kumar (2003). "Effect of seepage of caustic soda on foundation and remedial measure in alumina plant," *Indian Geotechnical Conference*, 1, Roorkee, India, 229–234.

Sivapullaiah, P.V. and Manju. (2005) "Kaolinite – alkali interactions and effects on Basic properties," *Geotechnical and Geological Engineering*, 23, Kluwer academic publishers, Netherlands, 601–614.

Sivapullaiah, P.V., Sridharan, A., and Prashanth, J.P. (1995) "Optimization of lime content of fly ash," *ASTM Journal of Testing and Evaluation*, 23, 222–227.

Sivapullaiah, P.V., Prashanth, J.P., and Sridharan, A. (1998a) "Delay in compaction and importance of lime fixation point on strength and compaction characteristics of soil," *Ground Improvement*, 2, 27–32.

Sivapullaiah, P.V., Prashanth, J.P., Sridharan, A. and Narayana, B.V. (1998b) "Reactive silica and strength of fly ashes," *Geotechnical and Geological Engineering*, 16, 239–250.
Sivapullaiah, P.V., Sridharan, A., and Ramesh, H.N. (2000) "Strength behaviour of lime treated soils in the presence of sulphate," *Canadian Geotechnical Journal*, 37, 1358–1567.
Sivapullaiah, P.V., Subba Rao, K.S., and Gurumurthy, J.V. (2004) "Stabilisation of rice husk ash for use as cushion below foundations on expansive soils," *Ground Improvement*, 7, 137–149.
Sridharan, A., Prashanth, J.P., and Sivapullaiah, P.V. (1997) "Effect of fly ash on the unconfined strength of black cotton soil," *Ground Improvement*, 1, 169–175.
Stockmeyer, M.R. (1991) "Adsorption of organic compounds on organophilic bentonites," *Applied Clay Science*, 6, 39–57.

Chapter 30

Swelling characteristics and improvement of expansive soil with rice husk ash

Agus Setyo Muntohar[1]

Summary

The study presented in this chapter was aimed at providing further understanding and guidance on the use of rice husk ash as a soil stabilizer in particular for expansive soils. Results from two different locations were presented, one from Kuala Lumpur, Malaysia and the other from Yogyakarta, Indonesia.

Introduction

The engineering properties of the swelling soils may be improved to make them more suitable for construction. Recent projects illustrate that successful waste utilization can result in considerable savings in construction costs (Kamon and Nontananandh, 1990; Edil and Benson, 1998). Utilization of lime, cement, and fly ash, for example, is widely used as a means of chemically transforming unstable soils into structurally sound construction foundations. In clay-bearing soils, these stabilizers induce a textural change resulting in a greater ease of compaction and handling as well as a moderate improvement in strength.

Rice husks are a major agricultural by-product in tropical countries, such as Indonesia, Thailand, Philippines, and Brazil. It is generally considered as valueless (Figure 30.1). In Indonesia, Muntohar (2002) stated that around 50 million tons were produced annualy in the last 5 years. The amount of rice husk is 12.5 million tons; the ash produced is approximately 4 million tons.

Incineration, resulting in ashes, is a common way to eliminate the problem. Chemical analyses have shown that the rice husk ash (RHA) has a high reactive pozzolanic material. RHA contains a high amount of silica dioxide suitable for use in lime pozzolana mixes and for Portland cement replacement (Jauberthie *et al*., 2000; Payá *et al*., 2001). However, the contribution of RHA to these engineering application needs further investigation. The utilization of RHA in geotechnical application has not been readily accepted due to the low level of confidence in its effectiveness among geotechnical engineers. For this reason, there is a need to fill the gap currently hindering the full potential of this underutilized waste product.

The study presented in this chapter is aimed at providing further understanding and guidance on the use of RHA as a soil stabilizer in particular for expansive soils. Results

[1] Department of Civil Engineering, Muhammadiyah University of Yogyakarta Building F1, 3rd Floor. Jl. Ringroad Selatan, Taman Tirto, Yogyakarta, Indonesia 55183; email: muntohar@umy.ac.id

Figure 30.1 Rice husk ashes disposal of rice milling in Kuala Selangor, Malaysia.

from two different locations are presented, one from Kuala Lumpur, Malaysia and the other from Yogyakarta, Indonesia.

Literature review

Lime stabilization has been extensively applied to expansive clay soils (Boardman, *et al*., 2001). This stabilization results from base exchange and cementation processes between clay particles and lime. Lime stabilization is particularly important in road construction for modifying subgrade soils, subbase, and base materials. Lime modifies and immediately improves workability, placeability, compactability of soils, and effectively shrinks the construction (ICI, 1986). The initial modification reaction occurs as a result of cation exchange of calcium ions (Ca^{2+}). The result of cation exchange is increasing flocculation of clay particles and changes in the plasticity properties of clay (Boardman *et al*., 2001). The cementation process develops from the reaction between calcium present in lime and silica and alumina in the soil, forming calcium-silicate hydrate (CSH) and calcium-aluminate (CAH) or calcium-aluminate-silicate. The cementitious compounds produced are characterized by their high strength and low-volume change.

Various results were found by previous researchers concerning uses of blended RHA with lime or cement. Lazaro and Moh (1970) showed that the addition of RHA in combination with lime to both Thai and Philippine soils did not produce any significant increase in strength as compared to the use of lime alone. Whereas, Ali *et al*. (1992) found that by adding RHA, both lime-stabilized and cement-stabilized residual soils from Malaysia were enhanced in strength and durability. Balasubramaniam *et al*. (1999) and Muntohar and Hantoro (2000) showed that addition of RHA to lime-stabilized soils resulted in ductile behavior associated with high strain and low strength.

Stabilization of soil-mixtures: case study from Malaysia

In order to minimize variations in the test data due to the variability of soil samples and to facilitate a representative study of a large number of soils, it was decided to conduct tests on

samples artificially prepared in the laboratory. The expansive soil used in this study was prepared using kaolin and bentonite mixtures. This expansive clay was engineered for controlling the variability of soil composition and properties. Studies have shown that a mixture composed of 10% bentonite and 90% kaolin behaves as an expansive soil. This soil was designated as KB (Table 30.1). The grain size distributions of the soils needed in the study are presented in Figure 30.2.

Table 30.1 Properties of soil used

Soils description	*Sand (%)*	*Silt (%)*	*Clay (%)*	*D_{50} (μm)*	*Liquid limit (%)*	*Plastic limit (%)*	*Linear shrinkage*	*Activity, PI/CF*
Bentonite[a]	5.4	2.4	73.2	0.62	307.3	45.4	17.4	3.6
Kaolin	4.3	75.6	19.9	4.1	72.3	39.8	6.6	1.6
Sand[b]	71.5	4.0	0.0	820	NP	—	—	—
KB	6.6	30	63.4	3.7	89.7	42.2	12.3	0.75

Notes
a Wyoming bentonite, b Mining sand (24.5% gravel), NP = non-plastic, PI = plasticity index, CF = clay fraction.

Table 30.2 Chemical composition (XRF Test) of additives used

Chemical constituents	*Lime*	*RHA*
Silica (SiO_2)	0.07	86.71–8.82
Alumina (Al_2O_3)	0.18	0.33–0.46
Iron oxide (Fe_2O_3)	0.12	0.67–1.78
Calcium oxide (CaO)	67.46	0.58–0.67
Potassium oxide (K_2O)	0.01	2.90–2.91
Magnesium oxide (MgO)	0.18	0.44
Sodium oxide (Na_2O)	0.19	0.12–0.27
Other oxides	0.06	1.10–1.11
Loss on ignition	31.73	4.81–5.88

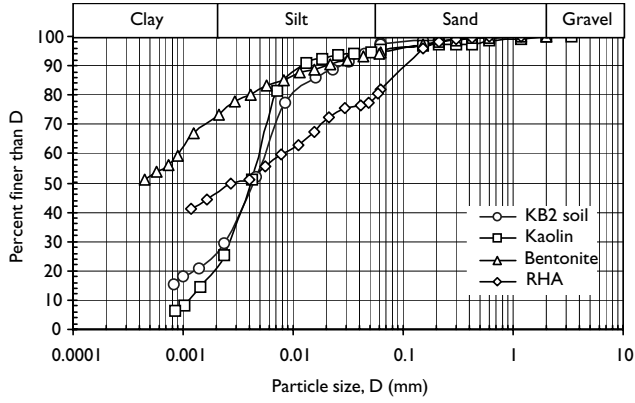

Figure 30.2 Grain size distribution curves of soil used and RHA.

Hydrated lime was used in this research. To reduce the carbonation effect, the lime was stored in an airtight container. RHA was obtained by burning the husks in an incinerator. The husks were collected from rice mill disposals in Kuala Selangor, Malaysia. The chemical compositions of the two additive materials are presented in Table 30.2.

Sample preparation for swelling tests

A conventional oedometer apparatus was used for the determination of the swelling and compressibility of soil mixtures. Required quantities of soil mixtures, at optimum moisture content, were transferred to a consolidation ring of 50 mm internal diameter and 20 mm height. All the soil mixtures were compacted statically to their maximum dry density and optimum moisture content. The calculated amount of soil was placed into a cylindrical mould and then compressed using a hydraulic jack (Figure 30.3).

Results and analysis

Effect of stabilization on consistency limits

Chemically, while RHA is lacking in cementitious materials, it does contain pozzolanics. The uses for soil stabilization alone would not yield a worthy improvement (Hossain, 1986). The effect of RHA addition on the consistency limit of lime-stabilized soil is presented in Figure 30.4. The plasticity index is reduced with addition of RHA (Figure 30.4c). Reduction of this index is an indicator of improvement which can be correlated with an increase in the strength and a reduction in swelling and compressibility.

RHA-treated soil significantly reduced the plasticity index because of a diminishing of the liquid limit. The liquid limit and plastic limit of lime-stabilized soil increased in conjunction with the addition of RHA as shown in Figures 30.4a and 30.4b respectively. The plastic limit increased steeply; concomitantly it reduced the plasticity index. Soil-lime-RHA mixtures are

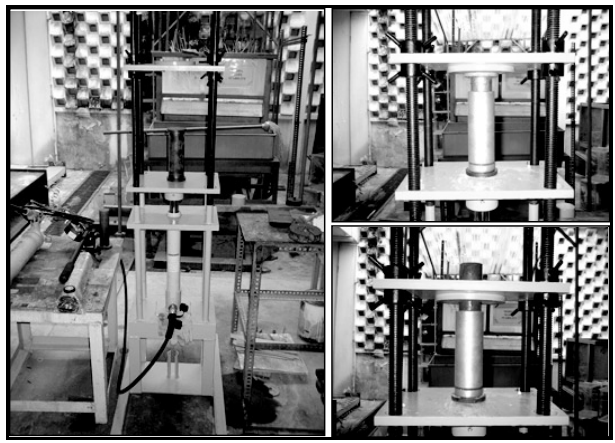

Figure 30.3 Static compaction equipment for preparation of swelling specimens.

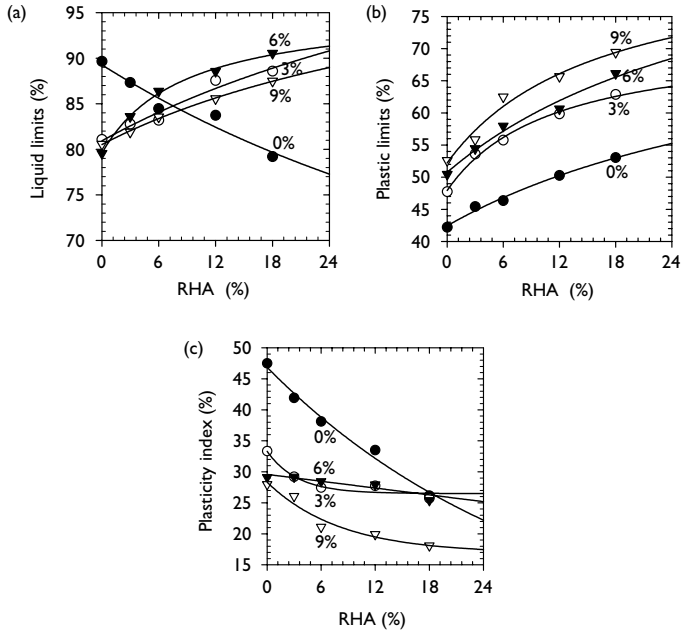

Figure 30.4 Effect of RHA addition on consistency limit of lime-stabilized expansive soil.

Note
Numbers in percents are referring to percentage of lime content.

recognized to favor the cementitious reaction to form cementing agents that coat and bind the clay to make coarser particles. These coarser particles would lead to a random/flocculated arrangement and alter the plasticity (Figure 30.5).

For treated-clay soil possessing montmorillonite clay mineral, a contributor to the liquid limit, water content arises from the water entrapped in the large void spaces of the flocculated soil fabric (Prakash *et al*., 1989). This explains the increase in the liquid limit. Stiffening (i.e. self-hardening) of lime-RHA treated soil requires more moisture to convey workability (i.e. to enable rolling to a 3 mm thread). Hence the plastic limit increases in conjunction with addition of lime and RHA. The overall effect is a diminishing of the plasticity index.

Effect of stabilization on swelling characteristics

The effect of addition of lime and RHA to expansive soils is shown in Figure 30.6. The swell is measured for 10 days of inundation after 1-day moist cured under a seating pressure. Then the swelling pressure is determined by increasing the load retrieve to the initial height of the specimen. The results show a decreasing of swelling and swelling pressure corresponding to the addition of lime.

When lime is added to a clay soil, it has an immediate effect on the properties of the soil. Cation exchange begins to take place between the ions associated with the surfaces of the

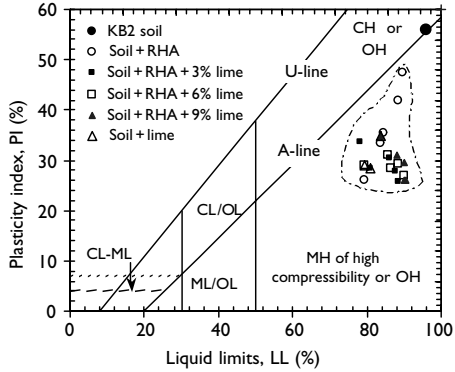

Figure 30.5 Plasticity chart of stabilized expansive soil.

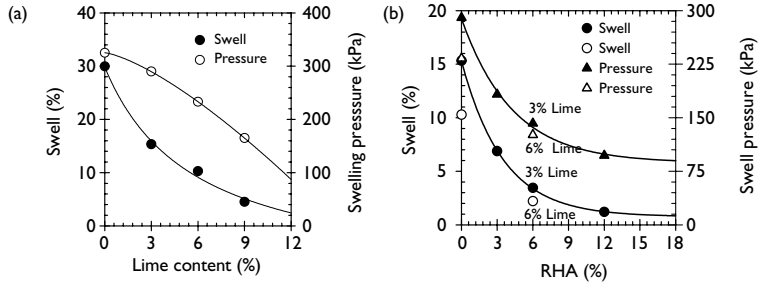

Figure 30.6 Effect of lime and RHA on the swelling and swelling pressure of stabilized soil.

clay particles and the calcium ions of the lime. Clay particles are surrounded by a diffuse hydrous double layer, which is modified by the ion exchange of calcium. This alters the density of the electrical charge around the clay particles, which leads to them being attracted closer to each other to form flocs. It is a process which is responsible for the loss of plasticity in clay. It reduces the tendency of clay to swell. In addition to cation exchange, reactions occur between the silica and the alumina of the lattices of the clay minerals, especially at the edges of the clay particles. The reaction products contribute to flocculation by bonding adjacent soil particles together and, as curing occurs, they strengthen the soils.

In the range of 6–9% lime-treated soil, cementation is the governing factor, causing formation of clods, which in turn act like coarse sand particles. These clods tend to reduce the permeability of the sample, thereby restricting the tendency of the clay to increase in volume (Bell, 1996; Azam *et al*., 1998). Addition of RHA to 3% lime-treated expansive soils considerably reduces the swelling (Figure 30.6b). This is due to the addition of non-plastic materials and the chemical constituents of the RHA/lime mixtures. These constituents, upon reaction with amorphous silica and clay in the presence of water, add cementitious properties which stabilize against swelling.

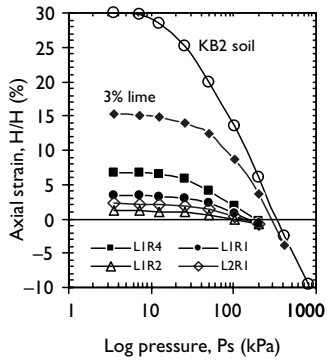

Figure 30.7 Typical of swelling–compressibility of stabilized expansive soils.

Notes
L1R4: 3% lime + 3% RHA, L1R1: 3% lime + 6% RHA, L1R2: 3% lime + 12% RHA, L2R1: 6% lime + 6% RHA.

Addition of RHA will fill in the intervoid of soil particles. This causes a reduction in permeability and compressibility. Concomitantly, the swelling and swelling pressure decrease appreciably. The compressibility, in this research, was performed after the soil had been allowed to cease its swell and then was loaded gradually. The typical swelling and compressibility of stabilized expansive soils with lime and RHA is illustrated in Figure 30.7. These results portray the swollen soils' (unstabilized) steep downward slope compared to stabilized expansive soil. Possibly, the swollen soil imbibed much water causing it to become plastic. Then the soil was easier to compress subject to load. A linear line was observed starting at 50 kPa pressure. Stabilized expansive soils with lime/RHA resulted in a denser soil structure as a result of cementitious reaction. The study (Figure 30.7) illustrated that addition of lime/RHA minimized the compressibility of stabilized expansive soils.

X-ray diffraction (X-RD) and scanning electron microscopy (SEM)

X-ray diffraction is the most widely used method to identify fine-grained soil minerals and to study their crystal structure. In swelling clay minerals, montmorillonite strongly appeared at 15.32 Å in tested soil (Figure 30.8). The presence of the kaolinite mineral was strongly found at 7.16 Å and 3.57 Å. Quartz and illite appeared at 3.35 Å and 3.19 Å, respectively. The montmorillonite peak disappeared at 15.32 Å of basalt spacing (CuKα radiation) when lime and RHA were blended with expansive soil. This was possibly attributed to the chemical reaction between clay mineral and lime-RHA mixtures that altered the mineral to other crystallized structures or reduced their intensities. The kaolinite and quartz minerals remained pronounced, but the intensities were reduced by addition of lime and RHA. The cementitious materials were detected as CSH gel at 3.04 Å and 2.79 Å (CuKα radiation) in both soils tested. Hydrated calcium aluminate silicates ($C_3AS_nH_{n-2}$) appeared strongly at 3.28 Å.

SEM techniques can be conveniently used to identify the formation of new products as a result of lime-induced changes. The SEM images in the current study depicted the different

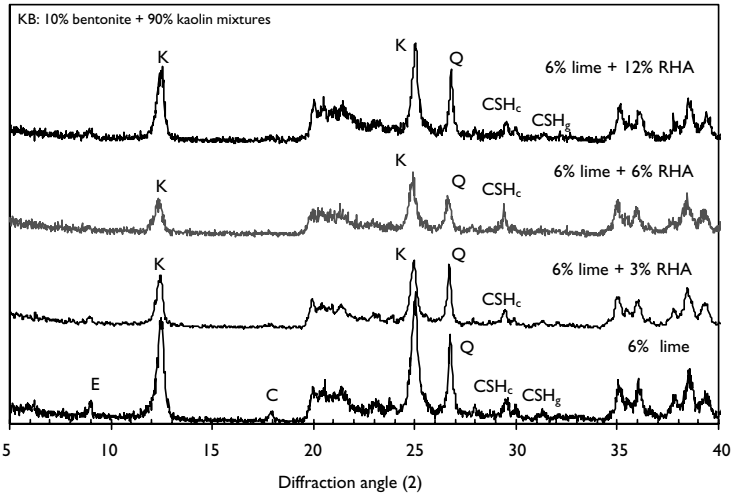

Figure 30.8 X-ray diffraction pattern (CuKα radiation) of stabilized expansive soil.

Notes
I: Illite, K: Kaolinite, M: Montmorillonite, Q: Quartz, E: Ettringite, CSH_g: Calcium silicates hydrate (gel), CSH_c: Calcium silicates hydrate (crystallized), CAS: Calcium aluminate silicates hydrate.

morphology between untreated and treated soils (Figure 30.9). SEM of untreated samples indicated the presence of a mixed layer between kaolinite and bentonite as a less distinct hexagonal plate (Figure 30.9a). Treated soil indicated a flocculated arrangement of soil particles with big floccules (Figure 30.9b). The SEM image of treated soil systems substantiated that the formation of cementation (CSH gel), which is shown as a cloud morphology, filled the pores and played a bridging role between hydrates and unhydrated cementitious particles. Well-crystallized CAS is shown distinctly in Figure 30.9b.

Mixtures design of lime-RHA stabilized expansive soil

Based on research results, we proposed a design chart for lime and RHA (Figure 30.10). The chart presents a mixture design based on the reduction in plasticity index. This parameter is well related to many geotechnical properties such as swelling and strength of soils (Wroth and Wood, 1978). The numbers shown on the chart refer to the ratio between the plasticity index of stabilized soil and unstabilized soil, where unstabilized soil has ratio equal to 1. Use of this chart will assist in the design of a lime-RHA mixture with the desired properties. For example, if the plasticity index needs to be 0.5, then 6% lime and 14% RHA can be mixed, or 10% lime and 6% RHA.

Stabilization of natural soil: case study from Indonesia

Indonesia has a significant amount of its land surface covered by Quaternary soft deposit. These soft deposit materials, which frequently exist in areas where developments have taken place or

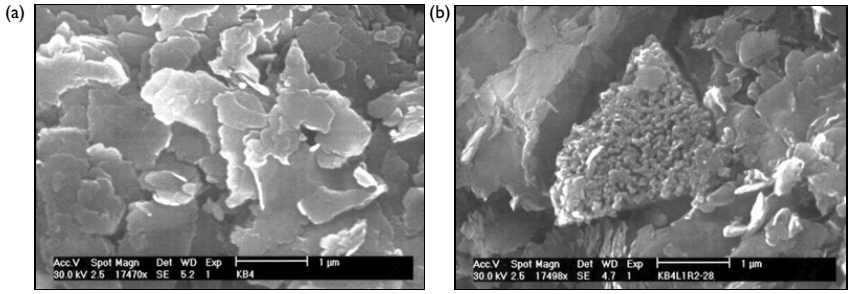

Figure 30.9 Scanning electron microscopy of stabilized soil.

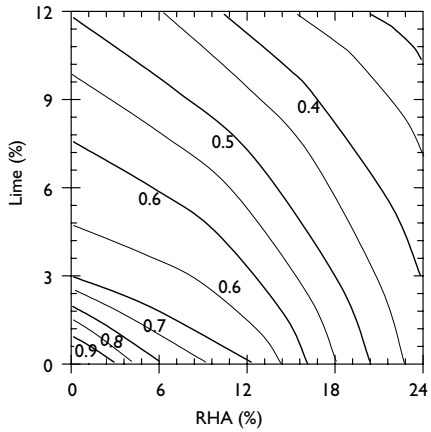

Figure 30.10 Mixtures design chart based on the reduction of plasticity index.

Note
Numbers on the chart are referring to the plasticity index ratio of stabilized to unstabilized soil.

are projected (Figure 30.11), contain many clay mineral. They are often problematic and do not perform satisfactorily (Younger, 1991). The soils have high compressibility, low strength, and potential to highly swell or shrink. Low-bearing capacity and high swelling–shrinkage of subgrade is inconvenient, and frequently has a detrimental impact on highway or roadway work.

Sample preparation and testing

Soil sampling was carried out in excavated pits, in the two locations, to a depth in excess of 0.5 m to expose fresh sample and avoid the influence of vegetation. The first location, Kasihan, contained predominantly silt (soil 1); the other location, Ngramang, contained primarily clay (soil 2). The properties of these soils are given in Table 30.3.

RHA was obtained from the brick stone industry in Godean, Yogyakarta. The fraction used for the test was that passing through an ASTM sieve size #200 (74 μm). The lime used

was hydrated. These additives were mixed with the soil individually or in a combination (by the dry weigh of soil) in which RHA content was varied from 8%, 10%, 12% for soil 1 and 2%, 4% for soil 2. The lime content was varied from 2% and 4%. The chemical constituents of these additives are presented in Table 30.4.

The CBR-laboratory test, unsoaked and four days soaked, was performed on samples compacted at optimum moisture content (OMC) and maximum dry density (MDD) using Standard Proctor energy. For soil 2, a Modified Proctor test was also employed. Each of the lime-RHA treated soils was cured for one day before performing the test. For soil 2, curing times of 3, 7, and 28 days were assessed.

Results and analysis

Table 30.3 describes the index and engineering properties of the original soil (untreated). It can be summarized that the soil samples had different classifications. Figure 30.12 shows that Soil 1 was classified into CL which is primarily silt. Soil 2 was categorized as CH that

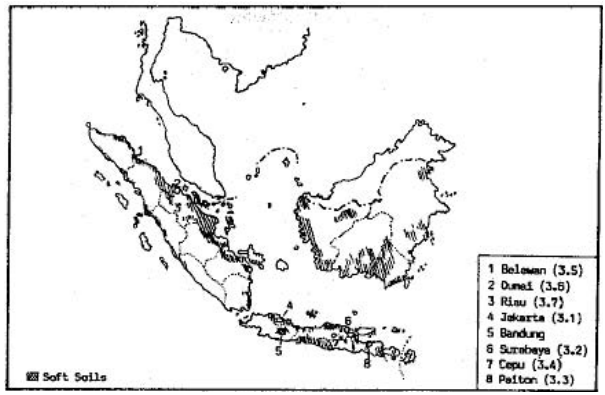

Figure 30.11 Location of major area of the soft soil in Indonesia.

Table 30.3 Properties of soil samples

Properties	*Soil 1*	*Soil 2*
Nature moisture content, w_N (%)	71.48	45.45
Specific gravity, Gs	2.63	2.62
Liquid limits, LL (%)	73.59	81.55
Plasticity index, PI (%)	35.25	58.40
Shrinkage limits, SL (%)	13.82	13.76
Maximum dry density (MDD), γ_d (kN/m^3)	13.20	13.53
Optimum moisture content, OMC (%)	34.00	26.62
Sand (%)	9.24	15.36
Silt (%)	80.76	40.64
Clay (%)	10.00	44.00
CBR unsoaked (%)	3.03	2.44
Activity	3.06	1.46
Color	Black–grey	Black

Table 30.4 Chemical composition of additives

Constituents	*Lime (%)*	*RHA (%)*
SiO_2	0.00	89.08
Al_2O_3	0.13	1.75
Fe_2O_3	0.08	0.78
CaO	59.03	1.29
MgO	0.25	0.64
Na_2O	0.05	0.85
K_2O	0.03	1.38
MnO	0.004	0.14
P_2O_5	0.00	0.61
H_2O	0.04	1.33
Loss of ignition	2.05	40.33

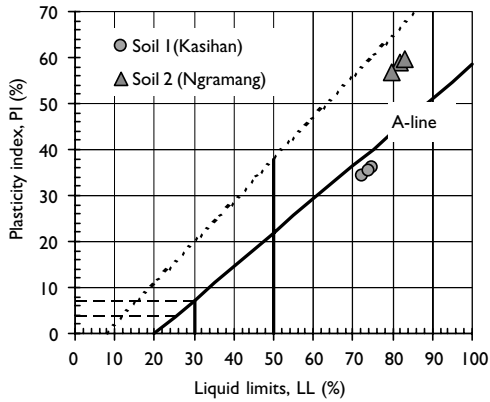

Figure 30.12 Plasticity chart of fine particles.

reveals an expansive soil (Seed *et al*., 1962). These soil samples had low strength and were unsuitable for subgrade.

Compaction

Compaction behavior of each soil is shown in Figure 30.13. It was observed that the MDD of soils decreased on the addition of additives. The OMC of treated soil increased. An exception for soil 1, was the addition of lime and lime-RHA mixture which decreased the OMC. RHA consumed much water to attain the MDD because the materials were very porous (Zhang *et al*., 1996).

In the case of soil 2, the MDD of soil treated with additives could be enhanced by greater compaction. Figure 30.13b shows that compacting the treated clay soil using the Modified Proctor (2700 kNm/m^3) method achieved a higher MDD than by the Standard Proctor.

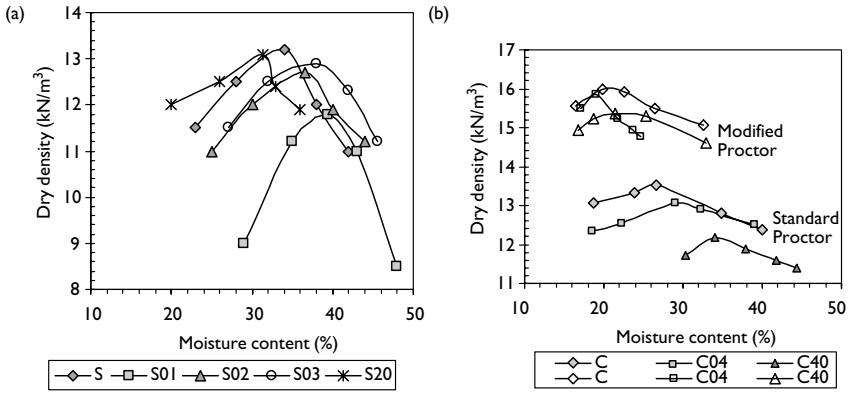

Figure 30.13 Dry density and moisture content relationship for varies admixtures (a) soil 1 and (b) soil 2.

However, it should be considered that dense clay soils will swell more when they become wetted, compared to the same clay soils at a lower density and with the same initial water content (Gromko, 1974). This is particularly advantageous in view of the need for strict density control during placing and subsequent compaction under exposed conditions.

California bearing ratio

California bearing ratio (CBR), values are closely related to both the compressive strength and the bearing capacity of compacted subgrade or fills. Therefore, this test is most appropriate to quantify the suitability of any compacted subgrade or fills (Indraratna, 1994). Stabilized soil with lime and RHA, generally, increased the CBR value for all soils. Lime enhanced the CBR more than RHA. However, when blended, both additives showed acceptable results. The highest CBR of soil 1 was 12%, which was attained at 4% lime and 10% RHA mixtures. In the case of soil 1, silt soil, the maximum CBR value was achieved at 10% RHA. Further addition of RHA in this soil decreased the CBR (Figure 30.14).

Compared to soil 2, the highest value of the unsoaked CBR (i.e. 11%) was attained by mixing 4% lime with 2% RHA and compacting with Standard energy (600 kNm/m^3). Furthermore, compared with Modified, a greater compaction effort gave higher strength (Figure 30.15). The highest of 31% was attained at 2% RHA and 2% lime mixture.

The influence of curing time and soaking on the CBR was also studied, especially for soil 2. The soaked condition simulates the behavior of subgrade under heavy rainfall or flooded situations. Nevertheless, the degree of saturation of the soaked specimen might be substantially higher than that of the subgrade soil under pavement (Chu and Chen, 1976). As illustrated in Figure 30.16, the effect of soaking is reflected by an increased penetration at the same stress levels for soil 2.

Considering the standard 2.5 mm penetration, a reduction in CBR from 2.4% to 0.7% was encountered as a result of four days soaking. This necessitated the requirement for surface water proofing of the road in order to maintain the desirable CBR. Figure 30.17 shows the

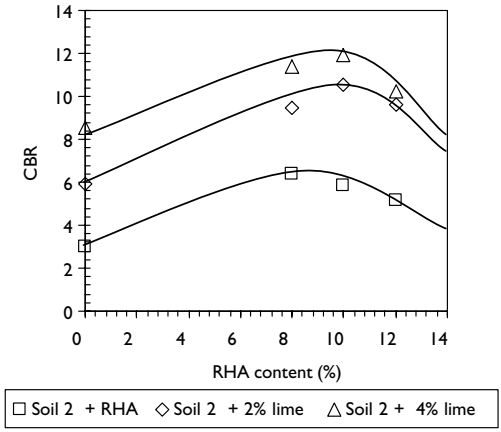

Figure 30.14 Effect of RHA content on the CBR of soil 1.

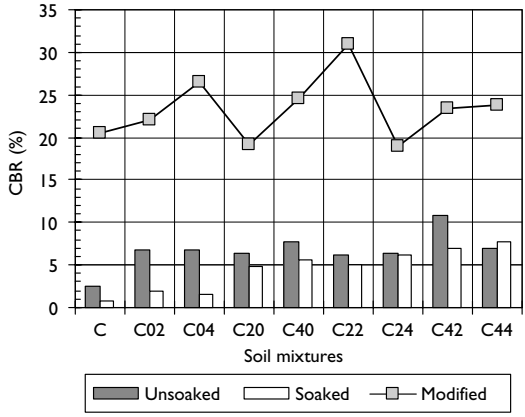

Figure 30.15 CBR values of soil 2 varies with treatment.

influence of curing on the four days soaked CBR of treated soil 2. Curing is important for chemically stabilized soils, particularly lime-stabilized soils, because lime-soil reactions are time and temperature dependent and continue for long periods of time (even years).

Swelling characteristics

The swelling of expansive soil (soil 2) was examined using soaked CBR test. Soil 1 was not assessed with the swell test because the soil did not exhibit potential to swell. In this test

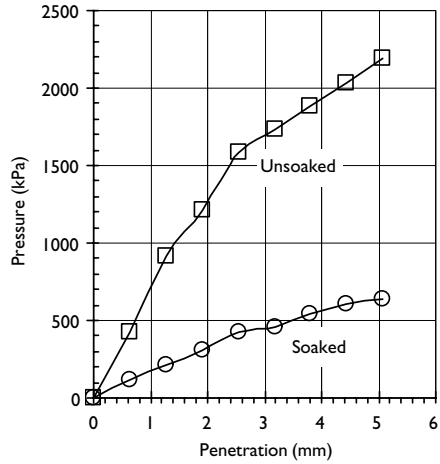

Figure 30.16 Effect of soaking on CBR values of soil 2.

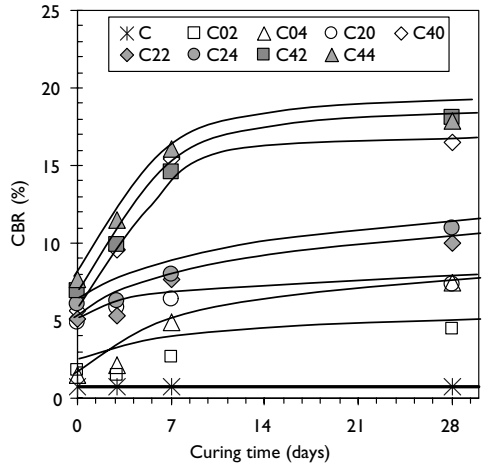

Figure 30.17 Effect of curing time on the four days soaked CBR value.

method, CBR specimens were submerged in water, under a simulated surcharge pressure, for four days prior testing. The swell was measured for each curing time. On the whole, curing diminished the heave of expansive soil (Figure 30.18). In the case of lime and lime-RHA treated soils, three days curing was enough to reduce swelling. RHA stabilized soil, indeed, demonstrated attractive swelling characteristics. Soil mixed with 4% RHA, actually

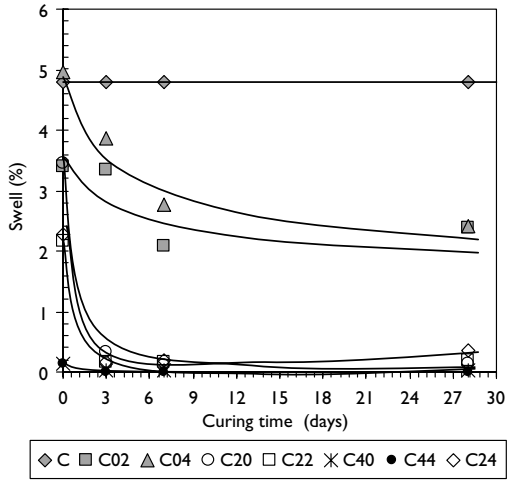

Figure 30.18 Effect of curing on the swelling of stabilized soil 2.

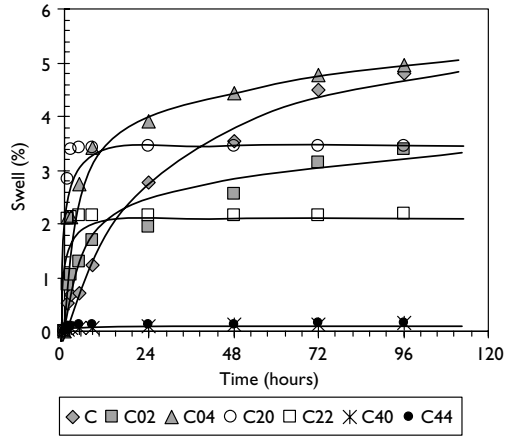

Figure 30.19 Time and swell relationship of stabilized soil 2.

augmented the swelling. In this case, lime was more effective in reducing the heave of soil. Figure 30.19 shows that heaving ceased by 24 hours after soaked. In contrast, with RHA treated soil, swelling only proceeded after the soil was inundated with water, and increased only marginally during four days soaking.

Gromko (1974) pointed out that the value of the swell depends on the same factors that influence the soil volume change: such as mineral type, density, load condition, and water

content. Dry clays will affect swell more than wet clays because of the direct relation between water content and suction pressures. It is important to blend RHA with lime, because that the former material cannot react solely with soil A cementatious material such as lime is required.

Conclusions

Addition of RHA decreased the plasticity of expansive soil as a result of a reduction in the liquid limit and an increase in the plastic limit. Addition of RHA significantly reduced the plasticity index, whereas as much as 80% of the reduction was achieved by addition of RHA in greater lime content. It was noticed that 6% lime addition was enough to improve the consistency limits of expansive soils. The swelling and swelling pressure of expansive soils decreased with the addition of lime and RHA. The swelling of expansive soil was almost zero when 6% lime and 6% RHA were used. Cementitious materials such as CSH gel and CAS were detected in lime-RHA treated expansive soil indicating that a pozzolanic reaction had taken place in the stabilized soil. The desired mixture between lime and RHA can be chosen by using a chart. This chart is useful as for preliminary mixture design in stabilizing an expansive soil. Finally, lime and RHA when added to soil in adequate amounts, have a beneficial effect on the soil strength. They have the potential to significantly increase the soil strength (CBR) and to decrease the swell in a relatively short time.

References

Ali, F.H., Adnan, A., and Choy, C.K. (1992), "Geotechnical properties of a chemically stabilised soil from Malaysia with rice husk ash as an additive," *Geotechnical and Geological Engineering,* 10, 117–134.

Azam, S., Abduljauwad, S.N., Al-Shayea, N.A., and Baghabra Al-Moudi, O.S. (1998), "Expansive characteristics of gypsiferous/anhydritics soil formations," *Engineering Geology*, 51, 89–107.

Balasubramaniam A.S., Lin D.G., Acharya S.S.S., and Kamruzzaman, A.H.M. (1999), "Behaviour of soft Bangkok clay treated with additives," *Proceedings of 11th Asian Regional Conference on Soil Mechanics and Geotechnical Engineering*, Seoul, 11–14.

Bell, F.G. (1996), "Lime stabilization of clay minerals and soils," *Engineering Geology*, 42, 223–237.

Boardman, D.I., Glendinning, S., and Rogers, C.D.F. (2001), "Development of stabilisation and solidification in lime–clay mixes," *Géotechnique*, 50 (6), 533–543.

Chu, T.Y. and Chen, S.N. (1976), "Laboratory preparation of specimen for simulating field moisture content conditions of partially saturated soils," *Soil Specimen Preparation for Laboratory Testing*, ASTM STP 599: 229–247, American Society for Testing and Materials, Philadelphia, PA.

Edil, T.B. and Benson, C.H. (1998), "Geotechnics of industrial by-products," in Vipulanandan, C. and Elton, D.J. (eds), *Recycled Materials in Geotechnical Applications*, ASCE, Geotechnical Special Publication No.79, ASCE Press, USA, pp. 1–18.

Gromko, G.J. (1974), "Review of expansive soils," *Journal of Geotecnical Engineering Division, ASCE*, 100 (6), 667–687.

Hossain, A.S.M.M (1986), *Cement and Cement-Rice Husk Ash Stabilization of Selected Local Alluvial Soils*, MS Thesis, Department of Civil Engineering, Bangladesh University of Engineering and Technology, Dhaka.

ICI (1986), *Lime stabilisation manual*, Imperial Lime Chemical Business Industries PLC, Derbyshire, UK.

Indraratna, B. (1994), "Geotechnical characterisation of blended coal tailings for construction and rehabilitation work," *Quarterly Journal of Engineering Geology*, 27, 353–361.

Jauberthie, R., Rendell, F., Tamba, S., and Cisse, I. (2000), "Origin of the pozzolanic effect of rice husks," *Constraction and Building Material*, 14, 419–423.

Kamon, M., and Nontananandh, S. (1990), "Combining industrial wastes with lime for soil stabilisation," *Journal of Geotechnical Engineering*, 117 (1), pp. 1–17.

Lazarov, R.C. and Moh, Z.C. (1970), "Stabilisation of deltaic clays with lime-rice husk ash admixtures," *Proceedings of Southeast Asian Conference on Soil Engineering*, Singapore, pp. 215–223.

Muntohar, A.S. (2002), "Improvement of the bearing of soil by using lime – rice husk ash," In Alawaji (ed.), *Geotechnical and Geoenvironmental Engineering in Arid Lands*, pp. 225–229.

Muntohar A.S. and Hantoro, G. (2000), "Influence of the rice husk ash and lime on engineering properties of clayey subgrade," *Electronic Journal of Geotechnical Engineering* 5, Paper#019. www.ejge.com

Payá, J., Monzó, J., Borrachero, M.V., Mellado, A., and Ordoñez, L.M. (2001), "Determination of amorphous silica in rice husk ash by rapid analytical method," *Cement and Concrete Research*, 31, 212–231.

Prakash, K., Sridharan, A., and Rao, S.M. (1989), "Lime addition and curing effects on the index properties and compaction characteristics of a montmorillonitic soil," *Geotechnical Engineering Journal*, 20, 39–47.

Seed, H.B., Woodward, R.J., and Lundgren, R. (1962), "Prediction of swelling pontential for compacted clays," *Journal of Soil Mechanics and Foundation Division ASCE*, 88 (MS3), 53–87.

Wroth, C.P. and Wood, D.M. (1978), "The correlation of index properties with some basic engineering properties of soils," *Canada Geotechnical Journal,* 15 (2), 137–145.

Younger, J.S. (1991), Geotechnical characteristics of soft soils in Indonesia, in Balasubramaniam *et al.* (eds), *Development in Geotechnical Aspects of Embankment, Excavations and Buried Structures*, Rotterdam, Balkema, 557–570.

Zhang, M.H., Lastra, R., Malhotra, V.M. (1996), Rice husk ash paste and concrete: some aspects of hydration and the microstructure of the interfacial zone between the aggregate and paste, *Journal of Cement and Concrete Research*, 26 (6): 963–977.

Chapter 31

Effects of addition of fly ash on swell potential of an expansive soil

Devrim Turker[1] *and Erdal Cokca*[2]

Summary

Most countries with arid and semi-arid climates have problems with expansive soils. Fly ash, this is an industrial by-product from coal burning thermal power plants, is accumulating in large quantities in many countries. In this study, utilization of fly ash for stabilizing expansive soils was assessed. F and C type fly ash (according to ASTM C618) were used on expansive soil for stabilization. Samples were tested for free swell and primary swell time. Degree of saturation-suction relationships for the expansive soil and stabilized expansive soil with F and C Type fly ash (F 75/25/0 and C 75/25/0) were also investigated. Samples with fly ash caused a decrease in free swell test results. C type fly ash was more effective in stabilization.

Introduction

Many countries with arid and semi-arid climates have problems with expansive soils. Problems with expansive soils have been reported for Australia, Argentina, Burma, China, Cuba, Ethiopia, Ghana, Great Britain, India, Iran, Israel, Kenya, Mexico, Morocco, South Africa, Spain, USA, and Venezuela (Fredlund and Rahardjo, 1993). Examples of expansive soil problems are cracking and break up of asphalt pavements, highway embankments, roadways, building foundations, slab on grade members, and channel and reservoir linings, irrigation systems, water lines, and sewer lines. If there is leakage in a water line, cracking progresses with swelling of soil which can cause damage to structures (Fredlund and Rahardjo, 1993).

Expansive soil deposits may range from lacustrine to bedrock shale deposits. In general, expansive soils have high plasticity (i.e. high liquid limit), and are relatively stiff or dense. The expansive nature of soil is most obvious near the ground surface where the profile is subjected to seasonal, environmental changes. The pore water pressure is initially negative and the deposit is generally unsaturated. These soils often have some montmorillonite clay mineral present. The higher the amount of monovalent cations absorbed to the clay mineral (e.g. sodium), the more severe the expansive soil problem (Fredlund and Rahardjo, 1993).

[1] BOTAS Baku – Tbilisi – Ceyhan Crude Oil Pipeline Project, Sogutozu Cad No: 27 Sogutozu, Ankara, Turkey; devrim.turker@btc.com.tr

[2] Department of Civil Engineering, Middle East Technical University, Ankara, Turkey; ecokca@metu.edu.tr

In Turkey, yearly amount of disposed fly ash-bottom ash is estimated as 21,390,000 tons. Due to transportation costs, most waste materials and by-products will need to be used within a relatively short distance from the source, unless located in an area with a shortage of construction material (NCHRP, 1994).

Fredlund *et al.* (1997) derived a relationship between grain size distribution and volume-mass properties. The graph shown in Figure 31.1 was derived by Zapata (1999) and cited in Fredlund *et al.* (2003).

In the study reported in this chapter, the reduction of free swell of expansive soil was examined by addition of F/C type fly ash and sand. The degree of saturation-suction relationships for stabilized expansive soil with F and C Type fly ash was also investigated.

Mechanism of swelling

Hydration and double layer repulsion are principal driving forces in swelling. In the first stage of hydration of the clay particles, water is adsorbed in successive monolayers on the surfaces and pushes the particles or the layers of montmorillonite clay apart. In this stage, surface hydration energy causes swelling (Figure 31.2). Interaction of water with clay

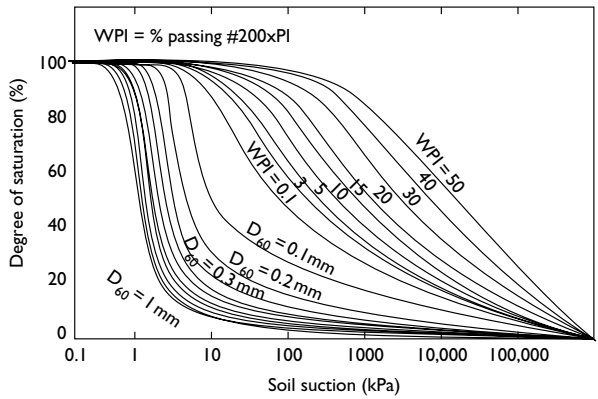

Figure 31.1 Correlation of the classification properties of a soil with previously measured soil-water characteristic curves.

Source: After Zapata (1999), cited in Fredlund *et al.* (2003).

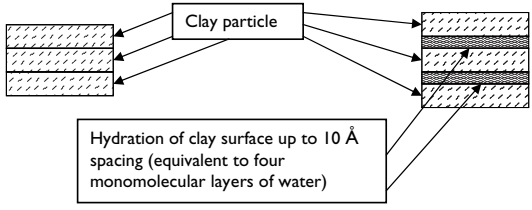

Figure 31.2 Intracrystalline swelling.

Source: After Van Olphen, 1977.

surface reduces the chemical potential of water, thereby generating a gradient in the chemical potential that causes additional water to flow into the system (Mitchell, 1993).

At plate distances beyond 10 Å (equivalent to four monomolecular layers of water), surface hydration energy is no longer important, and the electrical double layer repulsion becomes the major repulsive force between plates (Van Olphen, 1977). Exchangeable cations that are held to negatively charged clay surface have a higher concentration than in water. Since cations do not have the ability to move, water enters in between the mineral layers to equalize the concentration difference. Consequently, water exerts an osmotic pressure force to open up the mineral layers (Mitchell, 1993) (Figure 31.3).

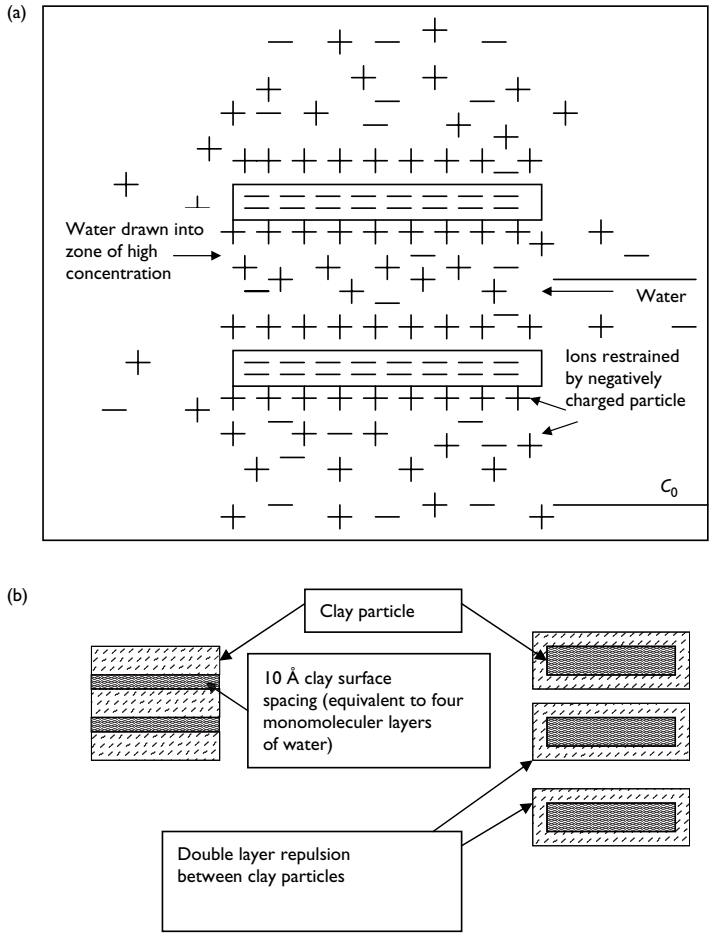

Figure 31.3 (a) Swelling of soil with entrance of water in between mineral layers (after Mitchell, 1993) (b) Interparticle swelling.

Source: After Mitchell, 1993.

From the theoretically derived distribution of ions in the double layers between the clay plates, and in the equilibrium liquid, the osmotic pressure can be computed according to procedures presented in Van Olphen (1977). This pressure is identical to double layer repulsion of the two plates as computed by other methods. Consequently, the swelling pressure as given by the applied confining pressure will be identical with the osmotic pressure only when the double layer repulsion is the single operating force, or by far the dominant force between plates (Van Olphen, 1977). Another operating force is when particles are very close together, the net positive charge at the edges can participate in an edge to face linkage between particles of an electrostatic type (Lambe and Whitman, 1969).

Stabilization with fly ash

The effect of fly ash can be assessed in the short and long term considering fly ash reactions. If soil is not of a good gradation and there is a gap of silt-sized particles in the gradation curve, fly ash application will improve soil gradation. The immediate effect of the introduction of fly ash to the soil (including the lime, CaO, already present in the fly ash) is to cause flocculation and agglomeration of the clay particles due to ion exchange at the surfaces of the soil particles (Nicholson and Kashyap, 1993).

The long-term reactions are accompanied over a period of time (i.e. many weeks, months, or even years may be required for completion of these reactions) depending upon the rate of chemical breakdown and hydration of silicates and aluminates. This results in further amelioration and binds the soil grains together by formation of cementitious materials. In order for cementation to occur, there must be a sufficient source of pozzolans available. Pozzolans are a source of silica and alumina with high surface area. These are a source of silica for hydration by alkali and alkali earth hydroxides to form cementitious products in the presence of moisture at ordinary temperatures. Fly ash stabilization is used in soils, which do not have sufficient pozzolans for lime stabilization (Nicholson and Kashyap, 1993).

Experimental

Materials

Kaolinite: Kaolinite clay was obtained in the form of gravel sized grains. These grains were crushed and passed through # 40 sieve. Specific gravity of kaolinite was 2.721. Bentonite: Bentonite clay (Na-Montmorillonite) was taken from Bentonite Factory. The specific gravity of bentonite was 2.32.Fly Ash (F type/C type according to ASTM D5239-98): F type fly ash was taken from electro filters of Catalagzi Thermal Power Plant. C type fly ash was taken from electro filters of Soma Thermal Power Plant. The coal particles were removed by sieving through # 200 sieve. Specific gravity of F type fly ash was 2.053 and C type fly ash was 2.107. Chemical composition and mineralogical analysis of fly ash was determined by laboratory of Association of Cement Producers of Turkey and is presented in Tables 31.1 and 31.2 respectively. Sand was taken from concrete plant. Sand remaining between # 30 and # 100 was used. Specific gravity of sand was 2.636.

ASTM free lime content (hydrated lime procedure) was used to distinguish between different fly ashes and quality control since it represented the lime reactions that take place in fly ash. Results of available lime tests, which were made according to ASTM C 25 hydrated lime procedures, are presented in Table 31.3.

Table 31.1 Chemical analysis of the materials used

Chemical composition (%)	*Kaolinite*	*Bentonite*	*F type fly ash*	*C type fly ash*
SiO_2	49.89	60.75	58.48	53.12
Al_2O_3	33.03	18.90	25.61	26.28
Fe_2O_3	1.78	3.05	6.00	4.46
TiO_2	1.33	—	1.34	1.09
MgO	0.03	2.10	0.38	0.33
CaO	0.42	2.75	1.97	10.78
Na_2O	0.08	2.70	0.52	0.43
K_2O	1.69	0.95	4.27	1.98
SO_3	0.13	—	0.13	0.61
Loss in ignition (%)	11.10	7.55	0.86	0.42

Table 31.2 Mineralogical analysis of fly ash

F type fly ash	*C type fly ash*
Quartz (SiO_2)	Quartz (SiO_2)
Hematite (Fe_2O_3)	Hematite (Fe_2O_3)
Mullite ($3Al_2O_3.2SiO_2$)	Mullite ($3Al_2O_3.2SiO_2$)
	Albite ($NaAlSi_3O_8$)
	Sanidine
	Free CaO
Glassy or amorphous phase	Glassy or amorphous phase

Table 31.3 Available lime test (ASTM C-25) results

Fly ash type	*Volume of HCl (ml) for titration*	*Available lime ($Ca(OH)_2$) (%)*
F	1	1.32
C	5	6.6

Preparation of test samples

Kaolinite, bentonite, fly ash, and sand were oven-dried at 50°C for one day. Sample A was composed of 85% kaolinite and 15% bentonite. Other samples were composed of 75% sample A, which corresponded to 63.75% kaolinite and 11.25% bentonite, and 25% fly ash mixture. Water, 10 g, was added to the mixtures to form samples. Then the samples were mixed with a trowel and passed through # 30 sieve (Figure 31.4). Samples were then placed in rings of 1.9 cm in height and 6.35 cm in diameter and compacted statically with a hydraulic jack. The percentages of the materials in the test samples are given in Table 31.4. Hydrometer test, Atterberg limit tests, and specific gravity test were done on the samples according to ASTM D 2435 (Specific gravity of bentonite was determined according to ASTM C 188).

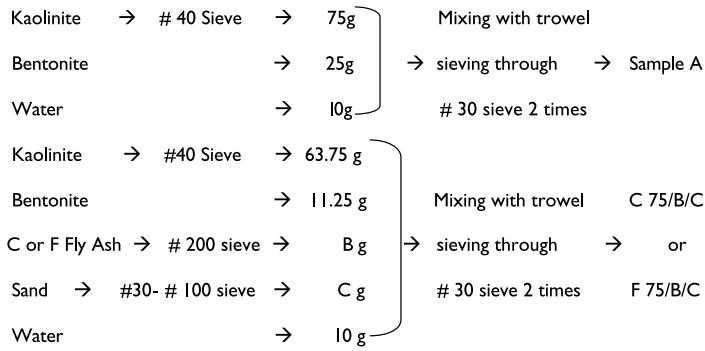

Figure 31.4 Preparation of the test samples.

Table 31.4 Mixture percentages of materials in the test samples

Sample A	*Expansive soil*	*F type fly ash*	*C type fly ash*	*Sand*
Sample A	100	0	0	0
F 75/25/0	75	25	0	0
F 75/24/1	75	24	0	1
F 75/22/3	75	22	0	3
F 75/20/5	75	20	0	5
F 75/17/8	75	17	0	8
F 75/15/10	75	15	0	10
C 75/25/0	75	0	25	0
C 75/24/1	75	0	24	1
C 75/22/3	75	0	22	3
C 75/20/5	75	0	20	5
C 75/17/8	75	0	17	8
C 75/15/10	75	0	15	10

Free swell test

ASTM D 4546–96 was used. The experimental setup is shown in Figure 31.5. Test samples were placed in rings of 6 cm in height. Then filter papers were placed at the bottom and top of the test samples. Two porous stones were placed over the filter paper, which was over the test sample, and one porous stone was placed below the filter paper, which was below the test sample. Porous stones were de-aired and saturated in water boiling on an electric heater before the experiment. There was a metal cover over the top porous stone. Rings were placed in modified Bishop device (higher than original Bishop sample containers). A vertical deflection dial gauge was mounted on the top metal cover. Grease was applied to the inner surface of the ring to eliminate friction. After taking the initial dial gauge reading, the test sample was inundated. Distilled water was preferred to eliminate effects of anions and cations in water.

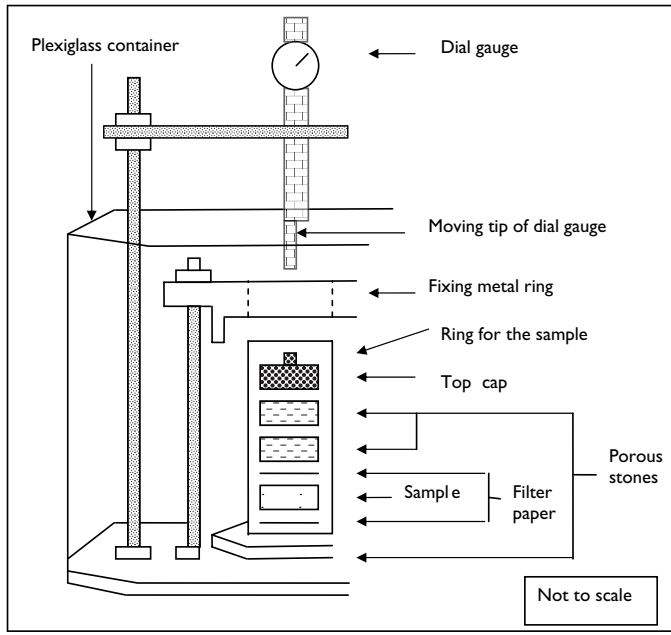

Figure 31.5 Experimental setup for free swell test.

Deflection values in dial gauge were recorded against time. Deflection values at 0.1, 1, 2, 4, 8, 15, 30, 60 minutes, 2, 4, 8 hours, 1, 2, 3, 4, and 8 days were used to plot free swell versus time graphs. After deflections had ceased or were less than 0.01 mm/day, the last reading of swell was recorded and the oedometer was dismantled. The filter papers were separated from the surface of the test samples. According to ASTM D 2435, the final weight of the test sample was measured and test sample was put into an oven to find the dry weight for final water content determination.

Results and discussion

Test sample properties measured (Turker and Cokca, 2004) are tabulated in Table 31.5. It can be observed from Table 31.5 that liquid limit (LL) of sample A was 90%, LL of C 75/25/0 drops to 74%. With increasing sand portion, in C 75/17/8, the LL reduced to 68%. LL of F 75/25/0 dropped to 74% with increasing sand portion. Immediate reactions of free lime in the form of CaO, which is more in C type fly ash, were effective in reduction of the LL of the test samples with F and C type fly ash. According to Ferguson (1993), the reduction in Atterberg limits is generally less than observed with lime stabilization due to lower calcium ion concentration.

From Table 31.5, it can be observed that the plastic limit (PL) of sample A was 20%, the PL of C 75/25/0 increased to 24%, then in presence of sand the PL was around 21%.

Table 31.5 Properties of the samples

Sample	*Clay (%)*	*Silt (%)*	G_s	*LL (%)*	*PL (%)*	*PI (%)*	*USCS*	*Activity*
Sample A	54.5	45.5	2.55	90.2	19.7	70.5	CH	1.29
F 75/25/0	41.1	58.9	2.32	73.5	20.5	53.0	CH	1.29
F 75/24/1	45.0	55.0	2.29	72.4	20.7	51.7	CH	1.15
F 75/22/3	42.4	57.6	2.32	74.5	20.8	53.7	CH	1.27
F 75/20/5	42.0	58.0	2.40	74.2	20.4	53.8	CH	1.28
F 75/17/8	42.4	57.6	2.36	71.6	20.6	51.0	CH	1.20
F 75/15/10	42.5	57.5	2.38	72.2	19.6	52.6	CH	1.24
C 75/25/0	42.5	57.5	2.36	73.5	23.6	49.9	CH	1.17
C 75/24/1	42.4	57.6	2.34	70.6	20.9	49.8	CH	1.18
C 75/22/3	39.4	60.6	2.35	67.8	19.6	48.2	CH	1.22
C 75/20/5	38.5	61.5	2.35	68.4	20.6	47.8	CH	1.24
C 75/17/8	41.0	59.0	2.42	68.0	21.7	46.3	CH	1.13
C 75/15/10	40.4	59.6	2.38	70.5	20.9	49.6	CH	1.23

Notes
Activity = PI/% clay;
PL = Plastic limit;
Sample A: Expansive soil sample (85% kaolinite + 15% bentonite);
Naming is explained with following example:
C 75/22/3 → 75% sample A, 22% C type fly ash, 3% sand;
F 75/20/5 → 75% sample A, 20% F type fly ash, 5% sand.

The PL of F 75/25/0 was 21% which was also higher than sample A but lower than C 75/25/0. The PL of samples with F type fly ash did not change as much as when sand replaced fly ash. Sample A could remain plastic at a lower water content. The addition of sand and fly ash increased PL.

From Table 31.5, it can be observed that plasticity index (PI) of sample A was 71%, the PI of C 75/25/0 decreased to 50%. The PI of samples with C type fly ash reduced to 46% as sand replaced fly ash. The PI of C 75/17/8 dropped to 46%. The PI of F 75/25/0 reduced to 53. The PI varied around 53% as sand replaced fly ash. It can be seen from Table 31.5 that with decreasing LL and increasing PL the range got narrower so the PI decreased. The decrease in PI was slightly more with C type fly ash and with increasing sand percentage.

From Table 31.5, it can be observed that the specific gravity, G_s, of sample A was 2.55. It decreased to 2.36 in C 75/25/0. The specific gravity did not change much with varying sand and fly ash proportions. The specific gravity of F 75/25/0 reduced to 2.32. The specific gravity was around 2.35 as sand replaced fly ash. Fly ash which had specific gravity of 2.05–2.10 reduced the specific gravity of the sample. Sand should have increased the specific gravity, however, its effect was not very great.

Sample A had an activity of 1.29 (Table 31.5). The activity dropped to 1.17 in C 75/25/0. The activity takes values around 1.22 as sand replaces fly ash. The activity started with a value 1.29 in sample F 75/25/0. When sand replaced fly ash, the activity reduced to around 1.24. A small amount of clay with high PI indicated high activity. A reduction of activity resulted in a lower swell potential.

The percent swell and primary swell time values for the samples are given in Table 31.6. From Table 31.6, it can be observed that in C 75/25/0 sample, compared to sample A, there was a 58% decrease in free swell. The F 75/25/0 sample had a 10% decrease of free swell

Table 31.6 Measured swell values for the test samples

Sample	*% Swell*	*% Change in free swell*	*Primary swell time (min)*	*% Change in primary swell time*
Sample A	49.0	0.0	4000	0.0
F 75/25/0	44.1	10.0	3720	7.0
F 75/24/1	41.7	14.8	3660	8.5
F 75/22/3	39.5	19.3	3630	9.3
F 75/20/5	37.6	23.3	3570	10.8
F 75/17/8	33.8	31.0	3540	11.5
F 75/15/10	30.9	37.1	3470	13.3
C 75/25/0	20.3	58.5	380	90.5
C 75/24/1	18.1	63.2	360	91.0
C 75/22/3	17.2	64.9	330	91.8
C 75/20/5	15.3	68.9	320	92.0
C 75/17/8	14.0	71.5	300	92.5
C75/15/10	12.1	75.3	280	93.0

Note
+ Decrease / + Increase.

compared to sample A. This ratio continued to decrease till 37% while sand replaced fly ash. From Table 31.6 it can be seen that the free swell of C 75/25/0 was 46% of F 75/25/0. Samples F 75/B/C and C 75/B/C contained 11.15% bentonite. Sample A contained 15% bentonite. Since the amount of expansive soil was less, the free swell should decrease. Samples F 75/B/C and C 75/B/C could be comparatively inspected, since they both had 75% sample A.

The swell potential of the material reported in this study was reduced to levels comparable to lime treatment. As indicated by Ferguson (1993), this reduction appeared to be the result of bonding of soil particles by cementitious products formed during hydration of the fly ash in addition to flocculation of the clay minerals. The effect is more in C type fly ash which was due to CaO. However, according to Ferguson (1993), for some applications, such as the use of a self-cementing ash as a drying agent or to reduce shrink-swell potential of clay soils, the hydration characteristics of a particular ash may have only minor influence on the desired results.

Higher proportion of sand and a corresponding lower clay content, reduced the tendency of the clay to swell. Abduljauwad (1993) indicated that sand addition can also cause larger capillary canals in the soil pores and a corresponding reduction in soil suction.

From Table 31.6, it can be observed that in sample C 75/25/0, there was a 90% decrease in primary swell time compared to sample A. Sample F 75/25/0 had a 7% decrease in primary swell time. It resulted in a 13.3% decrease when sand replaced fly ash. From Table 31.6, a decreasing trend of primary swell time with increasing sand replacing fly ash could be seen. Sand also retarded the primary swell as it caused more intervoid swelling (Sivapullaiah *et al.*, 1998).

It was observed that 22% swell, which is 50% of total free swell, took place in 100–1000 minutes log cycle for sample F 75/25/0. This was 54% of the total free swell, that took place in 10–100 minutes log cycle for the sample.

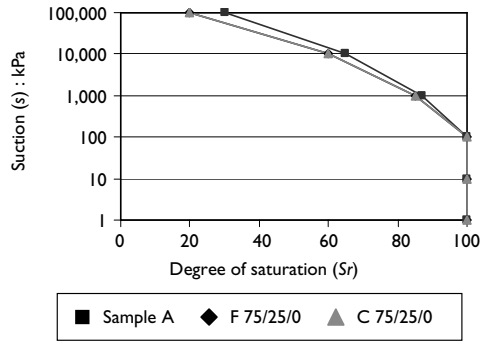

Figure 31.6 Soil water characteristic curve of samples.

A correlation of classification properties of soil with previously measured soil-water characteristic curves in Figure 31.1 (after Zapata (1999), cited in Fredlund *et al.* (2003)) was used to plot suction-degree of saturation relationships (Figure 31.6).

Conclusions

Free swell decreased as sand replaced fly ash. Free swell could be reduced up to 37.1% with 15% F type fly ash and 10% sand. While 15% C type fly ash and 10% sand could reduce free swell up to 75.3%. It was observed that in sample C 75/25/0, compared to sample A, there was a 58% decrease in free swell. Sample F 75/25/0 had a 10% decrease in free swell compared to sample A. The free swell of C 75/25/0 was 46% of F 75/25/0. In the experiments performed, C type fly ash was more effective than F type fly ash in reducing free swell. Primary swell was completed in a short time of six hours for C 75/25/0 which was 10% of the primary swell time of F 75/25/0.

On the basis of this research study, both class C and class F fly ash with sand can be recommended as effective stabilizing agents for improvement of expansive soils. The use of fly ashes as stabilizing agents can be economically attractive in regions where this industrial waste by-product is produced.

References

Abduljauwad, S.N. (1993), "Treatment of Calcareous Expansive Clays," *ASCE Geotechnical Publication No. 36*, New York, USA, pp. 100–117.

ASTM (1993), "Standard Specification for Fly Ash and Raw or Calcined Natural Pozzolan for Use as a Mineral Admixture in Portland Cement Concrete," *Annual Book of ASTM Standards, C 618–93*, Vol. 04.02, Philadelphia, PA, USA, pp. 310–312.

ASTM (1993), "Test Methods for Chemical Analyses of Limestone, Quicklime and Hydrated Lime," *Annual Book of ASTM Standards, C 25–93a*, Vol. 04.01, Philadelphia, PA, USA, pp. 9–36.

ASTM (1993), "Standard Test Method for Density of Hydraulic Cement," *Annual Book of ASTM Standards*, C 188, Vol. 04.01, Philadelphia, PA, USA, pp. 109–136.

ASTM (1999), "Standard Test Method for One-Dimensional Consolidation Properties of Soils," *Annual Book of ASTM Standards, D 2435–96*, Vol. 04.08, Philadelphia, PA, USA, pp. 210–219.

ASTM (1999), "Standard Test Method for One-Dimensional Swell or Settlement Potential of Cohesive Soils," *Annual Book of ASTM Standards, D 4546–96*, Vol. 04.08, Philadelphia, USA, pp. 672–678.

ASTM (1999), "Standard Practice for Characterizing Fly Ash for Use in Soil Stabilization," *Annual Book of ASTM Standards, D 5239–98*, Vol. 04.09, Philadelphia, PA, USA, pp. 130–132.

Ferguson, G. (1993), "Use of Self-Cementing Fly Ashes as a Soil Stabilizing Agent," *ASCE Geotechnical Publication No. 36*, New York, USA, pp. 1–15.

Fredlund, D.G. and Rahardjo, H. (1993), *Soil Mechanics for Unsaturated Soils*, John Wiley and Sons Inc., New York, USA.

Fredlund M.D. (1997), "Prediction of the Soil-Water Characteristic Curve from Grain-Size Distribution and Volume-Mass Properties," Proceedings of the Third Brazilian Symposium on Unsaturated Soils, NONSAT'97, Rio de Janeiro, Brazil.

Fredlund M.D., Fredlund G.F., Houston S.L., and Houston W.B.H. (2003), "Assessment of Unsaturated Soil Properties for Seepage Modeling Through Tailings and Mine Wastes," *Tailings and Mine Wastes*, Swets and Zeitlinger, Lisse, Eds, pp. 149–157.

Lambe T.W. and Whitman, R.V. (1969), *Soil Mechanics*, John Wiley and Sons Inc., New York, USA.

Mitchell, J.K. (1993), *Fundamentals of Soil Behavior*, John Wiley and Sons Inc., New York, USA.

NCHRP (1994), *Synthesis of Highway Practice 199, Recycling and Use of Waste Material and By-Products in Highway Construction*, National Academy Press, Washington, DC.

Nicholson, P.G. and Kashyap, V. (1993), "Fly Ash Stabilization of Tropical Hawaiian Soils," *ASCE Geotechnical Publication No. 36*, Sheng, D. and Sloan, S. W., Eds, New York, pp. 15–29.

Sivapullaiah, P.V., Prashanth, J.P., Sridharan, A., and Narayana, B.V. (1998), "Reactive Silica and Strength of Fly Ashes," *Geotechnical and Geological Engineering*, Chapman & Hall Press, Vol. 16, pp. 239–250.

Turker D. and Cokca E. (2004), "Stabilization of an Expansive Soil with Fly Ash and Sand," Proceedings of 6th International Congress on Advances in Civil Engineering, Istanbul, Turkey. pp 1613–1622.

Van Olphen, H. (1977), *Clay Colloid Chemistry, 2nd Ed.*, John Wiley and Sons Inc., New York, USA.

Zapata, C. E. (1999), Uncertainty in Soil-Water Characteristic Curves and Impacts on Unsaturated Shear Strength Predictions. PhD Dissertion, Arizona State University, AR, USA.

Chapter 32

Dynamic characterization of chemically modified expansive soil

Laureano R. Hoyos,[1] *Phonlawut Chainuwat,*[2] *and Anand J. Puppala*[3]

Summary

A series of resonant column tests was conducted on chemically stabilized specimens of sulfate-rich expansive clay from southeast Arlington, Texas. Specimens were tested for different stabilizer types, stabilizer dosages, compaction moisture contents, and confining pressures. Three chemical stabilization methods were used: sulfate resistant Type V cement, low calcium Class F fly ash, and lime mixed with polypropylene fibers. Results in the small-shear strain amplitude range (<0.0001%) were analyzed to assess the influence of compaction moisture content and confining pressure on the linear shear modulus G_{max} and material damping D_{min} of stabilized soil. Tests were also conducted at small- to mid-shear strain amplitude levels (0.0001–0.01%) to assess the threshold strain limit γ_{th} for each treatment method, and to study the effects of torsional shearing on the rate of degradation of normalized modulus G/G_{max} of treated soil. A 10%-by-weight dosage of sulfate resistant Type V cement was found to yield best performance. Results summarized herein further corroborate previous findings by authors on similar clayey soils and chemical stabilizers.

Introduction

Chemical stabilization of high-plasticity expansive soils using calcium-based stabilizers, such as lime and ordinary Portland cement, has been practiced over the last six decades. Its overall benefits include an increase in soil strength, stiffness, and durability, and a reduction in soil plasticity and swelling/shrinkage potential (Hausmann 1990; Sherwood 1995; Prusniski and Bhattacharya 1999). However, these stabilization methods present some serious limitations in soils containing large amounts of organic matter, sulfates, or salts. In the case of sulfate-rich soils, calcium components of lime- and cement-based stabilizers react with the free alumina of soils and sulfates to form ettringite mineral (Hunter 1988). Ettringite, a weak and unstable sulfate mineral, undergoes significant expansion when exposed to hydration, which results in differential heaving and distress-induced cracking of pavements and spread footings. This sulfate-induced heave is known to severely affect the

[1] Department of Civil & Environmental Engrg, University of Texas at Arlington, Arlington, Texas 76019. Tel: (817) 272 3879. Fax: (817) 272 2630; e-mail: lhoyos@uta.edu

[2] PSA Engineering, Dallas, Texas 75252.

[3] Department of Civil & Environmental Engrg, University of Texas at Arlington, Arlington, Texas 76019.

performance of residential and highway infrastructure in most southern and southwestern states of the US (Hunter 1988; Mitchell and Dermatas 1990; Nelson and Miller 1992; Petry and Little 1992; Kota *et al.*, 1996; Rollings *et al.*, 1999).

These sulfate-induced heave problems have led to new research efforts aimed at exploring novel, cost effective stabilization methods to treat natural, sulfate-rich soils. Recently, the University of Texas at Arlington conducted a study to evaluate the effectiveness of several sulfate resistant cementitious and recycled stabilizers for treating soft, high-plasticity, sulfate-rich expansive clays collected from various locations in the city. The study's testing program included Atterberg limits, linear shrinkage, one-dimensional swelling, and unconfined compression tests. All specimens were prepared and tested at or close-to optimum moisture content (Wattanasanticharoen, 2000; Puppala *et al.*, 2001, 2002).

Some of the investigated stabilizers were found to exert an immediate, positive influence on strength and swelling/shrinkage potential of treated soil. However, their effects on treated soil's dynamic response had not been addressed. The lack of experimental evidence of this kind on chemically-treated sulfate-rich clay has driven motivation for the present work. Dynamic soil properties, such as shear wave velocity V_s, shear modulus G, and material damping ratio D, are the key subsoil parameters for the design of geosystems resting on stabilized soils and dealing with heavy traffic or vibrating/impact machinery, and for the analysis of wave propagation in treated soils, as depicted schematically in Figure 32.1.

The main objective of the work reported in this chapter was to study the dynamic response of chemically stabilized, sulfate-rich expansive clay from southeast Arlington, Texas, using three selected stabilizers: sulfate resistant Type V cement, low calcium Class F fly ash, and lime mixed with polypropylene fibers. Type V cement was recommended for constructions in high-sulfate environments (i.e. sulfate content greater than 1,500 mg/l) and/or exposed to severe sulfate attack, such as seawater or salty circulating water (Atkins, 1983). Class F fly ash was recommended in sulfate-rich soil environments in order to minimize formation of ettringite mineral (Mamlouk and Zaniewski, 1999). Finally, polypropylene fibers have recently been used in conjunction with lime as a novel stabilization method to reduce shrinkage-induced soil cracking (Puppala *et al.*, 2001).

A series of free-fixed type of resonant column tests (Isenhower, 1979; Huoo-Ni, 1987; Stokoe *et al.*, 1991; ASTM D 4015–92, Test 1993) was conducted at small-shear strain amplitude levels ($<0.0001\%$) for different stabilizer types, stabilizer dosages, compaction moisture contents, and confining pressures. Dynamic soil properties investigated included

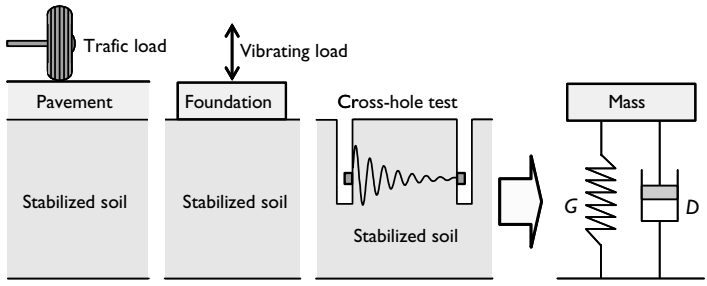

Figure 32.1 Idealization of stabilized soil under non-static loading.

linear shear modulus G_{max} and material damping ratio D_{min}. Tests were also conducted at small-to mid-shear strain amplitude levels (0.0001–0.01%) to assess the threshold strain limit γ_{th} for each treatment method, and to study the effects of torsional shearing on the rate of degradation of normalized modulus G/G_{max} of treated soil. The half-power bandwidth method was used to determine material damping D (Richart *et al*., 1970).

Test variables

Soil and stabilizers

The soil used in this study was sampled from the west side of South Cooper Estate Village in southeast Arlington, Texas. The soil was a high-plasticity, sulfate-rich clay, dark yellow in color, with natural moisture content w_n = 6.6%, fines content (minus No. 200) = 73%, clay fraction CF = 25%, standard Proctor optimum moisture content OMC = 21%, maximum dry unit weight $\gamma_{d\text{-}max}$ = 16.46 kN/m^3, specific gravity G_s = 2.85, liquid limit LL = 74%, plasticity index PI = 45%, and soluble sulfate content = 33,048 mg/l. The soil classified as A-7-6 and CH according to AASHTO and USCS, respectively, and it was selected because of its high plasticity index and sulfate content. Currently, low-to-moderate and high sulfate soils are identified as those containing soluble sulfates less than 2,000 mg/l and more than 2,000 mg/l, respectively (Mitchell and Dermatas, 1990; Kota *et al*., 1996).

Type V cement was provided by the Cement and Concrete Promotion Council (CCPC) of Texas. Its resistance to sulfate attack makes this product potentially feasible for treating sulfate-rich soils. It presented a 32,175-kPa (4,663-psi) compressive strength at seven days, and contained 62.6% calcium oxide (CaO). Class F fly ash was provided by Boral Material Technologies (BMT). It contained only 1.1% of CaO, which had the potential to minimize ettringite formation in sulfate-rich clays. Polypropylene fibers were also provided by BMT. They were made of 100% virgin, fibrillated polypropylene with normal fiber length = 1.9 cm (0.75 in.), tensile strength = 0.67 KN/mm^2 (97 ksi), and high resistance to alkali, salt, and acids (Puppala *et al*., 2001, 2002).

Experimental variables

Stabilizer dosages (by-weight of dry soil) used in this work, that is, 5% and 10% Type V cement, 20% Class F fly ash, and 8% lime + 0.3% fibers, yielded best performance, in terms of plasticity index, unconfined compressive strength, and swelling/shrinkage potential, in sulfate-bearing expansive clays from southeast Arlington. No noticeable change in any of these properties was observed after a 7-day curing period (Wattanasanticharoen, 2000). The 5% and 10% Type V cement dosage levels also represent those traditionally used by the Texas Department of Transportation in ordinary Portland cement-based treatments.

The range of compaction moisture contents, that is, 85% and 95% of maximum dry unit weight $\gamma_{d\text{-}max}$ on both sides of Proctor optimum, represents potential variations in moisture conditions during soil compaction operations in the field. The selected range of isotropic confining pressures, 17.25, 34.5, 69, and 138 kPa (2.5, 5, 10, and 20 psi), was aimed at reproducing in situ stress states at different locations within a pavement or shallow foundation system. Finally, each specimen was tested at different elapsed times under constant confinement, that is, at 0, 1, 2, 4, 8, 16, and 24 hours, in order to assess the change in dynamic properties with elapsed time. All specimens were tested after a 7-day curing period.

Specimen preparation

Standard Proctor compaction tests were first performed on natural (control) and treated soil for all stabilizer dosages described in the previous section. The desired compaction moisture content in a specific resonant column (RC) test specimen was determined via the Proctor compaction curve. The amounts of water and stabilizer, by weight of dry soil, were calculated from this required moisture content. Dry soil was then thoroughly mixed with the required amounts of water and stabilizer to ensure homogeneity. The mixed soil was then compacted in three equal layers into a 7.3-cm (2.875-in.) diameter, 14.6-cm (5.75-in.) height split miter box. Each layer was compacted using a 24.5-N (5.5-lb), 30.5-cm (12-in.) drop, US Army Corps hammer with 16 uniformly distributed blows, corresponding to a compactive effort of 593 kJ/m^3 (12,375 ft-lb/ft^3). After compaction, the specimen was covered with a non-woven geotextile, stored in a plastic bag, and kept under room temperature in a 100% humidity-controlled room for a 7-day curing period.

Test program

Specimen notation

A simple notation for specimen identification was adopted in order to facilitate the reading of all variables intervening in the fabrication/compaction of a RC test specimen, particularly those referring to stabilizer type, stabilizer dosage, and compaction moisture content. For instance, a specimen identified as 5V-85D implies that it was made of natural soil mixed with 5% Type V cement, and then compacted with a moisture content corresponding to 85% of $\gamma_{\text{d-max}}$ on the dry (*D*) side of Proctor optimum. Table 32.1 shows values of dry unit

Tables 32.1 Dry unit weights and compaction moisture contents of RC test specimens

RC test specimen (1)	γ_d *(kN/m^3) (2)*	*w (%) (3)*
Natural-OPT	16.46	21
5V-85D	13.30	10
5V-95D	14.87	15
5V-OPT	15.65	22
5V-95W	14.87	30
5V-85W	13.30	35
10V-98D	15.60	14
10V-99D	15.76	16
10V-OPT	15.92	20
10V-95W	15.12	29
10V-85W	13.53	36
FA-85D	14.34	13
FA-95D	16.03	15
FA-OPT	16.87	19
FA-95W	16.03	23
FA-85W	14.34	26
LF-85D	13.05	16
LF-95D	14.58	20
LF-OPT	15.35	26
LF-95W	14.58	30

weight γ_d and compaction moisture content w for all 20 RC test specimens used. For a 10% Type V cement dosage, a minimum water content of 14% was necessary for adequate soil-water-additive mixing.

Test procedure

After the 7-day curing period, the specimen was assembled into the RC apparatus and the remaining RC components were set into place. An initial isotropic confining pressure $\sigma_0' = 17.25$ kPa (2.5 psi) was then applied, and a series of RC tests were performed at 0, 1, 2, 4, 8, 16, and 24 hours elapsed from the time the initial pressure was applied. The pressure was kept constant during these first 24 hours. All RC tests were performed by sending a low-amplitude (250-mV peak-to-peak) sinusoidal signal from a dynamic signal analyzer (DSA) to the torsional driver fixed on top of the specimen. The frequency of the signal was incrementally changed by sweeping the frequency scale in the DSA until the frequency response curve was obtained, which allows for the determination of linear shear modulus G_{max} and damping ratio D_{min}. Right after the last RC test was completed, σ_0' was increased from 17.25 to 34.5 kPa (5 psi), and a new series of RC tests was performed at same elapsed times. The same test procedure was repeated for $\sigma_0' = 69$ kPa (10 psi) and $\sigma_0' = 138$ kPa (20 psi).

After the last RC test under $\sigma_0' = 138$ kPa (20 psi) was completed, this pressure was kept constant and an additional series of RC tests was conducted for different peak-to-peak amplitudes of the signal sent to the driver, that is, 0.75, 1, 1.5, 2, 3, 4, and 5 V. The purpose was to quantify the degree of stiffness degradation from small ($<0.0001\%$) to mid (0.01%) shear strain amplitude levels in treated soil. The entire procedure described here was identically followed for all 19 specimens of treated soil listed in Table 32.1. A specimen of natural soil, used as control soil, was prepared at optimum moisture content (OMC) and tested in the RC device for the same range of confining pressures and elapsed times described above.

Linear dynamic response

Time effect

Figure 32.2 shows the variation of G_{max} and D_{min} with time t, for different confining pressures σ_0', for natural (control) clay specimen. It can be noted that G_{max} increases with time, whereas D_{min} tends to decrease, for any σ_0'. It is also observed that G_{max} increases and D_{min} decreases with an increase in σ_0'. This can be explained by the fact that soil stiffness is directly related to shear wave velocity V_s, that is, $G = \rho(V_s)^2$, which increases sharply with an increase in confinement (Seed and Idriss, 1970; Kim and Stokoe, 1992). Both G_{max} and D_{min} reach approximately asymptotic values after the first five hours elapsed under constant σ_0'; hence, it can be concluded that, for the time frame investigated herein (up to 24 h), the effect of time is negligible after primary consolidation of the specimen, which was found to be achieved between 4 and 7 h (Wattanasanticharoen, 2000). Values of G_{max} and D_{min} obtained at 24 h are used herein for further analyses on natural soil.

Figure 32.3 shows the variation of G_{max} with time t, for different compaction moisture contents w and confining pressures σ_0', for specimens treated with 5% cement. Figures 32.4 to 32.6 show the same information for specimens treated with 10% cement, fly ash, and lime + fibers, respectively. As with natural (control) soil, no noticeable changes in G_{max} and D_{min} are observed after the first 5 h elapsed under constant σ_0' for any of the treatment

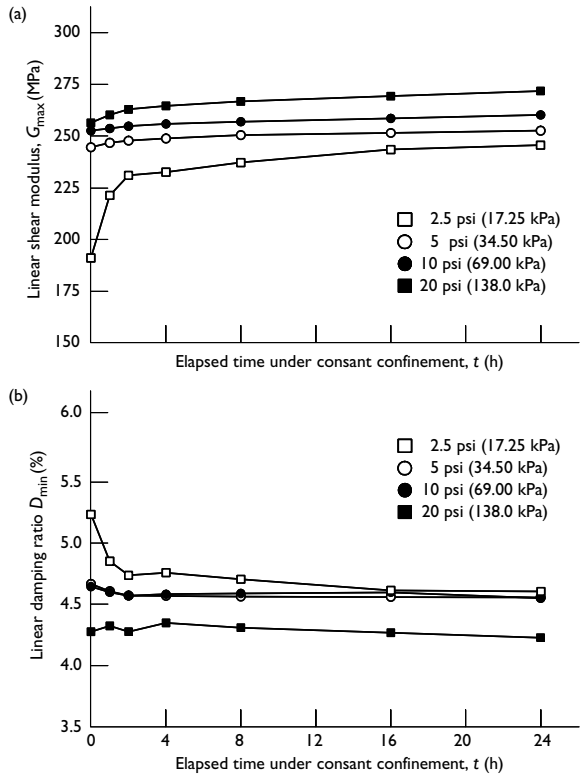

Figure 32.2 Variation in G_{max} and D_{min} with time t for natural sulfate-rich clay.

methods. Hence, values of G_{max} and D_{min} obtained at 24 h are also used herein for further analyses on treated soil.

Modulus response

The influence of compaction moisture content w on the dynamic response of treated specimens is clearly observed in Figure 32.7, where G_{max} has been plotted as function of σ_0', on the basis of w, for all treated specimens. As expected, in all cases G_{max} increases with an increase in σ_0', with a tendency to reach approximately asymptotic values for higher σ_0'. The influence of w, however, varies from one stabilizer to another. Treated specimens compacted at optimum moisture content do not necessarily yield highest G_{max}.

In general, G_{max} from all treatments is highly susceptible to even slight changes in w, with the most dramatic cases observed in cement-treated specimens. This can be attributed to the fact that stiffness enhancement in treated soils is highly dependent on the cementitious nature of each stabilizer. Chemical stabilizers, upon hydration, produce cementing gels and

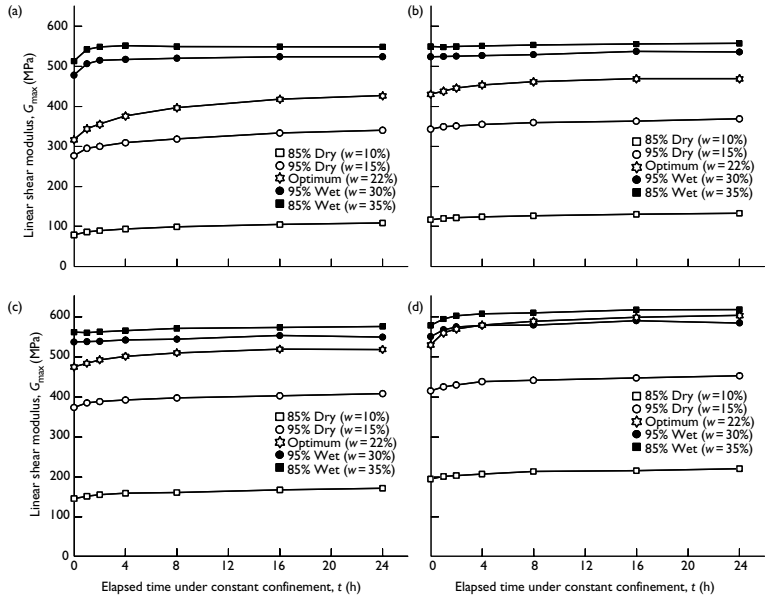

Figure 32.3 Variation in G_{max} and D_{min} with time t for 5% Type V cement-treated soil: (a) $\sigma_0' = 2.5$ psi (17.25 kPa); (b) $\sigma_0' = 5$ psi (34.5 kPa); (c) $\sigma_0' = 10$ psi (69 kPa); and (d) $\sigma_0' = 20$ psi (138 kPa).

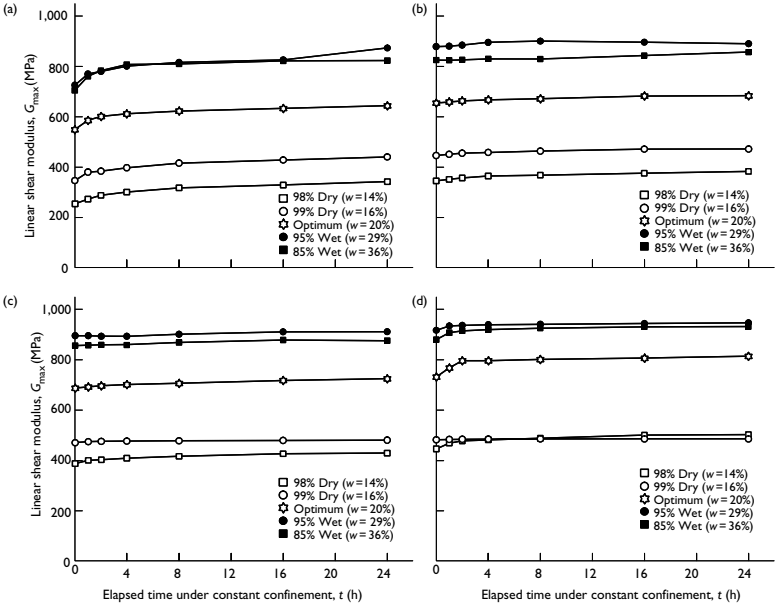

Figure 32.4 Variation in G_{max} and D_{min} with time t for 10% Type V cement-treated soil: (a) $\sigma_0' = 2.5$ psi (17.25 kPa); (b) $\sigma_0' = 5$ psi (34.5 kPa); (c) $\sigma_0' = 10$ psi (69 kPa); and (d) $\sigma_0' = 20$ psi (138 kPa).

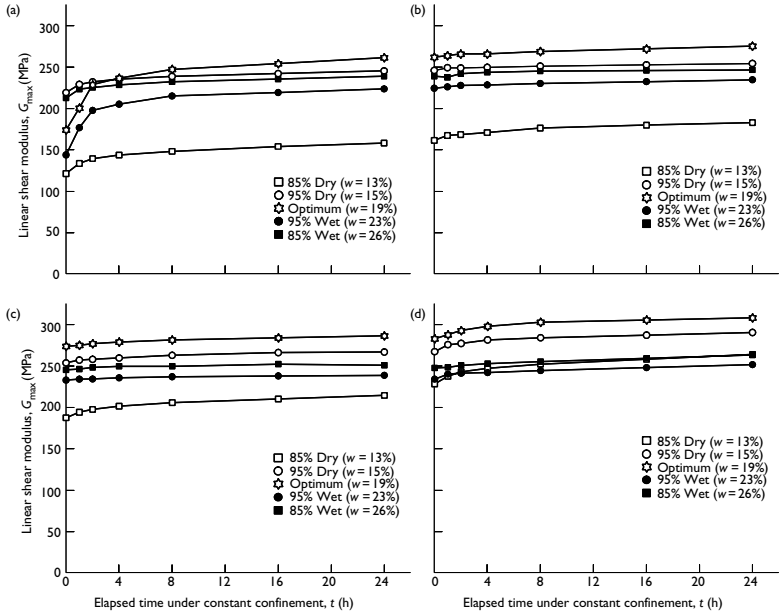

Figure 32.5 Variation in G_{max} and D_{min} with time t for class F fly ash-treated soil: (a) $\sigma_0' = 2.5$ psi (17.25 kPa); (b) $\sigma_0' = 5$ psi (34.5 kPa); (c) $\sigma_0' = 10$ psi (69 kPa); and (d) $\sigma_0' = 20$ psi (138 kPa).

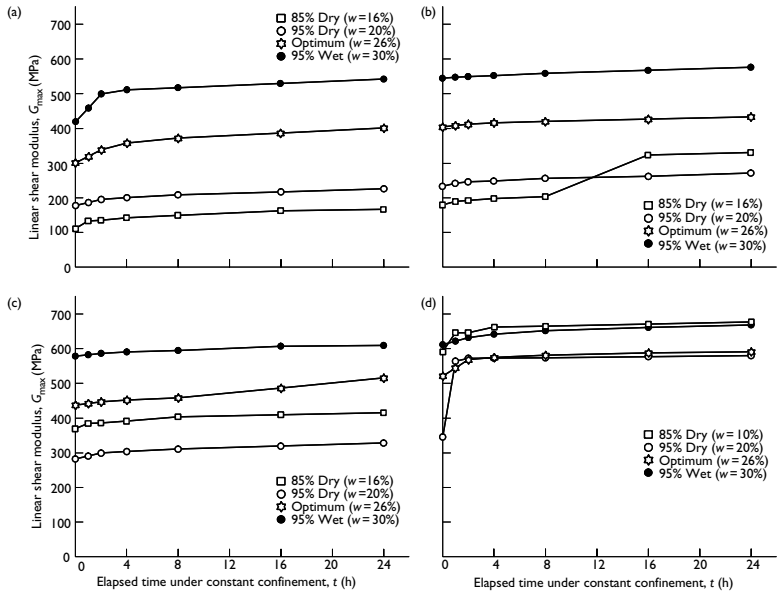

Figure 32.6 Variation in G_{max} and D_{min} with time t for lime + fibers-treated soil: (a) $\sigma_0' = 2.5$ psi (17.25 kPa); (b) $\sigma_0' = 5$ psi (34.5 kPa); (c) $\sigma_0' = 10$ psi (69 kPa); and (d) $\sigma_0' = 20$ psi (138 kPa).

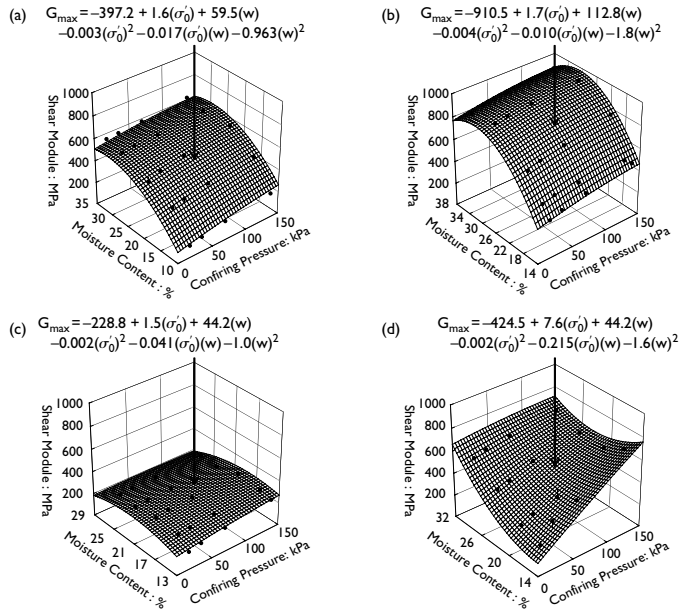

Figure 32.7 Variation of G_{max} with σ_0' for specimens treated with: (a) 5% Type V cement; (b) 10% Type V Cement; (c) Class F fly ash; and (d) lime + fibers.

compounds that stiffen the structure of treated specimens. It can be noted that highly cementitious stabilizers, such as Type V cement, yield highest G_{max} at higher levels of hydration (wet of optimum). Cement-treated specimens prepared with moisture contents on the wet side of optimum give G_{max} values approximately two times higher than those prepared on the dry side.

On the other hand, less cementitious stabilizers, such as Class F fly ash, yield highest G_{max} at or close-to optimum on the dry side of Proctor curve. However, fly ash-based treatment does not contribute significantly to an increase in soil's moduli. Moreover, the 5% cement- and lime/fibers-based treatments yield similar G_{max} responses. All these observations stress the need for a cautious selection of compaction moisture content, and ought to be taken into account when potential variations in moisture conditions during soil compaction operations in the field are expected.

Solid lines in Figure 32.7 represent best-fit, power regression functions of the form:

$$G_{max} = A\,(\sigma_0')^B \tag{32.1}$$

where constant A represents G_{max} (MPa) at $\sigma_0' = 1$ kPa, and constant B is representative of the soil's susceptibility to changes in σ_0' (i.e. slope of best-fit solid curves in Figure 32.7). Power regression constants A and B from Equation 32.1 used in Figure 32.7 are summarized in Table 32.2. It can be noted that the soil's susceptibility to changes in σ_0' (constant B) tends to decrease as the treated specimen is compacted with the moisture content w that yields highest G_{max}. Again, this is more evident in cement-treated specimens.

Table 32.2 Values of best-fit power regression constants used in Equations 32.1 and 32.2

Treatment method (1)	*Density level (%) (2)*	*w (%) (3)*	*Equation 32.1*			*Equation 32.2*			
			A (4)	*B (5)*	r^2 *(6)*	*a (7)*	*b (8)*	*c (9)*	r^2 *(10)*
Natural soil	OPT	21	214	0.05	0.99	—	—	—	—
5% cement	85 D	10	41	0.34	0.99	145	1.28	0.25	0.99
	95 D	15	230	0.14	0.99	154	1.21	0.39	0.90
	OPT	22	266	0.16	0.98	159	1.15	0.65	0.97
	95 W	30	452	0.05	0.92	153	1.12	1.09	0.98
	85 W	35	464	0.05	0.90	148	1.08	1.22	0.97
10% cement	98 D	14	202	0.18	0.99	145	1.28	0.25	0.99
	99 D	16	395	0.04	0.85	154	1.21	0.39	0.90
	OPT	20	468	0.11	0.97	159	1.15	0.65	0.97
	95 W	29	782	0.04	0.98	153	1.12	1.09	0.98
	85 W	36	700	0.06	0.97	148	1.08	1.22	0.97
Fly ash	85 D	13	78	0.25	0.99	992	1.44	0.15	0.99
	95 D	15	193	0.08	0.96	992	1.44	0.15	0.99
	OPT	19	209	0.08	0.99	992	1.44	0.15	0.98
	95 W	23	192	0.05	0.97	985	1.43	0.12	0.92
	85 W	26	210	0.04	0.97	1,050	1.41	0.07	0.90
Lime + fibers	85 D	16	29	0.64	0.97	159	1.12	0.96	0.97
	95 D	20	104	0.27	1.00	159	1.15	0.69	0.94
	OPT	26	227	0.19	0.98	159	1.14	0.75	0.95
	95 W	30	408	0.10	0.98	159	1.13	0.89	0.92

Damping response

Figure 32.8 shows the variation of D_{min} with σ'_0, on the basis of w, for all treated specimens. Even though the behavioral trends of D_{min} are not as clearly defined as those of G_{max}, it is observed that the damping response in all cases is also highly susceptible to even slight changes in w. In general, an increase in σ'_0 causes a decrease in D_{min}, but its influence is not as pronounced as on G_{max} (Figure 32.7). Except for the case of fly ash-treated specimens, the scatter in D_{min} data makes it difficult to perform power regression analyses of the form given in Equation 32.1. Cement-based treatments give lowest D_{min}, whereas fly ash-based treatment does not affect soil's damping response. These stress-dependent G_{max} and D_{min} behavioral trends observed in chemically treated sulfate-rich clay are similar to those reported on weakly cemented and fiber-reinforced sands (Chang and Woods, 1987; Maher and Woods, 1990).

Non-linear dynamic response

Threshold strain

Dynamic properties measured at shear strain amplitude levels below a threshold limit γ_{th} are referred to as linear (low-amplitude) shear modulus G_{max} and damping ratio D_{min}. If soils are strained to levels greater than γ_{th}, the soil does not exhibit linear elastic behavior as it undergoes strain softening or degradation (Seed and Idriss, 1970; Isenhower, 1979;

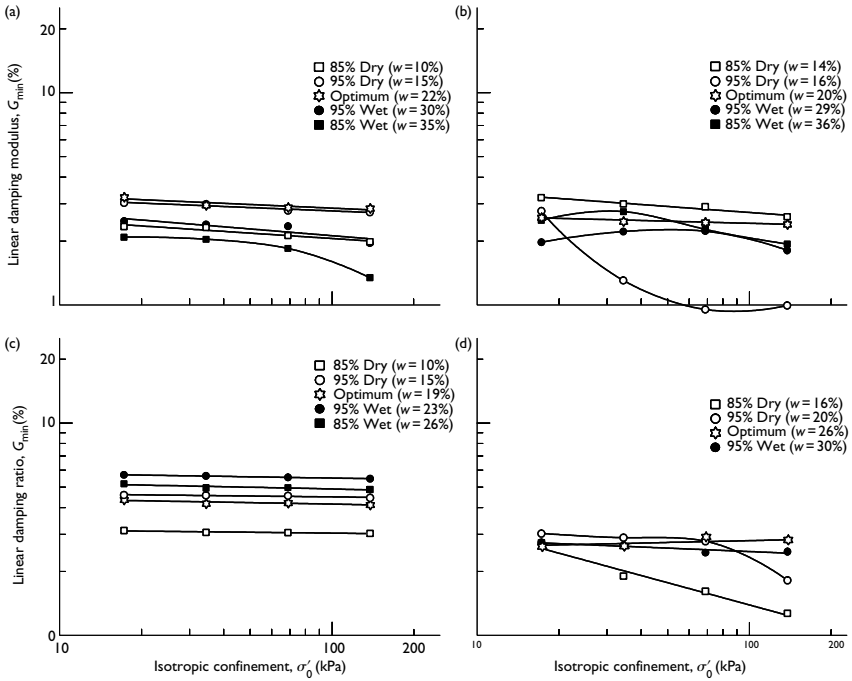

Figure 32.8 Variation of D_{min} with σ'_0 for specimens treated with: (a) 5% Type V cement; (b) 10% Type V cement; (c) Class F fly ash; and (d) lime + fibers.

Dobry *et al*., 1981, 1982; Huoo-Ni, 1987). In this work, G_{max} and D_{min} were found to remain constant when the specimens were strained at levels less than 0.0001% (10^{-6} cm/cm). To establish a threshold limit γ_{th} it is necessary to conduct small- to mid-shear strain amplitude RC testing, such that shearing strains γ surpass the linear range into a region where soil's response become strongly strain dependent. In this work, RC test specimens were subjected to different input-voltage amplitudes ranging from 0.25 to 5 V from the DSA, thus generating a family of frequency response curves with different resonant frequencies f_r and peak strain amplitudes A_{rms}, from which G and γ are calculated (Isenhower, 1979; Huoo-Ni, 1987; Stokoe *et al*., 1991).

A typical process of softening (degradation) of treated soil is illustrated in Figure 32.9(a) for specimen FA-85D (Table 32.1). The non-linearity of soil's response is manifested by the so-called back-bone curve in Figure 32.9(b). Even though past cycling at mid-to-high shear strain amplitudes has been reported not to have any effect on the recovery of G and D with an increase in σ'_0 (Hardin and Drnevich, 1972; Stokoe *et al*., 1980), small- to mid-shear strain amplitude RC tests were conducted at $\sigma'_0 = 138$ kPa (20 psi), since the only two-fold purpose was to determine an apparent γ_{th} for treated soil and to study the influence of w on the rate of degradation of normalized modulus G/G_{max}.

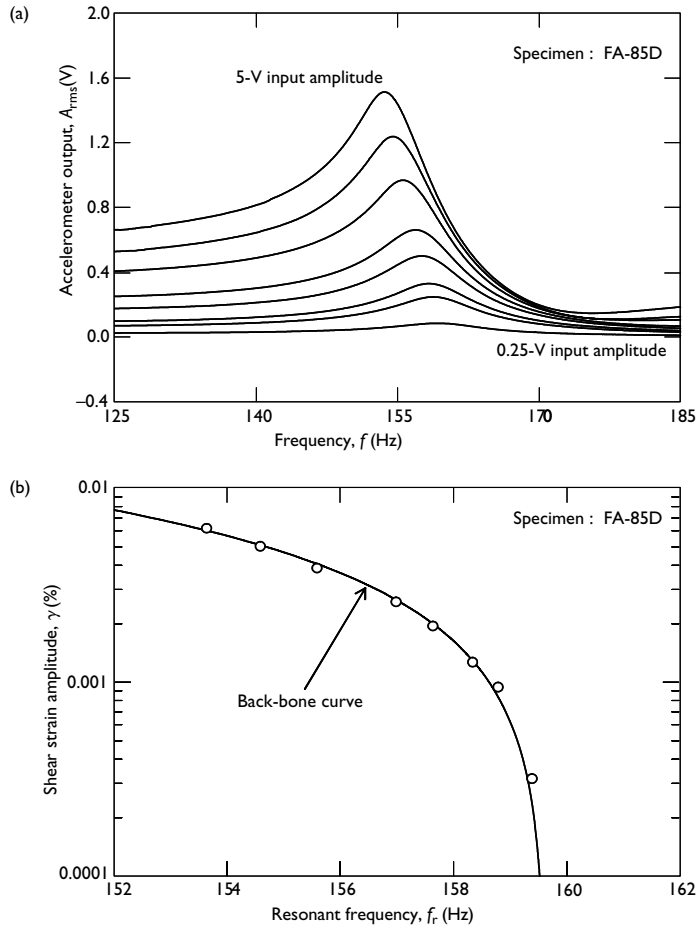

Figure 32.9 Material softening: (a) typical response at small- to mid-shear strain amplitude; and (b) back-bone curve.

Modulus degradation

Figure 32.10 shows the variation of normalized shear modulus G/G_{max} with shear strain amplitude γ, on the basis of compaction moisture content w, for all treated specimens. The influence of w on the rate of degradation of G varies from one stabilizer to another, with the most dramatic cases observed in cement-treated specimens, which are highly susceptible to even slight changes in w. For the case of fly ash- and lime/fibers-based treatments, values of G/G_{max} fall into a narrow band, hence, the influence of w was almost negligible.

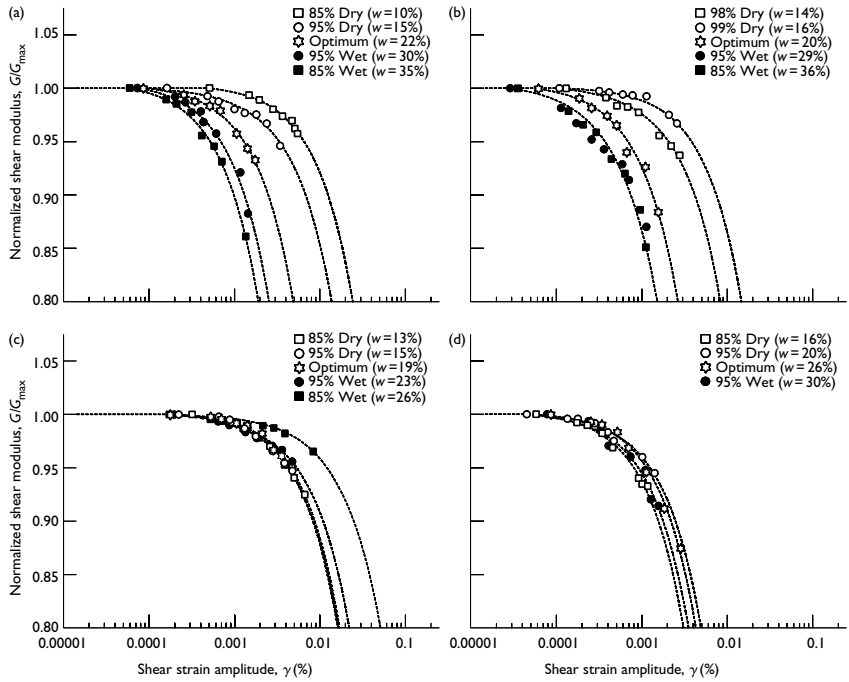

Figure 32.10 Variation of G/G_{max} with γ for specimens treated with: (a) 5% Type V cement; (b) 10% Type V cement; (c) Class F fly ash; and (d) lime + fibers.

Moreover, specimens treated at moisture contents corresponding to highest values of G_{max} present lower values of induced shear strain γ (i.e. higher torsional shear resistance).

Dotted lines in Figure 32.10 represent best-fit, power regression functions of the form:

$$\frac{G}{G_{max}} = \frac{1}{\{1 + a(\gamma)^b\}^c} \tag{32.2}$$

where constants *a, b*, and *c* represent the decay rate of G/G_{max} with an increase in shear strain amplitude γ (Borden *et al*., 1996). Power regression constants *a, b*, and *c* from Equation 32.2 used in Figure 32.10 are also summarized in Table 32.2. Even though the coefficients of determination r^2 in Equation 32.2 ranged from 0.90 to 0.99, the torsional shear (TS) approach will be the correct choice to obtain further data beyond the 0.01% strain level achieved in this study, facilitating a more reliable calculation of constants *a, b*, and *c* (Seed and Idriss, 1970; Kim and Stokoe, 1992; Borden *et al*., 1996).

From Figure 32.10, the apparent threshold strain limit γ_{th} for all treatment methods appears to range from 0.001% (10^{-5} cm/cm) to 0.01% (10^{-4} cm/cm). Figure 32.11 shows the variation of

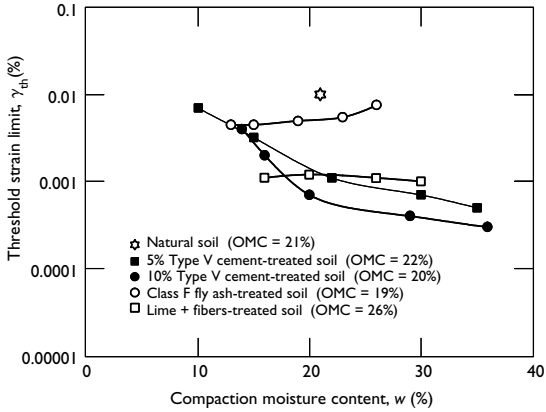

Figure 32.11 Influence of compaction moisture content w on threshold strain limit γ_{th}.

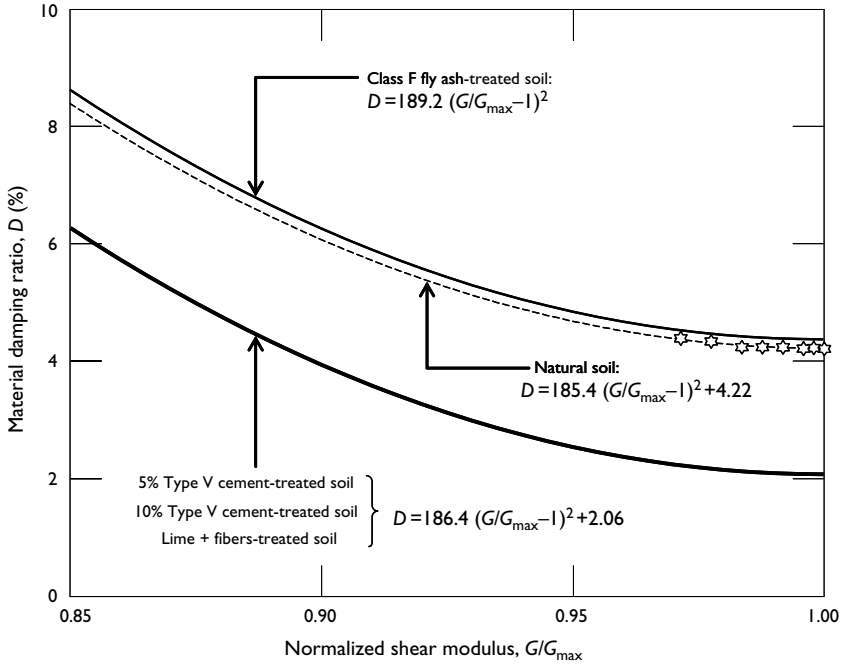

Figure 32.12 Best-fit variation of damping D with G/G_{max} for natural and treated specimens.

γ_{th} with compaction moisture content w, for all treatment methods, using the $G = 0.95(G_{max})$ criterion in Figure 32.10. It was observed that all treatment methods tended to decrease the γ_{th} limit of natural soil, except for the fly ash-based treatment, which gave similar γ_{th} to that of natural soil at high w. As with G_{max} and D_{min}, the influence of w on γ_{th} values varied from one stabilizer to another, with the most drastic changes in cement-treated specimens, which, again, were highly susceptible to even slight changes in w. The influence of w on γ_{th} values for fly ash- and lime/fibers-treated soils was almost negligible. In general, specimens treated at moisture contents corresponding to highest values of G_{max} present lower values of induced γ_{th}.

Useful D-G/G_{max} relationships can also be devised from the series of small- to mid-shear strain amplitude RC tests, as shown in Figure 32.12. This figure shows the variation of damping ratio D with G/G_{max}, on the basis of w, for all treated specimens. Even though w exerts a remarkable influence on individual values of D, with a $+/-$ 1% standard deviation in all treatment methods, its influence on the rate of increase in D, as the material softens, was almost negligible.

Solid lines in Figure 32.12 represent best-fit regression functions of the form:

$$D = m(G/G_{max} - 1)^2 + n \tag{32.3}$$

where constant n represents values of damping D(%) for $G/G_{max} = 1$ (i.e. D_{min}), and constant m is representative of the rate of increase in D as the material softens when sheared from small- to mid-shear strain amplitude levels (Borden *et al.*, 1996; Hoyos and Macari, 1999). Coefficients of determination r^2 ranged from 0.93 to 0.95. In general, all treatment methods yield similar m values, that is, similar rate of increase in D as the material softens. However, a remarkable decrease in D (i.e. constant n) is observed for cement-and lime/fibers-treated soils.

Concluding remarks

G_{max} from all treatment methods was highly susceptible to even slight changes in compaction moisture content w, with the most dramatic cases observed in Type V cement-treated specimens. Even though behavioral trends for D_{min} were not as clearly defined as those for G_{max}, all treated specimens were highly susceptible to changes in w when it comes to damping response. The 10% Type V cement-treated soil, compacted at 95% $\gamma_{d\text{-}max}$ wet of optimum, gave highest G_{max} values among all treated specimens.

The influence of w on the rate of decay of G from small- to mid-shear strain amplitudes varied from one stabilizer to another, with the most dramatic cases observed in cement-treated specimens. Specimens treated at moisture contents corresponding to highest values of G_{max} gave lower values of induced shear strain γ. Most treatment methods tended to decrease the threshold strain limit γ_{th} of natural soil. Apparent γ_{th} values from all treatment methods ranged from 0.001% (10^{-5} cm/cm) to 0.01% (10^{-4} cm/cm). The influence of compaction moisture content w on γ_{th} varied from one stabilizer to another, with the most drastic changes occurring in cement-treated specimens. Results summarized herein further corroborate previous findings by authors on similar clayey soils and chemical stabilizers.

Notation

The following symbols are used in this chapter:

A, B best-fit power regression constants for $G_{max} = A(\sigma'_0)^B$;

A_{rms} peak strain amplitude (V);

a, b, c best-fit power regression constants for $G/G_{max} = G/G_{max}(\gamma)$;
CF clay fraction (%);
D material damping ratio (%);
D_{min} linear (low-amplitude) damping ratio (%);
f frequency (Hz);
f_r resonant frequency (Hz);
G dynamic shear modulus (MPa);
G_{max} linear (low-amplitude) shear modulus (MPa);
G_s soil specific gravity;
LL liquid limit (%);
m, n best-fit power regression constants for $D = D(G/G_{max})$;
OMC optimum moisture content (%);
PI plasticity index (%);
PL plastic limit (%);
r^2 coefficient of determination;
t elapsed time (h);
V_s shear wave velocity (cm/s);
w compaction moisture content (%);
w_n natural moisture content (%);
γ shear strain amplitude (% or cm/cm);
γ_d soil dry unit weight (kN/m^3);
$\gamma_{d\text{-}max}$ maximum dry unit weight (kN/m^3);
γ_{th} threshold strain limit (% or cm/cm);
ρ soil mass density (Mg/m^3); and
σ'_0 effective isotropic confining pressure (kPa).

Acknowledgments

This research work was funded by the UTA Research Enhancement Program and the Cement and Concrete Promotion Council of Texas. This support is gratefully acknowledged. The writers also thank BMT for providing the polypropylene fibers.

References

Atkins, H.N. (1983). *Highway Materials, Soils and Concretes*. 2nd Edn, Reston Publishing Co., Reston, VA.

Borden, R.H., Shao, L., and Gupta, A. (1996). "Dynamic properties of Piedmont residual soils." *J. Geotech. Eng., ASCE*, 122(10), 813–821.

Chang, Y.J. and Woods, R.D. (1987). "Effect of confining stress on shear modulus of cemented sands." *Soil-Structure Interaction*. A.S. Cakmak, ed., Elsevier Science, New York.

Dobry, R., Yokel, F.Y., and Ladd, R.S. (1981). "Liquefaction potential of over-consolidated sands in moderately seismic areas." *Proceedings, Conference on Earthquake and Earthquake Engrg in the Eastern US*, Knoxville, TN, Vol. 2, 643–664.

Dobry, R., Ladd, R.S., Yokel, F.Y., Chung, R.M., and Powell, D.J. (1982). "Prediction of pore pressure buildup and liquefaction of sands during earthquakes by the cyclic strain method." *Nat. Bur. Stand. Build. Sci. Series*, 138.

Hardin, B.O. and Drnevich, V.P. (1972). "Shear modulus and damping in soils: design equations and curves." *J. Soil Mech. Found. Div., ASCE*, 98(7), 667–692.

Hausmann, M.R. (1990). *Engineering Principles of Ground Modification*. McGraw-Hill, New York.

Hoyos, L.R. and Macari, E.J. (1999). "Influence of in situ factors on dynamic response of Piedmont residual soils." *J. Geotech. Geoenviron. Eng., ASCE*, 125(4), 271–279.

Hunter, D. (1988). "Lime-induced heave in sulfate-bearing clay soils." *J. Geotech. Eng., ASCE*, 114(2), 150–167.

Huoo-Ni, S. (1987). "Dynamic properties of sand under true triaxial stress states from resonant column/torsional-shear tests," PhD dissertation, University of Texas, Austin, TX.

Isenhower, W.M. (1979). "Torsional simple shear/resonant column properties of San Francisco Bay mud," Thesis GT80–1, Geotech. Engrg Ctr., Univerity of Texas at Austin, Austin, TX.

Kim, D.S. and Stokoe, K.H. (1992). "Characterization of resilient modulus of compacted subgrade soils using resonant column and torsional shear tests." *Transportation Research Record No. 1369*, Transportation Research Board, Washington, DC, 83–91.

Kota, P.B.V.S., Hazlett, D., and Perrin, L. (1996). "Sulfate-bearing soils: problems with calcium based stabilizers." *Transportation Research Record No. 1546*, Transportation Research Board, Washington, DC, 62–69.

Maher, M.H. and Woods, R.D. (1990). "Dynamic response of sands reinforced with randomly distributed fibers." *J. Geotech. Eng., ASCE*, 116(7), 1116–1131.

Mamlouk, M.S. and Zaniewski, J.P. (1999). *Materials for Civil and Construction Engineers*. Addison Wesley, Manlo Park, CA.

Mitchell, J.K. and Dermatas, D. (1990). "Clay soil heave caused by lime-sulfate reactions." *ASTM Specification Publication No. 1135*, ASTM, 41–64.

Nelson, D.J. and Miller, J.D. (1992). *Expansive Soils: Problems and Practice in Foundation and Pavement Engineering*, John Wiley & Sons, New York.

Petry, M.T. and Little, N.D. (1992). "Update on sulfate-induced heave in treated clays: problematic sulfate levels." *Transportation Research Record No. 1362*, Transportation Research Board, Washington, DC, 51–55.

Prusniski, J. and Bhattacharya, S. (1999). "Effectiveness of Portland cement and lime in stabilizing clay soils." *Transportation Research Record No. 1652*, Transportation Research Board, Washington, DC, 215–227.

Puppala, A.J., Hoyos, L.R., Viyanant, C., and Musenda, C. (2001). "Fiber and fly ash stabilization methods to treat soft expansive soils." *Proceedings, Soft Ground Technology Conference*, Noordwijkerhout, The Netherlands, ASCE Geotech. Spec. Pub. No. 112, 136–145.

Puppala, A.J., Griffin, J.A., Hoyos, L.R., and Chomtid, S. (2002). "Assessments of sulfate resistant stabilization methods to counter sulfate induced heave problems." *CD-ROM Proceedings, 81st TRB Annual Meeting*, Transportation Research Board, Washington, DC.

Richart, F.E., Hall, Jr. J.R., and Woods, R.D. (1970). *Vibrations of Soils and Foundations*. Prentice-Hall, Inc., Englewood Cliffs, NJ.

Rollings, R.S., Burkes, J.P., and Rollings, M.P. (1999). "Sulfate attack on cement-stabilized sand." *J. Geotech. Geoenviron. Eng., ASCE*, 125(5), 364–372.

Seed, H.B. and Idriss, I.M. (1970). "Soil moduli and damping factors for dynamic response analysis." *Report EERC 70-10*. Earthquake Engineering Research Center, University of California at Berkeley, Berkeley, CA.

Sherwood, P.T. (1995). *Soil Stabilization with Cement and Lime*. HMSO Publication Center, London, 14–55.

Stokoe, K.H., Isenhower, W.M., and Hsu, J.R. (1980). "Dynamic properties of offshore silty samples." *OTC 3771*, Offshore Technology Conference, Houston, TX.

Stokoe, K.H., Nasir, S.H., and Andrus, R.D. (1991). "In-situ and laboratory measurements of the dynamic properties of cemented granular soils: a case history." *US/Brazil Geotech. Engrg. Workshop*, A.S. Nieto, ed., University of Illinois, Urbana, IL, 1–39.

"Test methods for modulus and damping of soils by the resonant column method." (1993). *Standard D 4015–92*, ASTM, Philadelphia, PA, 581–593.

Wattanasanticharoen, E. (2000). "Laboratory investigations on four novel treatment methods to stabilize soft subgrade soils of southeast Arlington." MS thesis, University of Texas at Arlington, Arlington, TX.

Chapter 33

Assessment of seasonal effects on engineering behavior of chemically treated sulfate-rich expansive clay

Laureano R. Hoyos,[1] *Arthit Laikram*,[2] *and Anand J. Puppala*[3]

Summary

A comprehensive series of unconfined compression (UC), unconsolidated undrained (UU) triaxial, and resonant column (RC) tests were conducted on chemically stabilized specimens of sulfate-rich expansive clay from southeast Arlington, Texas, after being subjected to repeated wetting-drying (w-d) cycles artificially induced in the laboratory. Results were used to assess the influence of cyclic w-d on long-term strength, stiffness, and one-dimensional (1-D) swell-shrink response of treated soil, including unconfined compressive strength, undrained shear strength parameters, dynamic shear modulus, and material damping. Stabilization methods included sulfate-resistant type V cement, low-calcium class F fly ash, and quick lime mixed with polypropylene fibers. Treated soil specimens were cured for 7 days and then subjected to 0, 1, 2, 4, 8, 16, and 32 w-d cycles prior to UC, UU, and RC testing. A w-d cycle consisted of 12-h immersion in a potable-water bath at room temperature followed by 12-h drying in oven at 140°F. Custom made w-d chambers allow for the monitoring of 1-D swell-shrink response during repeated w-d. A 10%-by-weight dosage of type V cement appears to yield best overall performance under cyclic w-d.

Introduction

Chemical stabilization of high-plasticity expansive soils using calcium-based stabilizers, such as lime and ordinary Portland cement, presents some limitations in soils containing large amounts of sulfates. Calcium in lime or cement-based stabilizers react with sulfates and reactive alumina liberated in the natural soil to form ettringite mineral, a weak and unstable crystalline mineral that undergoes significant heaving when exposed to hydration. This sulfate-induced heave is known to severely affect the performance of residential and highway infrastructure in most southern and southwestern states of the US (Hunter, 1988; Mitchell and Dermatas, 1990; Petry and Little, 1992; Kota *et al.,* 1996; Rollings *et al.*, 1999).

A series of studies have recently been conducted at The University of Texas at Arlington to evaluate the effectiveness of several sulfate-resistant cementitious and recycled stabilizers

[1] Department of Civil & Environmental Engrg, University of Texas at Arlington, Arlington, Texas 76019. Tel: (817) 272 3879. Fax: (817) 272 2630; e-mail: lhoyos@uta.edu

[2] Department of Civil & Environmental Engrg, University of Texas at Arlington, Arlington, Texas 76019.

[3] Department of Civil & Environmental Engrg, University of Texas at Arlington, Arlington, Texas 76019.

for treating soft, sulfate-rich expansive clays from various locations in the city of Arlington, Texas. Testing programs have included Atterberg limits, linear shrinkage, 1-D, and 3-D swelling, unconfined compression, unconsolidated undrained triaxial, and resonant column testing (Wattanasanticharoen, 2000; Chainuwat, 2001; Puppala *et al.*, 2001, 2004; Hoyos *et al.*, 2004).

Investigated stabilizers were found to exert an immediate, positive influence on the strength-stiffness response and swell-shrink potential of treated soil. However, all treated soil specimens were prepared and tested at or close-to optimum moisture content. As moisture conditions in the field are expected to change drastically throughout the year, a thorough study on potential effects of cyclic wetting-drying (w-d) on the long-term performance of treated soil is greatly needed. The present work is motivated by this research need.

Findings from a recent work by Takkabutr (2002) showed decreasing strength-stiffness trends in all treated soils after being subjected to eight w-d cycles artificially induced in the laboratory. Strength reductions were on the order of 30% but lacked a definite trend, while none of the treated specimens reached a well-defined swell-shrink equilibrium state, all of which made it difficult to draw substantial conclusions as to the full effects of sustained cyclic w-d on soil strength and volume change behavior. The present research work is an attempt to overcome these limitations by further increasing the number of w-d cycles while thoroughly monitoring the swell-shrink and strength-stiffness response of treated soils under repeated w-d.

The main objective of the research work reported in this chapter was to investigate the effects of cyclic w-d on strength, stiffness, and swell-shrink response of chemically stabilized specimens of sulfate-rich expansive clay from southeast Arlington, Texas. In order to achieve this goal, a comprehensive series of UC (ASTM D2166), UU triaxial (ASTM D2850), and RC (ASTM D4015-92) tests were conducted on compacted specimens of natural and treated clay after being subjected to repeated w-d cycles artificially induced in the laboratory.

Three stabilization methods were used: sulfate resistant type V cement, low calcium class F fly ash, and lime mixed with polypropylene fibers. Soil specimens were prepared at best-performance stabilizer dosages, moisture contents, and curing period assessed from previous studies at UT-Arlington (Wattanasanticharoen, 2000; Chainuwat, 2001). Custom made w-d chambers allow for the monitoring of vertical swell-shrink during cyclic w-d. Results from the series of UC, UU, and RC tests are used to assess the influence of cyclic w-d on unconfined compressive strength, undrained shear strength parameters, and dynamic shear modulus and material damping of both untreated and treated soils.

Test variables

Test soil and chemical stabilizers

Test soil was sampled from southeast Arlington, Texas. It is a high-plasticity, sulfate-rich clay, dark yellow in color, with natural moisture content $w_n = 6.6\%$, fines content (minus No. 200) = 73%, clay fraction (CF) = 25%, standard Proctor optimum moisture content (OMC) = 21%, maximum dry unit weight $\gamma_{d\text{-}max} = 16.46$ kN/m^3, specific gravity $G_s = 2.85$, liquid limit (LL) = 74%, plasticity index (PI) = 45%, and soluble sulfate content = 33,048 ppm (mg/l). The soil classifies as A-7-6 and CH according to AASHTO (American Association of State Highway and Transportation Officials) and USCS (Unified Soil Classification System) respectively.

Table 33.1 Best-performance stabilizer dosages and compaction moistures

Treatment method	*Moisture content, w(%)*	*Dry unit weight, γ_d (kN/m^3)*	*Curing period (days)*
Natural (control) soil	21	16.4	7
5% type V cement	35	13.3	7
10% type V cement	29	15.1	7
20% class F fly ash	15	16.0	7
8% lime + 0.3% fibers	30	14.6	7

Sulfate-resistant Type V cement used in this research work has a 32,175-kPa (4,663-psi) compressive strength at 7 days, and contains 62.6% of Calcium oxide (CaO). Low-calcium class F fly ash contains only 1.1% of CaO. Polypropylene fibers are made of 100% virgin, fibrillated polypropylene with normal fiber length = 1.9 cm (0.75 in.), tensile strength = 0.67 KN/mm^2 (97 ksi), and high resistance to alkali, salt, and acids. Further details on selected stabilizers are presented by Chainuwat (2001) and Hoyos *et al.* (2004).

Experimental variables

Stabilizer dosages (by-weight of dry soil) and compaction moisture contents used herein are reported to yield best performance after a seven-day curing period (Chainuwat, 2001). Best-performance stabilizer dosages and compaction moistures are summarized in Table 33.1. Cement dosage levels also represent those traditionally used by the Texas Department of Transportation in ordinary Portland cement-based treatments. Natural and treated soil specimens were subjected to repeated w-d cycles (0, 1, 2, 4, 8, 16, and 32 w-d cycles) in custom fabricated w-d chambers prior to UC, UU, and RC testing. A w-d cycle consisted of 12-h immersion in a potable-water bath at room temperature followed by 12-h placing in an oven. During drying stage, oven temperature was set to 140°F, artificially creating a "quick-aging" environment in the laboratory. This is also the temperature at which soil-lime mixtures are dried in Texas SDHPT Test Method Tex-121-E (Rogers and Wright, 1986). The range of confining pressures during UU and RC testing, that is 17.25, 34.5, 69, and 138 kPa (2.5, 5, 10, and 20 psi), is aimed at reproducing in situ stress states within subgrade foundation systems supporting highways.

Test program

Specimen preparation

Standard Proctor compaction tests were first performed on natural and treated soils. In each case, the desired moisture (Table 33.1) was determined via the obtained Proctor curve (Hoyos *et al.*, 2004). Pulverized air-dry soil was then thoroughly mixed with required amounts of water and stabilizer until ensuring homogeneity. Mixed soil was then compacted in three equal layers into a 3.5-cm (1.4-in.) diameter, 8.0-cm (3.2-in.) height, stainless steel, split miter box using a 10-mm (0.4-in.) diameter spring hammer. After compaction, the specimen was gently extruded, covered with geotextile, stored in a sealed plastic bag, and kept under room temperature in a 100% humidity room for seven-day curing.

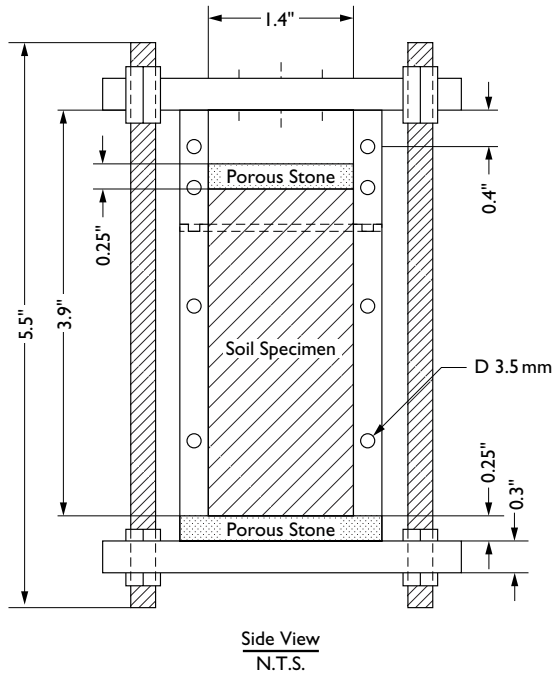

Figure 33.1 Cross sectional view of w-d chamber.

The cured specimen was then placed into a custom made, stainless steel, split w-d chamber (Figure 33.1). Top and bottom porous stones facilitate soil hydration during water-immersion stage. The top plate accommodates an analog dial gauge for continuous monitoring of vertical swell-shrink response. The gauge is attached to the top plate via a mounted extension rod, allowing the gauge to interact with the top stone inside the chamber. A total of 5 w-d chambers were fabricated for simultaneous testing of five identically prepared specimens.

Test procedure

A wetting stage was first initiated by soaking all 5 w-d chambers in a potable-water bath for 12 h at room-temperature conditions (72°F), as shown in Figure 33.2(a). Swell response was then recorded at 0, 1, 2, 4, 8, 16, 32, 60, 120, 240, 480, and 720 minutes (12 h). Immediately after wetting, a drying stage was initiated by transferring all 5 w-d chambers into an oven set at 140°F for 12 h, as shown in Figure 33.2(b). Shrink response was then recorded at same time intervals.

The above 24-h w-d process constitutes 1 w-d cycle, which aims to reproduce extreme wet-dry conditions in the field during any given day. After the desired number of w-d cycles

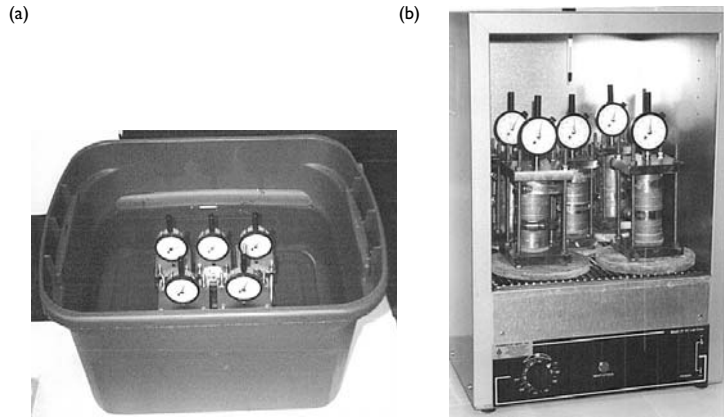

Figure 33.2 Cyclic w-d process: (a) 12-h wetting stage, and (b) 12-h drying stage.

was accomplished (i.e. 0, 1, 2, 4, 8, 16, or 32 w-d cycles), all 5 w-d chambers were soaked again in water for an additional 12 h. The main intent was to induce highest amount of saturation in all specimens prior to UC, UU, and RC testing. After this final 12-h wetting, all 5 chambers were retrieved from the water bath and allowed to come to equilibrium at room temperature for 1 h. Specimens were then trimmed to a 7.0-cm (2.8-in.) height and removed from the split chambers for UC, UU, and RC testing. One specimen was devoted to UC testing. Three others were devoted to UU testing at 17.25, 34.5, and 69 kPa (2.5, 5, and 10 psi) confinements. One last specimen was devoted to RC testing. All specimens were tested within 15 minutes after trimming.

During RC testing, an initial confinement, $\sigma_0' = 17.25$ kPa (2.5 psi), was applied to the specimen and kept constant for 2 h prior to testing. Upon test completion, σ_0' was increased to 34.5 kPa (5 psi) and kept constant for 2 h prior to testing. Same process was repeated for $\sigma_0' = 69$ and 138 kPa (10 and 20 psi). After the last test was completed, the specimen was immediately transferred to the triaxial cell for performing one more UU test at $\sigma_0' = 138$ kPa (20 psi). A total of 35 UC, 140 UU, and 140 RC tests were conducted. Soil's pH and moisture content, before and after cyclic w-d, were also monitored in order to assess any potential leaching of stabilizers.

Swell-shrink response

Figure 33.3 shows the 1-D swell-shrink response of natural and treated soil during cyclic w-d. Vertical axis represents the ratio of change in specimen height (ΔH) to initial height (H_0) in both swell and shrink test conditions. Plots correspond to experimental runs with 32 w-d cycles, and only the best representative sample of the five monitored is plotted (a maximum of $\pm 5\%$ variation in swell-shrink response was observed among all five specimens).

In general, the bandwidth of movement of treated soils decreases as the w-d cycles increase, with a tendency to reach a constant amplitude known as the "equilibrium bandwidth" of

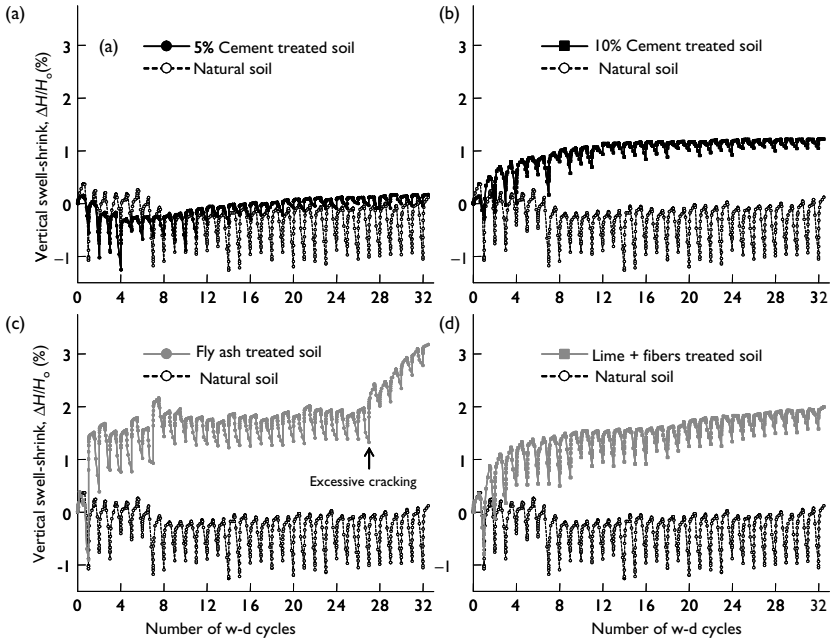

Figure 33.3 Swell-shrink response during cyclic w-d of soil treated with: (a) 5% type V cement, (b) 10% type V cement, (c) class F fly ash, and (d) lime + fibers.

movement (Rao and Tripathy, 2003). Although the natural soil specimen remains close to its original height after the last 12-h wetting, the equilibrium bandwidth is considerably high compared to that of any treated soil (over 280% that of the poorest performing stabilizer). This can be clearly seen in Figure 33.4 where the absolute amounts of swell at the end of each w-d cycle, relative to natural soil, are plotted. Similar findings have been reported by Day (1994) and Al-Homoud *et al.* (1995).

Treated soils show a tendency toward increase in overall specimen height after 32 w-d cycles. This can be attributed to moderate cracking observed within treated soil specimens during the first few w-d cycles, with the most extreme case observed in 10% cement treated soil, in which the highest amount of swell occurs after the first drying stage, as shown in Figures 33.3(b) and 33.4(b). Response of 5% cement treated soil appears to be excellent in terms of equilibrium bandwidth and overall $\Delta H/H_0$ after 32 w-d cycles. A relatively constant bandwidth was reached after 4 w-d cycles. This behavior may be indicative of continuing pozzolanic reactions (further curing) taking place during cyclic w-d.

Fly ash treated soil performed poorly, reaching equilibrium near 10 w-d cycles. Before reaching equilibrium, large amplitudes of movement and high overall swelling occurred. After 28 w-d cycles, further swelling develops, the extent of which is not fully devised. This can be attributed to both excessive cracking and possible stabilizer flush-out during cyclic w-d.

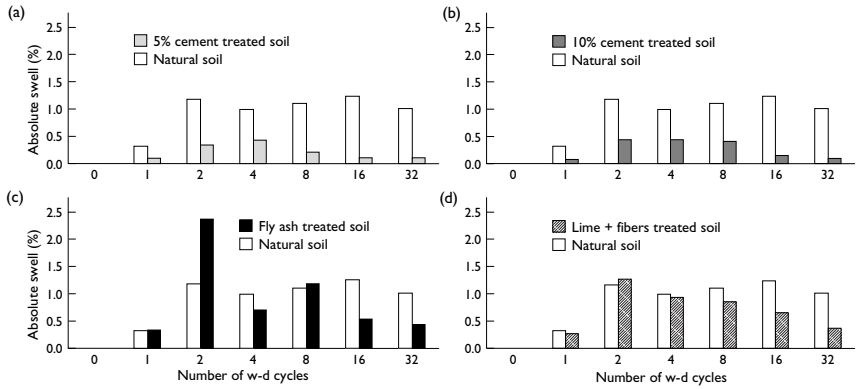

Figure 33.4 Absolute swell response of soil treated with: (a) 5% type V cement, (b) 10% type V cement, (c) class F fly ash, and (d) lime + fibers.

Table 33.2 Swell-shrink response relative to natural soil after 32 w-d cycles

Treatment method	*Vertical swell-shrink, $\Delta H/H_0$(%)*	*Equilibrium bandwidth relative to NS (%)*
Natural (control) soil	+0.12	100.0
5% type V cement	+0.17	18.5
10% type V cement	+1.22	15.0
20% class F fly ash	+3.18	33.8
8% lime + 0.3% fibers	+2.00	35.6

Response of lime + fibers treated soil followed that of fly ash treated soil, excluding the sudden swell increase after 28 w-d cycles. This can be attributed to the presence of fibers, which are known to enhance shrinkage cracking resistance (Puppala *et al.*, 2001). Lime + fibers treated soil, however, performed poorly relative to cement treated soils. It can be noted that prior to reaching equilibrium around 10 w-d cycles, a great amount of swelling occurred. Table 33.2 summarizes the overall swell-shrink performance of treated soils relative to that of natural soil.

In summary, type V cement provided best enhancements, followed by lime + fibers and fly ash treatments. It can be inferred from Figures 33.3 and 33.4 that both type V cement and lime + fibers treatments resulted in less shrinkage-related cracking of soil under sustained w-d, whereas a great deal of shrinkage-related cracking was observed in fly ash treated soils.

Unconfined compressive strength

Table 33.3 summarizes all UCS values obtained from natural and treated soils. The pH and moisture content of soil, before and after cyclic w-d, are also reported. Figure 33.5 shows change in UCS with w-d cycles for all treated soils, relative to natural soil. It can be noted

Table 33.3 Unconfined compressive strength (UCS) from UC tests

Number of w-d cycles	*UCS (psi)*	*UCS (kPa)*	*% Change*	*Initial w (%)*	*Final w (%)*	*Final pH (−)*	*Final pH (−)*
Natural soil							
0	26.5	182.9	0.0	21.0	21.0	7.4	7.4
1	16.9	116.6	−36.2	21.0	27.3	7.1	7.1
2	14.6	100.5	−45.1	21.0	28.2	7.6	7.0
4	12.1	83.5	−54.3	21.0	27.5	7.4	6.8
8	11.2	77.3	−57.7	21.0	26.9	7.1	6.6
16	10.7	73.6	−59.8	21.0	28.6	7.8	6.0
32	9.3	64.3	−64.8	21.0	26.2	7.5	5.6
5% Type V cement treated soil							
0	145.6	1004.6	0.0	35.0	34.3	9.9	9.6
1	82.4	568.5	−43.4	35.0	31.8	9.9	9.3
2	62.6	431.6	−57.0	35.0	34.9	10.1	9.6
4	59.3	409.4	−59.2	35.0	35.9	10.2	8.6
8	57.7	398.0	−60.4	35.0	31.8	9.9	8.4
16	48.8	336.8	−66.5	35.0	30.4	10.0	9.3
32	90.7	625.6	−37.7	35.0	36.8	10.3	8.3
10% Type V cement treated soil							
0	252.5	1742.3	0.0	29.0	29.5	10.1	10.0
1	174.2	1201.7	−31.0	29.0	30.8	10.1	9.7
2	198.3	1368.5	−21.5	29.0	30.2	10.1	9.5
4	210.7	1454.1	−16.5	29.0	28.8	10.0	9.4
8	277.7	1915.8	+10.0	29.0	32.3	10.1	9.2
16	279.3	1927.3	+10.6	29.0	33.2	10.0	8.7
32	310.6	2143.0	+23.0	29.0	36.1	10.0	9.4
20% Fly ash treated soil							
0	111.5	769.1	0.0	15.0	15.8	9.4	9.2
1	62.5	431.5	−43.9	15.0	18.7	9.4	8.4
2	55.8	384.9	−50.0	15.0	21.1	9.4	8.7
4	48.8	337.0	−56.2	15.0	23.2	9.0	8.6
8	47.7	328.9	−57.2	15.0	18.8	9.1	8.3
16	41.2	284.5	−63.0	15.0	21.1	9.3	7.9
32	30.9	213.2	−72.3	15.0	20.5	9.2	8.2
Lime + fibers treated soil							
0	201.1	1387.8	0.0	30.0	31.0	10.7	10.5
1	125.1	863.4	−37.8	30.0	32.4	10.7	9.7
2	159.8	1102.6	−20.5	30.0	32.9	10.5	9.6
4	169.4	1168.9	−15.8	30.0	31.9	11.3	9.5
8	161.3	1113.2	−19.8	30.0	33.3	10.6	9.5
16	183.6	1266.5	− 8.7	30.0	33.1	10.6	9.7
32	254.2	1754.0	+26.4	30.0	33.3	10.4	9.4

that cyclic w-d exerts a greatly detrimental effect on natural soil's UCS. Further cyclic w-d, however, is necessary to devise an absolute lower bound. Even though moisture remains close to that of compaction (21%), the pH slightly decreases with cyclic w-d. Similar findings were reported by Rogers and Wright (1986) on expansive clay from Beaumont, Texas.

Overall strength trend for 5% cement treated soil is indicative of decreasing UCS upon cyclic w-d. Despite a 38% strength loss after 32 w-d cycles, UCS of treated soil remains about seven times higher than that of natural soil. Similar findings were reported by

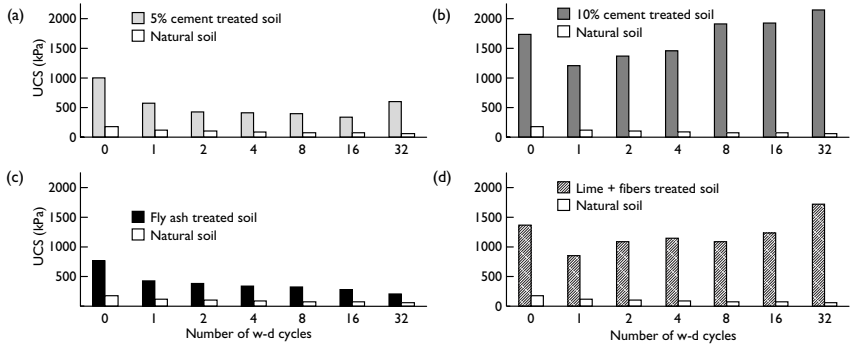

Figure 33.5 Change in UCS with w-d cycles for soil treated with: (a) 5% type V cement, (b) 10% type V cement, (c) class F fly ash, and (d) lime + fibers.

Santoni *et al.* (2002) on cement treated sand, and by Nunan and Humphrey (1990) on cement treated base aggregates. The pH of treated soil shows a slight tendency to decrease upon cyclic w-d, indicating potential leaching-out of stabilizer.

Overall strength trend for 10% cement treated soil indicates a continuous increase in UCS upon cyclic w-d. Both UCS and swell-shrink responses are indicative of continued bonding (pozzolanic reactions) taking place during cyclic w-d. The pH of treated soil remained practically same, which reconfirms the continued pozzolanic reactions. It is worth noting, however, that the final moisture tends to increase with an increase in w-d cycles (Table 33.3), a possible indication of increased pore space within treated soil after the cementation and agglomeration reactions.

Fly ash treated soil performed poorly, with a 72% loss in UCS after 32 w-d cycles. However, the benefits from fly ash treatment are not completely lost, as the UCS of treated soil is still more than three times that of natural soil after 32 w-d cycles. The pH of treated soil tends to decrease under sustained w-d, indicating possible leaching-out of stabilizer.

Overall strength trend for lime + fibers treated soil is indicative of sustained UCS recovery after an initial decrease during the first few w-d cycles. Best-fit trend in Figure 33.5(d) has a slightly positive slope, implying that cyclic w-d has a moderate effect on UCS of treated soil. Moreover, pH and moisture of treated soil remained practically same during cyclic w-d. Lime + fibers treated soil is the second best-performing method after 10% cement treatment.

Previous work reported by Laguros and Keshawarz (1987) and Miller *et al.* (1999) has shown considerable strength decrease upon cyclic w-d in soils treated with lime treatment alone, which underscores the benefits of fibers inclusion. However, field applications with fibers are far from standardized, especially specifications related to compaction procedures are not yet established (Puppala *et al.*, 2001).

Undrained shear strength

Strength of highway subgrade materials is often characterized via UC testing. However, UU triaxial testing in a cylindrical cell provides a more reliable measure of shear strength.

This is especially true for testing of fissured and compacted soils, where confining pressure keeps the specimen intact during shearing (Rauch *et al*,. 2002). Peak response (at failure) of natural and treated soils from the series of UU tests performed at different w-d cycles as shown in Figure 33.6 using modified Mohr-Coulomb *p-q* plots. Values of mean stress, $p = (\sigma_1 + \sigma_3)/2$, and deviator stress, $q = (\sigma_1 - \sigma_3)/2$, were determined using either peak axial deviator stress or, when no peak was reached, deviator stress at 15% axial strain.

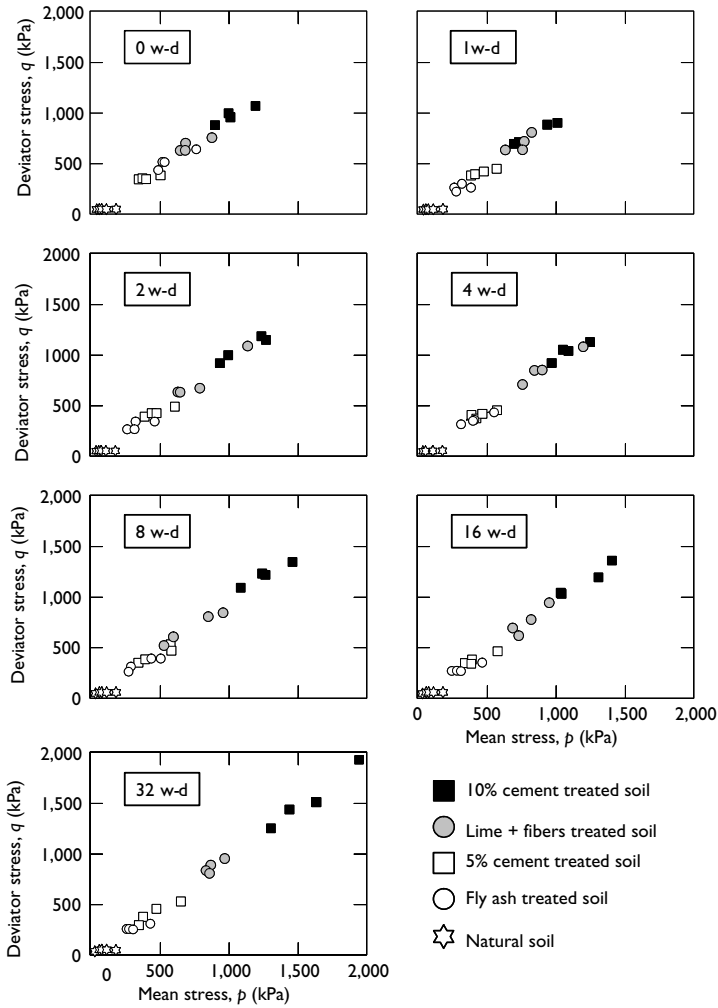

Figure 33.6 Variation in *p-q* response of natural and treated soils with w-d cycles.

Overall trends for 10% cement and lime + fibers treated soils in Figure 33.6 suggest that the stress state at failure becomes increasingly higher with increased w-d cycles, in agreement with UC test results. It is worth noting that all UU test specimens were unsaturated, which results in strength envelopes with overestimated values of friction angle ϕ from the p-q plots. UU triaxial tests would yield a $\phi = 0$ condition only if the soil were fully saturated.

In an attempt to devise the effect of cyclic w-d on treated soil's strength parameters (c and ϕ), the Mohr circles resulting from all UU tests on natural and treated soil were re-plotted in τ-σ plane. Since all specimens were tested under unsaturated conditions, the c-ϕ analysis presented herein is intended only for a qualitative assessment of the influence of cyclic w-d on soil strength. Figure 33.7 shows typical response of 5% cement treated soil in τ-σ plane from UU tests conducted after 0 and 32 w-d cycles. It can be noted that cyclic w-d exerts a paramount influence on the final positioning (intercept c and slope ϕ) of the failure envelope.

Table 33.4 summarizes all c-ϕ values obtained from natural and treated soils. Cyclic w-d caused little change in c-ϕ response of natural soil. Overall trends for 5% and 10% cement treated soils are indicative of decreasing c (plasticity) and increasing ϕ with increased w-d cycles. Values of c and ϕ are substantially higher than those of natural soil. An increase in cementation can be attributed to continued bonding from cementing gels at particle contacts, whereas an increase in friction angle can be attributed to agglomeration within treated soils.

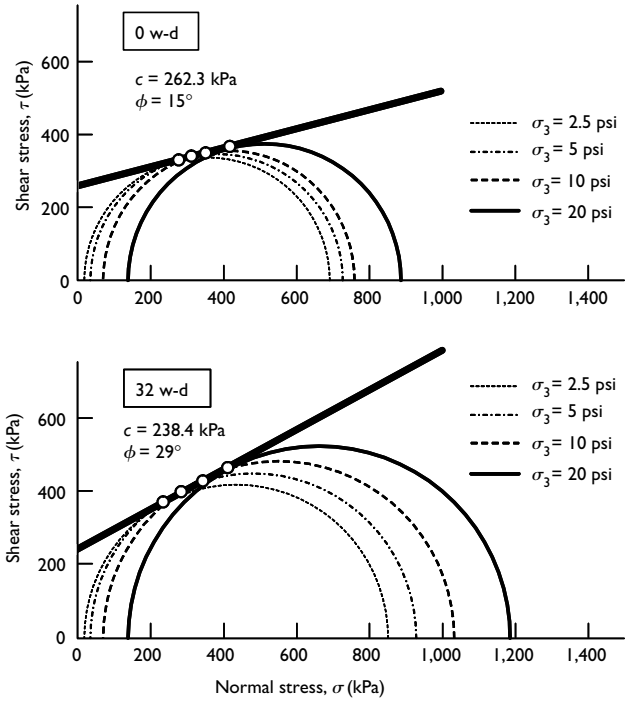

Figure 33.7 Response of 5% cement treated soil from UU tests conducted at 0 and 32 w-d cycles.

Table 33.4 Shear strength parameters (c and ϕ) from UU triaxial tests

Number of w-d cycles	*c (psi)*	*c (kPa)*	*% change*	*ϕ (°)*	*% change*
Natural soil					
0	6.8	46.9	0.0	0.6	0.0
1	6.5	44.9	−4.4	0.6	0.0
2	6.7	46.2	−1.5	0.6	0.0
4	6.3	43.5	−7.4	0.6	0.0
8	6.9	47.6	+1.5	0.6	0.0
16	6.9	47.3	+0.7	0.6	0.0
32	6.9	47.6	+1.5	0.6	0.0
5% Type V cement treated soil					
0	38.0	262.3	0.0	15.0	0.0
1	37.9	261.5	−0.3	17.8	+18.7
2	37.4	257.9	−1.7	21.5	+43.3
4	37.0	255.3	−2.7	24.5	+63.3
8	36.4	250.9	−4.4	26.9	+79.3
16	35.6	245.6	−6.4	28.0	+86.7
32	34.6	238.4	−9.1	29.0	+93.3
10% Type V cement treated soil					
0	97.0	669.3	0.0	20.5	0.0
1	78.9	544.4	−18.7	28.9	+41.0
2	60.0	414.0	−38.1	32.5	+58.5
4	57.9	399.4	−40.3	37.9	+84.8
8	54.7	377.2	−43.6	39.0	+90.2
16	49.0	338.1	−49.5	37.7	+83.9
32	50.0	345.0	−48.5	39.7	+93.5
20% Fly ash treated soil					
0	43.0	296.7	0.0	20.0	0.0
1	16.8	115.9	−60.9	16.0	+20.0
2	14.4	99.4	−66.5	10.5	+47.5
4	13.0	89.7	−69.8	10.5	+47.4
8	13.2	91.1	−69.3	10.4	+48.3
16	14.8	102.1	−65.6	10.7	+46.5
32	17.6	121.4	−59.1	10.5	+47.5
Life + fibers treated soil					
0	42.0	289.8	0.0	32.0	0.0
1	34.0	234.6	−19.0	34.7	+ 8.4
2	29.0	200.1	−31.0	36.9	+15.3
4	50.0	345.0	+19.0	38.0	+18.8
8	30.0	207.0	−28.6	42.5	+32.8
16	36.0	248.4	−14.3	43.0	+34.4
32	39.0	269.1	− 7.4	41.0	+28.1

Fly ash shows poor performance among all stabilizers, with a sharp simultaneous decrease in c and ϕ under sustained w-d. Although ϕ values from lime + fibers treated soil tend to increase with repeated w-d, overall c-ϕ trends are far from definitive. In general, however, all treated soils outperformed natural soil after 32 w-d cycles, with 10% type V cement treated soil showing best c-ϕ performance. Similar findings were reported by Laguros and Keshawarz (1987) on shale treated with cement, fly ash, and quicklime.

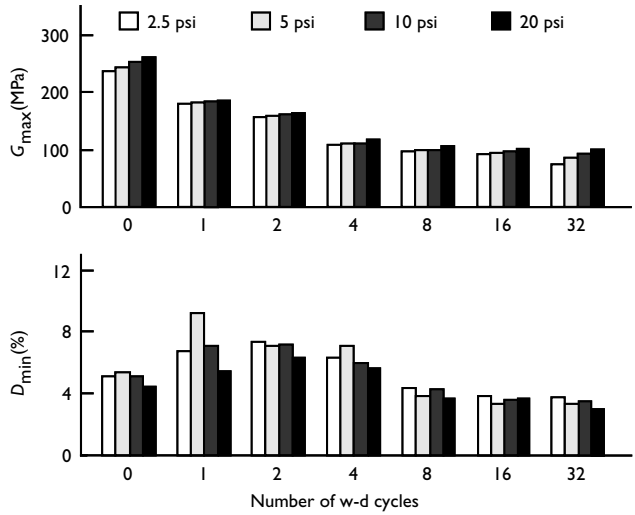

Figure 33.8 Change in G_{max} and D_{min} with w-d cycles for natural soil.

Shear modulus and damping ratio

Cyclic W-D effects

Figure 33.8 shows change in linear (small-strain) shear modulus G_{max} and damping ratio D_{min} with w-d cycles from the series of RC tests performed on natural soil at different confining pressures σ_0'. It can be noted that cyclic w-d exerts a greatly deleterious effect on G_{max} of natural soil (more than 50% reduction after 32 w-d cycles), reaching a lowest constant value after 4 w-d cycles. Confinement, however, does not have a paramount influence on G_{max} response, regardless of w-d cycles, which is typical of soft, high-plasticity clays (Seed and Idriss, 1970).

Damping ratio of a material indicates its capacity to absorb energy. If a material has a high damping ratio, it is most suitable for a vibration attenuation foundation (Zhong *et al.*, 2002). Hence, Figure 33.8 suggests that cyclic w-d also has a detrimental effect on natural soil's D_{min}. Similar to G_{max} response, confinement σ_0' does not have a paramount influence on D_{min} of natural soil.

Figure 33.9 shows change in G_{max} with w-d cycles for all treated soils. Contrary to natural soil behavior, G_{max} response of treated soils is highly susceptible to changes in σ_0', with the most evident cases observed in cement and lime + fibers treated soils. This can be partly attributed to the loss in plasticity of these treated soils upon cyclic w-d (Table 33.4). Similar G_{max} behavioral trends have been reported on weakly cemented sands by Chang and Woods (1987). Results from RC tests on lime + fibers treated soil after 32 w-d cycles are not reported in this work. Excessive exposure of fibers after 32 w-d cycles made it difficult to secure the torsional driving mechanism (spider) onto the top of the RC specimen, which rendered unreliable frequency response curves.

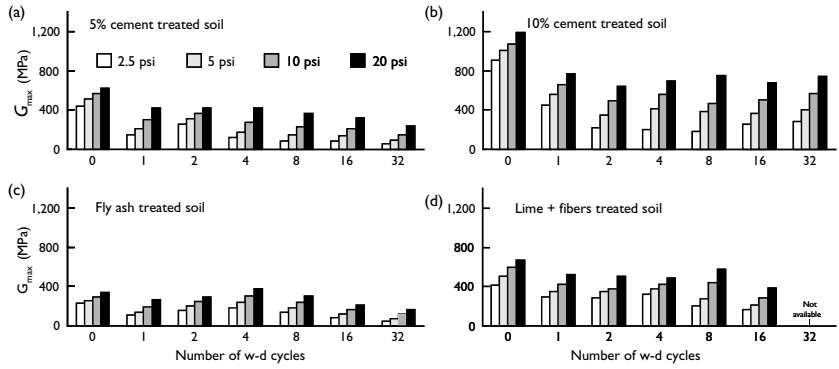

Figure 33.9 Change in G_{max} with w-d cycles for soil treated with: (a) 5% type V cement, (b) 10% type V cement, (c) class F fly ash, and (d) lime + fibers.

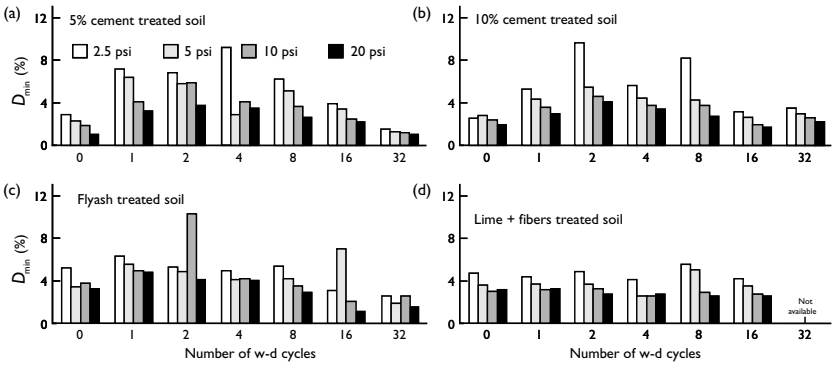

Figure 33.10 Change in D_{min} with w-d cycles for soil treated with: (a) 5% type V cement, (b) 10% type V cement, (c) class F fly ash, and (d) lime + fibers.

In general, cyclic w-d has a slightly detrimental effect on G_{max} response of all treated soils, though long-term G_{max} trends are far from definitive in most cases. Treated soils, however, outperform natural soil after 32 w-d cycles, with 10% type V cement treatment yielding best G_{max} performance, in agreement with findings from swell-shrink response and UC and UU tests.

Figure 33.10 shows change in D_{min} with w-d cycles for all treated soils. In general, cyclic w-d has a slightly detrimental effect on long-term D_{min} response of all treated soils after an initial increase in damping within the first few w-d cycles. As with G_{max}, confinement σ_0' does have a paramount influence on D_{min} response of treated soil. It appears that 10% cement and lime + fibers treated soils yield slightly better D_{min} performance over the other treatment methods.

Confinement effects

The influence of cyclic w-d on natural soil's susceptibility to changes in confinement σ_0' is clearly observed in Figure 33.11, where G_{max} has been plotted as function of σ_0' for different w-d cycles. As expected, in all cases G_{max} increases with an increase in σ_0', with a tendency to reach approximately asymptotic values for higher σ_0'. However, the rate at which G_{max} increases with σ_0' is slightly influenced by the number of w-d cycles.

This effect is better seen in Figure 33.12(a), where solid lines represent best-fit, power regression functions of the form, $G_{max} = A(\sigma_0')^B$, where A represents G_{max} (MPa) at $\sigma_0' = 1$ kPa, and B is representative of soil's susceptibility to changes in σ_0', that is, slope of best-fit solid curves in Figure 33.12(a). It can be observed that the soil's susceptibility to

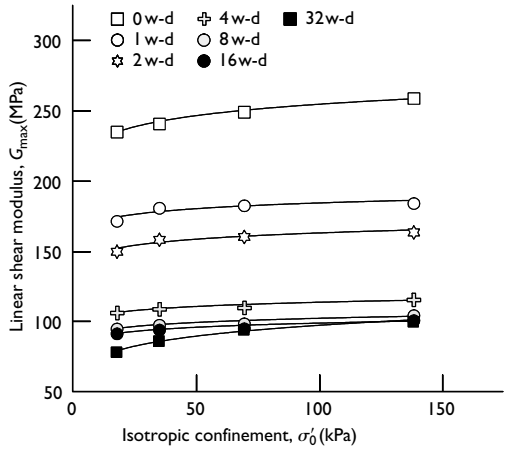

Figure 33.11 Variation in $G_{max} - \sigma'_o$ response of natural soil with w-d cycles.

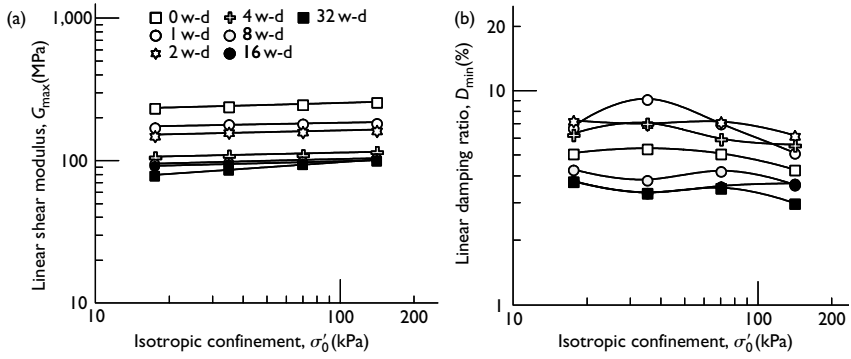

Figure 33.12 Influence of cyclic w-d on $G_{max} - \sigma_0'$ and $D_{min} - \sigma_0'$ response of natural soil.

changes in σ_0' (constant B) tends to increase with an increase in w-d cycles. Similar findings were reported by Khoury and Zaman (2002) in testing the resilient modulus of class C coal fly ash-stabilized base aggregates. Even though behavioral trends of D_{min} shown in Figure 33.12(b) are not as clearly defined as those of G_{max}, they do highlight the detrimental effect of cyclic w-d on natural soil's material damping.

Figure 33.13 shows the $G_{max} - \sigma_0'$ response of all treated soils for different w-d cycles. Values of G_{max} and power regression constants A and B for natural and treated soils are summarized in Table 33.5. In general, treated soil's susceptibility to changes in σ_0' (constant B) tends to increase as w-d cycles increase. This is more evident in cement treated soils, which can be regarded as additional evidence of the "aging" effects induced by cyclic w-d, making the treated soil more frictional and less cohesive, therefore more susceptible to any increase in σ_0'.

Behavioral trends of D_{min} shown in Figure 33.14 for treated soils are not as well defined as those of G_{max}, but they confirm best performance of 10% type V cement treated soil in terms of long-term material damping. All values of D_{min} are summarized in Table 33.6.

Concluding remarks

Soils treated with sulfate-resistant type V cement showed best swell-shrink performance under repeated w-d. Fly ash treated soil performed poorly, showing large amount of swelling

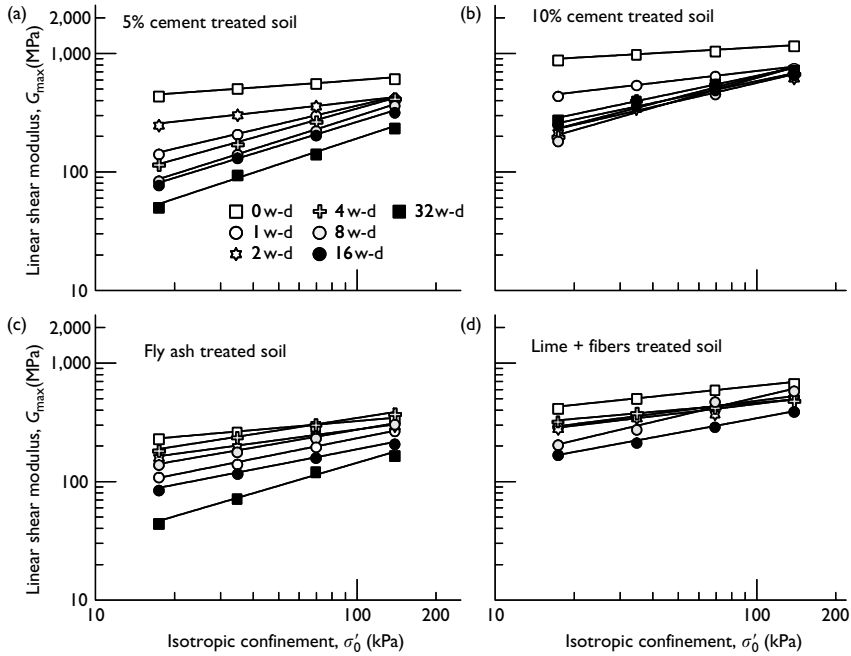

Figure 33.13 Influence of cyclic w-d on $G_{max} - \sigma_0'$ response of soil treated with: (a) 5% type V cement, (b) 10% type V cement, (c) class F fly ash, and (d) lime + fibers.

Table 33.5 Small-strain shear modulus (G_{max}) from RC tests

Number of w-d cycles	*Small-strain shear modulus, G_{max} (MPa)*				*Eq. (1)*		
	$\sigma'_0 = 17.25$ MPa	$\sigma'_0 = 34.5$ MPa	$\sigma'_0 = 69$ MPa	$\sigma'_0 = 138$ MPa	*A*	*B*	r^2
Natural soil							
0	235.7	241.6	249.9	259.6	205.7	0.047	0.98
1	179.5	181.7	183.4	185.0	159.4	0.032	0.81
2	157.2	159.4	161.3	164.5	136.3	0.039	0.89
4	107.2	109.9	110.9	116.7	95.9	0.038	0.91
8	95.9	98.6	99.6	105.3	84.7	0.042	0.91
16	92.4	95.1	96.1	101.9	81.3	0.044	0.91
32	79.0	86.8	94.9	100.6	56.9	0.118	0.98
5% Type V cement treated soil							
0	443.7	514.5	566.8	622.0	285.8	0.160	0.97
1	144.1	211.7	304.8	423.8	33.3	0.519	0.98
2	252.7	309.5	366.9	420.1	128.0	0.245	0.98
4	118.1	174.5	271.9	423.7	20.1	0.617	0.98
8	85.7	143.6	226.9	370.0	11.8	0.699	0.98
16	78.9	133.6	207.9	324.4	11.8	0.676	0.98
32	51.0	95.8	144.2	239.0	6.7	0.728	0.98
10% Type V cement treated soil							
0	896.3	998.9	1065.8	1178.0	626.9	0.128	0.98
1	444.4	552.9	655.7	761.0	217.5	0.257	0.98
2	219.0	348.5	490.9	632.7	54.3	0.509	0.97
4	202.6	407.9	555.9	687.9	45.3	0.574	0.91
8	185.7	378.6	462.4	746.0	34.0	0.631	0.94
16	253.5	364.9	498.8	669.0	68.7	0.465	0.98
32	279.2	403.2	560.4	737.5	75.3	0.468	0.98
20% Fly ash treated soil							
0	231.6	262.8	295.6	346.0	133.8	0.191	0.98
1	110.2	137.7	195.9	269.7	30.6	0.438	0.98
2	161.7	200.2	247.6	299.2	69.8	0.297	0.98
4	184.5	239.4	305.8	377.0	70.0	0.345	0.98
8	140.1	181.3	238.1	307.8	47.4	0.38	0.98
16	85.4	121.8	162.4	209.4	25.8	0.430	0.98
32	44.7	72.4	122.0	167.0	7.3	0.646	0.97
Lime + fibers treated soil							
0	419.4	506.6	599.3	676.4	220.6	0.231	0.98
1	292.1	350.8	429.7	524.2	130.0	0.282	0.98
2	283.8	350.1	377.3	511.6	132.5	0.266	0.94
4	322.3	383.1	426.5	486.8	188.2	0.194	0.98
8	206.4	278.0	444.8	588.4	46.1	0.521	0.97
16	169.9	214.5	292.0	393.6	52.0	0.408	0.98
32	—	—	—	—	—	—	22.0

before reaching equilibrium at near 10 w-d cycles. Response of lime + fibers treated soil followed that of fly ash treated soil, excluding the sudden swell increase after 28 w-d cycles. Lime + fibers treated soil, however, performed poorly relative to cement treated soils.

Cyclic w-d exerts a great detrimental effect on UCS of natural soil. Overall trend for 10% cement treated soil indicates a continuous increase in UCS under repeated w-d. Final

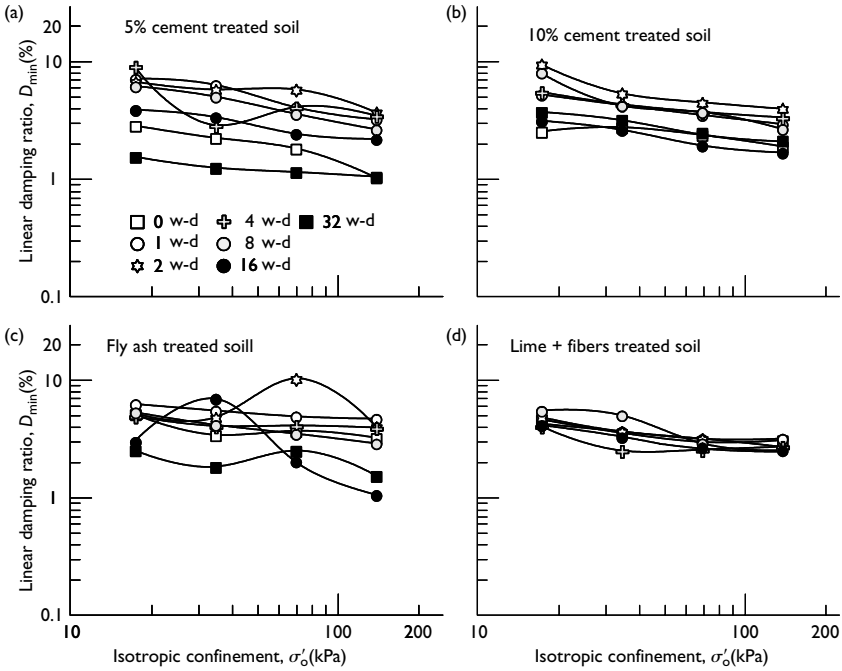

Figure 33.14 Influence of cyclic w-d on $D_{min} - \sigma'_0$ response of soil treated with: (a) 5% type V cement, (b) 10% type V cement, (c) class F fly ash, and (d) lime + fibers.

moisture, however, tends to increase with an increase in w-d cycles, a possible indication of increased pore space within treated soil. Fly ash treated soil performed poorly, with a 72% loss in UCS after 32 w-d cycles. Overall trend for lime + fibers treated soil is indicative of sustained UCS recovery after an initial decrease during the first few w-d cycles. Lime + fibers treated soil is the second best-performing method after 10% cement treatment.

Overall trends for type V cement treated soils are indicative of decreasing cohesion (plasticity) and increasing friction angle with increased w-d cycles. Fly ash treated soil shows poor performance among all stabilizers, with a sharp simultaneous decrease in c and ϕ under sustained w-d. In general, all treated soils outperformed natural soil after 32 w-d cycles, with 10% type V cement treated soil showing best c-ϕ performance.

In general, cyclic w-d has a slightly detrimental effect on G_{max} of all treated soils. Treated soils, however, outperform natural soil after 32 w-d cycles, with 10% type V cement treatment yielding best G_{max} performance, in agreement with findings from swell-shrink readings and UC and UU tests. Cyclic w-d also has a detrimental effect on long-term material damping of treated soil.

Table 33.6 Small-strain material damping (D_{min}) from RC tests

Number of w-d cycles	*Small-strain damping ratio, D_{min}(%)*			
	$\sigma'_0 = 17.25$ *kPa*	$\sigma'_0 = 34.5$ *kPa*	$\sigma'_0 = 69$ *kPa*	$\sigma'_0 = 138$ *kPa*
Natural soil				
0	5.1	5.4	5.1	4.3
1	6.8	9.2	7.1	5.2
2	7.3	7.1	7.2	6.2
4	6.3	7.1	6.0	5.6
8	4.3	3.9	4.3	3.7
16	3.8	3.4	3.6	3.7
32	3.8	3.4	3.5	3.0
5% Type V cement treated soil				
0	2.9	2.3	1.8	1.0
1	7.2	6.4	4.1	3.3
2	6.8	5.8	5.8	3.7
4	9.2	2.9	4.1	3.5
8	6.2	5.1	3.6	2.7
16	3.9	3.4	2.5	2.2
32	1.6	1.3	1.2	1.1
10% Type V cement treated soil				
0	2.6	2.8	2.4	1.9
1	5.3	4.3	3.5	3.0
2	9.5	5.4	4.5	4.0
4	5.6	4.4	3.8	3.4
8	8.1	4.2	3.7	2.7
16	3.2	2.7	2.0	1.7
32	3.7	3.2	2.5	2.2
20% Fly ash treated soil				
0	5.2	3.5	3.8	3.3
1	6.4	5.6	5.0	4.8
2	5.3	4.9	10.5	4.1
4	5.0	4.2	4.2	4.0
8	5.4	4.2	3.6	3.0
16	3.1	7.1	2.1	1.1
32	2.6	1.9	2.6	1.6
Lime + fibers treated soil				
0	4.7	3.6	3.0	3.2
1	4.4	3.7	3.2	3.2
2	5.0	3.7	3.2	2.8
4	4.2	2.6	2.6	2.8
8	5.6	5.1	3.0	2.6
16	4.2	3.5	2.8	2.6
32	—	—	—	—

An additional series of scanning electron microscope (SEM) and X-ray diffraction (XRD) tests are currently being conducted on treated soils in order to assess potential changes in soil's microstructural, physical, and chemical properties upon being subjected to cyclic w-d. Preliminary SEM and XRD data have substantiated the macro-behavioral observations drawn from the series of UC, UU, and RC tests presented herein.

Notation

A, B = best-fit power regression constants for $G_{max} = A(\sigma_0)^B$
c = cohesion (kPa)
D_{min} = linear (small-strain) damping ratio (%)
G_{max} = linear (small-strain) shear modulus (MPa)
G_s = soil specific gravity (−)
H_o = initial specimen height (cm)
p = mean stress (kPa) = $(\sigma_1 + \sigma_3)/2$
q = deviator stress (kPa) = $(\sigma_1 - \sigma_3)/2$
r^2 = coefficient of determination
w = compaction moisture content (%)
w_n = natural moisture content (%)
ϕ = friction angle (°)
γ_d = dry unit weight (kN/m^3)
$\gamma_{d\text{-}max}$ = maximum dry unit weight (kN/m^3)
ΔH = change in specimen height (cm)
σ = normal stress (kPa)
σ_0' = isotropic confining pressure (kPa)
σ_1 = major principal stress (kPa)
σ_3 = minor principal stress (kPa)
τ = shear stress (kPa)

Acknowledgment

This research work was partly sponsored by the Department of Engineering Services of the City of Arlington. This support is gratefully acknowledged. The authors would also like to thank BMT (Boral Material Technologies) and CCPC (Cement and Concrete Promotion Council) of Texas for providing the polypropylene fibers and type V cement used in this study, respectively.

References

Al-Homoud, A.S., Basma, A.A., Malkawi, A.I.H., and Bashabsheh, M.A.A. (1995). "Cyclic swelling behavior of clay." *J. Geotech Engrg*, ASCE, 121(7), 562–565.

Chainuwat, P. (2001). "Effects of compaction moisture content on stiffness properties of chemically stabilized sulfate-rich expansive clays using the resonant column testing device." MS thesis, Univ. of Texas at Arlington.

Chang, Y.J., and Woods, R.D. (1987). "Effect of confining stress on shear modulus of cemented sands." *Soil-structure interaction*. A.S. Cakmak, Editor, Elsevier Science, NY.

Day, R.W. (1994). "Swell-shrink behavior of compacted clay." *J. Geotech. Engrg*., ASCE, 120(3), 618–623.

Hoyos, L.R., Puppala, A.J., and Chainuwat, P. (2004). "Dynamic properties of chemically stabilized sulfate rich clay." *J. Geotech. and Geoenv. Engrg*, ASCE, 130(2), 153–162.

Hunter, D. (1988). "Lime-induced heave in sulfate-bearing clay soils." *J. Geotech. Engrg*., ASCE, 114(2), 150–167.

Khoury, N.N. and Zaman, M.M. (2002). "Effect of wet-dry cycles on resilient modulus of class C coal fly ash-stabilized aggregate base." *TRR 1787*, Transportation Research Board, Washington, DC, 13–21.

Kota, P.B.V.S., Hazlett, D., and Perrin, L. (1996). "Sulfate-bearing soils: problems with calcium based stabilizers." *TRR No. 1546*, Research Board, Washington, DC, 62–69.

Laguros, J.G. and Keshawarz, M.S. (1987). "Construction performance of the stabilized base course on U.S. 77 Ponca City, Kay County." *Final Report ODOT No. 83-07-02*, University of Oklahoma, Norman, OK.

Miller, A.G., Zaman, M.M., Rahman, J., and Tan, K.N. (1999). "Laboratory and field evaluation of soil stabilization using cement kiln dust." *Draft Report ORA 125–5693*, Oklahoma Department of Transport, Oklahoma.

Mitchell, J.K. and Dermatas, D. (1990). "Clay soil heave caused by lime-sulfate reactions." *ASTM Spec. Pub. No. 1135*, ASTM, 41–64.

Nunan, T. and Humphrey, D. (1990). "A review and experimentation of gravel stabilization methods." *Technical Report 90–2*, Technical Services Division, Maine Department of Transport.

Petry, T.M. and Little, N.D. (1992). "Update on sulfate-induced heave in treated clays: problematic sulfate levels." *TRR No. 1362*, Transportation Research Board, Washington, DC, 51–55.

Puppala, A.J., Hoyos, L.R., Viyanant, C., and Musenda, C. (2001). "Fiber and fly ash stabilization methods to treat soft expansive soils." *Proc., Soft Ground Technology Conf.*, Noordwijkerhout, Netherlands, ASCE Geotech. Spec. Pub. 112, 136–45.

Puppala, A.J., Griffin, J.A., Hoyos, L.R., and Chomtid, S. (2004). "Studies on sulfate resistant cement stabilization methods to address sulfate induced heave problems." *J. Geotech. and Geoenv. Engrg*., ASCE, 130(4), 391–402.

Rao, K.S. and Tripathy, S. (2003). "Effect of aging on swelling and swell-shrink behavior of a compacted expansive soil." *Geotech. Testing J*., ASTM, 26(1), 1–11.

Rauch, A.F., Harmon, J.S., Katz, L.E., and Lijestrand, H.M. (2002). "Measured effects of liquid soil stabilizers on engineering properties of clay." *TRR No. 1787*, Transportation Research Board, Washington, DC, 33–41.

Rogers L.E. and Wright S.G. (1986). "The effects of wetting and drying on the long-term shear strength parameters for compacted Beaumont clay." *Research Report 436–2F*, Center for Transportation Research, The University of Texas at Austin.

Rollings, R.S., Burkes, J.P., and Rollings, M.P. (1999). "Sulfate attack on cement-stabilized sand." *J. Geotech. and Geoenvir. Engrg*., ASCE, 125(5), 364–372.

Santoni, R.L., Tingle, J.S., and Webster, S.L. (2002). "Stabilization of silty sand with nontraditional additives." *TRR 1787*, Transportation Research Board, Washington, DC, 61–70.

Seed, H.B. and Idriss, I.M. (1970). "Soil moduli and damping factors for dynamic response analysis." *Report EERC 70–10*, Earthquake Engineering Research Center, Univ. of California at Berkeley, Berkeley, CA.

Takkabutr, P. (2002). "Effects of cyclic drying and wetting on strength and stiffness properties of chemically stabilized sulfate-rich expansive clay." MS thesis, Univ. of Texas at Arlington.

Wattanasanticharoen, E. (2000). "Laboratory investigations on four novel treatment methods to stabilize soft subgrade soils of southeast Arlington." MS thesis, Univ. of Texas at Arlington.

Zhong, X.G., Zeng, X., and Rose, J.G. (2002). "Shear modulus and damping ratio of rubber-modified asphalt mixes and unsaturated subgrade soils." *J. of Materials in Civil Engrg.*, ASCE, 14(6), 496–502.

Part 9

Construction techniques and remedial measures

Chapter 34

Granular pile-anchors

An innovative foundation technique for expansive soils

Bhyravajjula R. Phanikumar[1] *and Radhey S. Sharma*[2]

Summary

The cost of repairs to damage caused by expansive soils to civil engineering structures per annum is estimated at one billion USD and many billion dollars worldwide. Hence, there is an imperative need to counteract the problems posed by these soils by devising innovative foundation techniques. This chapter reports on the development of granular pile-anchors as an innovative foundation technique for counteracting the effects of expansive soils. It was found that the load-carrying capacity of an expansive clay bed increased by the installation of the granular pile-anchors. The loading intensity for a settlement of 25 mm in the case of a reinforced clay bed increased by $2\frac{1}{2}$ times over that for the same settlement in the case of an unreinforced clay bed.

Introduction

Expansive soils are a worldwide challenge. They pose problems for civil engineers in general and for geotechnical engineers in particular (Chen, 1988). Such soils cause damage to structures founded in them because of their potential to react to changes in moisture. They undergo severe volume changes corresponding to changes in moisture content. Expansive soils swell or increase in their volume when they imbibe water and shrink or reduce in their volume on evaporation of water (Holtz and Gibbs, 1956; Johnson and Snethen, 1978; Chen, 1988; Sharma, 1998; Sharma, 2000, Sharma, 2001; Wheeler *et al.*, 2003; Rao *et al.*, 2004a). Due to their alternate swelling and shrinkage, they result in detrimental cracking of lightly loaded civil engineering structures such as foundations, retaining walls, pavements, airports, side walks, canal beds, and linings (Wray, 1980; Chen, 1988). As the lightly loaded structures cannot counteract the swelling pressure caused by expansive soils, they are subjected to severe cracking (Department of the Army USA, Technical Manual TM 5-818-7, 1983; Chen, 1988).

The hazards caused by expansive soils have been recorded in countries all over the world, including America, Australia, Canada, India, Israel, Iran, Mexico, and South Africa (Chen, 1988). The cost of repairs to damage caused by expansive soils to civil engineering

[1] Department of Civil engineering, GMR Institute of Technology, GMR Nagar, Rajam – 532 127, Srikakulam district, Andhra Pradesh, India; email: phanikumar_29@yahoo.com

[2] Department of Civil and Environmental Engineering, CEBA Building 3505B, Louisiana State University, Baton Rouge, LA 70803, USA; email: rsharma@lsu.edu

structures per annum is estimated at one billion USD and many billion dollars worldwide (Gourley *et al.*, 1993). Hence, there is an imperative need to counteract the problems posed by these soils by devising innovative foundation techniques. This chapter reports on the development of granular pile-anchors as an innovative foundation technique for counteracting the effects of expansive soils.

Existing foundation practices in expansive soils

The various foundation practices currently adopted to minimize heave in expansive soils can be broadly grouped into two categories: mechanical, physical, or chemical alteration, and special foundation techniques.

Minimizing heave

Mechanical alteration

This involves excavation of expansive soil and replacement with non-expansive material, where the depth of active zone (depth from ground surface wherein seasonal moisture fluctuations occur) is small and where a suitable replacement material is available. Sand cushion method (Satyanarayana, 1966) and cohesive non-swelling (CNS) layer method (Katti, 1978) are very popular.

In the sand cushion method, the entire depth of the expansive clay stratum if it is thin, or a part thereof, if it is deep enough, is removed and replaced by a sand cushion compacted to the desired density and thickness (Figure 34.1). It was reported that swelling pressure varies inversely as the thickness of the sand layer and directly as its density (Satyanarayana, 1966). Hence, sand cushions are formed in their loosest state to avoid the possibility of excessively increasing the swelling pressure without, however, violating the criterion of bearing capacity. The basic philosophy of this method is that, in monsoon, the saturated sand occupies less volume, accommodating some of the heave of underlying expansive soil, and in summer, unsaturated sand bulks and occupies the extra space left by the shrinkage of the soil. This technique, however, has some limitations. First, the high permeability of sand creates accumulation of water, and second, the thickness of the sand cushion depends on the depth of active zone, which itself is difficult to determine. Besides, effects of fatigue in swelling have to be considered in designing the thickness of the sand cushion.

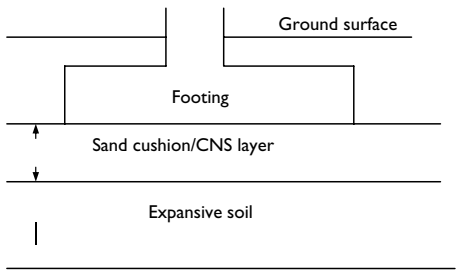

Figure 34.1 Sand cushion/CNS layer.

With the CNS layer method, the top 1 to 1.2 m of the expansive soil is removed and replaced by a cohesive non-swelling soil layer (Figure 34.1). According to Katti (1978), with saturation of expansive soil cohesive forces are developed up to a depth of about 1.0–1.2 m and counteract heave. The electrical charge of clay particles produces absorbed water bonds and develops this cohesion. CNS layer creates an environment similar to that around 1m deep in an expansive soil with equivalent cohesion to counteract heave. The disadvantage with this system, however, is that it is not easy to get a material, which conforms to the specifications laid down by Katti (1978) for an ideal CNS material.

Physical and chemical alteration

In physical alteration, granular material is mixed with expansive clay to minimize heave (Satyanarayana, 1966). However, the disadvantage with this method is that the permeability of the resulting blend would be more than that of the expansive soil. Hence, ingress of water into the soil would be faster due to increased permeability and heave would occur suddenly.

Chemical alteration involves addition of chemicals to expansive clay to reduce heave by altering the nature of expansive clay minerals (Chen, 1988). Of all the chemicals tried, lime is the most effective and economical additive. Lime treatment of expansive soils is the most widely used technique and the most effective technique of chemical alteration to minimize volume changes and to increase the shear strength of foundation expansive soils. Lime treatment is applied to minimize the volume changes of soils in railroad beds, pavement sub-grades, and slopes and to strengthen them. The usefulness of the treatment depends on the reactivity of the soil to lime treatment and the extent of dispersion of lime into the soil. However, the limitation of this technique is that only the top few layers of the soil are modified by the infiltration of lime into the soil.

In pavements, a technique called Lime-Slurry Pressure Injection (LSPI) is also used for minimizing swelling of soils. In this technique, lime-slurry is injected into drill-holes under a pressure of 15 kg/cm^2 (Department of the Army USA, Technical Manual TM 5-818-7, 1983; Chen, 1988). In this technique, lime-slurry penetrates into the fissures in the soil mass to a sufficient depth (usually 8 to 10 ft), and the lime-filled seams help control the soil water content, reduce volumetric changes, and increase soil strength. However, for LSPI to be an effective technique, the expansive clay soil must contain an extensive network of fissures. Otherwise, lime cannot penetrate into the relatively impermeable soil to an appreciable distance from the injection hole to form a continuous lime seam moisture barrier (Department of the Army USA, Technical Manual TM 5-818-7, 1983). Lime-soil columns were also tried to stabilize expansive clays in situ (Rao, 1984). It was reported (Shanker and Maruthi, 1989) that diffusion of lime into the ambient soil is effective up to a radial distance of about three times the diameter of the lime-soil column.

Addition of calcium chloride ($CaCl_2$) to expansive soil has also proved efficacious in altering the swelling properties of the soil (Desai and Oza, 1997; Phanikumar and Sastry, 2001). Calcium chloride is a hygroscopic material and hence, is preeminently suited for stabilization of expansive soils, because it absorbs water from the atmosphere and prevents shrinkage cracks occurring in expansive soils during summer. Research showed that addition of calcium chloride to expansive soils reduced plasticity index (PI), free swell index (FSI%), heave or increase in thickness of the expansive clay layer, ΔH, where H is the initial thickness of the layer, swell potential, $\Delta H/H$ (%), and swelling pressure, p_s, significantly. It was found that addition of 4% of calcium chloride rendered the soil non-expansive

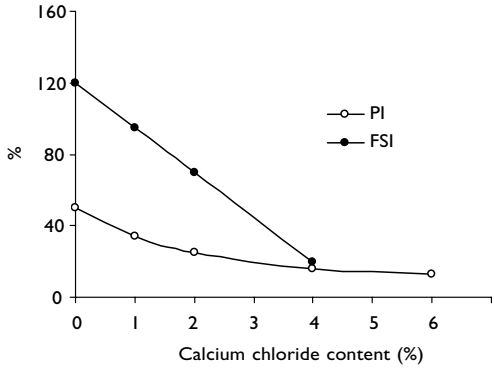

Figure 34.2 Effect of calcium chloride.

Table 34.1 Effect of fly ash on swelling characteristics

	Fly ash content				
Property	*0*	*5*	*10*	*15*	*20*
Free swell index (FSI)	250	200	165	140	125
Swell potential (%)	10.8	8.75	7.2	6.0	5.5
Swelling pressure (kPa)	90	72	60	50	45

(Phanikumar and Sastry, 2001). Figure 34.2 shows the effect of calcium chloride on FSI and PI. It was also reported that the unconfined compressive strength and the initial tangent modulus of the expansive soil increased with the content of calcium chloride (Phanikumar and Sastry, 2001). The unconfined compressive strength increased up to 4% calcium chloride, and thereafter decreased.

Another additive that has been found to be quite promising in reducing the swelling characteristics and improving the engineering behavior of expansive soils is fly ash. The efficacy of fly ash as an additive to expansive soils in ameliorating their properties was reported (Phanikumar and Sharma, 2004). A laboratory experimental program revealed that FSI, swell potential ($\Delta H/H$), swelling pressure (p_s), and plasticity decreased considerably with increasing fly ash content. Table 34.1 shows the significant effect of fly ash content on swelling characteristics, namely, FSI, swell potential, and swelling pressure. It can be seen from the table that, incidentally, all the swelling characteristics of the soil used decreased by 50% at a fly ash content of 20% for the type of the fly ash used. Figure 34.3 shows the influence of fly ash on Proctor compaction characteristics of the soil. While the optimum water content decreased, the maximum dry density increased with increasing fly ash content. Hence, compaction curves are shifted upward and toward the left. Addition of fly ash is, therefore, equivalent to increased compactive effort. This establishes that expansive soils can be effectively stabilized with fly ash.

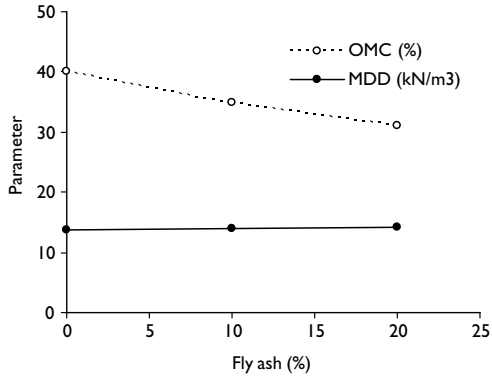

Figure 34.3 Influence of fly ash on compaction characteristics.

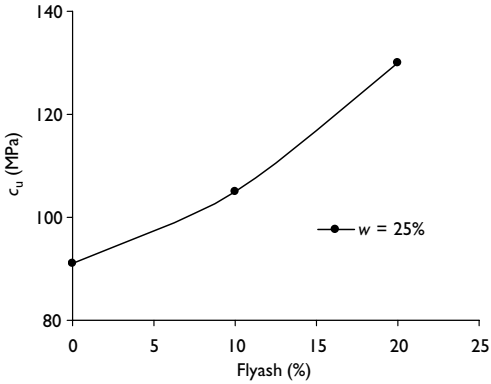

Figure 34.4 Influence of fly ash on undrained shear strength.

Figure 34.4 shows the variation of undrained shear strength of the expansive soil-fly ash blend at different contents of fly ash for given water content of 25%. Undrained shear strength of the blend increased with increasing fly ash content. Figure 34.5 shows the influence of fly ash on the value of hydraulic conductivity, k (cm/s), of expansive soil-fly ash blends prepared at the respective MDD and OMC. As MDD increased with increasing fly ash content, void ratio decreased. Hence, hydraulic conductivity decreased with increasing fly ash content (Phanikumar and Sharma, 2004). The foregoing observations reveal that fly ash is an effective additive to expansive soils for reducing the swelling properties of expansive soils, stabilizing them and improving their engineering behavior.

Special foundation techniques

The problem of heave or uplift of foundations caused by expansive soils is one of tension developed in the soil due to swelling. Hence, tension-resistant foundations are required for

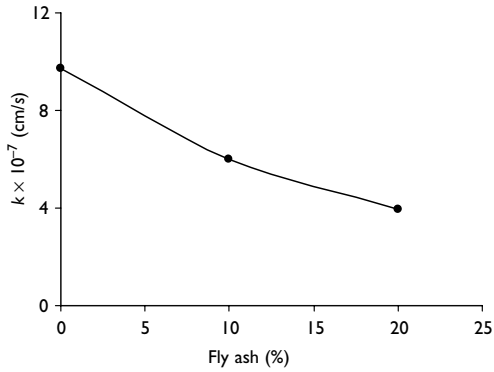

Figure 34.5 Variation of *k* with fly ash content.

counteracting the heave problem. Various special foundation techniques, which are going to be explained, are all tension-resistant foundations. However, some of them counteract swelling through skin friction also. Some of the special foundation techniques employed to counteract heave in expansive soils are explained in the following section.

Drilled piers Drilled piers are piers of small diameter but of considerable length, which are drilled (Figure 34.6) into expansive soils up to the zone unaffected by moisture change (Chen, 1988), or beyond active zone. Both the end-bearing resistance, E (psf), and skin friction resistance increase with depth at the rate of about 10% per meter, or 3% per foot. Therefore, the load-carrying capacity, Q (kips) of a pier is given (Chen, 1988) as:

$$Q = [A(E = 0.03\ EL) + 0.1\ (E + 0.03\ EL)\ CL\backslash] \tag{34.1}$$

where

A = Area of cross-section of the pier (sq.ft),
L = Depth of penetration into the bearing stratum (ft),
C = Perimeter of the pier (ft).

The uplift force, U (lb) is given by:

$$U = 2\pi rfu\ (D - d) \tag{34.2}$$

where

r = radius of the pier (ft),
d = depth of the zone of soil unaffected by wetting (ft),
D = total length of the pier (ft),
u = Swelling pressure (psf),
f = coefficient of uplift between concrete and soil.

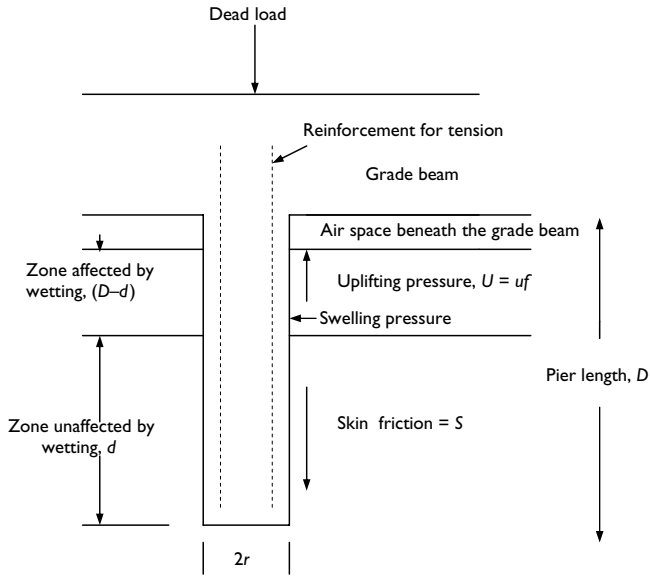

Figure 34.6 Drilled pier foundation.

The resisting force comprises of the dead load of the pier and the skin friction and is given by:

$$W = (\pi r^2 P + 2\pi rsd) \tag{34.3}$$

where

P = unit dead-load pressure (psf),
s = skin friction surrounding the pier (psf),
W = total withholding force (lb),
d = depth of the zone of soil unaffected by wetting (ft),
r = radius of the pier (ft).

A rational pier formula is obtained by equating the uplift force and the resisting force.

$$2\pi rfu\,(D - d) = (\pi r^2 p + 2\pi rsd) \tag{34.4}$$

$$\text{or} \qquad p = 2/r[\,fu(D - d) - sd\,] \tag{34.5}$$

Friction piers Where the bedrock is very deep and the upper layers of the soil are expansive, friction piers can be used (Chen, 1988). In these piers, resistance to uplift is basically by shaft friction. If the stratum is homogeneous clay, the ultimate shaft resistance

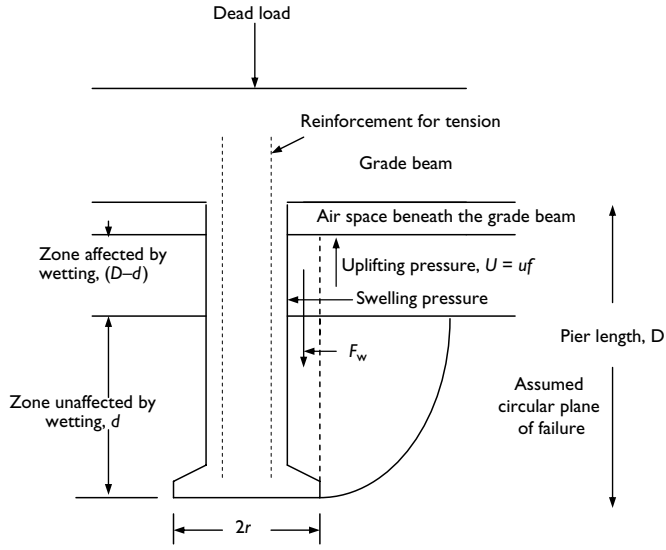

Figure 34.7 Belled pier foundation.

(S) is given by

$$S = \pi r^2 \infty S_u \tag{34.6}$$

where

r = radius of the pier,
S_u = undrained shear strength,
∞ = a reduction factor, obtained from field load tests.

The disadvantage is that soft soil should not be encountered within the length of the pier.

Belled piers Belled piers (Chen, 1988) are piers with enlarged base adopted to increase the carrying capacity (Figure 34.7). The uplift force, U, exerted on the belled pier is given by:

$$U = (P + F_w + F_s) \tag{34.7}$$

where

P = total vertical pressure on the pier,
F_W = total weight of the soil above the bell,
F_S = total shearing resistance along the assumed circular failure surface.

Under-reamed piles These piles, developed by Central Building Research Institute (CBRI), Roorkee, are an extension of belled-pier technique and are most efficacious in isolating the structure from the foundation soil. Sharma *et al.* (1978) brought out a handbook on under-reamed piles. Under-reamed piles are bored cast in situ piles with

enlarged bases and connected at their top by plinth beams. In the case of multi under-reamed piles, frictional resistance is mobilized over a larger perimeter and reduces heave.

While some of the aforesaid techniques are efficacious, they suffer from serious limitations. Moreover, the installation of some of these foundations is not foolproof. The solution may not be often economical, particularly for lightly loaded structures as the cost of the foundation may be very high. Hence, a simple solution in the form of granular pile-anchors was also tried as a possible innovative foundation technique for expansive soils. In this technique, foundations are anchored to granular piles to reduce heave. The technique and its efficacy are explained in detail in the following section:

Granular pile-anchors

Granular piles, also called stone columns, have been used during the last few decades, as a technique to improve the engineering behavior of soft cohesive soils and also loose cohesionless deposits (Thorburn and Mc Vicar, 1968; Greenwood, 1970; Hughes and Withers, 1974; Datye and Nagaraju, 1981; Ranjan and Rao, 1986). Granular piles have been used as an effective technique for improving the load-carrying capacity and decreasing the settlement of soft clays and loose sand deposits (Priebe, 1976; Ranjan, 1989). The response of the composite ground (granular pile and soil together) is assessed in terms of its load-carrying capacity and settlement.

The use of granular piles, therefore, has been so far confined to non-swelling soils only. Recently, the efficacy of granular pile-anchor foundation (GPAF) system has been investigated in reducing the amount of heave and improving the engineering behavior of expansive clay beds (Phanikumar, 1997; Phanikumar and Sharma, 2004; Phanikumar *et al.*, 2004; Sharma *et al.*, 2004; Sharma and Phanikumar 2005). A series of tests were performed to study the heave behavior, compressive load response, and pull-out behavior of granular pile-anchors and shear strength characteristics of the ambient expansive soil by varying the length, diameter, and relative density of the granular pile-anchors and initial water content and dry unit weight of the expansive clay bed. The basic philosophy, the tests conducted, results obtained, and the efficacy of the GPAF technique are dealt with in the following sections:

Basic philosophy of granular pile-anchors

The problem with expansive soils, as has already been mentioned, is one of tension. A mere granular pile will not be able to resist the uplift force exerted by the swelling soil on the foundation, which is tensile in nature. On the other hand, if the foundation is anchored at the bottom of the granular pile to a mild steel plate through a mild steel rod, the granular pile becomes tension-resistant by the effect of anchor and is able to counteract the uplift force exerted on the foundations. In a granular pile-anchor, the resistance to uplift is developed mainly due to the weight of the granular pile acting in the downward direction, and the uplift resistance due to friction mobilized along the cylindrical pile-soil interface, and precludes the possibility of heave of foundations.

Figure 34.8 illustrates the concept of a granular pile-anchor showing the various forces acting on it. The upward force acting on the foundation tending to lift it up is because of swelling of the expansive soil on imbibition of water. The resisting force acting in the

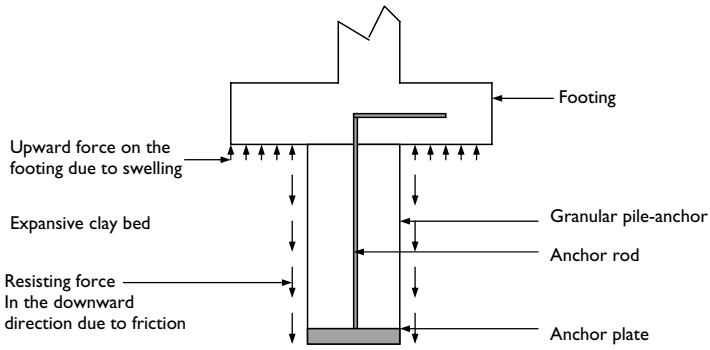

Figure 34.8 Concept of granular pile-anchor foundation system.

downward direction and counteracting the uplift force is due to friction mobilized along the pile-soil interface, which depends on the shear strength parameters of the interface.

Test program and results

Heave tests The expansive clay used in this investigation was collected from Amalapuram, of the State of Andhra Pradesh, India, from a depth of about 1.5 to 2.0 m below the ground level. The granular material used for the installation of the granular piles was a mixture of 20% stone chips with particle size varying between 6 and 10 mm and 80% coarse sand with size varying between 2.4 and 4.8 mm. Heave tests were performed in metal tanks of size 300 × 300 × 900 mm^3. Figure 34.9 shows the experimental set-up. The initial water content (w_i) of the expansive clay was kept constant at 14% in all the tests, but the initial dry unit weight (γ_{di}) was varied as 13, 14, and 15 kN/m^3. With regard to granular pile-anchor, the length was varied as 300, 400, and 500 mm and the diameter as 30, 40, and 50 mm. A total of 81 tests were conducted for studying the heave behavior. The relative density of the granular pile was varied as 50%, 60%, and 70%. The height of the expansive clay bed and the granular pile-anchor were the same in all the tests. A square mild steel plate of size 100 × 100 mm^2 was used as the surface footing in the heave tests.

The rate and amount of heave of the unreinforced clay bed are compared with those of the clay bed reinforced with granular pile-anchor. The unreinforced expansive clay bed attained a final heave of 9% in nine days. However, the heave of the expansive clay bed reinforced with granular pile-anchor attained a reduced amount of heave of 1.15% in a short period of three days. The percent heave, S, is the ratio of increase in thickness of the expansive clay bed to the initial thickness and is expressed as

$$S = \frac{\Delta H}{H} \times 100 \tag{34.8}$$

where ΔH is the heave, and H is the initial thickness of clay bed.

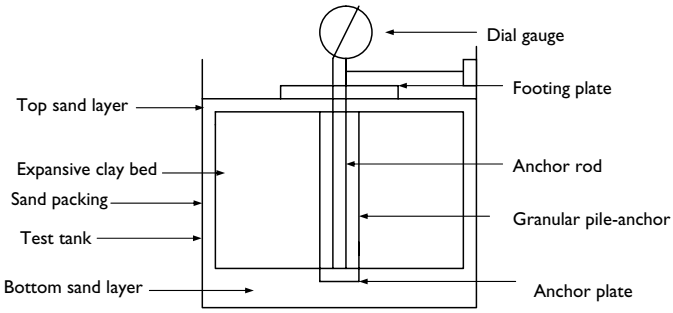

Figure 34.9 Experimental set-up for heave tests using GPAF system.

Table 34.2 % heave of expansive clay bed reinforced by granular pile-anchors

D_r	0.50			0.60			0.70		
L_g (m)	D_g (mm)			D_g (mm)			D_g (mm)		
	30	40	50	30	40	50	30	40	50
(a) % Heave for γ_{di} = 13 kN/m^3 and w_i = 14% (Original % heave = 6%)									
0.30	1.26	0.95	0.73	1.15	0.82	0.60	1.04	0.70	0.48
0.40	1.08	0.78	0.63	0.95	0.65	0.50	0.82	0.52	0.38
0.50	0.87	0.65	0.50	0.75	0.52	0.38	0.62	0.40	0.25
(b) Swell potential at γ_{di} = 14 kN/m^3 and w_i = 14% (Original % heave = 9%)									
0.30	1.75	1.25	0.92	1.60	1.15	0.87	1.44	1.04	0.80
0.40	1.52	1.12	0.86	1.41	1.04	0.80	1.30	0.96	0.72
0.50	1.35	1.00	0.81	1.24	0.94	0.76	1.14	0.82	0.62
(c) Swell potential at γ_{di} = 15 kN/m^3 and w_i = 14% (Original % heave = 14%)									
0.30	2.25	1.70	1.35	2.10	1.60	1.25	1.98	1.50	1.15
0.40	1.95	1.45	1.16	1.82	1.35	1.05	1.70	1.26	0.95
0.50	1.65	1.20	0.95	1.55	1.10	0.85	1.45	1.00	0.75

Table 34.2 summarizes the values of the % heave of the expansive clay bed reinforced with granular pile-anchors for various dry unit weights of the clay, different lengths (L_g) and diameters (D_g), and relative densities (D_r) of the granular pile. For a given diameter of the granular pile, % heave decreases with increasing length and that for a given length of the granular pile decreases with increasing diameter of the pile because the frictional resistance increases with increasing surface area of the granular pile, reducing the heave. Heave could be reduced to negligible values of 0.25%, 0.62%, and 0.75% respectively for the different dry unit weights of the clay beds (13, 14, and 15 kN/m^3) whereas the heave of the unreinforced clay beds were 6%, 9%, and 14%, respectively.

Hence, it can be summarized that heave of expansive clay beds decreased significantly on being reinforced with granular pile-anchors. A maximum of 96% reduction in the heave of the expansive clay beds was obtained (see Table 34.2). The rate of heave also became faster on the installation of granular pile-anchors in the expansive clay beds. Expansive clay beds

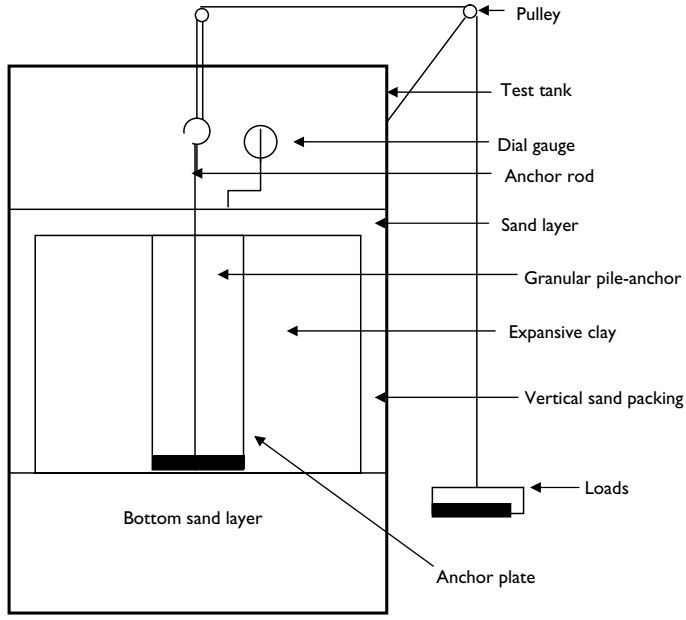

Figure 34.10 Experimental set-up for pull-out test.

reinforced with granular pile-anchors adjusted quickly to changes in moisture because of the higher hydraulic conductivity of the granular material. The time period required for attaining the final amount of heave in the case of reinforced clay bed was 1/3 of that for unreinforced clay bed. Increase in the relative density of the granular material in the granular pile-anchor enhanced reduction of heave.

Pull-out tests Figure 34.10 shows the experimental set-up for pullout tests. The pull-out capacity of the granular pile-anchors increased with increasing length of the pile-anchor and relative density of the granular material. For a pile of length of 250 mm, the load for 30 mm upward movement was about 250 N, whereas for a pile of length of 350 mm, it was equal to about 510 N, indicating an increase of about 100%. The percent increase in the pull-out load when the relative density was increased from 50% to 70% was about 30% for an upward movement of 30 mm.

Strength tests For the determination of undrained shear strength, c_u, of the clay, vane shear tests were conducted on samples obtained at different depths of the saturated expansive clay bed in both the reinforced and the unreinforced conditions. Undrained shear strength, c_u, was directly obtained from the results of the vane shear tests. Penetration tests were also conducted on the expansive clay bed in both reinforced and unreinforced conditions. A Proctor needle to which a shoe of diameter 20 mm was attached was kept vertically on the clay bed and pushed into the soil up to depths of 75, 150, and 225 mm and the penetration

Table 34.3 Improvement of engineering properties of expansive clay beds on installation of granular pile-anchors (c_u, in kN/m^2) *(w_f is the final water content)*

Dry unit weight γ_{di} *(kN/m^3)*	*Unreinforced clay bed*		*Reinforced clay bed*	
	c_u	w_f *(%)*	c_u	w_f *(%)*
13.00	15	45.00	18	41.00
14.00	18	42.00	21	36.00
15.00	21	40.00	25	31.10

force read. The penetration resistance was measured at different depths and radial distances from the center of the granular pile-anchor.

It was observed that the undrained shear strength of the expansive clay bed reinforced with granular piles also increased as evidenced by vane shear tests and Proctor needle penetration tests. A maximum increase of about 20% was observed in the undrained strength of the expansive clay bed as well as in the penetration resistance. Table 34.3 summarizes the improvement in the engineering behavior of expansive clay beds reinforced with granular pile-anchors as evidenced by increase in the undrained strength of the surrounding soil.

Compressive load tests Load tests were conducted on expansive clay beds alone (unreinforced), granular pile-anchors alone, and composite ground (granular pile and clay together) to assess and compare the compressive load response. The tests were conducted by placing the bearing plate on the saturated expansive clay bed alone, on the granular pile-anchor alone, and on both the clay and the granular pile-anchor (the bearing plate resting on both).

In all the load tests, the dry unit weight and the initial water content of the expansive clay bed were kept constant at 14 kN/m^3 and 14%, respectively. Load was applied after complete saturation of the expansive clay bed. Granular piles of length 300 mm, diameter 40 mm and relative density 60% were used for conducting load tests on the granular pile-anchor alone and the expansive clay bed reinforced with granular pile-anchor. In the case of load test on the expansive clay bed alone, a bearing plate of size 40 mm was used. In the load test in which the granular pile-anchor alone was tested, a bearing plate of diameter equal to that of the granular pile-anchor was used. In the case of load test on composite ground (expansive clay and granular pile-anchor together), a bearing plate of diameter 60 mm was used. The load was applied in increments of 1/5 of the expected safe bearing capacity in all the tests. The settlements of the plates under each increment were measured with the help of dial gauges of sensitivity 0.02 mm at time intervals of 1, 2.25, 4, 6.25, 9, 16, and 25 minutes, and thereafter, at hourly intervals for 24 hours. The tests were continued until a maximum load of two times the safe bearing pressure was applied.

It was found that the load-carrying capacity of the expansive clay bed increased by the installation of granular pile-anchors. The loading intensity for a settlement of 25 mm in the case of the reinforced clay bed increased by 2½ times over that for the same settlement in the case of the unreinforced clay bed.

It may be mentioned here that the proposed granular pile-anchor system has also been tested in field conditions by performing in situ tests (Rao *et al.*, 2004b). It was found that heave reduction and the rate of heave were similar to those obtained in the laboratory model tests. Hence, granular pile-anchors can be recommended for use in situ as an innovative foundation technique in expansive clay beds.

References

Chen, F.H. (1988). *Foundations on Expansive Soils*, Elsevier Scientific Publishing Co., Amsterdam, Edition ??

Datye, K.R. and Nagaraju, S.S. (1981). "Design Approach and field Control for stone columns," Proceedings. 10th International Conference on Soil Mechanics and Foundation Engineering, Stockholm.

Desai, I.D. and Oza, B.N. (1997). "Influence of anhydrous calcium chloride on shear strength of expansive soils," Proceedings, 1st International Symposium on Expansive Soils, HBTI, Kanpur, India.

Gourley, C.S., Newill, D., and Schreiner, H.D. (1993). "Expansive soils: TRL's research strategy," Proceedings, 1st International Symposium on Engineering Characteristics of Arid Soils, London.

Greenwood, D.A. (1970). "Mechanical improvement of soils below ground surface," Proceedings, Ground Engineering Conference, Institution of Civil Engineers, London, pp. 9–20.

Holtz, W.G. and Gibbs, H.J. (1956), "Engineering properties of expansive clays," *Transactions, ASCE*, Vol. 121, pp. 641–677.

Hughes, J.M.O. and Withers, N.J. (1974). "Reinforcing of soft cohesive soils with stone columns," *Ground Engineering*., London, Vol. 17, No. 3, 42–49.

Johnson, L,D. and Snethen, D.R. (1978). "Prediction of potential heave of swelling soil," *Geotechnical Testing Journal*, Vol. 1, No. 3, 117–124.

Katti, R.K. (1978), "Search for solutions to problems in black cotton soils," First I.G.S. Annual lecture, Indian Geotechnical society at I.I.T, Delhi.

Phanikumar, B.R. (1997). A study of swelling characteristics of and granular pile-anchor foundation system in expansive soils, Ph. D Thesis submitted to JN Technological University, Hyderabad, India.

Phanikumar, B.R. and Sastry, M.V.B.R. (2001). Stabilizing swelling subgrades with calcium chloride, Highway Research Bulletin, Vol. 65, Indian Roads Congress, pp. 77–82.

Phanikumar, B.R. and Sharma, R.S. (2004). "Effect of fly ash on engineering properties of expansive soils." *Journal of Geotechnical and Geoenvironmental Engineering, ASCE*, Vol. 130, No. 7, pp. 764–767.

Phanikumar, B.R., Sharma R.S., Rao A.S., and Madhav M.R. (2004). "Granular pile-anchor foundation (GPAF) system for improving the engineering behavior of expansive clay beds," *Geotechnical Testing Journal*, ASTM. Vol. 27, No. 3, pp. 279–287.

Priebe, A. (1976). "Abschalzung des satzung sverha mens eines duren stopverditchtung varbesserten," *Baugrudes Die Bautechnik*. H.5. 1946.

Ranjan, G. (1989), "Ground treated with granular piles and its response under load," *Indian Geotech, Journal*. Vol. 19, No.1, pp. 1–86.

Ranjan, G. and Rao, B.G. (1986), "Granular piles for ground improvement," Proceedings, International Conference on Deep Foundations, Beijing, China, Vol. 1, pp. ??

Rao, A.S. (1984), "A study of swelling characteristics and behavior of expansive soils," Ph.D thesis submitted to the Kakatiya University, Warangal, India.

Rao, A.S., Phanikumar B.R., and Sharma, R.S. (2004a). "Prediction of swelling characteristics of remoulded and compacted expansive soils using free swell index," *The Quarterly Journal of Engineering Geology and Hydrogeology*, Vol. 37, No. 3, pp. 217–226.

Rao, A.S., Phanikumar, B.R., Suresh, K., and Sudhakar, V. (2004b). "Compression test on granular pile-anchors embedded in expansive soils," Indian Geotechnical Conference, Warangal, India, pp. 141–144.

Satyanarayana, B. (1966), "Swelling pressure and related mechanical properties of black cotton soils," PhD Thesis, IISc, Bangalore.

Shanker, N.B. and Maruti, G. (1989). "Use of lime-soil piles for in-situ stabilization of black cotton soils," Proceedings, Indian Geotechnical Conference, Vol. 1, pp. 149–153.

Sharma, D., Jain, M.P., and Prakash, C. (1978), "Handbook on under-reamed and bored compaction pile foundations," Central Building Research Institute, Roorkee.

Sharma, R.S. (1998). "Mechanical behavior of unsaturated highly expansive clays," D.Phil. (Doctor of Philosophy) thesis, University of Oxford, England.

Sharma, R.S. (2000). "Recent advances in constitutive modeling of unsaturated soils," Keynote paper. Proceedings of International Conference on Geotechnical, Geoenvironmental Engineering, and Management in Arid Lands, Al Ain, UAE, A.A. Balkema, pp. 25–34.

Sharma, R.S. (2001). "Constitutive modeling of unsaturated soils: stress variables and strain increment parameters," Proceedings, 10th International Conference of International Association for Computer Methods and Advances in Geomechanics (IACMAG), Tucson, Arizona. A.A. Balkema, Vol. 1, pp. 395–400.

Sharma, R.S., and Phanikumar, B.R. (2005). "Laboratory Study of Heave Behavior of Expansive Clay Reinforced with Geopiles," *Journal of Geotechnical and Geoenvironmental Engineering, ASCE*, Vol. 131, No. 4, pp. 512–520.

Sharma, R.S., Phanikumar B.R., and Nagendra, B. (2004). "Compressive load response of geogrid-reinforced granular piles in soft clays," *Canadian Geotechnical Journal*, Vol. 41, pp. 187–192.

Technical Manual, TM 5-818-7. (1983). Department of the Army, USA.

Thorburn, S. and Mc Vicar, R.S.L. (1968), "Soil stabilization employing surface and depth vibrators," *The Structural Engineer*, Vol. 46, No. 10.

Wheeler, S.J., Sharma, R.S., and Bussien, M.S.R. (2003). "Coupling hydraulic hysteresis and stress-strain behavior in unsaturated soils," *Géotechnique,* Vol. 53, No. 1, pp. 41–54.

Wray, W.K. (1980). "Analysis of stiffened slabs on ground over expansive soil," Proceedings, 4th International Conference on Expansive Soils, American Society of Civil Engineers, Vol. 1, Denver, CO.

Index

Acrylic resin additive 405
Advanced techniques 185; digital imaging technology 260–266; finite element analysis of piers in expansive soils 231–244; neural networks for predicting swelling pressure (artificial neural networks) 245; remote sensing of expansive soils 187; spectroscopy for studying expansive soils 211–230
Air entrapment: model describing soil swelling 73
Al-Qatif clay 85
Anisotropic behavior of swelling soils (assessment of anisotropic behavior) 371
Ankara clay 289; coefficients of volume compressibility 293; compacted clay 289–294; damage details 149; dry density versus moisture content 291; oedometer test 290; predictive techniques 149; soil properties 290; swelling maps 149; swell potential 292; with lime 317–340
Ankara clay with lime 317–348; engineering properties 321; lime column technique 327–332; mineralogy and physicochemical properties 319
ANNs (artificial neural networks, advanced techniques) 245
Arabian Gulf coastal region 86; geology 87; soil characteristics 88
Argentina: non-vertisols of Pampas region 56
Argillite 81; permeability anisotropy 83
Artificial neural networks for predicting swelling pressure 245; applications in geotechnical engineering 246; charts for estimation of swelling pressure 253–255; modeling of swelling pressure 248; prediction equations 246
Assessment of anisotropic behavior of swelling soils: chemical stabilization 381; compaction 380; constant water content 380; factors affecting volume change 375; geotechnical problems 376; global distribution of expansive soils 372–374; mechanism of soils expansion 374; prewetting 380; protecting structures 381

Bentonites: geographic location of clay deposits 102; overview of mineralogy 37–54; principal deposits 49; swelling–shrinkage 117–126; water sorption and dilatation 101–114; world production 49
Black cotton soil: India 237; Sudan 238

Cement and lime 385–398; compression index versus sand content 403; compressive strength versus sand content 402; fly ash 395; influence of clay minerals 386; physical and engineering properties 405; porosity versus sand content 403; sand-resin treated soil 399–404; slaking versus sand content 402; treated with acrylic resin additive 405–414
Cement stabilized soil 369–416; assessment of anisotropic behavior 371; factors affecting volume change 375; geotechnical problems with construction work 376; mechanism of soils expansion 374; protecting structures from disturbances 381
Chemical composition: of bentonites 43; of smectites 43
Chemically modified sulfate-rich expansive clay 465, 483; dynamic properties 465–482; linear dynamic response 469; non-linear dynamic response 474; seasonal effects on behavior 483–504; shear modulus and damping ratio 495; swell-shrink response 487; test variables 467; unconfined compressive strength 489; undrained shear strength 491
Classification of expansive soils 3, 15, 25; degree of swell 33
Clay with lime 341–348
Clay mapping 187
Clay mineralogy in topsoil 63
Combined lime and polypropylene fibers stabilization 349–368; compaction

Combined lime and polypropylene fibers stabilization (*Continued*) relationships 354; properties of fibers 353; repeatability 355; X-ray diffraction studies 362
Compaction water content 22
Consolidation behavior 85
Construction techniques and remedial measures 505; assessment of anisotropic behavior of swelling soils 371; existing foundation practices 508; granular pile anchors 507–522; minimizing heave 508; special foundation techniques 511
Czech Republic: geographic location of clay deposits 102

Digital imaging technology: accessories 262; applications in geotechnical fields 261; digital imaging 261; hardware and software 262; linear shrinkage bar test 260; linear shrinkage strain 263, 265; measurement of shrinkage 262; mechanism of crack formation 259; for shrinkage strain characterization 257; volumetric shrinkage strain 264, 266
Distribution of expansive soils (classification) 3, 15, 25
Dynamic properties of expansive clay 465–482

Empirical models (finite element analysis): for predicting swelling potential 30–33
ESEM–DIA method: absolute error 122; aggregate deformation 125; to estimate swelling–shrinkage 117–126; hysteresis between swelling–shrinkage 124; MX80 bentonite 118; shrinkage potential isotherms 121; swelling potential isotherms 121
ESEM study of argillite 81–84; hydration/dehydration cycles 81; structural modifications 81
Existing foundation practices 508; minimizing heave 508
Expansive classification 19
Expansive shale 273–288

Finite element analysis of piers in expansive soils (advanced techniques) 231–244; displacement 235; distribution of stress 242; pier–grade beam configuration 232; pier length, diameter, and slip 239–240
Fly ash 359, 428, 453–464
Free swell index 173–184
Fuller's earth 50

Genesis of smectite-rich rocks 44; hydrothermal deposits 45; sedimentary deposits 45; volcano sedimentary deposits 44
Geology of expansive soils 3; from the Arabian Gulf 3–14
Geotechnical problems with construction work 376; buildings 376; canals 379; earth dams 377; retaining walls 379; roads 376; slopes 378; underground construction 379
Global distribution of expansive soils 372–374
Granular pile-anchors 507–522; basic philosophy 515; heave of reinforced clay bed 517; improvement of engineering properties of clay beds 519

Hazard assessment 187
Hydration/dehydration cycles of argillite 81; structural modifications 81
Hyperspectral imagery (advanced techniques) 188

Identification of expansive soils 15
Improvement of expansive soils: with rice husk ash 435
Indirect evaluation of swell potentials 19; Van Der Merwe method 20
Influence of sand content on cement-acrylic resin treated soil 399–404
Influence of trees on expansive soils 295; on clay 297; current footing design practice 300; national guidelines 296; reactive clay sites 301; sampling of sap pressure 308; soil suction 297, 304; streetscape 307; water potential of plants 300; wilting point 299; xylem pressures 309–311

Laboratory swell tests 278; comparison 284–286; constant volume 280; swell overburden 280; triaxial swell 281
Lime and polypropylene fiber stabilization 349–368; compaction relationships 354; cost analysis 364; free swell strain 359; linear shrinkage strain 361; physical properties of soil 352; plasticity 356; properties of fibers 353; repeatability 355; shear strength 356; soil specimen preparation 353; specifications for field mixing 365; statistical analysis 363; uniformity of specimens 355; X-ray diffraction studies 362
Lime column technique 327–332; performance 332–337
Lime stabilization 315; Ankara clay 317–340, 341–348; pozzolanic 419; SEMs 347; using cement and lime 385–398

Minimizing heave 508; mechanical 508; physical and chemical 509
Models describing process of: soil structural destabilization due to drying 74; soil swelling 73
Montmorillonite-rich clays: water sorption and dilatation 101–114

Natric soils 65; air entrapment 65; soil volume change 65
Neural networks (ANNs) for predicting swelling pressure (advanced techniques) 245; modeling 248; network architecture 252; prediction equations 246
Non-vertisolic soil swelling 55–78; causes and importance 55; clay mineralogy in topsoil 63; clod shrinkage characteristics 61, 63; shrinkage curves and indices 60–64; soil specific volume–water content 71; soil volume change caused by air entrapment 65; theory 58; X-diffractograms 59

Oedometer for assessing swelling 85–100; Al-Qatif clay 85; consolidation behavior 85; test procedures 16
Oman 3; geographic distribution of expansive soils 12; soil properties 10
Other soil stabilization treatment methods 417; California bearing ratio 446; case study from Indonesia 444; case study from Malaysia 436; chemical modification 465; linear dynamic response 469; non-linear dynamic response 474; pozzolanic agents 419
Overview of mineralogy of bentonites 37–54; genesis 37; industrial uses 37; physicochemical properties 37; world production 37

Permeability anisotropy 83
Piers in expansive soils 231–244
Plasticity index 27; correlation with swelling potential 28
Potential expansiveness of soil 26
Pozzolanic stabilization of expansive soils 419–432; applications 428; chemical stabilization 422; fly ash 428; mechanism of swelling 420; methods of incorporating lime into soil 424; rice husk ash 429; use of lime 429
Prediction of swelling characteristics with free swell index 173–184; direct measurement 175; effect of surcharge 180; free swell index and correlations 178, 181; identification of expansive soils 174; indirect correlations 175; mineralogical composition 174; neural networks 245; swelling pressure 245–256; validation 181
Protecting structures 381; footing size and depth 381; preventing uplift swelling pressures 382; use of rigid frames 383

Reactive clay sites, climate data, 301; influence on soil suction 304; rail corridor 301
Remolding techniques: compaction curves for soil 128; compression test 131; effect of initial water content on swelling pressure 134; effect on soil swelling and shear strength properties 127–138; swell potential test 132; zero swell test 131
Remote sensing of expansive soils (advanced techniques) 187; clay mapping 187; hazard assessment 187; hyperspectral imagery 188
Rice husk ash 435; California bearing ratio 446; case study from Indonesia 444; case study from Malaysia 436; swelling characteristics 447

Sand-resin treated soil 399–404; compression index versus sand content 403; compressive strength versus sand content 402; porosity versus sand content 403; slaking versus sand content 402
Seasonal effects on engineering behavior 483–504; shear modulus and damping ratio 495; swell-shrink response 487; unconfined compressive strength 489; undrained shear strength 491
Shrinkage strain characterization of expansive soils 257–270; digital imaging technology (advanced techniques) 257; measurement 262
Site characterization 271; on clay 297; current footing design practice 300; influence of soil suction 304; influence of trees 295; laboratory swell tests 278; map of case study area 274; national guidelines 296; rail corridor 301; research on reactive clay sites 301; soil characterization 277; soil suction 297, 304; streetscape 307–311; swelling behavior of expansive shale 273; water potential of plants 300; wilting point 299; volume change of Ankara clay 289
Smectite-rich rocks: classification 41; of commercial interest 39; crystal structure 40; industrial applications 48; mineralogy and chemistry 40; nuclear waste treatment 47; physical and physico-chemical properties 46; principal deposits and world production 49; *see also* Bentonites
Soil profiles 7

Soil shrinkage curves 64, 69
Soil specific volume–water content 71
Soil volume change caused by air entrapment 65; sources of trapped air 70
Solutions to geotechnical problems due to swelling: chemical stabilization 381; compaction 380; constant water content 380; prewetting 380
Special foundation techniques 511; belled piers 514; drilled piers 512; friction piers 513; granular pile anchors 507–522; under-reamed piles 514
Spectroscopy for studying expansive soils 211–230; clay minerals spectral properties 216–221; conventional remote sensing 223; conventional soil swelling determination 220; Gilgai topography 224; integration into potential mapping 221; soil spectra 220; spectral data interpretations 215; swelling potential mapping 213–215
Stabilization of expansive soils: Ankara clay with lime 317–340; clay with lime 341–348; effect of combined lime and polypropylene fibers 349–368; pozzolanic 419; using cement and lime 385–398
Swelling behavior: of Ankara clay 149–172; assessment of damage 163, 167; comparison 284–286; constant volume 280; damage details 149; effect of addition of fly ash 453–464; effect of climatic conditions 152; empirical equations 164; of expansive shale 273; of expansive soils with rice husk ash 435–452; geological setting 153; laboratory swell tests 278; mineralogy and physicochemical properties 154; predictive techniques 149; soil characterization 277; swell overburden 280; swelling maps 149, 168; swelling tests 159; triaxial swell 281
Swelling characteristics: free swell index 173–184
Swelling in non-vertisolic soils 55–78; caused by air entrapment 65; its causes and importance 55; clay mineralogy in topsoil 63; clod shrinkage characteristics 61, 63; different kinds 75; ESEM–DIA method 122; factors influencing 21; Pampas silty loams 55, 62–65; shrinkage curves and indices 60–62; soil shrinkage curves 64; soil specific volume-water content 71; soil volume change 55, 65–74; theory 58; X-diffractograms 59
Swelling pressure 16, 245–256; comparison of methods 137; compression test 131; effect of initial water content on swelling pressure 134; effect on soil swelling and shear strength properties 127–138; neural networks 245; swell potential test 132; zero swell test 131
Swelling rate 139–148; coefficients 144; particle size distribution 140; physical properties of soils 141; plasticity chart 141; rate of swelling and maximum swelling 144; swelling mechanism 142–143; swelling pressure 146; water absorption 145
Swell potential measurement of expansive soil: advanced techniques 185; Ankara clay 149–172; assessment of damage 163, 167; classification chart 29; climatic conditions 152; damage details 149; effect of fly ash 453; effect of surcharge 180; empirical equations for predicting swelling parameters 164; free swell index and correlations 178, 181; geological setting 153; identification of expansive soils 174; mineralogy and physicochemical properties 154; neural networks 245; prediction of swelling characteristics with free swell index 173–184; predictive techniques 149; remolding techniques 128; swelling maps 149, 168; swelling pressure 245–256; swelling rate of expansive clay soils 139–148; swelling tests 159; validation 181; water absorption 145

Trees and expansive soils 295

Void ratio–effective stress relationship 92
Volume change characteristics 79; absorption experiments 104; Al-Qatif clay 96; Ankara clay 289–294; of bentonites 101–114; coefficients of volume compressibility 293; correlation of experimental data 109; desorption experiments 103; dilatation experiments 105; dry density versus moisture content 291; effect of sample geometry 94–95; ESEM–DIA method 289–294; ESEM study of argillite 81–84; to estimate swelling–shrinkage of bentonite 117–126; hydration/dehydration cycles 81; montmorillonite-rich clays 101–114; oedometer for assessing swelling 85–100; oedometer test 290; soil properties 290; structural modifications 81; swell potential 292; vertical swelling pressure 93; void ratio–effective stress relationship 92; water sorption and dilatation 101–114

Water sorption and dilatation: of bentonites 101–114; montmorillonite-rich clays 101–114
Water table depth 72

X-ray diffraction studies 362